

**The characterisation of lignin-rich residues and their  
valorisation as biosolvents and adsorbents**

Daniel Steven Chernick

Submitted in accordance with the requirements for the degree of  
**Doctor of Philosophy as part of the Integrated PhD with MSc in  
Bioenergy**

**The University of Leeds  
School of Chemical and Process Engineering**

**October 2024**

The candidate confirms that the work submitted is his own, and that appropriate credit has been given where reference has been made to the work of others.

This copy has been supplied on the understanding that it is copyright material and that no quotation from the thesis may be published without proper acknowledgement.

## Acknowledgements

Amongst the pantheon of thanks that I must give, I could not have completed this PhD without Dr Andrew B Ross and Dr Valerie Dupont. Since I returned to the PhD after a year away due to the COVID-19 pandemic, Andy and Valerie helped me to re-focus, re-structure, and to make my work as strong as it possibly could be.

When I began my programme at the Bioenergy Centre for Doctoral Training (CDT) in 2018, Professor Richard Bourne and Professor John Blacker were present to support me in the development of the work plan and were always on-hand to discuss any issues that I had.

This thesis was proof-read before submission by a third-party proof-reader. The PGR confirms that the third-party proof-reading undertaken was in accordance with the Postgraduate Researcher Proof-reading policy.

In the weeks preceding the first COVID-19 lockdown in the United Kingdom in 2021, I was hosted by Dr Jessica Adams at Aberystwyth University for a placement. Although I could not complete the placement due to the first lockdown, Jess was always kind, thoughtful and an honour to work for.

I would like to acknowledge the Engineering and Physical Sciences Research Council (EPSRC), with Grant No. EP/L014912/1, for their funding in support of this research degree.

In the last 6 years, my knowledge and competence in the laboratory has grown due to the expertise of the technical staff (Simon Lloyd, Dr Adrian Cunliffe, and Karine Alves Thorne) and other PhD students (Dr Iram Razaq, Dr Jeanine Williams, Dr Aaron Brown, and Dr James Hammerton), without which the cost to replace broken lab consumables would be infinitely higher.

I must also thank the admin team for the CDT, James McKay and Emily Bryan-Kinns, who supported me at the start of the PhD, put me at ease and inspired me to enhance my personal development.

In addition to those mentioned previously, I must express gratitude to my colleagues and friends who I met whilst they were also completing their PhDs (Dr Scott Wiseman, Katherine Graves, Dr Gillian Finnerty, Karim Ismail, Katterin Hernandez, and Betul Esen). They were the people that I interacted with during the good days, the stressful days, and the very stressful days. Their lab support and emotional support during the last 6 years cannot be overstated.

My thanks must also go to everyone based at the School of Chemical and Process Engineering and Energy Building, in particular Jenny Jones, Ed Woodhouse, and Alastair Baker for their support.

Thank you to my immediate family (Felicia, Bernard, Jonathan, and Richard), who always asked me to explain my work in a single sentence to tell their friends. Your continued support in the last (nearly) three decades has allowed me to become the person I am today, for both bad and good (hopefully mostly good).

The greatest level of thanks must go to Oana. Without your support every single day, I would not have been able to complete this PhD, let alone complete this sen...

## Abstract

Since the industrial revolution, economies throughout the world have pursued greater capital at the cost of greater environmental pollution, energy consumption and waste accumulation.

To combat this, numerous countries' governments have set net zero greenhouse gas emission targets. As of 2016, notable emitters of greenhouse gas emissions were chemical and petrochemical manufacturing (3.6%), the burning of agricultural residues (3.5%), and agricultural soils due to synthetic nitrogen fertiliser applications (4.1%).

Therefore, in this thesis, a selection of biomass residues have been investigated for their potential applications as lignin-rich feedstocks to replace synthetic nitrogen fertilisers and petroleum-derived chemicals.

The lignin-rich nature of the biomass residues were explored through a variety of characterisation methods: proximate analysis, ultimate analysis, fibre analysis, atomic absorption spectroscopy and pyrolysis-gas chromatography/mass spectrometry (py-GC/MS). Here, the feedstock that performed best was a tree bark of an unknown species. This work necessitated the characterisation of a selection of identifiable tree barks.

From the characterisation of eleven different species of tree barks, the noble fir sample was found to have the greatest potential as a lignin-rich residue due to its high lignin content, low ash, and low alkaline earth metal content.

The properties of the lignin-rich residues after pyrolysis were investigated for their potential as bio-based solvents. The data from the py-GC/MS was used for the theoretical upgrading (by methylation and hydrogenation) of the key pyrolysis oil-derived components. The hazardousness and solubility of the three types of components were then assessed, with potential applications of lignin-rich residue-derived bio-based solvents being discussed.

The biomass residues were also explored for their application as ammonia adsorbents. The tree barks were tested both untreated and treated, as slow pyrolysis biochars and solvent-extracted samples. The untreated barks performed best and were found to be comparable in performance to costly gamma-alumina sorbents from the literature, but not as well as the most expensive zeolite catalysts. The untreated tree barks, as low-cost residues, may therefore be a good prospective ammonia adsorbent.

## Table of Contents

<b>Acknowledgements .....</b>	<b>iii</b>
<b>Abstract .....</b>	<b>iv</b>
<b>List of Tables .....</b>	<b>ix</b>
<b>List of Figures .....</b>	<b>xx</b>
<b>List of Equations .....</b>	<b>xxvi</b>
<b>List of Acronyms and Abbreviations .....</b>	<b>xxix</b>
<b>Chapter 1 – Introduction .....</b>	<b>1</b>
1.1 Background .....	1
1.1.1 Valorisation as a bio-based chemical .....	4
1.1.2 Valorisation of agricultural residues as ammonia adsorbents for the reduction of synthetic fertiliser use .....	8
1.2 Research gap .....	11
1.3 Aims and Objectives .....	13
1.4 Organisation of chapters .....	15
<b>Chapter 2 - Literature Review .....</b>	<b>17</b>
2.1 Lignin .....	17
2.1.1 Structure and properties of lignin .....	18
2.1.2 Extraction of lignin from biomass .....	23
2.2 Agricultural residues .....	27
2.2.1 Arising of agriculture by-products .....	27
2.2.2 Treatment methods of residues .....	29
<b>Chapter 3 - Materials and Methods .....</b>	<b>38</b>
3.1 Materials .....	38
3.1.1 Lignin products .....	38
3.1.2 Digestates .....	38
3.1.3 Other feedstocks .....	39
3.1.4 Tree barks .....	39
3.2 Proximate Analysis .....	41
3.3 Ultimate Analysis .....	43
3.4 Fibre Analysis .....	45
3.5 Crude Protein .....	51
3.6 Atomic absorption spectroscopy (AAS) .....	52
3.7 Thermal analysis .....	53
3.7.1 Derivative Thermogravimetry .....	53
3.7.2 Pyrolysis-Gas Chromatography/Mass Spectrometry .....	54

3.8	Thermal conversion .....	57
3.8.1	Slow pyrolysis .....	57
3.9	Extractions.....	60
3.9.1	Mild acid wash.....	60
3.9.2	Soxhlet solvent extraction .....	60
3.9.3	Accelerated Solvent Extraction .....	61
3.9.4	Rocket Evaporator .....	62
3.10	Liquid Injection Gas Chromatography/Mass Spectrometry.....	63
3.11	Solvent Hazardousness Assessment .....	65
3.12	Ammonia adsorption.....	67
3.12.1	Set-up of the experiments .....	67
3.12.2	Calculation of ammonia adsorption capacity in the fresh adsorbents .....	69
3.12.3	Comparison of adsorption capacity to literature data .....	71
3.13	Assessment of error and statistical analysis.....	75
3.14	Methods limitations.....	76
3.14.1	Atomic absorption spectroscopy .....	76
3.14.2	Fibre analysis.....	76
3.14.3	Ammonia adsorption experiments.....	76
3.15	Concluding remarks.....	77
<b>Chapter 4 – The screening and characterisation of lignin-rich feedstocks.....</b>		<b>78</b>
4.1	Introduction.....	78
4.1.1	Background.....	79
4.2	Results and Discussion .....	82
4.2.1	Proximate and Ultimate Analysis.....	82
4.2.2	Atomic Absorption Spectroscopy .....	85
4.2.3	Fibre Analysis.....	89
4.2.4	Pyrolysis-Gas Chromatography/Mass Spectrometry.....	91
4.2.5	Proximate Analysis, Ultimate Analysis and Derivative Thermogravimetry (DTG) of the acid-washed samples.....	105
<b>Chapter 5 – The characterisation and pyrolysis behaviour of tree barks.....</b>		<b>116</b>
5.1	Introduction.....	116
5.1.1	Background.....	117
5.2	Results and Discussion .....	125
5.2.1	Proximate and Ultimate Analysis.....	125

5.2.2	AAS.....	129
5.2.3	Fibre Analysis.....	130
5.2.4	Py-GC/MS of raw barks .....	132
5.2.5	Solvent Extraction .....	143
5.3	Conclusion.....	156
<b>Chapter 6 – The potential to produce bio-based solvents from the pyrolysis of lignin-rich residues .....</b>		<b>158</b>
6.1	Introduction.....	158
6.1.1	Background.....	159
6.2	Results and Discussion .....	166
6.2.1	Pyrolysis-Gas Chromatography/Mass Spectrometry.....	167
6.2.2	Comparison of pyrolysis oil components with common solvents 184	
6.3	Conclusion.....	200
<b>Chapter 7 – The potential to produce bio-based ammonia adsorbents from lignin-rich residues .....</b>		<b>202</b>
7.1	Introduction.....	202
7.1.1	Background.....	203
7.2	Results and Discussion .....	211
7.2.1	Ammonia Sorption Capacities .....	212
7.2.2	Comparison between this work and literature’s data.....	215
7.2.3	Statistical analysis of the effect of treatment on the samples’ adsorption capacity .....	223
7.3	Conclusion.....	228
<b>Chapter 8 – Conclusions and recommendations for further work .....</b>		<b>230</b>
8.1	Conclusions.....	230
8.2	Recommendations for further work .....	234
8.2.1	Limitations of the analysed tree barks.....	234
8.2.2	Further investigation of the valorisation of lignin-rich samples as bio-based solvents .....	235
8.2.3	Further investigation of the valorisation of lignin-rich samples as ammonia adsorbents.....	236
8.3	Closing Statement .....	238
<b>References.....</b>		<b>239</b>
<b>Appendix .....</b>		<b>292</b>
A.1	Solvent Hazardousness Justification tables .....	292
A.2	Ammonia adsorption appendices .....	302

A.2.1	Characterisation data for samples ran specifically for ammonia adsorption testing .....	302
A.2.2	Calculation of the partial pressures from the mass of ammonia. 321	
A.2.3	List of inputs for D-A models from Helminen et al.'s data. ....	325
A.2.4.	Calculation of the partial pressure of ammonia .....	326
A.3	Pyrolysis-Gas Chromatography/Mass Spectrometry peak tables...	333

## List of Tables

Table 1-1 - The global markets for all solvents and bio-based solvents (as of 2024) (51, 52). .....	6
Table 2-1 – Common metallic elements found in biomass (119), and their typical concentrations. ....	21
Table 2-2 - Summary of technical lignin recovery processes (100). ....	24
Table 2-3 - Conditions and products of different pyrolysis methods (260, 261). ....	34
Table 3-1 – Use of each material across this work. ....	40
Table 3-2 – Collection of Dumas conversion factors used in this work, adapted from literature. ....	51
Table 3-3 – Equipment and conditions used for the pyrolyser to perform pyrolysis-gas chromatography/mass spectrometry. ....	56
Table 3-4 – Equipment and conditions used for the GC/MS to perform pyrolysis-gas chromatography/mass spectrometry. ....	56
Table 3-5 – Accelerated Solvent Extraction conditions for the extraction of fats. ....	61
Table 3-6 – Equipment and conditions used to perform liquid-injection gas chromatography/mass spectrometry. ....	63
Table 3-7 – CHEM21 Safety Criteria. ....	65
Table 3-8 – CHEM21 Health Criteria. CMR = carcinogen, mutagen or reprotoxic. STOT = single target organ toxicity. ....	66
Table 3-9 – CHEM21 Environment Criteria. If chemical has H420, the score = 10. E.g. water: score = 1. ....	66
Table 3-10 – Ammonia sorption capacity testing conditions. ....	68
Table 3-11 – An example of the data presented by Helminen et al (380) for the generation of the Dubinin-Astakhov adsorption equilibrium model. This data are the isotherm parameters for the alumina sorbent. ....	72
Table 3-12 – Antoine equation component-specific constants for ammonia (382). ....	73
Table 3-13 – Thermodynamics data of ammonia, taken from Haar and Gallagher (385). ....	74
Table 4-1 - Feedstocks analysed in this chapter. ....	78
Table 4-2 - Proximate and Ultimate Analysis of lignin products, digestates and residues, with higher heating values (HHV) estimated with 3 methods. Error values were calculated by 1x standard deviation. 2 replicates were run for each sample. ....	84

<b>Table 4-3 - Metals Analysis of all untreated feedstocks. Error values were calculated by 1x standard deviation. 2 replicates were run for each sample .....</b>	<b>87</b>
<b>Table 4-4 - Metals Analysis of acid-washed feedstocks compared to the untreated feedstocks. Error values were calculated by 1x standard deviation. 2 replicates were run for each sample .....</b>	<b>87</b>
<b>Table 4-5 - Fibre Analysis (results in weight%). Error values were calculated by 1x standard deviation. 2 replicates were run for each sample. Moisture content (M) results are on an 'as analysed' (a.a) basis. Crude protein calculated by Table 2-2.....</b>	<b>90</b>
<b>Table 4-6 - The lignocellulosic composition of coconut husk in this study compared to in literature. Error values were calculated by standard deviation.....</b>	<b>90</b>
<b>Table 4-7 - Proportions of key and shared peaks of Lignoboost and organsolv lignin from fast pyrolysis at 550 °C by py-GC/MS. RT = Retention Time. The top 25 peaks of each chromatogram were identified using the NIST mass spectral database versions 147 and 27. ....</b>	<b>93</b>
<b>Table 4-8 - Proportions of key and shared peaks of untreated Alkali Lignin and acid-washed Alkali Lignin from fast pyrolysis at 550 °C by py-GC/MS. The top 25 peaks of each chromatogram were identified using the NIST mass spectral database versions 147 and 27. ....</b>	<b>94</b>
<b>Table 4-9 - Proportions of key and shared peaks of untreated and acid-washed agricultural residue digestate (AGRdig) and untreated vegetable, garden, and fruit residue digestate (VGFdig) from fast pyrolysis at 550 °C by py-GC/MS. The top 25 peaks of each chromatogram were identified using the NIST mass spectral database versions 147 and 27. ....</b>	<b>96</b>
<b>Table 4-10 - Proportions of key and shared peaks of untreated and acid-washed sewage sludge digestate (SSdig) and Municipal Solid Waste digestate (MSWdig) from fast pyrolysis at 550 °C by py-GC/MS. The top 25 peaks of each chromatogram were identified using the NIST mass spectral database versions 147 and 27. ....</b>	<b>98</b>
<b>Table 4-11 - Proportions of key and shared peaks of untreated and acid-washed coconut husk (CH) and Pakistani sugarcane bagasse (PKBag) from fast pyrolysis at 550 °C by py-GC/MS. The top 25 peaks of each chromatogram were identified using the NIST mass spectral database versions 147 and 27.....</b>	<b>100</b>
<b>Table 4-12 - Proportions of key peaks of SP Bark from fast pyrolysis at 550 °C by py-GC/MS. The top 25 peaks of each chromatogram were identified using the NIST mass spectral database versions 147 and 27. ....</b>	<b>101</b>
<b>Table 4-13 - Proximate and Ultimate Analysis of acid-washed samples. Error values were calculated by 1x standard deviation. 2 replicates were run for each sample.....</b>	<b>106</b>
<b>Table 4-14 - Proximate and Ultimate Analysis of acid-washed digestate samples. Error values were calculated by 1x standard deviation. 2 replicates were run for each sample. ....</b>	<b>106</b>

**Table 4-15 - Temperatures (°C) at which the cellulose volatilisation phase occurred for each untreated and acid-washed sample. ....113**

**Table 5-1 - Data of proximate and ultimate analysis taken from the Phyllis database (426). ....122**

**Table 5-2 - Range of lignocellulosic compositions for softwoods and hardwoods in the literature (428-431, 521). Values given as weight% on a dry basis. ....123**

**Table 5-3 - Stocked areas of tree species in Great Britain (88). ....124**

**Table 5-4 - Proximate and Ultimate Analysis of cypress barks, with higher heating values (HHV) estimated with 3 methods. Error values were calculated by 1x standard deviation. WRC = Western red cedar, NC = Nootka cypress, LC = Lawson cypress. ....125**

**Table 5-5 - Proximate and Ultimate Analysis of pine barks, with higher heating values (HHV) estimated with 3 methods. Error values were calculated by 1x standard deviation. NF = Noble fir, L = Larch, DF = Douglas fir, SS = Sitka spruce, NS = Norway spruce, ESF = European silver fir, GF = Grand fir, WH = Western hemlock. ....126**

**Table 5-6 - Estimated planting density of trees in the UK compared to the Netherlands. ....128**

**Table 5-7 - Metals analysis of raw tree barks. Error values were calculated by 1x standard deviation. Each tree bark was run in duplicate. NF = Noble fir, L = Larch, DF = Douglas fir, SS = Sitka spruce, NS = Norway spruce, ESF = European silver fir, GF = Grand fir, WH = Western hemlock, WRC = Western red cedar, NC = Nootka cypress, LC = Lawson cypress. ....129**

**Table 5-8 - Fibre analysis of raw tree barks. Moisture content (MC) is analysed on an 'as analysed (a.a.) basis, as it underwent oven drying at 60 °C after being received. Crude protein (wt%) calculated using Dumas conversion factors provided in Equation 3-6. All variables are presented on a wt% basis. Error values were calculated by 1x standard deviation. Fibre analysis was repeated in duplicate for each sample. NF = Noble fir, L = Larch, DF = Douglas fir, SS = Sitka spruce, NS = Norway spruce, ESF = European silver fir, GF = Grand fir, WH = Western hemlock, WRC = Western red cedar, NC = Nootka cypress, LC = Lawson cypress. Crude protein calculated by Table 2-2. ....130**

**Table 5-9 - Comparison of larch bark fibre analysis data in this work to the literature. ....131**

**Table 5-10 - Proportions of key and shared peaks of noble fir (NF), larch (L), Douglas fir (DF) and Sitka spruce (SS) tree bark from fast pyrolysis at 550 °C by py-GC/MS. RT = Retention Time. The top 25 peaks of each chromatogram were identified using the NIST mass spectral database versions 147 and 27. ....136**

<b>Table 5-11 - Proportions of key and shared peaks of Norway spruce (NS), European silver fir (ESF), grand fir (GF) and Western hemlock (WH) tree bark from fast pyrolysis at 550 °C by py-GC/MS. The top 25 peaks of each chromatogram were identified using the NIST mass spectral database versions 147 and 27.....</b>	<b>137</b>
<b>Table 5-12 - Proportions of key and shared peaks of Western red cedar (WRC), Nootka cypress (NC) and Lawson cypress (LC) tree bark from fast pyrolysis at 550 °C by py-GC/MS. The top 25 peaks of each chromatogram were identified using the NIST mass spectral database versions 147 and 27.....</b>	<b>140</b>
<b>Table 5-13 - Fibre Analysis of suberin-containing tree barks before and after solvent extraction (wt%). Moisture content (MC) data given on an ‘as analysed’ (a.a.) basis. Errors are presented with 1x standard deviation, and each sample was run in duplicate. ....</b>	<b>144</b>
<b>Table 5-14 - Fibre Analysis of non-suberin-containing tree barks before and after solvent extraction (wt%). Moisture content data given on an ‘as analysed’ (a.a.) basis. Errors are presented with 1x standard deviation, and each sample was run in duplicate. ....</b>	<b>144</b>
<b>Table 5-15 - Mass losses of tree barks after Soxhlet extraction. Errors are presented with 1x standard deviation, and each sample was run in duplicate.....</b>	<b>146</b>
<b>Table 5-16 - Distribution of pyrolysis-GC/MS compounds of bark samples to the solid and liquid phase after solvent extraction (in % peak area).....</b>	<b>152</b>
<b>Table 5-17 - Distribution of pyrolysis-GC/MS compounds of bark samples to the solid and liquid phase after solvent extraction (in % peak area).....</b>	<b>153</b>
<b>Table 5-18 - Comparison of compound classification peak areas from the py-GC/MS of post-Soxhlet extraction and post-ASE liquid residues. ....</b>	<b>154</b>
<b>Table 5-19 - Comparison of compound classification peak areas from the py-GC/MS of post-Soxhlet extraction and post-ASE liquid residues. ....</b>	<b>155</b>
<b>Table 6-1 - Hansen Solubility Parameter values for sorting into non-polar, polar aprotic and polar protic solvents. ....</b>	<b>162</b>
<b>Table 6-2 – List of samples explored for their potential as bio-based solvent precursors. ....</b>	<b>166</b>
<b>Table 6-3 – Compounds with the top 10 peak areas across all pyrolysis oil samples. ....</b>	<b>184</b>
<b>Table 6-4 – Hansen Solubility Parameters (HSPs) and CHEM21 hazardous scores of common pyrolysis oil compounds (PYx), methylated pyrolysis oil compounds (PYxM), and hydrogenated pyrolysis oil compounds (PYxH).....</b>	<b>190</b>
<b>Table 6-5 – Hansen Solubility Parameters (HSPs) and CHEM21 hazardous scores of common pyrolysis oil compounds (PYx), methylated pyrolysis oil compounds (PYxM), and hydrogenated pyrolysis oil compounds (PYxH).....</b>	<b>191</b>

**Table 6-6 – Comparison of similarities between non-polar common solvents and pyrolysis oil-derived components. Scores of 7 or above are deemed hazardous (and highlighted in red). ‘Peak areas’ are the combined totals and errors (calculated by 1x standard deviation of the peak areas of the base pyrolysis oil-derived component’s values) standard deviation) from each individual compound. Further information on PY codes can be found in Table 6-4 and Table 6-5.....194**

**Table 6-7 – Comparison of similarities between polar protic common solvents and pyrolysis oil-derived components. Scores of 7 or above are deemed hazardous (and highlighted in red). No hydrogenated PY compounds were similar to common solvents. ‘Peak areas’ are the combined totals and errors (calculated by 1x standard deviation of the peak areas of the base pyrolysis oil-derived component’s values) from each individual compound. Further information on PY codes can be found in Table 6-4 and Table 6-5.....195**

**Table 6-8 – Comparison of similarities between polar aprotic common solvents and pyrolysis oil-derived components. Scores of 7 or above are deemed hazardous (and highlighted in red). NMP = n-methyl pyrrolidone. DMF = dimethyl formamide. No hydrogenated PY compounds were similar to common solvents. ‘Peak areas’ are the combined totals and errors (calculated by 1x standard deviation of the peak areas of the base pyrolysis oil-derived component’s values) from each individual compound. Further information on PY codes can be found in Table 6-4 and Table 6-5.....196**

**Table 6-9 – List of the non-hazardous (where no CHEM21 categories’ score is above 7) pyrolysis oil-derived components that are considered similar to hazardous common solvents. ‘Peak areas’ are the combined totals and errors (calculated by 1x standard deviation of the peak areas of the base pyrolysis oil-derived component’s values) from each individual compound. ....197**

**Table 7-1 - Range of proximate and ultimate analysis values for peat in the literature (735-738). Moisture content on an ‘as received’ (a.r) basis. All other values given on a ‘dry basis’ (d.b). ....209**

**Table 7-2 - List of samples explored for their ammonia adsorption capacity in Chapter 7. ....211**

**Table 7-3 - Ammonia sorption capacity (mgNH<sub>3</sub>/g fresh adsorbent) of raw tree bark samples compared to treated barks and activated carbons. Errors presented as 1x standard deviation. Adsorption testing run in duplicate. Ultimate analysis samples run in duplicate. ....213**

**Table 7-4 - Change in base nitrogen contents of biochars before and after hot-water washing. Errors presented as 1x standard deviation. Ultimate analysis samples run in duplicate. ....213**

**Table 7-5 - Ammonia sorption capacity (change in nitrogen contents, in mgN/g sample) of tree bark samples from this work and Dorward’s study (691). Errors presented as 1x standard deviation. Adsorption testing run in duplicate. Ultimate analysis samples run in duplicate. NM = not measured. NF = noble fir, ESF = European silver fir, GF = grand fir, DF = Douglas fir, NC = nootka cypress. ....214**

**Table 7-6 - Ammonia sorption capacity (mgNH<sub>3</sub>/g fresh adsorbent) of non-bark samples. Errors presented as 1x standard deviation. Adsorption testing run in duplicate. Ultimate analysis samples run in duplicate. CH = coconut husk, PeatSEPO = Irish peat, PeatMoss = moss sphagnum peat, MSWdig = municipal solid waste digestate, VGFdig = vegetable, garden, fruit residue digestate.....214**

**Table 7-7 - Ammonia sorption capacity (mgNH<sub>3</sub>/g fresh adsorbent) of commercial lignin products. Errors presented as 1x standard deviation. Adsorption testing run in duplicate. Ultimate analysis samples run in duplicate. ....215**

**Table 7-8 – Summary of the main results calculated for the constant parameters before and after ammonia adsorption reactions. ....216**

**Table 7-9 – Adsorption capacities of untreated biosolid samples from this study at 1.442 kPa.....218**

**Table 7-10 - Comparison of this study’s adsorption capacities to Helminen (380). All unspecified values are given in mgNH<sub>3</sub>/g of fresh adsorbent. Errors presented as 1x standard deviation, from 4 datapoints for each sample in this study R<sup>2</sup> is given for data interpolated by the Dubinin-Astakhov equilibrium model. Conversion of gaseous ammonia masses to partial pressures are presented in the Appendix (A1.2.2).....221**

**Table 7-11– Univariate statistical analysis outputs of ammonia adsorption capacity (mgNH<sub>3</sub>/ g fresh adsorbent) against sample treatment, outlined as [a] Descriptive Statistics and [b] Pairwise Comparisons. ....223**

**Table 7-12 – Multivariate statistical analysis outputs of [a] Descriptive Statistics and [b] Pairwise Comparisons of untreated (Treatment=0) and treated samples (Treatment=1) for molar H/C, molar O/C, and volatile matter/fixed carbon (VM/FC) ratios.....225**

**Table 7-13 – Numbering of biomass types for the comparison of differences in proximate and ultimate analysis values.....226**

**Table A1-1 – Environmental scoring of pyrolysis oil-derived components...293**

**Table A1-2– Safety scoring of pyrolysis oil-derived components.....293**

**Table A1-3 – Health scoring of pyrolysis oil-derived components. ....294**

**Table A1-4 – Environmental scoring of methylated pyrolysis oil-derived components. ....294**

**Table A1-5 – Safety scoring of methylated pyrolysis oil-derived components. ....295**

<b>Table A1-6 – Health scoring of methylated pyrolysis oil-derived components.</b>	<b>295</b>
<b>Table A1-7 – Environmental scoring of hydrogenated pyrolysis oil-derived components.</b>	<b>296</b>
<b>Table A1-8 – Safety scoring of hydrogenated pyrolysis oil-derived components.</b>	<b>296</b>
<b>Table A1-9 – Health scoring of hydrogenated pyrolysis oil-derived components.</b>	<b>297</b>
<b>Table A1-10 – Environmental scoring of non-polar common solvents.</b>	<b>298</b>
<b>Table A1-11 – Safety scoring of non-polar common solvents.</b>	<b>299</b>
<b>Table A1-12 – Health scoring of non-polar common solvents.</b>	<b>300</b>
<b>Table A1-13 – Environmental scoring of non-polar common solvents.</b>	<b>301</b>
<b>Table A1-14 – Safety scoring of non-polar common solvents.</b>	<b>301</b>
<b>Table A1-15 – Health scoring of non-polar common solvents.</b>	<b>301</b>
<b>Table A2-1 – Proximate Analysis of raw tree barks used in Chapter 7. Error calculated by 1x standard deviation. Samples run in duplicate.</b>	<b>302</b>
<b>Table A2-2 – Proximate Analysis of treated tree barks and activated carbons used in Chapter 7. ‘bc’ = biochar, ‘HW’ = hot water-washed, ‘Sox’ = solvent extraction solid residue. Error calculated by 1x standard deviation. Samples run in duplicate.</b>	<b>303</b>
<b>Table A2-3 – Proximate Analysis of ‘miscellaneous’ samples used in Chapter 7. Error calculated by 1x standard deviation. Samples run in duplicate.</b>	<b>303</b>
<b>Table A2-4 – Ultimate Analysis of raw tree barks used in Chapter 7. Error calculated by 1x standard deviation. Samples run in duplicate.</b>	<b>304</b>
<b>Table A2-5 – Ultimate Analysis of treated tree barks and activated carbons used in Chapter 7. ‘bc’ = biochar, ‘HW’ = hot water-washed, ‘Sox’ = solvent extraction solid residue. Error calculated by 1x standard deviation. Samples run in duplicate.</b>	<b>304</b>
<b>Table A2-6 – Ultimate Analysis of ‘miscellaneous’ samples used in Chapter 7. Error calculated by 1x standard deviation. Samples run in duplicate.</b>	<b>304</b>
<b>Table A2-7 – Ultimate Analysis of coconut husk after each ammonia adsorption experiment. In XX-A-B-C, A = ammonium sulphate concentration (AMS), B = ammonia adsorption experiment replicate number, C = ultimate analysis replicate number. Uncorr H = hydrogen uncorrected for moisture content.</b>	<b>305</b>
<b>Table A2-8 – Ultimate Analysis of European silver fir tree bark after each ammonia adsorption experiment. In XX-A-B-C, A = ammonium sulphate concentration (AMS), B = ammonia adsorption experiment replicate number, C = ultimate analysis replicate number. Uncorr H = hydrogen uncorrected for moisture content.</b>	<b>305</b>

**Table A2-9 – Ultimate Analysis of noble fir tree bark after each ammonia adsorption experiment. In XX-A-B-C, A = ammonium sulphate concentration (AMS), B = ammonia adsorption experiment replicate number, C = ultimate analysis replicate number. Uncorr H = hydrogen uncorrected for moisture content.....306**

**Table A2-10 – Ultimate Analysis of nootka cypress tree bark after each ammonia adsorption experiment. In XX-A-B-C, A = ammonium sulphate concentration (AMS), B = ammonia adsorption experiment replicate number, C = ultimate analysis replicate number. Uncorr H = hydrogen uncorrected for moisture content.....306**

**Table A2-11 – Ultimate Analysis of grand fir tree bark after each ammonia adsorption experiment. In XX-A-B-C, A = ammonium sulphate concentration (AMS), B = ammonia adsorption experiment replicate number, C = ultimate analysis replicate number. Uncorr H = hydrogen uncorrected for moisture content.....307**

**Table A2-12 – Ultimate Analysis of Douglas fir tree bark after each ammonia adsorption experiment. In XX-A-B-C, A = ammonium sulphate concentration (AMS), B = ammonia adsorption experiment replicate number, C = ultimate analysis replicate number. Uncorr H = hydrogen uncorrected for moisture content.....307**

**Table A2-13 – Ultimate Analysis of oak after each ammonia adsorption experiment. In XX-A-B-C, A = ammonium sulphate concentration (AMS), B = ammonia adsorption experiment replicate number, C = ultimate analysis replicate number. Uncorr H = hydrogen uncorrected for moisture content.....308**

**Table A2-14 – Ultimate Analysis of peat moss after each ammonia adsorption experiment. In XX-A-B-C, A = ammonium sulphate concentration (AMS), B = ammonia adsorption experiment replicate number, C = ultimate analysis replicate number. Uncorr H = hydrogen uncorrected for moisture content.....308**

**Table A2-15 – Ultimate Analysis of PeatSEPO after each ammonia adsorption experiment. In XX-A-B-C, A = ammonium sulphate concentration (AMS), B = ammonia adsorption experiment replicate number, C = ultimate analysis replicate number. Uncorr H = hydrogen uncorrected for moisture content.....309**

**Table A2-16 – Ultimate Analysis of European silver fir tree bark biochar after each ammonia adsorption experiment. In XX-A-B-C, A = ammonium sulphate concentration (AMS), B = ammonia adsorption experiment replicate number, C = ultimate analysis replicate number. Uncorr H = hydrogen uncorrected for moisture content.....310**

**Table A2-17 – Ultimate Analysis of noble fir tree bark biochar after each ammonia adsorption experiment. In XX-A-B-C, A = ammonium sulphate concentration (AMS), B = ammonia adsorption experiment replicate number, C = ultimate analysis replicate number. Uncorr H = hydrogen uncorrected for moisture content.....310**

<b>Table A2-18 – Ultimate Analysis of Douglas fir tree bark biochar after each ammonia adsorption experiment. In XX-A-B-C, A = ammonium sulphate concentration (AMS), B = ammonia adsorption experiment replicate number, C = ultimate analysis replicate number. Uncorr H = hydrogen uncorrected for moisture content.....</b>	<b>311</b>
<b>Table A2-19 – Ultimate Analysis of nootka cypress tree bark biochar after each ammonia adsorption experiment. In XX-A-B-C, A = ammonium sulphate concentration (AMS), B = ammonia adsorption experiment replicate number, C = ultimate analysis replicate number. Uncorr H = hydrogen uncorrected for moisture content.....</b>	<b>311</b>
<b>Table A2-20 – Ultimate Analysis of Lawson cypress tree bark biochar after each ammonia adsorption experiment. In XX-A-B-C, A = ammonium sulphate concentration (AMS), B = ammonia adsorption experiment replicate number, C = ultimate analysis replicate number. Uncorr H = hydrogen uncorrected for moisture content.....</b>	<b>312</b>
<b>Table A2-21 – Ultimate Analysis of larch tree bark biochar after each ammonia adsorption experiment. In XX-A-B-C, A = ammonium sulphate concentration (AMS), B = ammonia adsorption experiment replicate number, C = ultimate analysis replicate number. Uncorr H = hydrogen uncorrected for moisture content.....</b>	<b>312</b>
<b>Table A2-22 – Ultimate Analysis of Norway spruce tree bark biochar after each ammonia adsorption experiment. In XX-A-B-C, A = ammonium sulphate concentration (AMS), B = ammonia adsorption experiment replicate number, C = ultimate analysis replicate number. Uncorr H = hydrogen uncorrected for moisture content.....</b>	<b>312</b>
<b>Table A2-23 – Ultimate Analysis of NORIT activated carbon after each ammonia adsorption experiment. In XX-A-B-C, A = ammonium sulphate concentration (AMS), B = ammonia adsorption experiment replicate number, C = ultimate analysis replicate number. Uncorr H = hydrogen uncorrected for moisture content.....</b>	<b>313</b>
<b>Table A2-24 – Ultimate Analysis of SIGMA activated carbon after each ammonia adsorption experiment. In XX-A-B-C, A = ammonium sulphate concentration (AMS), B = ammonia adsorption experiment replicate number, C = ultimate analysis replicate number. Uncorr H = hydrogen uncorrected for moisture content.....</b>	<b>313</b>
<b>Table A2-25 – Ultimate Analysis of oak biochar after each ammonia adsorption experiment. In XX-A-B-C, A = ammonium sulphate concentration (AMS), B = ammonia adsorption experiment replicate number, C = ultimate analysis replicate number. Uncorr H = hydrogen uncorrected for moisture content.....</b>	<b>314</b>
<b>Table A2-26 – Ultimate Analysis of hot water-washed Douglas fir tree bark biochar after each ammonia adsorption experiment. In XX-A-B-C, A = ammonium sulphate concentration (AMS), B = ammonia adsorption experiment replicate number, C = ultimate analysis replicate number. Uncorr H = hydrogen uncorrected for moisture content.....</b>	<b>314</b>

<b>Table A2-27 – Ultimate Analysis of hot water-washed noble fir tree bark biochar after each ammonia adsorption experiment. In XX-A-B-C, A = ammonium sulphate concentration (AMS), B = ammonia adsorption experiment replicate number, C = ultimate analysis replicate number. Uncorr H = hydrogen uncorrected for moisture content.....</b>	<b>315</b>
<b>Table A2-28 – Ultimate Analysis of Soxhlet-extracted grand fir tree bark after each ammonia adsorption experiment. In XX-A-B-C, A = ammonium sulphate concentration (AMS), B = ammonia adsorption experiment replicate number, C = ultimate analysis replicate number. Uncorr H = hydrogen uncorrected for moisture content.....</b>	<b>315</b>
<b>Table A2-29 – Ultimate Analysis of Soxhlet-extracted Douglas fir tree bark after each ammonia adsorption experiment. In XX-A-B-C, A = ammonium sulphate concentration (AMS), B = ammonia adsorption experiment replicate number, C = ultimate analysis replicate number. Uncorr H = hydrogen uncorrected for moisture content.....</b>	<b>316</b>
<b>Table A2-30 – Ultimate Analysis of municipal solid waste digestate after each ammonia adsorption experiment. In XX-A-B-C, A = ammonium sulphate concentration (AMS), B = ammonia adsorption experiment replicate number, C = ultimate analysis replicate number. Uncorr H = hydrogen uncorrected for moisture content.....</b>	<b>316</b>
<b>Table A2-31 – Ultimate Analysis of vegetable, garden, and fruit residue digestate after each ammonia adsorption experiment. In XX-A-B-C, A = ammonium sulphate concentration (AMS), B = ammonia adsorption experiment replicate number, C = ultimate analysis replicate number. Uncorr H = hydrogen uncorrected for moisture content.....</b>	<b>317</b>
<b>Table A2-32 – Fibre Analysis of raw tree barks used in Chapter 7. Error calculated by 1x standard deviation. Samples run in duplicate. ....</b>	<b>320</b>
<b>Table A2-33 – Fibre Analysis of ‘miscellaneous’ samples used in Chapter 7. Error calculated by 1x standard deviation. Samples run in duplicate... </b>	<b>320</b>
<b>Table A2-34 – Dilutions of ammonium sulphate and NaOH at each ammonia adsorption experiment. ....</b>	<b>321</b>
<b>Table A2-35 – Total volumes of water used in the dilutions of ammonium sulphate and NaOH at each ammonia adsorption experiment. ....</b>	<b>321</b>
<b>Table A2-36 – The isotherm parameters of the sorbents investigated by Helminen et al. (380) for the Dubinin-Astakhov ammonia adsorption equilibrium model. ....</b>	<b>325</b>
<b>Table A3-1 – Peak tables of samples representing each category of sample. ....</b>	<b>333</b>
<b>Table A3-2 – Peak table for py-GC/MS of lignoboost at 550 °C. Highlighted cells denote compounds discussed in the results chapters. ....</b>	<b>334</b>
<b>Table A3-3 – Peak table for py-GC/MS of MSW digestate at 550 °C. Highlighted cells denote compounds discussed in the results chapters. ....</b>	<b>335</b>

<b>Table A3-4 – Peak table for py-GC/MS of coconut husk (CH) at 550 °C. Highlighted cells denote compounds discussed in the results chapters.</b>	<b>336</b>
<b>Table A3-5 – Peak table for py-GC/MS of acid-washed MSW digestate at 550 °C. Highlighted cells denote compounds discussed in the results chapters.</b>	<b>337</b>
<b>Table A3-6 - Peak table for py-GC/MS of grand fir (GF) tree bark at 550 °C. Highlighted cells denote compounds discussed in the results chapters.</b>	<b>338</b>
<b>Table A3-7 - Peak table for py-GC/MS of solvent-extracted solid grand fir (GFSox) tree bark at 550 °C. Highlighted cells denote compounds discussed in the results chapters.</b>	<b>339</b>

## List of Figures

Figure 1-1 – Global greenhouse gas emissions by sector for the year 2016. Sourced from (8). .....	1
Figure 1-2 – Illustration of the building blocks of lignin’s structure, connected via several linkages. Sourced from (32). .....	4
Figure 1-3 – Potential routes for valorising agricultural residues, producing bio-based chemicals, and recovering excess nitrogen or ammonia.....	11
Figure 1-4 - Scope of the work in this thesis. ....	14
Figure 2-1 – The oxidative polymerisation of lignin’s three main monolignols. Sourced from (100). .....	18
Figure 2-2 – Images showing lignin colour lightening as the molecular weight decreases. Sourced from (109). .....	19
Figure 2-3 - Glass transition temperatures of native lignin from herbaceous plants, softwoods, and hardwoods. Sourced from (116). .....	20
Figure 2-4 – The structure of a rice grain. Sourced from (218).....	28
Figure 2-5 – Simple scheme of anaerobic digestion pathways. Sourced from (243). .....	31
Figure 3-1 – Example of a thermogravimetric curve. The mass loss that occurs across the regions outlined represent the moisture (M), volatile matter (VM), fixed carbon (FC), and ash content of the sample. ....	42
Figure 3-2 – Image of the Fibretherm equipment used for fibre analysis. ....	46
Figure 3-3 – Images of [a] the glass spacer and quartz crucible, and [b] the Fibrebag around the glass spacer used for fibre analysis.....	46
Figure 3-4 - Carousel used within the Fibretherm equipment for fibre analysis. ....	47
Figure 3-5 – Small steel carousel used for the fibre analysis acid step.....	48
Figure 3-6 – Example of a thermogravimetric analysis (TGA) curve, overlaid with a derivative thermogravimetric (DTG) curve. Sourced from (357)...	53
Figure 3-7 – TGA/DTG heating programme used in this work, with illustrations of lignocellulosic components degradation temperature ranges.....	54
Figure 3-8 – Diagram of a platinum-coil pyrolyser. Sourced from (361). ....	55
Figure 3-9 – Diagram of char production using a kiln reactor. Sourced from (315). .....	57
Figure 3-10 – Fixed bed reactor for batch processes. Sourced from (315). ....	58
Figure 3-11 - Fixed-bed slow pyrolysis reactor used for production of biochar. ....	59
Figure 3-12 – Diagram of the split/splitless injector commonly used in liquid-injection GC/MS. Adapted from (375). .....	63

<b>Figure 3-13 – Chromatogram output from a GC or GC/MS. Sourced from (376).</b> .....	<b>64</b>
<b>Figure 3-14 - Batch set-up of ammonia adsorption tests.....</b>	<b>67</b>
<b>Figure 3-15 - The graphical representation of Helminen et al's (380) ammonia adsorption data for alumina. ....</b>	<b>71</b>
<b>Figure 3-16 – Change in saturated liquid density of ammonia against the natural log of the saturated pressure. ....</b>	<b>74</b>
<b>Figure 4-1 –The overall scope of this study. The work covered in Chapter 4 is denoted by red dotted lines. ....</b>	<b>78</b>
<b>Figure 4-2 - Relative change of metals concentration between acid-washed and untreated samples. ....</b>	<b>88</b>
<b>Figure 4-3 - Fast pyrolysis chromatograms of [a] Lignoboost and [b] organosolv lignin at 550 °C by py-GC/MS. Pyrolysis heating rate of 20 °C/ms, then held for 20s. Column temperature program of 40 °C for 2 min, 6 °C/min ramp to 280 °C, then hold for 10 min.....</b>	<b>92</b>
<b>Figure 4-4 - Fast pyrolysis chromatogram of untreated Alkali Lignin at 550 °C by py-GC/MS. Pyrolysis heating rate of 20 °C/ms, then held for 20s. Column temperature program of 40 °C for 2 min, 6 °C/min ramp to 280 °C, then hold for 10 min.....</b>	<b>94</b>
<b>Figure 4-5 - Fast pyrolysis chromatogram of [a] untreated AGRdig and [b] untreated VGFdig at 550 °C by py-GC/MS. AGRdig and VGFdig are presented at different y-axis scales due to the large difference in absolute intensities measured. Pyrolysis heating rate of 20 °C/ms, then held for 20s. Column temperature program of 40 °C for 2 min, 6 °C/min ramp to 280 °C, then hold for 10 min. ....</b>	<b>95</b>
<b>Figure 4-6 - Fast pyrolysis chromatogram of [a] untreated SSdig and [b] untreated MSWdig at 550 °C by py-GC/MS. SSdig and MSWdig are presented at different y-axis scales due to the large difference in absolute intensities measured. Pyrolysis heating rate of 20 °C/ms, then held for 20s. Column temperature program of 40 °C for 2 min, 6 °C/min ramp to 280 °C, then hold for 10 min. ....</b>	<b>97</b>
<b>Figure 4-7 - Proportions of key and shared peaks of untreated and acid- washed sewage sludge digestate (SSdig) and Municipal Solid Waste digestate (MSWdig) from fast pyrolysis at 550 °C by py-GC/MS. The top 25 peaks of each chromatogram were identified using the NIST mass spectral database versions 147 and 27. ....</b>	<b>98</b>
<b>Figure 4-8 - Fast pyrolysis chromatogram of [a] untreated coconut husk and [b] untreated PKBag at 550 °C by py-GC/MS. CH and PKBag are presented at different y-axis scales due to the large difference in absolute intensities measured. Pyrolysis heating rate of 20 °C/ms, then held for 20s. Column temperature program of 40 °C for 2 min, 6 °C/min ramp to 280 °C, then hold for 10 min. ....</b>	<b>99</b>

**Figure 4-9 - Fast pyrolysis chromatogram of SP Bark at 550 °C by py-GC/MS. Pyrolysis heating rate of 20 °C/ms, then held for 20s. Column temperature program of 40 °C for 2 min, 6 °C/min ramp to 280 °C, then hold for 10 min. ....101**

**Figure 4-10 - DTG of the lignin products (alkali lignin, Lignoboost, organosolv lignin). Conditions: Starting mass ≈ 10 mg, pyrolysed in a nitrogen atmosphere of 30 ml/min with a heating rate of 25 °C/min.....108**

**Figure 4-11 - DTG of PKBag, coconut husk and SP Bark. Conditions: Starting mass ≈ 10 mg, pyrolysed in a nitrogen atmosphere of 30 ml/min with a heating rate of 25 °C/min.....109**

**Figure 4-12 - DTG of Vegetable, Garden and Fruit residue digestate (VGFdig). Conditions: Starting mass ≈ 10 mg, pyrolysed in a nitrogen atmosphere of 30 ml/min with a heating rate of 25 °C/min.....109**

**Figure 4-13 - DTG of untreated and acid-washed alkali lignin. Conditions: Starting mass ≈ 10 mg, pyrolysed in a nitrogen atmosphere of 30 ml/min with a heating rate of 25 °C/min. ....110**

**Figure 4-14 - DTG of untreated and acid-washed [a] Municipal Solid Waste digestate (MSWdig), [b] agricultural residue (AGRdig) and [c] sewage sludge digestate (SSdig). Conditions: Starting mass ≈ 10 mg, pyrolysed in a nitrogen atmosphere of 30 ml/min with a heating rate of 25 °C/min. ....111**

**Figure 4-15 - DTG of untreated and acid-washed coconut husk. Conditions: Starting mass ≈ 10 mg, pyrolysed in a nitrogen atmosphere of 30 ml/min with a heating rate of 25 °C/min. ....112**

**Figure 4-16 - DTG of untreated and acid-washed sugarcane bagasse from Pakistan (PKBag). Conditions: Starting mass ≈ 10 mg, pyrolysed in a nitrogen atmosphere of 30 ml/min with a heating rate of 25 °C/min. ....112**

**Figure 5-1 – The overall scope of this study. The work covered in Chapter 5 is denoted by red dotted lines. ....116**

**Figure 5-3 - Fast pyrolysis chromatograms of pine family barks, including [a] noble fir (NF), [b] larch (L), [c] Douglas fir (DF), [d] sitka spruce (SS) at 550 °C by py-GC/MS. Samples are presented at different y-axis scales due to the large difference in absolute intensities measured. Pyrolysis heating rate of 20 °C/ms, then held for 20s. Column temperature program of 40 °C for 2 min, 6 °C/min ramp to 280 °C, then hold for 10 min.....133**

**Figure 5-4 - Fast pyrolysis chromatograms of pine family barks, including [a] Norway spruce (NS), [b] European silver fir (ESF), [c] grand fir (GF) and [d] Western hemlock (WH) at 550 °C by py-GC/MS. Samples are presented at different y-axis scales due to the large difference in absolute intensities measured. Pyrolysis heating rate of 20 °C/ms, then held for 20s. Column temperature program of 40 °C for 2 min, 6 °C/min ramp to 280 °C, then hold for 10 min. ....135**

Figure 5-5 - Fast pyrolysis chromatograms of cypress family barks, including [a] Western red cedar (WRC), [b] Nootka cypress (NC) and [c] Lawson cypress (LC) at 550 °C by py-GC/MS. Pyrolysis heating rate of 20 °C/ms, then held for 20s. Column temperature program of 40 °C for 2 min, 6 °C/min ramp to 280 °C, then hold for 10 min.....	139
Figure 5-6 - Derivative Thermogravimetric curves of raw and Soxhlet residues of [a] Douglas fir and [b] European silver fir tree bark.....	147
Figure 5-7 - Derivative Thermogravimetric curves of raw and Soxhlet residues of [a] grand fir and [b] noble fir tree bark.....	147
Figure 5-8 - Derivative Thermogravimetric curves of raw and Soxhlet residues of [a] larch and [b] Western hemlock tree bark.....	148
Figure 5-9 - Derivative Thermogravimetric curves of [a] raw Norway spruce and raw and Soxhlet residues of [b] Lawson cypress tree bark.....	148
Figure 5-10 - Derivative Thermogravimetric curves of raw and Soxhlet residues of [a] Western red cedar, [b] Nootka cypress tree bark, and [c] Lawson cypress.....	149
Figure 6-1 –The overall scope of this study. The work covered in Chapter 6 is denoted by red dotted lines. ....	158
Figure 6-2 - Common solvents organised into polar protic, polar aprotic and non-polar. Sourced from (559).....	160
Figure 6-3 - Considerations for environmental, health and safety in solvent selection guides. Sourced from (568).....	161
Figure 6-4 - Peak areas (%) of 2-methoxy phenol across [a] commercial lignin products, [b] biomass residues, [c] fir tree barks, [d] pine tree barks, [e] cypress tree barks and [f] the average of all categories. Each sample was run once. Errors in [f] are 1x standard error, taken from collating the data points in [a] – [e]. Individual peak areas have been normalised.....	169
Figure 6-5 – Peak areas (%) of phenol across [a] commercial lignin products, [b] biomass residues, [c] fir tree barks, [d] pine tree barks, [e] cypress tree barks and [f] the average of all categories. Each sample was run once. Errors in [f] are 1x standard error, taken from collating the data points in [a] – [e]. Individual peak areas have been normalised.....	170
Figure 6-6 - Peak areas (%) of trans-isoeugenol across [a] commercial lignin products, [b] biomass residues, [c] fir tree barks, [d] pine tree barks, [e] cypress tree barks and [f] the average of all categories. Each sample was run once. Errors in [f] are 1x standard error, taken from collating the data points in [a] – [e]. Individual peak areas have been normalised.....	171
Figure 6-7 - Peak areas (%) of creosol across [a] commercial lignin products, [b] biomass residues, [c] fir tree barks, [d] pine tree barks, [e] cypress tree barks and [f] the average of all categories. Each sample was run once. Errors in [f] are 1x standard error, taken from collating the data points in [a] – [e]. Individual peak areas have been normalised.....	172

Figure 6-8 - Peak areas (%) of furfural across [a] commercial lignin products, [b] biomass residues, [c] fir tree barks, [d] pine tree barks, [e] cypress tree barks and [f] the average of all categories. Each sample was run once. Errors in [f] are 1x standard error, taken from collating the data points in [a] – [e]. Individual peak areas have been normalised.....	174
Figure 6-9 - Peak areas (%) of 5-methyl-2-furancarboxaldehyde (MFCA) across [a] commercial lignin products, [b] biomass residues, [c] fir tree barks, [d] pine tree barks, [e] cypress tree barks and [f] the average of all categories. Each sample was run once. Errors in [f] are 1x standard error, taken from collating the data points in [a] – [e]. Individual peak areas have been normalised. ....	175
Figure 6-10 - Peak areas (%) of lignin-derived compounds of raw and solvent-extracted [a] fir tree barks, [b] pine tree barks, and [c] cypress tree barks at 550 °C. Individual peak areas have been normalised.....	177
Figure 6-11 - Peak areas (%) of holocellulose-derived compounds of raw and solvent-extracted [a] fir tree barks, [b] pine tree barks, and [c] cypress tree barks at 550 °C. Individual peak areas have been normalised. ....	179
Figure 6-12 - Peak areas (%) of [a] lignin-derived and [b] holocellulose-derived compounds of acid-washed samples at 550 °C. Individual peak areas have been normalised. ....	181
Figure 6-13 – Comparison of peak areas of [a] 2-methoxy phenol, [b] phenol, [c] trans-iso Eugenol, [d] creosol, [e] furfural and [f] 5-methyl-2-furancarboxaldehyde with the average values of all sample categories at each temperature (450, 550 and 650 °C). Error bars were calculated using 1x standard deviation of all values. Number of data points were 13 (U@450, U@550, U@650), 3 (A@550), and 10 (S@550). ....	183
Figure 6-14 – Example mechanism of the methylation of alcohol-containing compounds. Sourced from (59). ....	185
Figure 6-15 – Hydrogenation of catechol via highly reactive intermediates. Sourced from (599). ....	185
Figure 6-16 – Hydrogenation reactions of the compounds with the top 10 peak areas from py-GC/MS.....	186
Figure 6-17 – Methylation reactions of the compounds with the top 10 peak areas from py-GC/MS. [b] is empty as the structure of furfural would not change after methylation.....	187
Figure 6-18 – Example of a HSP Sphere. Modified from (609). ....	192
Figure 7-1 – The overall scope of this study. The work covered in Chapter 7 is denoted by red dotted lines. ....	202
Figure 7-2 – The graphical representation of Helminen et al's (380) ammonia adsorption data for alumina. ....	217
Figure 7-3- Screenshot of the Microsoft Excel workbook where Helminen et al's data (in this case, gamma-alumina) is converted to the conditions presented in this study.....	218

**Figure 7-4 - Screenshot of the Microsoft Excel workbook where Helminen et al.'s activated carbon data is converted to the conditions presented in this study (1.8M, 20°C and 1.44 kPa). .....219**

**Figure 7-5 – The graphical representation of Helminen’s (380) ammonia adsorption data for activated carbon. ....220**

**Figure 7-6 – Comparison of the averages of ammonia adsorption capacities of the untreated samples (raw barks, oak, and peats) and treated samples (biochars and activated carbons). .....222**

**Figure 7-7 – Comparison of the averages of ammonia adsorption capacities of the untreated samples (raw barks, oak, and peats) and treated samples (biochars and activated carbons). .....224**

**Figure 7-8 – Means of molar H/C, molar O/C, and volatile matter/fixed carbon ratio values for the untreated and treated biosolids. Error bars are 1× standard deviation. ....226**

**Figure 7-9 – Comparison of (a) molar H/C and (b) molar O/C ratios for untreated and treated biosolids. Each number on the x axis represent one type of biosolid for which untreated and treated elemental analysis was carried out. Experiments were carried out in duplicate in some cases for both levels of treatment, e.g. there are 2 points for both untreated and treated types 3 and 7. Key of biosolids type: 1-NC, 2-CH, 3-NF, 4-ESF, 5-GF, 6-DF, 7-Oak, 8-PeatSEPO, 9-PeatMoss, 10-SIGMA AC, 11-NORIT-AC. ....227**

**Figure A2-1 – Screenshot of the Microsoft Excel worksheet (in particular the calculation of mgN/g fresh adsorbent) used for calculating the adsorption capacity of this study’s samples after ammonia adsorption testing.....318**

**Figure A2-2– Screenshot of the Microsoft Excel worksheet (in particular the calculation of mgNH<sub>3</sub>/g fresh adsorbent) used for calculating the adsorption capacity of this study’s samples after ammonia adsorption testing.....319**

**Figure A2-3 [a] and [b] – Screenshot of the Microsoft Excel worksheet used for calculating the partial pressure of ammonia (in this case, for 1.8M of ammonium sulphate). .....323**

**Figure A2-4 – Screenshot of Solver used in the Microsoft Excel worksheet used for calculating the partial pressure of ammonia (in this case, for 1.8M of ammonium sulphate). .....324**

**Figure A2-5 – Validation of Helminen’s adsorption capacity of alumina as an adsorbent to values generated by Microsoft Excel in this study. ....324**

## List of Equations

Equation 3-1 - Friedl's equation for estimating higher heating values (327). C, H and N represent carbon, hydrogen and nitrogen contents, respectively (on a dry basis). .....	43
Equation 3-2 - Dulong's equation for estimating higher heating values (331). C, H and O represent carbon, hydrogen and oxygen contents, respectively (on a dry basis). .....	43
Equation 3-3 - Channiwala and Parikh's equation (329) for estimating higher heating values. C, H, O, N, S and A represent carbon, hydrogen, oxygen, nitrogen, sulphur and ash contents, respectively (on a dry basis). .....	43
Equation 3-4 - Correction of H-content for moisture. a.r. denotes 'as received'. M denotes 'moisture content' in wt% from the proximate analysis.....	44
Equation 3-5 - Calculation of oxygen content (O%), by difference, from the values given from ultimate analysis. C, H, N and S refer to carbon, hydrogen (calculated from Equation 3-4), nitrogen and sulphur on a dry basis. ....	44
Equation 3-6 – Calculation of %NDF, %ADF, and %ADL proportions from fibre analysis.....	49
Equation 3-7 – Calculation of %Cellulose, %Hemicellulose, %Lignin proportions from fibre analysis. ....	49
Equation 3-8 - Calculation of crude protein utilising Dumas conversion factors.....	51
Equation 3-9 – Calculation for the normalisation of gas chromatography peak areas. ....	64
Equation 3-10 - Chemical reaction of ammonia gas production for ammonia adsorption tests.....	67
Equation 3-11 - Sum of spent adsorbent mass ( $m_s$ ), as a function of fresh ( $m_f$ ) and adsorbent nitrogen ( $m_N$ ).....	69
Equation 3-12 - Calculation of the nitrogen content (wt%) for spent adsorbent. ....	69
Equation 3-13 - Calculation of the nitrogen content (wt%) in the fresh adsorbent, defined as %N <sub>f</sub> .....	69
Equation 3-14 - Substitution and re-organisation of spent adsorbent nitrogen content (wt%). ....	69
Equation 3-15 - Calculation for the grams of nitrogen per gram of fresh adsorbent. ....	70
Equation 3-16 – Conversion of $\alpha$ from gN/g fresh adsorbent to mgNH <sub>3</sub> /g fresh adsorbent. ....	70
Equation 3-17 – Antoine's equation to calculate the vapour pressure of a sorbate, as a function of equilibrium temperature. ....	73
Equation 3-18 - Dubinin-Astakhov isotherm equations for calculating adsorption capacity. ....	73

Equation 3-19 - The ideal gas law.....	73
Equation 3-20 – Calculation of the condensed adsorbate density of ammonia, where $P_0$ is given in ‘bar’.....	74
Equation A2-1 – Application of Henry’s law for the calculation of the post-reaction ammonia gas molar fraction ( $y$ ). .....	326
Equation A2-2 – The temperature-dependent polynomial equation to calculate the density of pure liquid water (784). .....	327
Equation A2-3 – Calculation of the mass of liquid water. ....	328
Equation A2-4 – Calculation of the number of moles from component masses. $W_i$ is molar mass. This equation is valid for NaOH ( $N_{NaOH}$ ), ammonium sulphate ( $N_{AMS}$ ) and water ( $N_{H_2O}$ ). .....	328
Equation A2-5 – Calculation of the number of moles of sodium sulphate ( $N_{NS}$ ) and water in the reaction ( $N_{H_2O,R}$ ), relative to the moles of ammonia ( $N_{NH_3}$ ). .....	328
Equation A2-6 – Calculation of the number of moles of NaOH present after reaction.....	328
Equation A2-7 – Calculation of the total number of moles present in the liquid phase after reaction.....	328
Equation A2-8 – Calculation of mole fraction of ammonia in the liquid phase. ....	328
Equation A2-9 – Calculation of error after application of Henry’s law.....	329
Equation A2-10 – Calculation of the molar amount of ammonia present in the gas phase. ....	329
Equation A2-11 – Calculation of the total volume of gas present before reaction.....	329
Equation A2-12 – Application of the ideal gas law for the calculation of the number of moles present in the gas phase before reaction. ....	329
Equation A2-12 – Raoult’s law .....	330
Equation A2-14 – Application of the ideal gas law for water held in the moisture after sealing the reaction bottle. ....	330
Equation A2-15 – Calculation of number of moles in the gas phase after reaction.....	330
Equation A2-16 – Calculation of mole fractions of ammonia in the gas phase. ....	330
Equation A2-17 – Calculation of mass of liquid water produced from the reaction.....	330
Equation A2-18– Calculation of volume of liquid water produced from the reaction.....	330
Equation A2-19 – Calculation of volume of liquid contained in the Duran bottle after reaction. ....	330

Equation A2-20 – Calculation of volume of gas contained in the Duran bottle after reaction. ....	331
Equation A2-21 – Calculation of the total pressure in the Duran bottle after reaction.....	331
Equation A2-22 – Calculation of the partial pressure of ammonia in the Duran bottle after reaction, according to Dalton’s law, as a function of the right hand side term of Henry’s law ( $xH = yP_{tot} = P_{NH_3}$ ). ....	331
Equation A2-23 – Calculation of Henry’s constant (783). $T^\ominus$ is 298.15K. ....	331
Equation A2-24 – Value of Henry’s constant (783) at 20 °C, where $T^\ominus$ is 298.15K. ....	331
Equation A2-25– Calculation of error in applying Henry’s law. ....	332

## List of Acronyms and Abbreviations

<b>1,3-DL</b>	1,3-dioxolane
<b>1,4-D</b>	1,4-dioxane
<b>A</b>	Ash
<b>a.a.</b>	As analysed
<b>a.r.</b>	As received
<b>AAS</b>	Atomic absorption spectroscopy
<b>AC</b>	Activated Carbon
<b>AD</b>	Anaerobic Digestion
<b>ADF</b>	Acid Detergent Fibre
<b>ADL</b>	Acid Detergent Lignin
<b>AEM</b>	Alkaline Earth Metal
<b>AGRdig</b>	Agricultural residue digestate
<b>AlkLig</b>	Alkali Lignin
<b>ASE</b>	Accelerated Solvent Extraction
<b>Cell</b>	Cellulose
<b>CH</b>	Coconut Husk
<b>CMR</b>	Carcinogen, Mutagen or Reprotoxic
<b>D</b>	Polanyi adsorption potential
<b>d.b.</b>	Dry basis
<b>D-A</b>	Dubinin-Astakhov
<b>daf</b>	Dry ash free basis
<b>DCF</b>	Dumas conversion factors
<b>DEE</b>	Diethyl ether
<b>DF</b>	Douglas fir
<b>DTG</b>	Derivative Thermogravimetry
<b>E</b>	Characteristic energy of the adsorbent-adsorbate system
<b>EHS</b>	Environmental, Health and Safety
<b>ESF</b>	European silver fir
<b>FC</b>	Fixed Carbon
<b>FTIR</b>	Fourier Transform Infrared Spectroscopy
<b>GF</b>	Grand fir
<b>GHS</b>	Global Harmonised System
<b>H</b>	Henry's constant
<b>HHV</b>	Higher heating value
<b>HSP</b>	Hansen Solubility Parameter
<b>ID</b>	Internal Diameter
<b>L</b>	Larch
<b>LB</b>	Lignoboost
<b>LC</b>	Lawson cypress
<b>LCA</b>	Life Cycle Analysis
<b>LOME</b>	Lignin oil methyl ether
<b>M</b>	Moisture content
<b>MDC</b>	Methylene dichloride
<b>MEK</b>	Methyl Ethyl Ketone
<b>m<sub>f</sub></b>	Mass of fresh adsorbent
<b>MFCA</b>	5-methyl-2-furancarboxaldehyde
<b>m<sub>N</sub></b>	Mass of adsorbed nitrogen

<b>m<sub>Nf</sub></b>	Mass of nitrogen in fresh adsorbent
<b>m<sub>s</sub></b>	Mass of spent adsorbent
<b>MSWdig</b>	Municipal solid waste digestate
<b>n</b>	Heterogeneity parameter
<b>NC</b>	Nootka cypress
<b>NDF</b>	Neutral Detergent Fibre
<b>NF</b>	Noble fir
<b>NMP</b>	n-methylpyrrolidone
<b>NORIT-AC</b>	NORIT Activated Carbon
<b>NS</b>	Norway spruce
<b>Oakbc450</b>	Oak biochar pyrolysed at 450 °C
<b>Org</b>	Organosolv lignin
<b>OWS</b>	Organic Waste Systems
<b>P</b>	Pressure
<b>PAH</b>	Polyaromatic hydrocarbon
<b>PA</b>	Peak area
<b>PeatMoss</b>	Irish sphagnum moss peat
<b>PeatSEPO</b>	Peat turf
<b>PKBag</b>	Sugarcane bagasse from Pakistan
<b>PY</b>	Pyrolysis oil
<b>Py-GC/MS</b>	Pyrolysis-Gas Chromatography/Mass Spectrometry
<b>q</b>	Adsorption capacity
<b>R</b>	Universal gas constant
<b>RBF</b>	Round-bottomed flask
<b>SDS</b>	Safety Data Sheets
<b>SIGMA-AC</b>	Activated Carbon from Sigma-Aldrich
<b>Sox</b>	Soxhlet-extracted residue
<b>SP Bark</b>	Softwood pine tree bark
<b>SS</b>	Sitka spruce
<b>SSdig</b>	Sewage sludge digestate
<b>STOT</b>	Single Target Organ Toxicity
<b>T<sub>ads</sub></b>	Adsorption temperature
<b>TEA</b>	Technoeconomic Analysis
<b>TGA</b>	Thermogravimetric analysis
<b>THF</b>	Tetrahydrofuran
<b>tot</b>	Total
<b>TS</b>	Total Solids
<b>UV</b>	Ultraviolet
<b>VGFDig</b>	Vegetable, garden, fruit digestate
<b>VM</b>	Volatile Matter
<b>VOC</b>	Volatile Organic Compounds
<b>W<sub>i</sub></b>	Molar mass
<b>W<sub>0</sub></b>	Limiting pore volume of adsorber bed material
<b>WRC</b>	Western red cedar
<b>WWTP</b>	Wastewater treatment plant
<b>x</b>	NH <sub>3</sub> liquid molar fraction
<b>y</b>	NH <sub>3</sub> gas molar fraction
<b>α</b>	Adsorption capacity, in g <sub>N</sub> /g <sub>fresh adsorbent</sub>
<b>ρ</b>	Condensed adsorbate density



agricultural soils due to synthetic nitrogen fertiliser application (4.1%), chemical and petrochemical manufacturing emissions from energy inputs (3.6%) and the burning of agricultural residues (3.5%) (8).

The levels of NO<sub>x</sub> emissions from agricultural soils are expected to increase in the following years as chemical fertiliser and poor manure management continue to grow (9). As well as aiming to reduce NO<sub>x</sub> emissions, organic soil amendments such as biochars and animal manure have been adopted for the enhancement of soil organic matter stocks (10). Here, the manure and biochars act as nitrogen-rich amendments (11). The highest levels of NO<sub>x</sub> emissions occur where the soil amendment is scattered on the soil surface, as the nitrogen compounds desorb over time (12). These emissions can be alleviated by burying the soil amendment under the topsoil, however, individual countries have their own practices regarding this (13).

In the chemical and petrochemical industry, around two-thirds of greenhouse gas emissions are due to fuel combustion, whilst one-third is linked to industrial processes and product use (14). Fuel combustion takes up a large proportion of emissions as it is necessary for heat generation, electricity, and steam production (15). These can be electrified, to an extent (16), but it is more difficult with the chemical production-side.

The consumption of fossil fuels drives the emissions from the chemical productions side, with 90% of the raw materials arising from natural gas, coal or oil (17). In addition, as the production and consumption of fossil-derived resources do not occur at the same rate, the price and availability can be significantly variable (18). In the long-term, this variability can be stabilised through the valorisation of a variety of renewable feedstocks (18).

Although chemicals from renewable feedstocks (also known as bio-based chemicals) can be produced in single-product processes, they can also feature in biorefineries. As with oil refineries, the primary chemical product can be produced alongside secondary energy carriers (such as power, heat and fuel), to maximise the efficiency of the process (19).

In China, the largest energy consumer and carbon dioxide emitter of the chemicals industry is the production of synthetic ammonia. Approximately 54 million tonnes of ammonia is estimated to be produced in China each year (20). One avenue for reducing these emissions is the recycling of ammonium ions that are currently present in nitrogen-rich waste streams (21). The most common streams that contain ammonium ions are anaerobic digestates and wastewaters (22, 23).

The capturing of ammonium, either gaseous or aqueous, can be performed by absorption and adsorption. In absorption, aqueous ammonia is stripped into the air (as gaseous ammonia) by aeration and adjustment of the temperature and pH (24, 25). The gaseous ammonia is then reacted with sulphuric acid, which stabilises as ammonium sulphate. In adsorption, carbon-rich materials such as biochars and catalysts adsorb gaseous ammonia onto their surface due to their particular physical and chemical properties (26).

As discussed, the burning of agricultural residues has led to 3.5% of greenhouse gas emissions (Figure 1-1). Through the valorisation of these agricultural residues, the emissions from the chemicals industry and applications of synthetic nitrogen fertilisers may also be reduced. Agricultural residues cover a wide range of biomass, from straws to bagasses to husks (27). In 2030, there is expected to be 139 million tonnes of agricultural residues across the European Union (28). An alternative residue is tree bark, where an estimated 0.7 – 2.0 million tonnes of bark are generated each year in the United Kingdom.

As lignocellulosic biomass, the structure of agricultural residues is predominantly composed of cellulose, hemicellulose and lignin (29). Through the maturation of the biorefinery concept, hemicellulose and cellulose are widely extracted for valorisation (30). The last main constituent of lignocellulose, lignin, remains to be valorised to the same degree and upgraded into higher-value products.

During the mass extraction processes of cellulose and hemicellulose, the lignin (which makes up about 15-40% of lignocellulose) (31) that remains is considered to have a low economic value, and is therefore used as a fuel. Instead, the 'waste' lignin could be valorised to exploit its high-value aromatic structure.

The individual monomers of lignin are connected by a variety of linkages (32). The structure of lignin differs from one sample to the next, based on the connections between different linkages and monomers (Figure 1-2). Due to this somewhat randomised construction of building blocks, lignin can be valorised in a variety of industries.

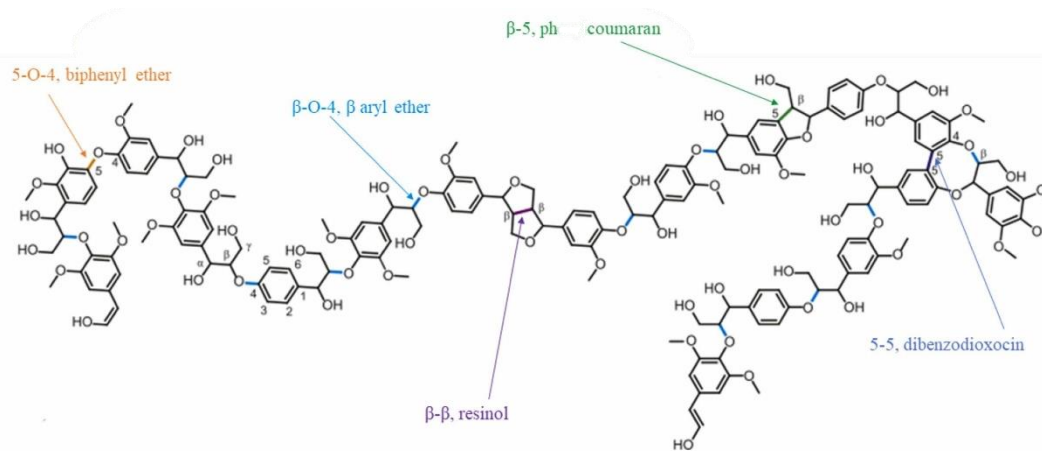


**Figure 1-2** – Illustration of the building blocks of lignin’s structure, connected via several linkages. Sourced from (32).

As discussed, some of the main emitters of greenhouse gases, by sector, are the petrochemical and chemical manufacturing industry, agricultural soils by way of synthetic nitrogen fertiliser applications, and the burning of agricultural residues. Therefore, this work considers the potential applications of lignin as alternatives to petrochemicals and synthetic nitrogen fertilisers by valorising agricultural residues rather than burning them.

### 1.1.1 Valorisation as a bio-based chemical

The current global market of bio-based chemicals is considered to be approximately 90 million tonnes (33). Despite this, a large majority of organic chemicals are still derived from petrochemical feedstocks, with a global production around 330 million tonnes (19). One of the key issues that slows the growth of the bio-based chemicals market is that the cost of bio-based chemicals production is greater than the cost of petrochemicals production. Bio-based chemicals are expected to both have a lower environmental impact than petrochemicals, and for their performance to at least be on par with them.

The substitution of petrochemicals with bio-based chemicals are currently being sought by companies in the manufacturing of products such as detergents, paints, plastics, solvents and pesticides (34).

Bio-based plastics have a share of 0.4% across all plastics produced in the EU, with around 268 kilotons of bio-based plastics produced each year (35). These are of high importance to the EU, with mid-level production maturity. The drivers of bio-based plastics are consumer demand and widespread activity across research and development

departments (36). However, there is currently a lack of investment and infrastructure, with the plastic recycling sector not being in line with the bio-plastics reduction (35).

Around 1,002 kilotons of bio-based paints (in addition to inks, dyes and coatings) are produced each year in the EU, with around 1,293 kilotons consumed (35). Although the bio-based share in the market's production is 12.5%, it is currently of low importance to the EU and at low maturity of production. This market is expected to grow in the future, although not by greater than a few percent (37). The slow uptake is expected due to uncertainty regarding sales of the bio-based products, because of perceived reduction in quality compared to petrochemical-based products (37), and the potential risk of investing in this market (35).

Bio-based surfactants are compounds that are used in the production of detergents, fabric softeners, and paper (35, 38). Around 50% of all surfactants produced are from bio-based routes, with an annual production in the EU of 1,500 kilotons (of approximately 3,000 kilotons of all surfactants produced). The high proportion of bio-based surfactants of the total market is due to the high level of production maturity, whilst being of medium-level importance to the EU (35). One of the barriers that is preventing further interest in bio-based surfactants is the necessary purity of the compounds leading to high production costs (39).

Bio-based pesticides account for approximately 2.5% (3 ktons) of the global pesticide market (120 ktons) (40). In some areas, local use of bio-based pesticides is avoided by farmers due to limited market availability and a lack of knowledge (41). The sustainable use of pesticides is considered to be of high importance to the EU, as laid out in the Farm-to-Fork and EU Green Deal strategies (42). The production maturity of bio-based pesticides is considered to be at a moderate level, with there being an expectation of the market proportions being equal between bio-based and synthetic pesticides by the late 2040s (43).

Bio-based solvents can be used in a range of industries, across cosmetics, adhesives, paints, thinners and inks (44). Currently, only about 1.5% of all solvents in the EU are produced via bio-based routes, with around 75 kilotons of bio-based solvents produced each year (35). One of the constraints surrounding the increased uptake of bio-based solvents is the apparent lack of biomass available because of the significant volumes of solvent required across the different industries (45). In addition, bio-based solvents are currently of low importance to the EU, and of low production maturity (35).

From the different applications of bio-based chemicals discussed above, solvents have the greatest room for growth. This is due to the low production maturity and need for high production volumes.

#### 1.1.1.1 Bio-based solvents

Solvents are chemicals which are used for the dispersal, dissolution, or dilution of other compounds. In recent years, there has been an increased drive towards “green” or ‘bio-based’ solvents, as society has greater knowledge of the impacts of the synthesis and disposal of petrochemical-derived solvents (46).

The power of the solvent against the solute is dependent on the physical properties and molecular structure of both components (47). In the chemical manufacturing industry, solvents are the components with the greatest consumption, and make up a large proportion of the waste generated (48). As of 2024, bio-based solvents make up 5.7% of the overall global solvent market (by valuation) (49, 50), and 12% by volume consumed (51, 52) (Table 1-1).

**Table 1-1** - The global markets for all solvents and bio-based solvents (as of 2024) (51, 52).

<b>Solvent</b>	<b>Market Value (US\$ Mn)</b>	<b>Volumes Consumed (Million Metric Tonnes, MMT)</b>
<b>Global Market</b>	36,300	30.7
<b>Bio-based Global Market</b>	2,100	3.7

The applications of solvents are dependent on their chemical structure. Their solubility is affected by the solvent’s polarity, which is the ability of the individual atoms and molecules within the structure to attract an electron bonding pair. In addition to polarity, chemical structures can also have aprotic and protic functionality, depending on whether the solvent contains acidic hydrogens or not. Solvents can therefore be separated into three categories: non-polar, polar protic, and polar aprotic.

As large volumes of solvents are needed for industry (48), large volumes of raw materials are needed to fulfil this demand. Each year, approximately five billion metric tonnes of agricultural residues are produced globally (53), most of which are burned. The scale of agricultural residues could subsequently be potentially valorised as bio-based solvents.

Non-polar solvents are molecules containing bonds that are predominantly between two or more atoms with similar electronegativities like carbon and hydrogen. These bonds

therefore have an absence of charge, and the overall structure is referred to as being non-polar. As the key rule for understanding solubility is “like dissolves like”, non-polar solvents are best for dissolving non-polar solutes like hydrocarbons. Common non-polar bio-based solvents are terpenes (54) such as D-limonene and  $\alpha$ -Pinene, which can be obtained from plant-derived essential oils (44). However, terpenes tend to be toxic towards fish, amongst other environmental risks (54, 55).

Polar solvents contain bonds between atoms with large differences in electronegativities (e.g. hydrogen and oxygen). Polar protic solvents (such as water,  $H_2O$ ) have acidic hydrogens, so can participate in hydrogen bonding and act as a source of protons. The common applications of polar protic solvents is as solvents for their conjugate base, such as water being used for the solvation of alcohol groups (-OH). Bioethanol is the most commercialised bio-based polar protic solvent, which is predominantly made from sugarcane and corn. Polar aprotic solvents are not as commercially established as the other solvent categories, but have been explored in literature with dihydrolevoglucosenone (Cyrene) and 2-methyl tetrahydrofuran (2-MeTHF) (56). These polar aprotic solvents do not have N-H or O-H bonds (which include acidic hydrogens), and are unable to hydrogen bond. Therefore, they tend to be better as solvents across a large range of reactions due to their limited effectiveness at bonding.

In addition to essential oils, pyrolysis oils can also be a source of bio-based solvents. This is generated by the pyrolysis of raw materials. Pyrolysis oils are very complex and unstable polar (57) mixtures made up of over a hundred compounds (58), with the individual compounds generally having similar properties such as boiling point and polarities, so compound separation and isolation is difficult. Pyrolysis oils, therefore, do not have many applications in its initial state. For this reason, upgrading routes including methylation (59, 60) and hydrogenation (61) are necessary for ensuring a stable and simpler mix with a wider range of potential applications.

There is therefore the most scope for commercialising bio-based polar aprotic and non-polar solvents, as bioethanol is a platform chemical that can be upgraded into a wide variety of other chemicals (62).

### **1.1.2 Valorisation of agricultural residues as ammonia adsorbents for the reduction of synthetic fertiliser use.**

As discussed earlier, organic fertilisation has been identified as augmenting soil organic matter (SOM) content and nutrient status, thereby improving soil fertility and structure (63). The use of crop, or agricultural, residues as a source of organic carbon can favour the accumulation of soil organic matter in soil, whilst recycling and retaining farm-sourced nutrients (64).

For nitrogen-rich organic matters such as manure and other sludges, there may be concerns, when looking to apply them as fertilisers, regarding the presence of pathogens (65). This can be rectified through the methods such as heat-treating or anaerobic digestion (66). Different sources of organic fertilisers include composts, biosolids, industrial wastes and anaerobic digestates (67, 68).

Organic fertilisers can also be applied as liquid or granular fertilisers, which come with their own benefits and difficulties.

Liquid-phase organic fertilisers, such as manures, composts and liquid anaerobic digestates, are readily absorbed by plants, so can provide an immediate boost to nutrient-deficient soils. They are also uniform in nature as the nutrients within are evenly distributed across the liquid-phase, and they are more versatile as they can be diluted, if needed, depending on the application. However, due to the power of absorption, liquid fertilisers do not last that long, and must be reapplied to the soil fairly often. In addition, they cannot be applied in hot weather or sunny conditions due to the risk of leaf scorch (69).

Granular organic fertilisers, such as biosolids and solid-phase anaerobic digestates, are less likely than liquid-phase fertilisers to be washed away by rain, so do not need to be applied as frequently to the soil. This increased longevity can aid in the sustaining of plants over a longer period too. In contrast to liquid organic fertilisers, granular fertilisers tend to be easier to transport and sold in bulk. Therefore, they are considered to be more cost-effective. Most importantly, granular fertilisers are easier to spread over larger areas than liquid fertilisers, by using equipment such as a broadcast spreader (70). However, granular fertilisers cannot simply be spread over soils, as they must be worked into the soil. Also, common granular fertilisers, when improperly applied, may burn plant tissue due to their high concentrations (69).

In the UK, liquid fertilisers (including liquid urea and ammonium nitrate) are less expensive per tonne than granular fertilisers (71). This is likely due to liquid fertilisers being less

concentrated. The cheaper fertilisers are generally those that are animal-based (manure, fish meal, blood meal, bone meal and feather meal) (72). However, the use of animal-based granular fertilisers carries an increased risk of drawing in pests (69), as they remain accessible to animals due to their slow absorption into the soil. Therefore, plant-based (or bio-based) granular fertilisers are valuable alternatives for their long-lasting properties and lack of attracting pests (73).

The quality of soil can be enhanced through the co-application of biochar (biomass that has undergone pyrolysis) with the fertiliser. The combination of the two substances has been shown to reduce the loss of soil nitrogen, increasing soil carbon storage and overall improving soil fertility (74).

Alternatively, the biochar could be used as an organic granular fertiliser by itself through the prior adsorption of nutrients. Adsorption can occur chemically and physically and is dependent on the properties of the adsorbent. Physical adsorption is determined by factors including specific surface area, pore size distribution, and pore volume, whilst chemical adsorption is dependent on functional groups within the adsorbent's structure (75). For example, surface-level biochar functional groups (e.g. carboxyl and hydroxyl, C=O and O-H) can form chemical bonds with the nitrogen and oxygen functional groups in the sorbent (75).

The global adsorbent market, as of 2024, is estimated to currently be worth between US \$ 3,600 – 4,800 million (76-79). Each year, around 5300 thousand tons of adsorbents are traded globally (80).

The most widely used adsorbents for the treatment of emissions and nitrogen-rich wastewaters are activated carbons. These are defined as carbonaceous materials with high internal surface areas and porosities (81). As they are produced by pyrolysis at higher temperatures, activated carbons have high-temperature resistance, as well as resistance to strong acids and bases and good chemical stability (82). The carbonised materials can be activated physically or chemically. Physical adsorption utilises a mixture of carbon dioxide, air and steam, whilst chemical adsorption uses oxidative chemicals to react with the carbonaceous material to improve its surface area, surface functionality and carbon yield (83).

The most common materials used to generate activated carbons include coal, peat and petroleum (81). However, these are non-renewable, so research has investigated their production from industrial byproducts and agricultural wastes (83). Although waste or

residue-derived activated carbons may come from more renewable sources, the energy intensity of the carbonisation process and sustainability of the activation of the raw materials requires greater optimisation.

Another group of adsorbents, zeolitic materials, were among the first to be commercialised. These are microporous catalysts, where the structure and composition are designed in such a way where the adsorption properties can be fine-tuned depending on the specific application (84). However, their high performance comes at a cost. In addition to their higher price (between US\$ 10-100 per kg) (85), the production process is energy-intensive and is not very sustainable (86).

The adsorption performance of zeolites compared to activated carbons are dependent on several factors, including the pressure, adsorption temperature, and sorbate (87). Activated carbons appear to perform better than zeolites at pressures below 350 kPa (87).

## 1.2 Research gap

Through exploring the literature, several gaps were identified in the literature. Some of these are presented in Figure 1-3.

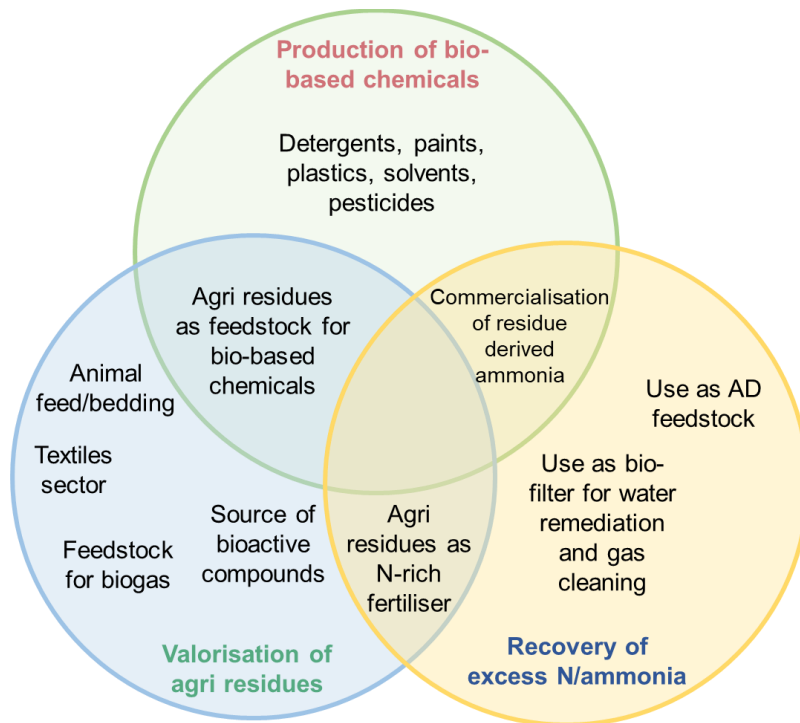


**Figure 1-3** – Potential routes for valorising agricultural residues, producing bio-based chemicals, and recovering excess nitrogen or ammonia.

Although different forms of biomass have been characterised individually in the research before, there are limited sources where a variety of samples have been characterised for their valorisation as high-lignin feedstocks. In addition, literature could not be found where the applications of biomass residues were compared to established commercial lignin products.

Regarding the characterisation of biomass, literature could not be found that investigated the effect of acid-washing or solvent extraction on the proximate, ultimate and fibre analysis data. In addition, research could not be found on how the treatment of biomass impacts its valorisation.

Tree barks have been characterised across the literature. However, none of the published research has explored tree barks from the United Kingdom. This is expected due to the greater level of resources in Scandinavia and the U.S.A. Nevertheless, the UK is thought to have 1357 thousand hectares of conifer (softwood) trees (88). Assuming that 50 tonnes worth of conifer trees are thinned every 5-10 years (89), and that bark makes up around

10 wt% of tree stem volume (90), approximately 0.7 – 2.0 million tonnes of bark from lumbered roundwood are generated each year in the United Kingdom.

The valorisation of biomass residues as bio-based solvents via fast pyrolysis has been considered in the literature previously, predominantly with each peer-reviewed paper focusing on a single biomass residue. No individual paper has looked at a range of residues and a range of pyrolysis temperatures, to attempt to optimise the process based on the available feedstocks. There has also been limited literature that assesses the hazardousness and solubility to compare biomass residue-derived pyrolysis oil to common industrial solvents, to discuss the potential applications of the prospective bio-based solvents.

In the literature, most research regarding the valorisation of biomass as ammonia adsorbents uses activated carbons or biochars, due to them being established as good adsorbents. However, only limited literature could be found that tested the (gaseous) ammonia adsorption capacity of raw/untreated biomass residues (91). Only one piece of literature (92) was sourced that looked at the ammonia adsorption capacities of biomass that been treated in different ways to slow pyrolysis, this being hydrothermal carbonisation to produce hydrochars. Limited literature could be found that explored tree barks as gaseous ammonia adsorbents, with none of the papers considering the difference between individual tree bark species.

The gaps in the literature that were identified were distilled into the aims and objectives for this thesis which are described in Section 1.3.

### 1.3 Aims and Objectives

Lignin has been recognised as a promising source of high-value products. However, there is a current need for more lignin-rich feedstocks to both be discovered and valorised. The aim of this research is to identify biomass that are lignin-rich and explore their performances in high-value applications.

This aim will be accomplished through the completion of the following research objectives:

#### 1. To identify high-lignin feedstocks

- A wide variety of biomass will be characterised to determine its lignin content and other composites. The lignin content will be estimated by fibre analysis.
- The results of the characterisation will aid in the understanding of which are actually “high-lignin”, and how their composition may impact different valorisation routes.

#### 2. To explore the valorisation and upgrade of high-lignin feedstocks to bio-based solvents

- A selection of biomass will undergo fast pyrolysis to identify the valuable aromatic compounds that would be present in the pyrolysis oil.
- The benefits of upgrading pyrolysis oil-derived compounds will be explored through theoretical methylation and hydrogenation.
- The properties of the different forms of pyrolysis oil-derived compounds will be assessed by utilising the CHEM21 hazardousness criteria and estimating their solubility.
- The pyrolysis oil-derived compounds will then be compared to common industrial solvents, to assess their potential applications as bio-based solvents.

#### 3. To explore the valorisation of high-lignin feedstocks as an adsorbent of ammonia

- The ammonia adsorption capacity of the lignin-rich feedstocks will be investigated through laboratory work at three different conditions.
- The lignin-rich samples will be thermally treated under slow pyrolysis conditions to generate biochars.
- The correlation and causation of lignin to ammonia adsorption capacity will be explored.

- The effect of biomass pre-treatment on ammonia adsorption capacity will be tested.
- The correlation and causation of other components of biomass that will be characterised, will be explored.

The aims and objectives, described above, were distilled into Figure 1-4 to summarise the scope of the work to be done.

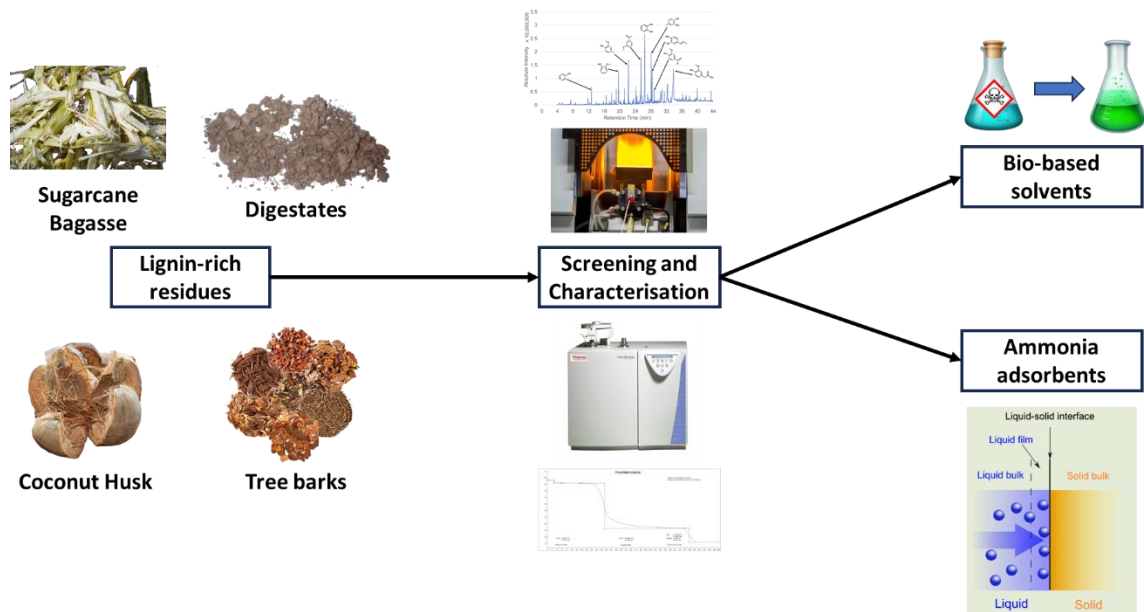


Figure 1-4 - Scope of the work in this thesis.

## 1.4 Organisation of chapters

This thesis is composed of 8 chapters and an appendix, organised as follows:

**Chapter 1 – Introduction.** This chapter outlines the background, purpose, and necessity of this work, whilst detailing the thesis' structure.

**Chapter 2 – Literature Review.** This chapter describes the background and research that pertains to more than two or more chapters in this thesis.

**Chapter 3 – Materials and Methods.** This chapter illustrates both the materials utilised in this study, and the methods of how they were examined for their characterisation and valorisation. Characterisation methods include proximate analysis, ultimate analysis, fibre analysis, atomic absorption spectroscopy, and pyrolysis-gas chromatography (py-GC/MS). Valorisation methods include additional py-GC/MS at different temperatures, solvent extraction, and finally, ammonia adsorption testing and modelling.

**Chapter 4 – The screening and characterisation of lignin-rich feedstocks.** This chapter assesses a wide variety of biomass for its elemental composition (ultimate analysis), proximate analysis, alkaline earth metals content (atomic absorption spectroscopy), lignocellulosic content (fibre analysis), and pyrolysis products. Several of the biomass samples underwent a mild acid-washing and were then re-characterised.

**Chapter 5 – The characterisation and effect of solvent extraction on bark.** This chapter characterises barks by the same methods as Chapter 4, with the addition of solvent extraction by Soxhlet apparatus and Accelerated Solvent Extraction.

**Chapter 6 – The potential to produce bio-based solvents from the pyrolysis of lignin-rich residues.** This chapter explores the valorisation of lignin-rich residues as bio-based solvents. Samples undergo fast pyrolysis (via pyrolysis-gas chromatography/mass spectrometry), and the prevalent pyrolysis oil-derived components are assessed and compared to common solvents for their hazardousness and solubility.

**Chapter 7 – The potential to produce bio-based ammonia adsorbents from lignin-rich residues.** This chapter measures the ammonia adsorption capacity of untreated tree barks, treated tree barks, and a selection of other samples. After adsorption capacity testing, the characteristics of the untreated and treated samples were compared to explore what led to the measured differences.

**Chapter 8 – Conclusions, Research Limitations, Recommendations and Direction.**

This chapter brings together the results of the previous chapters and relates them to how they met the objectives discussed in **Section 1.4**. The limitations of the research presented is discussed, with recommendations for further work presented.

**Appendix.** This section outlines the data whereby the absolute values were not used, but where it was applied onto other figures or tables discussed within the main chapters.

## Chapter 2 - Literature Review

In this chapter, the literature pertaining to lignins, its sources, properties, extraction methods and its applications are discussed. Throughout this study, materials are investigated for their lignin contents, with the properties of lignin, and the different processes for extracting and purifying lignin discussed in Section 2.1. The arising of agricultural residues and the treatment methods to generate lignin-rich residues are outlined in Section 2.2.

### 2.1 Lignin

The maturation of the biorefinery concept has led to the mass extraction of hemicellulose and cellulose from lignocellulosic biomass (30). The last main constituent of lignocellulose, lignin, remains to be valorised to the same degree and upgraded into higher-value products.

Lignin, which makes up between 15-40% of lignocellulose (31), tends to be used as an energy supply for the cellulose and hemicellulose extraction process by burning (93). This is because once the lignin is cleaved from the desired cellulose and hemicellulose, its economic value is so low that the lignin is used as a fuel. The 'waste' lignin could instead be valorised to exploit it being a source of high-value aromatic compounds due to its complex three-dimensional structure.

However, not all batches of lignin are the same. The composition of lignin is dependent on both the biomass it's coming from, and the batch of that biomass. For this reason, there is not an agreed model for its chemical and physical structure. The complexity and diversity of lignin structures add importance to the characterisation of the biomass itself. It is important to understand how the lignin composition fits into the overall structure of the biomass through characterisation.

Lignin can be referred to as native, residual or technical, which is conditional on whether the biomass is untreated (native), treated with the lignin still present (residual) or treated with the lignin having been extracted (technical) (94).

### 2.1.1 Structure and properties of lignin

The structure of lignin is a complex matrix of guaiacyl (G), p-hydroxyphenyl (H) and syringyl (S) units (Figure 2-1). These three subunits are produced by the oxidative radical polymerisation of the mono-lignols: p-coumaryl alcohol, coniferyl alcohol, and sinapyl alcohol. The main categories of lignin-rich native biomass are herbaceous plants (such as rice, sugarcane, bamboo, maize, and other cereals), hardwoods (oak, ash, beech, birch) and softwoods (pine, fir, spruce, cedar, larch) (95). Softwoods have the highest proportion of G units, whilst hardwoods consist of S and G units (96). According to the literature, softwood lignins do not vary much across different species, whilst the syringyl-to-guaiacyl ratio (S/G ratio) of hardwoods can vary significantly between species (97). In herbaceous plants and grasses, there is known to be equal amounts of S and G units. In contrast to the softwoods and hardwoods, which have trace or low levels of H units, herbaceous plants have higher levels of H units, though still less than the S and G units (98). In the sphere of sugar production from feedstocks, a lower S/G ratio has been linked to higher release of sugars (99) by increasing their solubilisation.

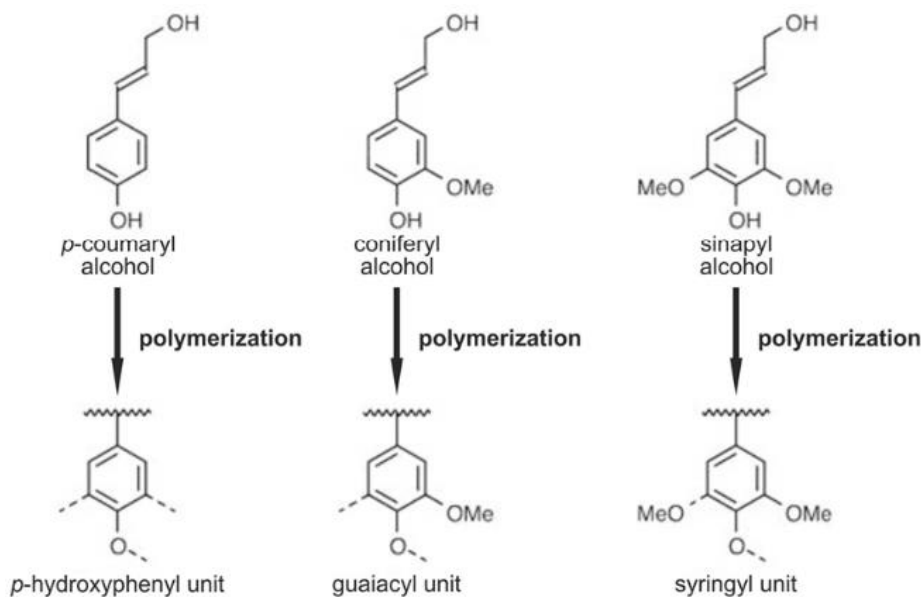


**Figure 2-1** – The oxidative polymerisation of lignin’s three main monolignols. Sourced from (100).

Due to high proportions of aromatics within lignin’s structure, it is overall considered to be hydrophobic. By contrast, hemicellulose and cellulose are hydrophilic because of the lack of aromatic structures (101, 102). However, as lignin’s structure is so complex, it may contain a not insignificant proportion of polar functional groups (amide, carboxyl, hydroxyl,

carbonyl), which are hydrophilic (103). Therefore, some research has looked at the modification of the functional groups present in a lignin's structure, or the creation of new functional groups, to strengthen the hydrophobic or hydrophilic nature of the lignin depending on the desired application (103). These applications have included lignin-elastomer composites (104, 105), lignin sub-micro spheres (106, 107), and polymers.

The molecular weights of lignin differ between the different categories of lignin-rich biomass. Softwood lignins have the greatest molecular weight ( $\approx 20,000$  g/mol) (98), with hardwoods having lower molecular weights. The molecular weight of a lignin can impact its physico-chemical properties. Lignins with higher molecular weights are likely to have lower levels of alcohol hydroxyl, phenolic hydroxyl, and carboxyl functional groups (98).

However, higher molecular weight lignins are known to contain more conjugated carbonyls and benzoquinone, leading to the lignin having a darker colour (Figure 2-2) (108).

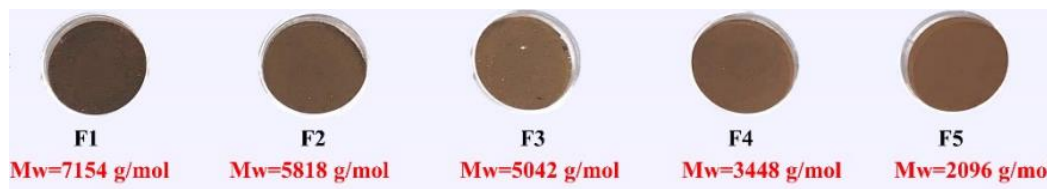


**Figure 2-2** – Images showing lignin colour lightening as the molecular weight decreases. Sourced from (109).

All lignins (unmodified and modified) have UV-protecting properties. The darker coloured lignin is of less interest to the cosmetics industry; therefore, research has looked at lightening lignin for its application as a sunscreen (108, 110, 111). In some papers, the molecular weight of lignin has been increased by its polymerisation in acidic aqueous solutions with acrylic-containing compounds, to improve the lignin's performance as a flocculant and additives (112-114). In addition, the antibacterial and antioxidant properties of lignin changes with its molecular weight (115).

Higher molecular weights are also known to lead to higher glass transition temperatures. The glass transition temperature ( $T_g$ ) is the region whereby a polymer (such as lignin) changes from a glassy to a rubbery state without a phase transformation in between. The  $T_g$  increases for polymers that are highly cross-linked with high levels of crystallinity, a lower moisture content, and a higher polarity (98). The  $T_g$  values therefore differ across the three main categories of lignin-rich biomass, with herbaceous plants having the lowest and hardwoods having the greatest (116). Herbaceous plants have a  $T_g$  at approximately 150 °C, softwoods have a  $T_g$  of 164 °C, and hardwoods have a  $T_g$  around 238 °C (Figure 2-3).

In the thermal pretreatment of lignin, it would become softer at temperatures which are higher than its  $T_g$  (117) and will thermally expand at an increasing rate (118). Where

lignins could be used in the production of adhesives, the  $T_g$  is a key factor. Above the  $T_g$ , the tensile strength and shear strength of the adhesive reduces (118). Therefore, in these cases, it is better to have an adhesive with high  $T_g$  values.

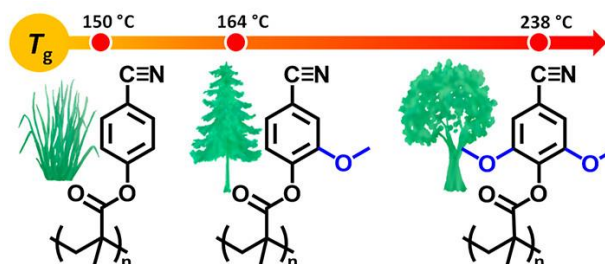


**Figure 2-3** - Glass transition temperatures of native lignin from herbaceous plants, softwoods, and hardwoods. Sourced from (116).

In addition to the other properties of lignin that have been discussed, the alkali, alkaline earth, and transition metals that are inherent to lignocellulosic biomass impact the thermal degradation of the lignin (119) by increasing its thermal reactivity. The common alkali metals, potassium and sodium (Table 2-1), are mostly present in biomass either as dissociated ions or as salts (alongside chloride ions). For example, potassium tend to exist as free  $K^+$  in solution within the cells. Magnesium tends to be present as organically bound materials within organic compounds, whilst calcium is likely to occur from its precipitation via natural processes, as calcium oxalate ( $CaC_2O_4$ ). Transition metals are not always present in biomass, and different transition metals can exist in different forms in varying types of biomass (119). In impurities, such as nitrates and sulphates, the transition metal elements are likely to be in ionic form. However, they can also be bonded to semi-crystalline or amorphous cellulose in an organically bound form. Iron can be present in precipitated forms such as  $FePO_4$  and  $Fe_2(SO_4)_3$ , but can also be found in organic compounds as a bonded  $Fe^{2+}$  ion.

**Table 2-1** – Common metallic elements found in biomass (119), and their typical concentrations.

<b>Alkali metal</b>	<b>Alkaline earth metal</b>	<b>Transition metal</b>
Potassium – K (1-22 mg/g)	Calcium – Ca (1-50 mg/g)	Copper – Cu (0.001-0.1 mg/g)
		Iron – Fe (0.05-0.25 mg/g)
Sodium – Na (0.1-10 mg/g)	Magnesium – Mg (0.9-7 mg/g)	Manganese – Mn (0.02-0.3 mg/g)
		Zinc – Zn (0.4-6.6 mg/g)

Whilst undergoing pyrolysis, the presence of alkali metals in lignin can lead to increased levels of coke (or char) and permanent gases (predominantly CO and CO<sub>2</sub>), with tar (condensable gases) levels reducing (120, 121). The overall reduction in tar may be due to secondary reactions during pyrolysis, favoured by the existence of the alkali metals, potentially converting generated tars into char (122).

Alkaline metals have the opposite effect, with coke/char and permanent gases reducing, whilst tar levels increase (123, 124). Transition metals generally increase the levels of coke/char and gases (125, 126), but the change in tar levels depend on the specific transition metal. Iron and nickel oxides have been seen to weakly promote tar promotion, however cobalt, copper and manganese oxides appear to inhibit tar promotion (127, 128). The synergistic impacts on lignin's thermal degradation when two or more of these groups of metals are present are unknown.

The inherent metals within lignin impact the thermal degradation of the material, as discussed. The addition of alkali metals to lignin has been used in the literature to aid in controlling the porosity and reactivity of the lignin (129, 130), as well as to further increase the char yield of feedstocks (122). In cases where the solid char was not the favoured product of pyrolysis, potassium and sodium has been removed from lignin by acid washing, reducing the char yields (131).

Once lignocellulosic biomass has been combusted, for example as a source of energy in biorefineries, the inherent alkali metals are retained in the ash. The alkali metals within the ash, such as potassium and phosphorous, have been considered in the literature as a sustainable nutrient supply by applying the ash onto farmland (132).

Regarding alkaline metals such as calcium and magnesium, their addition to lignocellulose has been shown to reduce the crystallinity of cellulose (133) and increase the yields of the oil generated after fast pyrolysis (134).

The majority of the literature that was found pertaining to the effect of the presence of transition metals on biomass regards the pulping process (135-137). Ordinarily, lignin-rich materials are pulped for the production of paper. As mentioned earlier, lignin is known to be a coloured material. Therefore, the lignin-rich materials must also be bleached to remove the darker colours and increase its brightness (135). The presence of transition metal ions within lignin-rich materials, however, reduces the effectiveness of the bleaching process by both catalysing the decomposition of the bleaching chemicals, and causes the formation of coloured compounds (136). In addition, when transition metals have been added during the pulping process, the viscosity of the pulps generated are greater than those without additional transition metals (137).

The addition of iron, as a transition metal, to lignin has been explored as a method for improving its thermal resistance and stability during the production of carbon fibres (138). The addition of manganese to lignin-derived biochars has been investigated for the potential adsorption capacity enhancement of methylene blue (139). The benefit of manganese in this field was through the addition of ion exchange functional groups on activated carbon's surface, and by improving the surface electron transfer (139). Manganese has also been noted to enhance lignin's degradation (140), which has been applied in areas which include saccharification (the breakdown of polymers into monomers).

As the complex structure of lignin is predominantly made up of carbon, dissolution requires organic solvents. Solvents that are commonly used to solubilise lignin are dimethyl formamide (DMF), dimethyl sulphoxide (DMSO), and 2-methoxyethanol (141). The performance of the solvents in dissolving the lignin can be improved by prior fractionation to disentangle the polymeric chains (142). This fractionation produces technical lignins with greater solubilities, and is discussed later (Section 2.1.2). The power of the organic solvents can be quantified by solubility parameters, which include Hansen solubility parameters (HSP) (141) and Hildebrand solubility parameters (142). These are discussed in Section 6.1.

Lignin's solubility is affected by a wide range of factors. Lignin has higher solubility when it has a lower molecular weight and polydispersity (the ratio of the weight-average molar mass and the number-average molar mass) (143), a decrease in aliphatic hydrocarbon

side chains (such as alkanes and alkenes), or an increase in acid-base interaction capability (142).

### **2.1.2 Extraction of lignin from biomass**

As well as lignin's structure changing depending on the biomass it's coming from, it can be recovered from biomass from a large variety of routes as technical lignins, which all have different benefits and drawbacks (100). These recovery processes have been summarised in the table below.

Regarding the potential environmental impacts of the technical lignin recovery processes, the use of ionic liquids and the organosolv lignin process both utilise relatively low temperatures (< 120 °C). The energy requirements of these two recovery processes are therefore a lot lower than the pyrolysis and hydrolysis processes.

The sources, production route, and disposal route of the substances used in the recovery processes would also affect the environmental impacts of the technical lignins. In organosolv lignin, the impact would depend on the organic solvent used, and whether it's petroleum-derived or bio-based. Several of the technical lignin recovery processes utilise acids or bases, so understanding their production and disposal route is paramount to quantifying their impacts.

Due to the processes below including various types of processes, including thermal, acidic, and basic, the structure of the technical lignins vary greatly from native lignin. For example, alkaline processes like soda and Kraft pulping leads to the breakdown of protolignin, lignin fragment dissolution, and recondensation. The organosolv process leads to a lignin with lower residual carbohydrates and ash (144).

**Table 2-2** - Summary of technical lignin recovery processes (100).

<b>Lignin types</b>	<b>Summary of process</b>	<b>Benefits</b>	<b>Drawbacks</b>
<b>Alkali Lignin</b>	Hydrolytic degradation of Kraft lignin	High lignin yield	High sodium from processing
<b>Ionic Liquids</b>	Temp: 70-100 °C Hydrothermal solvent fractionation	Sulphur-free Limited changes to lignin's structure	Cost of ionic liquids
<b>Hydrolysis</b>	Temp: 170-210 °C Acidic or enzymatic hydrolysis	Sulphur-free High-quality lignin Minor degradation	Acid treatment is expensive Acid treatment has severe conditions
<b>Kraft</b>	Temp: 150-180 °C Na <sub>2</sub> S and NaOH treatment	Lignin recovered is soluble in polar solvents and alkali solutions Low ash content	Black liquor that is generated has high sugar concentrations Processing time is long (1-2 hours)
<b>Klason</b>	Acid hydrolysis with concentrated H <sub>2</sub> SO <sub>4</sub>	High lignin yield Low carbohydrate levels	Acid treatment is expensive Structure of the lignin changes
<b>Lignoboost</b>	Utilises black liquor from the Kraft process Two-stage acid treatment, then filter pressed	Kraft pulp load increases (145) Can be valorised as a feedstock	Long processing time
<b>Organosolv</b>	Temp: 90-120 °C Hydrothermal treatment with a solvent (25-75 %)	Alkali-soluble lignin Limited changes to lignin's structure Sulphur-free	Additional solvent cost The solvent recovery that is required adds additional steps
<b>Pyrolysis</b>	Temp: >450 °C Thermal treatment	Sulphur-free Short vapour residence time (2s)	Low average molecular weight High consumption of carbohydrate
<b>Soda</b>	Temp: 90-150 °C Alkali treatment with NaOH/KOH	Low ash Sulphur-free	Low purity of lignin, due to carbohydrate content Structure of the lignin changes

Common commercial applications of lignin products are in dispersants, additives, and surfactants (31, 146-152). The lignin products that tend to be used for these applications are alkali lignin (153-155) and Kraft lignin (152, 153).

In the literature, Kraft lignin (156-165), soda lignin (165-167), alkali lignin (165, 168-170), organosolv lignin (162, 163, 167, 171, 172) and Klason lignin (173) have been explored as binders for adhesives (165). However, organosolv lignin is not used extensively in the production of binders or adhesives due to its low molecular weight (174). Other areas that utilise lignin-based binders include wiring boards, hydrogels, soil suppressants, battery binds, and lignin-based paper and coatings (165).

In the field of tissue engineering and regenerative medicine, alkali lignin (175-178), Kraft lignin (152, 179-183), Klason lignin (152) and organosolv lignin (152, 179) has been researched for their performance as nanoparticles via ultrasonication. These exhibit high activity and large specific surface area, whilst providing the additional bioresource utilisation and sustainability (178). Thermo-sensitive gels, which are used in drug release, tissue repair and water purification, have been synthesised using lignin products. The lignin products utilised for thermo-sensitive gels include alkali lignin (184) and organosolv lignin (185).

Lignin products have been considered, in the literature, as a biosorbent for the removal of dyes from wastewater (186). A key site where dye removal is necessary is in paper mills, where any dye effluent can lead to harming flora and fauna. Hajkova et al (2023) considered the performance of alkali lignin as a dye-removing biosorbent, due to its pre-existing presence as a waste from paper milling (186).

The valorisation of depolymerised lignin is predominantly done with Kraft and organosolv lignin (187). This is due to the processing method not being severe, allowing the lignin to still be reactive enough for the depolymerisation (188). Hydrolysis lignin does not tend to be utilised for polymerisation because the hydrolysis method renders the product with low reactivity (187).

Due to the dye sorbency properties of lignin, liginosulfonate products (Kraft and alkali lignin) are known to be used as dye dispersants (153, 189). Technical lignins have potential applications as dispersants due to their hyperbranched polymer structure (190). Chemically modified alkali lignin has been studied for its performance as an adsorber of cellulase (cellulose-degrading enzymes) (191). Lignins are thought to be competent adsorbers due to their aromatic structure, allowing for strong interactions with other molecules. Soda lignin has been reported as having limited industrial applications due to its lack of reactivity and insolubility in water (192). The applications that it would be suitable for include dispersants, animal nutrition as a binding agent due to the binding properties of lignin, and the production of phenolic resins. Their use in the production of phenolic resins is due to lignin's complex structure leading to good tensile strength and thermal properties (174). Ionic liquid-extracted lignin, although not available at industrial scale, has been seen to have properties similar to organosolv lignin (174).

Predominantly, the Klason method is used for the quantification of lignin in lignocellulosic structures (193-195). As a relatively new type of industrial lignin (196), LignoBoost does not yet appear to have common applications. However, it is believed that, as it is a high

purity lignin, it has a wide scope of applications. These cover thermal and chemical conversions into hydrocarbons, phenols and oxidised products. As discussed throughout this section, the high-purity lignin can also be used in thermoset resins, polymers, adhesives, binders, preservatives and carbon fibres (197).

## **2.2 Agricultural residues**

In this section, the various types and treatments of agricultural residues are discussed. The distinctions between primary and secondary by-products are outlined, and their main applications industrially and in the literature. In addition, the background and valorisation of agricultural residues by different treatment methods (biochemical and thermochemical) are discussed.

### **2.2.1 Arising of agriculture by-products**

The by-products of agriculture can be separated into primary and secondary by-products. Common primary by-products are the residues that remain after the harvesting of crops and include straws and other crop residues. Secondary by-products arise from the processing of products into consumable forms, and consist of shells, husks, pulps, peels and seeds (198).

#### **2.2.1.1 Primary agricultural by-products**

Crop residues are the parts of plants and crops that remain after the financially valuable sections have been harvested (199). Example of crop residues include straw and bagasse. The main applications of crop residues are that they are generally left on the field (40-70%), burned (0-10%) or used by animals (0-40%) (200), with the proportions of each changing across individual cropland, regions and countries.

The most common sources of husks and straws discussed in the literature arise from rice and other cereals (201, 202), predominantly in Asian countries (203). Within the EU, maize and wheat straws are the most abundant types of cereal straw (204). Once cereal grains are grown and harvested, the straw is the remaining residue left to dry on the field. The straw is then harvested and baled, before being used across the agricultural sector. The main use of harvested straw is as animal bedding (205). Although illegal in the EU, unused straw is burned in the field, as this does not include additional costs such as handling or transportation (206). Excusing the reduced costs, the generation of smoke from straw burning is sometimes used by farmers as a method of pest and disease control (207). Another key use of straw is as a source of organic matter for soil. In Italy and Ireland, there are financial incentives for farmers to leave straw on fields, as the straw incorporation leads to increased soil fertilisation and soil organic carbon accumulation (205). In the literature, straw has been explored for its use in the production of particleboards (208),

fibreboards (209), concrete reinforcement (210, 211), and in the cultivation of mushrooms (212-214).

### 2.2.1.2 Secondary agricultural by-products

In the growing season of cereals such as rice, husks are the coating that protect the seeds (215) (Figure 2-4). After the harvesting of the cereals, the grains are dried, ground, peeled, and milled, which separates the husks from the cereal seed (216). As with straws, agricultural husks can be used as a soil amendment by aiding the retention of nutrients and moisture in the soil. The widespread uses of husks are as energy sources, either to be burned in power plants to generate electricity, or as a fuel source for heating and cooking (217). Less common applications are in packaging, paper production and insulation (217).

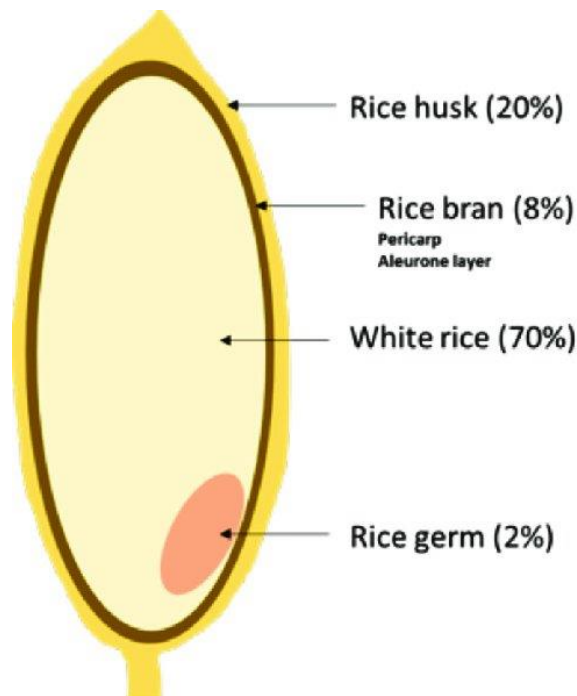


**Figure 2-4** – The structure of a rice grain. Sourced from (218).

Cereal brans are a part of the outer layer of cereal grains that is often discarded during milling (219). The key difference between the bran and the husk is that where the bran is the broken seed coat, the husk is the hard, protective cover of grains that must be removed before consumption (220). Whilst the husk has no nutritional value, the bran has plenty of proteins, vitamins, and fibres (220). The main applications of brans are as low-value animal feed, or being discarded as waste (221). About 10 % of generated bran is used to supplement human food. This small percentage is due to the transportation and processing costs, and with the poor functional and textural properties of the bran (222).

Bagasse is a residue of sugarcane and sorghum. After the sugarcane or sorghum is crushed for extraction of its sugar content, the bagasse is the remains, present as a dry fibrous waste (223, 224). The bagasse is high in cellulose content, so is used as a feedstock in the paper industry, as a biofuel, and is also burned for its energy content (225). Bagasse is also a fibrous material. Consequently, the fibres have been investigated for their use in the textile and civil engineering sectors (225).

Similar to bagasse, pulps are the remains after a fruit or vegetable have been crushed, or where the desired content has been extracted. Within the EU, the largest vegetable processing by-product is sugar beet pulp (204). The main applications of vegetable pulps, such as sugar beet pulp, is to be used as an animal feed (226), or as a feedstock for biogas via fermentation or anaerobic digestion (227).

The peels of potatoes are the third largest vegetable processing by-product in the EU (204). In contrast to the other types of residues that have been discussed, peels are more likely to be generated in households rather than in processing facilities (228), so they are only present in high volumes at waste facilities and referred to as food waste (229). There are only limited industrial-scale applications of vegetable or fruit peels, or seeds, but literature has looked to study and find uses for their high bioactive contents (229, 230). The peels of fruit including mangosteen, mango, papaya, and dragon fruit appear to have greater levels of phenolics than the flesh (between 13-47%) (230). Seeds contain phenolics to a lesser extent than the peels but contain a larger variety of bioactive components also including tannins, triterpenoids, flavonoids, steroids, fatty acids, oils, and saponins (230). These chemicals are mostly used in the cosmetic and food industries due to their anti-inflammatory, antimicrobial, antioxidant properties (231).

### **2.2.2 Treatment methods of residues**

Due to the limited applications of agricultural residues, as discussed, the biomass can be converted to exploit its lignocellulosic content (232). As the focus of this study is on lignin-rich residues, only the methods that concentrate the lignin in the agricultural residues will be discussed.

The common types of conversion routes for biomass are biochemical and thermochemical. In biochemical conversion, the biomass can be upgraded via routes including anaerobic digestion, fermentation, saccharification and transesterification (233). The thermochemical conversion routes consist of pyrolysis, gasification, combustion, hydrothermal liquefaction and hydrothermal carbonisation (233).

### **2.2.2.1 Biochemical conversion**

As discussed, the biochemical conversion of biomass is commonly accomplished by anaerobic digestion, fermentation, saccharification and transesterification.

Saccharification is a key form of pre-treatment prior to fermentation. This process depolymerises the constituents of biomass into their fermentable sugar monomers. However, lignin reduces the severity and scale of saccharification, leading to a lower fermentable sugar yield (234). It is for this reason that lignin would need to be depolymerised and separated from the biomass to improve the process. Therefore, saccharification will be discussed alongside anaerobic digestion and fermentation, which require similar pre-treatments.

Transesterification is the change of ester groups within a structure under basic or acidic conditions (235). In the literature, transesterification has not been done on biomass due to its complex structure, but has been done on extracted and processed lignin (such as Kraft lignin) (236). Due to the process not being performed on the biomass, but on pre-extracted lignin, it will not be discussed in detail in this section.

#### **2.2.2.1.1 Anaerobic Digestion**

Anaerobic digestion (AD) is the microbial digestion of a substrate (in this case, lignocellulosic biomass) in the absence of oxygen to produce a biogas that can be upgraded into biomethane (237). Biomethane can be used as an energy source in the generation of steam and heat, in combined heat and power (CHP) production, and as a replacement for natural gas (in the transportation sector and in the natural gas grid) (238).

One of the barriers for the use of lignocellulosic biomass in anaerobic digesters is its structure. The interactions between the hemicellulose, cellulose and lignin leads to a biomass structure which is both resistant and recalcitrant (239). Therefore, improving the digestibility of the organic matter contained within the biomass has been explored through chemical, physical, and biological pre-treatments.

Physical pre-treatments, including milling and grinding, are performed to reduce the cellulose content's crystallinity, increasing its availability for AD (240).

The lignin components of lignocellulosic biomass can be removed through chemical pre-treatments with ozone (240). During ozonation, the lignin is depolymerised into degradation products including phenols, benzenes, and fatty acids (241). However, ozone's selectivity is poor, so it may react with the carbohydrates (predominantly cellulose

and hemicellulose) to produce inhibitory compounds that can negatively impact the anaerobic digestion process downstream, but these are only generally produced in small amounts. One of the key reasons that ozonation is used is due to its operation at ambient temperature and pressure. Additional chemical pre-treatments are the use of acids such as hydrochloric acid or sulphuric acid, as it is an inexpensive process to degrade the biomass' structure and enhance the enzymatic hydrolysis process (240).

The enzymatic hydrolysis processes are biological pre-treatments which degrade hemicellulose and cellulose through the addition of enzymes, into the monomer forms (glucose and xylose) that are more readily available for anaerobic digestion (242).

After the necessary pre-treatment has been performed, the degraded biomass is introduced to the microbes, beginning the four-stage anaerobic digestion process. In a typical single-stage batch reactor, the four stages: hydrolysis, acidogenesis, acetogenesis, and methanogenesis, occur sequentially (243). These four stages break down carbohydrates, proteins, and lipids in various ways as to generate biogas (Figure 2-5).

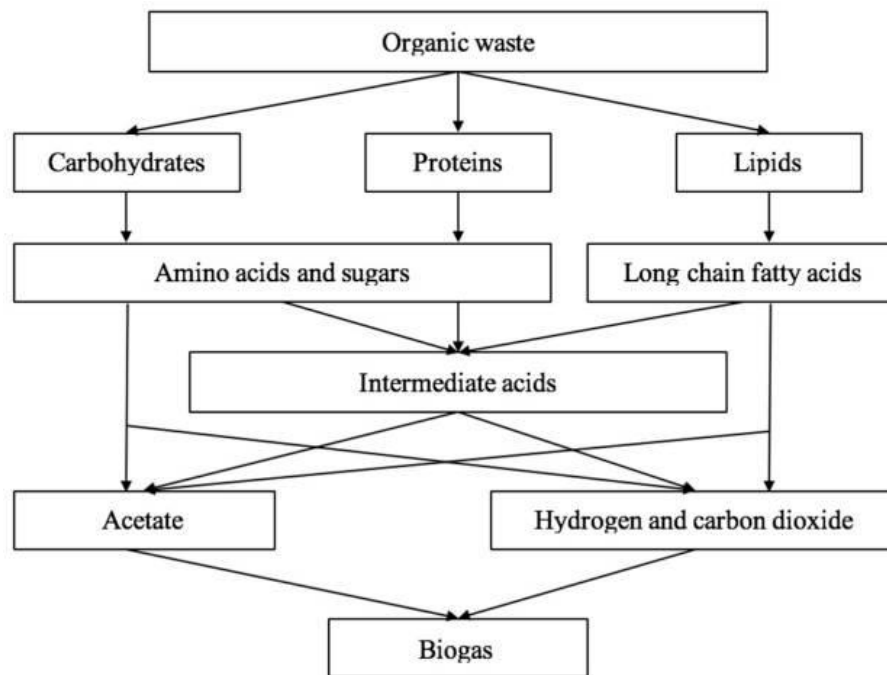


**Figure 2-5** – Simple scheme of anaerobic digestion pathways. Sourced from (243).

Where the lignin content of the biomass was not removed during the pre-treatment by ozonation, and alternative pre-treatments were performed, the residue from the AD process leaves behind a digestate. Typically, the digestate is considered to be rich in lignin

due to the degradation of the other lignocellulosic components (244). However, this is more likely when the biomass began with a high lignin content.

In addition to the lignin that would be concentrated within the digestate, the nutrient content (nitrogen, phosphorous and potassium) is also concentrated. For this reason, around 95% of agricultural digestate in Europe is utilised as fertiliser (245). However, the volume of digestate used can lead to downstream issues because of the high concentrations of nutrients, potentially leading to run-off to waterways, negatively impacting the water quality (246).

The mass of the digestate generated from AD can range from 38-84 wt% of the fresh matter (247). The digestate also has a high water content, which leads to large transport volumes and costs (248). Therefore, digestates tend to undergo solid-liquid separation, generating a low-solids liquid fraction, and a thick solid fraction (249). The liquid fraction ideally consists of the bulk of the water, total potassium, and ammonium nitrogen contents, whilst the solid fraction comprises the organic nitrogen, total phosphorous, recalcitrant fibres, and the remaining undigested substrates (248).

As the liquid phase carries the most mass due to the large water content, this tends to still be applied as a fertiliser locally. The solid phase, however, is more easily exported to other farms to be used as a P/N fertiliser (250).

#### **2.2.2.1.2 Fermentation**

Whilst anaerobic digestion is a biological intracellular process, fermentation is a similar but different process where chemical reactions are induced by micro-organisms for the conversion of sugars into alcohols and carbon dioxide (251).

As with AD, fermentation requires the pre-treatment of lignocellulosic biomass to either extract the valuable sugars, or to allow them to be accessible by microbes (252). This pre-treatment, as discussed earlier, can either include the delignification of the biomass (with the use of ozone) or not. Here, it will be assumed that the lignin content of the biomass has not been removed prior to fermentation.

General methods of biomass pre-treatment prior to AD or fermentation include enzymatic and fungal pre-treatment, particle size reduction, and chemical pre-treatment (with acids, alkalis, and solvents). For fungal and enzymatic pre-treatment, the fungi and enzymes used varies depending on the target. Regarding fungi, if the aim is to degrade cellulose, a cellulolytic fungus such as brown-rot fungi, is used. For the degradation of lignin, white rot fungi can be used. However, fungal pre-treatment require extended incubation periods

from weeks to months. Enzymatic pre-treatments only need a few hours. The effectiveness of the degradation of lignocellulose by enzymes depends on the enzymes' activity, the enzyme's specificity to the substrate, the presence of any inhibitory components (such as humins), and the temperature and pressure of the process (253).

The size reduction of particles by milling or grinding of biomass makes its structure more accessible to microbial and enzymatic exposure, whilst chemical treatments solubilise the hemicellulose and lignin present within the structure. The most common form of chemical treatment is dilute acid treatment, whereby dilute sulphuric acid digests the biomass over a range of temperatures (< 131 °C) for between 1 hour to 2 days (253).

In the most common route of fermentation, the hemicellulose and cellulose contents are partially converted into ethanol. The residue that remains after the fermentation consists of the unconverted cellulose and hemicellulose, proteins (including the yeast and enzymes used in the fermentation), and lignin (254).

In the literature, the valorisation of fermentation residues have been explored as a potential animal feed, in the production of biofuels, biopolymers, bioplastics, and in nanomaterials (255, 256). Research has also discussed its use as a precursor of lignin-based resin adhesives (254), and to exploit the remaining unconverted cellulose and hemicellulose by anaerobic digestion (255).

### **2.2.2.2 Thermochemical conversion**

The different routes of thermochemical conversion of lignocellulosic biomass are pyrolysis, gasification, combustion, hydrothermal liquefaction and hydrothermal carbonisation.

In this study, the focus is on the valorisation of lignin and lignin-rich residues into higher value products. As the purpose of combustion and gasification is commonly for the generation of low value gases including hydrogen, carbon dioxide and carbon monoxide, and heat and power (257, 258), it is not of interest to this work.

#### **2.2.2.2.1 Pyrolysis**

Pyrolysis is the heating of organic matter in the absence of oxygen. In this section, the concepts behind the various types of pyrolysis are explored. The literature pertaining to the pyrolysis of the specific samples are covered in the respective chapters (i.e. the fast pyrolysis of general biomass residues, digestates, and commercial lignin products can be found in Section 4.1, the fast pyrolysis of tree barks can be found in Section 5.1, and the slow pyrolysis of samples is located in Section 7.1).

The pyrolysis process set up and conditions that are chosen are based on the desired products. There are three types of pyrolysis products: a liquid (bio oil, aka condensable gases), a gas (non-condensable gases including H<sub>2</sub>, CO, CH<sub>4</sub> and CO<sub>2</sub>) and a solid (char) (259). The range of conditions for each pyrolysis type can be seen in Table 2-3.

**Table 2-3** - Conditions and products of different pyrolysis methods (260, 261).

Method	Temperature (°C)	Residence Time (s)	Heating Rate	Major products
<b>Slow pyrolysis</b>	< 500	600 – 172,800	10 °C/min	Char (< 35 wt%) Liquid (< 35 wt%) Gas (< 30 wt%)
<b>Fast pyrolysis</b>	425 - 650	0.5 – 5	100 °C/s	Char (15 – 25 wt%) Liquid (60 – 75 wt%) Gas (10 – 20 wt%)
<b>Ultra-fast/flash pyrolysis</b>	900 - 1300	< 0.5	>1000 °C/s	Char (15 – 25 wt%) Liquid (60 – 75 wt%) Gas (10 – 20 wt%)

The pyrolysis of lignocellulosic biomass is normally consolidated into three key steps. First, the moisture that is present in the biomass is evaporated. Following this is the degradation of the primary biomass, and secondary reactions. In the primary degradation, the majority of the biomass' decomposition occurs at 200-400 °C, leading to the char formation. The secondary reactions include the cracking of the pyrolysis oils and repolymerisation. This happens in the interior surface of the biomass.

The individual components of lignocellulosic biomass pyrolyse at different temperatures due to the differences in structure.

Cellulose pyrolysis occurs at 325-400 °C. The main groups of compounds found in cellulose-derived pyrolysis oils are furans, pyrans, and small linear molecules, with levoglucosan, 5-hydroxymethylfuran and glycolaldehyde as the core products (262).

The decomposition of hemicellulose by pyrolysis arises between 250-350 °C (263), leading to noticeable proportions of aromatic compounds, C5 molecules, predominantly furans, and acids including as acetic acid (264).

Due to its increased stability, lignin degrades at higher temperatures between 300-550 °C (263). The main types of compounds in lignin-derived pyrolysis oils are aromatic hydrocarbons and phenols, featuring functional groups such as methoxy, carbonyl, and carboxyl (265).

Proteins within lignocellulosic biomass, when pyrolysed, leads to amine and amide groups that join other pyrolysis products to form groups including pyrazoles, indoles, pyrroles, and imidazoles (266).

The char that is produced from pyrolysis differs greatly between slow and fast pyrolysis (267). In fast pyrolysis, the char is more alkaline (high pH), has greater aromaticity and a larger surface area (268). Slower heating rates and lower temperatures produce a char in higher quantities, and high cation-exchange capacities and electric conductivity (269). These allow the slow pyrolysis biochar to provide a greater adsorption capacity. In slow pyrolysis, the bio-char contains larger amounts of oxygen and volatiles, which is held in the liquid phase during fast and flash pyrolysis (270).

Although the fast and flash pyrolysis major products appear to be the same in Table 2-3, the composition of the liquid phases are different (271). After undergoing flash pyrolysis, the generated bio-oil would have a reduced water content compared to fast pyrolysis oils (261). For the heating rates and high heat transfer necessary for flash pyrolysis, intense mechanical pre-treatment is needed as the particle size must be small (105 – 250  $\mu\text{m}$ ) (261). With shorter residence times, the liquid yield can be maximized. This can occur by preventing secondary cracking reactions, whilst volatiles are still emitted (272). The contents of the pyrolysis oil change depending on the pyrolysis temperature, heating rate, and lignocellulosic composition.

At larger scales, the economic effectiveness of fast and flash pyrolysis are determined by several factors separate to the actual pyrolysis process. These include feedstock availability and variety, biomass logistics, and location of the plant (273). The key challenge with scaling flash pyrolysis is the reactor design that allow extreme heating rates (in  $^{\circ}\text{C}/\text{ms}$ ) with ultra-short residence times (< 5 secs) (274). With fast pyrolysis, although the heating rate is lower (in  $^{\circ}\text{C}/\text{s}$ ), there is still difficulty in ensuring sufficient heat transfer (275).

Regarding the feasibility of fast pyrolysis processes, the literature includes some papers on the techno-economic analysis of the production of pyrolysis oil leading to an estimated cost of pyrolysis oil between  $0.94 \pm 0.24$  USD/L across various feedstocks and feed rates (274). However, no literature could be found that estimated the cost of flash pyrolysis oil. The range of prices for crude oil across 2024 was 0.41-0.55 USD/L (276). This is clearly a lot lower than the price of pyrolysis oils. However, as crude oils and pyrolysis oils are immiscible with each other due to the difference in polarities, their applications are different, and so the difference in prices is not as important.

Hydropyrolysis is a process where a reducing H<sub>2</sub> gas is used to pyrolyse biomass under pressures between 1-52 bar (277). The main products are hydrocarbons from the reaction of hydrogen radicals with volatiles. The oxygen contained within the biomass' structure is removed by the pyrolysis as CO, CO<sub>2</sub> and water (278). The production of hydrocarbons is not desirable for the bio- oil components of interest, so this method will not be considered any more.

#### **2.2.2.2.2 Hydrothermal conversion**

Hydrothermal liquefaction and hydrothermal carbonisation are processes which operate under above-saturated pressure and elevated temperatures to alter the physiochemical properties of water, allowing the processing of biomass into energy-dense fuels and chemicals (279). In comparison to pyrolysis, these two routes are more ideal for biomasses with higher moisture contents (70-90%) (279).

As the bulk of the agricultural residues discussed in Section 2.2 are left to dry after the harvesting of the main crop, the moisture contents are expected to be relatively low. For this reason, hydrothermal conversion would not be the best route for valorising the potential lignin-rich residues. Despite this, the two main routes of hydrothermal conversion have been used on lignin samples in the literature (280-282), so they will be discussed briefly below.

#### **Hydrothermal liquefaction**

Hydrothermal liquefaction (HTL) is a process whereby lignocellulosic biomass is converted into a solid residue (hydrochar), an aqueous phase, a gas, and an oil-phase referred to as bio-crude (283), at temperatures between 250 and 375 °C (284). In comparison to other thermal conversion routes, biomass can be fed directly (as received) into the conversion unit, and does not require drying prior to the process (285).

The aqueous phase has been researched for its potential valorisation in anaerobic digestion to produce biogas (286), as a feedstock for gasification to produce hydrogen-rich gas (287), and to be recycled to be used as a reaction medium in further hydrothermal liquefaction for the generation of bio-crude (288, 289). The CO<sub>2</sub>-rich gas phase of HTL has been explored for the cultivation of microalgae (290).

The bio-crude is the main product of HTL and contains a wide variety of aromatic compounds and hydrocarbons. Its key application is as a substitute for petroleum-derived transportation fuels but is also able to be refined into specialty chemicals and additional biochemicals (291, 292). As the lignin-derived aromatic contents is concentrated within the

bio-crude, the hydrochar that is generated has less of an aromatic structure, in addition to a smaller surface area and reduced porosity compared to pyrolysis biochars (293).

### **Hydrothermal carbonisation**

Hydrothermal carbonisation (HTC) is a thermochemical process that uses pressure and heat to convert lignocellulosic biomass into solid (hydrochar), liquid, and gas products. In contrast to HTL, the main target product of hydrothermal carbonisation is the hydrochar (294), with an expected mass yield between 35-80% (295). However, the energy density of the hydrochars are smaller than the chars produced from pyrolysis due to the high moisture contents.

The conditions used in HTC are similar to slow pyrolysis that has taken places over long residence times (5 min to 12 hrs) and slow heating rates (10-30 °C/min) (296). Yet, in contrast to slow pyrolysis, HTC takes place in acidic or neutral aqueous solutions. The hydrochar from HTC typically has lower ash contents, higher H/C and O/C molar ratios compared to slow pyrolysis biochars (297). In the literature, the hydrochars have been explored for their uses in gas adsorption (298, 299), composites (300), wastewater remediation (301, 302), flame retardancy (303), energy storage (304, 305), and in the biomedical field (297, 306, 307).

The aqueous phase of the HTC process (also known as process water) is generally comprised of inorganic salts and dissolved organic components, but is very dependent on the feedstock used and process conditions (308, 309). The process water phase has been investigated for their recirculation into later HTC batches (310). Although some work has suggested that this can enhance the hydrochars, carbon or energy yields, it can also lead to the accumulation of total acids, chemical oxygen demand (COD), and total organic carbon (TOC). The re-use of the process water can therefore become increasingly concentrated, so would require additional treatment prior to being discharged (311).

The gas phase that is produced from HTC is only about 1-3 wt% of the initial raw material, is predominantly carbon dioxide, with traces of carbon monoxide (312).

## Chapter 3 - Materials and Methods

In this section, the background of the samples tested in this work are outlined. The chapters where each sample was used can be found in Table 3-1. Following this, the different methods explored in this study will be described. These include the methods used for characterisation of the samples, the extraction of alkali metals, alkaline earth metals and suberin, the implementation of a solvent hazardousness assessment, and the ammonia adsorption experimental set-up. Lastly, the assessment of errors and method limitations are presented.

### 3.1 Materials

#### 3.1.1 Lignin products

LignoBoost (LB) from Innventia AB (Stockholm, Sweden) was produced from the black liquor generated in the Kraft lignin process. The black liquor was first filtered at high pH to precipitate out a crude lignin. After this, the material then underwent an additional stage of filtration and washing at low pH to produce a pure lignin (313). The specific conditions of the LignoBoost process is unknown due to it being a patented process (313). Alkali Lignin (AlkLig), which is generated from Kraft lignin that has undergone hydrolytic degradation from Merck, was purchased from Sigma-Aldrich. Organosolv lignin (Org) was purchased from Sigma-Aldrich. The organosolv process isolated lignin from other lignocellulosic components using low boiling point organic solvents.

#### 3.1.2 Digestates

Samples of dewatered digestates were supplied by Organic Waste Systems (OWS), Belgium and Yorkshire Water, UK. The four digestates (SSdig, VGFdig, MSWdig and AGRdig) were generated from the anaerobic digestion of different waste streams (314):

(i) Sewage sludge (SSdig), comprising of a homogenised mixture of pre-treated primary and secondary biosolids. This was gathered from a WWTP (wastewater treatment plant) with commercial-scale anaerobic digestion (AD) facility (Dewsbury, UK). Prior to AD, the SS digestate underwent thermal hydrolysis at 160 °C and 6 bar. After AD, the digestate was dewatered to increase the total solids (TS) concentration to 15-20 %. The material was then oven-dried at 60 °C.

- (ii) Vegetable, garden and fruit (VGFdig) material, collected from source separated organic household waste.
- (iii) Municipal solid waste (MSWdig), specifically the residual organic fraction after mechanical separation.
- (iv) Agricultural residue (AGRdig), combining fractions of manure, whole plant and grass silage, and >80% of maize.

The VGF, MSW and AGR digestates were produced at a lab-scale test digestion facility (DRANCO) that simulates a large-scale dry anaerobic composting processing plant.

### 3.1.3 Other feedstocks

Coconut husk (CH) was obtained by de-shelling whole coconuts purchased in Leeds, UK at a local supermarket. Sugarcane bagasse (*Saccharum officinarum*) was collected from sugar cane fields near to Faisalabad city, Pakistan (PKBag).

Bark-free holm oak wood (oak) and its biochar (produced at 450 °C) (Oakbc450) were provided by the Fertiplus Consortium (Grant Agreement N°: 289853), co-funded by the European Commission, Directorate General for Research & Innovation, within the 7th Framework Programme of RTD, Theme 2 – Biotechnologies, Agriculture & Food. The pyrolysis to produce the biochar was completed in a mono retort reactor for 60 min in the absence of oxygen. The retort-type reactor allows the recovery of oil and gas (315).

Two types of peat were analysed. An Irish sphagnum moss peat, and a peat turf. Two different types of commercial activated carbons were tested for their ammonia adsorption potential. These were a NORIT RO 3515 (NORIT-AC) and activated charcoal from Sigma-Aldrich (SIGMA-AC).

### 3.1.4 Tree barks

One softwood tree bark was obtained from Golden Acre Park, Leeds. 11 species of bark were provided by Abbey Timber (Scottish Borders, UK). The tree barks that were analysed were all softwoods from the pine and cypress family.

The pine family barks consisted of sitka spruce (*picea sitchensis*, SS), Douglas fir (*pseudotsuga menziesii*, DF), Norway spruce (*picea abies*, NS), noble fir (*abies procera*, NF), larch (*larix decidua*, L), grand fir (*abies grandis*, GF) and European silver fir (*abies alba*, ESF).

The cypress family samples were Western red cedar (*thuja plicata*, WRC), lawson cypress (*chamaecyparis lawsoniana*, LC) and nootka cypress (*chamaecyparis nootkatensis*, NC).

Table 3-1 – Use of each material across this work.

Sample	Abbreviation	Chapter 4	Chapter 5	Chapter 6	Chapter 7
Alkali Lignin	AlkLig	Y		Y	Y
Lignoboost	LB	Y		Y	Y
Organosolv Lignin	Org	Y		Y	
Municipal Solid Waste Digestate	MSWDig	Y			Y
Vegetable, Garden and Fruit Digestate	VGFDig	Y			Y
Agricultural Residue Digestate	AGRDig	Y			
Sewage Sludge Digestate	SSDig	Y			
Coconut Husk	CH	Y		Y	Y
Sugarcane bagasse from Pakistan	PKBag	Y		Y	
Golden Acre Park bark	SP Bark	Y		Y	
Nootka Cypress tree bark	NC		Y	Y	Y
Grand fir tree bark	GF		Y	Y	Y
Western hemlock tree bark	WH		Y	Y	
Norway spruce tree bark	NS		Y	Y	
Sitka spruce tree bark	SS		Y	Y	
European silver fir tree bark	ESF		Y	Y	Y
Douglas fir tree bark	DF		Y	Y	Y
Western red cedar tree bark	WRC		Y	Y	
Larch tree bark	L		Y	Y	
Noble fir tree bark	NF		Y	Y	Y
Lawson cypress tree bark	LC		Y	Y	
Cellulose	Cell				Y
Oak	Oak				Y
Oak biochar at 450C	Oakbc450				Y
Peat turf	PeatSEPO				Y
Irish sphagnum moss peat	PeatMoss				Y
NORIT Activated Carbon	NORIT-AC				Y
SIGMA Activated Carbon	SIGMA-AC				Y

## 3.2 Proximate Analysis

Proximate analysis is a key characterisation method, which can aid in determining:

1. Ash content – which can inform on the potential slagging, fouling and coking of the biomass from thermal conversion (316),
2. Fixed carbon – which provides an estimate of the proportion of char that would be produced if the biomass is pyrolysed (317),
3. Moisture content – which indicates the difficulty of storing the biomass, and
4. Volatile matter – which can be used as a measure of the biomass' combustion characteristics (318),

The proximate analysis is ordinarily performed at either 550 °C and 900 °C for the final step (ashing) (319). Although several standard test methods exist (ISO 17246:2024, ISO 18122:2022), there is not a clear reasoning for why each temperature is chosen. Commonly, ashing is done at 900 °C for thermally converted biomass, such as chars and coals (320), whilst 550 °C is done for non-thermally converted biomass (321). Lower temperatures are likely to be used to prevent the ash from melting or hardening (322). Some biomass, including miscanthus, have ash melting points around 700 °C (323), therefore the proximate analysis ashing is performed below this temperature in this case.

Historically, proximate analysis was completed in a furnace under the controlled conditions. However, this required a large amount of sample ( $\approx 1$  g) and long durations, as the furnace's scale effects its heating rate. The benefit of using the larger sample mass was that the results would be more accurate due to the greater sample size, but at the cost of time and precious sample (324). Within the last decade, methods have been developed to perform proximate analysis using thermogravimetry (325). This requires only 10 mg of sample, with programs lasting close to 30 minutes rather than several hours (326).

The proximate analysis of the solid materials in this study was determined by thermogravimetric analysis (TGA/DSC 1, Mettler Toledo GmbH, Greifensee, Switzerland).

All measurements were performed in duplicate, with the mean values being reported. The heating profile used on the TGA consisted of the sample initially being heated from room temperature to 120 °C in nitrogen, which was held for 10 minutes. Then, the sample was heated to 900 °C and held for 30 minutes. After this time, the gas was switched to air to combust the sample and produce ash. Error values were calculated by standard deviation. The balance used for this analysis had an error of  $\pm 0.005$  mg.

The four components of proximate analysis can be taken from the TGA curve, according to Figure 3-1. Here, the mass loss and temperature changes from the heating programme, are used to determine the moisture, volatile matter, fixed carbon, and ash content.

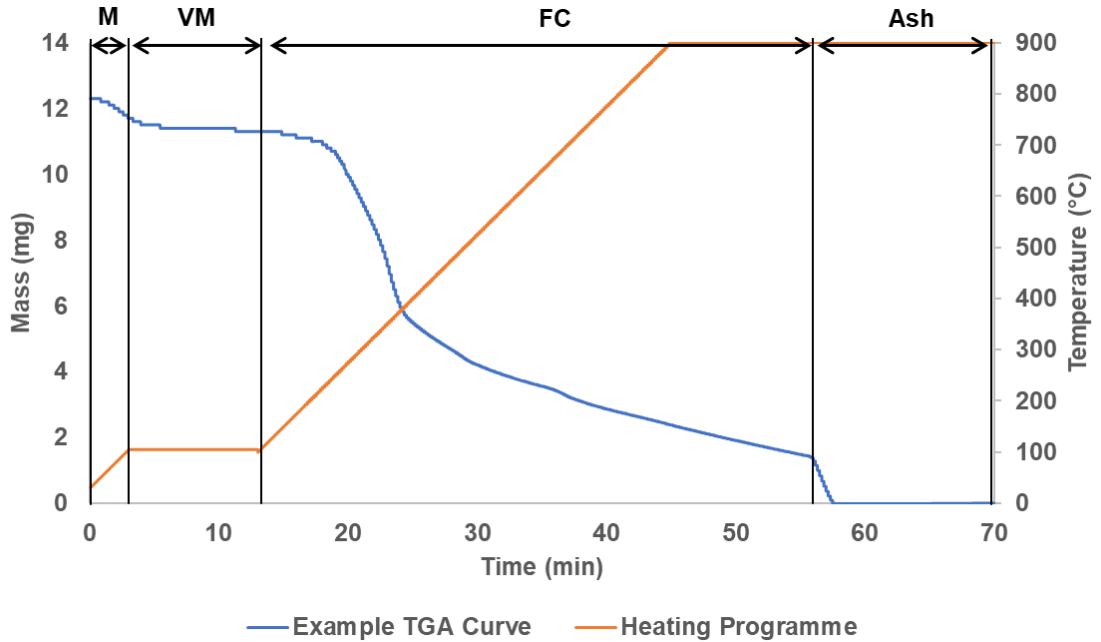


**Figure 3-1** – Example of a thermogravimetric curve. The mass loss that occurs across the regions outlined represent the moisture (M), volatile matter (VM), fixed carbon (FC), and ash content of the sample.

### 3.3 Ultimate Analysis

Ultimate analysis is another key characterisation method which can inform on the:

1. Calorific content of the biomass - which provides the biomass' value as an energy source by incineration,
2. Carbon/Hydrogen/Nitrogen/Sulphur/Oxygen content – which helps to estimate the gases produced by the pyrolysis or combustion of the biomass.

The calorific content of biomass can be estimated by a few different equations including Friedl and Dulong (327, 328). However, Channiwala and Parikh's (Equation 3-3) (329) is better validated and includes all of the terms measured by ultimate analysis. By comparison, Friedl and Dulong do not include the ash content. As the ash content of biomass can range from 5 wt% to over 40 wt% (330), it is important to consider all aspects of the ultimate analysis. The one true method for calculating HHV would be bomb calorimetry. However, this was unable to be done for this work as the equipment was not available. Values in the equations (Equation 3-1, Equation 3-2, and Equation 3-3) are used on a weight% dry basis (d.b).

**Equation 3-1** - Friedl's equation for estimating higher heating values (327). C, H and N represent carbon, hydrogen and nitrogen contents, respectively (on a dry basis).

$$HHV \left( \frac{kJ}{kg} \right) = 3.55C^2 - 232C - 2230H + 51.2C \times H + 131N + 20,600$$

**Equation 3-2** - Dulong's equation for estimating higher heating values (331). C, H and O represent carbon, hydrogen and oxygen contents, respectively (on a dry basis).

$$HHV \left( \frac{MJ}{kg} \right) = (0.3383 \times C) + (1.422 \times \left( H - \frac{O}{8} \right))$$

**Equation 3-3** - Channiwala and Parikh's equation (329) for estimating higher heating values. C, H, O, N, S and A represent carbon, hydrogen, oxygen, nitrogen, sulphur and ash contents, respectively (on a dry basis).

$$HHV \left( \frac{MJ}{kg} \right) = 0.4391C + 1.1783H + 0.1005S - 0.1034O - 0.0151N - 0.0211A$$

The calorific content states what the maximum expected energy output of the sample is on a per mass basis (332). This is useful as, in a scaled-up process, the biomass can be incinerated (if needed). The energy generated from this incineration can be recovered to help reduce the energy intensity of the process and therefore reduce costs (333).

The carbon content of the biomass is not the same as the fixed carbon content. Although a proportion of the biomass' carbon will migrate to the fixed carbon, when

combusted or pyrolysed, the carbon will be used to generate gaseous compounds including carbon dioxide (CO<sub>2</sub>) and carbon monoxide (CO) (334). These would be included in the volatile content of the proximate analysis.

In this study, the carbon, hydrogen, nitrogen, and sulphur content were analysed using an Elemental Analyser (Flash 2000, Thermo Scientific, Waltham, USA). The instrument was calibrated and checked using calibration standards and certified biomass reference materials (Elemental Microanalysis, Devon, UK). The oxygen content of the feedstocks was calculated by difference after correction for moisture and ash content measured by TGA. Error values were calculated by standard deviation. The instrument can measure the C, H, N and S contents in wt% above 0.2 wt%, however, this is very dependent on the sample being analysed. The balance used for this analysis had an error of ±0.005 mg.

Due to the moisture content of the samples, the hydrogen value must be corrected according to:

**Equation 3-4** - Correction of H-content for moisture. a.r. denotes 'as received'. M denotes 'moisture content' in wt% from the proximate analysis.

$$\text{Corrected H (\%)} = H_{a.r} - \left( M_{a.r} \times \frac{2}{18} \right)$$

**Equation 3-5** - Calculation of oxygen content (O%), by difference, from the values given from ultimate analysis. C, H, N and S refer to carbon, hydrogen (calculated from Equation 3-4), nitrogen and sulphur on a dry basis.

$$O (\%) = 100 - (C\% + \text{corrected H}\% + N\% + S\% + \text{Ash}\%).$$

### 3.4 Fibre Analysis

One key form of characterisation is fibre analysis. In this gravimetric method, the different fibrous fractions are removed from a sample so that lignocellulosic components such as cellulose, lignin and hemicellulose can be measured. There are two base methods of fibre analysis, “Van Soest’s acid detergent fibre method” (335) and “Weende’s Crude Fibre Determination method” (336). Van Soest’s method analyses the neutral detergent fibre (NDF) and acid detergent fibre (ADF) by a two-step process in which two different solutions are added to the sample. In Weende’s method, the crude fibre of the sample is measured after undergoing acid digestion, alkali digestion, and various washing steps. Each of these methods have their merits, depending on what the important component is, but previously they were very active methods that required a lot of input from the laboratory user.

A more recent piece of equipment (the Fibretherm) combines Van Soest and Weende’s methods and utilises a more automated methodology. The Fibretherm method is a four-step process which can sequentially separate the acid detergent fibre, neutral detergent fibre and acid detergent lignin (ADL) so that the lignocellulosic components can be measured. The results from the Fibretherm method can provide a good comparison between different types of biomasses (337). A review of the literature regarding the fibre analysis of samples explored in this study can be found in the respective chapter in which they are performed.

The Gerhardt Fibrecap system (as described by Fettweis and Kühl, 2015) (Figure 3-2) was used in this study to determine the neutral detergent fibre ( $\text{NDF}_{\text{om}}$ , or  $\text{aNDF}_{\text{om}}$  using amylase, STM 016), acid detergent fibre ( $\text{ADF}_{\text{om}}$ , STM 017) and acid detergent lignin ( $\text{ADL}_{\text{om}}$ , STM043) (338).



**Figure 3-2** – Image of the Fibretherm equipment used for fibre analysis.

Prior to beginning the method, the samples must be dry and have a particle size between 120  $\mu\text{m}$  and 1 mm. The glass spacer must be placed in the quartz crucible, and weighed. Then, the Fibrebag is placed around the glass spacer (in the quartz crucible) and re-weighed (Figure 3-3).

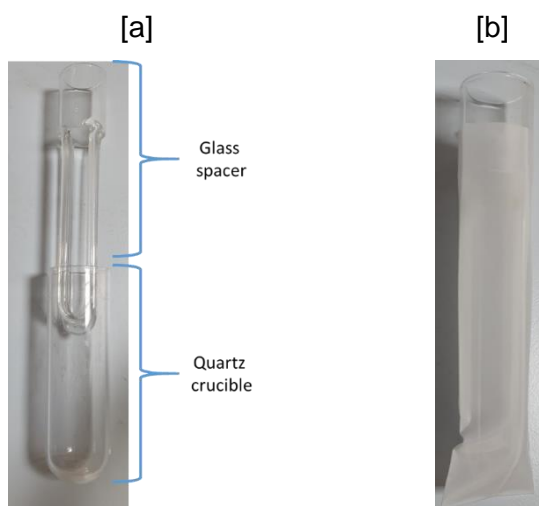


**Figure 3-3** – Images of [a] the glass spacer and quartz crucible, and [b] the Fibrebag around the glass spacer used for fibre analysis.

Then, around 1 g of sample is added to the Fibrebag and once again re-weighed. This is repeated for all samples.

The next steps of the method are outlined below step-by-step, to simplify the instructions.

1. The prepared sample in the glass spacers are removed from the quartz crucibles and are placed in the carousel (Figure 3-4). A full batch is made up of 12 samples. If less than 12 samples are run, it is advised to still add the empty glass spacers to the carousel to ensure balance.



**Figure 3-4** - Carousel used within the Fibretherm equipment for fibre analysis.

2. At this point, 5 drops of anti-foaming agent are added to the carousel. This makes sure that the solutions that are added to the carousel do not foam and lead to leakages in the system.
3. The Fibrecap equipment is turned on, and the localised cold water source connected to the equipment is opened. This allows the system to stay sufficiently cool, and perform any rinses necessary according to the method.
4. The neutral detergent fibre method, as programmed onto the system, is then executed.
5. Following the method, the equipment is turned off, and the glass spacers are placed inside the quartz crucible (held within a rack), which is put into a drying oven for at least 8 hours at 105 °C.
6. After the samples have sufficiently dried, the rack is placed within a desiccator to allow it to cool whilst minimising the moisture that will be adsorbed.
7. When cool (at approximately 20 °C), the masses of each quartz crucible (containing the glass spacer, Fibrebag and sample) are weighed.
8. Step 1 to 3 are repeated.
9. The acid detergent fibre method, as programmed onto the system, is then executed.
10. Step 5 to 7 are repeated.
11. Three wide 3-5 L glass beakers are rinsed, and then dried in a drying oven.

12. 2 L of 72% sulphuric acid are added to a 5 L glass beaker (whilst wearing a face shield, acid gloves, and a lab coat).
13. All glass spacers are placed into a small steel carousel (that is attached to a clamp and stand) (Figure 3-5), and the carousel is slowly submerged into the sulphuric acid-containing glass beaker.



**Figure 3-5** – Small steel carousel used for the fibre analysis acid step.

14. The small steel carousel is then slowly rotated for 1 minute every 5 minutes, for 30 minutes.
15. After 30 minutes, the carousel is left submerged into the sulphuric acid for at least 90 minutes.
16. Following this, the carousel is slowly taken out of the sulphuric acid, clamped, and left to drain for 15 minutes.
17. The two other 3-5 L glass beakers are filled with water (which can be normal tap water).
18. The used sulphuric acid is transferred to a spare bottle for re-use, if it is not exhausted.
19. The small steel carousel, containing the glass spacers, is slowly submerged into one of the water-containing glass beakers. The carousel is rotated for 1 minute.
20. The carousel is taken out of the water, and is then placed into the other water-containing glass beaker and rotated.
21. The carousel is again taken out of the water, and the glass spacers are transferred into the rack.
22. Steps 1 to 3 are repeated.
23. The washing method, as programmed onto the system, is then executed.

24. Steps 5 to 7 are repeated.
25. The rack is placed into a cold (below 50 °C) ashing furnace.
26. The ashing furnace is switched on and set to 550 °C.
27. The samples are left to ash. The furnace will take around 30 minutes to heat up, and the ashing will take at least 4 hours at 550 °C (although the necessary time is dependent on the specific sample). In this study, samples required at least 2 days to fully ash.
28. Once fully ashed, the rack is taken out of the furnace and left to cool for an hour before being moved to the desiccator to cool.
29. The cooled ashes are then weighed.

The calculations of the lignin, cellulose, and hemicellulose contents (in wt%) are calculated by Equation 3-6.

**Equation 3-6** – Calculation of %NDF, %ADF, and %ADL proportions from fibre analysis.

$$\%NDF = 100 \times \frac{(m_{NDF} - m_{bag} - m_{ash}) - blank_{NDF}}{m_{sample}}$$

$$\%ADF = 100 \times \frac{(m_{ADF} - m_{bag} - m_{ash}) - blank_{ADF}}{m_{sample}}$$

$$\%ADL = 100 \times \frac{(m_{ADL} - m_{bag} - m_{ash}) - blank_{ADL}}{m_{sample}}$$

Where:

$m_{NDF}$  = mass of NDF after step 7

$m_{ADF}$  = mass of ADF after step 10

$m_{ADL}$  = mass of ADL after step 24

$m_{bag}$  = mass of Fibrebag

$m_{ash}$  = mass of ash

$m_{sample}$  = mass of sample

Every 3-4 batches, two blank samples were run. The only difference between the blank and the normal samples, is that for the blanks no sample was added to the glass spacer (therefore  $m_{sample} = 0$  g). The blanks were run to check that, as the fibre analysis was a gravimetric method, that there was no undue mass gain across the methodology.

From Equation 3-6, the cellulose, hemicellulose, and lignin contents (in wt%) were calculated by Equation 3-7.

**Equation 3-7** – Calculation of %Cellulose, %Hemicellulose, %Lignin proportions from fibre analysis.

$$\%Cellulose = \%ADF - \%ADL$$

~ 50 ~

$$\%Hemicellulose = \%NDF - \%ADF$$

$$\%Lignin = \%ADL$$

Error values across this work were presented using 1x standard deviation, calculated using Microsoft Excel. The balance used for this analysis had an error of  $\pm 0.005$  g.

### 3.5 Crude Protein

From the fibre analysis, the unknown content includes waxes, fats, lipids, and proteins. The target components for the solvent extraction were the extractable content including the waxes, lipids and fats. Therefore, it was necessary to estimate the crude protein content in the samples so as to more accurately estimate the changes in extractable content from the solvent extraction. The crude protein contents were calculated by using the Dumas conversion factors (DCF) most relevant to the type of samples (Equation 3-8). The values of the DCFs were taken and estimated from the literature (Table 3-2).

**Equation 3-8** - Calculation of crude protein utilising Dumas conversion factors.

$$\text{Crude Protein (wt\%)} = N \text{ (wt\%)} \times \text{DCF}$$

**Table 3-2** – Collection of Dumas conversion factors used in this work, adapted from literature.

Sample Type	DCF	Reference
Lignin products	5.60	Mariotti, F., D. Tomé and P.P. Mirand (339)
Agricultural digestates	4.40	Mariotti, F., D. Tomé and P.P. Mirand (339)
Waste digestates	2.83	Amiri, A. (340), Zang, J., J.C.H. Shih, J.J. Cheng, Z. Liu, Y. Liu and W. Lu (341)
Bagasse or husks	5.83	Jones, D.B. (342)
Barks	5.60	Mariotti, F., D. Tomé and P.P. Mirand (339)

### 3.6 Atomic absorption spectroscopy (AAS)

Atomic absorption spectroscopy (AAS) is a method utilised for the analysis and quantification of trace metals.

In this work, the relevant trace metals to analyse were those known to influence the composition and yields of biomass-derived pyrolysis oils (343). These metals: aluminium, calcium, potassium, iron, sodium and magnesium, can be measured by atomic absorption spectroscopy (AAS). For biomass with high metal contents, the intensity of pyrolysis or combustion is greater at lower temperatures compared to biomass with low metal contents (344).

The contents of alkaline earth metals (AEMs), which include calcium and magnesium (345), can be removed during acid-washing. Acid-washing (or acid-digestion) is performed during the preparation of samples for AAS, ordinarily with 10 wt% (or 2.2M) nitric acid (346). The nitric acid breaks down the solid samples into the acidic solution. However, by utilising a milder acid-washing method, AEMs can be leached into solution whilst leaving the sample with its structural integrity intact.

The removal of calcium, sodium and potassium has been explored using a variety of acids including hydrochloric acid (346, 347), sulphuric acid (347-351), nitric acid (346, 347, 349, 352), and acetic acid (347-349, 352). However, hydrochloric acid was found to be the best at extracting calcium with a minimal impact on the structure of the sample (353, 354).

For this work, atomic absorption spectroscopy was used to determine the calcium (Ca), potassium (K), sodium (Na), magnesium (Mg), aluminium (Al) and iron (Fe) content in the feedstocks. All feedstocks were digested in 10 wt% nitric acid solution. The solution was then analysed by flame atomic absorption spectroscopy (Model: 240FS AA, Agilent, CA, US). Error values were calculated by standard deviation. The balance used for this analysis had an error of  $\pm 0.005$  g.

### 3.7 Thermal analysis

In this section, the two methods of thermal analysis used in this work has been presented. Derivative thermogravimetry (DTG) was used in Chapter 4 and Chapter 5, to explore how treatment of the samples (either mild acid-washing or solvent extraction) affected its thermal degradation.

Pyrolysis-Gas Chromatography/Mass Spectrometry (py-GC/MS) was used in Chapter 4, Chapter 5 and Chapter 6. This method was utilised to explore and analyse the change in fast pyrolysis products of the samples described previously.

#### 3.7.1 Derivative Thermogravimetry

The thermal behaviour of the feedstocks was studied by thermogravimetry (TGA/DTG, Mettler Toledo GmbH, Greifensee, Switzerland). In derivative thermogravimetry (DTG), a prepared sample (of around 10 mg) is positioned on a thermogravimetric balance within the equipment. As the sample is heated, according to the heating programme, the equipment measures the mass (either continuously, or at set points) (355).

Derivative thermogravimetry, in contrast to thermogravimetry analysis (TGA), can provide the precise decomposition temperature of a sample at each stage of the heating programme (Figure 3-6) (356). Here, the derivative refers to the derivatisation of the mass loss (taken from the TGA) against time.

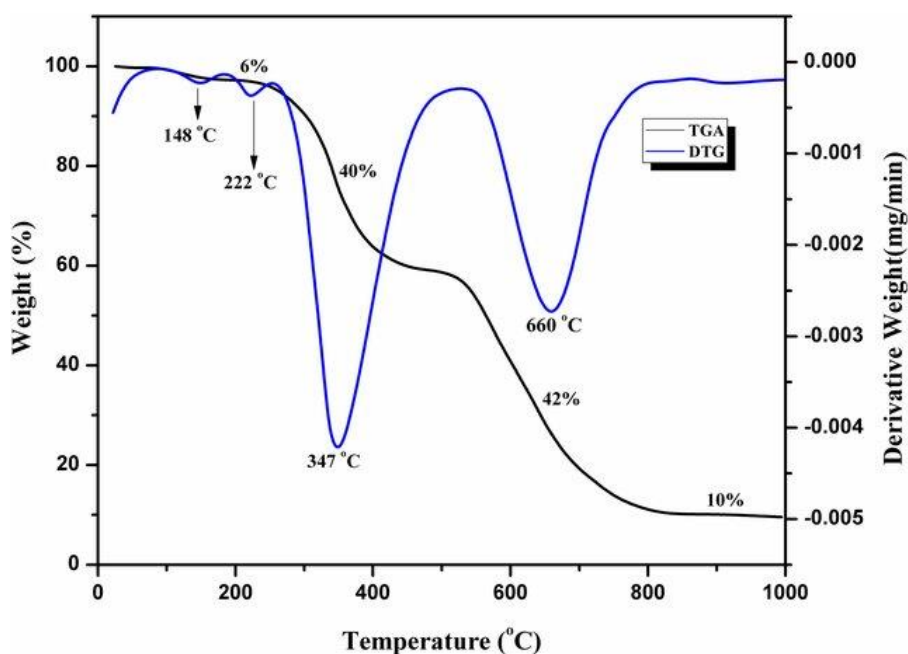


**Figure 3-6** – Example of a thermogravimetric analysis (TGA) curve, overlaid with a derivative thermogravimetric (DTG) curve. Sourced from (357).

For lignocellulosic biomass, the thermal degradation of the key three components (cellulose, hemicellulose, and lignin) can be subdivided into three phases. Where the mass loss is greatest, shown as a peak in Figure 3-6, is normally within the temperature range at which the component degrades. The most mass loss during DTG occurs during the devolatilization phase, between 180-420 °C. As discussed earlier, in Section 2.2, this temperature range is where cellulose and hemicellulose degrades. Lignin also degrades here but continues to degrade up to 1000 °C (Figure 3-7). The specific temperature at which the peaks occur, for each lignocellulosic component, varies depending on the sample, the heating programme (which includes heating rate, gas flow rate, gas, and sample mass) (358), and the presence and concentration of metallic elements (358).

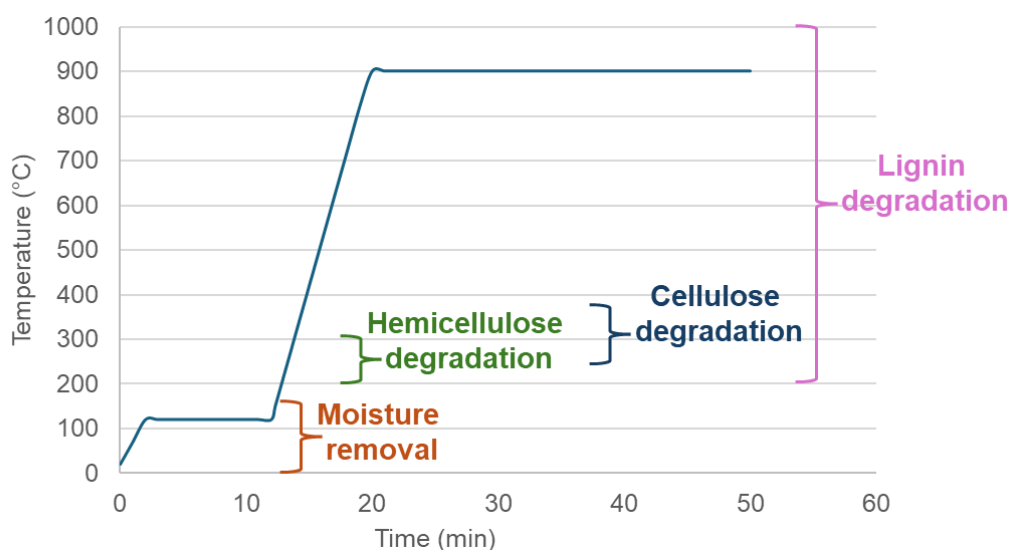


**Figure 3-7** – TGA/DTG heating programme used in this work, with illustrations of lignocellulosic components degradation temperature ranges.

The experiments were carried out under a nitrogen atmosphere at a flow rate of 50 ml/min, a temperature range of 25 – 900 °C and a heating rate of 25 °C/min in ceramic crucibles. The balance used for this analysis had an error of  $\pm 0.005$  mg.

### 3.7.2 Pyrolysis-Gas Chromatography/Mass Spectrometry

Fast pyrolysis coupled with Gas Chromatography/Mass Spectrometry (py-GC/MS) was performed to identify and semi-quantify the volatile pyrolysis products from the different feedstocks.

Fast pyrolysis involves the rapid heating of biomass in the absence of oxygen to decompose its polymeric fractions (359).

There are several types of lab-scale pyrolysis reactors commonly used for fast pyrolysis, namely fluidised-bed, fixed-bed, ablative, rotary kiln, and screw or auger reactors (360). However, in this work, fast pyrolysis was only able to be done at analytical scale (361), with a filament micro-pyrolyser .

In a filament pyrolyser, the sample is loaded into a pre-heated reaction zone (typically between 200 – 300 °C), before both are heated to the desired temperature simultaneously. The yellow zone in Figure 3-8 (the pyrolysis chamber) is pre-heated to prevent less-volatile pyrolysis products from condensing.

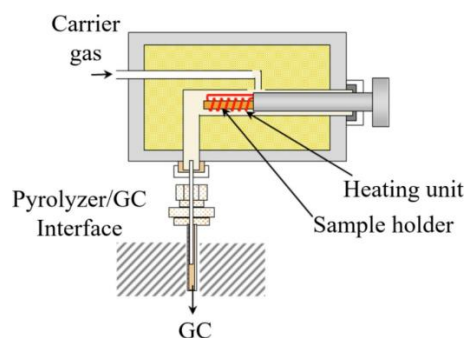


**Figure 3-8** – Diagram of a platinum-coil pyrolyser. Sourced from (361).

The shape of the filament is commonly either a coil or a ribbon. The decision over filament shape is dependent on the sample's physical state.

For purely solid samples, the sample is loaded into a quartz tube or boat into the middle of the coil filament. One issue with using the quartz tube or boat to house the sample is that the sample and filament are not directly in contact. Therefore, the set temperature for the fast pyrolysis may not be the actual temperature experienced by the sample (361).

If a sample can be dissolved in a volatile solvent, it is generally pyrolyzed with the ribbon filament. Here, the sample is spread on the surface of the ribbon filament (361).

The ideal filament material has high electrical resistance and a wide range of operating temperatures (362). Therefore, the materials used tend to be nickel, nichrome and platinum (363). From these materials, platinum has the greatest resistance and operating range (up to 1400 °C), so is employed more frequently. In this work, a platinum coil Pyroprobe was used.

The conditions of the py-GC/MS can be seen in Table 3-3 and Table 3-4. The balance used for this method had an error of  $\pm 0.005$  mg.

**Table 3-3** – Equipment and conditions used for the pyrolyser to perform pyrolysis-gas chromatography/mass spectrometry.

<b>Instrument</b>	<b>CDS Pyroprobe 5200 (Analytix Ltd, UK)</b>
<b>Pyrolysis Conditions</b>	20 °C/ms to 450/550/650 °C, hold for 20 s
<b>Pyrolysis Atmosphere</b>	Helium
<b>Transfer Line Temperature</b>	300 °C
<b>Valve Oven Temperature</b>	300 °C

**Table 3-4** – Equipment and conditions used for the GC/MS to perform pyrolysis-gas chromatography/mass spectrometry.

<b>Instruments</b>	<b>GCMS-QP2010SE (Shimadzu Corp, Japan)</b>
<b>Injector</b>	Split/Splitless, 300 °C
<b>Carrier Gas</b>	Helium, 25 ml/min, split ratio 20
<b>Column</b>	DB1701, 60m x 0.25mm x 0.25 um
<b>Column Temperature Program</b>	40 °C for 2 min, 6 °C/min ramp to 280 °C, hold for 10 min
<b>Transfer Line Temperature</b>	300 °C
<b>Scan Range</b>	50 – 600 amu
<b>Source Temperature</b>	260 °C

### 3.8 Thermal conversion

In this work, two forms of pyrolysis at vastly different scales were employed to generate thermally converted samples for further analysis. Fast pyrolysis was performed on a microgram analytical scale pyrolysis-Gas Chromatography/Mass Spectrometry unit, whilst slow pyrolysis was performed using 10-30g of sample to generate biochar for use in Chapter 7.

#### 3.8.1 Slow pyrolysis

Slow pyrolysis is a thermal process which favours the yield of the solid chars. The characteristics of the char produced by slow pyrolysis is dependent on the sample, its particle size, residence time, heating rate and process temperature (364).

The char yield is predominantly dependent on the final process temperature, with the yield decreasing as the temperature rises (365). The greatest factor which affects the char yield is the structure of cellulose and hemicellulose. Above 400 °C (the temperature at which cellulose and hemicellulose's thermal degradation has completed), the char yield reduces slowly (366). Between 400 - 600 °C, the char has lower levels of oxygen and hydrogen, whilst the degree of carbonisation increases (367).

Due to the low heating rate and relatively long residence time that is necessary, slow pyrolysis is mostly carried out in batch reactors, namely kiln or retort reactors (315). Continuous slow pyrolysis reactors have been investigated in the literature, mostly in retort reactors, but are not well-established (368-370).

Although both types of reactors are utilised for char production (371), the oil and gas phases can be recovered in retorts, but not in kilns. Kilns only have an air inlet, and oil and gas outlet, with the sample being enclosed within the brick, clay and metal vessel (Figure 3-9) (372).

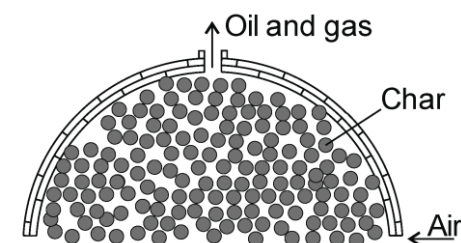


**Figure 3-9** – Diagram of char production using a kiln reactor. Sourced from (315).

A batch retort reactor can be operated in a horizontal or vertical mode. In laboratory scale studies, fixed bed reactors are commonly used. The sample is loaded into the

reactor, with the reactor being closed and heated to the necessary temperature. An inert gas is swept through the reactor throughout the process, to both ensure an oxygen-free atmosphere (to prevent combustion), and to remove the oil and gas-phase products from the main reaction region (Figure 3-10).

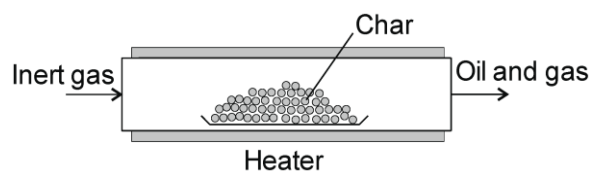


**Figure 3-10** – Fixed bed reactor for batch processes. Sourced from (315).

In this study, slow pyrolysis was performed at the University of Leeds in a vertical mode fixed-bed batch reactor at laboratory-scale (with a 1.2 kW sealed tube furnace of 95 mm internal diameter (ID) x 820 mm by length surrounding the sample) as shown in Figure 3-11. Depending on feedstock density, between 25 – 150g of sample was added to fill approximately 70 vol% of a stainless-steel tube. This tube was then placed inside a metal mesh basket (82 mm ID).

The feedstocks that were pyrolysed were tree bark samples: Douglas fir (DF), lawson cypress (LC), larch (L), European silver fir (ESF), noble fir (NF), norway spruce (NS) and nootka cypress (NC).

The feedstocks were pyrolysed at 450 °C and held for 1 hour. A nitrogen flow of 50 ml/min (to create an inert atmosphere) was maintained for 10 min prior to the heater being turned on and until the sample had been cooled to under 200 °C. The heating rate of the unit was approximately 10 °C. After this period, the heater was turned off and allowed to cool until the thermocouple recorded that the sample was below 50 °C. The long cooling time (approximately 0.14 °C/min) was due to the self-heating nature of bark (373).

The sample was weighed prior to being pyrolysed. After being cooled to under 50 °C, the char was weighed (with an associated balance error of  $\pm 0.005$  g), and then stored in airtight containers. Between sample runs, when the biomass basket was removed from the tube furnace, the sample holder was physically cleaned. The holder was not cleaned with chemicals, so as to not introduce any potential contaminants that would react with the sample during the pyrolysis of the next run.

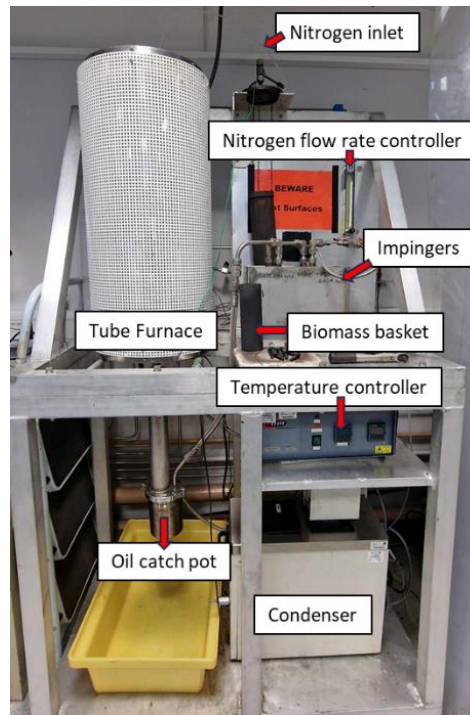


**Figure 3-11** - Fixed-bed slow pyrolysis reactor used for production of biochar.

## 3.9 Extractions

Across the four results chapters, a variety of methods were employed to extract different components from untreated biomass. A mild acid wash was performed to remove the metals content of several of the samples characterised in Chapter 4, whilst solvent extraction was performed to remove lipids from tree barks characterised in Chapter 5.

### 3.9.1 Mild acid wash

The samples with the highest metal contents from the Atomic Absorption Spectroscopy underwent a mild acid-washing with 2M HCl, according to the Nowakowski and Jones method (353). The balance used for this analysis had an error of  $\pm 0.005$  g.

### 3.9.2 Soxhlet solvent extraction

Soxhlet extraction was performed on the tree bark samples to extract lipids. Dependent on the density of the sample, between 3 – 7g were added to a cellulose thimble (25x80mm) up to 70 vol%. The solvent, ethanol, was added in excess ( $\approx 225$  ml) to a 250 ml round-bottomed flask (RBF) along with anti-bumping granules. The volume of solvent was chosen to be enough to cover the cellulose thimble during the extraction process, with over a third of the RBF still containing solvent solution.

After the cellulose thimble and RBF containing solvent were inserted into the Soxhlet equipment, the water for the cooling system was turned on. The heater was then set to approximately 78 °C (the boiling point of ethanol) as to start the evaporation of the solvent from the RBF. The purpose of the anti-bumping granules in the RBF were to ensure more consistent evaporation. The cooling water causes the evaporated solvent to condense into the section with the cellulose thimble for the extraction to occur.

As the extraction progresses, the extracted lipids turn the solvent solution from clear transparent to a darker colour. The extraction had finished when the solvent solution held around the cellulose thimble returns to clear transparency, whilst the RBF contains a dark solution.

After extraction, the heater is turned off and the RBF is left to cool. The RBF and cellulose thimble and then removed from the Soxhlet equipment. The solution in the RBF was then evaporated using the Rocket Evaporator (Section 3.9.4) until a 2 ml vial remained for GC/MS analysis. A sample of the concentrated solution (30  $\mu$ l) was added to a quartz tube and pyrolysed in the py-GC/MS according to the method outlined in Section 3.7.2. This was done in case any extracted compounds had molecular weights higher than the detector after liquid-injection.

The cellulose thimble was moved into a glass vial and left exposed in a fume cupboard for the solvent to evaporate. After 7 days, the thimble was weighed to estimate the mass loss due to extraction. The contents of the thimble were transferred to an airtight container for further analysis. Error values of mass loss were calculated by standard deviation. The balance used for this method had an error of  $\pm 0.005$  g.

### 3.9.3 Accelerated Solvent Extraction

The accelerated solvent extraction was performed on a Dionex™ ASE™ 350 Accelerated Solvent Extractor, Thermo Scientific™, USA. Samples (between 0.5 – 2.0 g) were mixed with an amount of calcined silicone dioxide up to 9 ml. The silicon dioxide acted as a drying agent and dispersant to ensure contact with the solvent and prevent compaction of the sample.

A cellulose filter was inserted into the bottom of a stainless-steel cell (10 mL), with the sample/sand mix then being added. Sand was then added to the cell up until 1 ml of headspace remained. The method used by the ASE (Table 3-5) is taken from Yang and Lopez' Application Note (374) for the extraction of unbound fats. The extracted material and solvent were washed into a collection vial, with the excess solvent to be evaporated via Rocket Evaporator.

**Table 3-5** – Accelerated Solvent Extraction conditions for the extraction of fats.

	<b>Method</b>
<b>Solvent: Hexane/Isopropanol (v/v)</b>	3:2
<b>Extraction Cell Material</b>	Stainless Steel
<b>Extraction Cell Size (mL)</b>	10
<b>Temperature (°C)</b>	125
<b>Static Extraction Time (min)</b>	15
<b>Number of Static Cycles</b>	1
<b>Purge Volume (%)</b>	100
<b>Purge Time (sec)</b>	100
<b>Total Extraction Time per Sample (min)</b>	24
<b>Total Solvent Volume per Sample (mL)</b>	25

### **3.9.4 Rocket Evaporator**

The Rocket Evaporator (Genevac Ltd, Suffolk, UK) was used for the evaporation of excess solvent after both Accelerated Solvent Extraction and Soxhlet Extraction. However, the evaporation program differed due to the different solvents used. The solvent and extracted material were placed into the equipment in a flip-flop vial, which allowed the solution to be distilled into a 2 ml GC/MS vial for analysis.

For the post-ASE solutions, the flip-flop vials were rinsed with isopropanol before the evaporation had finished to render it as the sole solvent. This was done to simplify the GC/MS chromatograms. The flip-flop vials for the post-Soxhlet solutions were rinsed with ethanol to wash any extracted material retained on the walls of the vial. The liquid solutions were analysed by GC/MS using the conditions in Table 3-6.

### 3.10 Liquid Injection Gas Chromatography/Mass Spectrometry

The post-solvent extraction solutions for the tree barks in Chapter 5 underwent liquid injection gas chromatography/mass spectrometry (liq-injection GC/MS), according to the instrument and conditions in Table 3-6.

**Table 3-6** – Equipment and conditions used to perform liquid-injection gas chromatography/mass spectrometry.

<b>Instruments</b>	GCMS-QP2010SE Shimadzu
<b>Injector</b>	Split/Splitless, 250 °C
<b>Carrier Gas</b>	Helium, 25 ml/min, split ratio 20
<b>Column</b>	DB1701, 60m x 0.25mm x 0.25 µm
<b>Column Temperature Program</b>	117 °C for 1.4 mins, 3 °C/min ramp to 280 °C, hold for 2.27 mins
<b>Scan Range</b>	50 – 600 amu
<b>Source Temperature</b>	260

In contrast to the py-GC/MS system, which has a heated transfer line to carry the resultant gases, the liq-injection GC/MS uses a split/splitless injector (Figure 3-12) to pass the sample solutions onto the column. As the samples that were analysed using liq-injection GC/MS were post-solvent extraction solutions, it was imperative that no solid particles were present in the sample vials. If solid particles were present, due to the thin size of the injector, the injector would likely be blocked and need to be replaced. This was rectified by filtering each sample solution through 0.45 µm filters.

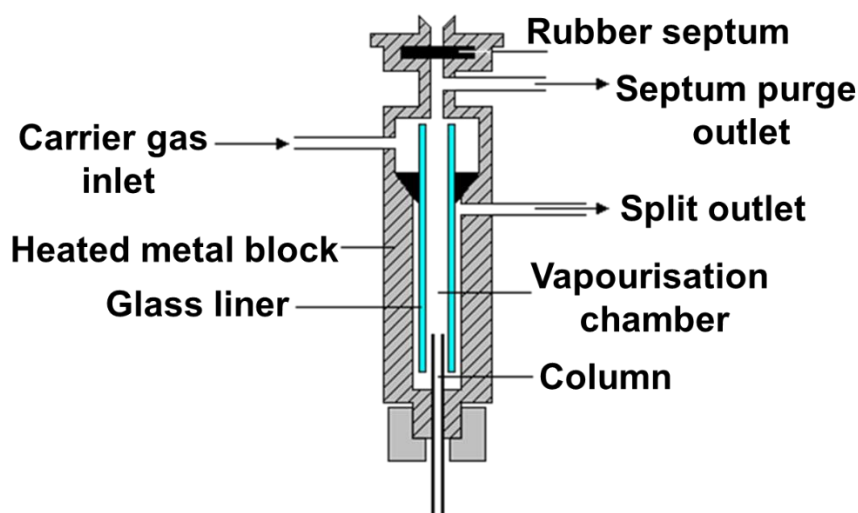


**Figure 3-12** – Diagram of the split/splitless injector commonly used in liquid-injection GC/MS. Adapted from (375).

The data from the GC-MS produces a chromatogram plotting the retention time against the response (commonly the absolute intensity) (Figure 3-13).

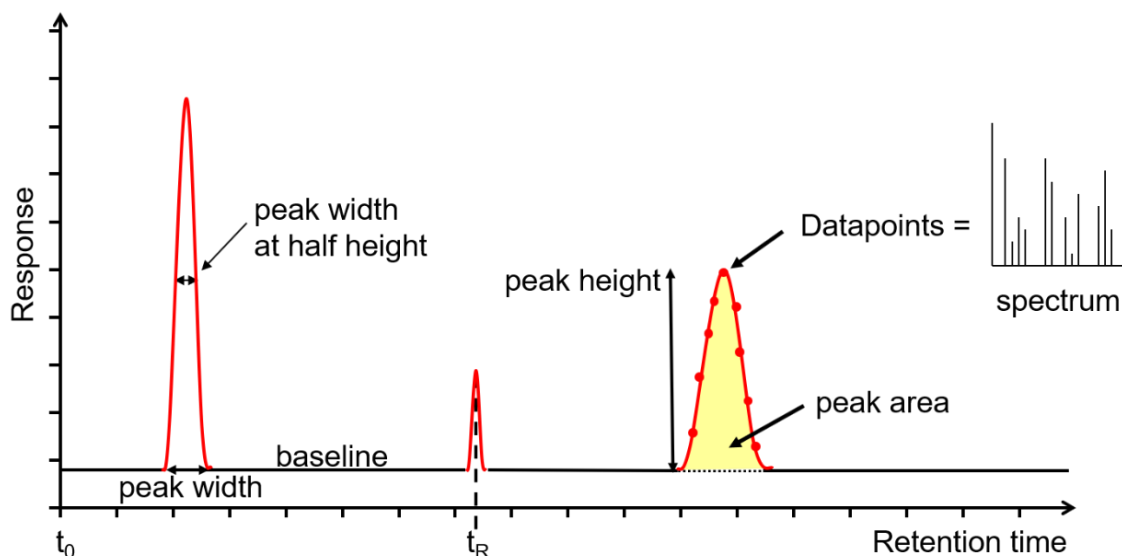


**Figure 3-13** – Chromatogram output from a GC or GC/MS. Sourced from (376).

In a typical chromatogram, there may be over a hundred different identified compounds. However, for ease of analysis in this work, the 25 peaks with the highest areas were chosen to be assessed further. Generally, the top 25 peaks accounted for around 93 % of the total peak area. With the treated samples (acid-washed and solvent-extracted), the top 25 peaks accounted for around 80 % due to the wider variety of compounds that were generated. The total peak area of all identified compounds were equivalent to 100%. Therefore, the areas of the top 25 peaks must be normalised to account for the loss of the peak area from the disregarded compounds.

For the normalised peak area, the most common method is to divide the area of each individual peak ( $PA_i$ ) by the total sum of the top 25 peak areas (Equation 3-9). In Equation 3-9, PA refers to 'peak area'.

**Equation 3-9** – Calculation for the normalisation of gas chromatography peak areas.

$$PA_{norm} = \frac{PA_i}{PA_{total}}$$

Then, this value is multiplied by 100 so that each identified compound can be expressed by their percentage contribution to the total area (377).

### 3.11 Solvent Hazardousness Assessment

In the chapter regarding bio-based solvents (Chapter 6), the guidelines from CHEM21 were imposed. These consider the safety, health and environmental impact of compounds, and requires the collation of their Safety Data Sheets (SDS).

CHEM21 contains certain criteria under the categories of safety, health and environment, where the maximum score for each category was 10. These criteria can be seen in Table 3-7, Table 3-8 and Table 3-9 (378). In each category, the greatest value is considered to be the 'score'.

Regarding the safety criteria (Table 3-7), this considers the flash point and the flammability of the chemicals (H2xx hazard statements). The safest chemicals are those with flash points above 60 °C, and non-flammable. Additional points (1 each) are added to the safety scores for a variety of reasons: the auto-ignition temperature is below 200 °C, resistivity is above 10<sup>8</sup> Ωm, and the chemical has the ability of form peroxides (the EUH019 hazard statement). However, resistivity was unable to be found for any of the chemicals, so this was not considered in the overall score. In the case of a chemical having high decomposition energies (> 500 Jg<sup>-1</sup>), these are automatically given a score of 10.

**Table 3-7 – CHEM21 Safety Criteria.**

<b>Base Safety Score</b>	<b>1</b>	<b>3</b>	<b>4</b>	<b>5</b>	<b>7</b>
<b>Flash Point (°C)</b>	>60	24 to 60	23 to 0	-1 to -20	< -20
<b>GHS (H2xx)</b>	-	H226	H225 or H224	-	-

The health category (Table 3-8) considers the H3xx hazard statements. These give a score to chemicals which may be carcinogenic, mutagenic, reprotoxic, irritants, and/or feature single target organ toxicity. An additional point is also given to the health score if the boiling point of the chemical was below 85 °C. For chemicals where toxicological data is not available, H3xx statements are not assigned. In these cases, a health score of 5 is attributed. This is done to ensure that there is not a bias towards solvents without the necessary toxicological data (378).

**Table 3-8 – CHEM21 Health Criteria.** CMR = carcinogen, mutagen or reprotoxic. STOT = single target organ toxicity.

Health Score	2	4	6	7	9
<b>CMR</b>	-	-	H341, H351, H361	-	H340, H350, H360
<b>STOT</b>	H304, H371, H373	H334	H370, H372	-	-
<b>Acute Toxicity</b>	H302, H312, H332, H336, EUH070	-	H301, H311, H331	-	H300, H310, H330
<b>Irritation</b>	H315, H317, H319, H335, EUH066	H318	-	H314	-

For the environmental scores (Table 3-9), the REACH registrations, boiling point, and H4xx hazard statements of each chemical were considered. The H4xx hazard statements relate to the chemical's toxicity to aquatic life (379).

**Table 3-9 – CHEM21 Environment Criteria.** If chemical has H420, the score = 10. E.g. water: score = 1.

Environment Score	3	5	7
<b>Boiling Point (°C)</b>	70 to 139	50 to 69	< 50
	-	140 to 200	>200
<b>GHS</b>	No H4xx after full REACH registration	H412, H413	H400, H410, H411
<b>Other</b>	-	No, or partial REACH registration	-

Once the CHEM21 criteria were imposed, the scores were categorised into Recommended, Problematic or Hazardous. With a maximum score of 10, a score between 1-3 would show a Recommended solvent, 4-6 for a Problematic solvent and 7 and above for a Hazardous solvent.

## 3.12 Ammonia adsorption

### 3.12.1 Set-up of the experiments

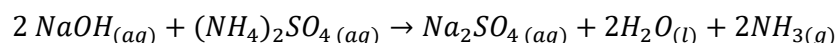
The adsorption capacity of ammonia onto a variety of samples was tested in a batch set-up (Figure 3-14). The samples that were tested included raw tree barks, solvent-extracted tree barks, commercial lignin products, tree bark biochars, activated carbons, and other biomass residues. In this method, an excess of sodium hydroxide (NaOH) is added to a Duran bottle (250 ml). Following this, a sample (approximately 0.3 g) was placed in a black lid then placed inside a bottle so that it would float. Prior to adsorption method, a variety of small caps were tested to see if they would float on water. Due to the small neck diameter of the Duran bottles, tweezers were used to gently lower and remove the sample-filled lids from the bottles.



**Figure 3-14** - Batch set-up of ammonia adsorption tests.

The Duran bottle was then fitted tightly with a septum to achieve a closed atmosphere. With a syringe, a known concentration of ammonium sulphate solution,  $(\text{NH}_4)_2\text{SO}_4$  was injected into the bottle. The reaction between the sodium hydroxide and ammonium sulphate produces gaseous ammonia as follows:

**Equation 3-10** - Chemical reaction of ammonia gas production for ammonia adsorption tests.



The ammonia sorption tests were run at three different concentrations of reagents (Table 3-10), so that a known amount of gaseous  $\text{NH}_3$  was produced. After 7 days, an excess volume of sulphuric acid was injected into the Duran bottles to end the reaction. Although the reaction would take approximately 2 hours to stop, the lids containing the samples were removed the following day. The samples were then analysed by

elemental analysis to yield the nitrogen values before and after the adsorption testing. For the first batch of ammonia adsorption testing, the ammonium concentration of the solution was tested with the LCK503 HACH kit (for concentrations between 10-100 mg/L NH<sub>4</sub>-N and 13-130 mg/L NH<sub>4</sub>). However, no differences were found between the ammonium concentrations of each sample's solutions, so this was stopped for the following batches.

The conditions of the three ammonia concentrations can be found in Table 3-10. Error values were calculated by 1x standard deviation using four datapoints (the adsorption was performed in duplicate, and the elemental analysis for each duplicate was again run twice). The balance used for this method had an error of ±0.005 mg.

**Table 3-10 – Ammonia sorption capacity testing conditions.**

<b>Experiment</b>	<b>1</b>	<b>2</b>	<b>3</b>
<b>NaOH concentration and volume</b>	0.1M, 60ml	1 M, 60ml	3 M, 60ml
<b>Ammonium sulphate concentration and volume</b>	0.05M, 25ml	0.5 M, 25ml	1.76M, 25ml
<b>Theoretical gaseous ammonia produced</b>	43 mg	430 mg	1500 mg
<b>Sulphuric acid concentration and volume</b>	0.05 M, 30ml	0.5 M, 30ml	1.76 M, 30 ml

### 3.12.2 Calculation of ammonia adsorption capacity in the fresh adsorbents

The nitrogen content measured by elemental analysis recorded the N in a 'spent adsorbent', necessitating the conversion to a 'fresh adsorbent' basis ( $\frac{m_{NH_3}}{m_f}$ ). The mass of the spent adsorbent ( $m_s$ ) was assumed to be the sum of the fresh adsorbent ( $m_f$ ) and the adsorbed  $NH_3$  ( $m_{NH_3}$ ) from the experiment (Equation 3-11), where  $W_{NH_3}$  and  $W_N$  are the molar masses of  $NH_3$  ( $17.04 \text{ gmol}^{-1}$ ) and N ( $14.01 \text{ gmol}^{-1}$ ) respectively. Here,  $\gamma$  is the ratio between these two molar masses.

**Equation 3-11** - Sum of spent adsorbent mass ( $m_s$ ), as a function of fresh ( $m_f$ ) and adsorbent nitrogen ( $m_N$ )

$$m_s = m_f + m_{NH_3} = m_f + \frac{W_{NH_3}}{W_N} m_N = m_f + \gamma m_N$$

The nitrogen values of the adsorbents could therefore be calculated according to Equation 3-12 and Equation 3-13, where  $m_{Nf}$  is the mass of N in the fresh adsorbent.

**Equation 3-12** - Calculation of the nitrogen content (wt%) for spent adsorbent.

$$\%N_s = \frac{m_{Nf} + m_N}{m_s} \times 100 = \frac{m_{Nf} + m_N}{m_f + \gamma m_N} \times 100 \therefore \frac{\%N_s}{100} \times (m_f + \gamma m_N) = m_{Nf} + m_N$$

**Equation 3-13** - Calculation of the nitrogen content (wt%) in the fresh adsorbent, defined as  $\%N_f$ .

$$\%N_f = \frac{m_{Nf}}{m_f} \times 100$$

By dividing all terms in Equation 3-12 by  $m_f$ , it was re-organised into Equation 3-14.

**Equation 3-14** - Substitution and re-organisation of spent adsorbent nitrogen content (wt%).

$$\text{Where } \alpha = \frac{m_N}{m_f},$$

$$\frac{\%N_s}{100} \times (1 + \gamma\alpha) = \frac{\%N_s}{100} + \gamma\alpha \frac{\%N_s}{100} = \frac{m_{Nf}}{m_f} + \alpha = \frac{\%N_f}{100} + \alpha$$

Following this,  $\frac{m_{Nf}}{m_f}$  in Equation 3-13 was substituted according to Equation 3-14, yielding Equation 3-15.

**Equation 3-15** - Calculation for the grams of nitrogen per gram of fresh adsorbent.

$$\frac{\%N_s}{100} + \gamma\alpha \frac{\%N_s}{100} = \frac{\%N_f}{100} + \alpha \quad \therefore \quad \alpha = \frac{\%N_s - \%N_f}{100 - \gamma\%N_s}$$

**Equation 3-16** – Conversion of  $\alpha$  from gN/g fresh adsorbent to mgNH<sub>3</sub>/g fresh adsorbent.

$$\text{Adsorption capacity of NH}_3 \text{ on fresh adsorbent (mg}_{\text{NH}_3}\text{/g}_{\text{ads}}) = 1000 \times \gamma\alpha$$

### 3.12.3 Comparison of adsorption capacity to literature data

After determining the adsorption capacities of the prospective adsorbents, the next step was to compare the capacities from this work to studies found in the literature. To do this, the adsorption capacities from the literature to this work must be compared under the same conditions, in particular the partial pressure of ammonia ( $P_{\text{NH}_3}$ ) and the adsorption temperature ( $T_{\text{ads}}$ ).

The literature usually presents the equilibrium adsorption capacities in the graphical form of adsorption isotherms (adsorption capacity versus pressure) in the adsorption temperature range typically between 15 °C to 50 °C and pressures of the adsorbate from 10 mbar (vacuum) to several hundreds/thousands of kPa. A typical example of adsorption isotherm is provided below for ammonia adsorption on  $\gamma$ -alumina from Helminen et al (380).

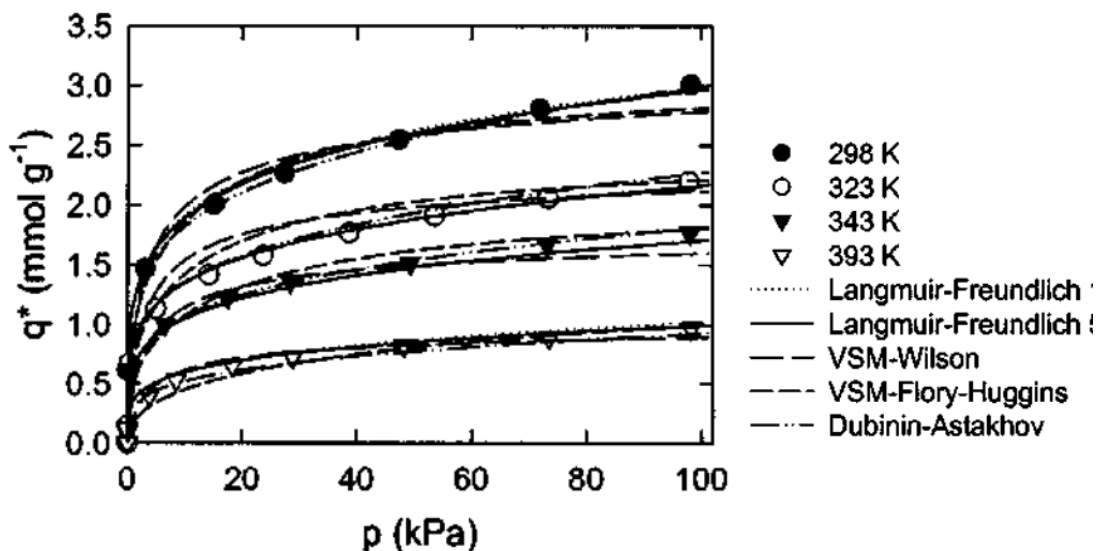


**Figure 3-15** - The graphical representation of Helminen et al's (380) ammonia adsorption data for alumina.

It can be seen (from Figure 3-15) that most of the experimental points are obtained for the higher partial pressures of the adsorbate ammonia (> 5 kPa), with only a few points at lower resolutions for partial pressure below 5 kPa. This is a common occurrence in isotherm data from the literature.

Therefore, in order to provided a comparison with the literature regarding ammonia adsorption capacities of common adsorbents at low partial pressures of  $\text{NH}_3$  (such as those in this study's experiments), accurate modelling of the equilibrium isotherms from the literature was required.

There are several different models of adsorption equilibrium, and varying sources of literatures uses different sets of equilibrium adsorption models. In Helminen et al (380), the Dubinin-Astakhov (D-A) model was used successfully (for example with the high  $R^2$  value shown in Table 3-11) on ammonia adsorption isotherms at 298, 323, 343 and 393 K for five different adsorbents ( $\gamma$ - $Al_2O_3$ ,  $SiO_2$ , activated carbon and two zeolites). In this thesis, the D-A model, with equation parameters derived by Helminen et al (380), were used to calculate the adsorption capacities of Helminen et al 's adsorbents at the adsorption temperature and partial pressures of ammonia from this study.

### 3.12.3.1 The Dubinin-Astakhov adsorption equilibrium model

The generation of an adsorption isotherm requires the fitting of several datapoints, and the identification of three isotherm parameters:  $W_0$  (the limiting pore volume of the adsorber bed material,  $cm^3g_{ads}^{-1}$ ),  $E$  (the characteristic energy of the adsorbent-adsorbate system,  $J/mol$ ), and  $n$  (the heterogeneity parameter, unitless). The fitting of the Dubinin-Astakhov adsorption equilibrium model, and the conversion of ammonia adsorption capacity values from the literature to the conditions in this study were performed using Microsoft Excel.

Helminen et al (380) had previously fitted an isotherm around their ammonia adsorption data, and had generated excellent fits ( $R^2 > 99.7$ , as shown in Table 3-11 for the alumina adsorbent).

**Table 3-11** – An example of the data presented by Helminen et al (380) for the generation of the Dubinin-Astakhov adsorption equilibrium model. This data are the isotherm parameters for the alumina sorbent.

Isotherm Model	Isotherm Parameters	$R^2$ (%)	Total SS	RSS	Standard Error of Estimate
Dubinin-Astakhov	$W_0 = 0.159 \pm 0.012 \text{ cm}^3\text{g}^{-1}$	99.78	24	0.05	0.042
	$E = 10.0 \pm 0.9 \text{ kJmol}^{-1}$				
	$n = 0.844 \pm 0.055$				

In the Dubinin-Astakhov model, it is assumed that the adsorbent houses the vapour adsorbate in a state similar to saturated liquid according to the Polanyi sorption potential theory (381).

The vapour pressure of the sorbate ( $P_0$ ) can be calculated through the use of the Antoine's Equation (Equation 3-17), where the equilibrium temperature ( $T_{eq}$ ) is in Kelvin, and A, B, and C are component-specific Antoine constants. The constants and the format of Antoine's equation are obtained from the NIST chemistry webbook (382). The values for A, B and C for ammonia can be seen in Table 3-12.

**Equation 3-17** – Antoine’s equation to calculate the vapour pressure of a sorbate, as a function of equilibrium temperature.

$$P_0 = 10^{\left(A - \frac{B}{T_{eq} + C}\right)}$$

**Table 3-12** – Antoine equation component-specific constants for ammonia (382).

Temperature (K)	A	B	C	Reference
164.0 – 239.6	3.18757	506.713	-80.78	(383)
239.6 – 371.5	4.86886	1113.928	-10.409	(383)

The adsorption capacity of a sample can be estimated, at a particular adsorption temperature ( $T_{ads}$ , K) and ammonia partial pressure ( $P$ , kPa), according to the Dubinin-Astakhov isotherm equations (Equation 3-18 and Equation 3-19) (384).

**Equation 3-18** - Dubinin-Astakhov isotherm equations for calculating adsorption capacity.

$$q = q_0 \times e^{\left[-\left(\frac{D}{E}\right)^n\right]}$$

$$D = RT_{ads} \ln \left(\frac{P_0}{P}\right)$$

$$q_0 = \rho W_0$$

**Equation 3-19** - The ideal gas law.

$$P_i(\text{Pa}) \times V(\text{ml}) = N_i(\text{mol}) \times R \times T(\text{K})$$

In Equation 3-18, ‘q’ is the adsorption capacity ( $g_{\text{adsorbate}}/g_{\text{adsorbent}}$ ), where the ‘adsorbate’ is  $\text{NH}_3$  and the adsorbent are the solids that have been tested. ‘ $q_0$ ’ is the limiting adsorption capacity ( $g_{\text{adsorbate}}/g_{\text{adsorbent}}$ ), ‘D’ is the Polanyi adsorption potential (J/mol), ‘E’ is the characteristic energy of the adsorbent-adsorbate system (J/mol), and ‘n’ is the heterogeneity parameter (or pore dimensions, no units). ‘R’ is the universal gas constant ( $8.314 \text{ J mol}^{-1}\text{K}^{-1}$ ), and  $P_i$  is the partial pressure when using the ideal gas law (Equation 3-19).  $T_{ads}$  is the adsorption temperature and  $P_0$  is the vapour pressure of the sorbate at the defined adsorption temperature (also known as  $T_{eq}$  and  $P_0$  in Antoine’s equation (Equation 3-17). Finally, in Equation 3-18, ‘P’ is the partial pressure of volatile organic compounds (VOC) upstream of the adsorber bed (Pa), ‘ $W_0$ ’ is the limiting pore volume of the adsorber bed material ( $\text{cm}^3 g_{\text{ads}}^{-1}$ ), and ‘ $\rho$ ’ is the condensed adsorbate density ( $\text{g cm}^{-3}$ ).

The condensed adsorbate density of the ammonia was determined with data by Haar and Gallagher (385) (Table 3-13 and Figure 3-16). This was calculated by the trendline in Figure 3-16 to be Equation 3-20.

**Table 3-13** – Thermodynamics data of ammonia, taken from Haar and Gallagher (385).

P (bar)	Specific Volume (liquid, cm <sup>3</sup> /g)	Saturated liquid density (g/cm <sup>3</sup> )	ln (P)
0.1	1.37611	0.72669	-2.30259
1	1.46636	0.68196	0.00000
10	1.65801	0.60313	2.30259
24	1.81336	0.55146	3.17805
38	1.94585	0.51391	3.63759

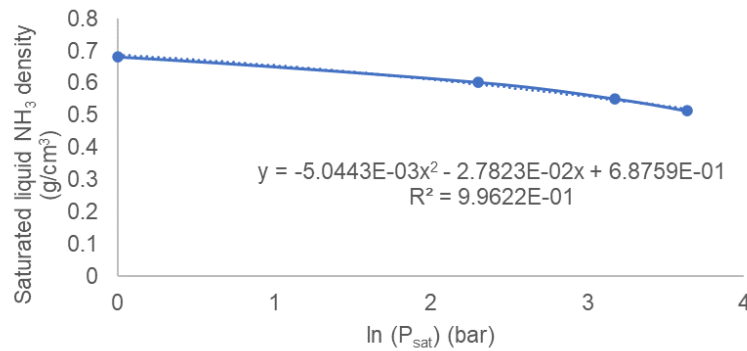


**Figure 3-16** – Change in saturated liquid density of ammonia against the natural log of the saturated pressure.

**Equation 3-20** – Calculation of the condensed adsorbate density of ammonia, where  $P_0$  is given in ‘bar’.

$$\rho_{NH_3,cond}(gcm^{-3}) = -5.0443 \times 10^{-3} \times \ln(P_0)^2 - 2.7823 \times \ln(P_0) + 0.68759$$

However, the last remaining unknown variable from Equation 3-17, Equation 3-18 and Equation 3-19 is the partial pressure of ammonia. This was calculated according to the method outlined in Section A.2.4.

### **Application of the partial pressure into the Dubinin-Astakhov equilibrium adsorption model**

Following the determination of the partial pressure, the values of A, B,C,  $P_0$ ,  $P_{NH_3}$ ,  $T_{ads}$ ,  $\rho_{NH_3,cond}$ ,  $W_0$ , E and n were fed back into Equation 3-17, Equation 3-18 and Equation 3-19 to calculate the adsorption capacity ( $q_0$ ) at the partial pressure of ammonia and adsorption temperature. This was then converted from gNH<sub>3</sub> per gram of adsorbent into mmol of NH<sub>3</sub> per gram of adsorbent so that it could be compared to Helminen et al (380)’s various common adsorbents, and that the calculated values are sensible when compared to the graphical adsorption isotherm data. Where the calculated values are consistent with Helminen et al’s trends, the values were then converted to mgNH<sub>3</sub>/g of fresh adsorbent. This allowed the values to be directly compared to the results of this study. An example of the conversion of Helminen et al’s data to the conditions in this study via the Microsoft Excel workbook can be found in the Appendix (A1.2.3).

### **3.13 Assessment of error and statistical analysis**

Throughout the laboratory work described in this chapter, each sample was performed in duplicate to ensure repeatability. In the cases where the error was greater than acceptable, a new replicate was run. Average mean values are stated together with the errors (calculated using 1x standard deviation) presented in the tables. By using 1x standard deviation, the error was presented with a 2x standard deviation range (i.e. plus 1x standard deviation, minus 1x standard deviation). This means that if another sample was run, there would only be a 5% chance that the values would fall outside of this range.

In Chapter 7, univariate and multivariate statistical analysis was conducted using SPSS Statistics 28 to analyse the effects of treatment on the samples' ammonia adsorption performances.

### **3.14 Methods limitations**

In this section, clear limitations from performing methods from across this study will be discussed.

#### **3.14.1 Atomic absorption spectroscopy**

As described in Section 3.6, prior to being analysed by the AAS, the samples must first undergo acid digestion. In some cases, where the samples are low density (coconut husk, LC and NC tree bark), greater volumes are needed to reach 0.2 g. In this method, 5 ml of nitric acid are added to the sample. With these particular samples, it was sometimes difficult to ensure that all of the sample was submerged in the nitric acid. This may have slightly impacted the AAS results. In future work, these particular samples (as well as the others) would be size reduced by cryomilling. Consequently, this would aid the sample in resembling a powder and simplify this process.

#### **3.14.2 Fibre analysis**

The equipment used to determine lignocellulosic composition in this study (Fibretherm) must be considered to be a semi-quantitative method. In the four-step gravimetric method, the reagents used are sensitive to different conditions. For example, when the temperature in the laboratory was below 15 °C, components of the NDF detergent precipitated out of solution. This was rectified by waiting for the temperature to raise again, or gently heat up the solution with warm water.

#### **3.14.3 Ammonia adsorption experiments**

Due to the neck diameter of Duran bottle used for the ammonia adsorption tests, there was a maximum lid diameter for floating the solid sample atop the solution. Therefore, with very light samples (such as nootka cypress tree bark), the full mass (0.3 g) was unable to fit inside the lid. In future work, the reagent concentrations for the very light samples should be adjusted to account for the mass of the low-density samples that can fit in the cap.

### **3.15 Concluding remarks**

All of the methods described in this chapter were verified and trained on by a professional technician for accuracy and repeatability. These methods and analytical techniques are valid approaches which have been chosen for their use in literature, in addition to the availability of equipment and resources. In the process of performing some of these techniques, more improved methods or standard operating protocols were realised. These should be employed in further work if possible.

## Chapter 4 – The screening and characterisation of lignin-rich feedstocks

### 4.1 Introduction

In this work, lignin residues from an array of sources (Table 4-1) were characterised (Figure 4-1). The methods of characterisation included proximate and ultimate analysis (Section 3.2-3.3), fibre analysis (Section 3.4), atomic absorption spectroscopy (AAS) (Section 3.6), and pyrolysis-gas chromatography/mass spectrometry (py-GC/MS) (Section 3.7.2).

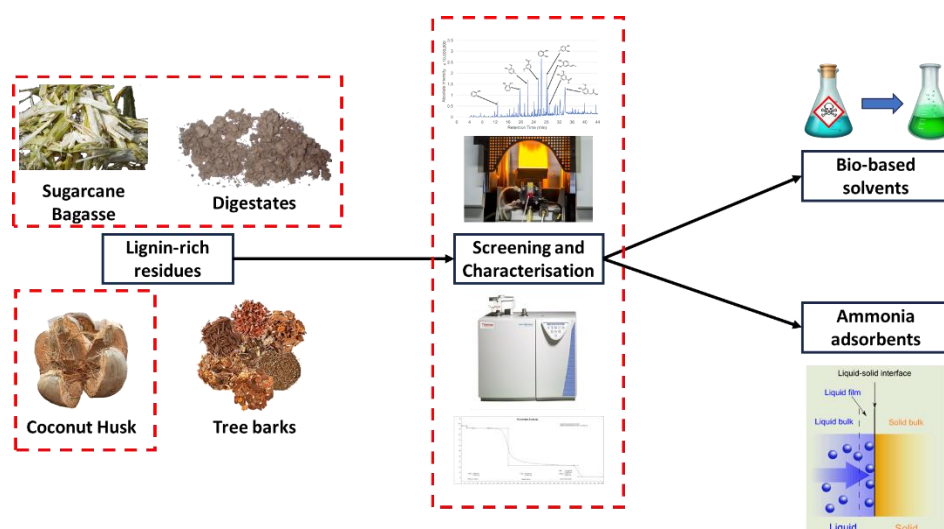


**Figure 4-1** –The overall scope of this study. The work covered in Chapter 4 is denoted by red dotted lines.

Based on the results from the AAS of several samples, a mild acid-wash was performed (Section 3.9.1), with the generated samples being further analysed by AAS, py-GC/MS, proximate and ultimate analysis and derivative thermogravimetry (DTG).

**Table 4-1** - Feedstocks analysed in this chapter.

Lignins	Digestates	Residues
Alkali lignin (AlkLig)	MSW Digestate (MSWdig)	Coconut husk (CH)
Lignoboost (LB)	VGF Digestate (VGFdig)	Sugarcane bagasse from Pakistan (PKBag)
Organosolv (Org)	AGR Digestate (VGFdig)	Tree bark from Golden Acre Park, Leeds (SP Bark)
	SS Digestate (SSdig)	

## **4.1.1 Background**

### **4.1.1.1 Lignin**

The maturation of the biorefinery concept has led to the mass extraction of hemicellulose and cellulose from lignocellulosic biomass (30). The last main constituent of lignocellulose, lignin, remains to be valorised to the same degree and upgraded into higher-value products.

Lignin, which makes up between 15-40% of lignocellulose (31), tends to be used as an energy supply for the cellulose and hemicellulose extraction process by burning (93). This is because once the lignin is cleaved from the desired cellulose and hemicellulose, its economic value is so low that the lignin is used as a fuel. The 'waste' lignin could instead be valorised to exploit it being a source of high-value aromatic compounds due to its complex three-dimensional structure.

However, not all batches of lignin are the same. The composition of lignin is dependent on both the biomass it's coming from, and the batch of that biomass. For this reason, there is not an agreed model for its chemical and physical structure. The complexity and diversity of lignin structures add importance to the characterisation of the biomass itself. It is important to understand how the lignin composition fits into the overall structure of the biomass through characterisation.

### **4.1.1.2 Methods of Characterisation**

Biomass can be characterised by a variety of methods depending on the information that is needed. These have been discussed in detail in the Methods section (Chapter 3).

Alkaline earth metals can be removed by acid-washing. High contents of these species, when burned, can induce ash deposits, slagging and corrosion on the equipment (343). By reducing or removing these metals, the thermal conversion products of the biomass may negatively impact the equipment less.

Pyrolysis-gas chromatography/mass spectrometry (py-GC/MS) is another method by which biomass can be screened. From the fibre analysis, the lignin content of biomass can be estimated. The proportion of high-value compounds derived from lignin structures can be provided by fast pyrolysis of the biomass. More details regarding the pyrolysis process can be found in Chapter 6.

The lignin products in Table 4-1 have previously been characterised by proximate analysis (386-388), ultimate analysis (386, 387, 389), py-GC/MS (387, 388), AAS (390) and DTG (387, 389). However, no literature could be found whereby lignin products

were characterised and employed as comparators for underutilised potential feedstocks for the valorisation of their lignin.

Digestates from a variety of sources have been characterised previously in the literature (391), but mostly for use as an energy source (392-395). Generally, digestate is predominantly used as a source of nutrients on farm and cropland (392, 393). The nutrient contents of nitrogen, phosphorous and potassium are regularly assessed in literature (392) and industry (396). Digestates have also been utilised and valorised as slow pyrolysis (397-399) and hydrothermally carbonised chars (393, 400, 401). The fast pyrolysis of digestate has been explored for the upgrading of its oil products (391, 402). Perez et al (2023) (391) stated that high levels of lignin-derived phenolic compounds were observed in the pyrolysis oil, which could be isolated and valorised.

Sugarcane bagasse is an abundant waste that is produced from the processing (403) of sugarcane by juicing. Commonly, the bagasse is incinerated to provide energy to the sugarcane milling process or disposed of as solid waste (404). However, it is known in literature as being particularly versatile regarding potential applications across numerous sectors (404). Characterisation of sugarcane bagasse has been presented in several papers (405), although mostly bagasse from India and Brazil (406). The fibre analysis has been characterised well, in at least 15 papers. The composition varies across the cellulose (30 wt% - 45 wt%), hemicellulose (20 wt% - 36 wt%) and lignin (9 wt% - 30 wt%) contents (225, 407). It is unknown why the content changes, but it is expected to be due to the differing growing conditions, seasonality of harvesting, and the sugarcane processing conditions.

Coconuts are made up of three layers which consist of an exocarp, a fibrous mesocarp (husk) and a hard endocarp (shell) (408). The majority of the husk and shells are generated as waste during commercial coconut processing. Commonly, the bulk of the coconut husk generated is mismanaged via open burning and direct disposal (409). Coconut husk has been characterised across several publications (409, 410). The proximate analysis values (fixed carbon, volatile matter, ash, and moisture content) vary between each. The variation is most likely due to the different countries of origin, time of harvesting and other factors (411). The lignocellulosic composition can range from 20-38 wt% cellulose, 15-30 wt% hemicellulose, and 40-50 wt% lignin (408, 412). The thermal degradation of coconut husk in the literature has mostly been regarding the production of biochar (409, 412-414). Several papers utilise coconut shell for fast pyrolysis (411, 415, 416), but not coconut husk.

Tree barks encompass around 20 vol% of above-ground tree biomass and 10-15 vol% of tree stems (417, 418), with approximately 300-400 million m<sup>3</sup> of being generated

each year (418). Although trees grow as they age, there may only be a limited impact on the vol% of the bark as a proportion of the tree. This is due to the trees becoming taller and thicker in wood as well as bark. The main applications of bark are as an energy source via incineration and as an aid for mulching in agriculture. Another key application of tree bark is cork. Although the main source of cork is from the outer bark of the cork oak (*Quercus suber L.*), other species have been considered in the research. These include Douglas fir, Turkey oak, and Chinese cork oak. In cork oak, the thickness of the cork is so substantial that it is able to be stripped from the tree without killing it. However, Douglas fir tree bark is different due to the bark being thinner, so the stripping of cork would damage the tree (419). Also, the only cork that is suitable for cork production are those from the lower part of the tree, and not from the higher branches due to them being more resinous. Therefore, as this study is looking at the valorisation tree bark residues, rather than from the stripping of live trees, cork is not a suitable valorisation route (420).

Various types of bark from across the world have been characterised before in the literature. The expected values from the proximate and ultimate analysis of barks are extremely variable due to the variety of tree species and growth conditions (418, 421-426). Volatile matter, fixed carbon and ash content can vary from 63 – 85 wt%, 11 – 27 wt% and 1.2 – 10.7 wt% respectively. Tree barks are known to accumulate alkaline earth metals including magnesium, calcium, potassium, sodium, iron, and aluminium. Calcium and potassium are essential for tree growth, which migrate into the bark over time (427). The lignocellulosic composition of bark has not been frequently clearly laid out in the literature, except for a few cases. These values can vary across the cellulose (17.4 – 35.2 wt% dry basis), hemicellulose (14.8 – 25.0 wt% dry basis) and lignin (13.4 – 51.2 wt% dry basis) contents (428-431). Although the fast pyrolysis of bark has been done for over a decade, limited literature was able to be found regarding this (432).

The characterisation of a wide variety of feedstocks has not been explored before, through the perspective of identifying which would be the best as a source of lignin-derived pyrolysis oil. Further to this, the investigation into the effect of mild acid-washing on the characterisation methods to reduce the alkaline earth metals content is also novel.

## 4.2 Results and Discussion

This section outlines and discusses the characterisation of the 10 samples listed in Table 4-1. After the characterisation by atomic absorption spectroscopy (AAS), it was decided to perform a mild acid-wash on the samples with high metals contents. The characterisation was then re-done on these acid-washed samples, and the results are laid out alongside the untreated samples in Section 4.2.4 and Section 4.2.5.

### 4.2.1 Proximate and Ultimate Analysis

In this section, the proximate and ultimate analysis results for the samples will be discussed. The moisture contents of the samples are not provided here (Table 4-2). This is because the samples were dried at 105 °C once received, to ease their storage and size reduction. Therefore, the moisture content cannot be on an 'as received' basis. They will, however, be included in the discussion of the fibre analysis (Section 4.2.3).

In Table 4-2, three of the digestate samples (SSdig, MSWdig and VGFdig) have a high ash content (> 40 wt%). It is known that the pyrolysis of high ash feedstocks leads to lower bio-oil yields, and a greater level of char (433). This is due to phase separation of the generated bio-oils, via a catalytic effect of the inorganic matter in the ash during fast pyrolysis reactions (434).

The softwood pine tree (SP Bark), organosolv lignin and the sugarcane bagasse (PKBag) have low ash contents (< 2.5 wt%). Higher concentrations of ash have been found to lead to fouling, corrosion, bed agglomeration and slagging problems during thermal degradation of biomass (435). AGRdig and PKBag have high volatiles contents (> 70 wt%). In the cases of fast pyrolysis, more volatile matter increases the pyrolysis oil yield, whilst also increasing how much of the sample will decompose (436).

LB, Org, AlkLig, and SP Bark have high fixed carbon contents (> 30 wt%). This is the solid carbon which remains once the volatile matter has been removed, and lignin has the greatest levels of fixed carbon out of the lignocellulosic components (437). These 4 samples are also expected to have higher lignin contents, with the fixed carbon providing more evidence of this.

The digestate samples have the lowest level of fixed carbon (< 15 wt%). For SSdig and MSWdig, the low fixed carbon is most likely due to the biochemical treatment of the waste (438). The high ash in the digestates is the key reason for their proximate and oxygen values being relatively lower than the other samples. These samples also have

the greatest nitrogen contents. Digestates are known to be nutrient-rich (phosphorous, nitrogen, and potassium) sources, so this is expected (439).

Alkali lignin, LB and SSdig have the greatest sulphur contents. Sulphur can be present within lignin structures as inorganic sulphur, organically bound sulphur, elemental sulphur or adsorbed polysulfide (440). In AlkLig and LB, their sulphur contents is most likely due to their derivation from Kraft lignin. Sodium sulphide is used in the processing of Kraft Lignin (440, 441). The higher sulphur content of SSdig is expected due to the abundance of sulphur in sewerage systems (442).

AlkLig, LB and MSWdig have the lowest H/C mole ratio values. A lower value signifies greater proportions of C=C and C≡C bonds in the feedstock structures, and less of simple bonds including C-C and C-H (443). For AlkLig and LB, this would be expected with higher levels of lignin due to its aromatic nature (the presence of benzene rings).

LB, org, and SP Bark have the greatest higher heating values (HHVs) of the feedstocks, which is due to the high carbon and hydrogen contents. This means that, although it is a low-value application, these feedstocks would be the most suited for incineration to regain energy in the process.

The digestate (excluding AGRdig) samples have the lowest HHV values due to their low carbon contents and high ash, so would not be a good option for the generation of energy by incineration.

Across the three equations used to calculate HHVs (Friedl, Dulong and Channiwala and Parikh), the ranges differ based on the type of biomass. The range is greater for those samples (such as the digestates) with low carbon, low volatile matter, and high ash contents.

The coconut husk values are different to those in the literature (409, 410), with higher ash (8 wt% compared to 4.6-5.3 wt%), fixed carbon (28.2 wt% compared to 14.7-18.7 wt%), and lower hydrogen contents (3.8 wt% compared to 7.5-8.0 wt%). There are not clear reasons for the different values.

**Table 4-2** - Proximate and Ultimate Analysis of lignin products, digestates and residues, with higher heating values (HHV) estimated with 3 methods. Error values were calculated by 1x standard deviation. 2 replicates were run for each sample.

Variable		Lignins			Digestates				Residues		
		AlkLig	LB	Org	AGRdig	VGfdig	SSdig	MSWdig	SP Bark	CH	PKBag
Proximates (%wt, dry basis)	Volatiles	47.6 ± 0.1	57.5 ± 0.9	61.4 ± 0.9	70.2 ± 0.3	47.2 ± 1.1	51.0 ± 0.1	36.2 ± 0.1	66.9 ± 0.0	63.7 ± 2.7	76.5 ± 0.2
	Fixed Carbon	31.8 ± 0.8	37.8 ± 0.1	36.5 ± 0.3	13.8 ± 0.0	9.0 ± 0.2	2.1 ± 0.1	8.3 ± 0.0	32.1 ± 0.1	28.2 ± 0.5	21.3 ± 0.1
	Ash	20.6 ± 0.8	11.0 ± 1.0	2.1 ± 1.3	16.0 ± 0.3	43.8 ± 0.8	46.9 ± 0.0	55.5 ± 0.1	1.1 ± 0.1	8.0 ± 3.2	2.2 ± 0.1
Ultimates (wt%, dry basis)	Carbon	47.2 ± 0.3	61.3 ± 0.5	49.1 ± 0.3	44.1 ± 0.1	29.5 ± 0.1	28.6 ± 0.3	24.1 ± 0.0	57.3 ± 2.5	48.4 ± 1.5	49.1 ± 0.1
	Hydrogen	3.5 ± 0.2	4.7 ± 0.3	5.7 ± 0.0	5.1 ± 0.0	3.0 ± 0.1	3.1 ± 0.1	1.7 ± 0.0	5.6 ± 0.5	3.8 ± 0.1	5.7 ± 0.5
	Nitrogen	0.0 ± 0.0	0.9 ± 0.0	1.3 ± 0.0	3.2 ± 0.0	2.0 ± 0.0	3.4 ± 0.0	1.5 ± 0.0	0.8 ± 0.0	0.8 ± 0.1	1.3 ± 0.0
	Sulphur	1.8 ± 0.2	1.2 ± 0.1	0.0 ± 0.0	0.3 ± 0.0	0.3 ± 0.0	1.5 ± 0.0	0.2 ± 0.0	0.0 ± 0.0	0.0 ± 0.0	0.0 ± 0.0
	Oxygen	26.9 ± 1.2	28.2 ± 1.2	41.7 ± 0.9	31.3 ± 0.3	21.3 ± 0.6	16.4 ± 0.3	16.9 ± 0.0	35.2 ± 3.0	38.9 ± 1.8	41.7 ± 1.2
HHV (MJ/kg)	Channiwala and Parikh	18.3	24.9	25.8	17.8	10.7	11.1	7.5	22.9	17.8	20.0
	Friedl	18.3	24.2	25.9	17.8	14.9	14.9	15.6	23.0	18.9	19.7
	Dulong	17.2	24.0	24.2	16.6	10.5	11.2	7.6	21.1	15.7	18.0
H/C Molar Ratio (dry ash free)		0.88	0.91	1.38	1.38	1.22	1.30	0.84	1.16	1.07	0.93

## 4.2.2 Atomic Absorption Spectroscopy

In this section, the data measured from the atomic absorption spectroscopy of the samples is laid out (Table 4-3). Due to the high alkaline earth metal contents for several of the samples, an acid wash (Section 3.9.1) was performed to reduce these concentrations. The comparison of the results for the untreated and acid washed samples are presented in Table 4-4, with the relative change in Figure 4-2.

Several of the samples tested had high concentrations of the metals analysed (Table 4-3), specifically AlkLig, AGRdig, VGFdig, SSdig, MSWdig, CH and PKBag. A key benefit of the presence of earth metals (such as those measured by AAS) is the lowering of temperatures needed for pyrolysis (344). In holocellulose (cellulose and hemicellulose) pyrolysis, the presence of alkaline earth metals catalyse the fragmentation of pyranose (a six-membered ring of five carbon atoms and one oxygen atom) and furanose (a five-membered ring of four carbon atoms and one oxygen atom) rings. In lignin structures, alkaline earth metals catalyse the cleavage of carbon-carbon bonds and side chains by reducing the activation energies necessary for the breakdown of the structure.

However, high concentrations of earth metals can catalyse the cracking of oxygen-containing compounds into a larger number of smaller compounds (444). The oxygen content arises from the complex lignocellulosic structures. In the interest of valorising the samples' phenolic content, it is more desirable to produce higher concentrations of fewer compounds, rather than low concentrations of a wide variety of compounds. It was for this reason that these samples were acid-washed according to Section 3.9.1. However, VGFdig was not acid-washed due to the limited supplies available. From Figure 4-2, all of the measured metals were decreased after the acid washing. For Al, Fe and Na, at least one of the samples (of AlkLig, CH and PKBag) seemed to gain in metal concentration after acid washing. This is discussed in more detail later in this section.

All of the digestate samples, and the sugarcane bagasse, had high levels of calcium. In the separation and recovery of phosphate and nitrogen, calcium is known to be added to digestates (445). In PKBag, the high calcium could be due to two scenarios. In the first, the soil in which the sugarcane grew in may naturally have high levels of calcium. An alternative scenario would be that the soil was quite acidic, so lime (an assortment of calcium and magnesium-containing materials) was added. The addition of lime to soil raises the pH and adds calcium and/or magnesium, depending on the specific lime used (446). However, it is difficult to know for sure the soil type that the sugarcane bagasse samples initially grew in, so a definitive reason for the high calcium cannot be

given. After acid-washing, the calcium levels were dramatically reduced in all of these samples.

The aluminium concentrations were greater in SSdig and MSWdig. The reasonable Al contents in VGFdig is most likely due to the presence of insoluble Al compounds within soil. As vegetation grows, the Al would be taken up into the plant (447). In SSdig and MSWdig, the high Al levels may occur from the use of aluminium sulphate and other precipitating agents. These are used frequently in the production of sewage sludge and in wastewater processing (448, 449). The acid-washing treatment did not have a large impact on the aluminium content of the samples, with most having a small reduction. In the case of CH and PKBag, which had 0 mg/g of aluminium when untreated, the aluminium contents appear to increase after acid-washing. This could be due to the acid-digestion step required for AAS preparation being of insufficient duration, or simply that there are only trace levels of Al which are concentrated slightly from the removal of the other metals and slight breakdown of the biomass' structures. Therefore, the changing in values of trace amounts will appear much larger when presented on a percentage change basis.

AGRdig and MSWdig have higher levels of potassium and magnesium. This is expected as, post-anaerobic digestion, the potassium and magnesium contents of digested material are concentrated into the digestate (450, 451). It is known that coconut husk has a high concentration of potassium (452). The potassium contents of all samples were dramatically reduced by acid-washing.

High iron (Fe) contents are only found in the digestates (excluding AGRdig). In SSdig and MSWdig, this may be due to the use of iron salts for sulphide control in sewer treatments and wastewater treatment plants (453, 454). The high iron in VGFdig is most likely from its iron-rich components, namely fruits (including watermelon, figs and raisins), vegetables (peas, broccoli and spinach) and garden waste (where it may have had nutritious soil conditioner added to increase the nutrient content, including iron) (455).

The high sodium content of alkali lignin is expected due to the presence of Na and K in the alkali processing streams used in its production (390). After acid-washing, the sodium content was noticeably reduced, but not to a negligible concentration.

The presence of calcium in biomass can be as three forms: acid-insoluble, acid-soluble and organically bound (456). As the majority of calcium from all samples was reduced from the acid-washing, it can be assumed that all of the calcium was acid-soluble.

**Table 4-3 - Metals Analysis of all untreated feedstocks. Error values were calculated by 1x standard deviation. 2 replicates were run for each sample**

Sample Type		Al (mg/g)	Ca (mg/g)	K (mg/g)	Fe (mg/g)	Na (mg/g)	Mg (mg/g)
Lignins	AlkLig	0.16 ± 0.01	0.43 ± 0.10	0.78 ± 0.10	0.00 ± 0.00	68.93 ± 0.40	0.39 ± 0.00
	LB	0.03 ± 0.00	0.05 ± 0.00	0.00 ± 0.00	0.00 ± 0.00	0.38 ± 0.05	0.37 ± 0.10
	Org	0.68 ± 0.00	1.18 ± 0.10	0.00 ± 0.00	0.02 ± 0.01	0.00 ± 0.00	0.07 ± 0.01
Digestates	AGRdig	0.20 ± 0.00	10.25 ± 0.10	14.45 ± 0.20	15.88 ± 0.67	0.50 ± 0.03	4.94 ± 0.20
	VGFdig	2.16 ± 0.46	24.28 ± 0.75	3.86 ± 0.29	3.79 ± 0.35	2.34 ± 0.16	3.74 ± 0.26
	SSdig	6.68 ± 0.02	17.44 ± 0.06	1.08 ± 0.03	14.21 ± 0.07	0.58 ± 0.02	4.30 ± 0.00
	MSWdig	4.55 ± 0.38	59.76 ± 1.46	8.91 ± 0.19	11.53 ± 0.12	2.84 ± 0.14	9.24 ± 0.05
Residues	CH	0.00 ± 0.00	0.69 ± 0.01	7.75 ± 0.98	0.07 ± 0.01	1.11 ± 0.09	0.72 ± 0.05
	PKBag	0.00 ± 0.00	6.08 ± 0.45	2.15 ± 0.02	0.12 ± 0.09	0.00 ± 0.00	0.81 ± 0.07
	SP Bark	0.05 ± 0.03	3.29 ± 0.36	0.45 ± 0.05	0.10 ± 0.02	0.00 ± 0.00	0.55 ± 0.12

**Table 4-4 - Metals Analysis of acid-washed feedstocks compared to the untreated feedstocks. Error values were calculated by 1x standard deviation. 2 replicates were run for each sample**

Sample Type		Al (mg/g)	Ca (mg/g)	K (mg/g)	Fe (mg/g)	Na (mg/g)	Mg (mg/g)
AlkLig	Untreated	0.16 ± 0.01	0.43 ± 0.10	0.78 ± 0.10	0.00 ± 0.00	68.93 ± 0.40	0.39 ± 0.00
	Acid-washed	0.24 ± 0.11	0.29 ± 0.16	0.41 ± 0.01	0.04 ± 0.00	18.00 ± 2.60	0.31 ± 0.03
AGRdig	Untreated	0.20 ± 0.00	10.25 ± 0.10	14.45 ± 0.20	15.88 ± 0.67	0.50 ± 0.03	4.94 ± 0.20
	Acid-washed	0.05 ± 0.03	0.00 ± 0.00	0.14 ± 0.01	3.40 ± 0.07	0.19 ± 0.19	0.50 ± 0.00
SSdig	Untreated	6.68 ± 0.02	17.44 ± 0.06	1.08 ± 0.03	14.21 ± 0.07	0.58 ± 0.02	4.30 ± 0.00
	Acid-washed	2.20 ± 0.35	0.00 ± 0.00	0.35 ± 0.13	6.29 ± 0.66	0.03 ± 0.03	0.95 ± 0.06
MSWdig	Untreated	4.55 ± 0.38	59.76 ± 1.46	8.91 ± 0.19	11.53 ± 0.12	2.84 ± 0.14	9.24 ± 0.05
	Acid-washed	1.93 ± 0.00	0.00 ± 0.00	0.78 ± 0.00	3.26 ± 0.00	0.13 ± 0.00	3.28 ± 0.00
CH	Untreated	0.00 ± 0.00	0.69 ± 0.01	7.75 ± 0.98	0.07 ± 0.01	1.11 ± 0.09	0.72 ± 0.05
	Acid-washed	1.54 ± 0.06	0.00 ± 0.00	0.25 ± 0.03	0.11 ± 0.05	0.29 ± 0.16	0.33 ± 0.01
PKBag	Untreated	0.00 ± 0.00	6.08 ± 0.45	2.15 ± 0.02	0.12 ± 0.09	0.00 ± 0.00	0.81 ± 0.07
	Acid-washed	1.08 ± 0.08	0.00 ± 0.00	0.11 ± 0.01	0.03 ± 0.01	0.21 ± 0.04	0.33 ± 0.00

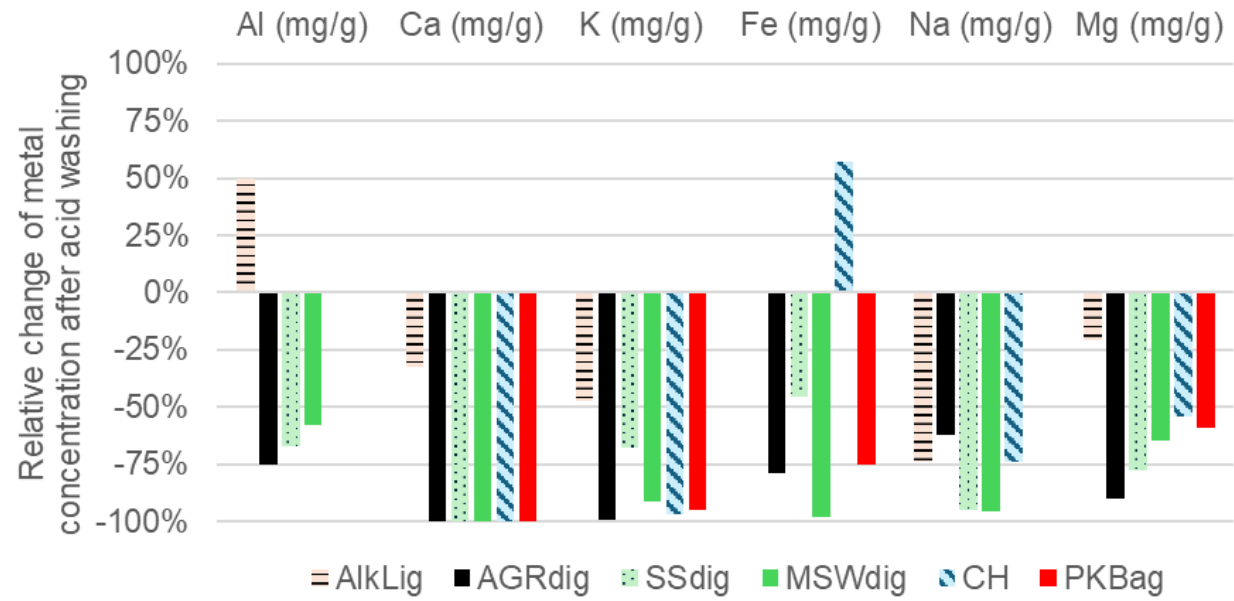


**Figure 4-2** - Relative change of metals concentration between acid-washed and untreated samples.

### 4.2.3 Fibre Analysis

In this section, the results of the fibre analysis are stated (Table 4-5). The moisture content of the samples, measured as a part of the proximate analysis, are featured here. The unknown content is calculated to be the remainder of the sample's weight% after summing up the cellulose, hemicellulose, lignin, and ash.

The samples (excluding the lignin products) with the greatest proportion of lignin was the coconut husk and the SP Bark. As stated previously (in Section 4.1), the results of the fibre analysis may be best used as semi-qualitative comparisons. These lignin contents are higher than the lignin products (AlkLig and LB), although organosolv lignin was unable to be analysed due to the limited supplies.

In addition to the high lignin contents, the SP Bark and PKBag also have a reasonably large 'unknown' content. These may include extractives such as resins, proteins, waxes, and fats. In addition to these extractives, SP Bark may contain tannins and flavonoids (457, 458). In the literature (225, 407), sugarcane bagasse has 30-40 wt% cellulose, 20-36 wt% hemicellulose and 9-30 wt% lignin. The lignin and cellulose content in the literature is similar to the result in this study. However, it is unknown why the hemicellulose content is lower in this work. For the SP Bark sample, the large 'unknowns' may be due to the presence of flavonoids and tannins (458, 459).

The samples with the lowest lignin contents are the digestates (AGRdig, VGFdig, SSdig, MSWdig) and PKBag. The low lignin in the digestates are expected, as lignin is known to negatively affect organic matter's biodegradability (460). Therefore, the matter chosen to undergo anaerobic digestion to produce the digestates would ideally have little lignin.

AGRdig, PKBag and CH have the greatest cellulose contents. This was not expected due to their pre-treatment methods, enzymatic hydrolysis, and anaerobic digestion (AD) respectively. The AD process is stated to be able to degrade up to 80% of the cellulose contained within crop residues (461). The agricultural residue that underwent AD must have had a substantial cellulose content. The results of AGRdig's fibre analysis is similar to that of Perez et al (391) although as it is a mix of various agricultural residues, it is dependent on the source and proportions of each type of residue.

**Table 4-5 - Fibre Analysis (results in weight%).** Error values were calculated by 1x standard deviation. 2 replicates were run for each sample. Moisture content (M) results are on an 'as analysed' (a.a) basis. Crude protein calculated by Table 2-2.

Sample Type		M	Cellulose	Hemi-cellulose	Lignin	Ash	Crude Protein	Not known
Lignins	AlkLig	6.0± 0.0	6.1± 0.0	24.5± 0.9	39.2± 1.7	20.6± 0.8	0.0± 0.0	9.6
	LB	2.8± 0.6	3.6± 1.5	29.8± 0.5	40.9± 0.5	11.0± 1.0	5.0± 0.0	14.6
Digestates	AGRdig	5.7± 0.2	24.3± 1.3	14.3± 0.1	26.4± 0.8	16.0± 0.3	14.1± 0.0	19.1
	VGFDig	4.4± 0.0	13.1± 1.2	3.8± 0.3	24.1± 0.3	43.8± 0.8	8.8± 0.0	15.2
	SSdig	6.7± 0.0	8.0± 0.6	8.9± 0.8	31.8± 1.1	46.9± 0.0	3.2± 0.0	4.4
	MSWdig	3.1± 0.0	6.5± 1.5	12.3± 0.0	17.5± 2.0	55.5± 0.1	1.4± 0.0	6.8
Residues	CH	4.5± 0.1	33.4± 1.5	2.6± 0.0	42.5± 2.9	8.0± 3.2	4.7± 0.6	13.5
	PKBag	3.7± 0.0	25.8± 4.9	8.6± 0.4	23.9± 8.7	2.2± 0.1	7.6± 0.0	39.5
	SP Bark	6.2± 0.1	7.6± 5.5	0.6± 0.0	68.7± 5.9	1.1± 0.1	4.5± 0.0	17.5

The coconut husk results are slightly different than in literature (Table 4-6). The lignin and cellulose values are close to those in literature; however, the hemicellulose content appears much lower in this study. As the errors for the coconut husk values are not abnormally large, it is unknown why this is so low. The composition across literature seems to change, dependent on the country it was sourced from and the time of year it was harvested.

**Table 4-6 - The lignocellulosic composition of coconut husk in this study compared to in literature.** Error values were calculated by standard deviation.

	Cellulose (wt%)	Hemicellulose (wt%)	Lignin (wt%)
<b>This study</b>	<b>33.4 ± 1.5</b>	<b>2.6 ± 0.0</b>	<b>42.5 ± 2.9</b>
Sangian and Widjaja (2018) (462)	26.60	17.74	41.18
Anuchi et al (2022) (408)	20-38	15-30	40-50

The lignin samples (AlkLig and LB) have the greatest hemicellulose contents. This is expected as, during Kraft pulping which occurs in the lignoboost and alkali lignin production processes, the lignin and some of the hemicellulose is dissolved into the black liquor. The liquor is then processed into the Lignoboost, which concentrates the lignin and hemicellulose content (hence the high levels of hemicellulose) (197).

#### **4.2.4 Pyrolysis-Gas Chromatography/Mass Spectrometry**

The pyrolysis chromatograms (or py-grams) generated at 550 °C (according to the method presented in Section 3.7.2) are illustrated below with the axes of retention time against the 'absolute intensity per mg of sample'. These were chosen to allow the different samples to be compared to each other, as it is then independent of the amount of sample prepared for the method.

The top 25 peaks of each chromatogram were identified by GC/MS using the NIST mass spectral database versions 147 and 27. For each identified molecule, its similarity to the actual molecule in the pyrolysis gas was compared (based on similarity of mass fragments) and given a similarity score out of 100. In this work, the identified molecule was considered to be trustworthy when the similarity score was above 66. Separately, the literature was consulted to see whether the identified molecule was likely to be found within the sample.

The axes for each group of py-grams have been kept the same where possible to aid comparison of the data. In some cases, such as Figure 4-5, this was not possible due to the large differences in scale. First, the py-grams of the untreated samples are illustrated. In the tables below, the proportions of the key peaks of the acid-washed samples (compared to the untreated samples) are outlined.

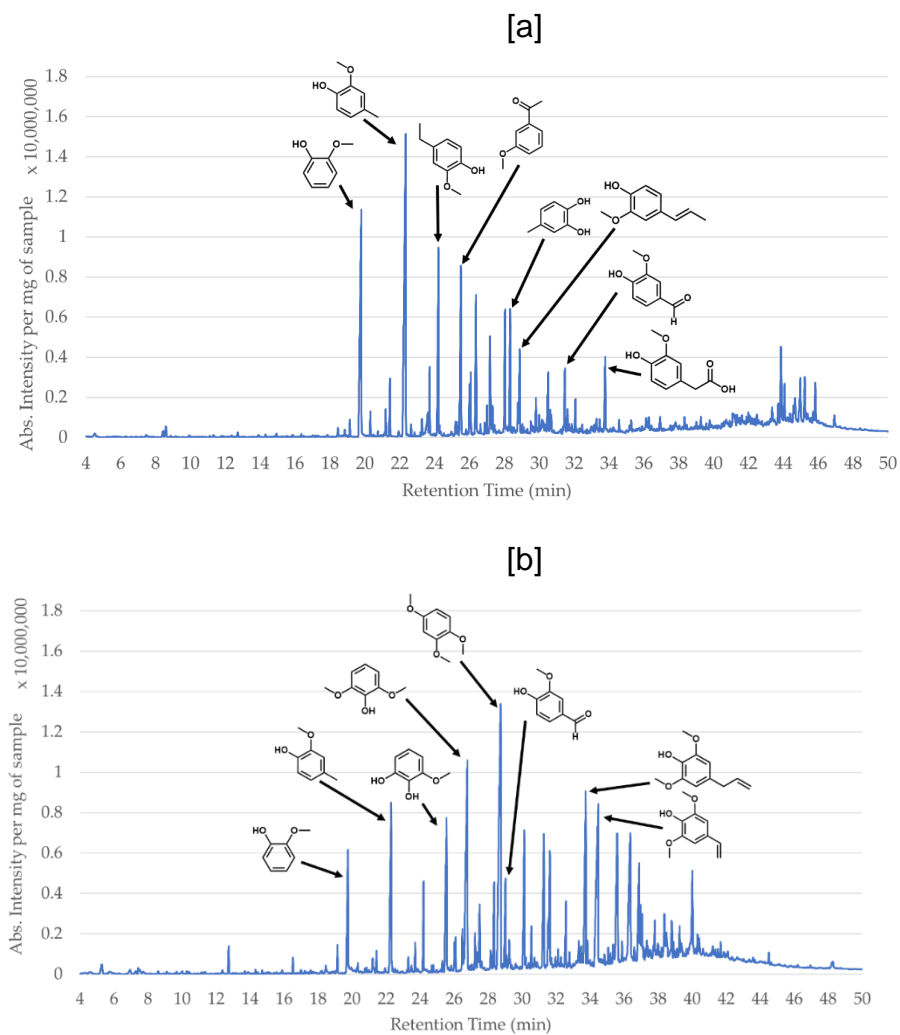


**Figure 4-3** - Fast pyrolysis chromatograms of [a] Lignoboost and [b] organosolv lignin at 550 °C by py-GC/MS. Pyrolysis heating rate of 20 °C/ms, then held for 20s. Column temperature program of 40 °C for 2 min, 6 °C/min ramp to 280 °C, then hold for 10 min.

**Table 4-7** - Proportions of key and shared peaks of Lignoboost and organsolv lignin from fast pyrolysis at 550 °C by py-GC/MS. RT = Retention Time. The top 25 peaks of each chromatogram were identified using the NIST mass spectral database versions 147 and 27.

RT (min)	Registered Peak	Lignoboost (%)	Organosolv (%)
19.9	Phenol, 2-methoxy-	13.6	3.6
22.4	Creosol	23.8	6.1
24.3	Benzene, 1,4-dimethoxy-2-methyl-	10.0	
25.6	1,2-Benzenediol, 3-methoxy-		5.8
25.6	Benzene, 1-methoxy-2-methyl-3-nitro-	8.3	
26.4	Catechol	4.3	0.8
26.8	Phenol, 2,6-dimethoxy-		11.3
27.1	Tran-isoeugenol	1.8	2.1
27.3	Phenol, 2-methoxy-4-(2-propenyl)-, acetate	3.1	0.9
28.7	1,2,4-Trimethoxybenzene		15.9
29.0	Vanillin	3.8	2.2
30.6	Apocynin	2.8	0.9
31.3	3',5'-Dimethoxyacetophenone		4.4
31.6	2-Propanone, 1-(4-hydroxy-3-methoxyphenyl)-	3.2	1.1
33.7	Phenol, 2,6-dimethoxy-4-(2-propenyl)-		6.4
34.5	Benzaldehyde, 4-hydroxy-3,5-dimethoxy-		9.7
35.6	Ethanone, 1-(4-hydroxy-3,5-dimethoxyphenyl)-		6.3
36.4	3-Amino-4-methoxybenzoic acid		6.6

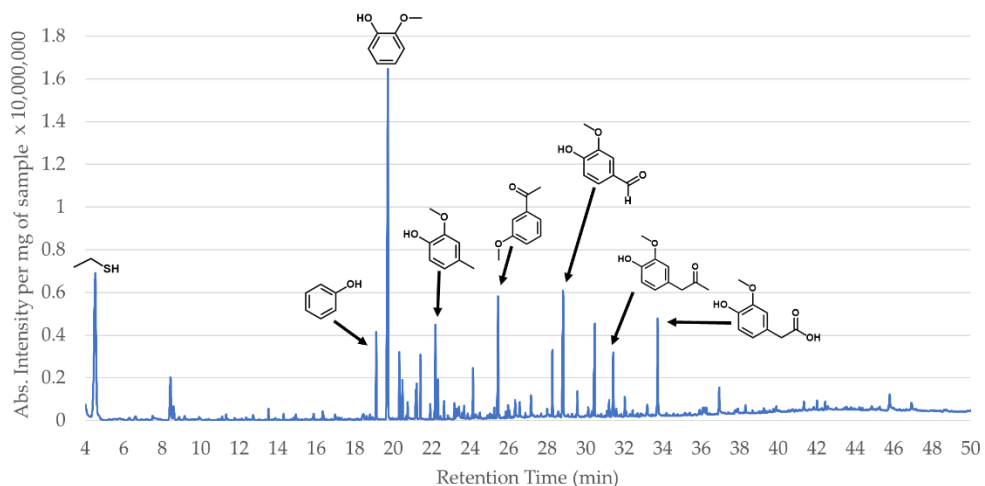


**Figure 4-4** - Fast pyrolysis chromatogram of untreated Alkali Lignin at 550 °C by py-GC/MS. Pyrolysis heating rate of 20 °C/ms, then held for 20s. Column temperature program of 40 °C for 2 min, 6 °C/min ramp to 280 °C, then hold for 10 min.

**Table 4-8** - Proportions of key and shared peaks of untreated Alkali Lignin and acid-washed Alkali Lignin from fast pyrolysis at 550 °C by py-GC/MS. The top 25 peaks of each chromatogram were identified using the NIST mass spectral database versions 147 and 27.

RT (min)	Registered Peak	AlkLig (%)	Acid AlkLig (%)
4.5	Ethanethiol	18.2	
5.3	Pentanal		5.7
5.7	Acetic acid		28.7
10.1	Furfural		9.7
14.0	2-Furancarboxaldehyde, 5-methyl-		7.9
19.7	Phenol, 2-methoxy-	24.8	
20.4	2-Furanmethanol		20.0
21.4	Creosol	6.9	
25.4	3-Methoxyacetophenone	5.5	
28.8	Vanillin	7.3	
30.5	Apocynin	4.6	
33.7	Homovanillic acid	4.8	

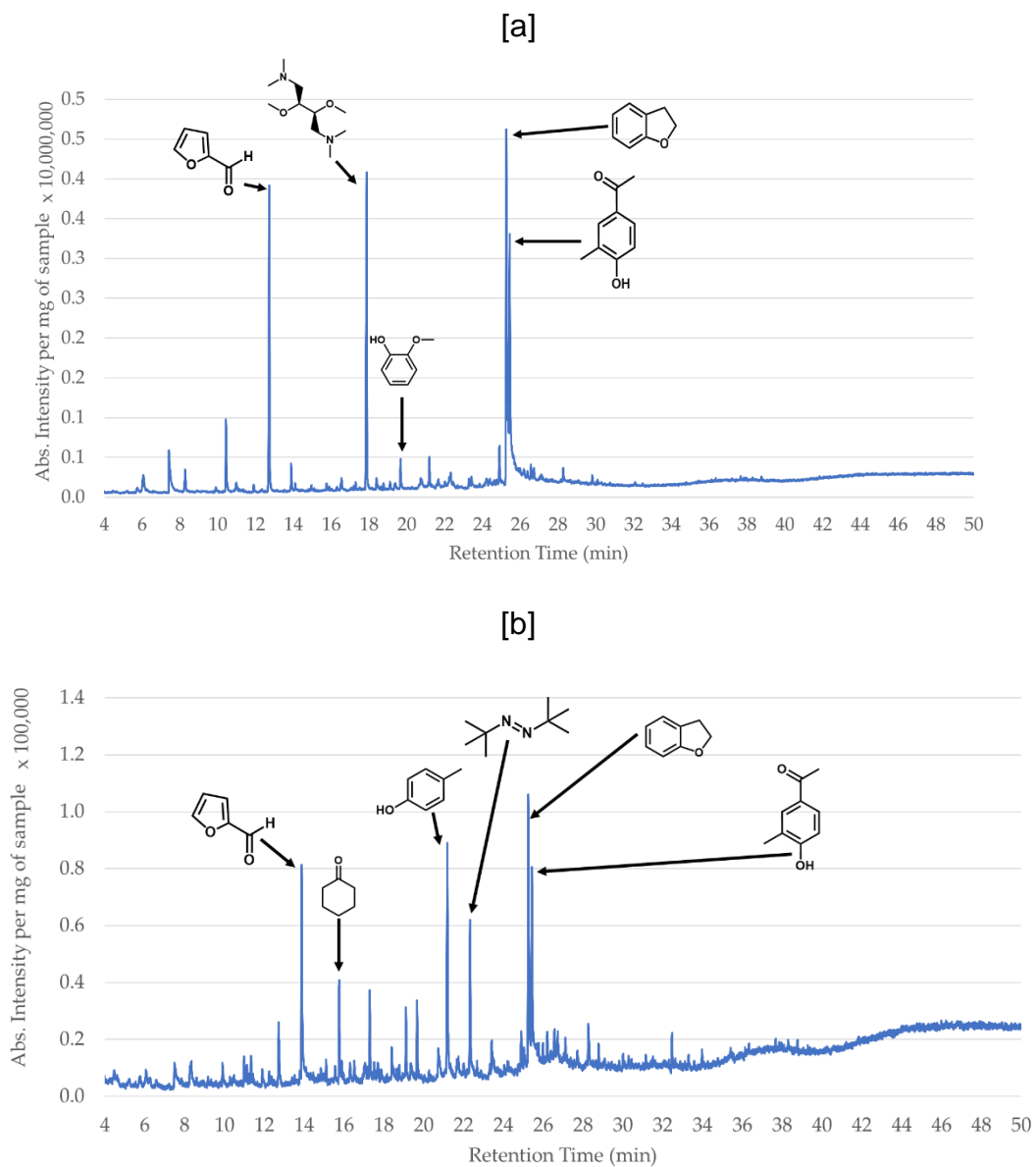


**Figure 4-5** - Fast pyrolysis chromatogram of [a] untreated AGRdig and [b] untreated VGFdig at 550 °C by py-GC/MS. AGRdig and VGFdig are presented at different y-axis scales due to the large difference in absolute intensities measured. Pyrolysis heating rate of 20 °C/ms, then held for 20s. Column temperature program of 40 °C for 2 min, 6 °C/min ramp to 280 °C, then hold for 10 min.

**Table 4-9** - Proportions of key and shared peaks of untreated and acid-washed agricultural residue digestate (AGRdig) and untreated vegetable, garden, and fruit residue digestate (VGFdig) from fast pyrolysis at 550 °C by py-GC/MS. The top 25 peaks of each chromatogram were identified using the NIST mass spectral database versions 147 and 27.

RT (min)	Registered Peak	AGRdig (%)	Acid AGRdig (%)	VGFdig (%)
3.8	Ethene, 1,1-difluoro-	2.2		7.0
5.7	Acetic acid	3.2	5.8	
12.7	Furfural	15.3	15.5	3.5
13.8	2-Furanmethanol	1.2		8.8
15.8	Cyclohexanone	15.8		5.2
16.5	2-Propenoic acid, 2-methyl-, 1-methylethyl ester		0.2	
17.0	Phenol		0.3	2.9
17.6	Phenol, 2-methoxy	1.4	0.6	2.9
17.9	1,4-Butanediamine, 2,3-dimethoxy-N,N,N',N'-tetramethyl-, [S-(R*,R*)]-	16.6	24.4	
19.2	Dodecanal		0.2	
21.2	p-Cresol	1.4	0.3	11.4
21.8	Phenol, 4-ethyl-	0.7	0.9	
22.3	Diazene, bis(1,1-dimethylethyl)-			7.2
22.8	Heptanal		0.4	
23.4	Benzoic acid	0.5		1.5
24.9	Methacrylic acid, ethyl ester	2.1		2.7
25.3	Benzofuran, 2,3-dihydro-	24.3	20.3	14.1
25.4	4-Hydroxy-3-methylacetophenone	18.5	22.0	9.2
26.3	trans-Isoeugenol	0.4	0.2	
26.7	Indole	0.6		2.4
27.7	Phenol, 2-methoxy-4-(1-propenyl)-		1.2	1.9
30.0	1-Dodecanol, 3,7,11-trimethyl-		0.3	
32.6	1-Octadecyne		0.7	

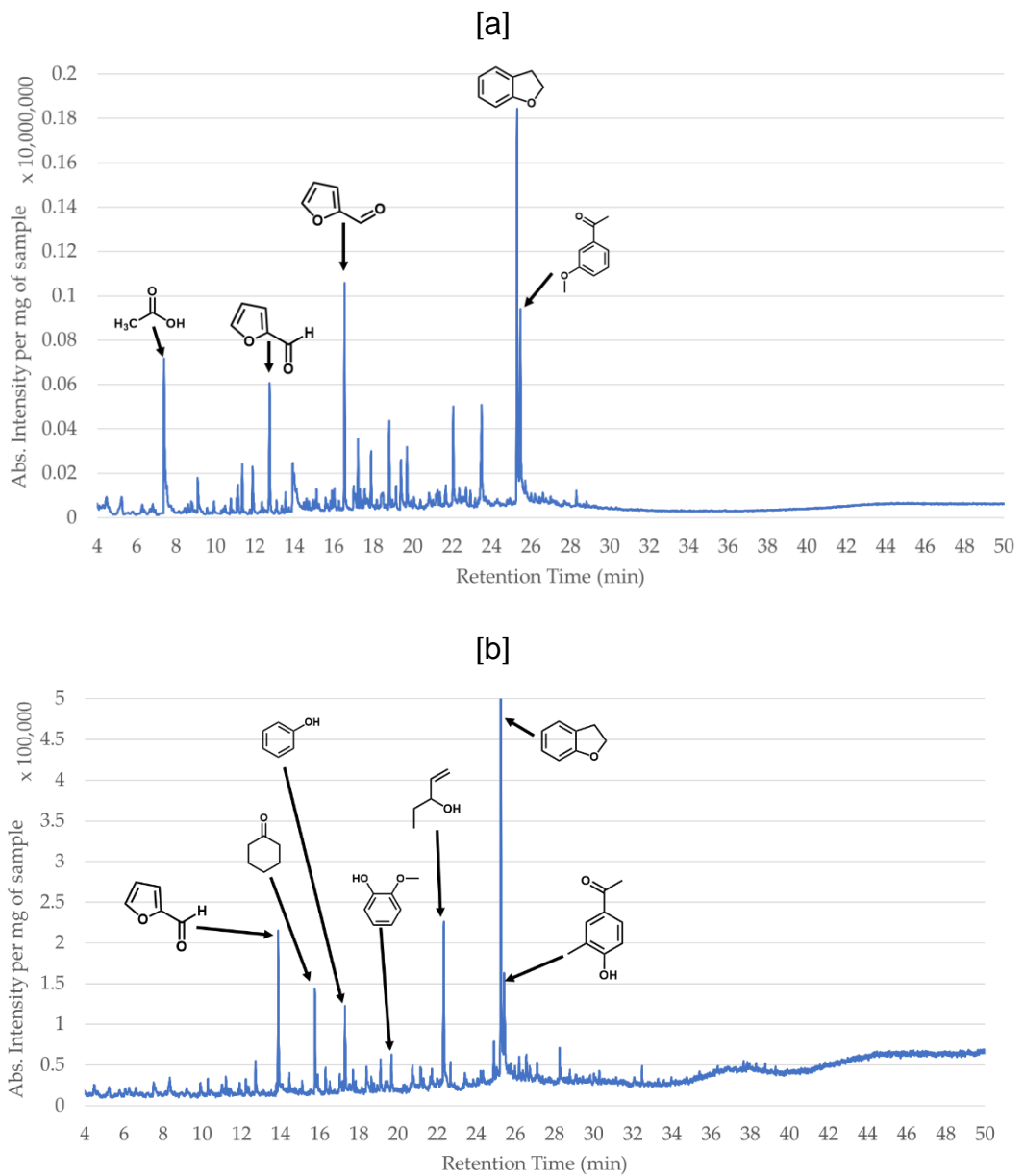


**Figure 4-6** - Fast pyrolysis chromatogram of [a] untreated SSdig and [b] untreated MSWdig at 550 °C by py-GC/MS. SSdig and MSWdig are presented at different y-axis scales due to the large difference in absolute intensities measured. Pyrolysis heating rate of 20 °C/ms, then held for 20s. Column temperature program of 40 °C for 2 min, 6 °C/min ramp to 280 °C, then hold for 10 min.

**Table 4-10** - Proportions of key and shared peaks of untreated and acid-washed sewage sludge digestate (SSdig) and Municipal Solid Waste digestate (MSWdig) from fast pyrolysis at 550 °C by py-GC/MS. The top 25 peaks of each chromatogram were identified using the NIST mass spectral database versions 147 and 27.

RT (min)	Registered Peak	SSdig (%)	Acid SSdig (%)	MSWdig (%)	Acid MSWdig (%)
3.8	Ethene, 1,1-difluoro-	3.1		2.2	
5.3	Pentanal		5.7		
5.7	Acetic acid	10.7			8.0
8.8	p-Xylene				0.5
9.3	Propanenitrile, 3,3'-oxybis-	2.6			2.0
10.1	Furfural	5.9	9.7	2.0	21.0
14.0	2-Furancarboxaldehyde, 5-methyl-	8.3	7.9		1.5
14.7	Cyclopentasiloxane, decamethyl-	2.5	0.9		
15.6	1,4-Butanediamine, 2,3-dimethoxy-N,N,N',N'-tetramethyl-, [S-(R*,R*)]-	2.5			17.1
15.8	Cyclohexanone			6.6	
18.8	7-Tridecanone	4.2			
20.3	2-Furanmethanol	6.9	20.0	10.2	27.0
22.2	Methacrylic acid, ethyl ester			2.9	1.1
22.3	1-Penten-3-ol			10.6	
23.5	Benzoic acid	6.5			
24.3	3-Methoxyacetophenone	9.9			3.6
24.8	4-Hydroxy-3-methylacetophenone			8.6	0.5
25.3	Benzofuran, 2,3-dihydro-	17.2		33.6	
27.7	Phenol, 2-methoxy-4-(1-propenyl)-			1.7	2.6

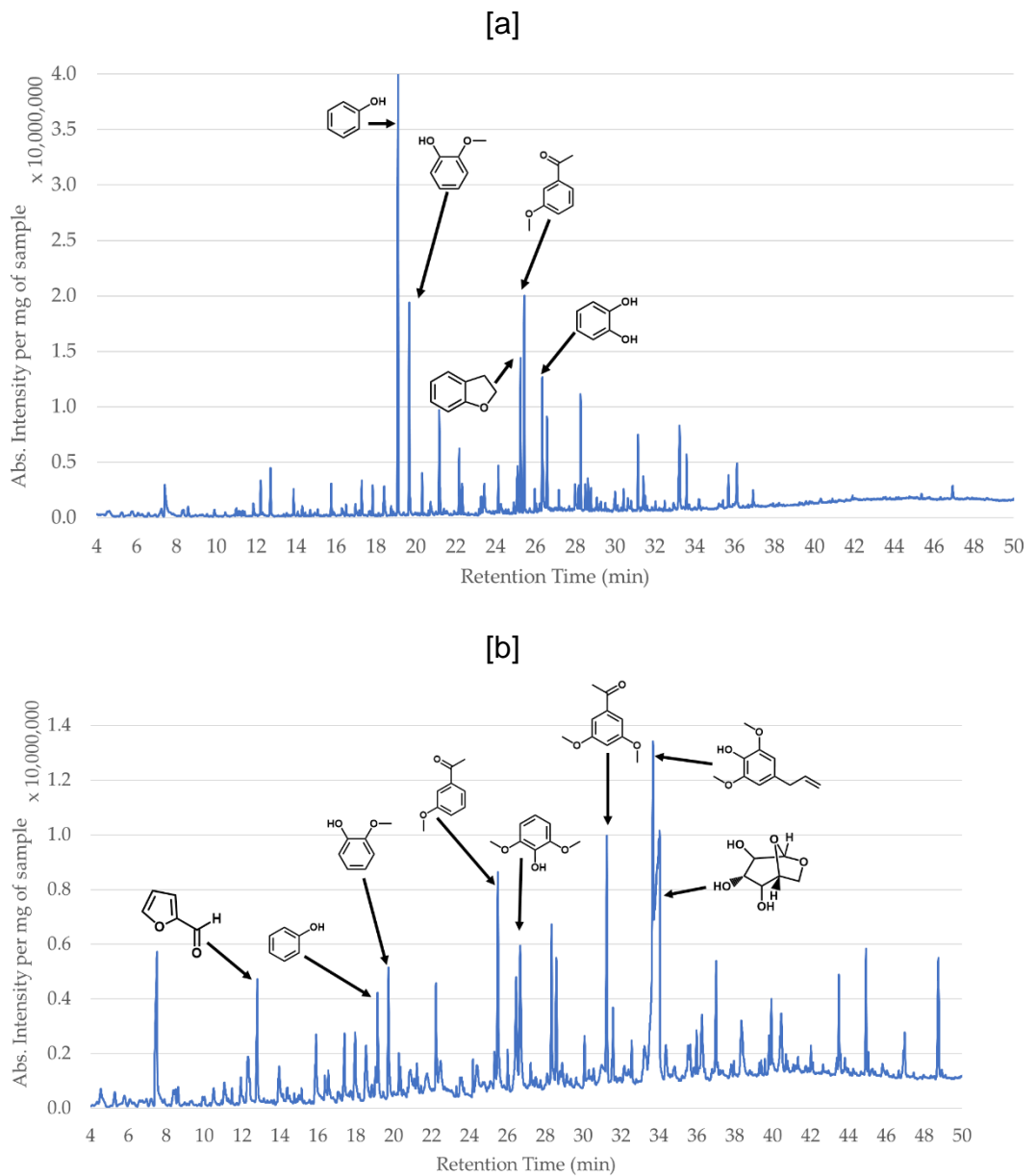


**Figure 4-7** - Fast pyrolysis chromatogram of [a] untreated coconut husk and [b] untreated PKBag at 550 °C by py-GC/MS. CH and PKBag are presented at different y-axis scales due to the large difference in absolute intensities measured. Pyrolysis heating rate of 20 °C/ms, then held for 20s. Column temperature program of 40 °C for 2 min, 6 °C/min ramp to 280 °C, then hold for 10 min.

**Table 4-11** - Proportions of key and shared peaks of untreated and acid-washed coconut husk (CH) and Pakistani sugarcane bagasse (PKBag) from fast pyrolysis at 550 °C by py-GC/MS. The top 25 peaks of each chromatogram were identified using the NIST mass spectral database versions 147 and 27.

RT (min)	Registered Peak	CH (%)	Acid CH (%)	PKBag (%)	Acid PKBag (%)
7.5	Acetic acid		13.7	6.0	13.3
12.7	Furfural	2.5	37.3	2.6	26.5
14.0	2-Furancarboxaldehyde, 5-methyl-		0.8		1.1
14.1	3-Chlorohexane				5.2
15.8	Cyclohexanone	1.4		1.9	
17.8	1,4-Butanediamine, 2,3-dimethoxy-N,N,N',N'-tetramethyl-, [S-(R*,R*)]-	1.3	25.0	1.6	30.1
19.1	Phenol	18.8	3.8	2.3	1.5
19.7	Phenol, 2-methoxy-	10.0		3.2	
20.3	2-Furanmethanol		4.5		4.7
22.2	Creosol	2.8	0.2	2.3	0.4
25.3	Benzofuran, 2,3-dihydro-	6.2	1.3		
25.4	3-Methoxyacetophenone	9.4		5.7	3.2
26.3	Catechol	6.2		2.8	
26.6	Phenol, 2,6-dimethoxy-	4.4		4.9	
28.3	trans-Isoeugenol	4.6	0.2	3.2	
31.2	3',5'-Dimethoxyacetophenone	3.0		5.8	
33.2	.beta.-D-Glucopyranose, 1,6-anhydro-	5.4		23.0	
33.6	Phenol, 2,6-dimethoxy-4-(2-propenyl)-	2.2		14.2	

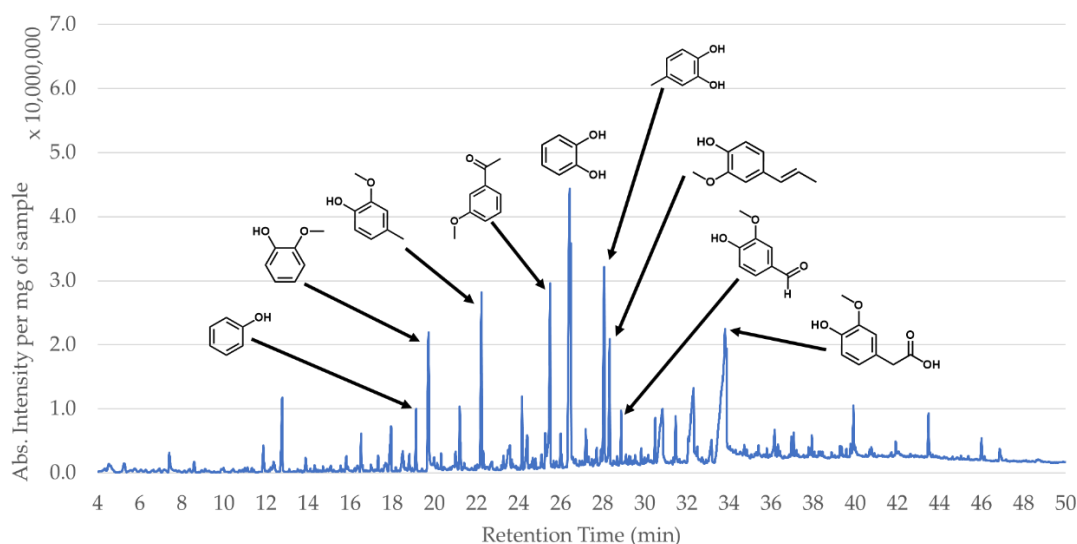


**Figure 4-8** - Fast pyrolysis chromatogram of SP Bark at 550 °C by py-GC/MS. Pyrolysis heating rate of 20 °C/ms, then held for 20s. Column temperature program of 40 °C for 2 min, 6 °C/min ramp to 280 °C, then hold for 10 min.

**Table 4-12** - Proportions of key peaks of SP Bark from fast pyrolysis at 550 °C by py-GC/MS. The top 25 peaks of each chromatogram were identified using the NIST mass spectral database versions 147 and 27.

RT (min)	Registered Peak	Bark (%)
12.8	Furfural	2.8
19.1	Phenol	2.1
19.7	Phenol, 2-methoxy-	8.4
21.2	p-Cresol	2.3
22.3	Creosol	8.8
24.2	Phenol, 4-ethyl-2-methoxy-	2.5
25.5	3-Methoxyacetophenone	8.0
26.4	Catechol	29.5
28.1	1,2-Benzenediol, 4-methyl-	10.5
28.3	trans-Isoegenol	5.1
33.8	Homovanillic acid	2.9
33.9	.beta.-D-Glucopyranose, 1,6-anhydro-	2.7

Generally, across all py-grams in this section, there are big differences between the untreated and acid-washed samples. This is most likely due to the addition of the acid potentially changing or breaking down the structure of the sample in addition to leaching the earth metals. The scales of the absolute intensities per mg of sample are generally higher for the acid-washed samples (except for alkali lignin). The presence of alkaline earth metals has been seen to generate more CO<sub>2</sub> and increase water production after pyrolysis, compared to those without alkaline earth metals. The alkali lignin intensities may not have been affected significantly due to its substantial

processing prior to the acid washing. The extractible contents originally in the 'lignin' may have been removed from the various processing steps, so that the acid washing did not additionally degrade its structure (compared to the other samples).

The compounds that are mentioned in the peak tables above are those with substantial peak areas (> 5%) or the identified compound is present in all of the samples mentioned in that table. There was therefore quite a few compounds that were not included in these peak tables after normalisation. Overall, for most of the peak tables, the compounds that are missing are complex aromatic compounds that had lower peak areas. Where the peak tables of the acid-washed samples were compared to the untreated samples, the unmentioned compounds included acids (other than acetic acid, such as formic acid) and other complex aromatics structures.

The acid-treated AlkLig, MSWdig, CH and PKBag have the highest proportions of furan-containing compounds (furfural, furanmethanol and 2-furancarboxylic acid, 5-methyl) (Table 4-7, Table 4-9, Table 4-11). The presence of some alkaline metals, such as potassium, has been seen to reduce the concentration of furfurals in pyrolysis oils, whilst increasing the formation of phenolic compounds (353). This may be one of the reasons why there is a greater furfural concentration in the acid-washed samples.

In addition, furan-containing compounds are known to be produced from the pyrolysis of cellulose, which correlates with the high cellulose content of CH and PKBag. AGRdig has a reasonable proportion of these furan compounds but has a negligible change after acid-washing. The cellulose content measured in the fibre analysis of the AGRdig is the highest of all of the digestates. This may mean that the cellulose of AGRdig is more easily accessible by external forces (i.e. chemicals or heat), compared to the other digestates. Due to this, the acid-washing may have simply removed the alkaline earth metals with limited structural degradation, whereas the degradation aided the other digestates by making its cellulose content more accessible.

Both AGRdig and VGFdig (untreated and acid-washed) have relatively high 1,4-Butanediamine, 2,3-dimethoxy-N,N',N'-tetramethyl-, [S-(R\*,R\*)]- (C<sub>10</sub>H<sub>24</sub>N<sub>2</sub>O<sub>2</sub>) (Table 4-9). This is likely due to the crude protein present in AGRdig and VGFdig (Table 4-5).

Acid AlkLig has high acetic acid and 2-furanmethanol (Table 4-8). Within lignocellulosic structures, hemicellulose and lignin have acetyl groups on the side chains (463). As the sample's structure is broken down during the acid-washing, these acetyl groups-containing side chains may be weakened. These may then be more easily volatilised during the fast pyrolysis process.

Despite the acid-washing clearly reducing the alkaline earth metal content of the AGRdig (Table 4-4), the registered compounds for its py-GC/MS (Table 4-9) did not change much. The main change is the loss of cyclohexanone (C<sub>6</sub>H<sub>10</sub>O), which, due to weaker bonds from the acid-washing, most likely fractured into a variety of simpler aromatic compounds.

The high proportions of 2-methoxy phenol ( $\approx$  25 wt% of the alkali lignin's volatilised products identified by the GC/MS) is likely to be due to the high alkaline earth metal content (in Table 4-3). This would lead to an increased pyrolysis severity and higher proportions of simple aromatics.

In the digestate samples (Table 4-9 and Table 4-11), the registered peaks of 'ethanethiol' and ethene, 1,1-difluoro' are most likely bleed from the TENAX adsorbent gas trap. Compared to the other samples, the digestate py-grams have a lot fewer noticeable peaks. The anaerobic digestion and other pre-treatment that they had undergone most likely had degraded and removed parts of the sample's structure, therefore reducing the sample contents and potential compounds that could be produced by fast pyrolysis.

The acid-washed SSdig has the lowest furfural proportion of all of the digestates. This is due to the cellulose and hemicellulose fragmentation mechanism leading to higher proportions of 2-furancarboxaldehyde, 5-methyl (464).

The presence of simple aromatic compounds (such as phenol and 2-methoxy phenol) can be seen as an indicator of pyrolysis severity (465). They are both used as typical compounds of lignin pyrolysis, with the largest proportions at higher temperatures.

Untreated CH (Table 4-11) has quite high phenol, which reduced once acid-washed. This may be due to the large increase in furfural content after acid-washing, leading to the proportional decrease in phenol.

The high proportion of .beta.-D-Glucopyranose, 1,6-anhydro- in PKBag's py-gram (Table 4-11) most likely occurs due to the high cellulose content (Table 4-5) (466), whilst the high phenol, 2,6-dimethoxy-4-(2-propenyl)- would be derived from the lignin content.

The SP Bark (Figure 4-8) does not have many peaks compared to the other samples, with the largest proportion coming from catechol. This is most likely due to several reasons. With high lignin and low cellulose and hemicellulose (Table 4-5), there would be higher selectivity of aromatic compounds, with less furan-containing compounds. Tree barks are known to be a rich source of phenolic compounds (467). SP Bark, compared to most of the other samples, has negligible nitrogen and sulphur, also

reducing the number of potential compounds. The intensities (per mg of sample) of SP Bark's peaks are greater than those of the lignin products. The compounds themselves in Table 4-12 are not all simple compounds like phenol. The presence of alkaline earth metals have been shown to affect the composition of pyrolysis oils (344). As the SP Bark has low metal contents compared to the other samples, the pyrolysis oil yield is likely to be greater at the same temperature.

#### **4.2.5 Proximate Analysis, Ultimate Analysis and Derivative Thermogravimetry (DTG) of the acid-washed samples**

After the comparison of alkaline earth metals reduction by AAS, and py-GC/MS of the raw and acid-washed samples, DTG, proximate and ultimate analysis of the acid-washed samples were performed. These were done to see, in addition to the fast pyrolysis of the py-GC/MS, how else the composition of the samples had changed. Fibre analysis was attempted on the acid-washed samples. However, some of the samples dissolved into the detergent used in the Fibretherm process, so the analysis was unable to be completed.

The key differences in the proximate analysis of the acid-washed samples compared to the raw samples (in Table 4-13 and Table 4-14) is the reduction in ash and the shared increase in volatile and fixed carbon content. Coconut husk has the greatest increase in volatiles after acid-washing (Table 4-13), which is due to the fixed carbon content reducing along with the ash content. Most of the digestates had a large difference in their proximate data values after acid-washing, mostly due to their initially large ash contents. MSWdig had a large increase in volatiles ( $\approx 20$  wt%), due to a 20 wt% reduction in its ash content.

**Table 4-13** - Proximate and Ultimate Analysis of acid-washed samples. Error values were calculated by 1x standard deviation. 2 replicates were run for each sample.

		AlkLig		CH		PKBag	
		Raw	Acid	Raw	Acid	Raw	Acid
<b>Proximates (%wt, dry basis)</b>	<b>Volatiles</b>	47.6 ± 0.1	54.4 ± 1.1	63.7 ± 2.7	85.1 ± 8.1	76.5 ± 0.2	79.4 ± 0.8
	<b>Fixed Carbon</b>	31.8 ± 0.8	42.0 ± 0.9	28.2 ± 0.5	14.6 ± 8.3	21.3 ± 0.1	19.7 ± 0.1
	<b>Ash</b>	20.6 ± 0.8	1.5 ± 0.1	8.0 ± 3.2	0.4 ± 0.1	2.2 ± 0.1	1.0 ± 0.9
<b>Ultimates (wt%, dry basis)</b>	<b>Carbon</b>	47.2 ± 0.3	51.4 ± 2.3	48.4 ± 1.5	32.3 ± 2.1	49.1 ± 0.1	42.0 ± 0.2
	<b>Hydrogen</b>	3.5 ± 0.2	4.6 ± 0.2	3.8 ± 0.1	3.2 ± 0.2	5.7 ± 0.5	5.0 ± 0.0
	<b>Nitrogen</b>	0.0 ± 0.0	0.6 ± 0.0	0.8 ± 0.1	0.6 ± 0.0	1.3 ± 0.0	1.1 ± 0.0
	<b>Sulphur</b>	1.8 ± 0.2	3.1 ± 0.2	0.0 ± 0.0	0.0 ± 0.0	0.0 ± 0.0	0.0 ± 0.0
	<b>Oxygen</b>	26.9 ± 1.2	38.9 ± 2.7	38.9 ± 1.8	63.5 ± 2.4	41.7 ± 1.2	50.9 ± 0.2

**Table 4-14** - Proximate and Ultimate Analysis of acid-washed digestate samples. Error values were calculated by 1x standard deviation. 2 replicates were run for each sample.

		AGRdig		SSdig		MSWdig	
		Raw	Acid	Raw	Acid	Raw	Acid
<b>Proximates (%wt, dry basis)</b>	<b>Volatiles</b>	70.2 ± 0.3	75.5 ± 0.9	51.0 ± 0.1	66.6 ± 0.2	36.2 ± 0.1	56.0 ± 1.5
	<b>Fixed Carbon</b>	13.8 ± 0.0	19.6 ± 0.2	2.1 ± 0.1	9.9 ± 0.2	8.3 ± 0.0	9.6 ± 0.2
	<b>Ash</b>	16.0 ± 0.3	4.9 ± 0.7	46.9 ± 0.0	28.5 ± 0.1	55.5 ± 0.1	34.4 ± 1.7
<b>Ultimates (wt%, dry basis)</b>	<b>Carbon</b>	44.1 ± 0.1	46.5 ± 3.1	28.6 ± 0.3	38.4 ± 0.8	24.1 ± 0.0	38.0 ± 1.0
	<b>Hydrogen</b>	5.1 ± 0.0	5.6 ± 0.5	3.1 ± 0.1	5.0 ± 0.1	1.7 ± 0.0	4.7 ± 0.0
	<b>Nitrogen</b>	3.2 ± 0.0	2.7 ± 0.5	3.4 ± 0.0	4.1 ± 0.1	1.5 ± 0.0	2.1 ± 0.0
	<b>Sulphur</b>	0.3 ± 0.0	0.2 ± 0.0	1.5 ± 0.0	0.6 ± 0.0	0.2 ± 0.0	0.4 ± 0.0
	<b>Oxygen</b>	31.3 ± 0.3	40.1 ± 4.1	16.4 ± 0.3	23.3 ± 0.9	16.9 ± 0.0	20.5 ± 1.0

The thermal degradation of biomass can be subdivided into 3 phases. Pure xylan and cellulose samples were run to illustrate 'ideal' thermal degradation curves. The temperatures at which the degradation of these occurred are visible on each DTG curve. The first phase occurs between room temperature and around 160 °C, where the moisture is driven from the biomass sample.

Past 180 °C until 420 °C is the devolatilisation phase where the majority of sample masses is lost, which is made up of two parts. The first part of the second phase features between 210 and 310 °C (for the samples in this work) and shows the decomposition of hemicellulose. AlkLig, LB and AGRdig have the greatest hemicellulose contents (Table 4-5) and have reasonable mass loss per second values until the primary shoulder (Figure 4-12 and Figure 4-13). However, several other samples also have high mass loss per second in this region (VGFdig, CH, and PKBag in Figure 4-11, Figure 4-14 and Figure 4-15).

The second part, displaying the decomposition of cellulose, occurs around 310 and 430 °C. This is evident with AGRdig, PKBag and CH, which have high cellulose content (Table 4-5). AlkLig and SSdig (Figure 4-9 and Figure 4-10) do not have secondary shoulders in this area. As their cellulose contents vary, the lack of secondary shoulders may be due to the higher metal contents (Table 4-3).

The third phase indicates the tailing section, highlighting the lignin decomposition and char residue degradation. The lignin decomposition is not limited solely to the 3rd phase (post-430 °C), as it begins during the devolatilisation phase and completes at the end of the DTG curve (468). The feedstocks with the highest lignin contents (AlkLig, LB, CH, SP Bark) do not have any humps after the cellulose shoulder, but a slow decrease of mass loss per second.

Lignoboost has the greatest mass loss of the untreated lignin samples (Figure 4-9), and its cellulose peak occurs at the latest temperature (408 °C). Alkali Lignin has the earliest cellulose peak of the lignin products, which is most likely due to the high sodium content (308 °C) (Table 4-3).

From the residue DTGs (Figure 4-10), PKBag and SP Bark have their cellulose peak at the same point (367 °C). This is probably due to the low metal contents (Table 4-3), with the CH having higher potassium, catalysing some of CH's structure to be volatilised at lower temperatures. The mass losses of CH and SP Bark are similar, but the shape of the curve is different. This is likely due to the differing fibre analysis values (Table 4-5). SP Bark has 25 wt% less cellulose than CH (hence less mass loss at the cellulose peak), and 25 wt% more lignin. The increased lignin is present in Figure 4-10 as a consistent decrease in mass loss from 500-900 °C. In samples with less lignin, like PKBag, there is a sudden drop in mass loss after around 400-500 °C. The PKBag mass losses are the greatest of the residues, likely due to the greater volatile matter that is present (Table 4-2).

The acid-washed samples appear to have greater mass losses throughout than their unwashed counterparts. As ash is the key component that is reduced by the acid-washing (which is more noticeable in Table 4-13), the mass lost during DTG for the acid-washed samples would be in greater proportions due to the ash being a smaller component than in the raw material.

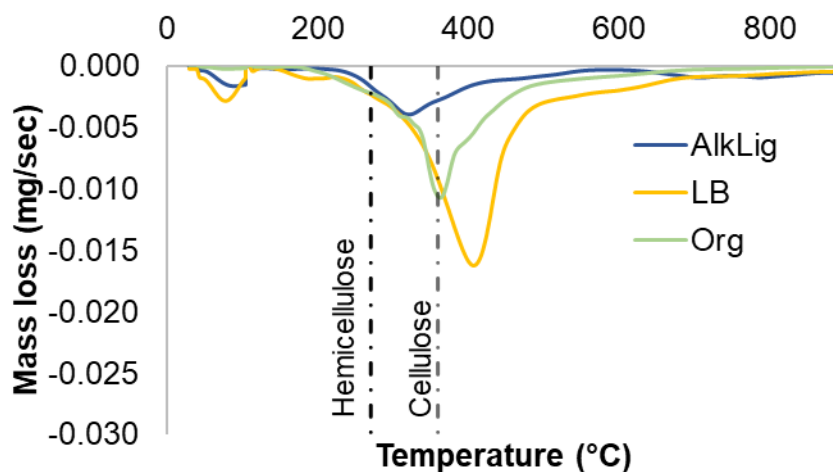


**Figure 4-9** - DTG of the lignin products (alkali lignin, Lignoboost, organosolv lignin). Conditions: Starting mass  $\approx$  10 mg, pyrolysed in a nitrogen atmosphere of 30 ml/min with a heating rate of 25 °C/min.

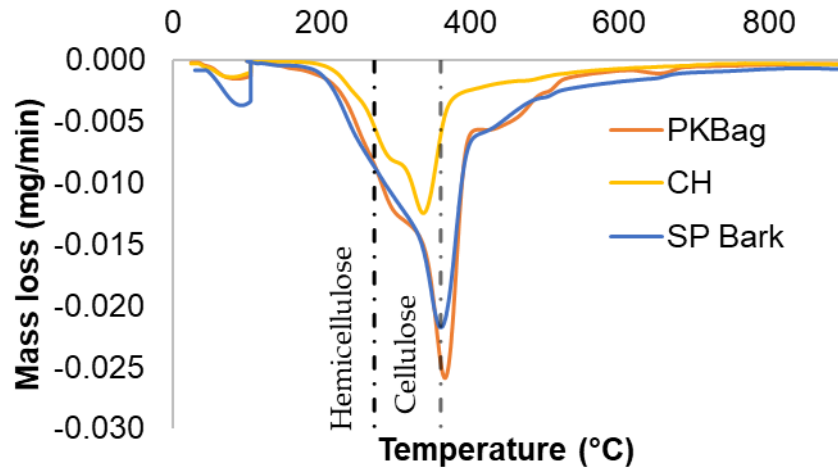


**Figure 4-10** - DTG of PKBag, coconut husk and SP Bark. Conditions: Starting mass  $\approx$  10 mg, pyrolysed in a nitrogen atmosphere of 30 ml/min with a heating rate of 25 °C/min.

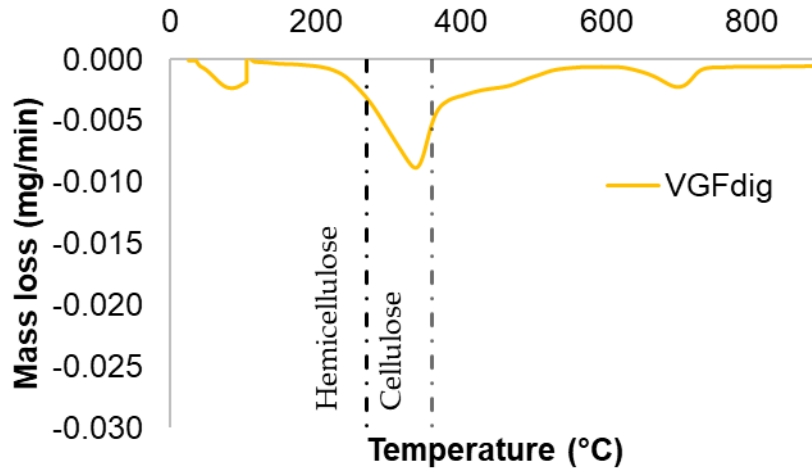


**Figure 4-11** - DTG of Vegetable, Garden and Fruit residue digestate (VGFdig). Conditions: Starting mass  $\approx$  10 mg, pyrolysed in a nitrogen atmosphere of 30 ml/min with a heating rate of 25 °C/min.

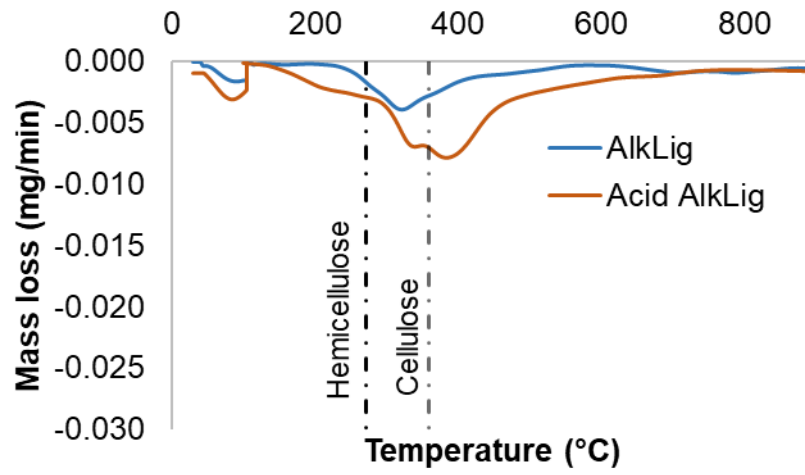


**Figure 4-12** - DTG of untreated and acid-washed alkali lignin. Conditions: Starting mass  $\approx$  10 mg, pyrolysed in a nitrogen atmosphere of 30 ml/min with a heating rate of 25 °C/min.

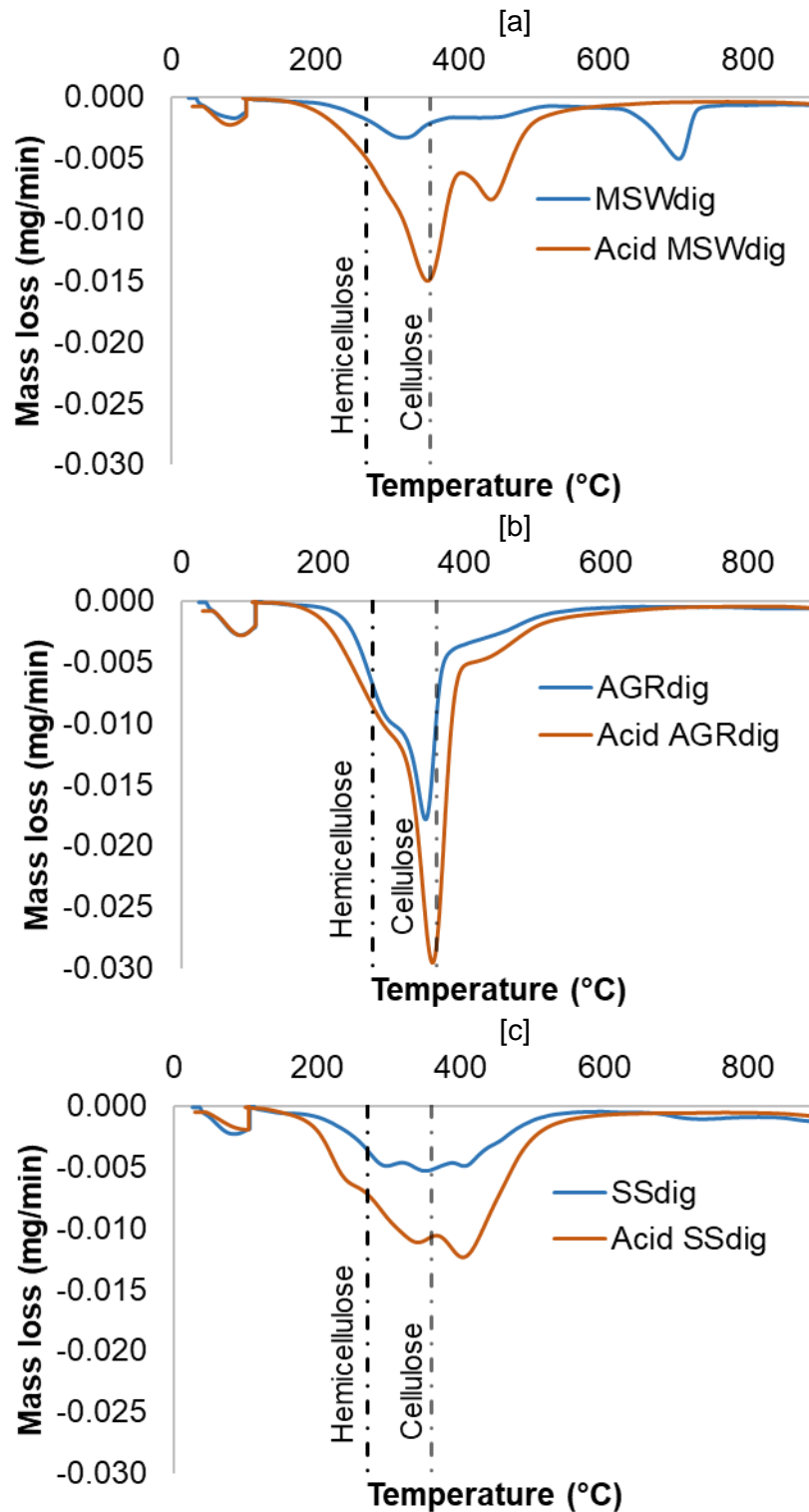


**Figure 4-13** - DTG of untreated and acid-washed [a] Municipal Solid Waste digestate (MSWdig), [b] agricultural residue (AGRdig) and [c] sewage sludge digestate (SSdig). Conditions: Starting mass  $\approx$  10 mg, pyrolysed in a nitrogen atmosphere of 30 ml/min with a heating rate of 25 °C/min.

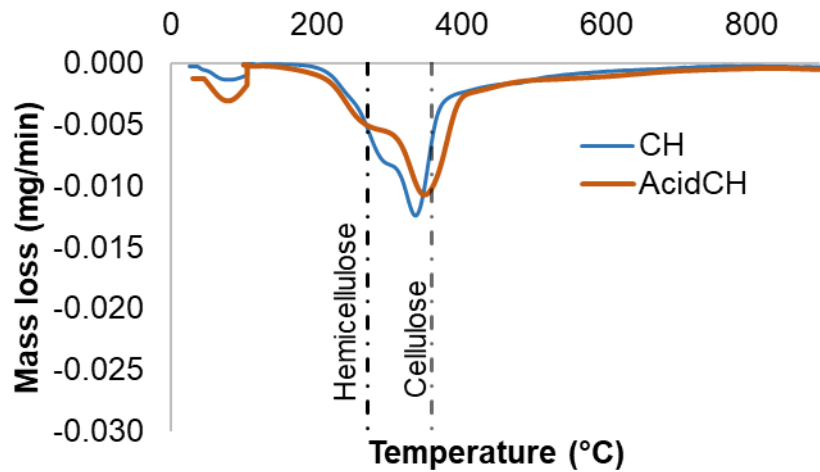


**Figure 4-14** - DTG of untreated and acid-washed coconut husk. Conditions: Starting mass  $\approx$  10 mg, pyrolysed in a nitrogen atmosphere of 30 ml/min with a heating rate of 25 °C/min.

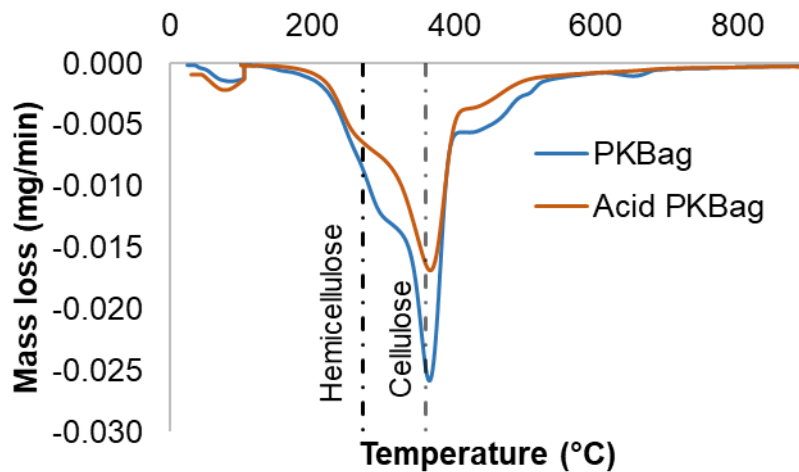


**Figure 4-15** - DTG of untreated and acid-washed sugarcane bagasse from Pakistan (PKBag). Conditions: Starting mass  $\approx$  10 mg, pyrolysed in a nitrogen atmosphere of 30 ml/min with a heating rate of 25 °C/min.

The main difference between the untreated and acid-washed CH (Figure 4-14) is the location of the cellulose peak, which occurs about 20 °C higher for the acid-washed sample (356 °C compared to 338 °C). Across all untreated and acid-washed samples (Table 4-15), the cellulose volatilisation phase (between 310 – 430 °C as stated earlier) takes place at a higher temperature once the samples have undergone acid-washing. This

temperature is unclear for SSdig and AlkLig (Figure 4-9 and Figure 4-13) as they have several small humps. For most of the samples, the temperature that this volatilisation appears to occur at is closer to that of pure cellulose (361 °C).

**Table 4-15** - Temperatures (°C) at which the cellulose volatilisation phase occurred for each untreated and acid-washed sample.

State of sample	PKBag	CH	SSdig	MSWdig	AGRdig	AlkLig	Cellulose
Raw	365	338	351	336	333	308	360
Acid wash	365	356	409	361	356	338	

The changes in cellulose volatilisation temperature in Table 4-15 were taken by locating the point in the DTG curves where the mass loss was greatest between 310 – 430 °C. They are most likely due to the removal of alkaline earth metals and their salts. The metals and metal salts would not appear in the DTG graphs as their boiling points are commonly above 1000 °C (469, 470), but the change in metal contents can be seen in atomic absorption spectroscopy as with Section 4.2.2. However, the organically-bound metals may form carbonates after thermal decomposition of the lignin-derived phenol groups have been produced. The boiling points of these are lower than the pure metal and metal salts, with K<sub>2</sub>CO<sub>3</sub> (as an example) being stable up until around 850 °C (456). Although the change in volatilisation temperature (between 0-58 °C) may not be a large proportion of fast pyrolysis temperatures (between 450-650 °C), the slight reduction in energy intensity would improve the feasibility of a large scale pyrolysis plant. This is due to the lower necessary temperature lowering the cost necessary to generate the heat requirements, and therefore reducing the pyrolysis plant's payback period.

### 4.3. Conclusion

In this chapter, a wide variety of potential feedstocks were screened by a selection of characterisation methods.

From the proximate and ultimate analysis, all of the samples had volatiles content above 45% (except MSWdig), which indicated a larger proportion of oil which would be generated by fast pyrolysis. In addition, the carbon and oxygen content were greatest for lignoboost (LB) and the SP Bark. The ash content was above 10 wt% for most samples, except organosolv (Org), SP Bark, coconut husk (CH) and sugarcane bagasse (PKBag). High ash increases the risk of coking, slagging, and fouling. The lignin products (alkali lignin, LB, and Org) and the SP Bark had the greatest HHVs.

With the atomic absorption spectroscopy, the digestates had consistently high alkaline earth metals (AEMs). The lignin products had low metal contents, except for high sodium levels in the alkali lignin. The residues had low levels of AEMs, predominantly calcium and potassium. These are likely to be found in biomass due to bioaccumulation.

After a mild acid-washing of the feedstocks with the highest AEMs, the metals contents decreased. It also led to a reduction in ash content.

In terms of the fibre analysis, the SP Bark, coconut husk, alkali lignin and lignoboost had the greatest lignin contents (>39 wt%). However, the coconut husk has high cellulose (along with the sugarcane bagasse).

This was also reflected in the pyrolysis-gas chromatography/mass spectrometry, whereby the lignin products have tall peaks of only lignin-derived compounds (those with phenolic groups including 2-methoxy phenol and phenol). The py-gram for the SP Bark is the most similar to the lignin products. The samples with higher holocellulose (cellulose and hemicellulose) contents include peaks for furfural and acetic acid. After the acid-washing, the furfural and acetic acids contents grow.

Across all of the samples, the softwood pine tree bark (SP Bark) was found to be the most ideal. This is because of the low alkaline earth metal contents, and its closeness in structure to expensive purer lignin products across a range of characterisation methods which would be accessible for a very low cost.

The least suitable feedstocks for the production and valorisation of fast pyrolysis oil were the digestates. This was assumed to be due to the high ash content and/or high alkaline

earth metals content. Owing to this, the feedstocks with high alkaline earth metals content underwent a mild acid-washing method. It was found that the high metal-containing samples endured more intensive pyrolysis at the same temperature as those with low metal contents. However, after acid-washing, the pyrolysis products were severely impacted. As the acid-washing severely decreased the mass of sample too, it was deemed to not be a necessary step in the valorisation of the high metal-containing lignin-rich residues.

The sugarcane bagasse (PKBag) can be considered to be a middling feedstock. The PKBag has lower levels of lignin compared to the more suitable samples (24 wt% compared to > 40 wt%), and minimal alkaline earth metal concentrations. However, from the fast pyrolysis-GC/MS, some of its tallest peaks are holocellulose-derived, rendering it less of an ideal lignin-rich feedstock.

Regarding the well-performing SP Bark, unfortunately, as the only known information about the tree bark from Golden Acre Park (Leeds) was its source, it seemed necessary to further explore tree barks. Therefore, the main conclusion from this study was that a selection of barks from a variety of species should be investigated in the following chapter (Chapter 5). This was done to see whether the bark explored in this chapter was a special case or characteristic of more barks. In addition, the characterisation covered in this work provides additional datasets to be used to explore valorisation routes of lignin-rich biomass residues.

## Chapter 5 – The characterisation and pyrolysis behaviour of tree barks

### 5.1 Introduction

The potential of tree bark as a feedstock for fast pyrolysis has been explored in Chapter 4, with its performance as a low-cost residue matching that of high-cost commercial lignin products. However, the specific species of bark tested in the previous chapter (SP Bark) was unable to be identified. In the present chapter, a wide variety of tree bark species will be characterised to explore whether the high performance of the unknown bark was a ‘one-off’, or a common trait of barks.

Samples of the 11 tree bark species were characterised by a variety of methods, including proximate and ultimate analysis (Section 3.2 and 3.3), atomic absorption spectroscopy (Section 3.6), fibre analysis (Section 3.4) and pyrolysis-gas chromatography/mass spectrometry (py-GC/MS) (Figure 5-1).

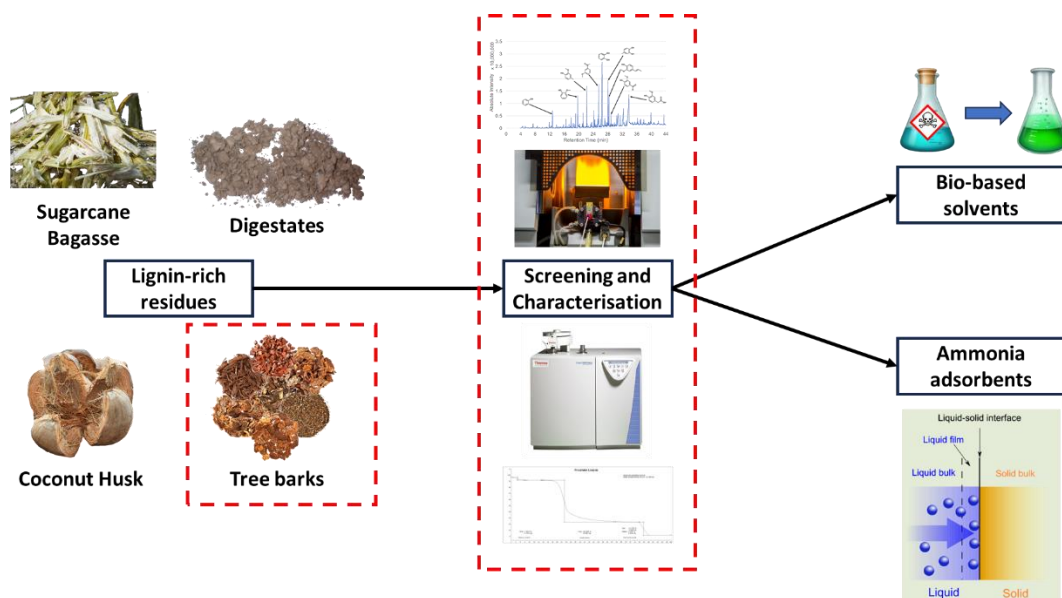


**Figure 5-1** – The overall scope of this study. The work covered in Chapter 5 is denoted by red dotted lines.

As most literature categorises bark by its family, this work is being done to show the differences of species within the same families through characterisation. Based on some of the results obtained from the fibre analysis and pyrolysis-gas chromatography/mass spectrometry, a selection of the barks underwent solvent extraction to remove the suberin

content. In these cases, this was done by both Soxhlet extraction (Section 3.9.2) and Accelerated Solvent Extraction (ASE) (Section 3.9.3). The post-solvent extraction solids were unable to be recovered after ASE due to the sample being mixed with sand, so the post-Soxhlet solids and liquids were analysed by py-GC/MS at 550 °C (Section 3.7.2). The post-ASE liquid was analysed by liquid-injection GC/MS (Section 3.10).

### **5.1.1 Background**

Bark is the internal tree's protection from the external environment, including attack from organisms (fungi, insects, birds and mammals) and damage from the sun (471). The structure of tree bark has evolved for each species based on the required protection. For example, in areas that are prone to wildfires, tree species such as Scots pines have evolved to have thick, plated bark to protect themselves. The bark of the silver birch tree is white, which enables it to reflect sunlight and protect itself from UV rays. Tree barks such as cork oak bark are known for having increased protection from heat and fire (472). However, this is dependent on the thickness of the bark. Cork oak barks can be harvested between 12-20 times throughout its life, with the fire protection decreasing as the bark thinness becomes more common (472).

In cases where a live standing tree has over 90% of its bark stripped (around the circumference of the tree), the whole tree normally dies. This is because of the loss of protection, with the tree becoming prone to infection and other forms of damage (473). Bark is composed of an inner bark (secondary phloem) and outer bark (periderm). The height along a tree determines the proportion of inner and outer bark. Near the top of the tree is where the most inner bark is found, whilst the greatest proportion of outer bark is located at the tree trunk's base. The structural composition of inner and outer bark is different, meaning that the composition of the overall bark changes at each point along the tree's height (417). In addition, due to the effect of the external environment on trees, the bark thickness and bark structure can differ across time of year but also the same species in different locations. However, although the composition of a tree bark may change based on the location on the tree, the focus of this study is on utilising tree bark residues rather than harvesting a live tree. Therefore, the tree bark that is accessible as a batch is likely to be the remains after debarking has already occurred (such as at a sawmill), so the specific location on the tree where the bark was generated does not necessarily matter.

The chemical components within bark differ to those found from the wood of the same tree. Compared to wood, bark has much higher chemical variability (474). Soluble substances in the lignin are nearly double in bark, whilst the polysaccharide content can be half that found in wood (475).

As both the structure and contents of tree bark can differ between the species, position on tree and source, it is necessary to explore a variety of tree bark species. This would help to validate whether the tree bark used in Chapter 4 was representative of all barks or was an independent sample.

Trees can be divided into two main categories. Conifers, or softwoods, and broadleaves, or hardwoods. Hardwoods are more hard-wearing, so are used in high-impact projects such as construction, cladding, fencing, and flooring. Softwoods make up 80 vol% of the timber that is used globally and are more versatile than hardwoods. These are used across a wider variety of applications including picture frames, paper manufacture, doors and carpentry (476). The bark density of softwood species (which include pines, yew and cypress trees) is relatively equal to wood density ( $100\text{-}400\text{ kg/m}^3$ ) (477), whilst the bark density of hardwood species (including oak, walnut, ash, beech, eucalyptus) is 40-50% lower than the density of the wood of that tree (418). Wood density has been found to be between  $400\text{-}800\text{ kg/m}^3$ . The wood contained in hardwoods is denser than the wood in softwoods.

Regarding the thermal conversion of biomass, woods are one of the most common biomasses used in fast pyrolysis literature (478) for the production of bio-oils. Tree barks, more specifically, are less established than woods but still common in literature. Many researched tree barks are from the pine species, as a representative of softwoods. Oak wood is generally used as a hardwood representative (478-482). The fast pyrolysis of cypress and yew family tree barks are not as present in the literature. Cypress wood, and its sawdust, another by-product of wood timber production, has been used in fast pyrolysis literature (483, 484). Here, increasing pyrolysis heating rates (between  $0.1\text{-}10\text{ }^\circ\text{C/s}$ ) was shown to increase the yields of aromatic compounds presents in the tar/pyrolysis oil, with the major tar components identified as phenols, furfural, acetic acid, catechol, and cellulose-derived glucose for woody biomass.

In addition to lignocellulosic components, barks also include high molecular weight tannins (485-487), pectic substances, and cross-linked polyesters (cutin and suberin) (487-492).

Tree bark can comprise 10-15% of tree stem volume (417), or around 20 vol% of the above-ground biomass of trees (418). Bark can be separated from the tree either through natural shedding, or by debarking. It is a normal part of the tree maturation process for bark to be shed. For species including pine, maple, ash and oak, the bark develops from the inside to the outside, so the older external bark is pushed out as the newer bark develops (493).

Trees are debarked primarily during the timbering process. The bark that is removed from trees tends to be greater during the growing season, compared to the dormant season (494). Prior to the 1970s, trees were commonly debarked in the forest where it was cut, but this action was moved to the sawmill due to the high costs. Although bark on a live tree is there to provide protection, once it has been felled, the bark can lead to damage of the tree. Some of the damage arises from the moisture trapped behind the bark, speeding up rotting of the wood. Once a tree has been cut into logs, there are a greater number of openings that allow insects to hide behind the bark. Bark removal can stop this from occurring (495).

Trees can be debarked by a variety of methods. Between the 1940s and 1970s, there was growing interest in the chemical debarking of trees. In this process, the bark around a small circumference of the tree was removed, and the chemical was applied directly onto the tree. After 4-12 months, and the tree had died, the bark became looser and easier to remove. Chemical debarking has not been wide-spread in the last half-century. This is because it was only effective when the sap is flowing in the tree, the chemicals used were extremely toxic, and the killing of trees up to a year before felling season leads to a reduction in tree growth, which can have a significant impact on timber volumes (494). In cases where labour costs are low, manual debarking is preferred over mechanised debarking. Manual debarking also has low environmental impacts, and no substantial fibre loss, but is very labour intensive (494). The two main environmental impacts associated with manual debarking occur due to the particulate environmental matter generated from the sawmilling itself, and the transportation of the bark (496). The particulates can lead to impacts including acidification, global warming, eutrophication, photo-oxidant formation and human toxicity (497).

Where woodchips are being generated from trees, bark can be removed by compression debarking. This can be done either on logs before they are chipped, or on the wood chips themselves. In this process, logs or bark-on woodchips are passed between two rotating

steel rolls. The intention of this debarking method is for the compression and shear forces to break the wood-bark bonds. The bark adheres to the roll's surface, then is removed later with roll scrapers (494).

Common debarking units that tend to be installed at sawmills are Rosser-head debarkers. In these units, a log is mounted onto a carriage. The log is then rotated around, whilst the Rosser-head saws off the bark (494). Debarking with harvester heads follow the compression principle so that the bark loosens. The harvester head also has delimiting knives to aid in bark removal. The use of these heads are well-established for *Eucalyptus* trees across the world (494).

If the volume of barks is conservatively estimated to be 10% of the tree, approximately 300-400 million m<sup>3</sup> of bark from lumbered roundwood is estimated to be generated each year (477). However, it is difficult to quantify the amount of bark that is produced due to large uncertainties. This is because only a small proportion is commercially utilised.

#### **5.1.1.1 Applications of tree bark**

The applications of tree bark can change based on the composition and structure of tree barks, due to these being entirely dependent on species and location of growth.

Historically, barks have been used as a form of medicine as they contain essential oils, antibiotics, vitamins, carbohydrates, and alkaloids. Some of these bark-derived medications offer the same protection as bark do on the trees themselves, namely for its antiviral, antibacterial and antifungal properties (477).

Most of the main timbered species of trees in the United Kingdom are hardwoods, followed by softwood pines.

A current application of bark is a source of energy through incineration. The heating value of bark is similar to wood ( $\approx 16.23$  MJ/kg), but it has a high moisture content. Bark can be briquetted or pelletised to increase caloric density. As a briquette, the bark is mixed with sawdust (another residue from timber processing) and straw to help to bind the briquette, with wax being added to reduce the moisture content and increase the solidity (477).

A low-value application of bark is to aid mulching in agriculture. The mixture of bark in heavy soil can increase absorption of water, reduce, or prevent compaction, lower soil erosion and aerify the soil. However, due to bark's low nitrogen content, composting is

needed to accelerate the decay. Some species of bark are unsuitable for mulching if they have high chemical contents (477).

Bark has also been used in the production of fibreboards. However, due to bark's slightly worse mechanical properties compared to wood, a 100% bark-derived piece of board is not possible. The bark is able to be present, but this is mixed with wood and resins (with the exact bark proportion being dependent on the specific application and bark species). As bark is a source of polyphenols (498), it has also been used in the production of plastics and aggregates, adhesives and tannings agents (96, 477).

Barks are a known natural source of flavonoids (459). These are bioactive compounds said to have anti-inflammatory, antioxidant and antiallergic properties (457). The proportions of flavonoids present in bark is dependent on, as discussed earlier, several different factors relating to how and where the bark was grown. Various types of solvents have been used to extract flavonoids, with a more recent interest in environmentally friendly solvents. These have included ethanol and water (486, 499, 500), as well as deep eutectic solvents (501) and ionic liquids (457). Extraction with ethanol and water have also been used in the extraction of tannins from bark (502, 503). Tannins are another bioactive compound that are commonly found in tree barks, leaves, seeds, and wood amongst others. The tannins stored in bark help to protect the tree from fungal or bacterial infections (458). Another form of extractives in bark are fatty acids. These have been identified in a variety of pine barks (429, 504, 505). They are most likely derived from suberin, a highly polymerised lipid material (506). The lipids content of barks is considered to be higher than those in woods (507). Although these may only make up 1-2 wt% of the bark's composition (429), the concentration of suberin-derived compounds increases in the pyrolysis products as the temperature increases (508). The suberin content volatilises at and over 650 °C, whilst lignin and carbohydrate-derived products decrease significantly after 750 °C (509).

#### **5.1.1.2 Characterisation of tree barks**

The barks that were characterised in this chapter were sourced by Abbey Timber (Duns, Scotland), and consisted of noble fir (NF), larch (L), Douglas fir (DF), Sitka spruce (SS), Norway spruce (NS), European silver fir (ESF), grand fir (GF), Western hemlock (WH), Western red cedar (WRC), Nootka cypress (NC) and Lawson cypress (LC) (Section 3.1.4).

Most of the literature regarding tree barks utilise Douglas fir, Norway spruce and Western hemlock, as they are considered representatives of fir and spruce species (510).

Douglas fir is so widely used as it is the second most common non-native trees species in European forests, due to its desirable wood properties and high growth rate (511). These desirable wood properties are for its suitability as timber, covering its density, bending stiffness, and bending strength. Douglas fir has been characterised by ultimate analysis on numerous occasions (422, 425, 426).

Norway spruce is native to Scandinavia and central Europe (512), and occupies around between 15-30% of central Europe's forests (513). Norway spruce characterisation has been done in some pieces of literature (423, 424, 426).

Noble fir, Western red cedar and Western hemlock are native to Canada and the west coast of north USA (512). Western red cedar (426) and Western hemlock have been characterised for their proximate and ultimate analysis values (422, 426). Although recorded in literature to a lesser extent, larch and grand fir tree bark has been characterised also (421).

Apart from these named species, a lot of literature simply refers to the barks by their family. From data collected by the Phyllis database (426), the range of proximate and ultimate analysis values show that within the tree families, there is a lot of variety (Table 5-1). One such reason for the large range of ash content (in Table 5-1) may be due to the presence of extraneous materials during the debarking and handling process (423).

**Table 5-1** - Data of proximate and ultimate analysis taken from the Phyllis database (426).

	<b>Variable</b>	<b>Softwood barks</b>	<b>Pine barks</b>	<b>Spruce barks</b>
<b>Proximates (%wt, dry basis)</b>	<b>Moisture content (wt%, a.r.)</b>	9 – 50	5 – 16	0.5 – 8.7
	<b>Volatile Matter</b>	N/A	63 – 73	70.3 – 85.0
	<b>Fixed Carbon</b>	N/A	24.2 – 26.6	11.2 – 25.5
	<b>Ash</b>	2.3 – 5.5	1.6 – 10.7	1.8 – 4.2
<b>Ultimates (wt%, db)</b>	<b>Carbon</b>	50.4 – 55.1	47.8 – 53.9	48.6 – 54.7
	<b>Hydrogen</b>	5.1 – 6.3	5.6 – 5.9	5.1 – 6.7
	<b>Oxygen</b>	35.8 – 40.1	35.4 – 39.7	36.3 – 42.0
	<b>Nitrogen</b>	0.0 – 0.6	0.0 – 0.7	0.0 – 0.7
	<b>Sulphur</b>	0.0 – 0.1	0.0 – 0.05	0.0 – 0.2

Fast pyrolysis of tree barks has been done across academia for nearly a decade (432). However, it is difficult to find literature regarding this (514).

No literature was found where British-grown tree barks were analysed. Most barks that have been analysed were sourced from the United States of America and Scandinavia. This is likely due to the volume of timbered forests in these countries (as discussed earlier), generating the residue during the debarking process.

The accumulation of alkaline earth metals has been established in tree barks (515). The concentration of magnesium is generally greater in the outer barks of trees (516). Depending on the species, the inner bark has either similar Mg concentration than the outer bark, or significantly lower (516). Calcium and potassium are essential for tree growth, so they are expected to be present within tree barks (427). Calcium is known to be higher in tree barks compared to the other parts of a tree (sapwood and heartwood) (517). The levels of potassium in barks are expected to be higher in low environmental stress sources (such as forests), and lower whilst in high environmental stress sources (urban areas) (475). Tree barks have been observed to be sources of sodium in countries including Uganda, as various species of apes chew them for their sodium content (518). Tree bark is known to contain iron, with them being utilised as a form of environmental monitoring (519). Some species of bark (such as *Simplocos*) have been observed to have high aluminium contents (520).

The lignocellulosic composition of tree barks can vary quite significantly. The values of cellulose, hemicellulose, lignin and extractive content change between tree species (428-431), location of bark on the tree (521), and location of the trees.

**Table 5-2** - Range of lignocellulosic compositions for softwoods and hardwoods in the literature (428-431, 521). Values given as weight% on a dry basis.

	<b>Softwoods</b>	<b>Hardwoods</b>
<b>Cellulose</b>	17.4 – 35.2	37.5 – 56.0
<b>Hemicellulose</b>	14.7 – 25.0	13.5 – 23.7
<b>Lignin</b>	13.4 – 51.2	16.9 – 30.1
<b>Extractives</b>	15.7 – 30.0	4.3 – 10.2

In Great Britain, Sitka spruce accounts for half of the stocked area (including those managed by the Forestry Commission, and on private land) (88) (Table 5-3).

**Table 5-3** - Stocked areas of tree species in Great Britain (88).

<b>Species</b>	<b>Stocked area (ha)</b>
<b>Sitka spruce</b>	682.1
<b>Scots pine</b>	241.3
<b>Larches</b>	133.3
<b>Lodgepole pine</b>	106.4
<b>Norway spruce</b>	61.6
<b>Corsican pine</b>	48.6
<b>Douglas fir</b>	45.4
<b>Other conifers</b>	39.4
<b>Total</b>	<b>1357.4</b>

## 5.2 Results and Discussion

In this results and discussion section, the characterisation of the 11 tree bark samples is outlined. After the fibre analysis (Section 3.4) and py-GC/MS (Section 3.7.2), solvent extraction was performed. The barks and their extracted contents (after solvent extraction) were analysed further by proximate analysis, ultimate analysis, fibre analysis and py-GC/MS.

### 5.2.1 Proximate and Ultimate Analysis

In this section, the values of the barks after proximate and ultimate analysis are outlined, according to the method in Section 3.2 and Section 3.3.

**Table 5-4** - Proximate and Ultimate Analysis of cypress barks, with higher heating values (HHV) estimated with 3 methods. Error values were calculated by 1x standard deviation. WRC = Western red cedar, NC = Nootka cypress, LC = Lawson cypress.

Sample Name		WRC	NC	LC
Proximates (%wt, dry basis)	Volatiles	80.7 ± 2.2	84.4 ± 0.0	77.2 ± 0.3
	Fixed Carbon	17.9 ± 1.5	13.4 ± 0.0	22.0 ± 0.1
	Ash	1.3 ± 0.8	2.2 ± 0.0	0.8 ± 0.4
Ultimates (%wt, dry basis)	Carbon	41.7 ± 6.7	50.0 ± 1.8	47.8 ± 0.0
	Hydrogen	7.1 ± 0.6	6.0 ± 0.3	6.2 ± 0.1
	Nitrogen	0.7 ± 0.1	0.7 ± 0.0	0.8 ± 0.0
	Sulphur	0.0 ± 0.0	0.0 ± 0.0	0.0 ± 0.0
	Oxygen	50.6 ± 8.8	43.3 ± 0.1	44.4 ± 0.1
HHV (MJ/kg)	Channiwala and Parikh	17.6	20.0	19.4
	Friedl	16.5	20.0	19.1
	Dulong	15.2	17.8	17.1
H/C Molar Ratio (daf)		2.01	1.43	1.54

**Table 5-5** - Proximate and Ultimate Analysis of pine barks, with higher heating values (HHV) estimated with 3 methods. Error values were calculated by 1x standard deviation. NF = Noble fir, L = Larch, DF = Douglas fir, SS = Sitka spruce, NS = Norway spruce, ESF = European silver fir, GF = Grand fir, WH = Western hemlock.

Sample Name		NF	L	DF	SS	NS	ESF	GF	WH
Proximates (wt%, d.b)	Volatiles	70.3 ± 0.3	70.1 ± 0.0	72.9 ± 0.4	69.8 ± 2.8	85.7 ± 0.0	78.9 ± 0.9	79.9 ± 0.0	70.1 ± 0.1
	Fixed Carbon	29.5 ± 0.3	28.7 ± 0.1	26.8 ± 0.5	26.5 ± 0.4	10.3 ± 0.0	20.5 ± 1.5	20.0 ± 0.0	28.9 ± 0.6
	Ash	0.2 ± 0.1	1.2 ± 0.1	0.4 ± 0.1	3.7 ± 2.4	4.0 ± 0.4	0.6 ± 0.6	0.1 ± 0.0	1.0 ± 0.5
Ultimates (wt%, d.b)	Carbon	54.1 ± 0.5	50.2 ± 0.4	49.7 ± 1.0	46.2 ± 0.3	46.0 ± 0.5	44.7 ± 4.5	47.8 ± 0.0	49.8 ± 0.3
	Hydrogen	5.7 ± 1.1	5.1 ± 0.5	5.1 ± 0.5	5.6 ± 0.3	5.4 ± 0.0	5.0 ± 0.5	5.9 ± 0.1	5.3 ± 0.0
	Nitrogen	0.7 ± 0.0	0.7 ± 0.0	0.6 ± 0.0	0.8 ± 0.0	0.8 ± 0.0	1.0 ± 0.0	0.7 ± 0.0	0.5 ± 0.0
	Sulphur	0.0 ± 0.0	0.0 ± 0.0	0.0 ± 0.0	0.0 ± 0.0	0.0 ± 0.0	0.0 ± 0.0	0.0 ± 0.0	0.0 ± 0.0
	Oxygen	39.4 ± 1.6	42.8 ± 0.1	44.3 ± 0.1	43.8 ± 0.5	43.7 ± 0.5	48.7 ± 0.5	45.6 ± 0.0	44.5 ± 0.0
HHV (MJ/kg)	Channiwala and Parikh	21.5	19.1	18.8	18.1	17.8	16.5	18.9	19.0
	Friedl	21.6	19.7	19.5	18.3	18.2	17.7	19.0	19.6
	Dulong	19.4	16.7	16.2	15.7	15.5	13.6	16.5	16.4
H/C Molar Ratio (daf)		1.25	1.21	1.23	1.43	1.41	1.34	1.48	1.26

In Table 5-4 and Table 5-5, the volatile matter (VM) for all tree barks were above 70 wt%. High volatile matter in biomass is likely to contribute to high pyrolysis oil yields from fast pyrolysis (436). ESF, GF and NS have volatile contents greater than that found in the literature for pine barks (63 – 73 wt%) (426). However, NS has the greatest, with 85.7 wt%. In literature pertaining to spruce barks, more specifically, they have VM between 70-85 wt% (423, 424). The volatiles content of the cypress barks are the second highest of the tree barks. The volatile matter of the barks is likely impacted by the accumulation of volatile organic compounds (VOCs) in the soil in which the trees have grown (522). In this scenario, the Scottish barks in this study are likely to have grown in higher VOC-contaminated soil than those in the literature. It is unknown why this might have occurred, but it may be due to slightly increased levels of pollution where the Scottish barks were sourced from, compared to the literature. No information could be found regarding pollution levels around these growth sites so a definitive answer cannot be given.

In addition, NS also has the lowest fixed carbon (FC) content (10 wt%). This adheres closely with the spruce bark FC range (11.2 – 25.5 wt%) (423, 424) from literature. For the other pine barks in this study, only SS (26.5 wt%) falls within the range for pine barks in the literature (24.2 – 26.6 wt%).

Both spruces (SS and NS) have the highest ash content, around 4 wt%. This has been observed in the literature (523).

The CHNSO values of the pine barks (Table 5-5) are very similar to each other. The Norway spruce CHNSO values are similar to that in the literature (524). The ultimate analysis of DF differs to that in the literature (422), with lower carbon and hydrogen present in this work. This may be due to international variations.

The density of bark relates to its carbon content (418). The three cypress barks were the lightest samples to hold, which corresponds with the carbon contents being among the lowest of the barks (in Table 5-6). In particular, WRC had the lowest C content (41.7 wt%).

In addition, the cypress family barks have consistently slightly higher H values (6-7 wt%) than the pine barks (5-6 wt%). The oxygen contents in the literature for pine barks had a range of 35.4 - 39.7 wt%. In the data outlined in this chapter, all of the pine barks have higher oxygen contents than in the literature (426) (above 42.8 wt%), except for NF (39.4 wt%). This difference is likely due to international variation. In the Netherlands (where the literature data was generated from), trees are planted in greater densities than in the UK

(Table 5-6). As oxygen is generated in plants and trees via photosynthesis, the increased tree planting density in the Netherlands may reduce the light getting to each tree individually. In turn, less photosynthesis may be occurring, reducing the oxygen content (compared to the Scottish trees). Although this may not be a considerable difference in planting density, it may have contributed to the change in the pine bark's oxygen contents.

**Table 5-6** - Estimated planting density of trees in the UK compared to the Netherlands.

	<b>Woodlands (hectares)</b>	<b>Number of trees (525)</b>	<b>Trees per hectare</b>
<b>United Kingdom</b>	3,250,000 (526)	3,004,205,568	924
<b>The Netherlands</b>	360,000 (527)	343,683,840	955

The larch bark data is similar to that in the literature (from China) (528). The volatile matter in the present work is 5 wt% lower, with the fixed carbon being 5 wt% higher. However, this variation is not unexpected as mentioned previously for the other barks.

The HHV of the bark samples in this study range from 13.6 – 21.6 MJ/kg. The HHV of ESF is particularly low, most likely due to the slightly lower C and higher O than the other barks when utilising the Channiwala and Parikh calculation (Equation 2-2).

However, the incineration of bark to exploit its energy content is seen to be difficult due to the minerals and resins present in its chemical composition (424). This appears to be mitigatable through appropriate moisture content management (424).

### 5.2.2 AAS

In this section, the alkaline earth metal contents of the tree barks were analysed by atomic absorption spectroscopy (AAS) (Table 5-7), according to the method laid out in Section 3.6.

Generally, the tree barks in this study do not have high levels of alkaline earth metals. The most variable alkaline earth metal throughout the barks in this work is calcium. Calcium is generally known to be the alkaline earth metal with the greatest concentration in barks (529). However, the calcium values for the barks analysed in this work (1.2 – 18.2 mg/g) are still on the low end of barks in the literature (4.6 – 34.9 mg/g) (529). The cause of the difference in calcium between this work and literature is unknown, although it is most likely due to the different compositions of the soils.

**Table 5-7** - Metals analysis of raw tree barks. Error values were calculated by 1x standard deviation. Each tree bark was run in duplicate. NF = Noble fir, L = Larch, DF = Douglas fir, SS = Sitka spruce, NS = Norway spruce, ESF = European silver fir, GF = Grand fir, WH = Western hemlock, WRC = Western red cedar, NC = Nootka cypress, LC = Lawson cypress.

Family	Spec.	Al (mg/g)	Ca (mg/g)	K (mg/g)	Fe (mg/g)	Na (mg/g)	Mg (mg/g)
Pine	NF	0.0 ± 0.0	2.7 ± 0.2	1.2 ± 0.1	0.0 ± 0.0	0.2 ± 0.1	0.7 ± 0.0
	L	0.0 ± 0.0	1.2 ± 0.0	1.5 ± 0.1	0.0 ± 0.0	0.1 ± 0.0	0.7 ± 0.0
	DF	0.6 ± 0.1	3.9 ± 0.7	1.6 ± 0.1	0.3 ± 0.0	0.6 ± 0.1	0.8 ± 0.0
	SS	0.3 ± 0.1	8.4 ± 0.3	2.7 ± 0.0	0.1 ± 0.0	0.7 ± 0.0	0.7 ± 0.0
	NS	0.5 ± 0.0	18.2 ± 0.1	1.2 ± 0.0	0.4 ± 0.0	0.9 ± 0.1	1.2 ± 0.0
	ESF	0.0 ± 0.0	5.0 ± 0.2	2.1 ± 0.0	0.1 ± 0.0	0.4 ± 0.1	0.7 ± 0.0
	GF	0.2 ± 0.0	2.2 ± 0.2	2.7 ± 0.1	0.0 ± 0.0	0.0 ± 0.0	0.6 ± 0.0
	WH	0.1 ± 0.0	3.1 ± 0.0	1.1 ± 0.0	0.1 ± 0.0	0.5 ± 0.1	0.7 ± 0.1
Cypress	WRC	0.0 ± 0.0	8.0 ± 0.0	0.7 ± 0.0	0.0 ± 0.0	0.1 ± 0.1	0.9 ± 0.0
	NC	0.3 ± 0.1	10.0 ± 0.5	2.8 ± 0.1	0.0 ± 0.0	0.3 ± 0.0	0.9 ± 0.2
	LC	0.0 ± 0.0	1.7 ± 0.0	2.1 ± 0.1	0.1 ± 0.0	0.2 ± 0.1	0.8 ± 0.0

### 5.2.3 Fibre Analysis

This section includes the data from the fibre analysis of the tree barks using the Fibretherm method (as discussed in Section 3.4). The moisture content of the samples, measured as a part of the proximate analysis, are featured here. The results from this method cannot be used as purely quantifiable data due to inaccuracies that can occur through using the Fibretherm equipment. However, the data collated is useful as an indication of the lignocellulosic composition of the tree barks.

**Table 5-8** - Fibre analysis of raw tree barks. Moisture content (MC) is analysed on an ‘as analysed (a.a.) basis, as it underwent oven drying at 60 °C after being received. Crude protein (wt%) calculated using Dumas conversion factors provided in Equation 3-6. All variables are presented on a wt% basis. Error values were calculated by 1x standard deviation. Fibre analysis was repeated in duplicate for each sample. NF = Noble fir, L = Larch, DF = Douglas fir, SS = Sitka spruce, NS = Norway spruce, ESF = European silver fir, GF = Grand fir, WH = Western hemlock, WRC = Western red cedar, NC = Nootka cypress, LC = Lawson cypress. Crude protein calculated by Table 2-2.

Family	Spec.	MC	Cellulose	Hemi-cellulose	Lignin	Ash	Crude Protein	Not known
Pine	NF	5.3± 0.0	23.4± 0.0	2.1± 0.5	48.3± 1.0	0.2± 0.1	3.9±0.0	22.1
	L	5.4± 0.0	24.8± 1.1	3.0± 0.4	28.4± 1.9	1.2± 0.1	3.9±0.0	38.8
	DF	5.3±0.1	20.0± 9.4	4.1± 0.3	32.3± 0.5	0.4± 0.1	3.4±0.0	39.8
	SS	6.4± 0.3	28.3± 9.4	7.5± 2.6	13.7± 3.6	3.7± 2.4	4.5±0.0	42.4
	NS	5.8± 1.3	28.7± 1.8	6.5± 0.9	29.5± 1.4	4.0± 0.4	4.5±0.0	26.8
	ESF	6.5± 0.6	38.9± 0.5	4.5± 0.0	45.0± 1.0	0.6± 0.6	5.6±0.0	5.5
	GF	4.8± 0.0	39.5± 0.1	8.1± 0.6	22.2± 0.2	0.1± 0.0	3.9±0.0	26.8
	WH	4.0± 0.3	23.6± 0.2	7.3± 0.4	29.6± 0.6	1.0± 0.5	2.8±0.0	35.8
Cypress	WRC	5.9± 1.3	29.6± 4.4	3.6± 0.2	44.7± 3.7	1.3± 0.8	3.9±0.6	17.0
	NC	3.8± 0.0	33.0± 0.2	8.8± 0.5	14.8± 0.6	2.2± 0.0	3.9±0.0	37.3
	LC	6.1± 0.0	35.0± 3.0	0.0± 0.0	46.9± 2.0	0.8± 0.4	4.5±0.0	12.8

In the fibre analysis of the tree barks, there are not meaningful differences between the samples except for the lignin and unknown contents. In barks, the unknown content may include waxes, resins, fats, flavonoids, and tannins. Tree bark is known to have a higher proportion of extractives than wood, hence the higher unknown values (530). The lignin content varies from 14-48 wt%. NF, ESF, LC and WRC have the highest lignin values. NC and SS have the lowest lignin contents, whilst also having the greatest unknown contents. Spruces have been seen to contain less lignin than other bark species (531). The SS tree bark has fibre analysis values closer to the literature (532). The main difference between

the SS and NS barks is the lower lignin content for the NS, which is similar to that in the literature (423).

In addition to NC and SS, DF and L have large unknown contents. In the literature, different species of barks can have between 10 – 30 wt% of extractives (430, 431, 521). However, the unknown content is not exclusively extractive content. For example, larch bark has 38.8 wt% of unknown content in this work, whilst having 12.6 wt% of extractives in the literature (528).

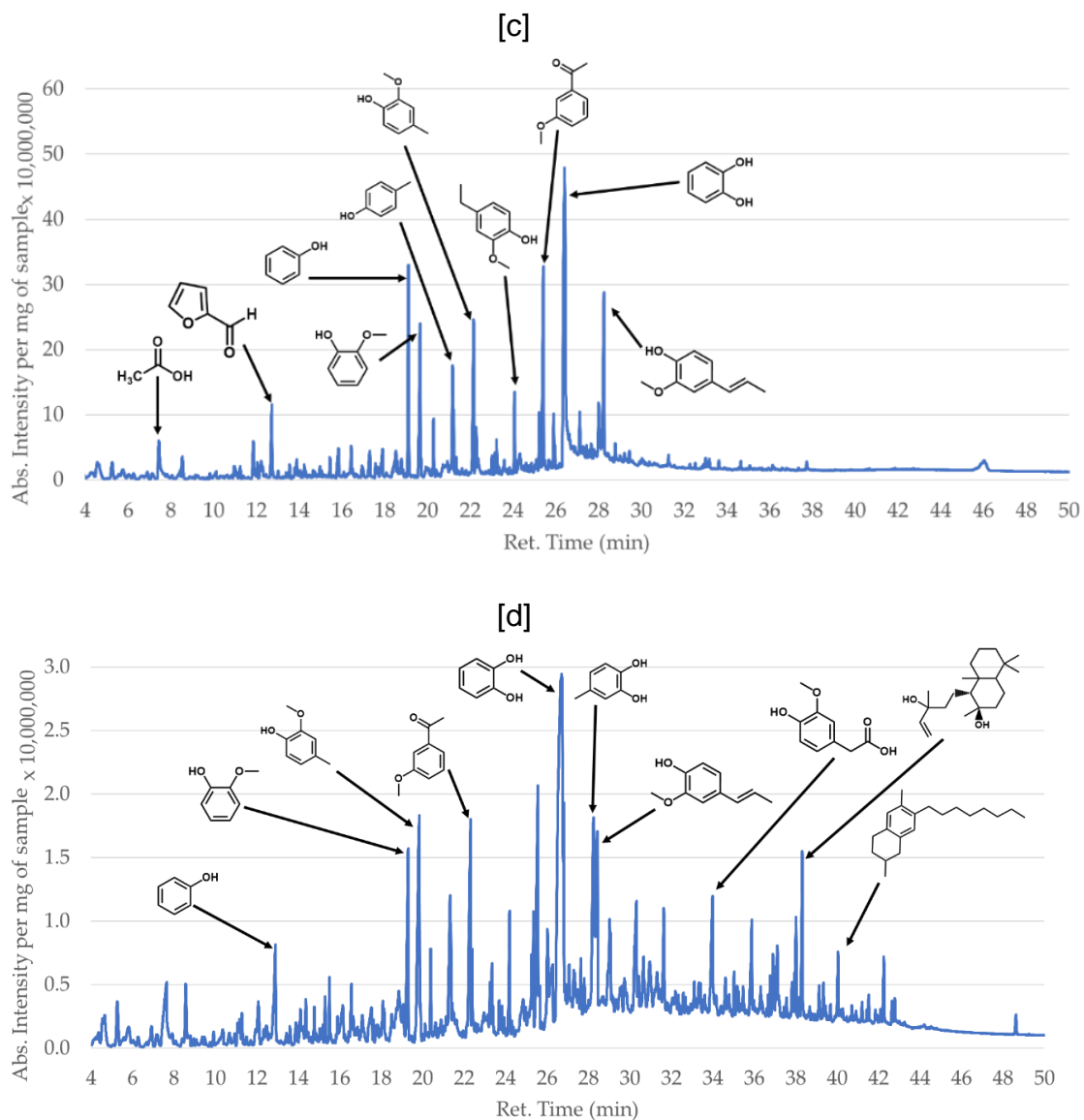
Regarding cellulose contents, all of the tree barks have between 20-40 wt% cellulose, with ESF and GF containing around 39 wt%. Fir barks have been found to have higher holocellulose (the sum of cellulose and hemicellulose) than spruces or cedars (531).

The hemicellulose contents are all below 10 wt%, with GF and NC having the largest. The fibre analysis data for larch bark is different to that found in the literature (Table 5-9) (528). Although the cellulose is similar, the hemicellulose and lignin are quite different. This may simply be due to international variation, with the bark being grown in China compared to Scotland.

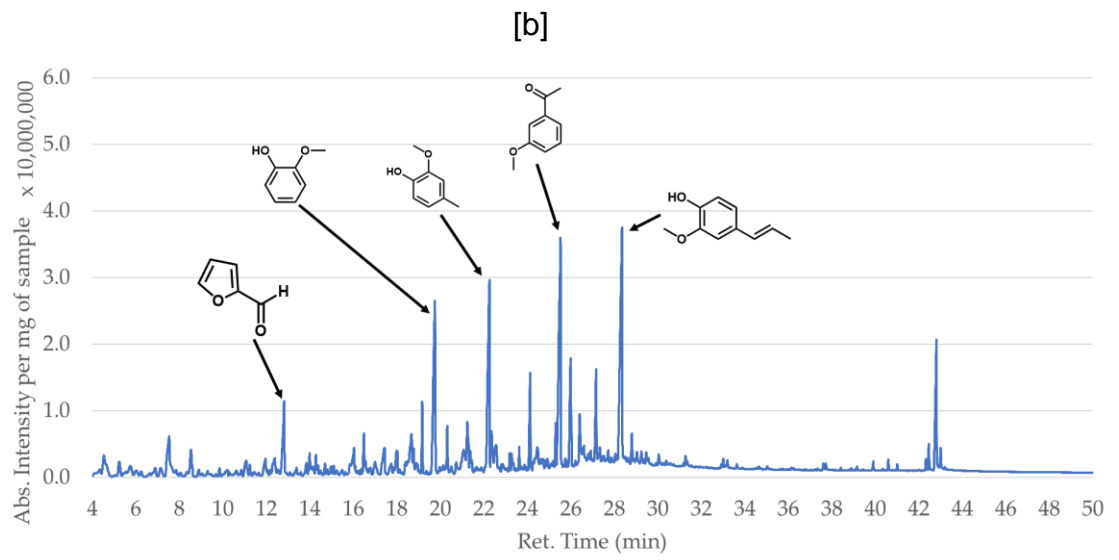
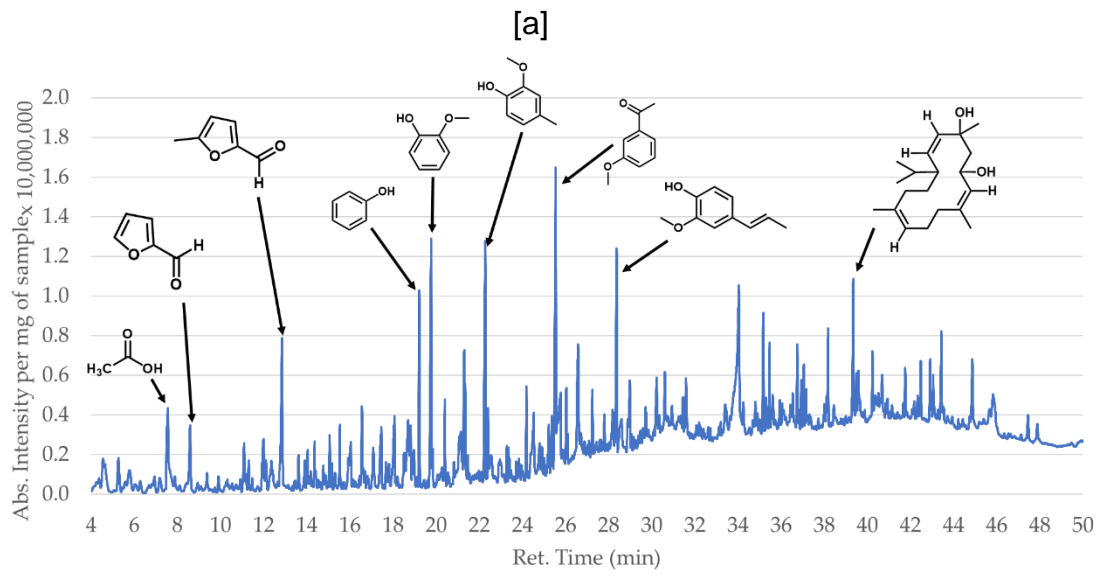
**Table 5-9** - Comparison of larch bark fibre analysis data in this work to the literature.

	<b>Cellulose (wt%)</b>	<b>Hemicellulose (wt%)</b>	<b>Lignin (wt%)</b>
<b>This study</b>	24.8	3.0	28.4
<b>Ren et al (2013) (528)</b>	28.8	13.2	45.4





**Figure 5-2** - Fast pyrolysis chromatograms of pine family barks, including [a] noble fir (NF), [b] larch (L), [c] Douglas fir (DF), [d] sitka spruce (SS) at 550 °C by py-GC/MS. Samples are presented at different y-axis scales due to the large difference in absolute intensities measured. Pyrolysis heating rate of 20 °C/ms, then held for 20s. Column temperature program of 40 °C for 2 min, 6 °C/min ramp to 280 °C, then hold for 10 min.



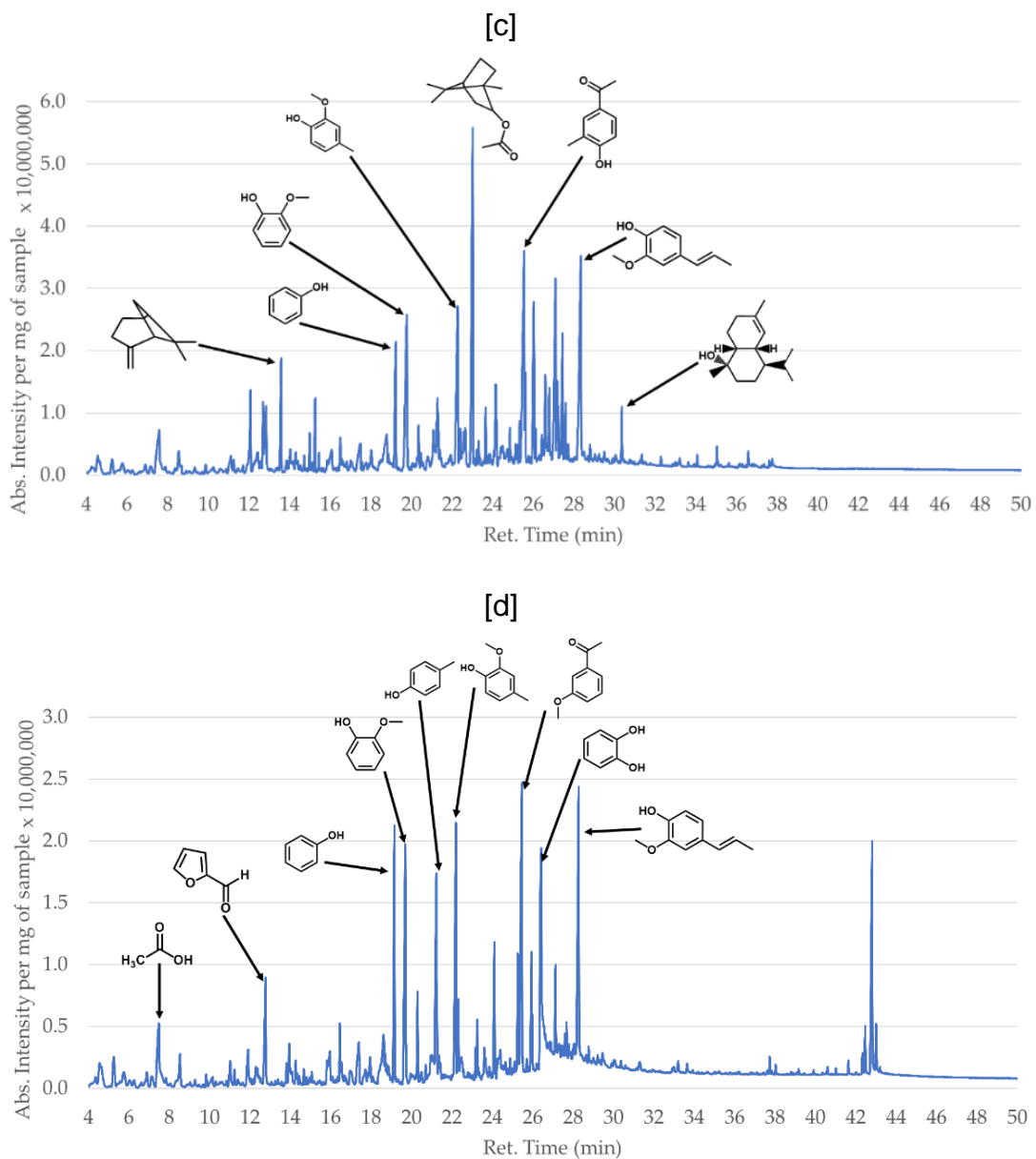


**Figure 5-3** - Fast pyrolysis chromatograms of pine family barks, including [a] Norway spruce (NS), [b] European silver fir (ESF), [c] grand fir (GF) and [d] Western hemlock (WH) at 550 °C by py-GC/MS. Samples are presented at different y-axis scales due to the large difference in absolute intensities measured. Pyrolysis heating rate of 20 °C/ms, then held for 20s. Column temperature program of 40 °C for 2 min, 6 °C/min ramp to 280 °C, then hold for 10 min.

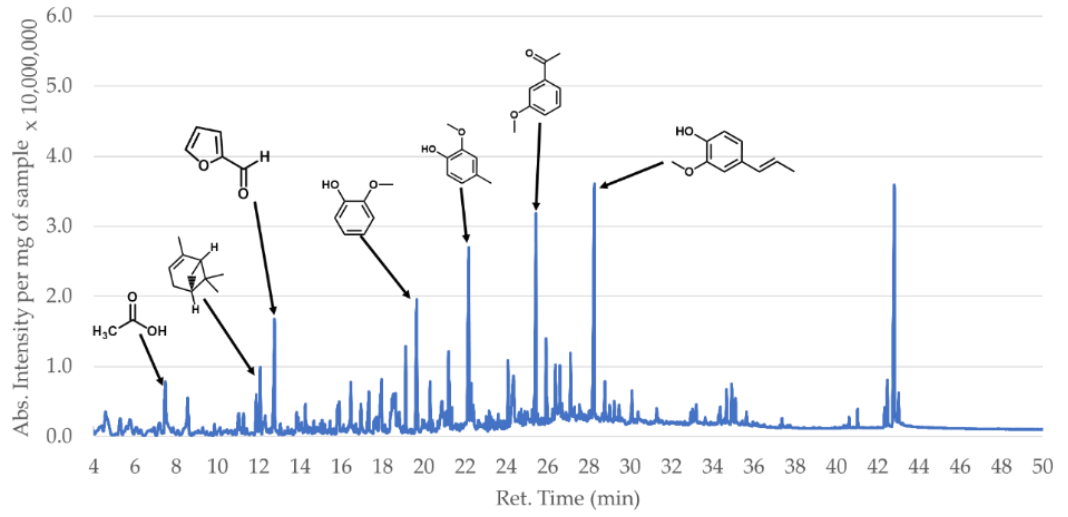
**Table 5-10** - Proportions of key and shared peaks of noble fir (NF), larch (L), Douglas fir (DF) and Sitka spruce (SS) tree bark from fast pyrolysis at 550 °C by py-GC/MS. RT = Retention Time. The top 25 peaks of each chromatogram were identified using the NIST mass spectral database versions 147 and 27.

RT (min)	Name	NF (%)	L (%)	DF (%)	SS (%)
7.4	Acetic acid	-	2.0	2.2	-
8.6	Toluene	0.6	-	-	1.1
12.7	Furfural	2.4	3.8	3.3	-
16.4	2-Furancarboxaldehyde, 5-methyl-	0.9	1.1	0.7	-
18.8	7-Tridecanone	-	0.7	0.6	-
19.3	Phenol	2.0	3.5	8.6	5.1
19.8	Phenol, 2-methoxy- (guaiacol)	8.3	10.7	8.3	7.7
20.4	Phenol, 2-methyl- (o-cresol)	1.1	-	1.7	1.4
21.3	p-cresol	-	2.3	4.6	3.7
21.4	Phenol, 3-methyl- (m-cresol)	2.5	0.6	1.5	1.0
22.3	Creosol (4-Methylguaiacol)	11.5	10.7	7.5	5.8
24.2	Phenol, 4-ethyl-2-methoxy-	3.3	4.1	2.6	10.9
25.2	Benzofuran, 2,3-dihydro-	-	2.3	2.2	-
25.4	3-Methoxyacetophenone	9.9	12.7	10.4	-
26.0	Phenol, 2-methoxy-4-(2-propenyl)-, acetate	5.6	1.8	1.8	1.3
26.8	Catechol	19.3	25.4	25.7	32.8
28.2	1,2-Benzenediol, 4-methyl-	7.2	0.6	2.9	7.8
28.4	trans-Isoeugenol	8.9	9.2	9.8	5.6
28.8	Vanillin	2.0	0.6	0.5	-
31.6	2-Propanone, 1-(4-hydroxy-3-methoxyphenyl)-	2.6	-	-	1.6
33.5	1-Naphthalenol, 4-methoxy-	0.6	-	-	-
34.0	Homovanillic acid	7.2	0.6	-	2.1
38.3	1-Naphthalenepropanol, .alpha.-ethenyldecahydro-2-hydroxy-.alpha.,2,5,5,8a-pentamethyl-, [1R-[1.alpha.(R*),2.beta.,4a.beta.,8a.	-	-	-	3.3
42.3	Naphthalene, 1,2,3,4-tetrahydro-2,6-dimethyl-7-octyl-	-	-	-	1.0

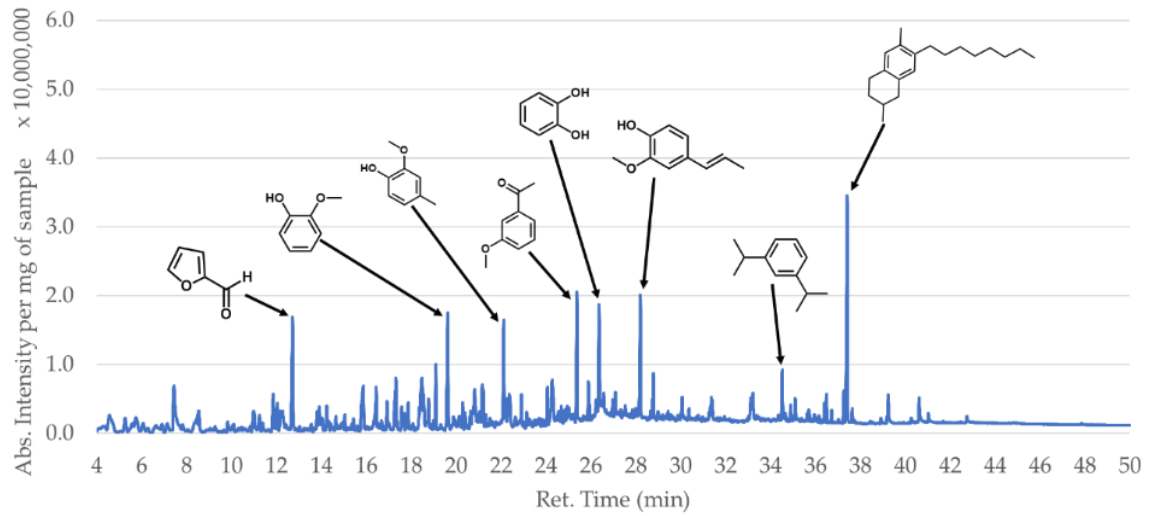
**Table 5-11** - Proportions of key and shared peaks of Norway spruce (NS), European silver fir (ESF), grand fir (GF) and Western hemlock (WH) tree bark from fast pyrolysis at 550 °C by py-GC/MS. The top 25 peaks of each chromatogram were identified using the NIST mass spectral database versions 147 and 27.

RT (min)	Name	NS (%)	ESF (%)	GF (%)	WH (%)
7.5	Acetic acid	3.7	2.6	-	3.1
8.5	Toluene	2.0	1.2	-	-
12.8	Furfural	5.2	3.7	-	3.8
16.5	2-Furancarboxaldehyde, 5-methyl-	2.2	1.2	-	1.3
19.2	Phenol	5.9	2.0	4.9	7.3
19.8	Phenol, 2-methoxy- (guaiacol)	10.5	11.5	7.3	9.5
20.3	Phenol, 2-methyl- (o-cresol)	3.7	1.3	1.0	1.7
21.2	p-Cresol	4.2	1.7	2.0	7.3
22.3	Creosol	9.3	12.2	7.5	9.3
22.4	Phenol, 2,3-dimethyl-	-	2.1	-	1.6
23.0	Acetic acid, 1,7,7-trimethyl-bicyclo[2.2.1]hept-2-yl ester	-	-	14.9	-
24.1	Phenol, 4-ethyl-2-methoxy-	2.4	3.6	2.2	3.1
25.3	Benzofuran, 2,3-dihydro-	-	1.1	-	2.6
25.5	4-Hydroxy-3-methylacetophenone	-	-	12.0	-
25.5	3-Methoxyacetophenone	10.6	16.2	-	11.6
26.0	Phenol, 2-methoxy-4-(2-propenyl)-, acetate	1.9	5.3	6.7	2.9
26.4	Catechol	5.3	2.3	-	8.0
27.1	Naphthalene, 1,2,3,5,6,8a-hexahydro-4,7-dimethyl-1-(1-methylethyl)-, (1S-cis)-	-	-	7.2	-
27.2	Naphthalene, 1,2,4a,5,8,8a-hexahydro-4,7-dimethyl-1-(1-methylethyl)-, [1S-(1.alpha.,4a.beta.,8a.alpha.)]-	-	-	0.9	-
27.4	Naphthalene, 1,2,3,4,4a,7-hexahydro-1,6-dimethyl-4-(1-methylethyl)-	-	-	3.7	-
27.6	Naphthalene, 1,2,3,4-tetrahydro-1,6-dimethyl-4-(1-methylethyl)-, (1S-cis)-	-	-	1.2	-
28.4	trans-Isoeugenol	6.6	19.9	9.8	11.5
28.8	Vanillin	-	0.9	-	-
30.4	1-Naphthalenol, 1,2,3,4,4a,7,8,8a-octahydro-1,6-dimethyl-4-(1-methylethyl)-, [1R-(1.alpha.,4.beta.,4a.beta.,8a.beta.)]-	-	-	1.3	-
34.0	.beta.-D-Glucopyranose, 1,6-anhydro-	3.3	-	-	-
35.2	Azulene, 1,2,3,3a,4,5,6,7-octahydro-1,4-dimethyl-7-(1-methylethenyl)-, [1R-(1.alpha.,3a.beta.,4.alpha.,7.beta.)]-	3.2	-	-	-
36.8	1-Naphthalenopropanol, .alpha.-ethenyldecahydro-2-hydroxy-.alpha.,2,5,5,8a-pentamethyl-, [1R-[1.alpha.(R*),2.beta.,4a.beta.,8a.	4.1	-	-	-
39.3	4,8,13-Cyclotetradecatriene-1,3-diol, 1,5,9-trimethyl-12-(1-methylethyl)-	4.8	-	-	-

[a]



[b]



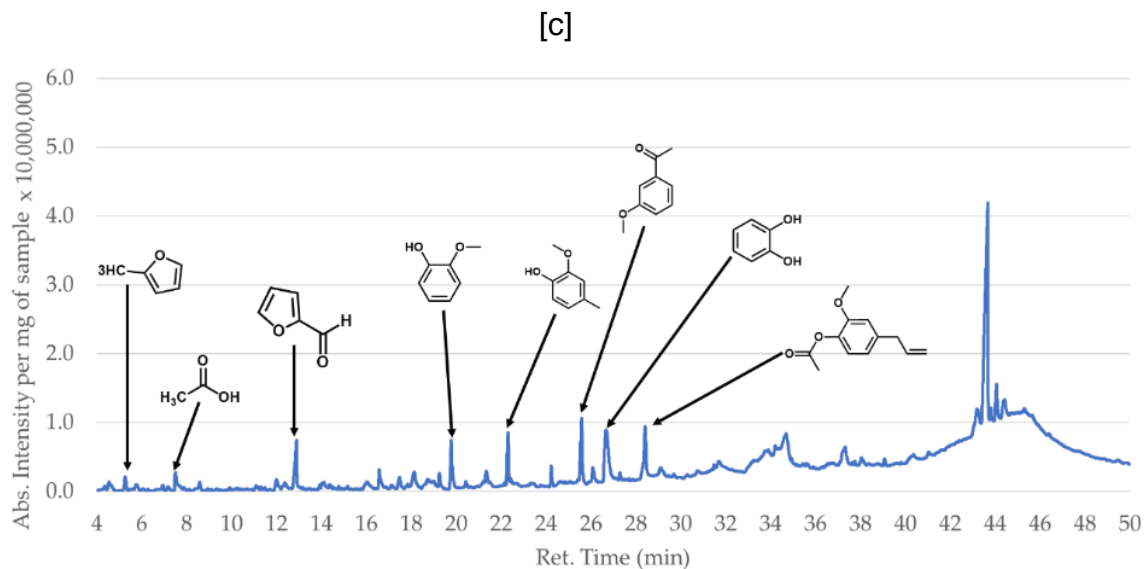


**Figure 5-4** - Fast pyrolysis chromatograms of cypress family barks, including [a] Western red cedar (WRC), [b] Nootka cypress (NC) and [c] Lawson cypress (LC) at 550 °C by py-GC/MS. Pyrolysis heating rate of 20 °C/ms, then held for 20s. Column temperature program of 40 °C for 2 min, 6 °C/min ramp to 280 °C, then hold for 10 min.

**Table 5-12** - Proportions of key and shared peaks of Western red cedar (WRC), Nootka cypress (NC) and Lawson cypress (LC) tree bark from fast pyrolysis at 550 °C by py-GC/MS. The top 25 peaks of each chromatogram were identified using the NIST mass spectral database versions 147 and 27.

RT (min)	Name	WRC (%)	NC (%)	LC (%)
7.5	Acetic acid	3.4	-	1.3
11.9	[1,1'-Bicyclopentyl]-2-one	1.3	-	-
12.0	(1R)-2,6,6-Trimethylbicyclo[3.1.1]hept-2-ene	2.8	1.6	-
12.9	Furfural	5.8	7.9	4.1
15.9	Cyclohexanone	3.2	5.9	-
16.6	2-Furancarboxaldehyde, 5-methyl-	1.5	-	1.6
18.5	1,2-Cyclopentanedione, 3-methyl-	1.0	5.3	-
19.3	Phenol	3.4	3.2	0.9
19.8	Phenol, 2-methoxy- (guaiacol)	7.0	7.9	4.1
21.2	Phenol, 3-methyl- (m-cresol)	1.4	1.7	-
21.4	p-Cresol	3.0	2.0	1.0
22.3	Creosol	9.4	5.7	3.3
24.2	Phenol, 4-ethyl-2-methoxy-	2.2	1.8	1.3
25.6	3-Methoxyacetophenone	11.2	7.5	5.1
26.1	Phenol, 2-methoxy-4-(2-propenyl)-, acetate	3.3	1.6	6.8
26.6	Naphthalene, 1,2,3,4,4a,5,6,8a-octahydro-4a,8-dimethyl-2-(1-methylethenyl)-, [2R-(2.alpha.,4a.alpha.,8a.beta.)]-	1.6	-	-
26.7	Catechol	2.3	7.1	9.4
28.2	Trans-Isoeugenol	15.0	6.6	-
29.1	Vanillin	1.6	-	1.4
33.9	.beta.-D-Glucopyranose, 1,6-anhydro-	-	-	5.4
37.4	Naphthalene, 1,2,3,4-tetrahydro-2,6-dimethyl-7-octyl-	-	15.7	-

In Table 5-11, the tree barks (except for SS) have low levels of furan-containing compounds. This is likely due to the lower cellulose and hemicellulose contents present in these samples (Table 5-8).

The levels of simple aromatic compounds are quite high for all tree barks in Table 5-10. DF has high phenol, whilst NF, L and SS have high 2-methyl phenol (o-cresol) and 2-methoxy phenol (guaiacol). DF may have higher proportions of the simplest aromatic compound (phenol) due to the slightly increased Al and Fe (Table 5-7) acting as a catalyst to increase the severity of the pyrolysis.

In all four tree barks in Table 5-10, the catechol content is between 20 – 30 wt% of the identified pyrolysis products. This is common in the pyrolysis of lignin and lignin-rich materials (58, 265, 533, 534).

From the tree bark data present in Table 5-11, GF is the only one that does not contain any furan-related compounds. This is unexpected as it has the greatest holocellulose (cellulose + hemicellulose) content of the tree barks (Table 5-8). However, GF has higher proportions of compounds that include naphthalene-type functional groups. NS also has several registered naphthalene-type compounds. NF and SS also have compounds including naphthalenols and naphthalenes (Table 5-10). These are likely to be derived from suberin (535).

GF has a relatively high proportion of acetic acid, 1,7,7-trimethyl-bicyclo[2.2.1]hept-2-yl ester. This compound and its stereoisomer, bornyl acetate, are known to be found in pine needle-derived essential oils (536-538).

All of the barks in Table 5-11 have large proportions of creosol, trans-isoeugenol and 3-methoxyacetophenone (or 4-hydroxy-3-methylacetophenone) (539-541). The trans-isoeugenol proportion of ESF is nearly double that of the other barks. This is likely because of the low unknown content from Table 5-8. As there are fewer types of extractants present within the ESF bark, the lignin-derived compounds such as trans-isoeugenol would be more concentrated.

WRC has larger proportions of creosol, 3-methoxyacetophenone and trans-isoeugenol compared to the other cypress barks (Table 5-12). ESF and WRC both have higher levels of trans-isoeugenol, with the only clear similarities being that they have the higher oxygen contents of the barks (Table 5-4 and Table 5-5).

NC has a large proportion of a naphthalene compound, whilst WRC only has a small proportion of one of them. This is expected as NC has over 30 wt% unknown content in Table 5-8, with WRC having 17 wt%.

GF, WH, WRC, LC have the same general peaks around 42-46 minutes. These are most likely phenanthrenes, aromatic secondary plant metabolites with beneficial biological properties (including anti-viral, antimicrobial, and antioxidant actions) (542).

Phenanthrenes is considered to be a polyaromatic hydrocarbon (PAH). PAHs are biopollutants, and phenanthrenes are one of the most concentrated PAHs present in pine tree barks in Isfahan (Iran) (543). Tree components have previously been recognised as a

form of biomonitoring to provide insight into the pollution in cities. Between the two bark layers (inner and outer), pollutants tend to be accumulated in the outer bark. From the analysis ran in this work, there is nothing common amongst the four barks, that differ with the other barks. Therefore, it is unknown why the GF, WH, WRC and LC barks have pronounced phenanthrene peaks. One reason may be that the collected samples for this work had higher proportions of outer bark than the remaining barks, hence greater proportions of bio-pollutants.

The tree bark that appears to have the most potential as a lignin-rich residue is the noble fir, due to its high lignin content, low ash, and relatively low extractives content (when compared to the other barks).

## **5.2.5 Solvent Extraction**

The high unknown contents in the fibre analysis (Section 3.4) and the naphthalene and naphthalenol compounds identified in the py-GC/MS (Section 3.7.2) led to an aim to remove extractible contents. The extraction was performed via Soxhlet extraction (Section 3.9.2) and Accelerated Solvent Extraction (ASE) (Section 3.9.3).

The ASE method was more efficient, but the solid sample was unable to be retained for analysis. Therefore, the Soxhlet method was run, with the solid being analysed afterwards. ASE was unable to be run on grand fir or Douglas fir due to the supply available.

Soxhlet extraction was run in duplicates for all samples, with a third replicate being performed when the error was considered significant. Norway spruce was not run due to limited supplies. Some data was collected for the Soxhlet extraction of Western red cedar, but due to the volume of sample available, this was not exhaustive.

### **5.2.5.1 Solvent Extraction Mass Loss and Fibre Analysis**

In this section, the fibre analysis data of the Soxhlet-treated tree barks are compared to the raw tree barks. After outlining the differences between the solvent extracted (and un-extracted) samples, the mass loss of the samples from the Soxhlet extraction are presented.

**Table 5-13** - Fibre Analysis of suberin-containing tree barks before and after solvent extraction (wt%). Moisture content (MC) data given on an 'as analysed' (a.a.) basis. Errors are presented with 1x standard deviation, and each sample was run in duplicate.

Sample	MC	Cellulose	Hemicellulose	Lignin	Ash	Crude Protein	Unknown
Noble Fir	5.31 ± 0.0	23.4 ± 0.0	2.1 ± 0.5	48.3 ± 1.0	0.2 ± 0.1	3.8± 0.0	22.2
Soxhlet-treated NF	4.99 ± 0.2	20.7 ± 0.3	7.6 ± 0.1	54.5 ± 0.1	0.8 ± 0.6	3.8± 0.1	12.6
Grand Fir	4.79 ± 0.0	39.5 ± 0.1	8.1 ± 0.6	22.2 ± 0.2	0.1 ± 0.0	4.1± 0.0	26.0
Soxhlet-treated GF	4.64 ± 0.4	42.9 ± 3.6	11.3 ± 0.6	23.6 ± 3.1	1.6 ± 0.8	6.7± 0.1	13.9
Nootka Cypress	3.78 ± 0.0	33.0 ± 0.2	8.8 ± 0.5	14.8 ± 0.6	2.2 ± 0.0	4.0± 0.0	37.2
Soxhlet-treated NC	5.05 ± 0.0	31.0 ± 2.5	10.3 ± 0.1	30.0 ± 3.0	3.1 ± 0.3	4.9± 0.4	20.7
Sitka Spruce	6.36 ± 0.3	28.3 ± 9.4	7.5 ± 2.6	13.7 ± 3.6	3.7 ± 2.4	4.5± 0.0	42.3
Soxhlet-treated SS	5.74 ± 0.1	28.5 ± 1.6	15.8 ± 0.4	23.7 ± 0.6	3.5 ± 0.6	5.7± 0.1	22.8

**Table 5-14** - Fibre Analysis of non-suberin-containing tree barks before and after solvent extraction (wt%). Moisture content data given on an 'as analysed' (a.a.) basis. Errors are presented with 1x standard deviation, and each sample was run in duplicate.

Sample	MC	Cellulose	Hemicellulose	Lignin	Ash	Crude Protein	Unknown
Lawson Cypress	6.12 ± 0.0	35.0 ± 3.0	0.0 ± 0.0	46.9 ± 2.0	0.8 ± 0.4	4.3± 0.0	12.9
Soxhlet-treated LC	4.19 ± 0.3	26.0 ± 0.1	5.4 ± 0.2	55.4 ± 0.1	0.7 ± 0.6	4.6± 0.2	7.9
European Silver Fir	6.53 ± 0.6	38.9 ± 0.5	4.5 ± 0.0	45.0 ± 1.0	0.6 ± 0.6	5.3± 0.0	5.7
Soxhlet-treated ESF	5.39 ± 0.2	19.6 ± 2.2	6.1 ± 1.9	57.1 ± 9.3	0.7 ± 0.3	5.6± 0.1	10.9
Douglas Fir	5.28 ± 0.1	20.0 ± 0.0	4.1 ± 0.0	32.3 ± 0.0	0.4 ± 0.1	3.2± 0.0	40.0
Soxhlet-treated DF	4.82 ± 0.0	22.9 ± 0.7	10.3 ± 0.0	43.6 ± 0.5	1.3 ± 0.4	6.8± 0.2	15.1
Larch	5.43 ± 0.0	24.8 ± 1.1	3.0 ± 0.4	28.4 ± 1.9	1.2 ± 0.1	3.9± 0.0	38.8
Soxhlet-treated L	4.40 ± 0.1	28.5 ± 2.7	8.8 ± 0.6	40.6 ± 1.8	1.4 ± 0.1	4.8± 0.0	15.9
Western Hemlock	4.02 ± 0.3	23.6 ± 0.2	7.3 ± 0.2	29.6 ± 0.6	1.0 ± 0.5	2.6± 0.0	36.0
Soxhlet-treated WH	4.74 ± 0.1	29.4 ± 8.3	8.9 ± 2.1	26.4 ± 5.9	1.4 ± 0.4	4.0± 0.1	29.9

Across the fibre analysis of the Soxhlet-treated tree barks, the unknown contents for most of the samples have reduced by at least 10 wt%. The samples which contained fatty acids (according to py-GC/MS) had consistent reductions in unknown content (Table 5-13) (from 22.2-42.3 wt% to 12.6-22.8 wt%). The DF and L samples, which did not seemingly include fatty acids, lost about 20 wt% from the Soxhlet extraction (Table 5-15) (from 38.8-40.0 wt% to 15.1-15. wt%). This mass loss is most likely due to the non-suberin derived content, including tannins and flavonoids.

Per gram of sample, the extraction has led to slight concentrations of the lignocellulosic contents, due to the removal of non-lignocellulosic components. In most of the tree barks, the cellulose content has increased slightly changed (by around 0-5 wt%, from 20.0-39.5 wt% to 20.7 – 42.9 wt%). Exceptions to this are LC and ESF, in which the cellulose content drops by 10-20 wt% (from 35.0-38.9 wt% to 19.6-26.0 wt%). These differences may be due to an overestimation in cellulose by the fibre analysis on the raw samples. In the literature, it is suggested that this is caused by the presence of ash and proteins (544). As LC and ESF have the greatest nitrogen contents of the barks (Table 5-4 and Table 5-5), and therefore crude protein contents (4.3-5.3 wt%), which may have disrupted the cellulose values estimated. Therefore, the cellulose is likely to be more accurate in the solvent-extracted barks.

The hemicellulose content has also been more concentrated, which is mostly noticeable for NF, SS, LC, DF, and L (from 0.0-7.5 wt% to 5.4-15.8 wt%). The proportional increase of hemicellulose is greater than for the other variables. This may be caused by the Soxhlet conditions slightly breaking down the structure of the barks, providing a more accurate estimate.

The lignin content has been concentrated by more than 10 wt% across most of the tree barks (from 13.7-48.3 wt% to 23.7 to 57.1 wt%). GF and WH did not share this concentration (from 22.2-29.6 wt% to 23.6-26.4 wt%). Lignin may be overestimated after solvent extraction. The extractives that remain, that are acid-insoluble, may condense and act as contaminants. These contaminants may register as lignin due to the gravimetric nature of the fibre analysis method (544), artificially increasing the lignin yield.

The ash content of NC and DF increase by 1 wt% after extraction (from 0.4-2.2 wt% to 1.3-3.1 wt%). This is not a significant amount, as it is likely that the ash wt% was concentrated in the sample after the removal of extractives.

**Table 5-15** - Mass losses of tree barks after Soxhlet extraction. Errors are presented with 1x standard deviation, and each sample was run in duplicate.

Sample	Mass loss from Soxhlet extraction (%)
<b>Suberin-containing barks</b>	
Noble Fir	14.2 ± 0.9
Grand Fir	15.6 ± 3.2
Nootka Cypress	23.2 ± 2.9
Sitka Spruce	30.8 ± 1.5
<b>Non-suberin-containing barks</b>	
Lawson Cypress	4.8 ± 0.0
European Silver Fir	3.0 ± 0.7
Douglas Fir	27.3 ± 0.5
Larch	30.6 ± 1.1
Western Hemlock	23.4 ± 0.0

From the mass losses of the samples after Soxhlet extraction (Table 5-15), there are several (NC, SS, DF, L and WH) in which over 23 wt% was lost. The mass loss could not be recorded when utilising the ASE method, due to the sample being mixed with sand as well as solvent being retained in the cell with the solid after extraction.

As DF, L and WH did not contain suberin-derived compounds in the py-GC/MS results, there must be other sources of extractives that could be lost. These likely include tannins, flavonoids and/or terpenoids, as discussed in Section 5.1. The particular types of extractives were attempted to be observed through further GC/MS of the extracted contents.

The high mass loss from the NC and SS was expected due to the presence of the fatty acids. According to the literature, extractives do not tend to exceed more than 30 wt% of the bark (457). In this case, the NC and SS appear to both have had the most extractives, whilst the Soxhlet extraction must have been completed to exhaustion.

#### **5.2.5.2 Derivative Thermogravimetry Curves of raw bark and post-solvent extraction solids**

In this section, the derivative thermogravimetry curves of the raw barks and solids (that remain after solvent extraction) are outlined. The change in lignocellulosic content may also be observed in the DTG curves.

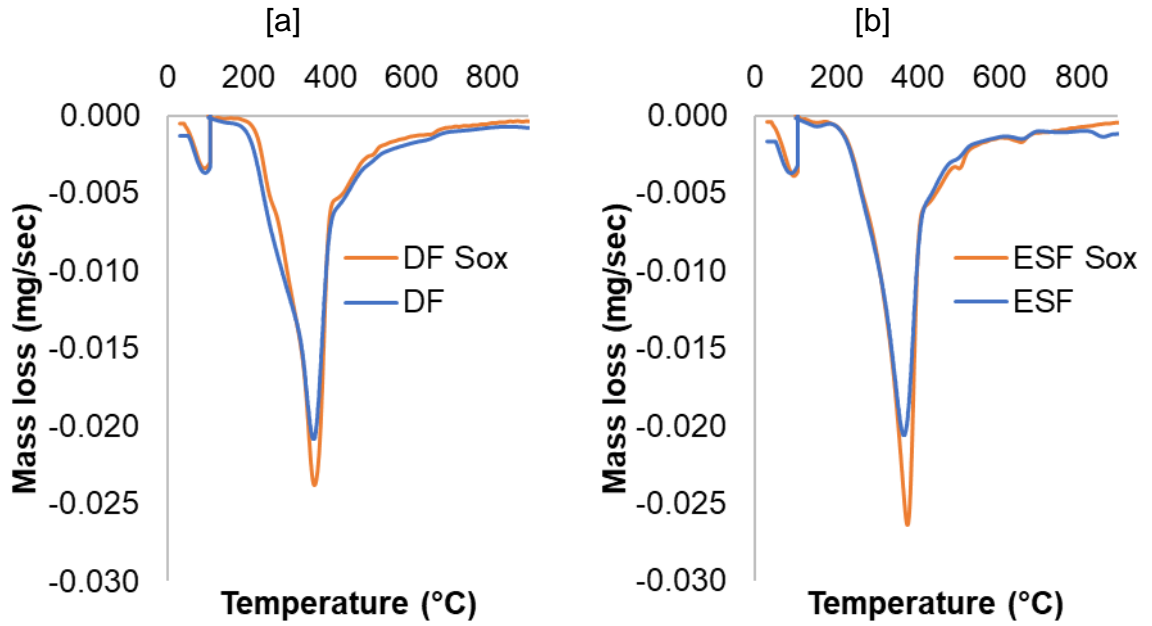


**Figure 5-5** - Derivative Thermogravimetric curves of raw and Soxhlet residues of [a] Douglas fir and [b] European silver fir tree bark.

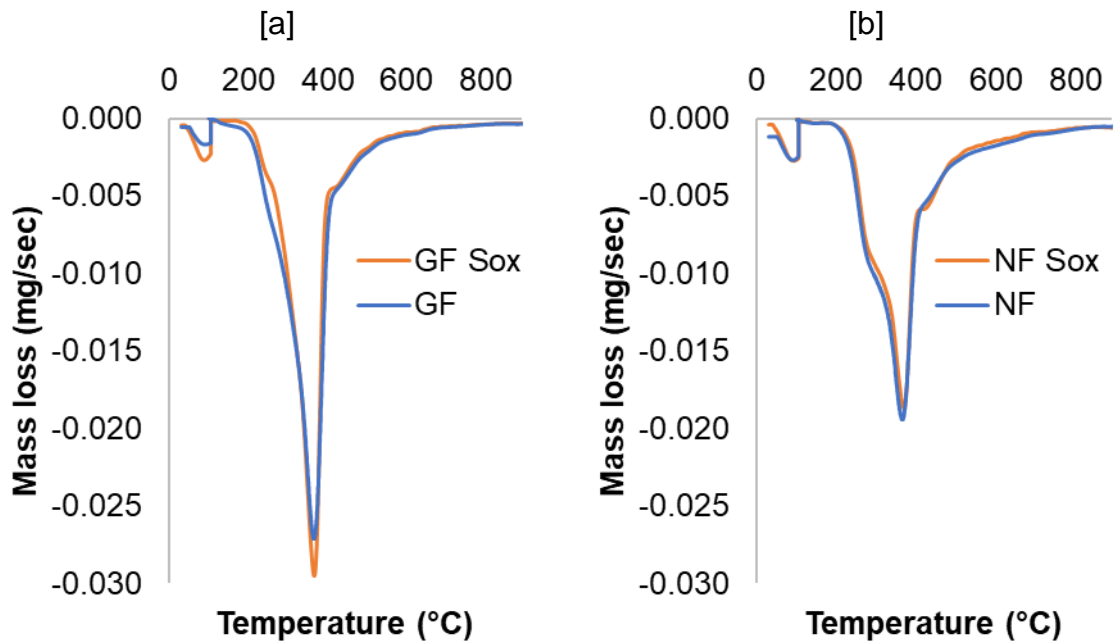


**Figure 5-6** - Derivative Thermogravimetric curves of raw and Soxhlet residues of [a] grand fir and [b] noble fir tree bark.

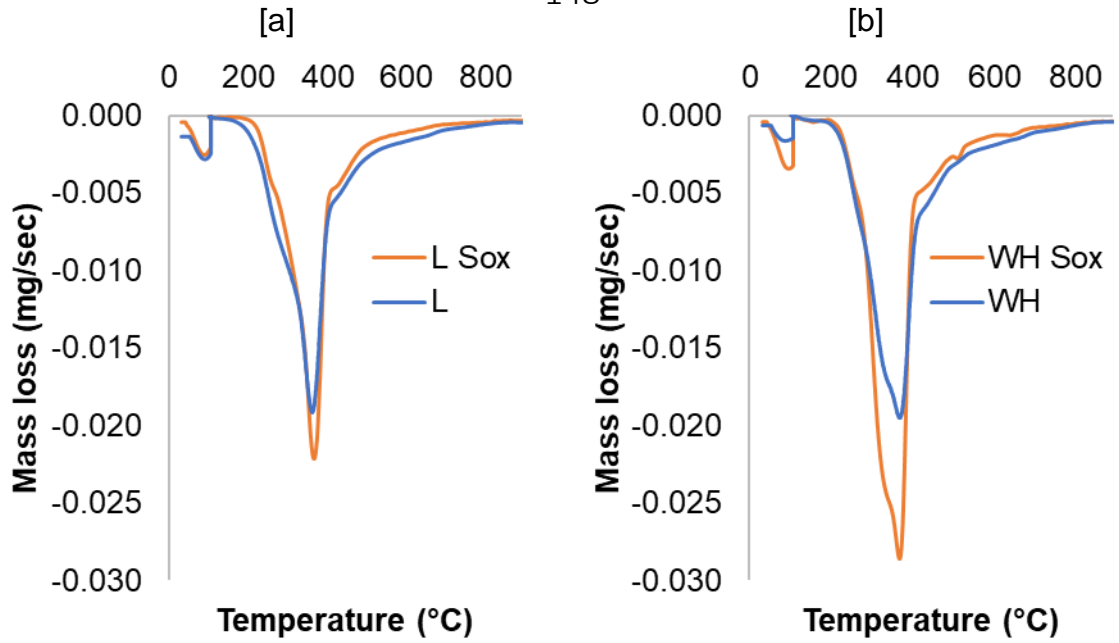


**Figure 5-7** - Derivative Thermogravimetric curves of raw and Soxhlet residues of [a] larch and [b] Western hemlock tree bark.

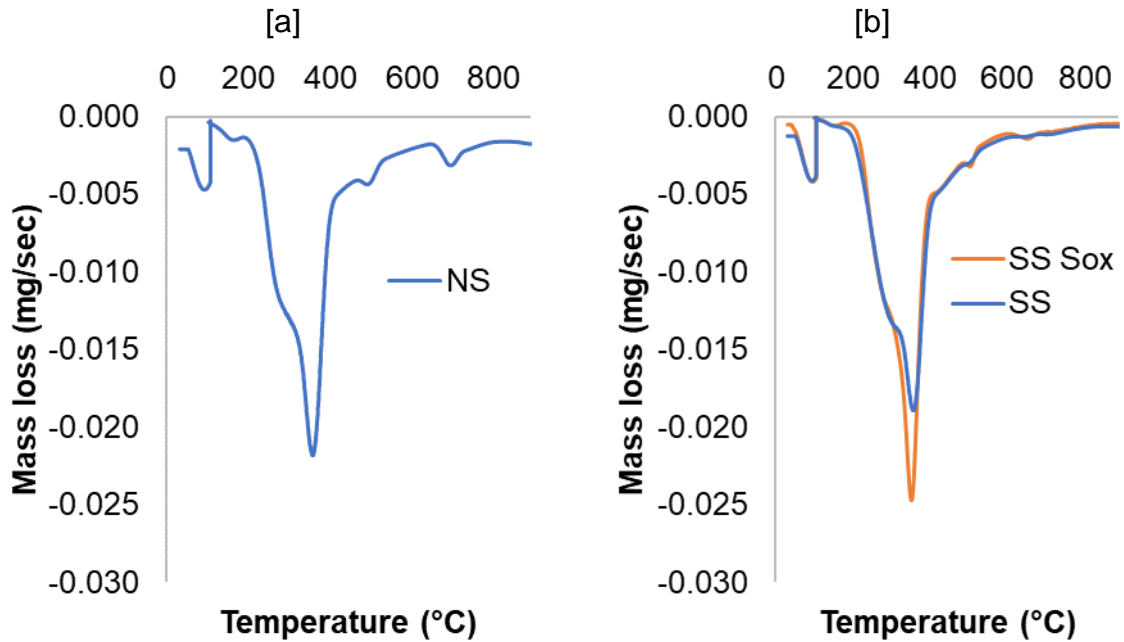


**Figure 5-8** - Derivative Thermogravimetric curves of [a] raw Norway spruce and raw and Soxhlet residues of [b] Lawson cypress tree bark.

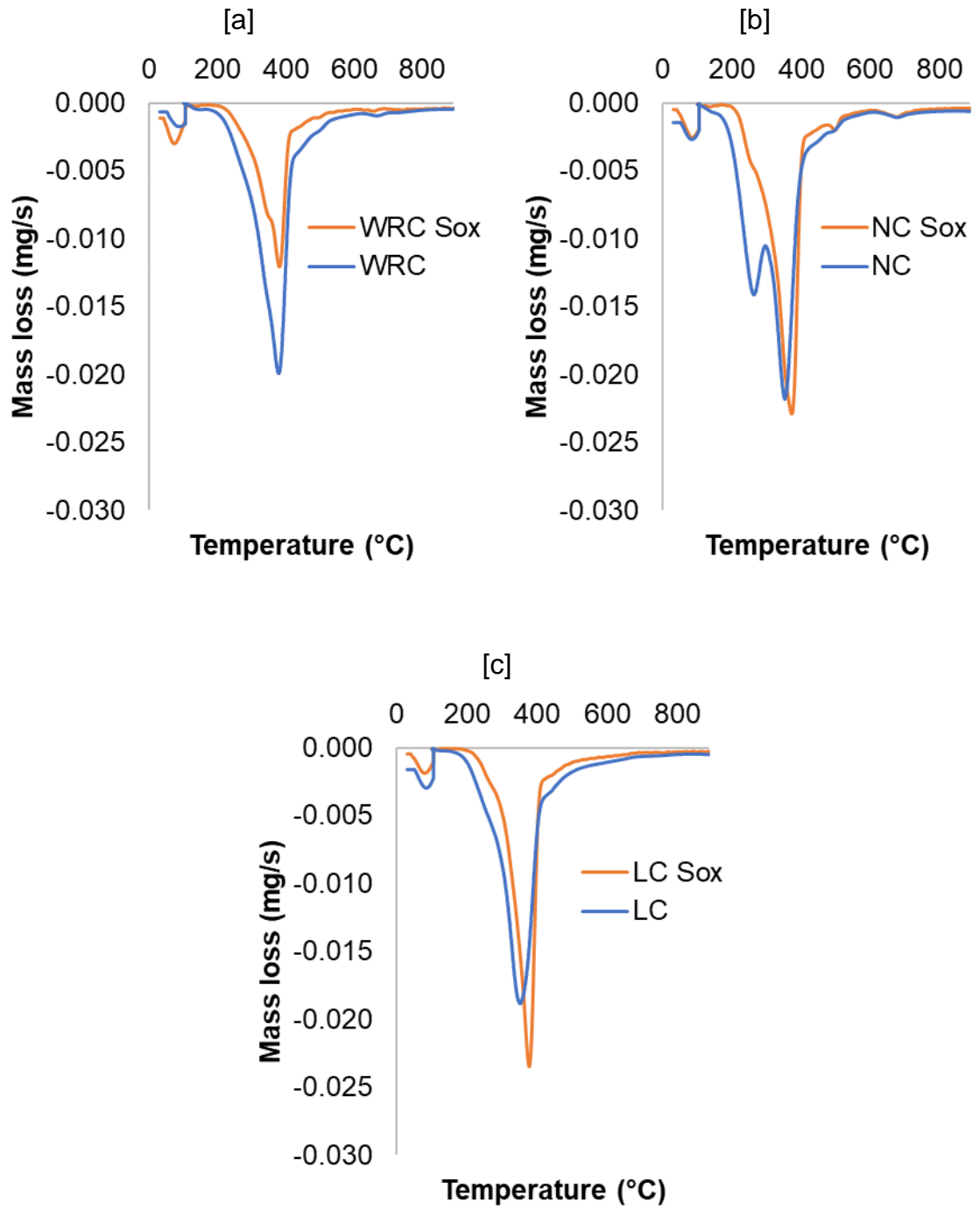


**Figure 5-9** - Derivative Thermogravimetric curves of raw and Soxhlet residues of [a] Western red cedar, [b] Nootka cypress tree bark, and [c] Lawson cypress.

From the raw barks DTG curves presented in Figure 5-5 to Figure 5-9, nootka cypress (NC) has the greatest mass loss for the section associated with hemicellulose content (at around 271 °C). NC has the largest hemicellulose content from the fibre analysis (Table 5-13), therefore this is expected.

The raw grand fir bark (GF) has the highest mass loss in the cellulose decomposition section (around 360 °C), as GF has the most cellulose according to the fibre analysis (Table 5-13). The raw LC bark has one of the highest cellulose contents from the fibre analysis, although it has the smallest cellulose mass loss in the DTG. It is unknown why this occurs, but one such reason may be from the potential overestimation of the cellulose in the raw bark from the ash and protein contents (544).

After solvent extraction, the shape of the DTG curves have generally remained the same except for the extent of mass loss changing. The only sample where the DTG curve changes is NC (Figure 5-9). In the unextracted sample, there is a clear hemicellulose peak around 260 °C. In the solvent extracted sample, this has disappeared. As the hemicellulose content (in Table 5-13) has not altered much, it is unknown what has caused this. This may be from the presence of suberin in the raw NC, as it degrades around 250 °C.

The DTG curves of L, NF, GF, and DF have not altered much after solvent extraction, which is expected as the fibre analysis values also did not change significantly.

A few of the samples experience significant additional mass loss after solvent extraction (ESF, WH, SS and LC). However, they do not share any similarities that would explain why this would occur. One reason may be that the solvent extraction removed some of the heavier non-lignocellulosic components. As the lignocellulosic components then made up a greater proportion of the mass of the sample, the DTG curve would show greater mass loss than its unextracted counterparts.

### 5.2.5.3 Distribution of compound classifications in py-GC/MS after solvent extraction

The fibre analysis of the solvent-extracted barks showed that the hemicellulose and cellulose content had been concentrated (to various extents). In this section, the distribution of different compound classifications (holocellulose-derived, lignin-derived, suberin-derived, and 'other') from the raw bark to the different phases post-Soxhlet extraction will be outlined. Py-GC/MS at 550 °C was performed independently on the solid and liquid residues, with the same conditions previously done on the raw barks. Analytical pyrolysis was performed on the liquid residues to break down any material with a molecular weight greater than the GC-MS measuring range (50 – 600 amu). This was pertinent due to the aim of identifying extracted long-chain compounds. However, this could not be run for the DF and GF post-Soxhlet liquid residues, due to the volume that was extracted.

Initially, the bulk of the peak areas for the raw barks were lignin-derived (> 45%) (Table 5-16 and Table 5-17). After solvent extraction, most of the pyrolysis products (> 65%) are holocellulose-derived, although this is predominantly from furfural and acetic acid. As intended, the liquid phase contains primarily suberin-derived compounds. However, the liquid-phase also contains lignin-derived compounds. These are almost all simple aromatics, including phenol and toluene.

Despite the aim to valorise the tree bark as a lignin-rich residue, the post-Soxhlet solid residues appear to be more valuable as holocellulose-rich residues. The additional processing cost to perform the solvent extraction may not be feasible, due to the low cost of alternative existing holocellulose-rich residues such as bagasse (545) and straws (546). Nonetheless, by using ethanol as the solvent in the Soxhlet extraction, which can be sourced renewably at increasingly cheaper costs (depending on the feedstock) (547), the environmental impact and financial viability can be positively affected. The ethanol should be able to be re-evaporated and isolated for re-use in the extraction (548), but this was not done in this study.

On a purely lignin-rich basis, NF and SS are the two tree barks for which their Soxhlet solid residues are the most potentially valuable. This is due to their high lignin-derived content, and low suberin, holocellulose and other extractives-derived content.

**Table 5-16** - Distribution of pyrolysis-GC/MS compounds of bark samples to the solid and liquid phase after solvent extraction (in % peak area).

<b>Bark</b>	<b>Type of bark analysed</b>		<b>Suberin-derived</b>	<b>Lignin-derived</b>	<b>Holocellulose-derived</b>	<b>Other extractives</b>
<b>NF</b>	<b>Raw</b>		5.18	85.93	3.28	0
	<b>Soxhlet Residue</b>	<b>Solid</b>	1.95	10.09	81.46	0
		<b>Liquid</b>	61.01	24.96	3.90	10.12
<b>GF</b>	<b>Raw</b>		14.23	56.65	14.88	8.57
	<b>Soxhlet Residue</b>	<b>Solid</b>	0	26.32	69.50	2.19
		<b>Liquid</b>	ND	ND	ND	ND
<b>ESF</b>	<b>Raw</b>		1.81	81.41	9.23	1.60
	<b>Soxhlet Residue</b>	<b>Solid</b>	2.12	0.00	93.59	3.55
		<b>Liquid</b>	66.22	15.58	7.87	0
<b>DF</b>	<b>Raw</b>		0.56	89.54	9.91	0
	<b>Soxhlet Residue</b>	<b>Solid</b>	0	10.73	79.91	5.31
		<b>Liquid</b>	ND	ND	ND	ND
<b>SS</b>	<b>Raw</b>		6.07	91.69	0.86	1.40
	<b>Soxhlet Residue</b>	<b>Solid</b>	1.83	4.80	87.66	0.61
		<b>Liquid</b>	44.33	33.00	6.27	16.28

**Table 5-17** - Distribution of pyrolysis-GC/MS compounds of bark samples to the solid and liquid phase after solvent extraction (in % peak area).

<b>Bark</b>	<b>Type of bark analysed</b>		<b>Suberin-derived</b>	<b>Lignin-derived</b>	<b>Holocellulose-derived</b>	<b>Other extractives</b>
<b>LC</b>	<b>Raw</b>		4.44	46.52	9.03	7.21
	<b>Soxhlet Residue</b>	<b>Solid</b>	1.91	2.75	82.40	11.69
		<b>Liquid</b>	65.72	20.00	1.74	0.00
<b>NC</b>	<b>Raw</b>		20.09	58.38	16.26	1.80
	<b>Soxhlet Residue</b>	<b>Solid</b>	0	0	82.18	0
		<b>Liquid</b>	71.32	4.53	0	0
<b>WH</b>	<b>Raw</b>		0	78.27	13.98	0
	<b>Soxhlet Residue</b>	<b>Solid</b>	1.46	10.60	80.15	5.87
		<b>Liquid</b>	40.89	52.75	6.35	0
<b>L</b>	<b>Raw</b>		0.66	87.15	9.23	2.98
	<b>Soxhlet Residue</b>	<b>Solid</b>	7.26	11.74	66.19	8.66
		<b>Liquid</b>	19.78	14.19	2.1	0

#### 5.2.5.4 Comparison of liquid residues after solvent extractions

In this section, the extracted liquid residues from the two used methods of solvent extraction are compared. These methods (from Section 3.9.2 and 3.9.3) utilise ethanol for Soxhlet extraction, and a hexane/isopropanol mix for the Accelerated Solvent Extraction (ASE) equipment.

From Table 5-18 and Table 5-19, the Soxhlet extraction had extracted mostly suberin-derived compounds (between 19.78-71.32 % peak area) , but also lignocellulosic-derived compounds (4.53-59.1 % peak area). After ASE, it appears that mostly non-suberin-derived extractives were taken into the liquid residues (between 89.59-99.5 % peak area). One such classification of extractives included in all of the liquid injection GC-MS results are phenanthrenes and phenanthrenols. These are known to be present in barks (549, 550), and have anti-cancer, anti-oxidative and anti-inflammatory activities (551, 552).

This shows that the ASE method was better, due in part to a more optimised solvent mix, enhanced extraction efficiency with the addition of sand, and a minimised volume of total solvent. The role of the sand is as an inert material that disperses the sample across the cell. As the Accelerated Solvent Extraction is a pressurised solvent extraction, the sample molecules would adhere tightly to each other under pressure, therefore the sand reduces the impact of this. However, the solid residue could not be retained for further analysis because of the mixture with sand. Future work in this area would be useful, that explored how the solid residue could be captured for analytical pyrolysis.

**Table 5-18** - Comparison of compound classification peak areas from the py-GC/MS of post-Soxhlet extraction and post-ASE liquid residues.

Type of bark analysed		Suberin-derived	Lignin-derived	Holocellulose-derived	Other extractives
NF	ASE	0.05	0.05	0.00	99.62
	Soxhlet	61.01	24.96	3.90	10.12
GF	ASE	3.12	0.35	0.10	89.3
	Soxhlet	ND	ND	ND	ND
ESF	ASE	0.80	0.25	0	97.8
	Soxhlet	66.22	15.58	7.87	0
SS	ASE	1.85	0.31	0.08	94.94
	Soxhlet	44.33	33.00	6.27	16.28

**Table 5-19** - Comparison of compound classification peak areas from the py-GC/MS of post-Soxhlet extraction and post-ASE liquid residues.

Type of bark analysed		Suberin-derived	Lignin-derived	Holocellulose-derived	Other extractives
LC	ASE	0.98	0.21	0	98.27
	Soxhlet	65.72	20.00	1.74	0.00
NC	ASE	10.41	0.20	0.04	87.53
	Soxhlet	71.32	4.53	0	0
WH	ASE	0.05	0.17	0.78	98.67
	Soxhlet	40.89	52.75	6.35	0
L	ASE	0.49	0.19	0	99.25
	Soxhlet	19.78	14.19	2.1	0

### 5.3 Conclusion

In this chapter, a selection of tree barks were analysed by a variety of characterisation methods including proximate and ultimate analysis, atomic absorption spectroscopy, fibre analysis and pyrolysis-gas chromatography/mass spectrometry.

In terms of the proximate and ultimate analysis, all of the tree barks have similar results. The volatile contents are consistently above 65 wt%. The ash content is below 4 wt% for all samples, with the two spruce samples (SS and NS) having the highest.

From the atomic absorption spectroscopy, the alkaline earth metals (AEMs) content is low for all tree barks. The only exception is for the calcium concentration of Norway spruce (NS) and nootka cypress (NC), which is higher (10-18 mg/g). Calcium is expected to be absorbed into the bark from bioaccumulation into the soil the tree is grown in.

The most notable observation that can be made from the fibre analysis is the higher level (20-40 wt% for most) of unknown content in the barks. For this reason, solvent extraction was performed to understand where the unknown content was coming from. Only European silver fir has an unknown content below 10 wt%. Four of the tree barks (noble fir, European silver fir, Western red cedar, and Lawson cypress) have lignin contents above 40 wt%, whilst two have lignin contents below 20 wt% (sitka spruce and nootka cypress). The cellulose content is consistently between 20-40 wt% for all barks, with Douglas fir, noble fir and Western hemlock having the lowest (20-24 wt%). It was posited that the source of the unknown content was from suberin, a known constituent of tree bark that protects its inner cell tissues.

The lignin and holocellulose (hemicellulose and cellulose) content is reflected in the pyrolysis-gas chromatography/mass spectrometry (py-GC/MS) chromatograms. Those with higher holocellulose content have more frequent peaks of furfural and acetic acid, derived from hemicellulose, and compounds such as levoglucosan that are derived from cellulose. The tree barks with the higher levels of unknown content from the fibre analysis contain peaks that include fatty acids such as naphthalenol. These are likely to be derived from suberin.

Two methods of solvent extraction were used to remove the suberin content, one with Soxhlet equipment and one utilising the ASE (Accelerated Solvent Extraction). Although the ASE method was more efficient, the solid sample could not be retained for further analysis, hence the Soxhlet extraction being performed.

From the fibre analysis performed on the Soxhlet extracted-solids, the unknown content was approximately halved for all samples that were run, except for Western hemlock. Due to the removal of the unknown content, the other components (lignin and holocellulose) were concentrated per gram of sample.

The liquid and solid residues after solvent extraction were also analysed by py-GC/MS. The liquids were initially analysed by liquid injection-GC/MS but were repeated by py-GC/MS in case large compounds outside of the mass spectrometer's atomic mass range register were present. From the solvent extraction, it appears that, in addition to the suberin-derived material, polyaromatic hydrocarbons (such as phenanthrenes and phenanthrenols) were extracted into the liquid phase.

The noble fir sample was found to be the bark with the most potential for valorisation as a lignin-rich residue. The solid residues retained after Soxhlet extraction with ethanol that may be the most value are those of NF and SS. For the other bark samples that underwent Soxhlet extraction, they may be able to be valorised as holocellulose (hemicellulose and cellulose) rich residues. However, a techno-economic analysis would be useful for determining the feasibility of the Soxhlet solid residue valorisation compared to the untreated barks. The Accelerated Solvent Extraction was seen to perform better in the overall extraction of non-lignocellulosic content than the Soxhlet extraction, whilst the Soxhlet was more focused in its removal of suberin-derived content.

Overall, this chapter characterised tree barks to explore the differences in composition between eleven species. This study found that the tree barks differed amongst species in fixed carbon (from proximate analysis), calcium contents (from atomic absorption spectroscopy), and lignin contents (from fibre analysis), providing valuable insight into the potential valorisation of tree barks.

## Chapter 6 – The potential to produce bio-based solvents from the pyrolysis of lignin-rich residues

### 6.1 Introduction

In this chapter, the composition of pyrolysis oil (generated by pyrolysis-Gas Chromatography/Mass Spectrometry) from the lignin-rich feedstocks explored in Chapter 4 and Chapter 5 were evaluated for their potential as bio-based solvents (Figure 6-1). The differences in oil composition at a variety of pyrolysis temperatures (450 – 650 °C) were compared. The most prevalent compounds in the pyrolysis oils were then considered if they had undergone established upgrading methods (methylation or hydrogenation) theoretically. The solvent potential of the three types of pyrolysis oil-derived compounds were screened by assessing their environmental, health and safety hazardousness (via the CHEM21 criteria, as described in Section 3.12) and solubility (via Hansen Solubility Parameters). The pyrolysis oil-derived compounds were then compared to common solvents, to determine the specific applications that the prospective bio-based solvents could be used for.

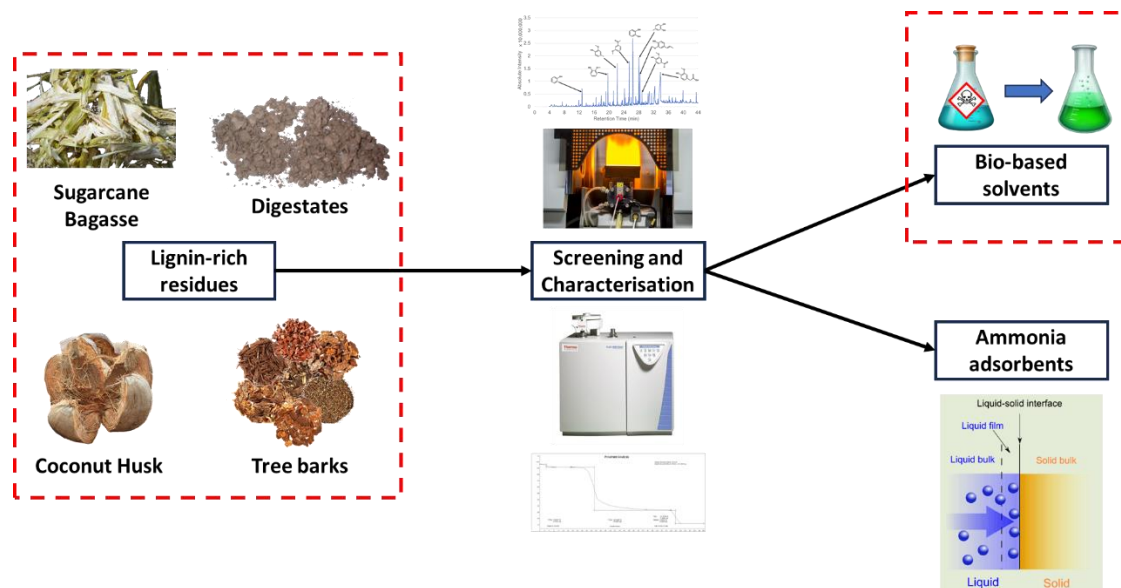


**Figure 6-1** –The overall scope of this study. The work covered in Chapter 6 is denoted by red dotted lines.

### 6.1.1 Background

Solvents are chemicals which are used for the dispersal, dissolution, or dilution of other compounds. In recent years, there has been an increased drive towards “green” or ‘bio-based’ solvents, as society has greater knowledge of the impacts of the synthesis and disposal of petrochemical-derived solvents (46).

An alternative route from changing petrochemical-based solvents to bio-based solvents are solvent-free systems. The potential negative impacts of solvent use on a process can include lower reaction rates, greater process costs, a less environmentally friendly process, and the need for solvent recovery and purification steps (553). Researchers that have looked at avoiding these negative impacts have considered solvent-free systems (554). This “mechanochemistry” occurs at solid-state and uses the constant mechanical force of heavy ball bearings to react two solids together. In comparison to solvent systems, these are considered by some to be comparatively cheaper to using a solvent, and easier to handle (553, 554).

Solvent-free systems may be a useful alternative for some processes, but they also present some challenges. This field remains relatively new, and so the majority of processes that currently utilise solvent systems are unexplored in a solvent-free system (555). Owing to mechanochemistry’s unexplored areas, solvent systems are still necessary across industrial processes. Until the time in which solvents are not needed, it is important to reduce their environmental impact, hence the need for bio-based solvents.

The key solvent property is its solubility, so that it is competent at dissolving a solute into solution (556). The solvent’s ability to do this is dependent on the physical properties and molecular structure of both the solvent and the solute (47).

Solvents’ application as a reaction medium are necessary for several reasons. They allow solid reagents to be used in solution, increase the efficiency of mixing and stirring, and enable the mixing of reagents at suitable concentrations.

The use of solvents in extractions and as a reaction medium is necessary across multiple industries. However, the ideal solvent is dependent on the application, due to the wide variety of properties that a chemical can exhibit.

In the chemical manufacturing industry, solvents are the components with the greatest consumption, and make up a large proportion of the waste generated (48).

The solubility of a solvent is affected by the polarity of its structure, which is related to its electronegativity. The electronegativity of a molecule or atom is its ability to attract an

electron bonding pair (557). For example, both carbons within a carbon-carbon bond have the same electronegativity, so the ability to attract another electron bonding pair is centred around the middle of the C-C bond. Amongst polar compounds with high electronegativities, there are also protic and aprotic functionality. Polar protic solvents contain acidic hydrogen and displays hydrogen bonding (558). The hydrogen bonding is still possible if the chemical is a weak acid. Polar aprotic solvents do not have acidic hydrogens, are not hydrogen bond donors, and so are able to accept hydrogen bonds (559).

Chemicals can therefore be generally organised into non-polar, polar aprotic and polar protic categories (560) (Figure 6-2).

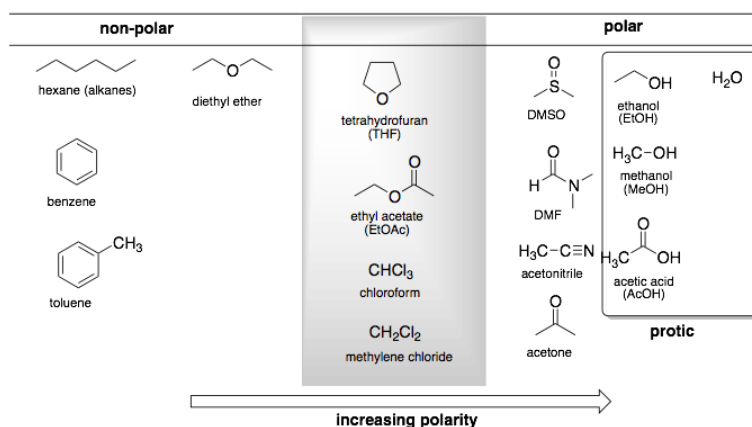


**Figure 6-2** - Common solvents organised into polar protic, polar aprotic and non-polar. Sourced from (560).

A solvent can be either organic or inorganic, whereby organic solvents are carbon-based (such as butanol, toluene, chloroform, acetone) and inorganic solvents are not (such as water, sulphuric acid and ammonia) (561).

### 6.1.1.1 Selection of a solvent

The solvent that is chosen for a particular application is dependent on the application's requirements. These requirements can consist of the physical and chemical properties of different solvents, and their solute and product (562). One of the key properties is polarity, so it is essential that a solvent has a similar polarity to the solute (556). In addition to the polarity, the solvent should preferably be unreactive with the solute molecules to reduce the formation of by-products that would be produced (563). One way to simplify solvent choice is to use a solvent with a boiling point that is lower than either the product or the solute, ensuring easier solvent separation after the reaction has completed (564).

Different factors that affect the selection of a solvent has been described in detail by pharmaceutical companies such as GlaxoSmithKline, Sanofi, Pfizer and AstraZeneca (565-568), and by CHEM21 (378). Their solvent selection guides consider solvent impacts on health, safety, and the environment (EHS) (Figure 6-3).

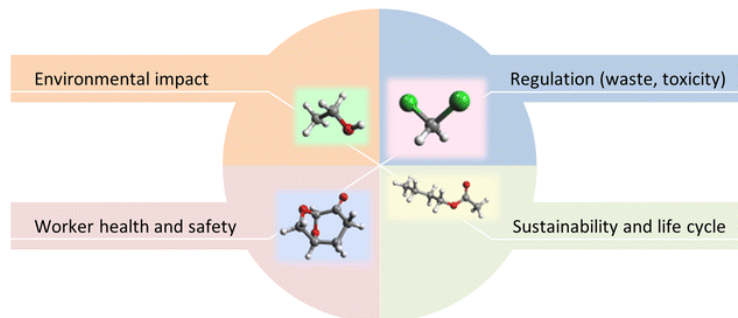


**Figure 6-3** - Considerations for environmental, health and safety in solvent selection guides. Sourced from (569).

At industrial scale, solvents are used in large amounts. At these scales, the potentially negative environmental, health and safety impacts can be significant. In a formulation or purification application where the solvent is not an active reaction component, some of the solvent's characteristics, including toxicity and flammability, are not part of the decision-making process (570).

Specific properties of solvents can benefit the process but may also increase the potential negative impacts. A volatile solvent can improve the levels of solvent recovery and purification post-reaction (571). However, increased volatility may lead to higher levels of volatile organic compounds (VOCs), which can increase worker exposure and undesirable air emissions (569). Solvents with amide functional groups tend to have high polarities, and so can solubilize very polar substrates (572). However, the amide functional group may be reprotoxic (570). Non-polar solvents that are effective in performing separations and dissolving oils include hydrocarbons (573). However, hydrocarbons are combustible and have low solubility in water, which can promote bioaccumulation and aquatic toxicity (574, 575).

The solubility between chemicals and solvents can be compared using the Hansen Solubility Parameters in Practice (HSPiP) database. This database allows for the solubility comparison of over 10,000 chemicals (576) using three factors (each measured in  $\text{MPa}^{0.5}$ ): the energy from dispersion forces between molecules ( $d_d$ ), the energy from dipolar intermolecular force between molecules ( $d_p$ ) and the energy from hydrogen bonds between molecules ( $d_h$ ). Using the HSPiP software, one could theoretically replace a

petrochemically-derived solvent with a bio-based solvent with similar Hansen Solubility Parameter values. Based on the three categories of solvents (as described in Figure 6-2), values for the three HSPs were grouped into non-polar, polar aprotic and polar protic solvents (Table 6-1).

**Table 6-1** - Hansen Solubility Parameter values for sorting into non-polar, polar aprotic and polar protic solvents.

Type of Solvent	dP (MPa <sup>0.5</sup> )	dH (MPa <sup>0.5</sup> )	dD (MPa <sup>0.5</sup> )
Non-polar	<3.5	-	-
Polar aprotic	>3.5	<12.49	
Polar protic	>3.5	>12.49	

### 6.1.1.2 Current commercial bio-based solvents

In the last decade, several bio-based solvents have come onto the market, predominantly as replacements to petroleum-derived solvents. In comparison to the production of petrochemical-derived solvents, the supply of bio-based solvents is independent of petrochemical production and is reliant on the availability of the feedstock. In addition, petrochemical-derived solvents contribute to environmental pollution throughout their life cycle (across their extraction, production to disposal), whereas this is not the case for bio-based solvents.

Non-polar solvents are those with zero (or very small) dipole moments across their structure (577). The most common groups of non-polar solvents are aromatics (such as benzene, toluene, and xylene) and alkanes (including hexane, pentane and heptane) (578). Due to the low (or lack of) polarity, these solvents have high solubility towards non-polar compounds. Therefore, non-polar solvents work best in applications that require good solubility against oils, fats and waxes (579).

One group of biobased non-polar solvents are terpenes (54), which can be obtained from plant-derived essential oils (44). Common terpene solvents are D-limonene and  $\alpha$ -Pinene. D-limonene, with a market demand currently expected to be around 65 kilotons per year, has been used to dissolve cholesterol-containing stones due to it acting as a strong solvent towards cholesterol, and to both degrease and grease wool and cotton wool (44).  $\alpha$ -Pinene is utilised in perfume production as insect repellent and as a household cleaning solvent (44). However, terpenes, in general, are known to be toxic towards fish, amongst other environmental risks (54, 55).

Polar protic solvents are chemicals which are able to participate in hydrogen bonding due to the presence of N-H or O-H bonds (580). These solvents commonly have high dipole moments and dielectric constants, and include ethanol, methanol, ammonia, acetic acid, and water. The most established polar protic bio-based solvent commercially is bioethanol, which is produced predominantly from sugarcane and corn (44). Both methanol and ethanol can be produced, in small amounts, from the gasification of biogas. Ethanol can then be produced by the fermentation of the carbohydrates (44), whilst methanol can be synthesised by the reaction between hydrogen and carbon dioxide (581). In comparison to the production of bioethanol process, biomethanol synthesis requires greater energy and material intensity (582).

Polar aprotic solvents do not have O-H or N-H bonds, so are unable to hydrogen bond (580). The properties of polar aprotic solvents can be separated into those with small dipole moments and dielectric constants (< 10, unitless), and those that are higher. For the solvents with the weaker of the properties, such as tetrahydrofuran, methylene dichloride and ethyl acetate, they are generally unreactive. Therefore, they are commonly only used as a reaction medium. The polar aprotic solvents with higher dielectric constants and dipole moments, by comparison, are reactive. Examples of these include acetonitrile, acetone, and N,N-dimethylformamide (580). Bio-based polar aprotic solvents have been explored in the literature (583), such as Cyrene (dihydrolevoglucosenone) and 2-methyl tetrahydrofuran (2-MeTHF). Cyrene has been noted as an alternative to dimethyl formamide, N-methyl pyrrolidone and dichloromethane (584, 585). 2-MeTHF has been explored for its similarity to tetrahydrofuran (56). Acetone can be produced, alongside ethanol and butanol, from biomass via ABE fermentation (44). However, this is not currently produced at large scales (586).

### **6.1.1.3 The potential for pyrolysis oil-derived solvents**

One potential route for the production of bio-based solvents precursors is pyrolysis. This thermochemical process covers a wide remit, such as hydrolysis, slow, fast and flash (587), as discussed in Section 2. The pyrolysis of lignocellulosic biomass can produce over a hundred individual compounds (58).

The pyrolysis oil, or bio-oil, which is produced from pyrolysis processes exhibit properties that are different from petroleum crude oils. Pyrolysis oils from biomass contain complex mixtures of oxygenated hydrocarbons with high polarity, whereas hydrocarbons from crude oil are generally non-polar by nature (57). The oxygenated hydrocarbons can be removed by hydrotreatment or hydrocracking, producing similar hydrocarbons to that from crude oil.

However, this requires H<sub>2</sub> for hydrotreatment and oxygen removal. Pyrolysis oils, dependent on the lignocellulosic composition, also contain alcohols, aldehydes/ketones, acids/esters, furans, lignin-derived methoxy groups, and phenolic compounds (588).

Petroleum crude oils and bio oil are immiscible with each other (589). This is due to bio-oil containing high levels of oxygen (from biomass), and is therefore polar. As crude oil does not contain high levels of oxygen, it is non-polar. If bio-oil was added to existing refinery equipment in which petroleum oil is used (including hydrotreaters and hydrocrackers), a separate feed system would be required (589).

However, the key challenge in the production of bio-oils is the identification of applications. In an ideal situation, each high-value compound within a bio-oil's composition could be separated out, and then sold as individual chemicals. Unfortunately, separation is difficult and is an expensive process. This was previously done for the commercial production of vanillin, but this is no longer the case (60). A more cost-effective solution is to use blends of the bio-oils as mixtures, but the mixtures would only be able to be used in lower-value applications. One example is that they are unlikely to be used in the pharmaceutical industry as there is a need for > 99% purity products with 100% reliability and conformity (590).

There are a few solvents that have been commercially produced from the fractionation and upgrading of pyrolysis oil. Turpentine oil is considered to be a specialised solvent. It is obtained by the distillation of the oleoresin of pine trees (591). The oil is used commercially in the production of varnishes and to thin oil-based paints. Turpentine oil is also upgraded by rectification for the pharmaceutical industry (591).

Mudraboyina et al (2016) (59) produced a pyrolysis oil-derived solvent referred to as lignin oil methyl ether (LOME) by the methylation and supercritical rectification (distillation under supercritical conditions) of pyrolysis oil. The solvent is aprotic and is seen as an alternative to dimethyl sulfoxide or dimethyl furan. Haseeb et al (2021) (60) then catalytically hydrogenated LOME, to generate a mixture of cyclohexyl methyl ethers (HLOME). The HLOME was produced as an aliphatic ether solvent, as a replacement for acetone, 2-butanone, ethyl acetate and tetrahydrofuran. The most common method for the upgrading of pyrolysis oil is hydrogenation, whereby molecular hydrogen is reacted chemically, typically with a catalyst (61). After hydrogenation, double bonded C=C may become saturated to single bonds, and the formation of alcohols from carbonyl groups (C=O) (592). One of the key reasons for hydrogenating pyrolysis oil is to improve its stability (593). Literature could be found whereby pyrolysis oil was hydrogenated (592, 594-597).

However, none could be found where the hydrogenated pyrolysis oil was considered as a solvent.

Independent of lignin-derived products' valorisation as a solvent, liquid smoke flavouring is used for the flavouring of cheese, meat and sausages, and is produced by the water extraction of bio oil in refineries (598).

Although the valorisation of pyrolysis oil-derived solvents has been explored, as discussed earlier, the literature has not considered a wide range of lignin-rich residues.

## 6.2 Results and Discussion

In this section, lignin-rich samples from a variety of sources (commercial lignin products, tree barks, and biomass residues) were investigated for their potential as precursors to bio-based solvents (Table 6-2).

**Table 6-2** – List of samples explored for their potential as bio-based solvent precursors.

Sample Type	Sample
<b>Commercial Lignin Products</b>	Lignoboost (LB)
	Alkali Lignin (AlkLig)
	Organosolv (Org)
<b>Biomass Residues</b>	Unknown Golden Acre tree bark (Bark)
	Sugarcane bagasse (PKBag)
	Coconut Husk (CH)
<b>Fir Tree Barks</b>	Noble fir (NF)
	Douglas fir (DF)
	European silver fir (ESF)
	Grand fir (GF)
<b>Pine Tree Barks</b>	Sitka spruce (SS)
	Norway spruce (NS)
	Larch (L)
	Western hemlock (WH)
<b>Cypress Tree Barks</b>	Western red cedar (WRC)
	Lawson cypress (LC)
	Nootka cypress (NC)
<b>Solvent-extracted tree barks</b>	Solvent-extracted Douglas fir (DFSox)
	Solvent-extracted European silver fir (ESFSox)
	Solvent-extracted noble fir (NFSox)
	Solvent-extracted grand fir (GFSox)
	Solvent-extracted sitka spruce (SSSox)
	Solvent-extracted Western hemlock (WHSox)
	Solvent-extracted larch (LSox)
	Solvent-extracted Lawson cypress (LCSox)
	Solvent-extracted nootka cypress (NCSox)
	Solvent-extracted Western red cedar (WRCSox)
<b>Acid-washed samples</b>	Acid-washed Alkali Lignin (AlkLigAcid)
	Acid-washed sugarcane bagasse (PKBagAcid)
	Acid-washed coconut husk (CHAcid)

The samples first underwent fast pyrolysis-gas chromatography/mass spectrometry (py-GC/MS) at analytical scale (< 10 mg) at a range of temperatures (450 - 650 °C) to identify the main components that would be present in the pyrolysis oils.

Following this, the theoretical upgrading of the main pyrolysis oil components (by methylation and hydrogenation) was explored, with their solubility and hazardousness

estimated through use of Hansen Solubility Parameters (HSP) and the CHEM21 criteria. The HSPs were collated from the HSPiP software, which contains the parameter values of over 1000 chemicals. The data for each chemical required for implementing the CHEM21 criteria was taken from safety data sheets and the literature. The three types of pyrolysis oil-derived components were then compared to common industrial solvents through the HSP values, with their potential applications discussed.

### **6.2.1 Pyrolysis-Gas Chromatography/Mass Spectrometry**

In this section, a wide variety of lignin-rich samples underwent fast pyrolysis by py-GC/MS at 450, 550 and 650 °C. The accuracy of the temperature for each analytical scale fast pyrolysis run was ensured through monitoring the readouts on the pyroprobe software. The software showed the current temperature of the platinum coil as the pyrolysis was occurring. As stated previously, the pyrolysis of a sample can produce over a hundred different compounds (58). Therefore, this section focuses on the compounds that were most prevalent across all of the py-GC/MS data. The py-GC/MS data, however, does not provide absolute values of compounds present in the samples, but it does give an indication. Regarding the absolute values and proportions of compounds identified by the GC/MS after py-GC/MS, they may not be identical in repeated runs. This is because, despite the samples being homogeneous, the sample may degrade slightly differently during the pyrolysis, leading to potentially different identification by GC/MS.

From Figure 6-4 to Figure 6-12, the change in peak areas of the six compounds across the three pyrolysis temperatures that appeared most often are illustrated. These were 2-methoxy phenol, phenol, trans-isoeugenol, furfural, creosol and 5-methyl-2-furancarboxaldehyde (MFCA). The peak areas taken from each sample have been normalised.

The presentation of the following data is subdivided between untreated samples and treated samples, as described in Table 6-2. The data is additionally separated into lignin-derived (2-methoxy phenol, phenol, trans-isoeugenol and creosol) and holocellulose-derived (furfural and MFCA) components. Holocellulose is a collective term of hemicellulose and cellulose.

#### **6.2.1.1 Py-GC/MS of untreated samples**

First, the peak areas of the lignin and holocellulose-derived components identified by the py-GC/MS of the untreated samples are outlined (from Figure 6-4 to Figure 6-9).

Alkali lignin has the greatest levels of 2-methoxy phenol, across all three temperatures in Figure 6-4. This is likely due to the high lignin content increasing the proportion of aromatic compounds, and high alkaline earth metal concentration increasing the pyrolysis severity (as discussed in Chapter 4). Therefore, alkali lignin would have greater proportions of simple aromatics at lower temperatures.

There is not a clear change of 2-methoxy phenol proportion as the temperature increases. In samples (such as NF, DF, NC, and WRC in Figure 6-4 [c] and [e]), the proportion decreases with temperature. With several samples (org and GF in Figure 6-4 [a] and [c]), the proportion of 2-methoxy phenol increases with the temperature.

For the phenol peaks (Figure 6-5), coconut husk (in [b]) had the greatest proportion of peak areas at all temperatures. Generally, as the pyrolysis temperature increased, the phenol proportion increased as well. This is expected due to phenol being the simplest aromatic compound (other than benzene), so is likely to be more prevalent as the functionalities of the larger aromatic structures break down at higher temperatures. The commercial lignin products (in [a]), other than alkali lignin, had negligible levels of phenol. This may be due to the high-lignin composition consisting of complex lignin polymeric structures, in addition to the low alkaline earth metal content, thereby raising the temperatures at which simple aromatics (such as phenol) are formed.

The proportions of trans-iso Eugenol in Figure 6-6 are consistently high for the fir tree barks (9-21%) (in [c]). The biomass residues (in [b]) and commercial lignin products (in [a]) have lower levels of trans-iso Eugenol. The greatest proportion of trans-iso Eugenol consistently occurs at 450 °C.

Lignoboost has the greatest levels of creosol of all samples (in Figure 6-7 [a]). This may be due to the commercial lignin product having more complex structures and is therefore more likely to contain benzene rings with multiple functionalities. The proportion of creosol does not seem to be consistently affected by pyrolysis temperature, apart from with NS (in [d]) and WRC (in [e]), where it decreases with temperature. The biomass residues (in [b]) have the lowest creosol proportions of all of the sample groups.

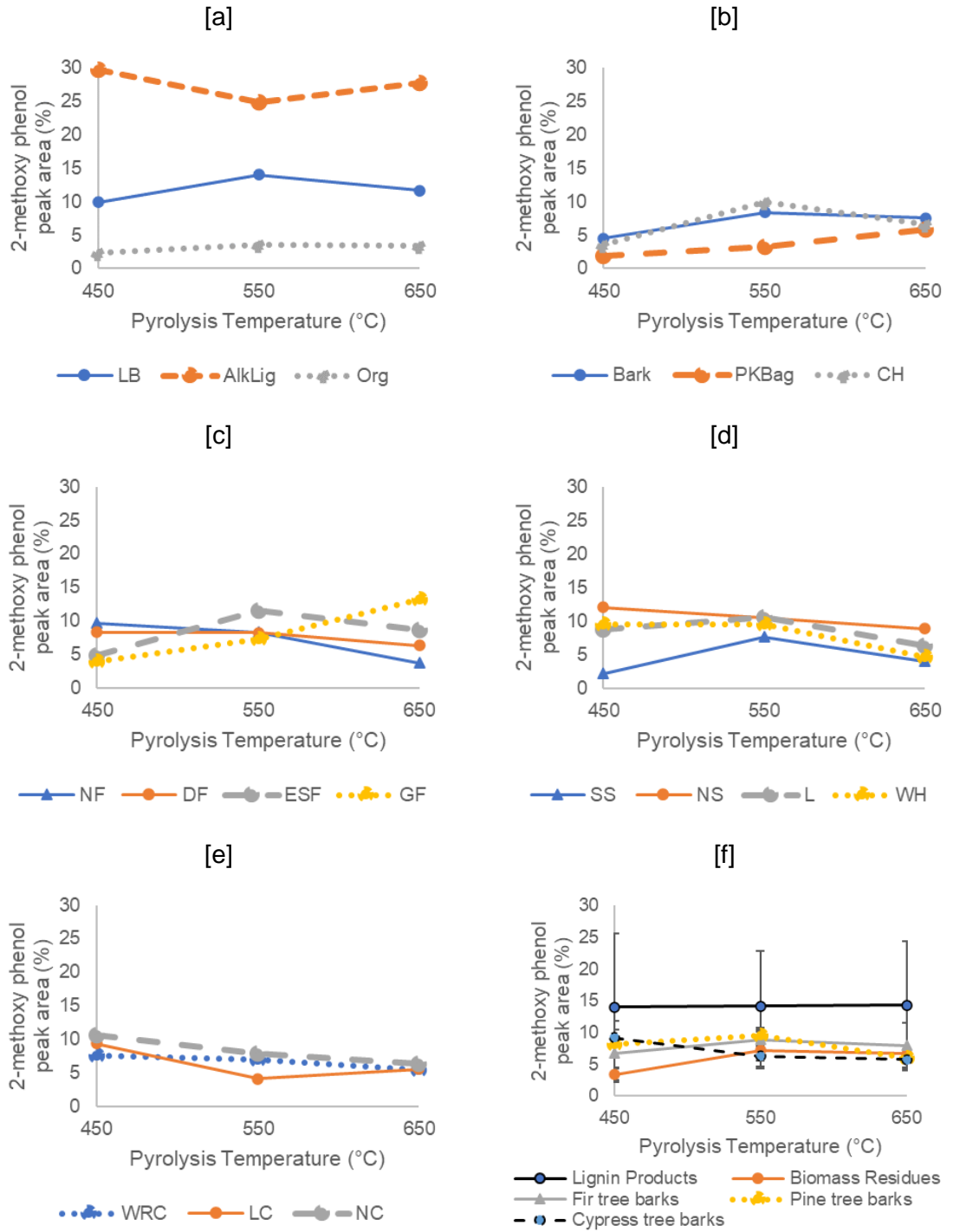


**Figure 6-4** - Peak areas (%) of **2-methoxy phenol** across [a] commercial lignin products, [b] biomass residues, [c] fir tree barks, [d] pine tree barks, [e] cypress tree barks and [f] the average of all categories. Each sample was run once. Errors in [f] are 1x standard error, taken from collating the data points in [a] – [e]. Individual peak areas have been normalised.

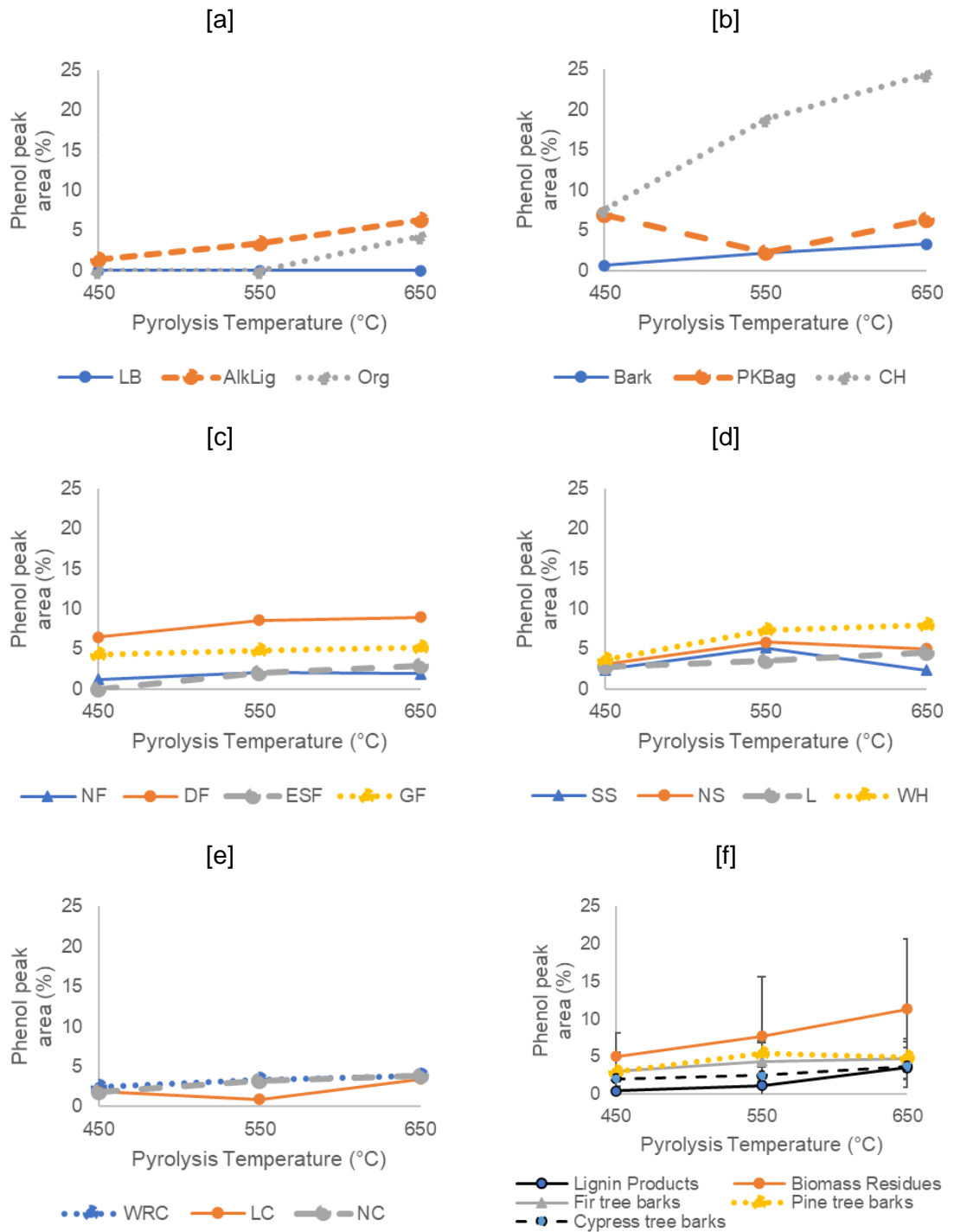


**Figure 6-5** – Peak areas (%) of **phenol** across [a] commercial lignin products, [b] biomass residues, [c] fir tree barks, [d] pine tree barks, [e] cypress tree barks and [f] the average of all categories. Each sample was run once. Errors in [f] are 1x standard error, taken from collating the data points in [a] – [e]. Individual peak areas have been normalised.

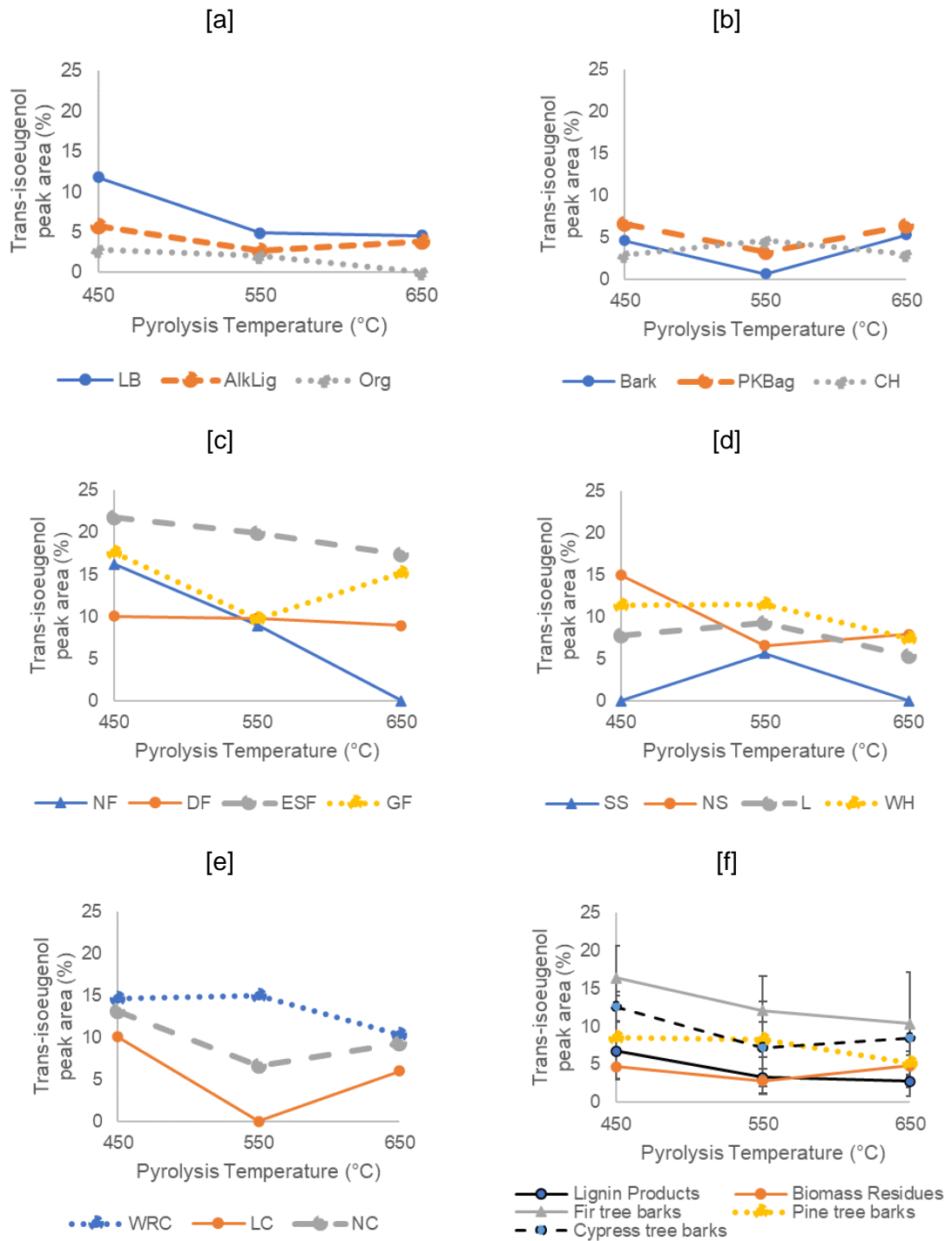


**Figure 6-6** - Peak areas (%) of **trans-iso Eugenol** across [a] commercial lignin products, [b] biomass residues, [c] fir tree barks, [d] pine tree barks, [e] cypress tree barks and [f] the average of all categories. Each sample was run once. Errors in [f] are 1x standard error, taken from collating the data points in [a] – [e]. Individual peak areas have been normalised.

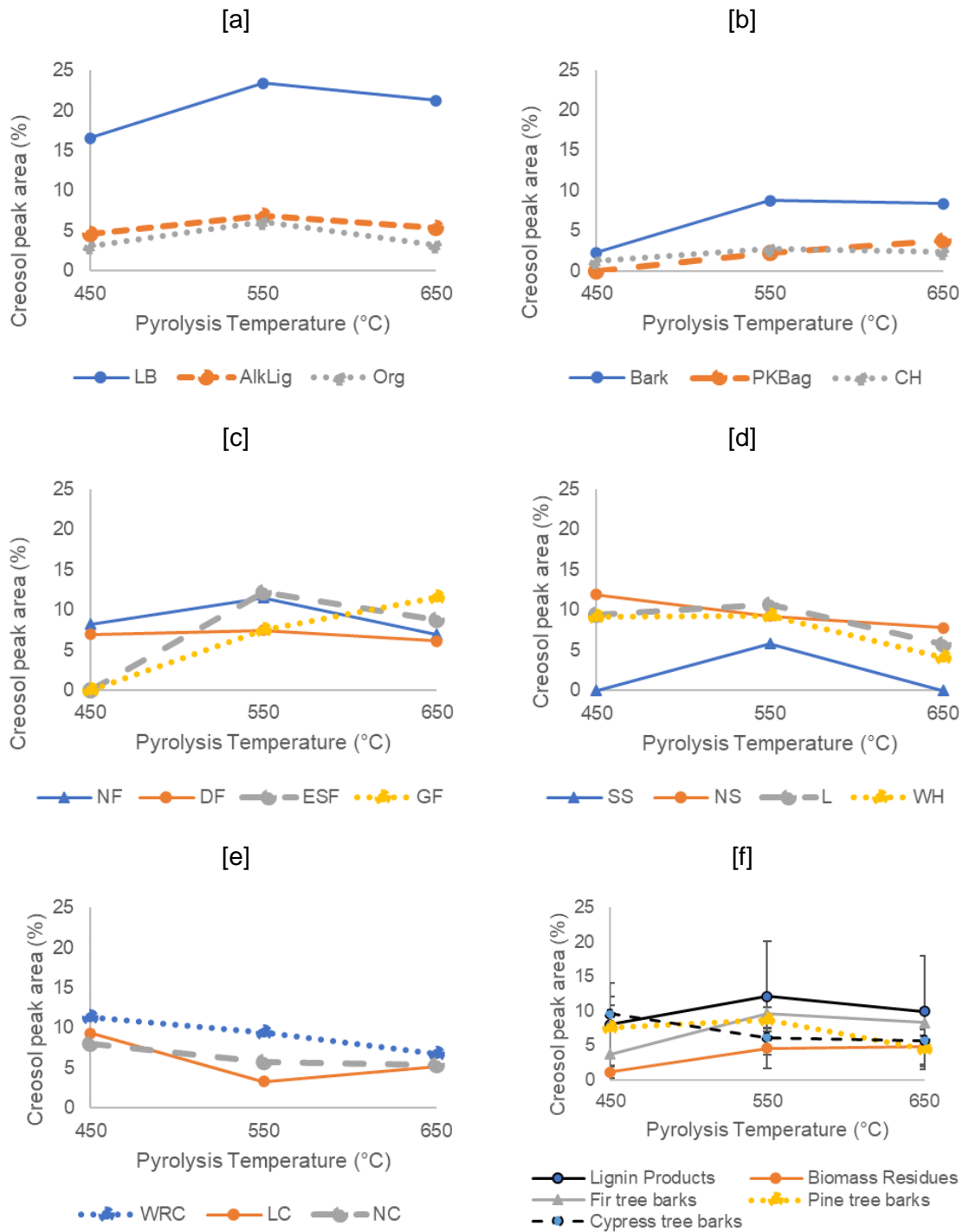


**Figure 6-7** - Peak areas (%) of **creosol** across [a] commercial lignin products, [b] biomass residues, [c] fir tree barks, [d] pine tree barks, [e] cypress tree barks and [f] the average of all categories. Each sample was run once. Errors in [f] are 1x standard error, taken from collating the data points in [a] – [e]. Individual peak areas have been normalised.

For the holocellulose-derived components presented in Figure 6-8, all of the untreated samples (Figure 6-8) have low levels of furfural. In addition, the majority of the tree bark samples, excluding SS (in [d]) and DF [in [c)], have 5-methyl-2-furancarboxaldehyde (MFCA) peaks (Figure 6-9).

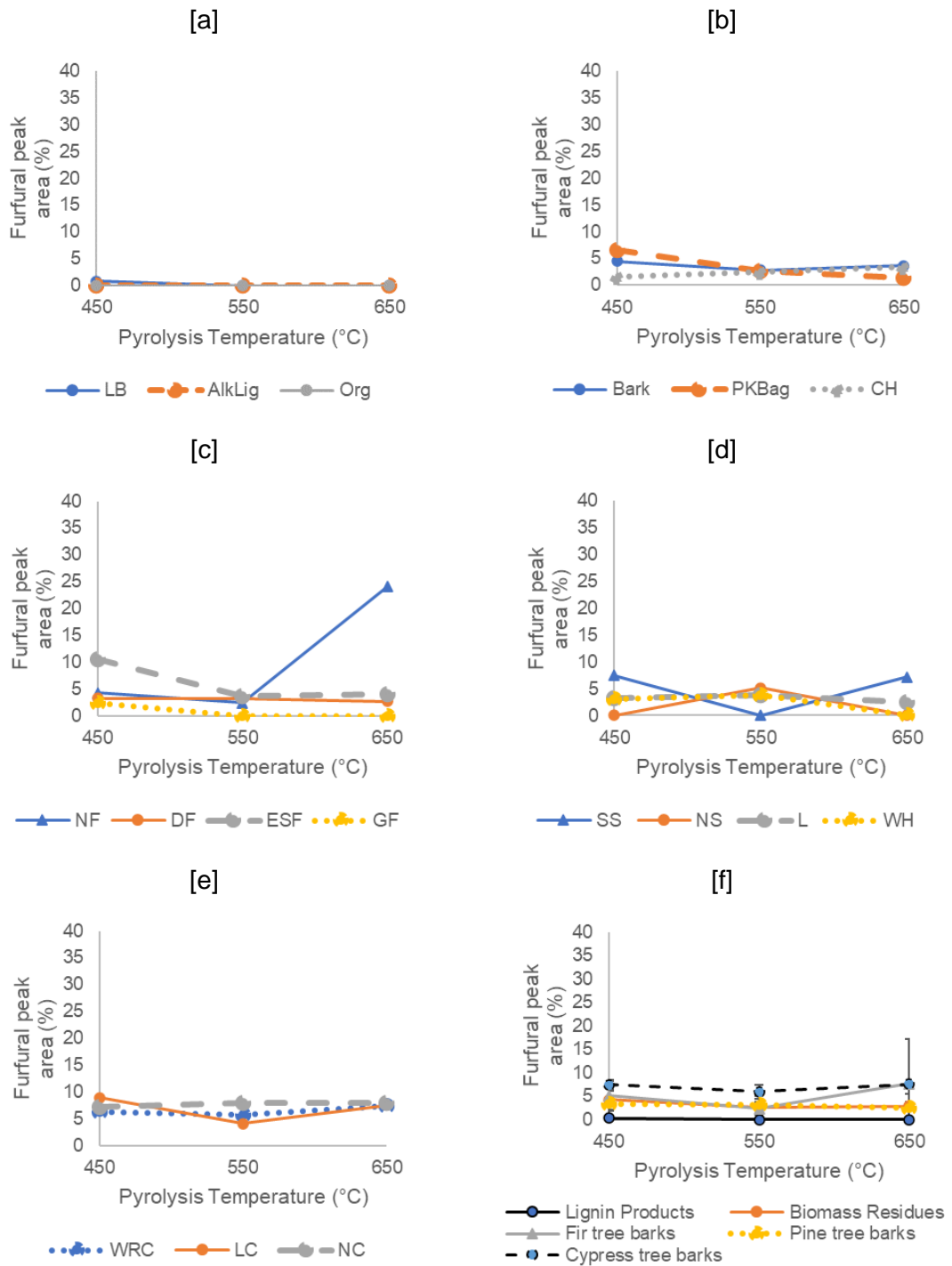


**Figure 6-8** - Peak areas (%) of **furfural** across [a] commercial lignin products, [b] biomass residues, [c] fir tree barks, [d] pine tree barks, [e] cypress tree barks and [f] the average of all categories. Each sample was run once. Errors in [f] are 1x standard error, taken from collating the data points in [a] – [e]. Individual peak areas have been normalised.

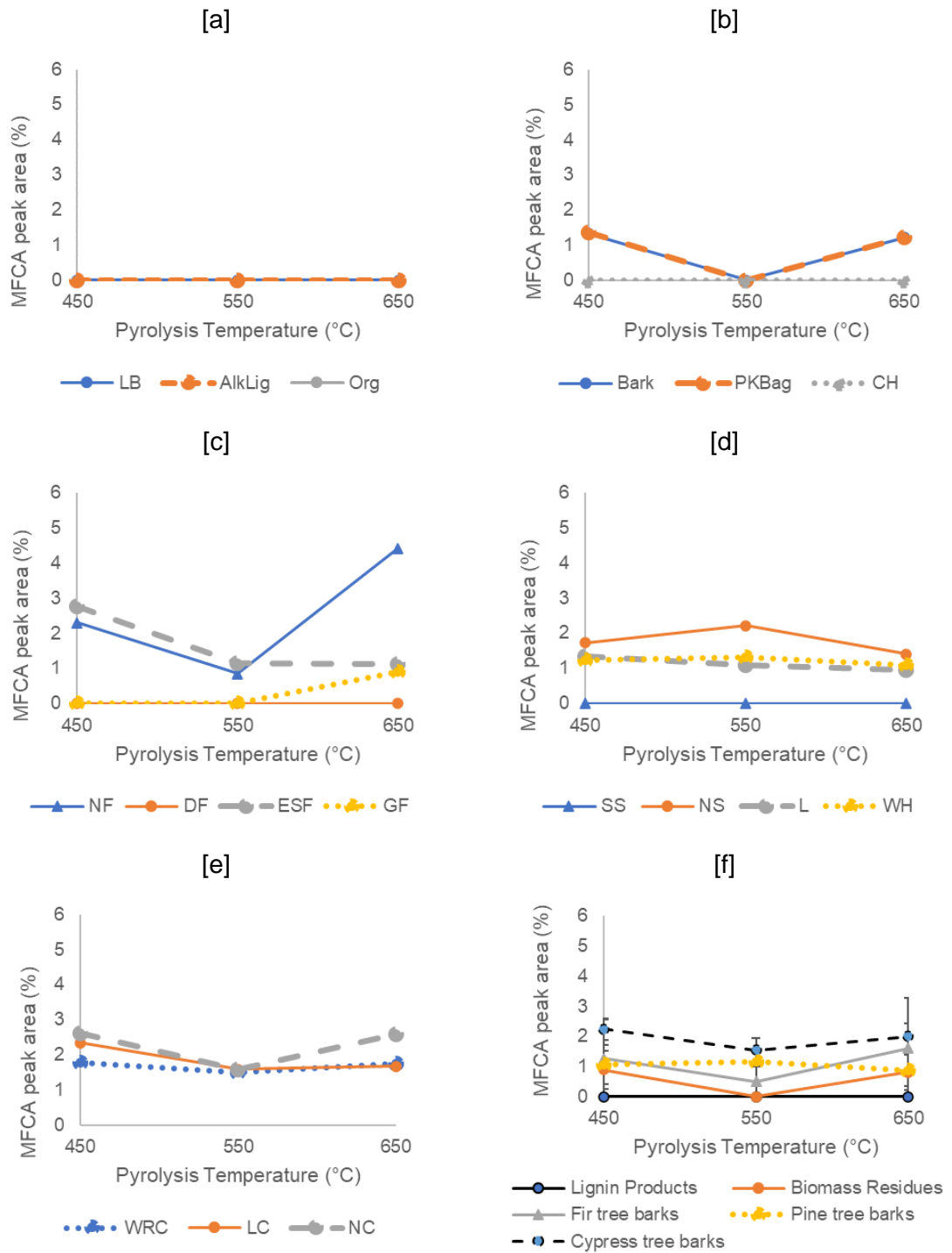


**Figure 6-9 - Peak areas (%) of 5-methyl-2-furancarboxaldehyde (MFCA) across [a] commercial lignin products, [b] biomass residues, [c] fir tree barks, [d] pine tree barks, [e] cypress tree barks and [f] the average of all categories. Each sample was run once. Errors in [f] are 1x standard error, taken from collating the data points in [a] – [e]. Individual peak areas have been normalised.**

### **6.2.1.2 Py-GC/MS of pre-treated samples**

In this section, the change in the key lignin-derived compounds (2-methoxy phenol, phenol, trans-isoeugenol and creosol) and holocellulose-derived compounds (furfural and 5-methyl-2-furancarboxaldehyde) after two forms of treatment will be discussed.

The treatments (acid-washing and solvent extraction) were outlined previously in Chapter 4 and Chapter 5.

#### **Py-GC/MS of solvent-extracted samples**

The treatment of the raw tree barks by solvent extraction has led to a general reduction in lignin-derived compounds (Figure 6-10), and an increase in holocellulose-derived compounds (Figure 6-11).

Across all solvent-extracted tree bark samples, the 2-methoxy phenol content significantly decreases after extraction. Only NFSox, GFSox, SSSox and WHSox still have 2-methoxy phenol after acid-washing, with NFSox, GFSox and WHSox having the highest proportion ( $\approx 2\%$  peak area).

The phenol peak areas are similar to 2-methoxy phenol, with an overall reduction after solvent extraction. However, here, only LSox and NCSox have no phenol. DFSox, GFSox, WHSox have the highest phenol proportions of the solvent-extracted samples, with around 1.5% peak area.

The trans-isoeugenol proportions were overall the highest of the untreated tree bark samples, but only three solvent-extracted samples still contained trans-isoeugenol (DFSox, ESFSox and NFSox, with around 1.5% peak area). The same can be said for creosol, but none of the solvent-extracted samples contained creosol after treatment.

One of the reasons for the phenol proportions reducing, but not reaching 0% peak area (other than LSox and NCSox) may be due to the solvent extraction weakening or breaking the bonds for the more complex aromatic compounds of trans-isoeugenol and creosol. This would then increase the likelihood of simple aromatics such as phenol after pyrolysis.

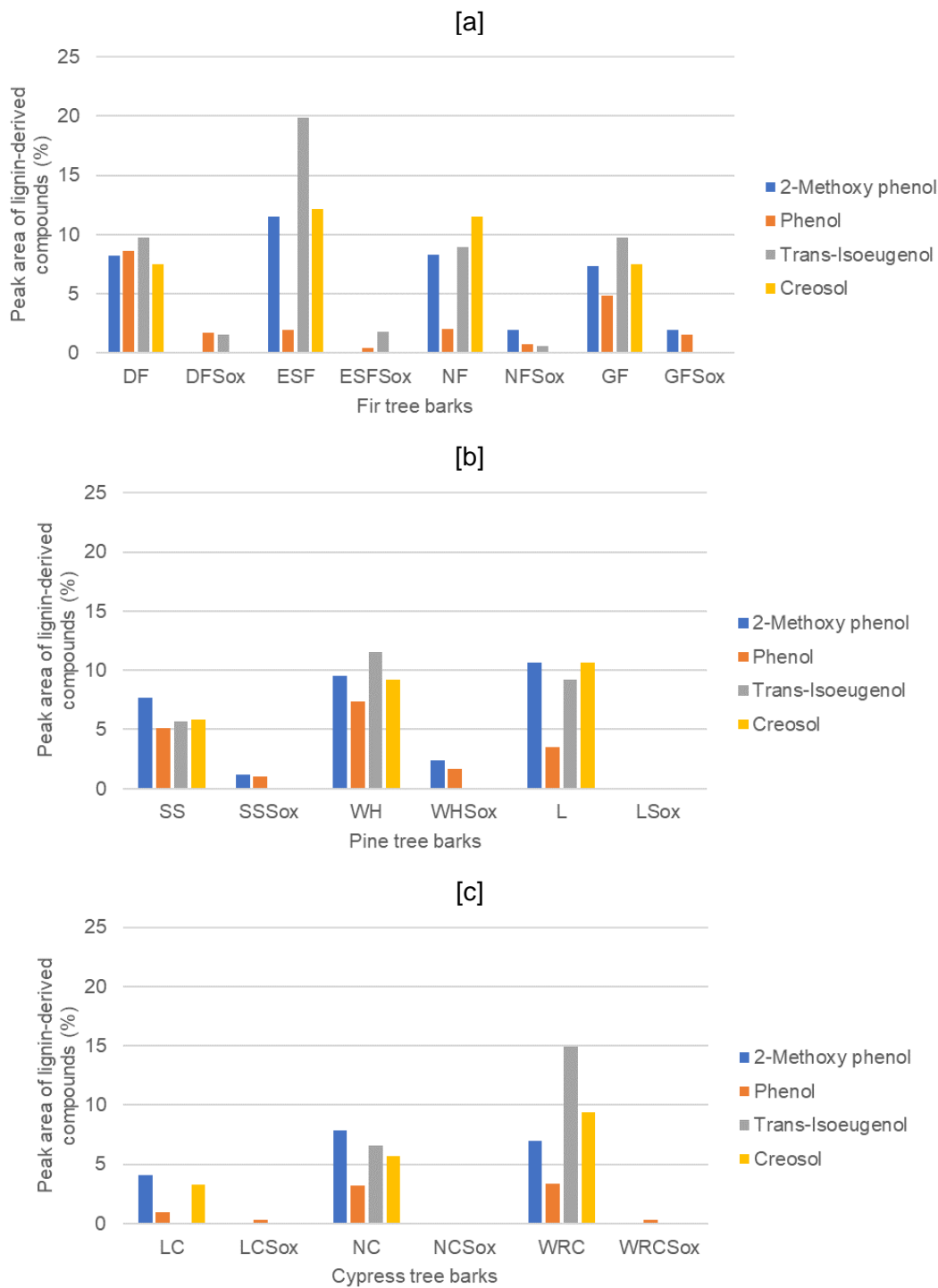


**Figure 6-10 - Peak areas (%) of lignin-derived compounds of raw and solvent-extracted [a] fir tree barks, [b] pine tree barks, and [c] cypress tree barks at 550 °C. Individual peak areas have been normalised.**

Regarding the change in holocellulose-derived compounds after solvent extraction (Figure 6-11), all of the tree barks gained furfural and 5-methyl-2-furancarboxaldehyde (MFCA).

LCSox had the highest level of furfural ( $\approx$  53% peak area), Most of the solvent-extracted samples had greater than 18% peak area of furfural, except for GFSox. This was more expected for GFSox and SSSox (which had 20.3% peak area) because their raw equivalent did not have any furfural to begin with.

NFSox and ESFSox had the greatest proportions of MFCA, with the highest value being around 5.5% peak area. This may be due to the treatment removing extractives or other material that was unrelated to the formation of MFCA, thereby concentrating the structural components that can form MFCA within the sample.

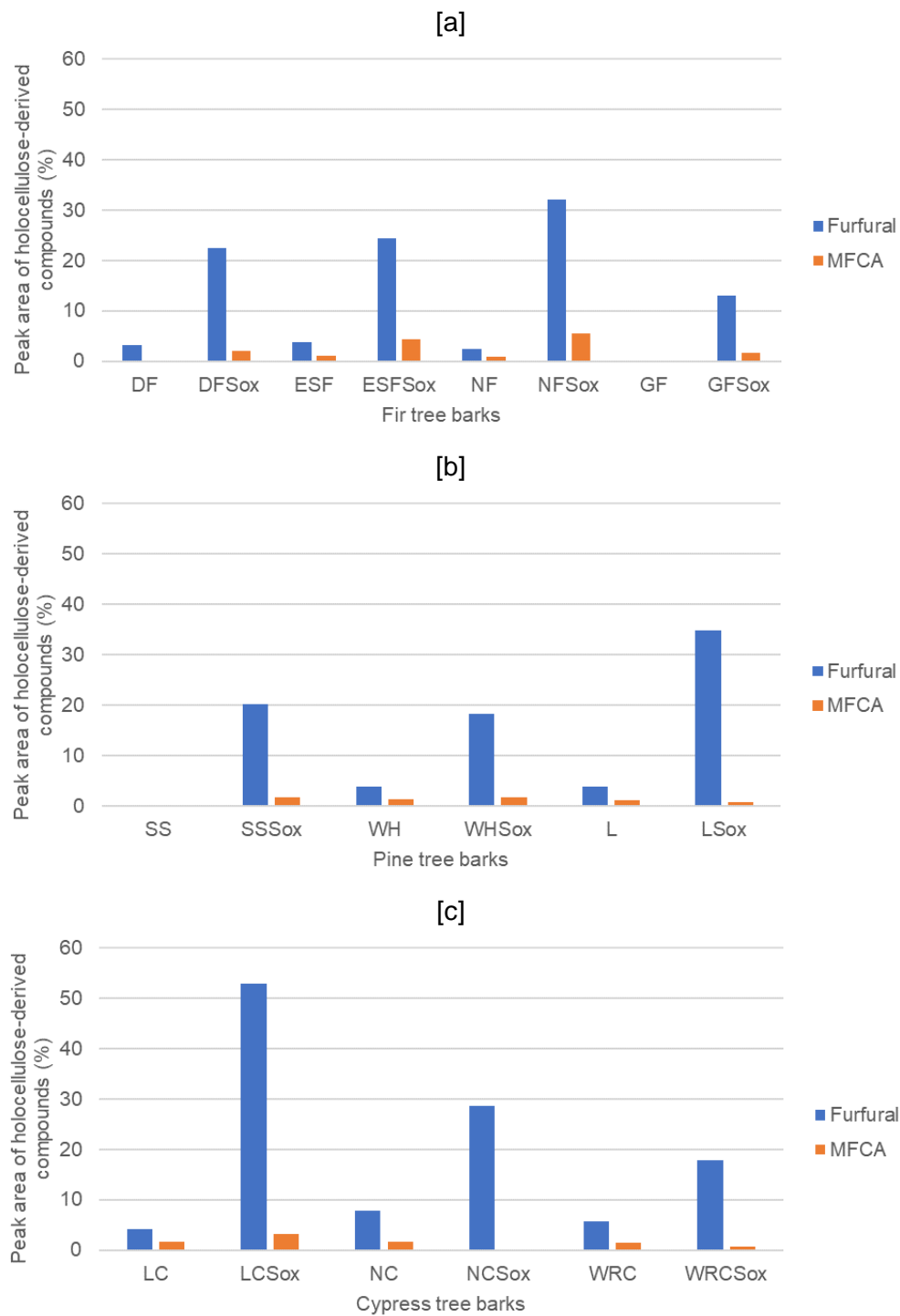


**Figure 6-11** - Peak areas (%) of holocellulose-derived compounds of **raw** and **solvent-extracted** [a] fir tree barks, [b] pine tree barks, and [c] cypress tree barks at 550 °C. Individual peak areas have been normalised.

### **Py-GC/MS of acid-washed samples**

When considering the changes in the key py-GC/MS peaks after acid-washing (Figure 6-12), the main differences appear to be the decrease in lignin-derived compounds, and the increase in holocellulose-derived compounds.

For the peak areas of 2-methoxy phenol, any that was present in the sugarcane bagasse (PKBag) and coconut husk (CH) has disappeared after acid-washing. The exception for this is the alkali lignin (AlkLig), though this is most likely due to the high initial peak area ( $\approx 25\%$ ). AlkLigAcid had the greatest level of 2-methoxy phenol of the acid-washed samples ( $\approx 11\%$  peak area), which was comparable to the 2-methoxy peak area of un-washed coconut husk ( $\approx 10\%$  peak area).

The phenol peak area consistently reduced also, but to a lesser extent than 2-methoxy phenol. This decreased reduction of peak area between phenol and 2-methoxy phenol may be due to the acid-washing, as it may have weakened or broken the bond between the phenol and methoxy functional group. Therefore, after acid-washing, the samples' structures would be more likely to generate phenol fragments after pyrolysis as the methoxy bond would be quicker to break, although the proportion of phenol present would be skewed by greater proportions of other compounds such as furfural (in Figure 6-12 [b]). CHAcid had the highest proportion of phenol ( $\approx 4\%$  peak area), though it is a similar peak area to unwashed AlkLig ( $\approx 3\text{-}4\%$  peak area).

AlkLigAcid has the greatest peak areas of trans-isoeugenol ( $\approx 7\%$  peak area) and creosol ( $\approx 4.5\%$  peak area) of the acid-washed samples. The trans-isoeugenol content decreases after acid-washing for the PKBag and CH samples but increases by around 5% for alkali lignin. The increase for AlkLig may be because this sample was already processed during its production, from the hydrolytic degradation of Kraft lignin. Therefore, the acid-washing may have had less of an impact compared to the untreated sugarcane bagasse and coconut husk, with the proportion of trans-isoeugenol increasing due to the reduction in other compound proportions.

Creosol also reduces after acid-washing. The change may be due to the same reason as trans-isoeugenol, where the bonds between the functional groups ( $\text{CH}_3$ ,  $\text{O-H}$  and  $\text{O-CH}_3$  in creosol) and the benzene ring are weakened from the treatment, producing similar aromatics with less functionality.

CHAcid has the highest proportion of furfural ( $\approx 36\%$  peak area). The furfural content (in Figure 6-12 [b]) has the greatest increase after acid-washing, with coconut husk gaining

the most ( $\approx 30\%$ ). This may be due to the lignocellulosic structure weakening from the acid-washing or solvent extraction, allowing the hemicellulose to degrade and volatilise during py-GC/MS, when it may not have done otherwise.

Regarding 5-methyl-2-furancarboxaldehyde (MFCA), the samples that had been treated either had a negligible difference or an increased peak area compared to their untreated versions. PKBagAcid and CHAcid had an increased level of MFCA (of around 1-2% peak area), compared to 0% before the acid-washing. PKBagAcid has the greatest level of MFCA ( $\approx 1\%$  peak area).

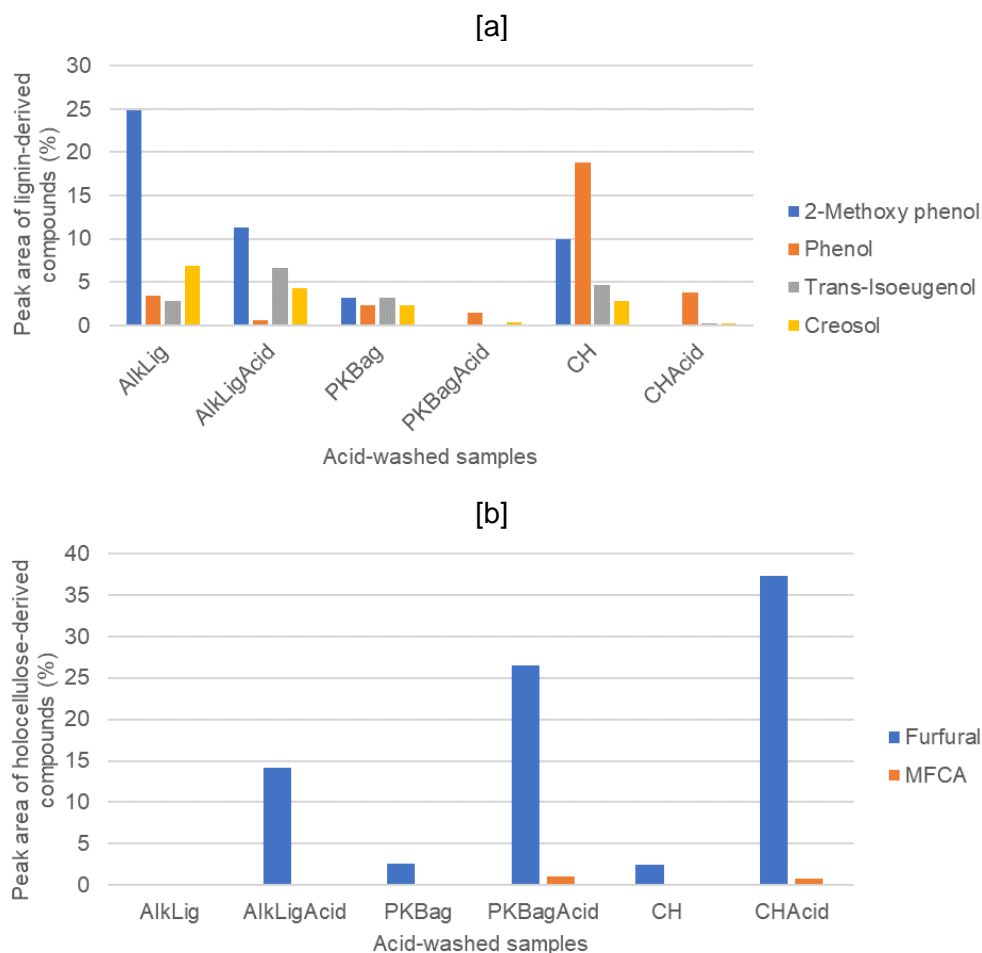


**Figure 6-12** - Peak areas (%) of [a] lignin-derived and [b] holocellulose-derived compounds of **acid-washed** samples at 550 °C. Individual peak areas have been normalised.

### 6.2.1.3 Effect of sample treatment and pyrolysis temperature on pyrolysis oil-derived compounds

Following the work in the previous section, the overall effects of pyrolysis temperature and sample treatment were explored in Figure 6-13.

Here, the peak areas of 2-methoxy phenol, phenol, trans-isoeugenol, creosol, furfural and 5-methyl-2-furancarboxaldehyde (MFCA) were averaged for each type of sample. The different categories are listed as: untreated samples pyrolysed at 450 °C (Untreated @ 450), untreated samples pyrolysed at 550 °C (Untreated @ 550), untreated samples pyrolysed at 650 °C (Untreated @ 650), acid-washed samples pyrolysed at 550 °C (Acid @ 550), and solvent-extracted samples pyrolysed at 550 °C (Sox @ 550).

As can be seen in Figure 6-13 for the lignin-derived compounds ([a] – [d]), the untreated samples, on average, had higher proportions than the treated samples. For 2-methoxy phenol (in [a]), there was not much difference between the peak areas of the untreated samples at the three pyrolysis temperatures. For phenol (in [b]), it can be seen that the peak area increased as the pyrolysis temperature increased. Regarding trans-isoeugenol (in [c]), the peak areas decrease as the pyrolysis severity increases. This is likely due to the bonds to the functional groups weakening to a greater extent through the higher pyrolysis temperatures or two forms of treatment, as discussed previously. There is not a linear change in creosol proportions with pyrolysis temperature. However, between the untreated and treated samples, there is a clear difference in creosol content.

For the holocellulose-derived compounds (Figure 6-13 [e] and [f]), the solvent-extracted samples have the greatest proportions of all sample categories. For furfural (in [e]), there is a clear difference between the treated and untreated samples, whereby the treated samples have peak areas around 25% and the untreated samples have peak areas less than 5%. The furfural data is the only case in this section where the treated samples clearly have greater proportions. This is due to there being no overlap in the error bars between the untreated and treated samples. The error bars were taken from the 1x standard deviation of the data. For MFCA, all of the average peak areas are below 2.1%. There is a noticeable difference between the solvent-extracted samples' average and the other sample categories, however, its error bar is also the greatest.

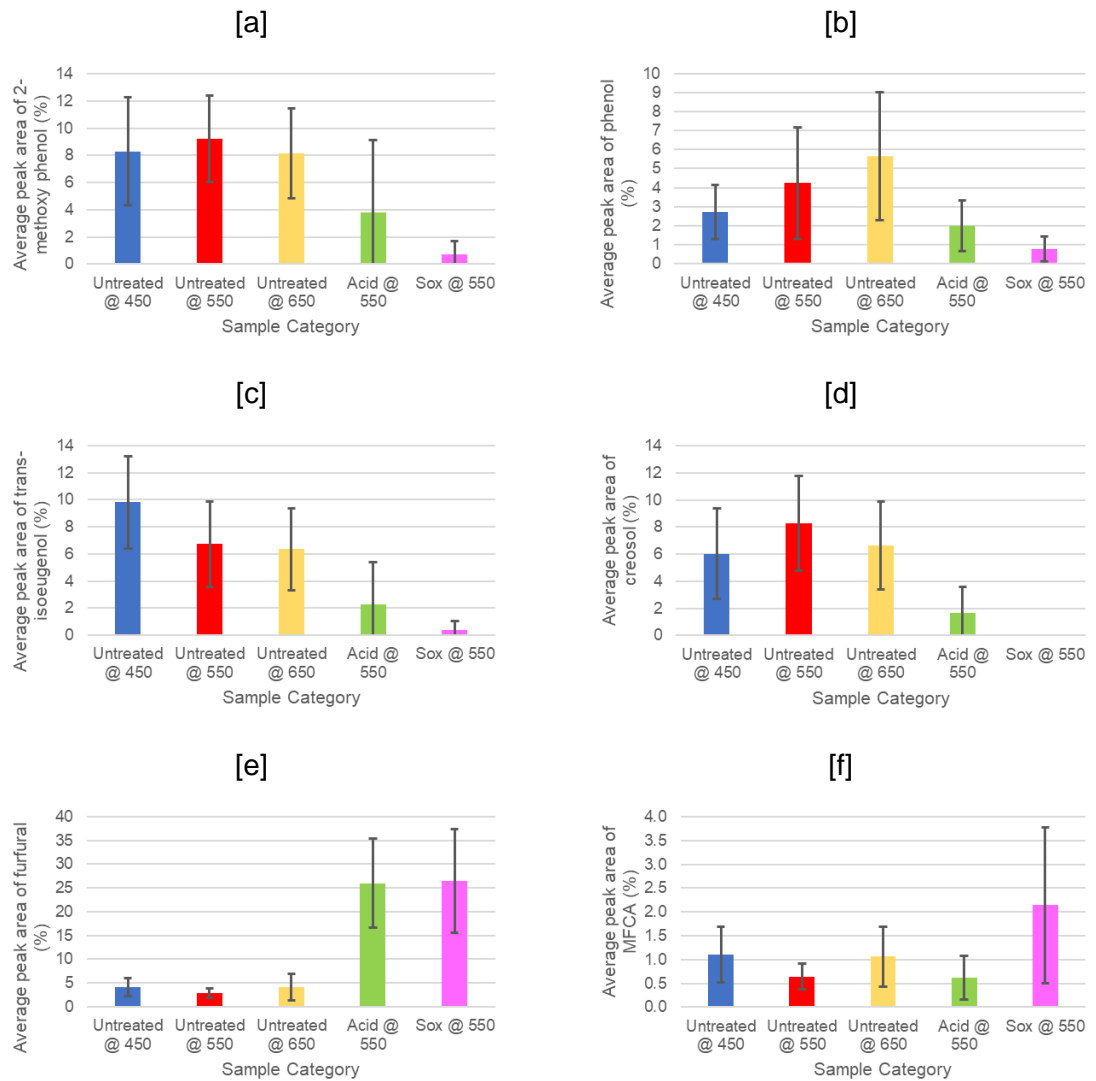


**Figure 6-13 – Comparison of peak areas of [a] 2-methoxy phenol, [b] phenol, [c] trans-isoeugenol, [d] creosol, [e] furfural and [f] 5-methyl-2-furancarboxaldehyde with the average values of all sample categories at each temperature (450, 550 and 650 °C). Error bars were calculated using 1x standard deviation of all values. Number of data points were 13 (U@450, U@550, U@650), 3 (A@550), and 10 (S@550).**

## 6.2.2 Comparison of pyrolysis oil components with common solvents

After discussion of the compounds that are both prevalent across most of the tested samples and in high proportions, it is necessary to explore their potential applications as solvents. However, the separation and isolation of pyrolysis oil-derived compounds is a difficult process due to the similarity in properties, predominantly the boiling point. In addition to the difficult separation, there are very few potential applications for pyrolysis oil where, as a whole, it could be utilised as a solvent due to its complex nature (271). Although some sources note that pyrolysis oil can be used as an industrial solvent (599), the current applications of pyrolysis oils where it is being used in industry could not be found.

Therefore, the upgrading of pyrolysis oil, as discussed earlier, has been investigated in the literature through methylation and hydrogenation (59, 60). Following this, this section will consider the potential solvent applications of the key pyrolysis oil components before and after theoretical upgrading.

The key pyrolysis oil components were chosen as the top 10 across all samples in terms of total peak areas (Table 6-3).

**Table 6-3** – Compounds with the top 10 peak areas across all pyrolysis oil samples.

Compound	CAS	Average peak area (%/sample)
Furfural	98-01-1	10.6
Catechol	120-80-9	10.2
Acetic acid	64-19-7	9.5
2-methoxy phenol	90-05-1	9.0
Trans-Isoeugenol	5932-68-3	8.3
Creosol	93-51-6	7.2
Phenol	108-95-2	4.6
Phenol, 4-ethyl-2-methoxy	2785-89-9	2.4
1,2-Benzenediol, 4-methyl	452-86-8	2.3
p-Cresol	106-44-5	2.0

The theoretical products of the methylation and hydrogenation of the pyrolysis oil components were predicted (in Table 6-4 and Table 6-5) by following a few assumptions. For the methylation, it was projected that any O-H functionality within the chemical's structure was converted into methoxy (O-CH<sub>3</sub>) groups (in accordance with Figure 6-14 (59)). For hydrogenation, any oxygen-containing functional groups or double-bonds were cleaved from the structure of the prospective solvent. This is in contrast to Figure 6-15, which demonstrates the selective hydrogenation of catechol. In selective hydrogenation, the hydrogen selectively breaks C=C bonds in the benzene ring, potentially forming four different structures. In this work, only exhaustive hydrogenation is being considered, to break all C=C in the compound's structures.

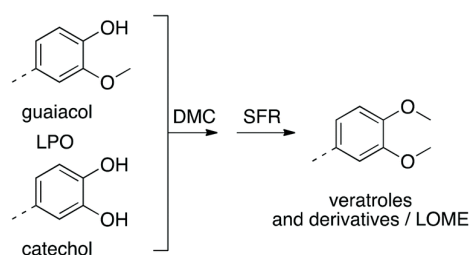


**Figure 6-14** – Example mechanism of the methylation of alcohol-containing compounds. Sourced from (59).

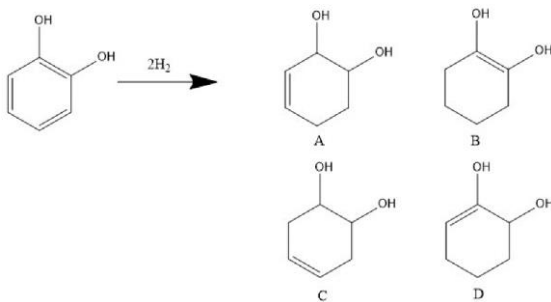


**Figure 6-15** – Hydrogenation of catechol via highly reactive intermediates. Sourced from (600).

The hydrogenation and methylation reactions for each compound with the top 10 peak areas can be seen in Figure 6-16 and Figure 6-17.

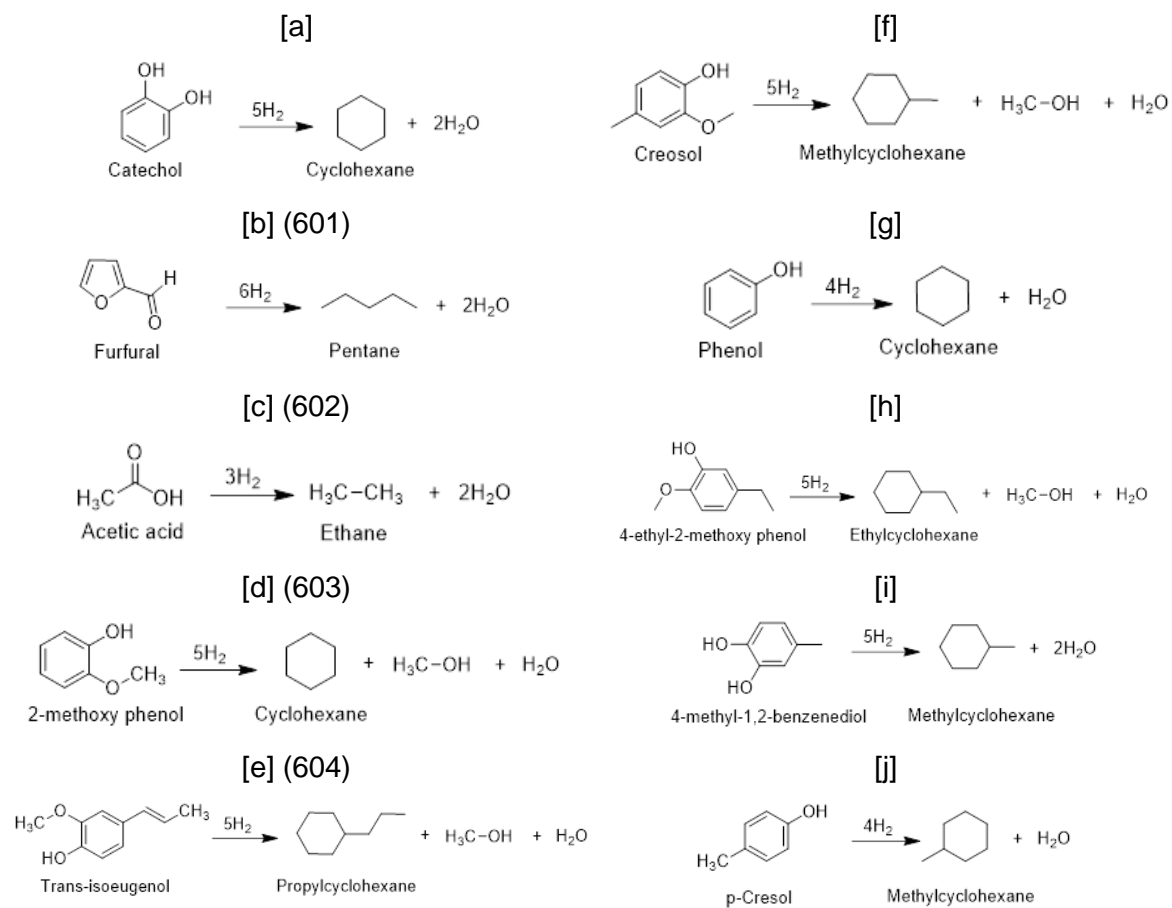


**Figure 6-16** – Hydrogenation reactions of the compounds with the top 10 peak areas from py-GC/MS.

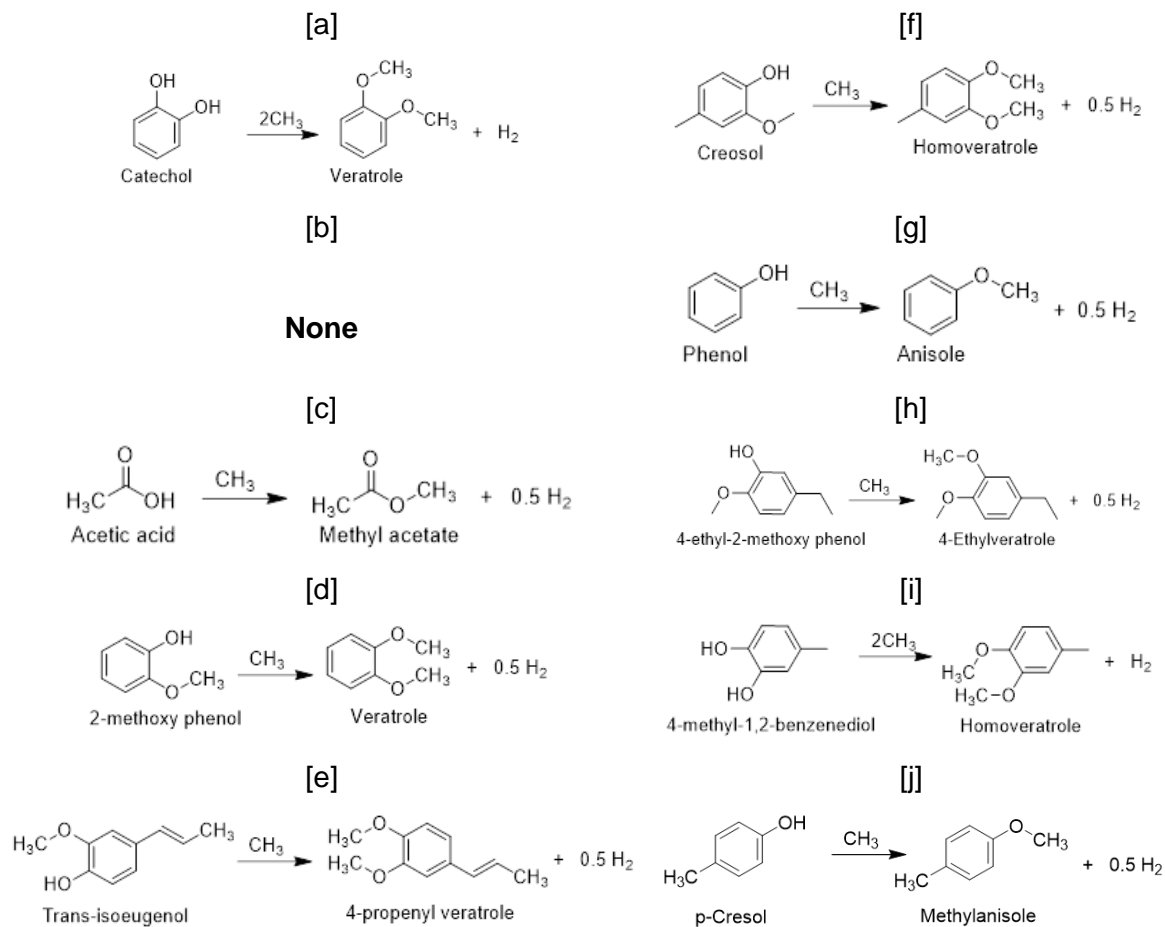


**Figure 6-17** – Methylation reactions of the compounds with the top 10 peak areas from py-GC/MS. [b] is empty as the structure of furfural would not change after methylation.

The Hansen Solubility Parameters (HSPs) and hazardousness of the three types of compounds (original pyrolysis oil, PY, methylated pyrolysis oil, PYM, and hydrogenated pyrolysis oil, PYH) were then considered to explore their potential applications as a solvent. The values of the Hansen Solubility Parameters for each compound were taken from the HSPiP database. The three HSPs act as co-ordinates in a three-dimensional space. The closer that two molecules are to each other in this space (Hansen space), the more likely they are to dissolve into each other. Therefore, regarding the solubility properties, one molecule (such as a bio-based solvent from this study) may be able to be used in similar applications to the other molecule (such as a hazardous petroleum-derived solvent). The hazardousness was scored by following the CHEM21 criteria using data taken from safety data sheets and the literature.

In the tables presented below (Table 6-4 and Table 6-5), the category score of a compound was deemed as hazardous when the score was 7 or above. In Table 6-4 and Table 6-5, the category score of a compound was deemed as hazardous when the score was 7 or above. In Table 6-4 and Table 6-5, after methylation, the dP and dH all drop, although the dD does not reduce significantly. The reduced dH from methylation shows that there is less hydrogen bonding occurring in the chemical structures. This is expected due to the exchange from the O-H to O-CH<sub>3</sub> group. Alcohol functionalities are known to exhibit hydrogen bonding (605), whilst methoxy (O-CH<sub>3</sub>) groups have not been seen to interact as either proton donor or acceptor in hydrogen bonding interactions (606). Regarding the change in dP, related to dipole moment, its slight reduction after methylation of the pyrolysis oil is expected due to the O-H group's strong polarity (607). For the effect of the hydrogenation of the pyrolysis oil on the Hansen Solubility Parameters, all three parameters (dD, dP and dH) reduce after upgrading. The dD is related to the strength of weak electrostatic forces between molecules in the chemical's molecular structure (608). Its reduction is likely due to the reduced polarity of saturated (single-bonded) molecules in the hydrogenated compounds compared to the unsaturated (double-bonded) molecules in the initial pyrolysis oil-derived compounds, as well as the high electronegativity of oxygen heteroatoms being lost (609). The loss of oxygen and double-bonded molecules are also the probable reason for the reductions of dP and dH. As a molecule is likely to experience stronger polarity when it contains a larger number of bonds with greater electronegativity (such as O-H, C=C, and C=O), the removal of oxygen and double-bonded molecules would reduce the polarity. In addition, hydrogen bonding is stronger with acidic hydrogens (H<sup>+</sup>), which are more likely to be present when bonded to strongly negative atoms (such as oxygen). This would therefore reduce the potential for hydrogen bonding with fewer oxygen molecules in the structure too.

The hazardousness was estimated using the CHEM21 guidelines (as described in Section 2.12). The only observation that is common across most of the compounds shown in Table 6-4 and Table 6-5 is that when methylated or hydrogenated, the health score of the pyrolysis oil-derived compound decreases. The health score is associated with the H3xx hazard statements of the chemicals. The highest score, 9, is given for those chemicals that are carcinogenic, mutagenic or reprotoxic, or have acute toxicity. Therefore, the upgrading of the pyrolysis oil appears to both increase its stability and reduce its toxicity. All of the hydrogenated compounds have at least one CHEM21 category with a hazardousness score, except for propylcyclohexane (PY5H). The Safety scores of all hydrogenated

compounds increase after upgrading, likely due to the reduction of flash point temperature (according to Table 3-7).

**Table 6-4** – Hansen Solubility Parameters (HSPs) and CHEM21 hazardous scores of common pyrolysis oil compounds (PYx), methylated pyrolysis oil compounds (PYxM), and hydrogenated pyrolysis oil compounds (PYxH).

Compound	Code	CAS	HSPs			CHEM21 Scores		
			dD	dP	dH	Env	Safety	Health
Catechol	PY1	120-80-9	20.0	11.3	21.8	7	1	9
Veratrole	PY1M	91-16-7	19.2	4.4	9.4	7	1	2
Cyclohexane	PY1H	110-82-7	16.8	0.0	0.2	7	7	3
Furfural	PY2	98-01-1	18.6	14.9	5.1	5	1	9
Pentane	PY2H	109-66-0	14.5	0.0	0.0	7	7	3
Acetic acid	PY3	64-19-7	14.5	8.0	13.5	3	3	7
Methyl acetate	PY3M	79-20-9	15.5	7.2	7.6	5	5	3
Ethane	PY3H	74-84-0	15.5	0.0	0.0	7	7	6
2-methoxy phenol	PY4	90-05-1	18.0	7.0	12.0	7	1	2
Veratrole	PY1M	91-16-7	19.2	4.4	9.4	7	1	2
Cyclohexane	PY1H	110-82-7	16.8	0.0	0.2	7	7	3
Trans-isoeugenol	PY5	5932-68-3	18.8	5.9	9.4	7	2	2
4-Propenyl Veratrole	PY5M	93-16-3	18.4	5.3	5.8	7	2	5
Propylcyclohexane	PY5H	1678-92-8	16.3	1.4	2.1	5	4	5

**Table 6-5** – Hansen Solubility Parameters (HSPs) and CHEM21 hazardous scores of common pyrolysis oil compounds (PYx), methylated pyrolysis oil compounds (PYxM), and hydrogenated pyrolysis oil compounds (PYxH).

Compound	Code	CAS	HSPs			CHEM21 Scores		
			dD	dP	dH	Env	Safety	Health
Creosol	PY6	93-51-6	18.9	6.7	10.8	5	1	7
Homoveratrole	PY6M	494-99-5	18.4	6.1	6.1	7	2	2
Methylcyclohexane	PY6H	108-87-2	16.0	0.0	1.0	7	5	2
Phenol	PY7	108-95-2	18.5	5.9	14.9	7	1	7
Anisole	PY7M	100-66-3	17.8	4.4	6.9	5	3	5
Cyclohexane	PY1H	110-82-7	16.8	0.0	0.2	7	7	3
Phenol, 4-ethyl-2-methoxy-	PY8	2785-89-9	18.5	6.3	9.7	7	2	2
Ethylcyclohexane	PY8H	1678-91-7	16.3	1.6	2.3	7	6	2
1,2-Benzenediol, 4-methyl	PY9	452-86-8	19.4	7.1	16.3	7	2	5
Homoveratrole	PY6M	494-99-5	18.4	6.1	6.1	7	2	2
Methylcyclohexane	PY6H	108-87-2	16.0	0.0	1.0	7	5	2
p-Cresol	PY10	106-44-5	19.0	5.8	10.8	7	1	7
Methyl anisole	PY10M	104-93-8	18.4	5.3	5.3	5	3	6
Methylcyclohexane	PY6H	108-87-2	16.0	0.0	1.0	7	5	2

Following the estimation of the CHEM21 scores and collation of HSPs, the pyrolysis oil-derived compounds were compared to common solvents. The purpose of comparing the solubility of the pyrolysis oil-derived components to common solvents was to look at the potential applications of the pyrolysis oil-derived components where they could replace petroleum-derived solvents. The list of common solvents were taken from the HSPIP database (576). The PY oil compound was deemed to be similar to a common solvent when the HSPs were within a 9.3-unit radius of a three-dimensional space where x, y, and z axes are the parameters (dD, dH, dP). As an example (Figure 6-18), the centre of the green sphere is the 'common solvent', in this case Methyl Ethyl Ketone (MEK). The diameter of the green sphere is 9.3 units. The 'full' blue spheres are chemicals with Hansen Solubility Parameters within the 9.3 units of MEK, whilst the dotted spheres with red dots are chemicals with HSPs outside of 9.3 units. Each common solvent was organised into the category of solvent, according to Table 6-1 (in Table 6-6 to Table 6-8). If a pyrolysis oil-derived component is not similar to any of the common solvents, they were not considered any further in this work. This is because, although they may have useful applications as a solvent, it is not likely to replace one of the common solvents.

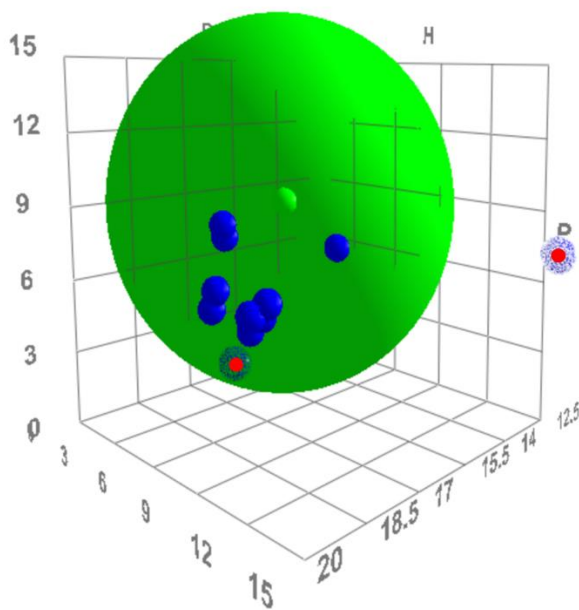


**Figure 6-18** – Example of a HSP Sphere. Modified from (610).

Across these three tables (Table 6-6 to Table 6-8), the combined peak areas were taken by averaging the peak areas across all 64 pyrolysis runs and adding together the average peak areas of the compounds that are considered similar to the same common solvent. As the peak areas of compounds, such as furfural, are widely variable between the treated and untreated samples, the errors (calculated by 1x standard deviation of the raw datapoints) are also high. Therefore, these values are only useful as an indication of the proportion of peak area that the compounds discussed make-up of the overall base or upgraded pyrolysis oil. The peak area of the upgraded pyrolysis oil-derived components is assumed to be the same as the base pyrolysis oil-derived component they were originally identified as (for example, the average peak area of veratrole is assumed to be the sum of the average peak areas of catechol and 2-methoxy phenol).

Regarding the similarity to common non-polar solvents (Table 6-6), most of the similar pyrolysis oil-derived compounds were hydrogenated. This is expected due to the lack of polar heteroatoms such as oxygen. Only two of the non-polar common solvents were not considered hazardous in any categories: xylene and toluene.

The methylated pyrolysis oil-derived compounds are consistently present as similar to polar aprotic common solvents (Table 6-8). The non-hazardous common solvents (Methyl Ethyl Ketone, pyridine, and acetonitrile) were also the solvents with the least similarity to the original pyrolysis oil compounds. In Table 6-7, none of the hydrogenated pyrolysis oil-derived compounds were considered similar to common solvents.

For polar protic common solvents (Table 6-7), the original pyrolysis oil compounds were most common, with veratrole (via methylation of catechol and 2-methoxy phenol) being the only similar methylated compound. Water, one of the non-hazardous common solvents does not have any similar pyrolysis oil-derived compounds. This is because of its exceedingly high dH value. Isoamyl alcohol, however, has many similar compounds from the original pyrolysis oil. In Table 6-6, none of the hydrogenated pyrolysis oil-derived compounds were considered similar to common solvents.

**Table 6-6** – Comparison of similarities between **non-polar** common solvents and pyrolysis oil-derived components. Scores of 7 or above are deemed hazardous (and highlighted in red). ‘Peak areas’ are the combined totals and errors (calculated by 1x standard deviation of the peak areas of the base pyrolysis oil-derived component’s values) standard deviation) from each individual compound. Further information on PY codes can be found in Table 6-4 and Table 6-5.

Common Solvent	CHEM21 Scores			HSP			Similar pyrolysis oil components					
	Env	Safety	Health	dD	dP	dH	Base PY	PYx Peak area	Methylated PY	PYxM Peak area	Hydrogenated PY	PYxH Peak area
Benzene	5	5	10	18.4	0.0	2.0					PY1H, PY2H, PY3H, PY5H, PY6H, PY8H	55.1±39.1
Cyclohexane	7	7	3	16.8	0.0	0.2					PY1H, PY2H, PY3H, PY5H, PY6H, PY8H	55.1±39.1
Hexane	7	7	3	14.9	0.0	0.0					PY1H, PY2H, PY3H, PY5H, PY6H, PY8H	55.1±39.1
Xylene	5	3	2	17.8	1.0	3.1			PY7M, PY10M	5.5±3.9	PY1H, PY2H, PY3H, PY5H, PY6H, PY8H	55.1±39.1
Toluene	5	5	6	18.0	1.4	2.0			PY10M	1.7±1.3	PY1H, PY2H, PY3H, PY5H, PY6H, PY8H	55.1±39.1
1,4-Dioxane	3	6	9	17.5	1.8	9.0	PY5, PY8, PY10	10.6±6.9	PY1M, PY6M, PY7M, PY10M	29.5±19.7		
Furan	5	1	9	17.0	1.8	5.3	PY5, PY8	8.9±5.6	PY1M, PY6M, PY7M, PY10M	29.5±19.7	PY5H, PY6H, PY8H	18.5±12.3
Diethyl ether	7	7	3	14.5	2.9	4.6			PY3M, PY5M, PY6M, PY7M, PY10M	28.1±24.7	PY1H, PY2H, PY3H, PY5H, PY6H, PY8H	55.1±39.1
Chloroform	5	1	7	17.8	3.1	5.7	PY5, PY8	8.9±5.6	PY1M, PY3M, PY6M, PY7M, PY10M	37.4±31.1	PY5H, PY8H	8.9±5.6
Isopropyl Ether	5	7	3	15.1	3.2	3.2			PY3M, PY5M, PY6M/PY9M, PY7M	26.4±23.4	PY1H, PY2H, PY3H, PY5H, PY6H, PY8H	55.1±39.1

**Table 6-7** – Comparison of similarities between **polar protic** common solvents and pyrolysis oil-derived components. Scores of 7 or above are deemed hazardous (and highlighted in red). No hydrogenated PY compounds were similar to common solvents. ‘Peak areas’ are the combined totals and errors (calculated by 1x standard deviation of the peak areas of the base pyrolysis oil-derived component’s values) from each individual compound. Further information on PY codes can be found in Table 6-4 and Table 6-5.

Common Solvent	CHEM21 Scores			HSP			Similar pyrolysis oil components			
	Env	Safety	Health	dD	dP	dH	Base PY	PYx Peak area	Methylated PY	PYxM Peak area
Ethanol	3	5	3	15.8	8.8	19.4	PY1, PY7, PY9	14.4± 10.5		
Methanol	5	5	7	14.7	12.3	22.3	None			
Water	3	5	5	15.5	16.0	42.3	None			
Isoamyl alcohol	3	3	4	15.8	5.2	13.3	PY3, PY4, PY5, PY6, PY7, PY8, PY9, PY10	37.6± 26.3	PY1M	16.4± 10.4
Hexafluoro Isopropanol	5	4	8	17.2	4.5	14.7	PY3, PY4, PY6, PY7, PY9, PY10	28.7± 20.7	PY1M	16.4± 10.4
m-Cresol	7	1	7	18.5	6.5	13.7	PY3, PY4, PY5, PY6, PY7, PY8, PY9, PY10	37.6± 26.3		

**Table 6-8** – Comparison of similarities between **polar aprotic** common solvents and pyrolysis oil-derived components. Scores of 7 or above are deemed hazardous (and highlighted in red). NMP = n-methyl pyrrolidone. DMF = dimethyl formamide. No hydrogenated PY compounds were similar to common solvents. 'Peak areas' are the combined totals and errors (calculated by 1x standard deviation of the peak areas of the base pyrolysis oil-derived component's values) from each individual compound. Further information on PY codes can be found in Table 6-4 and Table 6-5.

Common Solvent	CHEM21 Scores			HSP			Similar pyrolysis oil components			
	Env	Safety	Health	dD	dP	dH	Base PY	PYx Peak area	Methylated PY	PYxM Peak area
Methyl Ethyl Ketone	3	5	3	16.0	9.0	5.1	PY5, PY8	8.9± 5.6	PY1M, PY3M, PY5M, PY6M, PY7M	42.5± 29.6
Pyridine	3	5	2	19.0	8.8	5.9	PY5, PY8	8.9± 5.6	PY1M, PY3M, PY5M, PY6M, PY7M, PY10M	44.2± 30.9
Acetonitrile	3	5	3	15.3	18.0	16.1	PY2	8.8± 6.7		
Acetone	5	5	7	15.5	10.4	7.0	PY5, PY6, PY8, PY10	16.6± 10.5	PY3M, PY6M	15.8± 12.6
Methylene Dichloride	7	3	7	17.0	7.3	7.1	PY5, PY6, PY8, PY10	16.6± 10.5	PY1M, PY3M, PY5M, PY6M, PY7M, PY10M	44.2± 30.9
Ethyl acetate	3	5	7	15.8	5.3	7.2	PY5, PY6, PY8, PY10	16.6± 10.5	PY1M, PY3M, PY5M, PY6M, PY7M, PY10M	44.2± 30.9
NMP	7	5	10	18.0	12.3	7.2	None			
Tetrahydrofuran	5	7	7	16.8	5.7	8.0	PY4, PY5, PY6, PY8, PY10	24.0± 14.7	PY1M, PY3M, PY5M, PY6M, PY7M, PY10M	44.2± 30.9
1,3-Dioxolane	3	5	10	18.1	6.6	9.3	PY3, PY4, PY5, PY6, PY8, PY10	31.9± 21.9	PY1M, PY3M, PY5M, PY6M, PY7M, PY10M	44.2± 30.9
Dimethyl sulphide	7	7	6	18.4	16.4	10.2	None			
DMF	7	5	10	17.4	13.7	11.3	None			

Several of the common solvents, across Table 6-6 to Table 6-8, are hazardous according to the CHEM21 criteria. Therefore, they are most at need of being superseded by a bio-based solvent. These most hazardous common solvents and the non-hazardous pyrolysis oil-derived compounds that could potentially replace them are listed in Table 6-9. For simplicity, a chemical is considered hazardous when 1 of the 3 CHEM21 scores are 7 or more. All of the non-upgraded pyrolysis oils were considered as hazardous, due to their boiling points being above 200 °C (according to Table 3-9). Therefore, all of the pyrolysis oil-derived compounds listed in Table 6-9 are methylated or hydrogenated compounds. In addition, there were no non-hazardous pyrolysis oil-derived compounds considered to be similar to hazardous polar protic common solvents.

**Table 6-9** – List of the non-hazardous (where no CHEM21 categories' score is above 7) pyrolysis oil-derived components that are considered similar to hazardous common solvents. 'Peak areas' are the combined totals and errors (calculated by 1x standard deviation of the peak areas of the base pyrolysis oil-derived component's values) from each individual compound.

Type of Solvent	Non-hazardous pyrolysis oil-derived component	Combined peak area of PYx compounds
<b>Non-polar</b>		
Benzene	PY5H	6.9 ± 4.1
Cyclohexane	PY5H	6.9 ± 4.1
Hexane	PY5H	6.9 ± 4.1
1,4-Dioxane	PY7M, PY10M	5.5 ± 3.9
Furan	PY7M, PY10M, PY5H	12.3 ± 7.9
Diethyl ether	PY3M, PY7M, PY10M, PY5H	27.7 ± 19.3
Chloroform	PY3M, PY7M, PY10M, PY5H	27.7 ± 19.3
Isopropyl ether	PY3M, PY7M, PY5H	26.0 ± 18.0
<b>Polar aprotic</b>		
Acetone	PY3M	15.3 ± 11.4
Methylene dichloride	PY3M, PY7M, PY10M	20.8 ± 15.3
Ethyl acetate	PY3M, PY7M, PY10M	20.8 ± 15.3
Tetrahydrofuran	PY3M, PY7M, PY10M	20.8 ± 15.3
1,3-Dioxolane	PY3M, PY7M, PY10M	20.8 ± 15.3

As a solvent, 1,4-dioxane (1,4-D), tetrahydrofuran (THF) and methylene dichloride (MDC) are utilised in the manufacture of veterinary drugs, natural health products and pharmaceuticals (611-614). Discounting the obvious need for high solvent power solvents in these potential applications, the key property when considering human (or animal) use

is the purity (615). As the separation of pyrolysis oil into its individual components is difficult, it is likely that they would be ill-suited for applications including human/animal use.

1,4-D and furan are used as a stabiliser in chlorinated and ether solvents (including MDC, THF, and diethyl ether, DEE) (611, 614, 616, 617). The stabiliser aids these solvents by inhibiting reactions between the solvents and metals (such as aluminium) (614). The common stabiliser used for ethyl ether, butylated hydroxytoluene, does not have high optical purity due to its aromatic functionality (617). Therefore, pyrolysis-oil derived compounds may be good replacements for this application. However, an additional common stabiliser is ethanol. As there is already commercially available bio-based ethanol (618), there would be little demand for pyrolysis oil-derived chemicals to be used.

Furan, THF, 1,3-dioxolane (1,3-DL) and MDC are used as an extraction solvent for resins, oils, waxes, and lubricants (611, 616, 619-622). In the literature, 'green' solvents including terpenes have been looked at as alternatives to these hazardous chemicals due to its similar Hansen Solubility Parameter values (623). There is therefore scope for superseding the hazardous solvents for the extraction of substances akin to oils and waxes.

Furan is used as a solvent in the production of agricultural chemicals (nematicides, insecticides, and fungicides) and lacquers (611, 616, 624, 625). Safer common solvents that have been used in these applications are water and ethanol (626), so there is little motivation to explore the use of pyrolysis oil-derived compounds.

DEE, THF, and 1,3-DL are used as a solvent in the manufacture of plastics and synthetic dyes (624, 627-631). These applications occur between room temperature and 100 °C. The main property for the synthesis of the dyes and plastics is the solubility, so the non-hazardous pyrolysis oil-derived components may be good alternatives to explore further.

In research, DEE and THF are used as a solvent for the Grignard reaction (632, 633). DEE is also used as a solvent for several reactions involving organometallic reagents (633).

MDC and 1,3-DL are used as a process solvent in the manufacture of film coatings (613, 627). The key feature of solvents in this application is to dissolve waxes for use as the film coating. However, the melting point of wax is low (45 – 76 °C) so solvents are not necessarily needed. In the literature, the reduction of hazardous solvent use has been considered through solvent-free methods or using water as the main solvent (634).

MDC is used as a metal cleaning and finishing solvent in electronics manufacturing (611, 613, 624). This refers to the degreasing or washing of metal parts (635). Recently, metal

cleaning technologies have been explored using aqueous based technologies with water (636-638). However, some of the water-based technologies are not efficient at metal cleaning due to the hydrophobic nature of oil contaminants (635, 636). As the purpose of this application is to remove contaminants, a pyrolysis oil-derived bio-based solvent may not be the ideal substance.

MDC and 1,3-DL are used as a solvent in the production of paint strippers and paint removers (620, 622, 624). Since 2019, the United States' Environmental Protection Agency banned the use of MDC in paint removers. This was superseded by NMP (639), now recognised as a chemical of very high concern too (640). Regarding 1,3-DL, its market volume (where used as a solvent) is only around 3000 tons, in comparison to ethyl acetate or acetone (with a market volume of around 1 Mtons (621)). For this reason, there may be less of a market for finding an alternative bio-based solvent to 1,3-DL. In recent years, a few bio-based paint strippers have been commercialised (641). However, there does not appear to be any commercialised paint strippers or removers that are as cheap and effective as MDC. There is therefore a gap to explore low-cost alternatives such as biomass residue pyrolysis oil-derived components as paint strippers.

MDC is used as a solvent for active ingredients in hair spray formulations (642), but has been prohibited since 2015 in the EU (643). The most common solvent used in hairspray production is ethanol (644). As bio-based ethanol is an established solvent (618), there would be less of a drive to explore pyrolysis oil-derived components for this application.

## 6.3 Conclusion

This study has explored the potential of lignin-rich samples as precursors to bio-based solvents.

The samples were first pyrolysed at a micro-scale via pyrolysis-gas chromatography/mass spectrometry (py-GC/MS) under fast pyrolysis conditions between 450 and 650 °C. The components that were most prevalent across the py-GC/MS data were 2-methoxy phenol, phenol, furfural, trans-isoeugenol, creosol and 5-methyl-2-furancarboxaldehyde (MFCA).

The tree bark samples had the greatest proportions of MFCA. The samples that had undergone treatment, either solvent extraction (for the tree barks) or acid-washing (for alkali lignin and sugarcane bagasse (PKBag)), had either a similar value of MFCA or the peak area had increased. When comparing the treatment of samples with the pyrolysis temperature, the solvent-extracted samples had the greatest proportions of MFCA.

The levels of creosol were fairly consistent across the tree barks (5-10%), although the highest values were seen for all three lignoboost samples (LB450, LB550, LB650) with 15-23% peak areas of creosol. For creosol, when considering the different categories of sample explored in this chapter, the untreated samples (at all three pyrolysis temperatures) had higher levels than the treated samples.

Almost all of the samples had low-lying levels of furfural. However, both forms of treatment led to a significant increase (from around 5% to 20-50%), with the greatest value being seen by solvent-extracted larch bark (LSox550).

The trans-isoeugenol values were fairly consistent across the tree barks (5-15%), with the greatest proportion being at 450 °C. European silver fir (ESF) and grand fir (GF) had the largest values across all three temperatures (10-20%). The treatment of the samples led to a reduction in the trans-isoeugenol content, except for acid-washed alkali lignin, which slightly increased (from 4-7%), most likely due to the acid-washing removing non-trans-isoeugenol forming material such as ash.

The alkali lignin sample had the greatest proportions of 2-methoxy phenol across 450 – 650 °C. This may be due to the high lignin content increasing the proportion of aromatics. The 2-methoxy phenol levels also decreased for all of the treated samples.

Across most samples, the levels of phenol increased as the temperature increased. This was expected due to phenol being one of the simplest aromatic compounds. The coconut husk had the greatest proportion across the three temperatures, whilst the commercial

lignin products (lignoboost, organosolv, and alkali lignin) pyrolysis oil had negligible phenol content.

Due to the complex nature of pyrolysis oils, the individual components of upgraded pyrolysis oil (via methylation and hydrogenation) and the original product were investigated. The hazardousness and solubility of the three pyrolysis oil-derived component types were estimated by the CHEM21 criteria, which scored their environmental, health and safety impacts, and Hansen Solubility Parameters (HSPs). From assessing the pyrolysis oil-derived component's hazardousness, all of the original pyrolysis oil-derived components had at least one category that would be considered hazardous. The primary issue with using chemicals or solvents that may be considered hazardous is that the end-user may experience impacts to their health, such as skin/eye irritation, nausea, or loss of co-ordination. In addition, if the chemical is flammable, then there needs to be much stricter process control during its use in industry. It is for this reason why, in the methodology outlined in this work, a chemical was considered to be 'hazardous' even if only one of the categories had a hazardous score.

The health score (associated with toxicity of chemicals) decreased for most of the pyrolysis oil components after both methods of upgrading. Through collating the HSPs of the three types of pyrolysis oil-derived components, the methylation was observed as reducing the strength of hydrogen bonding and dipole moments. This is due to the power of the hydroxy (O-H) functional group, which was replaced by a methoxy (O-CH<sub>3</sub>) group. The hydrogenation of the pyrolysis oil leads to a reduction in all three parameters (dD, dP and dH) after upgrading.

The potential applications of the pyrolysis oil-derived components were then considered by comparing their solubilities to that of common solvents. The applications of hazardous common solvents where methylated or hydrogenated pyrolysis oil-derived components may be valuable alternatives are as extraction solvents for resins, oils, waxes, and lubricants, in the manufacturing of plastics, and in the production of paint strippers and removers.

## Chapter 7 – The potential to produce bio-based ammonia adsorbents from lignin-rich residues

### 7.1 Introduction

In this work, a range of raw barks selected from Chapter 5 were examined for their ammonia adsorption capacity (Section 3.13) (Figure 7-6). Tree barks, after different forms of treatment (Soxhlet solvent extraction [Section 3.9.2] and slow pyrolysis [3.8.1]), were also tested to investigate how the residues' performances would vary. In addition to tree barks, feedstocks from a series of sources were also tested. After the adsorption testing, the characteristics of the samples were compared to explore whether there was any correlation with the sorption capacity.

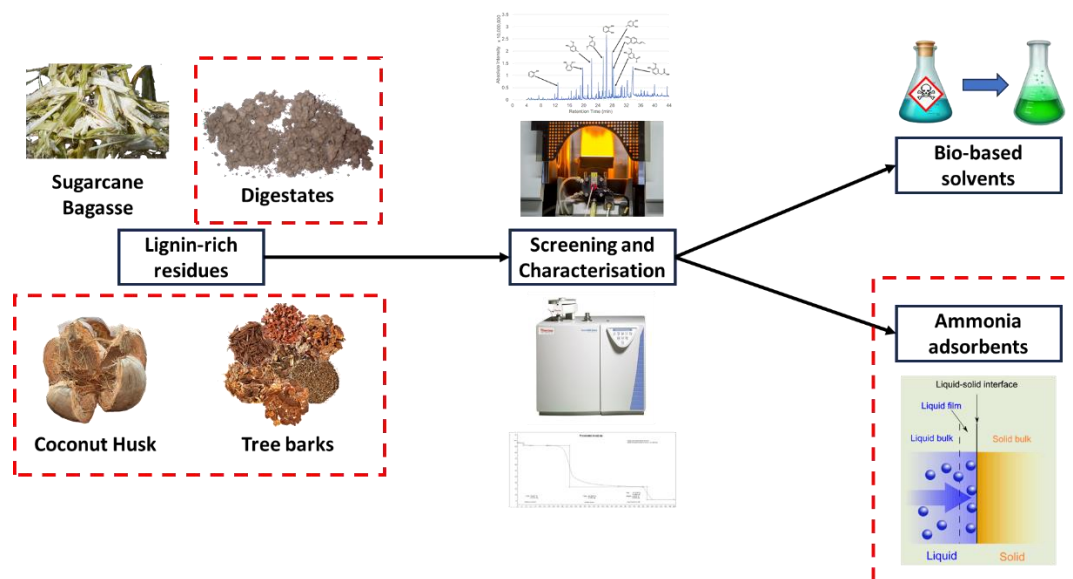


**Figure 7-1** – The overall scope of this study. The work covered in Chapter 7 is denoted by red dotted lines.

## 7.1.1 Background

### 7.1.1.1 Valorisation of ammonia

Ammonia ( $\text{NH}_3$ ) is a compound that is both present in nature (645) and is one of the most industrially produced chemicals in the world (by mass) (646). The traditional route to produce synthetic ammonia (otherwise known as 'grey ammonia') is the Haber-Bosch process (647). In this low-cost and high-emission process, hydrogen is stripped from natural gas and steam. The stripping process produces  $\text{CO}_2$  and excess methane and steam, with the hydrogen then being reacted with nitrogen from air at high temperature and pressure. For every ton of produced ammonia,  $\approx 2$  tons of  $\text{CO}_2$  is released into the atmosphere (648). Ammonia production is the largest emitting chemical industry process (649), with 47 % (about 340 Mt  $\text{CO}_2$  eq) of the total annual greenhouse gas of high production volume chemicals.

As of 2024, the global ammonia market is estimated to be worth around USD \$ 228.12 billion, growing at a compound annual growth rate of 5.4% (from 2022 to 2030) (650). The worldwide market volume of ammonia is projected to increase from 195 million tonnes (as of 2024) at a compound annual growth rate of 7.22% (from 2022 to 2030) (651).

Ammonia is used across several industries as a neutraliser, stabiliser, or a nitrogen source (652). It is one of the main ingredients in several household cleaning products as a surfactant and base (652, 653). In chemicals manufacturing, ammonia is a building block for polymers, such as nylon, and amines. However, the greatest consumption of ammonia ( $\approx 80$  vol%) is in the production of fertilisers including ammonium nitrate, ammonium hydrogen phosphate, ammonium sulphate and urea (654, 655). In the UK, 80-90% of emitted ammonia arises from agriculture (656), predominantly from the production and spreading of nitrate fertilisers for soil (649). Additionally, ammonia is used in industrial freezers and air conditioning systems as a common refrigerant (653). Ammonia is also present in cigarette smoke (657).

A developing research area for the valorisation of ammonia is using it as either an energy source or fuel source. The combustion of ammonia does not produce carbon dioxide, so ammonia fuel could be considered as a 'zero  $\text{CO}_2$ ' emitter (658). However, they do produce nitrous oxides ( $\text{NO}_x$ ), which are known air pollutants. One such  $\text{NO}_x$ ,  $\text{N}_2\text{O}$ , is a crucial component of acid rain and smog (659). It is also a greenhouse gas that is  $\approx 273$  times more potent than  $\text{CO}_2$  (658). Ideally, no reactive nitrogen species would be released by ammonia combustion, but this is possible through incomplete combustion or leaking

(akin to the production of carbon monoxide through incomplete coal combustion) (658). Ammonia combustion as a high hydrogen density fuel is currently not a perfect solution, due to its poor ignition and combustion performance (660).

The change from fossil fuels to ammonia fuel would positively impact levels of greenhouse gas emissions, but the main roadblock is the source of the ammonia that is used (661). Ammonia produced by water electrolysis (referred to as 'green ammonia') has been considered as an "energy" carrier (662). The green ammonia is transported by ship or pipeline and is combusted in power plants with turbines modified to run on ammonia (647). As the area of hydrogen fuel develops (663), there is growing interest in the use of ammonia as a hydrogen carrier. Here, ammonia is "cracked" by catalytic decomposition to produce atmospheric nitrogen and hydrogen for use as a fuel (646, 664).

Ammonia emissions are also prevalent from vehicles, including ships and cars. These are emitted as by-products of catalytic conversion to reduce sulphur and nitrogen oxide emissions (654, 657). The proportion of road transport-derived ammonia emissions has shrunk from 7% of total emissions in 2002 to 2% in 2022 (656).

Ammonia, in excess, poses a threat to human health, and leads to water body eutrophication (665) and environmental pollution. This occurs through the emitted ammonia depositing reactive nitrogen on surfaces (666). Due to the reactivity of the ammonia and nitrogen within air, gaseous ammonia only lasts for a few hours in the atmosphere (666). During this time, the gaseous ammonia can react chemically with aerosols and acidic gases already present in the atmosphere, contributing to greater levels of aerosol formation (667) and other secondary pollutants (656).

High levels of ammonia pollution can negatively affect biodiversity. Reduced biodiversity occurs due to fast-growing species that are able to thrive in nitrogen-rich environments being able to out-compete smaller and more sensitive species (649). The evidence pertaining to this, however, pertains to not just ammonia, but all nitrogen pollution (649).

Due to the effect of negative health impacts and loss of biodiversity from high levels of ammonia, the potential financial cost to the UK has previously been estimated to be over £700m per year (649).

The recycling of gaseous ammonia or aqueous ammonium from biowaste and biomass streams can help to reduce the impact of ammonia emissions and the net production of energy-intensive products.

Aqueous ammonium has been recovered from streams including wastewaters and anaerobic digestates by membrane-based electrochemical routes (22, 23, 668-670). Due to strict discharge regulations, many ammonia-rich wastewaters are prevented from being discharged or re-used (671). Through the removal of ammonia, wastewaters can be returned to the water source for further re-use, or is used further for non-potable purposes (irrigation, vehicle washing, agriculture or firefighting) (672). The membrane-based electrochemical routes utilise electrochemical stripping, bioelectrical systems or electrodialysis to diffuse and migrate ammonium ions ( $\text{NH}_4^+$ ) from the wastewater across the cation-exchange membrane. The transported ammonium ions are then available to be concentrated into high-value products (670).

One method for the capture of aqueous or gaseous ammonia is absorption. With aqueous ammonia, pH and temperature adjustment and aeration is performed to strip the ammonia into the air. The gaseous ammonia is then stabilised through contact with sulphuric acid, which stabilises the ammonia as ammonium sulphate. The crystals generated can be utilised as an agricultural fertiliser (24, 25).

#### **7.1.1.2 Common routes of ammonia adsorption**

Gaseous ammonia can also be captured through the use of adsorbents. These are materials which perform physical and/or chemical adsorption, due to their pore volumes and active functional groups (26), respectively. Desirable adsorbents have high thermal stability, strong mechanical properties, rich functional groups, and high pore volumes (673, 674). As carbon-rich materials share several of these properties, a variety of biomasses have been considered as low-cost adsorbents (675-677). These can also include carbon-silica composites, iron nanoparticles, and coal ash (678-681). Alternatively, catalysts, such as sepiolite and zeolite, have been used to remove gaseous ammonia (664).

In the literature, pre-treated biomass has been explored as sorbates of phenolic compounds (682-685), heavy metals (686-689), chlorofluorocarbon (690) and herbicides (683). When one or more of these substances are present in the same vicinity of an adsorbent, there is expected to be competition between them due to the limited active sites available for adsorption. Therefore, the adsorption capacity of a substance such as ammonia may decrease significantly if adsorbents with stronger affinities to the sorbent are present.

The pre-treatment of biomass has been seen to affect its sorption capacity. Previous unpublished work (691) found that in some cases, the raw feedstock exhibited a greater

sorption capacity than hydrothermally carbonisation-derived char. Alternative processing techniques such as slow pyrolysis have been explored in the literature. However, these compare biochars amongst themselves, rather than comparing to the raw feedstock (92, 692-694). According to Trazzi et al (2024) (695), ammonia adsorption capacity of biomass is dependent on the functional polar groups which are accessible at the surface.

In slow pyrolysis, solid samples are thermally decomposed in an inert atmosphere at a low heating rate (approximately 10 °C/min) (269). The key parameter that affects pyrolysis products is heating rate. The biochar that is produced from slow pyrolysis has higher surface areas and porosity than those from fast pyrolysis.

Biochar can be valorised in a variety of ways. The main established application is in soil conditioning and soil remediation (696). The fragments of biochar are said to act as an active site for useful soil microbes, whilst neutralising acidity and improving nutrient and water retention. However, in cases where the soil is already at an ideal pH, the change in pH through the addition of biochar is unnecessary (697).

The impacts of biochars on anaerobic digestion has been summarised by Tang et al (2020) (698). Biochar aids the stability of AD process stability through the prevention of ammonia production. However, a high dosage of biochar can have negative impacts on the performance of the AD process. This is due to the inhibition of microbial kinetics and activity, so biochar dose must be controlled carefully (698).

High ammonia concentrations in an AD system can lead to low efficiency, instability, or AD failure. There are a few strategies to reduce the inhibition that occurs in AD due to ammonia. Through nitrification or denitrification, ammonia nitrogen can be converted to N<sub>2</sub> (699). Nutrient addition can aid the micro-organism's ability to resist high NH<sub>3</sub> concentrations, whilst pH or temperature adjustment can convert ammonia into ammonium ions (NH<sub>4</sub><sup>+</sup>). This reduces the toxicity of the ammonia nitrogen (699). Biochars are a potentially valuable material for ammonium sorption. The sorption is reportedly a reversible process, therefore the ammonium is bioavailable if the biochar was to be used as a nitrogen-rich soil amendment (11). Although different countries have evolved different allowed practices (13), the ammonium-rich soil amendment (biochar) must be buried under the topsoil. If the biochar is scattered on the surface of the soil, the ammonia would desorb over time, generating the NH<sub>3</sub> emissions that are trying to be avoided (12).

In the valorisation of biochars in adsorbing ammonia, the key variables that impact its performance are the pyrolysis temperature, heating rate and raw material. Biochars

produced at different pyrolysis temperatures can have different surface properties, porosities, cation exchange capacities and final compositions. The higher the pyrolysis temperature, the lower the ammonia adsorption capacity. This is due to there being lower surface areas and fewer surface functional groups. Greater levels of adsorption capacity were found at temperature below 650 °C. The ammonia/ammonium adsorption capacity of biochar is also dependent on the washing processes and activation methods that it undergoes (700).

The purpose of the activation methods is to increase the porosity of the biochar, and hence its available surface area. After activation, biochar may be washed to remove any impurities (unwanted inorganic compounds) and increase the number of active sites that are available for adsorption (700).

Biochars require activation to induce adsorption behaviour, otherwise their ammonium adsorption capacity is subpar. Biochar activation can be completed by the use of steam (injecting water into a nitrogen gas flow), addition of phosphoric acid (692), the addition of  $K_2CO_3$  or  $CO_2$  (700, 701). In some cases, the washing of biochars can negatively impact the adsorption capacity. Washing with hot water reduces the adsorption capacity, whilst acid washing does not have much effect. Unwashed samples can in fact have the greatest capacities (700). A higher ammonium ion sorption was found to occur in biochars at near neutral pHs (7.0 – 7.5) (702).

Throughout the literature, the terms of 'activated carbons' and 'biochars' appear to be relatively interchangeable in the field of ammonia adsorption (703, 704). 'Biochar' is used in general research contexts, whilst 'activated carbon' is stated when discussing commercial applications of the biomass. 'Activated carbons' have been found to have high ammonia adsorption capacities (703, 705, 706).

The ammonia adsorption capacity of a sample can be tested by passing a known flow of a known concentration of ammonia gas through a sample of biochar (692). The total nitrogen content can be measured via a modified Berthelot method. In this, ammonium is chlorinated to monochloramine through the addition of salicylate, 5-aminosalicylate. Once this has oxidised, the absorption of the formed complex can be measured by Fourier Transform Infrared Spectroscopy (FTIR) at 660 nm (700). The change in nitrogen content can also be measured by the elemental analysis of the biochar before and after the adsorption (700).

The ammonium sorption ability of biochars can be evaluated by mixing the biochar with ammonia nitrogen solution in water, then measuring the ammonium concentration through the phenate method with a UV/VIS spectrophotometer (11). Alternative equipment for measuring this concentration can be HACH UV/Vis spectrophotometers. Some papers in the literature have determined the ammonium concentration via HACH equipment (707-709).

This work follows that of a previous University of Leeds' student's exploration of tree barks' ammonia sorption capacity (691). In the Dorward (2016) report (691), a pine bark and spruce bark were subjected to hydrothermal carbonisation, with the raw barks and hydrochars tested for their ammonia sorption capacity. The pine bark used by Dorward is the same as the unidentified bark used in Chapter 4. The conclusion of the report showed that the raw bark performed better than the thermally treated bark. It was also posited that the performance of the tree barks' ammonia sorption capacity may be linked to them being a lignin-rich residue.

#### **7.1.1.3 Valorisation of tree barks as adsorbents**

Untreated bark has been identified as a useful resource for water remediation, as a bio-filter, and in gas cleaning. Through thermal conversion to an activated carbon, the bark-derived carbon is able to remove metal ions from acidic wastewater and water solutions, and remove air contamination, whiten sugar and reclaim dissolvent (477). Bark-derived bio-filters were shown to effectively decontaminate odours, H<sub>2</sub>S and NH<sub>3</sub> from swine farms, and heavy metal ions from polluted waters (477). No literature could be found regarding utilising tree barks as ammonia adsorbents. The key extractives of tree barks are tannins, flavonoids and suberin (459, 485-492). The literature has not specifically mentioned the testing or use of barks as adsorbents, but tannins (a known extractive of tree barks) have been used as an adsorbent of precious metals (710, 711). Literature pertaining to any adsorption using flavonoids could not be found. Suberin has been seen in the literature as a sorbent for phenanthrene and polycyclic aromatic hydrocarbons (PAHs), with greater adsorption occurring for lower molecular weight PAHs (712-714).

#### **7.1.1.4 Valorisation of agricultural residues and wastes as ammonia adsorbents**

Agricultural wastes have been explored as ammonia adsorbents in the literature, with various peels and seeds being tested by Azreen et al (2017) (715). Limited literature was able to be found that utilised digestates as ammonia adsorbents. This is likely due to the

anaerobic digestion process leading to ammonia-rich liquid fractions (23, 716-721), so it would be less useful for the solid fraction to be used to adsorb ammonia from other samples.

Only limited commercial lignin products (such as Lignoboost or alkali lignin) have been tested for their ammonia adsorption capacity in the literature (722, 723). This is mostly due to aqueous ammonia being used as a form of pre-treatment for biomass to dissolve the lignin content for further isolation (724). A derivative of alkali lignin (demethylated alkali lignin nanospheres) was deemed to be a favourable ammonia adsorbent by Li et al (2024) (722).

A known ammonia sorbent in the literature is peat (723, 725-727). Peat is the organic layer on the surface of soil. It is composed of organic matter of primarily plant origin (728). Most of peat's organic component (60 – 85 wt%) are made up of humic substances (729), products from plant and animal residue decomposition (730). The remaining composition is made up of cellulose, lignins, wax, resins, and inorganic material (731). In peat moss (otherwise known as *sphagnum*), typical lignin is not one of the components. Here, the peat moss has polyphenolic compounds which resemble lignin (and are part of the acid detergent lignin phase) (732). The holocellulose (cellulose + hemicellulose) and lignin fractions of peats are expected to be between 5-40 wt% and 20-50 wt% respectively (733), although lignin contents can get as high as 93 wt% in the case of Indonesian peat (734).

The proximate and ultimate analysis values of peat were variable across the literature (735-738) (Table 7-1). The composition of peats greatly vary depending on the origin site and extraction depth (739, 740).

**Table 7-1** - Range of proximate and ultimate analysis values for peat in the literature (735-738). Moisture content on an 'as received' (a.r) basis. All other values given on a 'dry basis' (d.b).

<b>Proximate Analysis (wt%)</b>	<b>Moisture</b>	4.8 – 61.4
	<b>Volatile Matter</b>	32.8 – 74.0
	<b>Fixed Carbon</b>	21.1 – 41.1
	<b>Ash</b>	2.0 – 21.3
<b>Ultimate Analysis (wt%, dry basis)</b>	<b>Carbon</b>	33.2 – 53.6
	<b>Hydrogen</b>	3.9 – 7.0
	<b>Nitrogen</b>	2.1 – 2.9
	<b>Sulphur</b>	0.1 – 0.3
	<b>Oxygen</b>	29.1 – 49.4

Limited literature on the use of pure cellulose as an ammonia adsorber could be found (741), with coconut-derived material being considered a representative (742). In the

literature, coconut-derived materials have been seen to perform well as ammonia adsorbents (742-746). Coconut shells have been investigated mostly as biochars (744, 745, 747). Coconut wire/coir have been tested as a raw (746) and alkaline-activated material (748). Coconut husk has also been examined, though mainly as activated carbons (749).

#### **7.1.1.5 Synergistic effects between sample characteristics and adsorption performance**

As the most common adsorbents are activated carbons, formed by carbonisation processes, it is expected that ammonia sorption capacity increases with lower volatile matters. The products of carbonisation, compared to their precursors, have increased fixed carbon, decreased moisture content and reduced volatile matter (750). An increasing carbon content (from ultimate analysis) is expected to increase adsorption capacity (751), as an added benefit from carbonisation.

The moisture content of a medium or material has been observed as affecting ammonia sorption (752). However, a higher or lower moisture content does not appear to improve the sorption, but simply the presence of moisture (753). Moisture content has a greater positive impact on adsorption behaviour when the sample has low concentrations of oxygen-containing functional groups (754). This is due to water's affinity for adsorption (755), with ammonia's dissolution in water being relatively stronger at the surface of microporous carbon (756). Yet, adsorption capacity significantly reduces from the interaction and competition between adsorbates and moisture (757).

No literature could be found regarding any link between hydrogen, nitrogen, and sulphur and adsorption capacity. In the case of hydrogen, this is most likely due to ammonia containing hydrogen, with ammonia being considered a "hydrogen carrier" or as "hydrogen storage" (758-760).

## 7.2 Results and Discussion

The following section presents the data from the ammonia adsorption testing of a variety of samples (Table 7-2). The ammonia sorption capacities of the samples were calculated according to Section 3.13. Following this, the potential reasons for improved sorption capacities were explored.

**Table 7-2** - List of samples explored for their ammonia adsorption capacity in Chapter 7.

<b>Sample Type</b>	<b>Sample</b>
<b>Tree barks</b>	Nootka cypress (NC), noble fir (NF), European silver fir (ESF), grand fir (GF), Douglas fir (DF), oak
<b>Commercial Activated Carbons</b>	Commercial activated carbon from Sigma-Aldrich (SIGMA-AC)
	Commercial activated carbon from NORIT (NORIT-AC)
<b>Tree bark biochars</b>	Douglas fir tree bark biochar (DFbc)
	Nootka cypress tree bark biochar (NCbc)
	European silver fir tree bark biochar (ESFbc)
	Noble fir tree bark biochar (NFbc)
	Lawson cypress tree bark biochar (LCbc)
	Larch tree bark biochar (Lbc)
	Norway spruce tree bark biochar (NSbc)
	Hot water-washed noble fir tree bark biochar (HWNFbc)
	Hot water-washed noble fir tree bark biochar (HWDFbc)
Oak biochar (Oak450bc)	
<b>Solvent-extracted tree barks</b>	Solvent-extracted residue of Douglas fir tree bark (DFSox)
	Solvent-extracted residue of grand fir tree bark (GFSox)
<b>Lignin products</b>	Lignoboost (LB)
	Alkali Lignin (AlkLig)
<b>Digestates</b>	Municipal solid waste digestate (MSWdig)
	Vegetable, garden, and fruit residue digestate (VGFdig)
<b>Other residues</b>	Coconut husk (CH), Irish peat (PeatSEPO), sphagnum peat moss (PeatMoss)

### 7.2.1 Ammonia Sorption Capacities

In this section, the samples' ammonia sorption capacities are outlined. In Table 7-3, the performances of the DF, GF, NF, NC, ESF and oak wood (untreated and treated) were compared to the two commercial activated carbons (NORIT-AC and SIGMA-AC).

For the raw barks, the Douglas fir (DF) sample performed the best at 1500 mg (41.6 mgNH<sub>3</sub>/g fresh adsorbent). This was similar to the greatest performing sample, oak, which had an adsorption capacity of 41.9 mgNH<sub>3</sub>/g fresh adsorbent at 1500 mg).

GF and NF performed similarly at 1500 mg (27.7 – 28.8 mgNH<sub>3</sub>/g fresh adsorbent). NF and ESF have the best ammonia adsorption at the lowest concentration (20.2 – 23.4 mgNH<sub>3</sub>/g fresh adsorbent at 43 mg), but this doesn't improve much as the concentration increases.

After the adsorption, all of the biochars (except for oak) have negative values of ammonia mass adsorbed per gram of fresh adsorbent. This means that the adsorption method seemed to decrease the levels of nitrogen (and therefore ammonia) present on the samples. One theory for the poor biochar performance (compared to the other types of samples) was that, during the tree barks' slow pyrolysis, nitrogen had deposited onto the biochars. As the oak biochar was supplied externally and its post-pyrolysis nitrogen value was lower (1.3 wt%, compared to 2.4 – 2.7 wt% for the internally produced biochars) (Appendix – A1.2.2), the calculated adsorption will be higher.

Therefore, DFbc and NFbc were washed in hot water to attempt to remove the deposited nitrogen. The nitrogen values from ultimate analysis for the two biochars (before and after the hot water-washing) can be seen in Table 7-4. It can be seen that the nitrogen contents were lower after the wash, perhaps allowing more nitrogen to be adsorbed. Another reason for the poor biochar performance may be due to them being inactivated, which was not done due to the lack of available equipment.

Despite activated carbons being known for their adsorbency properties (698, 700, 702, 703, 705, 706), the two tested in Table 7-3 did not adsorb as much nitrogen as the hot water-washed biochars.

The Soxhlet-extracted tree bark solids performed fairly well, albeit less than the raw barks ( $\approx$  10 mgNH<sub>3</sub>/g fresh adsorbent less at 430 – 1500 mg than the raw barks). This could be from the extraction of suberin and phenanthrenes, which have been found to improve sorption capacity (712-714).

**Table 7-3 - Ammonia sorption capacity (mgNH<sub>3</sub>/g fresh adsorbent) of raw tree bark samples compared to treated barks and activated carbons. Errors presented as 1x standard deviation. Adsorption testing run in duplicate. Ultimate analysis samples run in duplicate.**

Sample	Form of Sample	Ammonia gas generated		
		43 mg	430 mg	1500 mg
DF	Raw	14.9 ± 1.6	34.9 ± 1.8	41.6 ± 1.0
	Biochar @ 400 °C	-15.6 ± 0.6	-12.8 ± 0.4	-11.5 ± 0.4
	Hot water-washed biochar	3.9 ± 1.3	17.5 ± 2.7	16.7 ± 1.0
	Soxhlet-extracted solid	2.4 ± 1.2	22.4 ± 1.2	31.0 ± 2.2
GF	Raw	13.3 ± 0.9	22.9 ± 2.2	28.8 ± 2.0
	Soxhlet-extracted solid	2.6 ± 1.0	11.7 ± 1.9	9.1 ± 1.3
NF	Raw	23.4 ± 3.7	26.5 ± 3.0	27.7 ± 1.2
	Biochar @ 400 °C	-9.2 ± 1.8	-7.2 ± 2.2	-5.3 ± 1.3
	Hot water-washed biochar	6.1 ± 0.6	18.1 ± 0.7	16.3 ± 0.9
NC	Raw	11.9 ± 4.9	14.4 ± 0.8	17.6 ± 0.1
	Biochar @ 400 °C	-16.2 ± 14.2	-12.3 ± 11.1	-9.9 ± 0.2
ESF	Raw	20.2 ± 1.3	20.2 ± 1.7	19.6 ± 1.2
	Biochar @ 400 °C	-12.9 ± 2.0	-8.1 ± 0.3	-7.1 ± 0.6
Oak	Raw	19.6 ± 2.5	28.0 ± 1.4	41.9 ± 0.5
	Biochar @ 450 °C	-2.4 ± 5.0	10.6 ± 1.9	11.6 ± 7.0
NORIT-AC		0.0 ± 0.6	2.7 ± 0.9	0.6 ± 1.2
SIGMA-AC		-8.2 ± 1.0	4.3 ± 0.3	5.9 ± 1.2

**Table 7-4 - Change in base nitrogen contents of biochars before and after hot-water washing. Errors presented as 1x standard deviation. Ultimate analysis samples run in duplicate.**

Sample	Form of sample	Nitrogen content from CHNS (wt%)
DF	Biochar	2.68 ± 0.05
	Hot water-washed biochar	0.67 ± 0.05
NF	Biochar	2.39 ± 0.08
	Hot water-washed biochar	0.57 ± 0.01

The raw data for Dorward's study was unable to be recovered, so herein the data is compared to the present work on a 'change in nitrogen contents' basis (Table 7-5). The noble fir (NF) and European silver fir (ESF) samples performed better than the Dorward pine bark (at 43 mg of ammonia). However, the Dorward spruce bark performed best. Spruce tree barks were not run in this study due to limited available supplies. Alongside the data presented above (in Table 7-3), the raw barks performed the best (as mentioned by Dorward (691)).

**Table 7-5** - Ammonia sorption capacity (change in nitrogen contents, in **mgN/g sample**) of tree bark samples from this work and Dorward's study (691). Errors presented as 1x standard deviation. Adsorption testing run in duplicate. Ultimate analysis samples run in duplicate. NM = not measured. NF = noble fir, ESF = European silver fir, GF = grand fir, DF = Douglas fir, NC = nootka cypress.

Sample	Ammonia gas generated		
	43 mg	430 mg	1500 mg
Pine bark (Dorward) (691)	15.5	NM	
Spruce bark (Dorward) (691)	24.5		
NF	23.4 ± 3.7	26.5 ± 3.0	27.7 ± 1.2
ESF	20.2 ± 1.3	20.2 ± 1.7	19.6 ± 1.2
GF	13.3 ± 0.9	22.9 ± 2.2	28.8 ± 2.0
DF	14.9 ± 1.6	34.9 ± 1.8	41.6 ± 1.0
NC	11.9 ± 4.9	14.4 ± 0.8	17.6 ± 0.1
Oak	19.6 ± 2.5	28.0 ± 1.4	41.9 ± 0.5

Following the work into the adsorption performances of tree barks, the data of the commercial lignin products and biomass residues are outlined.

In Table 7-6 and Table 7-7, the two peat samples, CH and lignoboost, performed similarly. This may be due to them sharing high lignin contents (> 40 wt%), ≈ 60 wt% volatile matter and ≈ 30 wt% fixed carbon. However, lignoboost had a stronger increase in ammonia adsorbed at the lowest concentration (43 mgNH<sub>3</sub>). The two lignin product samples (lignoboost and alkali lignin) both increase in ammonia adsorbed as the concentration increases, with AlkLig being the weaker adsorbent.

The two digestate samples performed the worst. This may be due to a number of reasons, including the high ash content and high alkaline earth metals content (Section A.2.1).

**Table 7-6** - Ammonia sorption capacity (**mgNH<sub>3</sub>/g fresh adsorbent**) of non-bark samples. Errors presented as 1x standard deviation. Adsorption testing run in duplicate. Ultimate analysis samples run in duplicate. CH = coconut husk, PeatSEPO = Irish peat, PeatMoss = moss sphagnum peat, MSWdig = municipal solid waste digestate, VGFdig = vegetable, garden, fruit residue digestate.

Sample	Ammonia gas generated		
	43 mg	430 mg	1500 mg
<b>Untreated biomass</b>			
CH	11.6 ± 5.2	24.1 ± 2.5	27.3 ± 2.8
PeatSEPO	4.4 ± 3.3	17.2 ± 0.9	29.2 ± 7.2
PeatMoss	5.6 ± 1.9	20.8 ± 2.1	27.4 ± 3.8
<b>Treated biomass</b>			
MSWdig	-1.7 ± 3.6	-3.5 ± 1.3	-3.7 ± 1.4
VGFdig	-9.0 ± 2.5	-1.6 ± 1.2	0.4 ± 5.9

**Table 7-7** - Ammonia sorption capacity (**mgNH<sub>3</sub>/g fresh adsorbent**) of commercial lignin products. Errors presented as 1x standard deviation. Adsorption testing run in duplicate. Ultimate analysis samples run in duplicate.

Sample	Ammonia gas generated		
	43 mg	430 mg	1500 mg
Lignoboost	14.7 ± 1.8	20.3 ± 0.9	24.8 ± 1.1
Alkali Lignin	6.5 ± 0.6	6.4 ± 0.4	15.6 ± 1.5

Overall, the raw Douglas fir tree bark and the oak wood had the greatest ammonia sorption capacities (based on ammonia adsorbed per gram of fresh adsorbent), with a high of 41.6-41.9 mgNH<sub>3</sub>/g fresh adsorbent when 1500 mgNH<sub>3</sub> was generated. Several of the potential adsorbents performed well, with a high between 27 – 29 mgNH<sub>3</sub>/g fresh adsorbent also at 1500 mgNH<sub>3</sub> generation. These were DFSox, PeatSEPO, GF, NF, PeatMoss, and CH.

## 7.2.2 Comparison between this work and literature’s data

The performance of the samples from this study were able to be compared to that of Helminen et al.(380) through extrapolation of the Dubinin-Astakhov adsorption equilibrium model and calculation of the ammonia partial pressure in each Duran bottle (as discussed in Section 3.13). The adsorption isotherm parameters to enable the comparison between each of Helminen et al.’s sorbents and those in this study are presented here and examples of how the D-A model was applied to Helminen’s data are shown below to illustrate the validity of the model in this thesis’s experimental conditions.

### 7.2.2.1.1 Calculation of literature data under this study’s adsorption conditions.

This section describes how the adsorption capacities for Helminen’s sorbents, at their adsorption temperature and partial pressures, were converted into the conditions from this study.

The partial pressures from this study were calculated according to Appendix Section A1.2.2. The intermediate values outlined in the Microsoft Excel worksheet illustrated in Section A1.2.2 are presented in Table 7-8.

**Table 7-8** – Summary of the main results calculated for the constant parameters before and after ammonia adsorption reactions.

Constant parameters before and after reaction	T <sub>ads</sub> = 20°C	Bottle 250 mL	
Before reaction – Conc of (NH <sub>4</sub> ) <sub>2</sub> SO <sub>4</sub>	0.05M	0.5M	1.8M
(NH <sub>4</sub> ) <sub>2</sub> SO <sub>4</sub> : (g) – (moles)	0.17 – 0.0013	1.68 – 0.0127	5.91 – 0.0447
NaOH: (g) – (moles)	0.25 – 0.0063	2.47 – 0.0618	7.42 - 0.1855
Volume H <sub>2</sub> O per expt (ml)	84.74	82.42	76.76
H <sub>2</sub> O density at T <sub>ads</sub> (g mL <sup>-1</sup> )	0.9978	0.9978	0.9978
H <sub>2</sub> O mass: (g) – (moles)	84.55 – 4.692	82.24 – 4.564	76.59 - 4.250
Total H <sub>2</sub> O <sub>(liq)</sub> before reaction: (moles) – (mol fraction)	4.6948 – 0.9983979	4.58916 – 0.9840395	4.3398 - 0.9496456
Volume before reaction (gas) (cm <sup>3</sup> )	165.2	167.1	171.6
Total Pressure before reaction (kPa)	100.00	100.00	100.00
Air before reaction and before water-moisture equilibrium: (moles)	6.7822E-03	6.8605E-03	7.0454E-03
Partial pressure H <sub>2</sub> O before reaction and after water - moisture equilibrium: (kPa)	2.3276	2.2942	2.2140
H <sub>2</sub> O moisture after water-moisture equilibrium and before reaction: (moles)	1.5778E-04	1.5731E-04	1.5590E-04
After reaction – Conc of (NH <sub>4</sub> ) <sub>2</sub> SO <sub>4</sub>	0.05M	0.5M	1.8M
NH <sub>3 tot</sub> – (assume no NH <sub>4</sub> <sup>+</sup> ) (moles)	2.57244E-03	2.54218E-02	8.94303E-02
NH <sub>3 (l)</sub> guestimate - adjusted by Solver: (moles) – (mol fraction)	2.56971E-03 – 0.0005465	2.53942E-02 – 0.0054452	8.93287E-02 - 0.0195473
NH <sub>3 (g)</sub> calc by difference with tot and (L): (moles)	2.73460E-06	2.75568E-05	1.01597E-04
Product reaction H <sub>2</sub> O <sub>R</sub> (moles)	2.57244E-03	2.54218E-02	8.94303E-02
Excess NaOH (l) (basic): (moles) – (mol fract)	3.67756E-03 – 0.0007821	3.63282E-02 – 0.0077897	9.60697E-02 - 0.0210224
Product Na <sub>2</sub> SO <sub>4 (l)</sub> (neutral): (moles) – (mol fract)	1.28622E-03 – 0.02735	1.27109E-02 – 0.0027256	4.47151E-02 - 0.0097847
Total (liq): (moles) – (mol fract)	4.70231 – 1.0	4.66360 – 1.0	4.56988 – 1.0
Mass H <sub>2</sub> O <sub>R</sub> (g)	4.63555E-02	4.58101E-01	1.61153E+00
Vol H <sub>2</sub> O <sub>R</sub> (mL)	4.64577E-02	4.59111E-01	1.61509E+00
Volume Liquid (mL)	84.786	82.879	78.375
Total gas after reaction (air+NH <sub>3(g)</sub> +moisture) (moles)	6.9427E-03	7.0453E-03	7.3029E-03
P <sub>tot</sub> Total Pressure after reaction (kPa)	102.37	102.69	103.65
Henry's constant <sub>aq</sub> NH <sub>3</sub> at T <sub>ads</sub> (kPa)	73.77	73.77	73.77
At equilibrium: Henry's law y P <sub>tot</sub> = x H = P <sub>NH3</sub>	0.05M	0.5M	1.8M
x H (kPa)	4.0311E-02	4.0167E-01	1.4419
y P <sub>tot</sub> (kPa) = P <sub>NH3</sub>	4.0320E-02	4.0168E-01	1.4420
% relative error Henry's law (after Solver)	0.022	0.001	0.008
Partial pressure: P <sub>NH3</sub> (kPa)	0.0403204	0.4016757	1.4420432

As shown in Table 7-8, the range of partial pressures in this study range from 0.04 – 1.44 kPa.

For the Dubinin-Astakhov data outlined by Helminen (380) for alumina, the closest graphical solution to this thesis is where  $T_{ads}$  is 25 °C and  $P_{NH_3}$  is 2 kPa. This provided an adsorption capacity ( $q$ ) of around 1.5  $mmol_{NH_3}/g$  (Figure 7-2).

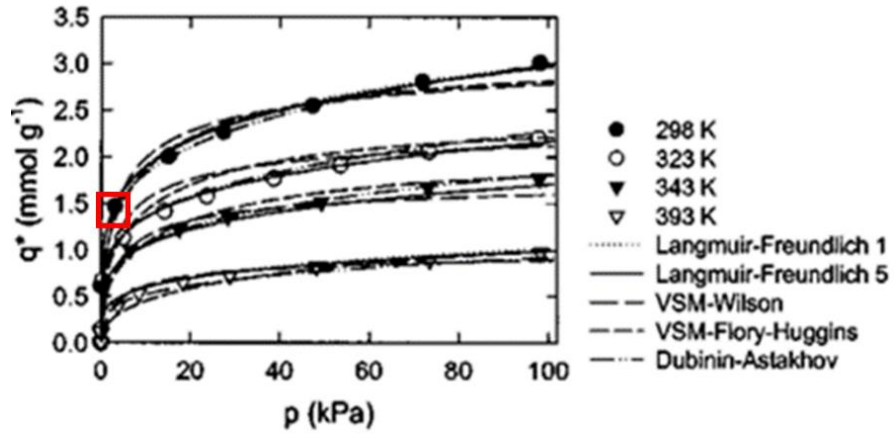


**Figure 7-2** – The graphical representation of Helminen et al's (380) ammonia adsorption data for alumina.

When this data was inputted into Microsoft Excel (Figure 7-3), where  $T_{ads} = 20$  °C, the solution of 1.59  $mmol_{NH_3}/g$  was given. As the adsorption capacity ( $q$ ) increased as the  $T_{ads}$  decreased, whilst  $q$  also decreased when the  $P_{NH_3}$  decreased, the value of 1.59  $mmol_{NH_3}/g$  was considered plausible. Validation of Helminen et al's data can be found in the Appendix (Section A1.2.2).

log 10 Vapour Pressure NH3 at T (bar) from Antoine's equation NIST	0.929113023	
Antoine cst A	4.86886	
Antoine cst B	1113.928	
Antoine cst C	-10.409	
P0 Vapour Pressure NH3 at T (bar)	8.49401499	
P0 Vapour Pressure NH3 at T (kPa)	849.401499	
P0/PNH3	589.0263954	
D = RT ln (P0/PNH3) in J/mol	15545.9227	
density liq NH3 at P0 (g/cm3)	0.725608	
W0 cm3/g	0.159	
Q0 (g NH3 / g ads)	0.115371668	
E (J/mol)	1.00E+04	
n	0.844	
(D/E) <sup>n</sup>	1.451190174	
exp -(D/E) <sup>n</sup>	0.234291275	
<b>q of NH3 on adsorbent at Tads (g NH3/g ads)</b>	<b>0.027030575</b>	
q in mol NH3/g ads	0.001586301	
<b>q in mmol of NH3 / g of ads</b>	<b>1.59</b>	check with relevant adsorbent Helminem isotherm
<b>Q in mg of NH3 / g of ads</b>	<b>27.03</b>	value for Helminem Ads to be compared to untreated biomass at same Tads and

**Figure 7-3-** Screenshot of the Microsoft Excel workbook where Helminen et al's data (in this case, gamma-alumina) is converted to the conditions presented in this study.

After converting the adsorption capacity from  $\text{mmol}_{\text{NH}_3}/\text{g}$  of fresh adsorbent to  $\text{mg}_{\text{NH}_3}/\text{g}$  of fresh adsorbent, Helminen et al.'s alumina sorbent at  $T_{\text{ads}}$  of 20 °C and  $P_{\text{NH}_3}$  of 1.44 kPa has a capacity of 27.03  $\text{mg}_{\text{NH}_3}/\text{g}$  of ads. The gamma-alumina sorbent performed similarly to the five untreated barks, coconut husk and two peats tested in this study (Table 7-9 ).

**Table 7-9 –** Adsorption capacities of untreated biosolid samples from this study at 1.442 kPa.

Adsorbent	Adsorption Capacity at $P_{\text{NH}_3}$ of 1.442 kPa ( $\text{mg}_{\text{NH}_3}/\text{g}_{\text{ads}}$ )
NC	17.6
NF	27.7
ESF	19.6
GF	28.8
DF	41.6
Oak	41.9
PeatSEPO	29.2
PeatMoss	27.4
CH	27.3
<b>Average untreated biosolids</b>	<b>29.0</b>

A further validation of the adsorption capacities in this study compared to the modelled data was performed by comparing the SIGMA-AC and NORIT-AC activated carbon samples with the sample used by Helminen et al. (Merck) (380) under the same conditions.

Once Helminen et al.'s data had been inputted into the Microsoft Excel Dubinin-Astakhov model calculator, the adsorption capacity of the Merck activated carbon was found to be 0.31 mmol<sub>NH3</sub>/g<sub>AC</sub> (Figure 7-4 ). From the graphical adsorption isotherm data (Figure 7-5), where the closest conditions were T<sub>ads</sub> = 25 °C and P<sub>NH3</sub> is 2 kPa, the adsorption capacity of the activated carbon was also around 0.3 mmol<sub>NH3</sub>/g<sub>AC</sub>. Therefore, the comparison of Helminen et al.'s data had been validated for use in this workbook.

log 10 Vapour Pressure NH3 at T (bar) from Antoine's	0.929113023
Antoine cst A	4.86886
Antoine cst B	1113.928
Antoine cst C	-10.409
P0 Vapour Pressure NH3 at T (bar)	8.49401499
P0 Vapour Pressure NH3 at T (kPa)	849.401499
P0/PNH3	589.0263954
RT ln (P0/PNH3) in J	15545.9227
density liq NH3 at P0 (g/cm3)	0.725608
W0 cm3/g	2.31
Q0 (g NH3 / g ads)	1.676154424
E (J/mol)	1.51E+03
n	0.751
(D/E) <sup>n</sup>	5.760926136
exp <sup>-</sup> (D/E) <sup>n</sup>	0.003148195
<b>q of NH3 on adsorbent at Tads</b>	<b>0.00527686</b>
Q in mol NH3/g ads	0.000309675
<b>mmol of NH3 / g of</b>	<b>0.31</b>
<b>Q in mg of NH3 / g of ads</b>	<b>5.28</b>

**Figure 7-4** - Screenshot of the Microsoft Excel workbook where Helminen et al.'s activated carbon data is converted to the conditions presented in this study (1.8M, 20°C and 1.44 kPa).

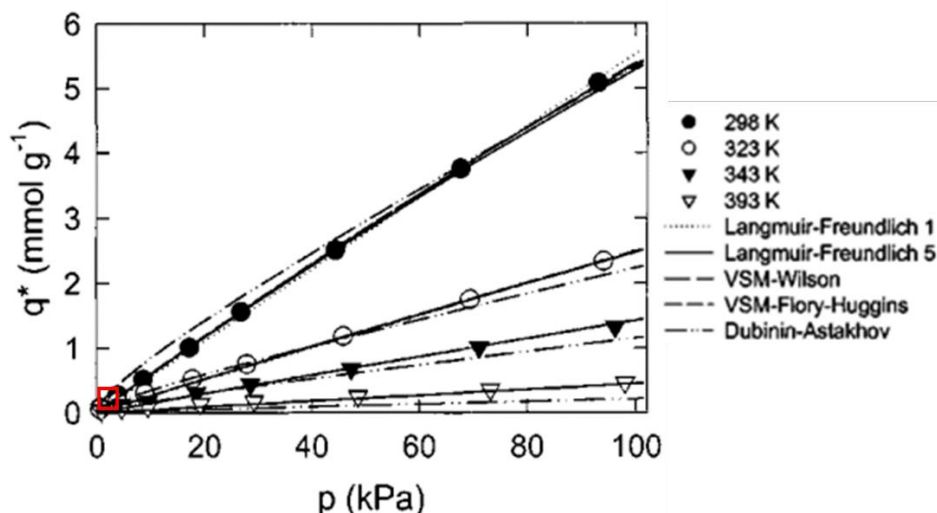


**Figure 7-5** – The graphical representation of Helminen’s (380) ammonia adsorption data for activated carbon.

The adsorption capacities obtained from this study, NORIT-AC ( $0.56 \text{ mg}_{\text{NH}_3}/\text{g}_{\text{AC}}$ ) and SIGMA-AC ( $5.8 \text{ mg}_{\text{NH}_3}/\text{g}_{\text{AC}}$ ) were then compared to Helminen et al.’s activated carbon from Merck. The SIGMA-AC samples measured in the experiments of the present thesis gave a value that was close to that obtained from Helminen et al.’s ( $5.28 \text{ mg}_{\text{NH}_3}/\text{g}_{\text{AC}}$ ).

#### 7.2.2.1.2 Direct comparison of this work to Helminen et al

The activated carbon samples (SIGMA-AC and NORIT-AC) from this study performed similarly to the activated carbon from Helminen (380), when interpolated to the same conditions (Table 7-10). The hot-water washed biochars are comparable to the alumina at the  $150 \text{ mg}_{\text{NH}_3}$  experiment, whilst the untreated samples are slightly stronger than the alumina sample across all three experiments. In comparison to the silica gel adsorption capacities in Table 7-10 ( $39.8 \text{ mg}_{\text{NH}_3}/\text{g}_{\text{ads}}$ ), the strongest adsorbents from this study (DF -  $41.6 \pm 1.0 \text{ mg}_{\text{NH}_3}/\text{g}_{\text{ads}}$ , oak -  $41.9 \pm 0.5 \text{ mg}_{\text{NH}_3}/\text{g}_{\text{ads}}$ ) are the only ones to surpass them, but not by a large margin.

None of the samples in this study outperform the zeolite catalytic samples as studied by Helminen et al. (380). However, in a real-world scenario, zeolite catalysts are not yet cost-effective (761, 762). Therefore, the valorisation of cheap biomass residues that have similar adsorption performances than commercial adsorbents is a valuable opportunity. Although the adsorption performance of the commercial adsorbents and the biomass residue-derived material have been compared, the desorption performance has not been

explored. In addition, the partial pressures of the experiments run in this work (0.04 – 1.44 kPa NH<sub>3</sub>) are a lot lower than those explored by Helminen et al. (2.7 – 27 kPa NH<sub>3</sub>). The higher partial pressures were unable to be explored using the method performed in this work, due to the specific scale of Duran bottle used (as described in Section 3.13). Further work should therefore look at the ammonia adsorption capacities of the samples at the higher partial pressures of NH<sub>3</sub>.

**Table 7-10** - Comparison of this study’s adsorption capacities to Helminen (380). All unspecified values are given in mgNH<sub>3</sub>/g of fresh adsorbent. Errors presented as 1x standard deviation, from 4 datapoints for each sample in this study R<sup>2</sup> is given for data interpolated by the Dubinin-Astakhov equilibrium model. Conversion of gaseous ammonia masses to partial pressures are presented in the Appendix (A1.2.2).

Gaseous Ammonia (mg)		43	150	1500	
Partial Pressure (kPa NH <sub>3</sub> )		0.04	0.4	1.44	
Adsorption Capacity (mgNH <sub>3</sub> /g fresh ads)					R <sup>2</sup>
Untreated Samples		13.9 ± 6.1	23.2 ± 5.8	29.0 ± 7.8	
Alumina	Helminen et al. (380)	11.7	17.9	22.7	99.8
4A Zeolite		58.5	92.8	111.4	99.0
13X Zeolite		61.7	94.5	112.9	99.1
Silica Gel		15.5	29.3	39.8	99.0
Activated Carbon	NORIT-AC	0.0 ± 0.6	2.7 ± 0.9	0.6 ± 1.2	
	SIGMA-AC	-8.2 ± 1.0	4.3 ± 0.3	5.9 ± 1.2	
	Helminen et al (380)	0.5	1.9	4.4	98.8
Biochars	Unwashed	-9.4 ± 4.7	-4.9 ± 3.2	-4.4 ± 1.9	
	Hot water-washed	5.0 ± 1.0	17.8 ± 1.7	16.5 ± 1.0	

Close examination of which biomass solids exhibited higher NH<sub>3</sub> adsorption in this work’s experiments indicated that raw barks, untreated oak, and untreated peats generally performed better than the biochars (unwashed, washed, Soxhlet treated) and the two activated carbons tested. This led to splitting the solid samples into two large categories: untreated vs. treated biomass solids. A statistical analysis was therefore performed to determine whether the treatment factor (untreated vs. treated) had a significant effect on the mean NH<sub>3</sub> adsorption.

This is summarised in Figure 7-6 where the means of untreated samples are superior to those of the treated samples at all three experiments conducted at different NH<sub>3</sub> concentrations, with non-overlapping error bars. This is further demonstrated in the results shown in the next section.

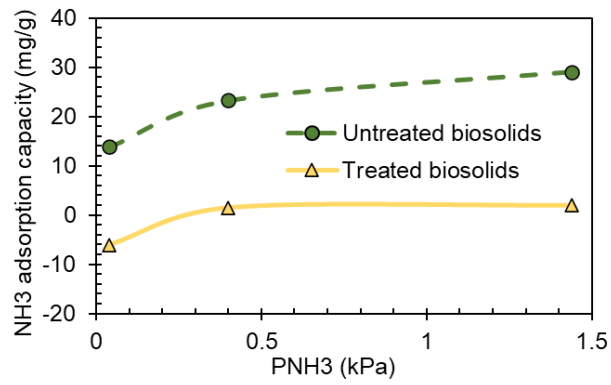


**Figure 7-6** – Comparison of the averages of ammonia adsorption capacities of the untreated samples (raw barks, oak, and peats) and treated samples (biochars and activated carbons).

### 7.2.3 Statistical analysis of the effect of treatment on the samples' adsorption capacity

The correlation between the samples' treatment and the adsorption capacity was explored using univariate analysis via SPSS. All unaveraged data was inputted into the software (SPSS Statistics 28), where the samples were separated into categories 'untreated' "Treatment=0" and 'treated' "Treatment=1" (Table 7-11[a]). Here, a generalised linear model was fitted around the inputted data.

From Table 7-11[b], it can be seen that the effect of treatment on the ammonia adsorption capacity is significant. This means that there is below a 0.01 probability that the null hypothesis is true (that there is no effect of sample treatment on the adsorption capacity) (763).

**Table 7-11**– Univariate statistical analysis outputs of ammonia adsorption capacity (mgNH<sub>3</sub>/ g fresh adsorbent) against sample treatment, outlined as [a] Descriptive Statistics and [b] Pairwise Comparisons.

[a]

Treatment	Mean	Standard Deviation	N
Untreated	22.03	9.40	112
Treated	-1.26	10.92	112
<b>Total</b>	<b>10.38</b>	<b>15.47</b>	<b>224</b>

[b]

Treatment	Treatment	Standard Error	Significance
Untreated	Treated	1.36	< 0.001

Due to the difference between the untreated and treated samples, Figure 7-6 was plotted again, but with the standard errors given by the statistical analysis (Figure 7-7). Here, there are clearly non-overlapping error bars. The lack of overlap between the error bars of the untreated and treated samples show that the differences between the two categories are significant.

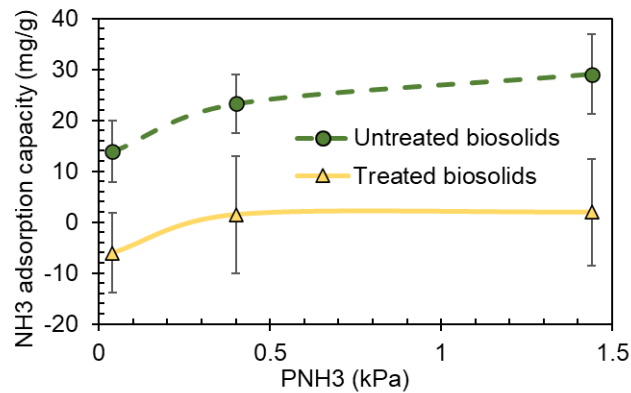


**Figure 7-7** – Comparison of the averages of ammonia adsorption capacities of the untreated samples (raw barks, oak, and peats) and treated samples (biochars and activated carbons).

As there is now a clear difference between the untreated and treated samples, in terms of adsorption capacity, the reason for this difference has been explored. Across this wider work, proximate and ultimate analysis have been run on all samples. When grouping the data, the solvent-extracted samples (DFSox, GFSox) were not included in the ‘treated’ group as their values were unmistakable outliers when compared to the biochars and activated carbons.

The statistical analysis of the proximate and ultimate analysis of the grouped untreated and treated samples were ran. However, the only statistically significant variables were the molar O/C, molar H/C, and the volatile matter/fixed carbon (VM/FC) ratios in Table 7-12.

**Table 7-12** – Multivariate statistical analysis outputs of [a] Descriptive Statistics and [b] Pairwise Comparisons of untreated (Treatment=0) and treated samples (Treatment=1) for molar H/C, molar O/C, and volatile matter/fixed carbon (VM/FC) ratios.

[a]

Variable	Treatment	Mean	Standard Deviation	N
Molar H/C	0	1.20	0.213	18
	1	0.33	0.131	18
	<b>Total</b>	<b>0.76</b>	<b>0.472</b>	<b>36</b>
Molar O/C	0	0.67	0.109	18
	1	0.16	0.056	18
	<b>Total</b>	<b>0.42</b>	<b>0.271</b>	<b>36</b>
Mass VM/FC	0	3.33	1.433	18
	1	0.40	0.312	18
	<b>Total</b>	<b>1.87</b>	<b>1.806</b>	<b>36</b>

[b]

Variable	Treatment	Treatment	Standard Error	Significance
Molar H/C	Untreated	Treated	0.059	< 0.01
Molar O/C	Untreated	Treated	0.029	< 0.01
Mass VM/FC	Untreated	Treated	0.346	< 0.01

The Means data provided above were used to produce Figure 7-8. The treated samples have a much higher fixed carbon and lower volatile matter than the untreated samples, with the VM/FC ratio also being lower after slow pyrolysis. In the pyrolysis process, volatile components are expected to leave the structure of the biomass, while the fixed carbon remains (764). This is why the volatile matter to fixed carbon ratio (VM/FC) is expected to be lower for biochars than untreated samples. In addition to surface area, a factor that is known to impact the ability of an adsorbent to adsorb is the amount of functional groups (765). Through pyrolysis, the functional groups that are present on the surface of the biomass, disappear (92). These groups are volatiles such as alkanes, alcohols, and aromatics (766). It can therefore be theorised that, as the volatile matter of the sample decreases, the extent of functional groups decreases also, reducing the VM/FC ratio and potentially the NH<sub>3</sub> adsorption capacity. The standard errors for VM/FC and molar O/C are

likely to be higher due them both being ratios, as the change in the individual variables would have a greater impact on the ratio value. Therefore, there would be a greater spread of values and thereby higher standard errors.

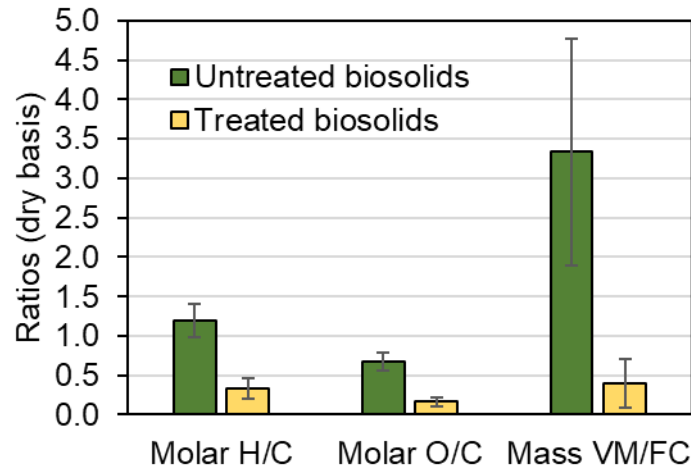


**Figure 7-8** – Means of molar H/C, molar O/C, and volatile matter/fixed carbon ratio values for the untreated and treated biosolids. Error bars are 1x standard deviation.

For a more in-depth look into the untreated and treated samples, they were compared directly with each other (where each sample came from the same source) (Table 7-13).

**Table 7-13** – Numbering of biomass types for the comparison of differences in proximate and ultimate analysis values.

Biomass Type	Untreated	Treated
1	NC	NCbc
2	CH	
3	NF	NFbc, HWNFbc
4	ESF	ESFbc
5	GF	
6	DF	DFbc, HWDFbc
7	Oak	Oak450bc
8	PeatSEPO	
9	PeatMoss	
10		SIGMA-AC
11		NORIT-AC

The ultimate analysis data has been converted into molar H/C and molar O/C ratios as presented in Figure 7-9. The change in molar H/C and O/C can be assumed to be due to the change in lignocellulosic composition. Although fibre analysis was not completed on

the treated biochars, the molar ratios provide an indication as to how they were affected by the pyrolysis process.

The untreated samples have higher molar H/C and molar O/C values than the treated samples. This is expected due to the increasing carbon contents gained by the carbonisation that occurs from pyrolysis.

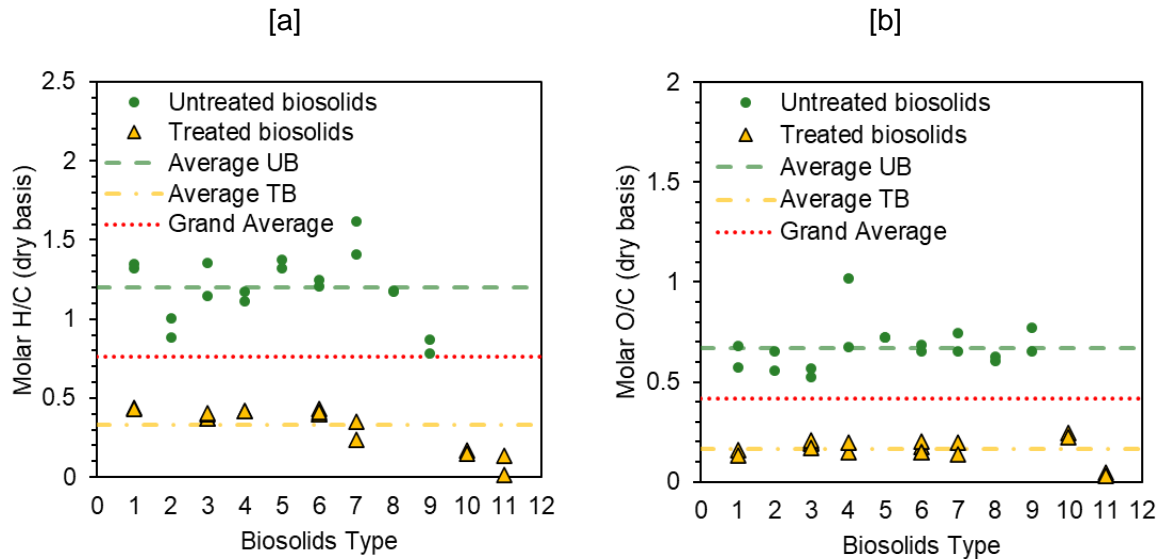


**Figure 7-9** – Comparison of (a) molar H/C and (b) molar O/C ratios for untreated and treated biosolids. Each number on the x axis represent one type of biosolid for which untreated and treated elemental analysis was carried out. Experiments were carried out in duplicate in some cases for both levels of treatment, e.g. there are 2 points for both untreated and treated types 3 and 7. Key of biosolids type: 1-NC, 2-CH, 3-NF, 4-ESF, 5-GF, 6-DF, 7-Oak, 8-PeatSEPO, 9-PeatMoss, 10-SIGMA AC, 11-NORIT-AC.

### 7.3 Conclusion

In this chapter, the ammonia adsorption capacity of raw tree barks, solvent-extracted tree barks, commercial lignin products, tree bark biochars, activated carbons, digestates, and other biomass residues were tested at three different concentrations. Here, the raw tree residues performed the best, particularly the Douglas fir tree bark and oak wood (41.6-41.9 mgNH<sub>3</sub>/g fresh adsorbent at 1500 mgNH<sub>3</sub>). Following this, the grand fir, and noble fir performed well (between 27.6 - 28.6 mgNH<sub>3</sub>/g fresh adsorbent at 1500 mgNH<sub>3</sub>).

All of the biochars were home-produced by slow pyrolysis at 400 °C, except for oak, which was supplied externally (and was pyrolysed at 450 °C). The home-produced biochars all had negative values of ammonia adsorption (-11.5 - -5.3 mgNH<sub>3</sub>/g fresh adsorbent at 1500 mgNH<sub>3</sub>). To examine if this was due to the deposition of nitrogen (as the inert gas used for the pyrolysis process), two of the samples were washed with hot water, and run again by the ammonia adsorption method. After the hot water-washing, the biochar samples (Douglas fir and noble fir) had increased capacities, with an adsorption capacity of 16.3 - 16.7 mgNH<sub>3</sub>/g fresh adsorbent. This was still lower than the raw samples but had improved on the previous values. The poor performance of the un-washed biochars was assumed to be due to the nitrogen deposit and the biochar's inactivation. The two activated carbons (SIGMA-AC and NORIT-AC) did not perform as well as the hot water-washed samples (0.6 - 5.9 mgNH<sub>3</sub>/g fresh adsorbent).

The solvent-extracted tree barks (Douglas fir and grand fir) had a slightly weaker performance than the raw tree barks (9.1 - 30.8 mgNH<sub>3</sub>/g fresh adsorbent) at 1500 mgNH<sub>3</sub>, which may be due to the extraction of compounds (phenanthrenes) that have a positive impact on ammonia sorption capacity.

The two digestate samples (derived from municipal solid waste, and vegetable, garden, and fruit residue), performed similarly to the un-washed biochars, with -3.7 - 0.4 mgNH<sub>3</sub>/g fresh adsorbent at 1500 mgNH<sub>3</sub>. The poor adsorption capacity may be due to a variety of reasons, such as the high alkaline earth metals content and high ash content. However, this has not been explored more deeply in this work.

For the remaining untreated biomass residues (peat moss, peat, and coconut husk) and commercial lignin products (alkali lignin and lignoboost), they performed reasonably strongly (15.5 - 28.8 mgNH<sub>3</sub>/g fresh adsorbent at 1500mgNH<sub>3</sub>). The order of overall ammonia adsorption performance across all samples were as follows: Raw tree barks >

Solvent-extracted tree barks > Biomass residues > Commercial lignin products > Hot-water washed tree bark biochars > Activated Carbons > Digestates > Unwashed biochars.

Through extrapolation of the Dubinin-Astakhov adsorption equilibrium model, the adsorption capacities of the samples in the work were compared to those of Helminen et al. (380) at the same partial pressure of ammonia and adsorption temperature. The method used in this study was validated by the similarity in results between the activated carbons from this work and Helminen et al.'s (380). Where Helminen et al. considered the ammonia adsorption capacities of two zeolites, alumina, silica and one activated carbon, the adsorption capacities of the untreated biomass samples in this study were comparable to that of the alumina at each partial pressure tested. The two zeolites in Helminen et al. had much stronger ammonia adsorption capacity throughout the three partial pressures tested, compared to any of the samples considered in this work. However, zeolites are expensive materials with poor sustainability (767). Therefore, low-cost materials with greater levels of sustainability, such as biomass residues, must be compared further when considering potential adsorbents.

Following the testing for all samples, the causation between the effect of slow pyrolysis of the samples and their adsorption capacities were explored using univariate and multivariate statistical analysis. The univariate statistical analysis showed that there was below a 0.01 probability that sample pyrolysis had no effect on adsorption capacity. The potential reasons for the effect of pyrolysis were investigated by considering the change in proximate and ultimate analysis values. From multivariate statistical analysis, the pyrolysis of the sample was shown to significantly impact the molar H/C, molar O/C, and mass volatile matter/fixed carbon ratios.

## Chapter 8 – Conclusions and recommendations for further work

The following section concludes how the research aims and objectives were met, discusses the research limitations, and recommends supplementary or replacement analysis to strengthen the performed work.

### 8.1 Conclusions

In this section, the findings of **Chapter 4** to **Chapter 7** will be viewed through the lens of the objectives laid out in **Chapter 1**.

**Objective 1: To identify high-lignin feedstocks.** Chapter 4 screened and characterised a wide variety of samples from a variety of sources. These samples consisted of anaerobic digestion digestates (from municipal solid waste, agricultural residue, sewage sludge, and vegetable, garden, and fruit residue), biomass residues (coconut husk, sugarcane bagasse, and a tree bark) and commercial lignin products (alkali lignin, organosolv lignin and Lignoboost) as comparators. Each sample was characterised by proximate analysis, ultimate analysis, atomic absorption spectroscopy and pyrolysis-gas chromatography/mass spectrometry.

Through proximate analysis, it was found that the ash contents of all samples (except for organosolv lignin, the tree bark, coconut husk and sugarcane bagasse) were above 10 wt%. High ash content can increase the risk of slagging, fouling and coking during thermochemical conversion.

Through ultimate analysis, the carbon and oxygen content of the tree bark and Lignoboost were the greatest. This implied a larger lignin content, which was confirmed by fibre analysis. Other high-lignin samples included coconut husk and alkali lignin, however, the coconut husk also had high levels of cellulose.

The alkaline earth metals' (aluminium, calcium, potassium, iron, sodium, magnesium) concentrations were measured by atomic absorption spectroscopy. The high-lignin samples, other than alkali lignin, had low levels of metal contents. The alkali lignin had very high levels of sodium. The biomass residues had low levels of calcium and potassium, which is expected due to bioaccumulation.

Due to the high levels of metal contents in some of the samples, the alkali lignin, sugarcane bagasse and digestates underwent mild acid-washing. After the acid-washing, the metals content decreased as well as the ash content.

From the py-GC/MS chromatograms at 550 °C, the commercial lignin products had larger peak areas of only lignin-derived compounds. These are compounds with phenolic groups, such as phenol or 2-methoxy phenol. From all of the samples tested, the py-GC/MS data of the tree bark was most similar to the commercial lignin products.

Only two of the biomass residue samples had high levels of lignin from the fibre analysis (coconut husk and the tree bark). However, the coconut husk had high levels of cellulose, which was also present in the pyrolysis fragments from py-GC/MS. The tree bark, as a cheap biomass residue, performed comparably to the commercial lignin products, especially Lignoboost. Alkali lignin is not an ideal lignin sample due to the high metal contents.

Therefore, Chapter 5 explored a wide range of tree barks to determine if the performance of the singular tree bark from Chapter 4 was representative of all samples. The 11 tree bark samples consisted of 4 fir pine tree barks (Douglas fir, noble fir, grand fir, and European silver fir), 2 spruce pine tree barks (Norway spruce and sitka spruce), 3 cypress tree barks (Lawson cypress, nootka cypress and Western red cedar) and 2 other pine tree barks (larch and Western hemlock).

The proximate and ultimate analysis results for the collection of tree barks were all similar, with volatile contents above 65 wt% and ash contents below 4 wt% (on a dry basis). The alkaline earth metal contents were also consistently low, except for a higher calcium concentration in the Norway spruce and nootka cypress.

The lignin content of the tree barks, from the fibre analysis, were more varied than expected. Four of the tree barks (European silver fir, Western red cedar, noble fir, and Lawson cypress) had lignin contents above 40 wt%, whilst two (nootka cypress and sitka spruce) had lignin contents below 20 wt%. The cellulose content for all tree barks was between 20-40 wt%, with noble fir, Douglas fir and Western hemlock having the lowest (20-24 wt%).

The extractives (or unknown) content from the fibre analysis was between 20-40 wt% for most of the tree barks. From the py-GC/MS chromatograms, the samples with the larger unknown contents contained peaks that included fatty acids such as naphthalenol. These were most likely to be derived from suberin. The extraction of these suberin-derived components was explored by two forms of solvent extraction. The Soxhlet-extracted residues, once measured by fibre analysis, had concentrated lignin and holocellulose (cellulose + hemicellulose) content from the removal of the extractives/unknowns.

The samples with the most potential for valorisation as a lignin-rich residue were the noble fir and Douglas fir tree barks. In addition, the Soxhlet-extracted noble fir and sitka spruce tree barks may be valuable as lignin-rich residues also.

**Objective 2: To explore the valorisation and upgrading of high-lignin feedstocks to bio-based solvents.** Chapter 6 investigated the applications of fast pyrolysis oil-derived components from the high-lignin samples tested in Chapter 4 and Chapter 5.

The samples underwent fast pyrolysis-GC/MS at 450, 550, and 650 °C. The most prevalent components were 2-methoxy phenol, phenol, furfural, trans-isoeugenol, creosol and 5-methy-2-furancarboxaldehyde (MFCA). However, pyrolysis oils have a complex nature, so separation and isolation is difficult. Therefore, the upgrading of the pyrolysis oil-derived components, by methylation and hydrogenation, were examined theoretically. The hazardousness and solubility of the three types of pyrolysis oil-derived components (original, methylated, and hydrogenated) were estimated by the CHEM21 criteria (for assessing the environmental, health and safety impacts of the prospective solvent) and Hansen Solubility Parameters. The original pyrolysis oil-derived components all had at least one CHEM21 category that would be considered as hazardous. After both methods of upgrading, the toxicity of the chemicals (considered as a part of the health score) reduced. In terms of the solubility, the methylation was seen to reduce the hydrogen bonding and dipole moments of the pyrolysis oil components, whilst all three of the solubility parameters reduced after hydrogenation.

Following the estimation of the pyrolysis oil-derived components' properties, they were compared to that of common industrial solvents. For the hazardous common solvents, the methylated and hydrogenated pyrolysis oil-derived components were thought to be valuable alternatives in the manufacturing of plastics, in the production of paint removers and strippers, and as extraction solvents for resins, oils, waxes and lubricants.

**Objective 3: To explore the valorisation of high-lignin feedstocks as an adsorbent of ammonia.** In Chapter 7, the ammonia adsorption capacity of biomass residues, commercial lignin products, digestates, activated carbons and various forms of tree barks were tested. The samples underwent ammonia adsorption in a closed environment, where ammonia gas was generated at three different masses (43mg, 150mg and 1500mg).

The tree barks were tested raw, as biochars (via slow pyrolysis at 400 °C), and as Soxhlet-extracted residues. Across all samples, the raw tree residues performed the best, in particular the Douglas fir bark and oak wood. Several of the other samples; grand fir, and

noble fir performed well. The internally produced biochars all had negative ammonia adsorption values, which was posited as being due to nitrogen deposition during the slow pyrolysis process. Therefore, two of the biochars were washed with hot water, dried, and re-tested. This led to increased adsorption capacities, but they still did not perform as well as the raw tree barks. The two activated carbon samples, despite being common adsorbents, did not perform as well as the hot water-washed samples. The solvent-extracted tree barks had a weaker performance than the raw tree barks.

The order of ammonia adsorption performance across all of the samples runs were as follows: Raw tree barks > Solvent-extracted tree barks > Biomass residues > Commercial lignin products > Hot-water washed tree bark biochars > Activated Carbons > Digestates > Unwashed biochars.

In comparing the performance of the samples in this study to that in the literature (via extrapolation of the Dubinin-Astakhov adsorption equilibrium model), it was found that the untreated samples had a similar performance to that of commercial gamma-alumina. The adsorption capacity of zeolites, however, was much higher than all of the samples tested. Despite the strong performance, zeolites are expensive materials with poor sustainability, so the cheaper biomass residues (including the raw tree barks) may be good low-cost adsorbent alternatives.

Following the testing, statistical analysis was run between the slow pyrolysis tree bark biochars and the raw tree barks to observe if there was any effect of slow pyrolysis on ammonia adsorption capacity. From the initial univariate analysis, it could be seen that there was below a 0.01 probability that sample pyrolysis had no effect on adsorption capacity, therefore there was a high probability that slow pyrolysis did effect adsorption capacity of a sample, with biochars produced by slow pyrolysis of barks exhibiting a statistically much lower ammonia adsorption capacity than their raw, untreated counterparts.

The structural differences between the biochars and untreated tree barks, from proximate and ultimate analysis, were then compared by multivariate statistical analysis. This showed that the slow pyrolysis had a high probability of impacting the molar H/C, molar O/C, and volatile matter/fixed carbon ratios. The biochars produced by slow pyrolysis of bark exhibited statistically lower molar H/C and O/C ratios, higher fixed carbon, lower volatile matter than the untreated counterparts. The ash content, however, had a low probability of being affected by slow pyrolysis.

## **8.2 Recommendations for further work**

This work has illustrated the potential of lignin-rich feedstocks to be used as ammonia adsorbents and as a source of bio-based solvents. However, there are a number of avenues that further work could follow to advance knowledge in the subject areas and the potential scaling-up of the applications.

### **8.2.1 Limitations of the analysed tree barks**

Although tree barks from eleven different species were analysed and tested in this work, how representative the tree barks are should be studied.

The tree barks were only sourced from one site (Abbey Timber) and were only collected during a single season. The structure of tree bark alters for each species (472), and is also dependent on the external environment (471). By varying the number of sites, time of the year, and tree ages where the bark is collected, the effect of the seasonality and environment on the bark's structure could be considered.

When considering the seasonality of tree barks, the carbohydrate content (hemicellulose and cellulose) appears to peak in July, with the contents lowering until February before growing again (768). However, the lignin contents and extractives content do not vary much throughout the year, thereby potentially concentrating the lignin in the winter months.

The thickness of bark, whilst still located on the tree, may be related to the temperature of the surrounding area, the precipitation, and soil nutrients (769). As the temperature increases, the relative bark thickness increases. Therefore, there may be value in comparing the change in temperature due to different site locations, whilst attempting to be independent of seasonality.

The age of trees can be separated into young, mature, over mature, and veteran (770). Literature could not be found to compare the lignocellulosic composition of barks from the same species in different age brackets. However, some of the contents, such as triterpenes, alkanolic acids and hydroxyacids are predominantly found in younger tree barks (771), so there are clear differences. There may be less interest in studying younger tree barks because for tree barks to be considered residues, they must fall off 'naturally'. This generally only occurs when rainfall is scarce, and younger trees become distressed due to the low moisture, but are also a part of the natural growth process (772). A greater volume of bark would be able to be collected from mature trees during the thinning process (773).

As discussed in Chapter 5, bark is composed of inner and outer bark, with the structural composition of each being different. The proportion of inner and outer bark changes along the height of the tree. The specific locations on the tree where this study's barks came from are unknown. Further work to explore the change in lignocellulosic composition, proximate analysis and ultimate analysis from bark sourced across different points along a tree's height would be useful for determining the optimal point for bark valorisation. However, as this work is focused on using tree bark residues, rather than harvesting live trees for bark, there would be limited options in deciding which specific point on a tree the bark should be taken from.

The causes for the levels of alkaline earth metals content (from atomic absorption spectroscopy) of the tree barks could also be explored through the analysis of the soils surrounding the trees that the bark was collected from. Although the fertility and composition of the soil is known to effect the composition of tree barks, it is currently unknown what these specific factors are that effect the soil fertility (774).

The optimisation of the solvent extraction could also be explored. In this study, the tree bark residue after Accelerated Solvent Extraction (ASE) was unable to be retained due its mixture with sand. There would be value in investigating how these residues could be further analysed, as ASE was better at extracting components than the Soxhlet extraction. The optimisation of the solvent extraction process can lead to increased concentrations of the desired components in barks (in this case, lignin), whilst reducing the energy intensity of the process (775).

### **8.2.2 Further investigation of the valorisation of lignin-rich samples as bio-based solvents**

In this study, after performing pyrolysis-gas chromatography/mass spectrometry (py-GC/MS), the assessment of the potential applications of the pyrolysis oil was purely theoretical. The main crux of any further research would be the testing of actual fast pyrolysis oil as bio-based solvents. Fast pyrolysis oil should be obtained either from commercial sources, or from the pyrolysis of samples in this study by external collaborators. Research could then investigate the routes of fractionation and upgrading that generate the pyrolysis oil-derived products which have similar solubilities to common solvents.

Where larger scale fast pyrolysis cannot be performed, microscale py-GC/MS should be run on a wider range of feedstocks and heating rates, to explore the full scale of fast

pyrolysis conditions. This would be necessary for ensuring the optimisation of the fast pyrolysis process.

The prospective bio-based solvents should be tested experimentally in the applications to which their solubility implies they would be effective, with the performance being compared to the hazardous petrochemical-based common solvents.

The quality, cost-effectiveness and impacts of the production and use of pyrolysis oil-derived solvents should be compared to the hazardous common solvents by technoeconomic analyses (TEA) and life cycle analyses (LCA). The different feedstock groups, such as the raw tree barks and the commercial lignin products, should be compared between each other. This would assess whether the impacts, quality, and cost-effectiveness of the higher cost purer lignins generate pyrolysis oils that outperform biomass residue-derived pyrolysis oils. The TEA and LCA would be especially valuable in outlining whether the separation of the pyrolysis oils, which may be using an additional solvent, is a feasible process step, or whether it undermines the production of the bio-based solvents from this study.

### **8.2.3 Further investigation of the valorisation of lignin-rich samples as ammonia adsorbents**

The study in Chapter 7 explored the ammonia adsorption capacities of a selection of samples including commercial lignin products, raw tree barks and treated tree barks (by slow pyrolysis and solvent extraction).

Regarding the feedstocks tested in Chapter 7, further work should be done to repeat the experiments at higher partial pressures of ammonia. The partial pressure of ammonia that was tested experimentally was lower than those found in the literature (1.44 kPa  $\text{NH}_3$  in this work, between 2.7 – 27 kPa  $\text{NH}_3$  by Helminen (380)). Although the literature values could be extrapolated by the Dubinin-Astakhov adsorption equilibrium model, it would be best practice to raise the partial pressure regardless. This would also be more beneficial by looking at the biomass residue's performance at a scale closer to the potential commercial applications. The partial pressure can be raised by increasing the concentration of the reagents and the adsorption temperature. Due to the scale of the experiment performed in this study (in a 250 ml Duran bottle), the highest partial pressure that is possible (at an adsorption temperature of 20 °C) is 13.3 kPa  $\text{NH}_3$ , i.e. 10 times the highest value used in this thesis' experiments.

The selection of samples that were tested in this work could also be refined for future studies. By selecting samples based on a wider range of characteristics (across proximate analysis, ultimate analysis, and fibre analysis), the statistical analysis would be more robust.

Although the raw tree barks performed best, slow pyrolysis could be done at lower temperatures (than 450 °C) to explore how the different pyrolysis temperatures affect the adsorption capacity. As stated in Chapter 7, biochar activation was unable to be completed on-site. Future work would explore more how could this be done internally, or how this could be done with collaborators. In addition, all biochars (rather than only two samples) would be hot water-washed, due to the improvement seen in Chapter 7 for Douglas fir and noble fir bark biochar. Separately to the biochar, the ammonia adsorption capacity of the acid-washed samples from Chapter 4 should be tested. This would allow the effect of another form of the treatment to be studied.

The most necessary further work is to study the impact of the ammonia adsorption on the samples. Besides the typical analysis that was not performed in Chapter 7 after the adsorption had been performed (proximate analysis and fibre analysis), the storage properties and desorption ability should be explored. One of the main properties that affect the storage of a sample is the moisture content. Materials with high moisture contents biologically degrade faster (776, 777), therefore, the raw tree bark adsorbents would be a risk compared to the biochars, despite the weaker performance. Pyrolysis should consequently be studied within the torrefaction temperature range (200 – 300 °C) and below (778). This would allow the optimal conditions where the ammonia adsorption capacity is sufficient to be found, while limiting the change to the biomass' structure.

The key property that would impact the commercial applications of the bio-based ammonia adsorbents is their ability to desorb the ammonia (779), and be regenerated for future adsorption. The main methods of desorption is pressure swing adsorption and temperature swing adsorption (780). Ordinarily, with temperature swing adsorption, ammonia would be adsorbed at room temperature, then desorbed by heating the adsorbent in an adsorption tower. This process, however, is very energy intensive, the adsorption performance decreases with repeated use and the tower has a complex design structure (781). Pressure swing adsorption also requires an adsorption tower, but the desorption and regeneration consumes a lot less energy than temperature swing adsorption (781). There are other methods of desorption in the literature, including moisture-swing adsorption and electro-swing adsorption, but these are in their early stages of development (782). The

desorption performance, and subsequent recycling of the adsorbent, should therefore be studied.

### **8.3 Closing Statement**

Although the studies described across this thesis have been completely in a closed laboratory environment, there is scope for this work to impact research at-large and the real world.

The main impacts of the ammonia adsorption work would be in aiding the reduction in waste ammonia that is present in agricultural run-off and wastewater treatment streams, the development of a low-cost methodology for screening adsorbents, and in the application of ammonia-rich biomass as natural N-fertilisers. The next steps of this work would be to test the adsorption of ammonia from these waste streams, and the effectiveness of ammonia-rich biomass as natural fertilisers on agricultural land.

Regarding the bio-solvents chapter, the key impact is in the development of a more holistic approach for screening replacement to hazardous petroleum-derived solvents with non-hazardous bio-based solvents with similar solubility properties, and adding valuable insights into the potential compositions of pyrolysis oils generated from biomass for their use as bio-based solvents. The following steps would consider the hazardousness and solubility of complex pyrolysis oil mixtures, in addition to the individual components considered in this work.

Lastly, the high-level and interdisciplinary impacts of this work overall is in the identification of lignin-rich residues, and the production of additional compositional datasets for a variety of biomass that have not been thoroughly presented in the literature. Further steps to investigate the seasonality and regionality of these biomass would allow more insight into their potential valorisation routes around the world.

## References

1. Casau, M., Dias, M.F., Matias, J.C.O. and Nunes, L.J.R. Residual Biomass: A Comprehensive Review on the Importance, Uses and Potential in a Circular Bioeconomy Approach. *Resources*. 2022, **11**(4), p.35.
2. Sun, P.T. and Peng, H. Valorisation of Biomass Waste for Sustainable Bioenergy and Biofuel Production. *Bioengineering (Basel)*. 2023, **10**(5).
3. Yıldız, İ. 1.12 Fossil Fuels. In: Dincer, I. ed. *Comprehensive Energy Systems*. Oxford: Elsevier, 2018, pp.521-567.
4. Ning, P., Yang, G., Hu, L., Sun, J., Shi, L., Zhou, Y., Wang, Z. and Yang, J. Recent advances in the valorization of plant biomass. *Biotechnology for Biofuels*. 2021, **14**(1), p.102.
5. Brack, D.B., Richard; Walker, Wayne. *Greenhouse gas emissions from burning US-sourced woody biomass in the EU and UK*. Chatham House, 2021.
6. IPCC. *Climate Change 2023: Synthesis Report. Contribution of Working Groups I, II and III to the Sixth Assessment Report of the Intergovernmental Panel on Climate Change*. Geneva, Switzerland: IPCC, 2023.
7. Carver, D. *Global net zero commitments*. [Online]. 2021. [Accessed 19th August]. Available from: <https://commonslibrary.parliament.uk/>
8. Ritchie, H. *Sector by sector: where do global greenhouse gas emissions come from?* [Online]. 2020. [Accessed July 30th]. Available from: <https://ourworldindata.org/>
9. Haider, A., Bashir, A. and Husnain, M.I.u. Impact of agricultural land use and economic growth on nitrous oxide emissions: Evidence from developed and developing countries. *Science of The Total Environment*. 2020, **741**, p.140421.
10. Shakoor, A., Shahzad, S.M., Chatterjee, N., Arif, M.S., Farooq, T.H., Altaf, M.M., Tufail, M.A., Dar, A.A. and Mehmood, T. Nitrous oxide emission from agricultural soils: Application of animal manure or biochar? A global meta-analysis. *Journal of Environmental Management*. 2021, **285**, p.112170.
11. Gao, F., Xue, Y., Deng, P., Cheng, X. and Yang, K. Removal of aqueous ammonium by biochars derived from agricultural residuals at different pyrolysis temperatures. *Chemical Speciation & Bioavailability*. 2015, **27**(2), pp.92-97.
12. Liu, F.-B., Ma, X., Zhang, F., Liang, T., Li, L.-W., Wang, J.-J., Chen, X.-P. and Wang, X.-Z. [Impact of Nitrification Inhibitors on Vegetable Production Yield, Nitrogen Fertilizer Use Efficiency and Nitrous Oxide Emission Reduction in China: Meta Analysis]. *Huanjing kexue*. 2022, **43**(11), pp.5140-5148.
13. Pan, Z., He, P., Fan, D., Jiang, R., Song, D., Song, L., Zhou, W. and He, W. Global impact of enhanced-efficiency fertilizers on vegetable productivity and reactive nitrogen losses. *Science of The Total Environment*. 2024, **926**, p.172016.
14. EEA. *Total greenhouse gas emissions in the chemical industry*. [Online]. 2024. [Accessed 16th August]. Available from: <https://www.eea.europa.eu/>

15. Bengtsson, W.K., Simon; Crispeels, Peter; Somers, Ken; Weihe, Ulriche; Weskamp, Thomas; Muhlbauer, Jonas. *Decarbonizing the chemical industry*. [Online]. 2023. [Accessed July 29th].
16. d'Amore, F., Nava, A., Colbertaldo, P., Visconti, C.G. and Romano, M.C. Turning CO<sub>2</sub> from fuel combustion into e-Fuel? Consider alternative pathways. *Energy Conversion and Management*. 2023, **289**, p.117170.
17. Durrani, J. *Biomass, plastic waste and carbon dioxide feedstocks key to cutting chemical industry's emissions*. [Online]. 2024. [Accessed July 29th]. Available from: <https://www.chemistryworld.com/>
18. Wegelin, S. and Meier, M.A.R. Bio-based aromatics for chemicals and materials: Advances in renewable drop-in and functional alternatives. *Current Opinion in Green and Sustainable Chemistry*. 2024, **47**, p.100931.
19. Jong, E.d.S., Heinz; Bell, Geoff; Jorgensen, Henning; de Bari, Isabelle; van Haveren, Jacco; Lindorfer, Johannes. *Bio-Based Chemicals: A 2020 Update*. IEA Bioenergy, 2020.
20. Rouwenhorst, K. *China: scaling-up "flexible" ammonia production powered by renewable energy*. [Online]. 2023. [Accessed August 20th]. Available from: <https://ammoniaenergy.org>
21. Strous, M., Van Gerven, E., Zheng, P., Kuenen, J.G. and Jetten, M.S.M. Ammonium removal from concentrated waste streams with the anaerobic ammonium oxidation (Anammox) process in different reactor configurations. *Water Research*. 1997, **31**(8), pp.1955-1962.
22. Iddya, A., Hou, D., Khor, C.M., Ren, Z., Tester, J., Posmanik, R., Gross, A. and Jassby, D. Efficient ammonia recovery from wastewater using electrically conducting gas stripping membranes. *Environmental Science: Nano*. 2020, **7**(6), pp.1759-1771.
23. Rivera, F., Muñoz, R., Prádanos, P., Hernández, A. and Palacio, L. A Systematic Study of Ammonia Recovery from Anaerobic Digestate Using Membrane-Based Separation. *Membranes (Basel)*. 2021, **12**(1).
24. Ma, H., Guo, Y., Qin, Y. and Li, Y.-Y. Nutrient recovery technologies integrated with energy recovery by waste biomass anaerobic digestion. *Bioresour Technol*. 2018, **269**, pp.520-531.
25. Jiang, A., Zhang, T., Zhao, Q.-B., Li, X., Chen, S. and Frear, C.S. Evaluation of an integrated ammonia stripping, recovery, and biogas scrubbing system for use with anaerobically digested dairy manure. *Biosystems Engineering*. 2014, **119**, pp.117-126.
26. Wei, Y., Wang, H., Zhang, X. and Liu, C. Ammonia-assisted hydrothermal carbon material with schiff base structures synthesized from factory waste hemicelluloses for Cr(VI) adsorption. *Journal of Environmental Chemical Engineering*. 2021, **9**(5), p.106187.
27. ETIPBioenergy. Agricultural residues as feedstocks for biofuels production. 2016. [Online]. Available from: <https://www.etipbioenergy.eu/>
28. Malins, C.S., Stephanie; Baral, Anil; Turley, David; Hopwood, Lucy; Baldock, David; Allen, Ben; Kretschmer, Bettina; Harrison, Pete. *Wasted: Europe's Untapped Resource. An Assessment of Advanced Biofuels from Wastes & Residues*. 2014.
29. Jayakumar, M., Gindaba, G.T., Gebeyehu, K.B., Periyasamy, S., Jabesa, A., Baskar, G., John, B.I. and Pugazhendhi, A. Bioethanol production from

- agricultural residues as lignocellulosic biomass feedstock's waste valorization approach: A comprehensive review. *Science of The Total Environment*. 2023, **879**, p.163158.
30. Takkellapati, S., Li, T. and Gonzalez, M.A. An Overview of Biorefinery Derived Platform Chemicals from a Cellulose and Hemicellulose Biorefinery. *Clean Technologies and Environmental Policy*. 2018, **20**(7), pp.1615-1630.
  31. Ragauskas, A.J., Beckham, G.T., Bidy, M.J., Chandra, R., Chen, F., Davis, M.F., Davison, B.H., Dixon, R.A., Gilna, P., Keller, M., Langan, P., Naskar, A.K., Saddler, J.N., Tschaplinski, T.J., Tuskan, G.A. and Wyman, C.E. Lignin Valorization: Improving Lignin Processing in the Biorefinery. *Science*. 2014, **344**(6185), p.1246843.
  32. Shah, S.W.A., Xu, Q., Ullah, M.W., Zahoor, Sethupathy, S., Morales, G.M., Sun, J. and Zhu, D. Lignin-based additive materials: A review of current status, challenges, and future perspectives. *Additive Manufacturing*. 2023, **74**, p.103711.
  33. Burns, C.H., Adrian; Hodgson, Edward. *Bio-based UK: Five Recommendations to Kick-Start Bioeconomy Innovation in the UK*. NNFCC, 2016.
  34. Wingard, C.W., Peter; Davis Winters, Amanda; Callahan, Morgan; Rosenblum, Danny; Marshall, Ian. *Identifying Growth Opportunities in Bio-based Chemicals*. LEK, 2023.
  35. Spekrijse, J.L., Tijss; Parisi, Claudia; Ronzon, Tevecia; Vis, Martijn. *Insights into the European market for bio-based chemicals*. European Commission, 2019.
  36. Bos, P., Ritzen, L., van Dam, S., Balkenende, R. and Bakker, C. Bio-Based Plastics in Product Design: The State of the Art and Challenges to Overcome. *Sustainability*. 2024, **16**(8), p.3295.
  37. Gagro, D. *Bio-based coatings: Small market, full of potential*. [Online]. 2019. [Accessed August 16th]. Available from: <https://www.european-coatings.com>
  38. Nur Liyana, I., Sara, S. and Jofry, O. Perspective Chapter: Overview of Bio-Based Surfactant – Recent Development, Industrial Challenge, and Future Outlook. In: Ashim Kumar, D. ed. *Surfactants and Detergents*. Rijeka: IntechOpen, 2022, p.Ch. 5.
  39. Hayes, D.G. and Smith, G.A. Chapter 1 - Biobased Surfactants: Overview and Industrial State of the Art. In: Hayes, D.G.Solaiman, D.K.Y.Ashby, R.D. eds. *Biobased Surfactants (Second Edition)*. AOCS Press, 2019, pp.3-38.
  40. Fusar Poli, E. and Fontefrancesco, M.F. Trends in the implementation of biopesticides in the Euro-Mediterranean region: a narrative literary review. *Sustainable Earth Reviews*. 2024, **7**(1), p.14.
  41. Fenibo, E.O., Ijoma, G.N. and Matambo, T. Biopesticides in Sustainable Agriculture: Current Status and Future Prospects. In: Mandal, S.D.Ramkumar, G.Karthi, S.Jin, F. eds. *New and Future Development in Biopesticide Research: Biotechnological Exploration*. Singapore: Springer Nature Singapore, 2022, pp.1-53.
  42. Wilson, A.N., Grieshop, M.J., Roback, J., Dell'Orco, S., Huang, J., Perkins, J.A., Nicholson, S., Chiaramonti, D., Nimlos, M.R., Christensen, E., lisa, K., Harris, K., Dutta, A., Dorgan, J.R. and Schaidle, J.A. Efficacy, economics,

- and sustainability of bio-based insecticides from thermochemical biorefineries. *Green Chemistry*. 2021, **23**(24), pp.10145-10156.
43. Umetsu, N. and Shirai, Y. Development of novel pesticides in the 21st century. *Journal of Pesticide Science*. 2020, **45**(2), pp.54-74.
  44. Novisi, K.O., Leah, C.M. and Banothile, C.E.M. Bio-Solvents: Synthesis, Industrial Production and Applications. In: Daniel, G.-M. and Magdalena, M. eds. *Solvents, Ionic Liquids and Solvent Effects*. Rijeka: IntechOpen, 2019, p.Ch. 1.
  45. Papadakis, E., Tula, A. and Gani, R. Solvent Selection Methodology for Pharmaceutical Processes: Solvent Swap. *Chemical Engineering Research and Design*. 2016, **115**.
  46. Capello, C., Wernet, G., Sutter, J., Hellweg, S. and Hungerbühler, K. A comprehensive environmental assessment of petrochemical solvent production. *The International Journal of Life Cycle Assessment*. 2009, **14**(5), pp.467-479.
  47. Bonventre, J.A. Solvents. In: Wexler, P. ed. *Encyclopedia of Toxicology (Third Edition)*. Oxford: Academic Press, 2014, pp.356-357.
  48. Sheldon, R.A. The E factor 25 years on: the rise of green chemistry and sustainability. *Green Chemistry*. 2017, **19**(1), pp.18-43.
  49. Polaris. *Green & Bio-Solvents Market Share, Size, Trends, Industry Analysis Report*. [Online]. 2023. [Accessed August 1st].
  50. GrandViewResearch. *Green Solvents Market Size, Share & Trends Analysis Report*. [Online]. 2023. [Accessed].
  51. ReportLinker. *Global Solvents Market to Reach 32.7 Million Metric Tons by the Year 2026*. [Online]. 2022. [Accessed August 1st].
  52. ReportLinker. *European Paint And Coating Trends in 2024*. [Online]. 2024. [Accessed 1st August].
  53. Krishna, V.V. and Mkondiwa, M. Economics of Crop Residue Management. *Annual Review of Resource Economics*. 2023, **15**(Volume 15, 2023), pp.19-39.
  54. Tobiszewski, M. Analytical chemistry with biosolvents. *Anal Bioanal Chem*. 2019, **411**(19), pp.4359-4364.
  55. Tobiszewski, M., Namieśnik, J. and Pena-Pereira, F. Environmental risk-based ranking of solvents using the combination of a multimedia model and multi-criteria decision analysis. *Green Chemistry*. 2017, **19**(4), pp.1034-1042.
  56. Englezou, G., Kortsen, K., Pacheco, A.A.C., Cavanagh, R., Lentz, J.C., Krumins, E., Sanders-Velez, C., Howdle, S.M., Nedoma, A.J. and Taresco, V. 2-Methyltetrahydrofuran (2-MeTHF) as a versatile green solvent for the synthesis of amphiphilic copolymers via ROP, FRP, and RAFT tandem polymerizations. *Journal of Polymer Science*. 2020, **58**(11), pp.1571-1581.
  57. Lee, H., Lim, H.K. and Kim, H. Hydration Thermodynamics of Non-Polar Aromatic Hydrocarbons: Comparison of Implicit and Explicit Solvation Models. *Molecules*. 2018, **23**(11).
  58. Supriyanto, Usino, D.O., Ylittervo, P., Dou, J., Sipponen, M.H. and Richards, T. Identifying the primary reactions and products of fast pyrolysis of alkali lignin. *Journal of Analytical and Applied Pyrolysis*. 2020, **151**, p.104917.

59. Mudraboyina, B.P., Farag, S., Banerjee, A., Chaouki, J. and Jessop, P.G. Supercritical fluid rectification of lignin pyrolysis oil methyl ether (LOME) and its use as a bio-derived aprotic solvent. *Green Chemistry*. 2016, **18**(7), pp.2089-2094.
60. Haseeb, S., Vanderveen, J.R., Elamaldeniya, D., Harris, J., Boniface, K.J., Lee, R., Champagne, P. and Jessop, P.G. Conversion of lignin pyrolysis oil to cyclohexyl methyl ethers as a promising biomass-derived solvent. *Green Chemistry*. 2021, **23**(6), pp.2457-2463.
61. Sedgwick, D.M. and Hammond, G.B. The history and future challenges associated with the hydrogenation of vinyl fluorides. *Journal of Fluorine Chemistry*. 2018, **207**, pp.45-58.
62. Xiang, H., Xin, R., Prasongthum, N., Natewong, P., Sooknoi, T., Wang, J., Reubroycharoen, P. and Fan, X. Catalytic conversion of bioethanol to value-added chemicals and fuels: A review. *Resources Chemicals and Materials*. 2022, **1**(1), pp.47-68.
63. Liang, Q., Chen, H., Gong, Y., Fan, M., Yang, H., Lal, R. and Kuzyakov, Y. Effects of 15 years of manure and inorganic fertilizers on soil organic carbon fractions in a wheat-maize system in the North China Plain. *Nutrient Cycling in Agroecosystems*. 2012, **92**(1), pp.21-33.
64. Dămățircă, C., Moretti, B., Bertora, C., Ferrarini, A., Lerda, C., Mania, I., Celi, L., Gorra, R. and Zavattaro, L. Residue incorporation and organic fertilisation improve carbon and nitrogen turnover and stabilisation in maize monocropping. *Agriculture, Ecosystems & Environment*. 2023, **342**, p.108255.
65. ERASPO. *Manure composting*. [Online]. 2024. [Accessed 19th August]. Available from: <https://www.eraspo.com/>
66. Naoki, M. and Kaori, M. An Overview of the Effects of Heat Treatments on the Quality of Organic Wastes as a Nitrogen Fertilizer. In: Amanullah and Shah, F. eds. *Nitrogen in Agriculture*. Rijeka: IntechOpen, 2017, p.Ch. 4.
67. DEFRA. Use less fertiliser, manure and lime. *Farming*. 2024. [Online]. Available from: <https://defrafarming.blog.gov.uk/>
68. Crooks, B.S., Alex; Litterick, Audrey; Williams, John. *Agricultural use of biosolids, composts, anaerobic digestates and other industrial organic fertilisers*. [Press release]. 2019. Available from: <https://www.fas.scot/>
69. Landers, L. *Liquid vs. Granular Fertilizer: Which One Is Better for Your Plants?* [Online]. 2023. [Accessed August 19th]. Available from: <https://www.bhg.com/>
70. Aphale, A., Bolander, N., Park, J., Shaw, L., Svec, J. and Wassgren, C. Granular Fertiliser Particle Dynamics on and off a Spinner Spreader. *Biosystems Engineering*. 2003, **85**(3), pp.319-329.
71. AHDB. *GB fertiliser prices*. [Online]. 2024. [Accessed]. Available from: <https://ahdb.org.uk/>
72. RHS. *Fertilisers*. [Online]. 2024. [Accessed August 19th]. Available from: <https://www.rhs.org.uk/>
73. Sun, J., Lu, X., Wang, S., Tian, C., Chen, G., Luo, N., Zhang, Q. and Li, X. Biochar Blended with Nitrogen Fertilizer Promotes Maize Yield by Altering Soil Enzyme Activities and Organic Carbon Content in Black Soil. *Int J Environ Res Public Health*. 2023, **20**(6).

74. Khan, Z., Zhang, K., Khan, M.N., Bi, J., Zhu, K., Luo, L. and Hu, L. How Biochar Affects Nitrogen Assimilation and Dynamics by Interacting Soil and Plant Enzymatic Activities: Quantitative Assessment of 2 Years Potted Study in a Rapeseed-Soil System. *Front Plant Sci.* 2022, **13**, p.853449.
75. Dong, X., Chu, Y., Tong, Z., Sun, M., Meng, D., Yi, X., Gao, T., Wang, M. and Duan, J. Mechanisms of adsorption and functionalization of biochar for pesticides: A review. *Ecotoxicology and Environmental Safety.* 2024, **272**, p.116019.
76. 24CR. *Adsorbent Market Size, Capacity, Demand & Supply 2022.* [Online]. 2022. [Accessed August 19th]. Available from: <https://www.24chemicalresearch.com>
77. MRF. *Global Adsorbents Market Overview.* [Online]. 2024. [Accessed August 19th]. Available from: <https://www.marketresearchfuture.com/>
78. MaM. *Adsorbents Market by Type, Application and Region - Global Forecast to 2026.* [Online]. 2021. [Accessed August 19th]. Available from: <https://www.marketsandmarkets.com/>
79. BR. *Adsorbent Market Size, Share, Growth and Industry Analysis By Type, By Application, Regional Insights, and Forecast to 2030.* [Online]. 2024. [Accessed August 19th]. Available from: <https://www.businessresearchinsights.com/>
80. Technavio. *Desiccant and Adsorbent Market Size to Grow by 3971.5 Thousand Tons, Activated Carbon to be Largest Revenue-generating Product Segment.* [Online]. 2022. [Accessed August 19th]. Available from: <https://www.prnewswire.com/>
81. Saleem, J., Shahid, U.B., Hijab, M., Mackey, H. and McKay, G. Production and applications of activated carbons as adsorbents from olive stones. *Biomass Conversion and Biorefinery.* 2019, **9**(4), pp.775-802.
82. Wang, J., Wang, R., Ma, J. and Sun, Y. Study on the Application of Shell-Activated Carbon for the Adsorption of Dyes and Antibiotics. *Water.* 2022, **14**(22), p.3752.
83. Njewa, J. and Shikuku, V. Recent advances and issues in the application of activated carbon for water treatment in Africa: A systematic review (2007-2022). *Applied Surface Science Advances.* 2023, **18**, p.100501.
84. Pérez-Botella, E., Valencia, S. and Rey, F. Zeolites in Adsorption Processes: State of the Art and Future Prospects. *Chemical Reviews.* 2022, **122**(24), pp.17647-17695.
85. TRM. *Speciality Zeolites Market.* [Online]. 2020. [Accessed August 19th]. Available from: <https://www.transparencymarketresearch.com/>
86. Parvulescu, A.-N. and Maurer, S. Toward sustainability in zeolite manufacturing: An industry perspective. *Frontiers in Chemistry.* 2022, **10**.
87. Kacem, M., Pellerano, M. and Delebarre, A. Pressure swing adsorption for CO<sub>2</sub>/N<sub>2</sub> and CO<sub>2</sub>/CH<sub>4</sub> separation: Comparison between activated carbons and zeolites performances. *Fuel Processing Technology.* 2015, **138**, pp.271-283.
88. Ditchburn, B. *Standing timber volume for coniferous trees in Britain: National Forest Inventory Report.* Forestry Commission, 2011.
89. Joshephi, J. *Thinnings from farm woodland.* [Leaflet]. 2024.

90. FAS. *Thinning for profit*. [Leaflet]. Scottish Rural Development Programme, 2019.
91. Wieczorek, S. Assessing the Influence of Adsorbent Bed (Tree Bark) Parameters on the Reduction of Ammonia Emissions from Animal Husbandry. *Polish Journal of Environmental Studies*. 2008, **17**(1), pp.147-154.
92. Takaya, C.A., Parmar, K.R., Fletcher, L.A. and Ross, A.B. Biomass-Derived Carbonaceous Adsorbents for Trapping Ammonia. *Agriculture*. 2019, **9**(1), p.16.
93. Chen, X., Zhang, K., Xiao, L.-P., Sun, R.-C. and Song, G. Total utilization of lignin and carbohydrates in *Eucalyptus grandis*: an integrated biorefinery strategy towards phenolics, levulinic acid, and furfural. *Biotechnology for Biofuels*. 2020, **13**(1), p.2.
94. Henrik-Klemens, Å., Caputo, F., Ghaffari, R., Westman, G., Edlund, U., Olsson, L. and Larsson, A. The glass transition temperature of isolated native, residual, and technical lignin. *Holzforschung*. 2024, **78**(4), pp.216-230.
95. Al-Naji, M., Brandi, F., Drieß, M. and Rosowski, F. From Lignin to Chemicals: An Expedition from Classical to Modern Catalytic Valorization Technologies. *Chemie Ingenieur Technik*. 2022, **94**(11), pp.1611-1627.
96. Kishimoto, T., Chiba, W., Saito, K., Fukushima, K., Uraki, Y. and Ubukata, M. Influence of Syringyl to Guaiacyl Ratio on the Structure of Natural and Synthetic Lignins. *Journal of Agricultural and Food Chemistry*. 2010, **58**(2), pp.895-901.
97. Jardim, J.M., Hart, P.W., Lucia, L. and Jameel, H. Insights into the Potential of Hardwood Kraft Lignin to Be a Green Platform Material for Emergence of the Biorefinery. *Polymers (Basel)*. 2020, **12**(8).
98. Kai, D., Chow, L.P. and Loh, X.J. Lignin and Its Properties. In: *Functional Materials from Lignin*. 2018, pp.1-28.
99. Davison, B.H., Drescher, S.R., Tuskan, G.A., Davis, M.F. and Nghiem, N.P. Variation of S/G ratio and lignin content in a *Populus* family influences the release of xylose by dilute acid hydrolysis. *Applied Biochemistry and Biotechnology*. 2006, **130**(1), pp.427-435.
100. Mennani, M., Kasbaji, M., Ait Benhamou, A., Boussetta, A., Mekkaoui, A.A., Grimi, N. and Moubarik, A. Current approaches, emerging developments and functional prospects for lignin-based catalysts – a review. *Green Chemistry*. 2023, **25**(8), pp.2896-2929.
101. Erfani Jazi, M., Narayanan, G., Aghabozorgi, F., Farajidizaji, B., Aghaei, A., Kamyabi, M.A., Navarathna, C.M. and Mlsna, T.E. Structure, chemistry and physicochemistry of lignin for material functionalization. *SN Applied Sciences*. 2019, **1**(9), p.1094.
102. Chami Khazraji, A. and Robert, S. Interaction Effects between Cellulose and Water in Nanocrystalline and Amorphous Regions: A Novel Approach Using Molecular Modeling. *Journal of Nanomaterials*. 2013, **2013**(1), p.409676.
103. Lisý, A., Ház, A., Nadányi, R., Jablonský, M. and Šurina, I. About Hydrophobicity of Lignin: A Review of Selected Chemical Methods for Lignin Valorisation in Biopolymer Production. *Energies*. 2022, **15**(17), p.6213.

104. Chang, B.P., Gupta, A., Muthuraj, R. and Mekonnen, T.H. Bioresourced fillers for rubber composite sustainability: current development and future opportunities. *Green Chemistry*. 2021, **23**(15), pp.5337-5378.
105. Shorey, R., Gupta, A. and Mekonnen, T.H. Hydrophobic modification of lignin for rubber composites. *Industrial Crops and Products*. 2021, **174**, p.114189.
106. Hong, N., Li, Y., Zeng, W., Zhang, M., Peng, X. and Qiu, X. Ultrahigh molecular weight, lignosulfonate-based polymers: preparation, self-assembly behaviours and dispersion property in coal–water slurry. *RSC Advances*. 2015, **5**(28), pp.21588-21595.
107. Li, B., You, S., Qi, W., Wang, Y., Su, R. and He, Z. Structure-tunable assembly of lignin sub-micro spheres by modifying the amphiphilic interfaces of lignin via n-alkane. *European Polymer Journal*. 2020, **126**, p.109539.
108. Li, Y., Zhao, S., Li, Y., Ragauskas, A.J., Song, X. and Li, K. Revealing the relationship between molecular weight of lignin and its color, UV-protecting property. *International Journal of Biological Macromolecules*. 2022, **223**, pp.1287-1296.
109. Liu, X., Zhao, S., Chen, X., Han, X., Zhang, J., Wu, M., Song, X. and Zhang, Z. The effect of lignin molecular weight on the formation and properties of carbon quantum dots. *Green Chemistry*. 2024, **26**(6), pp.3190-3201.
110. Li, Y., Zhao, S., Song, X., Cao, D., Li, K., Hassanpour, M. and Zhang, Z. UV-Shielding Performance and Color of Lignin and its Application to Sunscreen. *Macromolecular Materials and Engineering*. 2022, **307**(2), p.2100628.
111. Li, Y., Zhao, S., Hu, D., Ragauskas, A.J., Cao, D., Liu, W., Si, C., Xu, T., Zhao, P., Song, X. and Li, K. Role Evaluation of Active Groups in Lignin on UV-Shielding Performance. *ACS Sustainable Chemistry & Engineering*. 2022, **10**(36), pp.11856-11866.
112. Meister, J.J., Patil, D.R. and Channell, H. Properties and applications of lignin–acrylamide graft copolymer. *Journal of Applied Polymer Science*. 1984, **29**(11), pp.3457-3477.
113. Lim, S.-H. and Ibrahim, D. Utilization of Palm Kernel Cake as a Novel Substrate for Phytase Production by *Aspergillus niger* USM AI1. *BioResources*. 2014, **9**, pp.1488-1497.
114. Kong, F., Wang, S., Gao, W. and Fatehi, P. Novel pathway to produce high molecular weight kraft lignin–acrylic acid polymers in acidic suspension systems. *RSC Advances*. 2018, **8**(22), pp.12322-12336.
115. Ma, Q. and Zhang, X. An integral method for determining the molecular composition of lignin and its application. *Scientific Reports*. 2022, **12**(1), p.19136.
116. Bonjour, O., Nederstedt, H., Arcos-Hernandez, M.V., Laanesoo, S., Vares, L. and Jannasch, P. Lignin-Inspired Polymers with High Glass Transition Temperature and Solvent Resistance from 4-Hydroxybenzotrile, Vanillonitrile, and Syringonitrile Methacrylates. *ACS Sustainable Chemistry & Engineering*. 2021, **9**(50), pp.16874-16880.
117. Vural, D., Smith, J.C. and Petridis, L. Dynamics of the lignin glass transition. *Physical Chemistry Chemical Physics*. 2018, **20**(31), pp.20504-20512.

118. Mach, P., Geczy, A., Polanský, R. and Bušek, D. Glass transition temperature of nanoparticle-enhanced and environmentally stressed conductive adhesive materials for electronics assembly. *Journal of Materials Science: Materials in Electronics*. 2019, **30**(5), pp.4895-4907.
119. Leng, E., Guo, Y., Chen, J., Liu, S., E, J. and Xue, Y. A comprehensive review on lignin pyrolysis: Mechanism, modeling and the effects of inherent metals in biomass. *Fuel*. 2022, **309**, p.122102.
120. Guo, D.-l., Wu, S.-b., Liu, B., Yin, X.-l. and Yang, Q. Catalytic effects of NaOH and Na<sub>2</sub>CO<sub>3</sub> additives on alkali lignin pyrolysis and gasification. *Applied Energy*. 2012, **95**, pp.22-30.
121. Peng, C., Zhang, G., Yue, J. and Xu, G. Pyrolysis of lignin for phenols with alkaline additive. *Fuel Processing Technology*. 2014, **124**, pp.212-221.
122. Richa, L., Colin, B., Pétrissans, A., Wallace, C., Hulette, A., Quirino, R.L., Chen, W.-H. and Pétrissans, M. Catalytic and char-promoting effects of potassium on lignocellulosic biomass torrefaction and pyrolysis. *Environmental Technology & Innovation*. 2023, **31**, p.103193.
123. Eom, I.-Y., Kim, J.-Y., Kim, T.-S., Lee, S.-M., Choi, D., Choi, I.-G. and Choi, J.-W. Effect of essential inorganic metals on primary thermal degradation of lignocellulosic biomass. *Bioresource Technology*. 2012, **104**, pp.687-694.
124. Cui, Y., Wang, W. and Chang, J. Study on the Product Characteristics of Pyrolysis Lignin with Calcium Salt Additives. *Materials*. 2019, **12**(10), p.1609.
125. Li, J., Sun, H., Liu, J.-x., Zhang, J.-j., Li, Z.-x. and Fu, Y. Selective reductive cleavage of CO bond in lignin model compounds over nitrogen-doped carbon-supported iron catalysts. *Molecular Catalysis*. 2018, **452**, pp.36-45.
126. Zhu, C., Cao, J.-P., Zhao, X.-Y., Xie, T., Ren, J. and Wei, X.-Y. Mechanism of Ni-catalyzed selective CO cleavage of lignin model compound benzyl phenyl ether under mild conditions. *Journal of the Energy Institute*. 2019, **92**(1), pp.74-81.
127. Ma, Z., Custodis, V. and van Bokhoven, J.A. Selective deoxygenation of lignin during catalytic fast pyrolysis. *Catalysis Science & Technology*. 2014, **4**(3), pp.766-772.
128. Rutkowski, P. Pyrolysis of cellulose, xylan and lignin with the K<sub>2</sub>CO<sub>3</sub> and ZnCl<sub>2</sub> addition for bio-oil production. *Fuel Processing Technology*. 2011, **92**(3), pp.517-522.
129. Supanchaiyamat, N., Jetsrisuparb, K., Knijnenburg, J.T.N., Tsang, D.C.W. and Hunt, A.J. Lignin materials for adsorption: Current trend, perspectives and opportunities. *Bioresource Technology*. 2019, **272**, pp.570-581.
130. Suhas, Carrott, P.J.M. and Carrott, M.M.L.R. Using alkali metals to control reactivity and porosity during physical activation of demineralised kraft lignin. *Carbon*. 2009, **47**(4), pp.1012-1017.
131. Li, T. and Takkellapati, S. The current and emerging sources of technical lignins and their applications. *Biofuel Bioprod Biorefin*. 2018, **0**, pp.1-32.
132. Liu, G. and Bao, J. Maximizing phosphorus and potassium recycling by supplementation of lignin combustion ash from dry biorefining of lignocellulose. *Biochemical Engineering Journal*. 2019, **144**, pp.104-109.

133. Zhou, H.Z., L; Fu, X; Zhu, Y; Pan, Y. Effects of typical alkaline earth metal salts on cellulose torrefaction: Solid products and thermal gravimetric analysis. *BioResources*. 2020, **15**(1), pp.1678-1691.
134. Patel, M., Hill, N., Mullen, C.A., Gunukula, S. and DeSisto, W.J. Fast Pyrolysis of Lignin Pretreated with Magnesium Formate and Magnesium Hydroxide. *Energies*. 2020, **13**(19), p.4995.
135. Assessment, O.o.T. Chapter 4 - Pulp Bleaching Technology. In: Congress, U. ed. *Technologies for Reducing Dioxin in the Manufacture of Bleached Wood Pulp*. Washington, DC, 1989.
136. Peart, C. and Ni, Y. UV-VIS Spectra of Lignin Model Compounds in the Presence of Metal Ions and Chelants. *Journal of Wood Chemistry and Technology*. 2001, **21**(2), pp.113-125.
137. Kangas, H., Robertsen, L. and Vuorinen, T. The effect of transition metal ions on the kraft pulping process. *Paperi ja Puu/Paper and Timber*. 2002, **84**, pp.473-477.
138. Parot, M., Rodrigue, D. and Stevanovic, T. Effect of Iron Chloride Addition on Softwood Lignin Nano-Fiber Stabilization and Carbonization. *Polymers*. 2024, **16**(6), p.814.
139. Liu, X.-J., Li, M.-F. and Singh, S.K. Manganese-modified lignin biochar as adsorbent for removal of methylene blue. *Journal of Materials Research and Technology*. 2021, **12**, pp.1434-1445.
140. Fu, X., Zhang, J., Gu, X., Yu, H. and Chen, S. A comprehensive study of the promoting effect of manganese on white rot fungal treatment for enzymatic hydrolysis of woody and grass lignocellulose. *Biotechnology for Biofuels*. 2021, **14**(1), p.176.
141. Ruwoldt, J., Tanase-Opedal, M. and Syverud, K. Ultraviolet Spectrophotometry of Lignin Revisited: Exploring Solvents with Low Harmfulness, Lignin Purity, Hansen Solubility Parameter, and Determination of Phenolic Hydroxyl Groups. *ACS Omega*. 2022, **7**(50), pp.46371-46383.
142. Dastpak, A., Lourençon, T.V., Balakshin, M., Farhan Hashmi, S., Lundström, M. and Wilson, B.P. Solubility study of lignin in industrial organic solvents and investigation of electrochemical properties of spray-coated solutions. *Industrial Crops and Products*. 2020, **148**, p.112310.
143. Marx, S. and Venter, R.J. 5.09 - Alternative Bio-Refinery Products From Hydrothermal Liquefaction of Waste☆. In: Letcher, T.M. ed. *Comprehensive Renewable Energy (Second Edition)*. Oxford: Elsevier, 2022, pp.187-212.
144. Constant, S., Wienk, H.L.J., Frissen, A.E., Peinder, P.d., Boelens, R., van Es, D.S., Grisel, R.J.H., Weckhuysen, B.M., Huijgen, W.J.J., Gosselink, R.J.A. and Bruijninx, P.C.A. New insights into the structure and composition of technical lignins: a comparative characterisation study. *Green Chemistry*. 2016, **18**(9), pp.2651-2665.
145. Hermansson, F., Janssen, M. and Svanström, M. Allocation in life cycle assessment of lignin. *The International Journal of Life Cycle Assessment*. 2020, **25**(8), pp.1620-1632.
146. Oveissi, F. and Fatehi, P. Characterization of four different lignins as a first step toward the identification of suitable end-use applications. *Journal of Applied Polymer Science*. 2015, **132**(32).

147. Aro, T. and Fatehi, P. Production and Application of Lignosulfonates and Sulfonated Lignin. *ChemSusChem*. 2017, **10**(9), pp.1861-1877.
148. Qian, Y., Qiu, X. and Zhu, S. Lignin: a nature-inspired sun blocker for broad-spectrum sunscreens. *Green Chemistry*. 2015, **17**(1), pp.320-324.
149. Ksibi, M., Ben Amor, S., Cherif, S., Elaloui, E., Houas, A. and Elaloui, M. Photodegradation of lignin from black liquor using a UV/TiO<sub>2</sub> system. *Journal of Photochemistry and Photobiology A: Chemistry*. 2003, **154**(2), pp.211-218.
150. Kubo, S. and Kadla, J.F. The Formation of Strong Intermolecular Interactions in Immiscible Blends of Poly(vinyl alcohol) (PVA) and Lignin. *Biomacromolecules*. 2003, **4**(3), pp.561-567.
151. Song, Y., Wang, Z., Yan, N., Zhang, R. and Li, J. Demethylation of Wheat Straw Alkali Lignin for Application in Phenol Formaldehyde Adhesives. *Polymers*. 2016, **8**(6), p.209.
152. Rao, X., Liu, Y., Zhang, Q., Chen, W., Liu, Y. and Yu, H. Assembly of Organosolv Lignin Residues into Submicron Spheres: The Effects of Granulating in Ethanol/Water Mixtures and Homogenization. *ACS Omega*. 2017, **2**(6), pp.2858-2865.
153. Yang, D., Li, H., Qin, Y., Zhong, R., Bai, M. and Qiu, X. Structure and Properties of Sodium Lignosulfonate with Different Molecular Weight Used as Dye Dispersant. *Journal of Dispersion Science and Technology*. 2015, **36**(4), pp.532-539.
154. Ouyang, X., Ke, L., Qiu, X., Guo, Y. and Pang, Y. Sulfonation of Alkali Lignin and Its Potential Use in Dispersant for Cement. *Journal of Dispersion Science and Technology*. 2009, **30**(1), pp.1-6.
155. Khan, J., Mariatti, M., Zubir, S.A., Rusli, A., Manaf, A.A. and Khironudin, R.K. Eco-friendly alkali lignin-assisted water-based graphene oxide ink and its application as a resistive temperature sensor. *Nanotechnology*. 2024, **35**(5), p.055301.
156. Scarica, C., Suriano, R., Levi, M., Turri, S. and Griffini, G. Lignin Functionalized with Succinic Anhydride as Building Block for Biobased Thermosetting Polyester Coatings. *ACS Sustainable Chemistry & Engineering*. 2018, **6**(3), pp.3392-3401.
157. Strzemieska, B., Klapiszewski, Ł., Jamrozik, A., Szalaty, T.J., Matykiewicz, D., Sterzyński, T., Voelkel, A. and Jesionowski, T. Physicochemical Characterization of Functional Lignin–Silica Hybrid Fillers for Potential Application in Abrasive Tools. *Materials*. 2016, **9**(7), p.517.
158. Afewerki, S., Wang, X., Ruiz-Esparza, G.U., Tai, C.-W., Kong, X., Zhou, S., Welch, K., Huang, P., Bengtsson, R., Xu, C. and Strømme, M. Combined Catalysis for Engineering Bioinspired, Lignin-Based, Long-Lasting, Adhesive, Self-Mending, Antimicrobial Hydrogels. *ACS Nano*. 2020, **14**(12), pp.17004-17017.
159. Batista, K.B., Padilha, R.P.L., Castro, T.O., Silva, C.F.S.C., Araújo, M.F.A.S., Leite, L.F.M., Pasa, V.M.D. and Lins, V.F.C. High-temperature, low-temperature and weathering aging performance of lignin modified asphalt binders. *Industrial Crops and Products*. 2018, **111**, pp.107-116.

160. Xie, S., Li, Q., Karki, P., Zhou, F. and Yuan, J.S. Lignin as Renewable and Superior Asphalt Binder Modifier. *ACS Sustainable Chemistry & Engineering*. 2017, **5**(4), pp.2817-2823.
161. Lu, H., Cornell, A., Alvarado, F., Behm, M., Leijonmarck, S., Li, J., Tomani, P. and Lindbergh, G. Lignin as a Binder Material for Eco-Friendly Li-Ion Batteries. *Materials*. 2016, **9**(3), p.127.
162. Kosbar, L.L., Gelorme, J.D., Japp, R.M. and Fotorny, W.T. Introducing Biobased Materials into the Electronics Industry. *Journal of Industrial Ecology*. 2000, **4**(3), pp.93-105.
163. Podschun, J., Stücker, A., Buchholz, R.I., Heitmann, M., Schreiber, A., Saake, B. and Lehnen, R. Phenolated Lignins as Reactive Precursors in Wood Veneer and Particleboard Adhesion. *Industrial & Engineering Chemistry Research*. 2016, **55**(18), pp.5231-5237.
164. Danielson, B. and Simonson, R. Kraft lignin in phenol formaldehyde resin. Part 1. Partial replacement of phenol by kraft lignin in phenol formaldehyde adhesives for plywood. *Journal of Adhesion Science and Technology*. 1998, **12**(9), pp.923-939.
165. Mili, M., Hashmi, S.A.R., Ather, M., Hada, V., Markandeya, N., Kamble, S., Mohapatra, M., Rathore, S.K.S., Srivastava, A.K. and Verma, S. Novel lignin as natural-biodegradable binder for various sectors—A review. *Journal of Applied Polymer Science*. 2022, **139**(15), p.51951.
166. Zhu, H., Li, Y., Pettersson, B., Zhang, L., Lindström, M. and Henriksson, G. Technical soda lignin dissolved in urea as an environmental friendly binder in wood fiberboard. *Journal of Adhesion Science and Technology*. 2014, **28**(5), pp.490-498.
167. Mansouri, N.-E.E. and Salvadó, J. Structural characterization of technical lignins for the production of adhesives: Application to lignosulfonate, kraft, soda-antraquinone, organosolv and ethanol process lignins. *Industrial Crops and Products*. 2006, **24**(1), pp.8-16.
168. Jiang, B., Chen, C., Liang, Z., He, S., Kuang, Y., Song, J., Mi, R., Chen, G., Jiao, M. and Hu, L. Lignin as a Wood-Inspired Binder Enabled Strong, Water Stable, and Biodegradable Paper for Plastic Replacement. *Advanced Functional Materials*. 2020, **30**(4), p.1906307.
169. Kunitski, M., Eicke, N., Huber, P., Köhler, J., Zeller, S., Voigtsberger, J., Schlott, N., Henrichs, K., Sann, H., Trinter, F., Schmidt, L.P.H., Kalinin, A., Schöffler, M.S., Jahnke, T., Lein, M. and Dörner, R. Double-slit photoelectron interference in strong-field ionization of the neon dimer. *Nature Communications*. 2019, **10**(1), p.1.
170. Luo, C., Du, L., Wu, W., Xu, H., Zhang, G., Li, S., Wang, C., Lu, Z. and Deng, Y. Novel Lignin-Derived Water-Soluble Binder for Micro Silicon Anode in Lithium-Ion Batteries. *ACS Sustainable Chemistry & Engineering*. 2018, **6**(10), pp.12621-12629.
171. Wang, W., Wang, F., Zhang, C., Tang, J., Zeng, X. and Wan, X. Versatile value-added application of hyperbranched lignin derivatives: Water-resistance adhesive, UV protection coating, self-healing and skin-adhesive sensing. *Chemical Engineering Journal*. 2021, **404**, p.126358.
172. Çetin, N.S. and Özmen, N. Use of organosolv lignin in phenol-formaldehyde resins for particleboard production: II. Particleboard production and

- properties. *International Journal of Adhesion and Adhesives*. 2002, **22**(6), pp.481-486.
173. Tran, N.T., Ko, Y., Kim, S., Moon, J., Choi, J.-W., Kim, K.H., Kim, C.S., Ha, J.-M., Kim, H., Jeong, K., Lee, H. and Yoo, C.-J. Microwave-assisted phenolation of acid-insoluble Klason lignin and its application in adhesion. *Green Chemistry*. 2022, **24**(5), pp.2051-2061.
  174. Nakagame, S., Chandra, R.P., Kadla, J.F. and Saddler, J.N. The isolation, characterization and effect of lignin isolated from steam pretreated Douglas-fir on the enzymatic hydrolysis of cellulose. *Bioresource Technology*. 2011, **102**(6), pp.4507-4517.
  175. Frangville, C., Rutkevičius, M., Richter, A.P., Velev, O.D., Stoyanov, S.D. and Paunov, V.N. Fabrication of Environmentally Biodegradable Lignin Nanoparticles. *ChemPhysChem*. 2012, **13**(18), pp.4235-4243.
  176. Deng, Y., Feng, X., Zhou, M., Qian, Y., Yu, H. and Qiu, X. Investigation of Aggregation and Assembly of Alkali Lignin Using Iodine as a Probe. *Biomacromolecules*. 2011, **12**(4), pp.1116-1125.
  177. Qian, Y., Deng, Y., Qiu, X., Li, H. and Yang, D. Formation of uniform colloidal spheres from lignin, a renewable resource recovered from pulping spent liquor. *Green Chemistry*. 2014, **16**(4), pp.2156-2163.
  178. Zhang, Z., Belda Marín, C., Lefebvre, M., Lefebvre, C., Terrasson, V. and Guénin, E. The preparation of stable spherical alkali lignin nanoparticles with great thermal stability and no cytotoxicity. *International Journal of Biological Macromolecules*. 2022, **222**, pp.1830-1839.
  179. Richter, A.P., Bharti, B., Armstrong, H.B., Brown, J.S., Plemmons, D., Paunov, V.N., Stoyanov, S.D. and Velev, O.D. Synthesis and Characterization of Biodegradable Lignin Nanoparticles with Tunable Surface Properties. *Langmuir*. 2016, **32**(25), pp.6468-6477.
  180. Nair, S.S., Sharma, S., Pu, Y., Sun, Q., Pan, S., Zhu, J.Y., Deng, Y. and Ragauskas, A.J. High Shear Homogenization of Lignin to Nanolignin and Thermal Stability of Nanolignin-Polyvinyl Alcohol Blends. *ChemSusChem*. 2014, **7**(12), pp.3513-3520.
  181. Lievonen, M., Valle-Delgado, J.J., Mattinen, M.-L., Hult, E.-L., Lintinen, K., Kostianen, M.A., Paananen, A., Szilvay, G.R., Setälä, H. and Österberg, M. A simple process for lignin nanoparticle preparation. *Green Chemistry*. 2016, **18**(5), pp.1416-1422.
  182. Tortora, M., Cavalieri, F., Mosesso, P., Ciaffardini, F., Melone, F. and Crestini, C. Ultrasound Driven Assembly of Lignin into Microcapsules for Storage and Delivery of Hydrophobic Molecules. *Biomacromolecules*. 2014, **15**(5), pp.1634-1643.
  183. Li, H., Deng, Y., Liu, B., Ren, Y., Liang, J., Qian, Y., Qiu, X., Li, C. and Zheng, D. Preparation of Nanocapsules via the Self-Assembly of Kraft Lignin: A Totally Green Process with Renewable Resources. *ACS Sustainable Chemistry & Engineering*. 2016, **4**(4), pp.1946-1953.
  184. Jiang, P., Sheng, X., Yu, S., Li, H., Lu, J., Zhou, J. and Wang, H. Preparation and characterization of thermo-sensitive gel with phenolated alkali lignin. *Scientific Reports*. 2018, **8**(1), p.14450.

185. Jõul, P., Ho, T.T., Kallavus, U., Konist, A., Leiman, K., Salm, O.S., Kulp, M., Koel, M. and Lukk, T. Characterization of Organosolv Lignins and Their Application in the Preparation of Aerogels. *Materials (Basel)*. 2022, **15**(8).
186. Hájková, K., Filipi, M., Fojtík, R. and Dorieh, A. Application of Alkali Lignin and Spruce Sawdust for the Effective Removal of Reactive Dyes from Model Wastewater. *Molecules*. 2023, **28**(10), p.4114.
187. Schutyser, W., Renders, T., Van den Bosch, S., Koelewijn, S.F., Beckham, G.T. and Sels, B.F. Chemicals from lignin: an interplay of lignocellulose fractionation, depolymerisation, and upgrading. *Chemical Society Reviews*. 2018, **47**(3), pp.852-908.
188. Pappa, C.P., Cailotto, S., Gigli, M., Crestini, C. and Triantafyllidis, K.S. Kraft (Nano)Lignin as Reactive Additive in Epoxy Polymer Bio-Composites. *Polymers*. 2024, **16**(4), p.553.
189. Tang, Q., Chen, Q., Zhou, M. and Yang, D. Preparation of nano disperse dyes using sulfomethylated lignin: Effects of sulfonic group contents. *International Journal of Biological Macromolecules*. 2023, **234**, p.123605.
190. Yang, J., Wang, X. and Liu, H. Lignins and Lignin Derivatives as Dispersants for Copper Phthalocyanine Pigment Nanoparticles. *ACS Sustainable Chemistry & Engineering*. 2023, **11**(22), pp.8199-8207.
191. Mou, H., Huang, J., Li, W., Wu, X., Liu, Y. and Fan, H. Study on the chemical modification of alkali lignin towards for cellulase adsorbent application. *International Journal of Biological Macromolecules*. 2020, **149**, pp.794-800.
192. Abdulkhani, A., Khorasani, Z., Hamzeh, Y., Momenbeik, F., zadeh, Z.E., Sun, F., Madadi, M. and Zhang, X. Valorization of bagasse alkali lignin to water-soluble derivatives through chemical modification. *Biomass Conversion and Biorefinery*. 2024, **14**(7), pp.8639-8647.
193. Fagerstedt, K.V., Saranpää, P., Tapanila, T., Immanen, J., Serra, J.A. and Nieminen, K. Determining the Composition of Lignins in Different Tissues of Silver Birch. *Plants (Basel)*. 2015, **4**(2), pp.183-195.
194. Ibáñez, A.B. and Bauer, S. Downscaled method using glass microfiber filters for the determination of Klason lignin and structural carbohydrates. *Biomass and Bioenergy*. 2014, **68**, pp.75-81.
195. Wang, H., Pu, Y., Ragauskas, A. and Yang, B. From lignin to valuable products—strategies, challenges, and prospects. *Bioresource Technology*. 2019, **271**, pp.449-461.
196. Journal, M. *Valmet-supplied LignoBoost plant now handed over to Stora Enso's Sunila mill in Finland*. [Press release]. 2024. Available from: <https://www.manufacturing-journal.net/press-release/3431-valmet-supplied-lignoboost-plant-now-handed-over-to-stora-enso-s-sunila-mill-in-finland>
197. Durruty, J. *On the local filtration properties of LignoBoost: Lignin studies of the influence of xylan and ionic strength*. Doctor of Philosophy thesis, Chalmers University of Technology, 2017.
198. Schilling, K. *Agricultural By-Products*. [Online]. 2024. [Accessed September 7th]. Available from: <https://www.bio-powder.com/>
199. Shinde, R., Shahi, D.K., Mahapatra, P., Singh, C.S., Naik, S.K., Thombare, N. and Singh, A.K. Management of crop residues with special reference to

- the on-farm utilization methods: A review. *Industrial Crops and Products*. 2022, **181**, p.114772.
200. Smerald, A., Rahimi, J. and Scheer, C. A global dataset for the production and usage of cereal residues in the period 1997–2021. *Scientific Data*. 2023, **10**(1), p.685.
201. Wu, J., Elliston, A., Le Gall, G., Colquhoun, I.J., Collins, S.R.A., Wood, I.P., Dicks, J., Roberts, I.N. and Waldron, K.W. Optimising conditions for bioethanol production from rice husk and rice straw: effects of pre-treatment on liquor composition and fermentation inhibitors. *Biotechnology for Biofuels*. 2018, **11**(1), p.62.
202. Goodman, B.A. Utilization of waste straw and husks from rice production: A review. *Journal of Bioresources and Bioproducts*. 2020, **5**(3), pp.143-162.
203. Zhang, D.Q., Tan, S.K. and Gersberg, R.M. Municipal solid waste management in China: Status, problems and challenges. *Journal of Environmental Management*. 2010, **91**(8), pp.1623-1633.
204. NNFCC. *Vegetable Waste Factsheet*. [Press release]. 2020. Available from: <https://www.nfccc.co.uk/>
205. Huy, P., Göswein, V. and Habert, G. Climate-effective use of straw in the EU bioeconomy - Comparing avoided and delayed emissions in the agricultural, energy and construction sectors. *Environmental Research Letters*. 2023, **18**.
206. Singh, J. Identifying an economic power production system based on agricultural straw on regional basis in India. *Renewable and Sustainable Energy Reviews*. 2016, **60**, pp.1140-1155.
207. Palmieri, N., Forleo, M.B., Giannoccaro, G. and Suardi, A. Environmental impact of cereal straw management: An on-farm assessment. *Journal of Cleaner Production*. 2017, **142**, pp.2950-2964.
208. Chen, B., Mohrmann, S., Li, H., Gaff, M., Lorenzo, R., Corbi, I., Corbi, O., Fang, K. and Li, M. Research and Application Progress of Straw. *Journal of Renewable Materials*. 2023, **11**(2), pp.599--623.
209. Shi, L., Zhang, H., Li, Z., Man, X., Wu, Y., Zheng, C. and Liu, J. Analysis of moisture buffering effect of straw-based board in civil defence shelters by field measurements and numerical simulations. *Building and Environment*. 2018, **143**, pp.366-377.
210. Cao, F., Qiao, H., Li, Y., Shu, X. and Cui, L. Effect of highland barley straw ash admixture on properties and microstructure of concrete. *Construction and Building Materials*. 2022, **315**, p.125802.
211. Zhang, Q., Li, Y., Xu, L. and Lun, P. Bond strength and corrosion behavior of rebar embedded in straw ash concrete. *Construction and Building Materials*. 2019, **205**, pp.21-30.
212. Zhang, R., Li, X. and Fadel, J.G. Oyster mushroom cultivation with rice and wheat straw. *Bioresource Technology*. 2002, **82**(3), pp.277-284.
213. Singh, S., Raj, C., Singh, H.K., Avasthe, R.K., Said, P., Balusamy, A., Sharma, S.K., Lepcha, S.C. and Kerketta, V. Characterization and development of cultivation technology of wild split gill *Schizophyllum commune* mushroom in India. *Scientia Horticulturae*. 2021, **289**, p.110399.
214. Solovyev, N., Prakash, N.T., Bhatia, P., Prakash, R., Drobyshev, E. and Michalke, B. Selenium-rich mushrooms cultivation on a wheat straw

- substrate from seleniferous area in Punjab, India. *Journal of Trace Elements in Medicine and Biology*. 2018, **50**, pp.362-366.
215. NetZero.VN. *Rice husks: From waste to new green energy*. [Online]. 2023. [Accessed September 7th]. Available from: <https://netzero.vn/>
216. Kordi, M., Farrokhi, N., Pech-Canul, M.I. and Ahmadikhah, A. Rice Husk at a Glance: From Agro-Industrial to Modern Applications. *Rice Science*. 2024, **31**(1), pp.14-32.
217. IDT. *The Rise of Agriculture Husk as a Sustainable Alternative to Wood*. [Online]. 2023. [Accessed September 7th].
218. Shafie, N. and Me, N. The Healing Components of Rice Bran. In, 2017.
219. Coda, R., Katina, K. and Rizzello, C.G. Bran bioprocessing for enhanced functional properties. *Current Opinion in Food Science*. 2015, **1**, pp.50-55.
220. Lakna. *What is the Difference Between Husk and Bran*. [Online]. 2019. [Accessed 7th September]. Available from: <https://pediaa.com/>
221. Feng, Q., Zhang, S., Lin, J., Yang, J., Zhang, Y., Shen, Q., Zhong, F., Hou, D. and Zhou, S. Valorization of barley (*Hordeum vulgare* L.) brans from the sustainable perspective: A comprehensive review of bioactive compounds and health benefits with emphasis on their potential applications. *Food Chemistry*. 2024, **460**, p.140772.
222. Saini, P., Islam, M., Das, R., Shekhar, S., Sinha, A.S.K. and Prasad, K. Wheat bran as potential source of dietary fiber: Prospects and challenges. *Journal of Food Composition and Analysis*. 2023, **116**, p.105030.
223. ETIPBioenergy. *Sugar crops for production of advanced biofuels*. [Online]. 2024. [Accessed September 7th]. Available from: <https://www.etipbioenergy.eu/>
224. Meghana, M. and Shastri, Y. Sustainable valorization of sugar industry waste: Status, opportunities, and challenges. *Bioresource Technology*. 2020, **303**, p.122929.
225. Mahmud, M.A. and Anannya, F.R. Sugarcane bagasse - A source of cellulosic fiber for diverse applications. *Heliyon*. 2021, **7**(8), p.e07771.
226. Usmani, Z., Sharma, M., Diwan, D., Tripathi, M., Whale, E., Jayakody, L.N., Moreau, B., Thakur, V.K., Tuohy, M. and Gupta, V.K. Valorization of sugar beet pulp to value-added products: A review. *Bioresource Technology*. 2022, **346**, p.126580.
227. Tomaszewska, J., Bieliński, D., Binczarski, M., Berłowska, J., Dziugan, P., Piotrowski, J., Stanishevsky, A. and Witońska, I.A. Products of sugar beet processing as raw materials for chemicals and biodegradable polymers. *RSC Advances*. 2018, **8**(6), pp.3161-3177.
228. Kumar, H., Bhardwaj, K., Sharma, R., Nepovimova, E., Kuča, K., Dhanjal, D.S., Verma, R., Bhardwaj, P., Sharma, S. and Kumar, D. Fruit and Vegetable Peels: Utilization of High Value Horticultural Waste in Novel Industrial Applications. *Molecules*. 2020, **25**(12).
229. Hussain, H., Mamadalieva, N.Z., Hussain, A., Hassan, U., Rabnawaz, A., Ahmed, I. and Green, I.R. Fruit Peels: Food Waste as a Valuable Source of Bioactive Natural Products for Drug Discovery. *Curr Issues Mol Biol*. 2022, **44**(5), pp.1960-1994.
230. Nirmal, N.P., Khanashyam, A.C., Mundanat, A.S., Shah, K., Babu, K.S., Thorakkattu, P., Al-Asmari, F. and Pandiselvam, R. Valorization of Fruit

- Waste for Bioactive Compounds and Their Applications in the Food Industry. *Foods*. 2023, **12**(3).
231. Albuquerque, B.R., Heleno, S.A., Oliveira, M., Barros, L. and Ferreira, I. Phenolic compounds: current industrial applications, limitations and future challenges. *Food Funct.* 2021, **12**(1), pp.14-29.
  232. Rowan, M., Umenweke, G.C., Epelle, E.I., Afolabi, I.C., Okoye, P.U., Gunes, B. and Okolie, J.A. Anaerobic co-digestion of food waste and agricultural residues: An overview of feedstock properties and the impact of biochar addition. *Digital Chemical Engineering*. 2022, **4**, p.100046.
  233. Velvizhi, G., Jacqueline, P.J., Shetti, N.P., K, L., Mohanakrishna, G. and Aminabhavi, T.M. Emerging trends and advances in valorization of lignocellulosic biomass to biofuels. *Journal of Environmental Management*. 2023, **345**, p.118527.
  234. dos Santos, W.D., Gonzaga, D.E.R., Salvador, V.H., Freitas, D.L., Joia, B.M., Oliveira, D.M., Leite, D.C.C., Bido, G.S., Finger-Teixeira, A., de Souza, A.P., Polizeli, M.d.L.T.M., Constantin, R.P., Marchiosi, R., Rios, F.A., Ferrarese-Filho, O. and Buckeridge, M.S. Natural lignin modulators improve lignocellulose saccharification of field-grown sugarcane, soybean, and brachiaria. *Biomass and Bioenergy*. 2023, **168**, p.106684.
  235. Ashenhurst, J. *Transesterification*. [Online]. 2022. [Accessed September 9th]. Available from: <https://www.masterorganicchemistry.com/>
  236. Chauhan, K., Kumar, A., Goswami, K., Negi, L., Chauhan, A., Madan, K. and Jain, S. Lignin extraction from lignocellulosic biomass (sugarcane bagasse) and its potential application as a feedstock for fuel production. *Materials Today: Proceedings*. 2023, **78**, pp.688-694.
  237. Manyi-Loh, C.E. and Lues, R. Anaerobic Digestion of Lignocellulosic Biomass: Substrate Characteristics (Challenge) and Innovation. *Fermentation*. 2023, **9**(8), p.755.
  238. Cryospain. *Biomethane: industrial uses and particularities*. [Online]. 2022. [Accessed September 9th]. Available from: <https://cryospain.com/>
  239. Sawatdeenarunat, C., Surendra, K.C., Takara, D., Oechsner, H. and Khanal, S.K. Anaerobic digestion of lignocellulosic biomass: Challenges and opportunities. *Bioresour Technol*. 2015, **178**, pp.178-186.
  240. Parvathy Eswari, A., Ravi, Y.K., Kavitha, S. and Rajesh Banu, J. Recent insight into anaerobic digestion of lignocellulosic biomass for cost effective bioenergy generation. *e-Prime - Advances in Electrical Engineering, Electronics and Energy*. 2023, **3**, p.100119.
  241. Travaini, R., Martín-Juárez, J., Lorenzo-Hernando, A. and Bolado-Rodríguez, S. Ozonolysis: An advantageous pretreatment for lignocellulosic biomass revisited. *Bioresour Technol*. 2016, **199**, pp.2-12.
  242. Romano, R.T., Zhang, R., Teter, S. and McGarvey, J.A. The effect of enzyme addition on anaerobic digestion of Jose Tall Wheat Grass. *Bioresour Technol*. 2009, **100**(20), pp.4564-4571.
  243. Meegoda, J.N., Li, B., Patel, K. and Wang, L.B. A Review of the Processes, Parameters, and Optimization of Anaerobic Digestion. *Int J Environ Res Public Health*. 2018, **15**(10).

244. Khan, M.U. and Ahring, B.K. Lignin degradation under anaerobic digestion: Influence of lignin modifications -A review. *Biomass and Bioenergy*. 2019, **128**, p.105325.
245. Cathcart, A., Smyth, B.M., Lyons, G., Murray, S.T., Rooney, D. and Johnston, C.R. Optimising mechanical separation of anaerobic digestate for total solids and nutrient removal. *Journal of Environmental Management*. 2023, **345**, p.118449.
246. Smith, V.H., Tilman, G.D. and Nekola, J.C. Eutrophication: impacts of excess nutrient inputs on freshwater, marine, and terrestrial ecosystems. *Environmental Pollution*. 1999, **100**(1), pp.179-196.
247. Negri, M., Bacenetti, J., Fiala, M. and Bocchi, S. Evaluation of anaerobic degradation, biogas and digestate production of cereal silages using nylon-bags. *Bioresource Technology*. 2016, **209**, pp.40-49.
248. Carraro, G., Tonderski, K. and Enrich-Prast, A. Solid-liquid separation of digestate from biogas plants: A systematic review of the techniques' performance. *Journal of Environmental Management*. 2024, **356**, p.120585.
249. Lukehurst, C.T.F., Peter; Al Seadi, Teodorita. *Utilisation of digestate from biogas plants as biofertiliser*. IEA Bioenergy, 2010.
250. Tambone, F., Orzi, V., D'Imporzano, G. and Adani, F. Solid and liquid fractionation of digestate: Mass balance, chemical characterization, and agronomic and environmental value. *Bioresource Technology*. 2017, **243**, pp.1251-1256.
251. AMZCO. *Is anaerobic digestion the same as fermentation?* [Online]. 2024. [Accessed September 10th]. Available from: <https://www.amzco.co.uk/>
252. Taylor, M.J., Hornsby, K., Cheah, K.W., Hurst, P., Walker, S. and Skoulou, V. Repurposing lignin rich biorefinery waste streams into the next generation of sustainable solid fuels. *Sustainable Chemistry for the Environment*. 2024, **7**, p.100123.
253. Prasad, R.K., Sharma, A., Mazumder, P.B. and Dhussa, A. A comprehensive pre-treatment strategy evaluation of ligno-hemicellulosic biomass to enhance biogas potential in the anaerobic digestion process. *RSC Sustainability*. 2024, **2**(9), pp.2444-2467.
254. Pang, B., Cao, X.-F., Sun, S.-N., Wang, X.-L., Wen, J.-L., Lam, S.S., Yuan, T.-Q. and Sun, R.-C. The direct transformation of bioethanol fermentation residues for production of high-quality resins. *Green Chemistry*. 2020, **22**(2), pp.439-447.
255. Radhika, N.L., Sachdeva, S. and Kumar, M. Microbe assisted depolymerization of lignin rich waste and its conversion to gaseous biofuel. *Journal of Environmental Management*. 2021, **300**, p.113684.
256. Faria, D.J., Carvalho, A.P.A.d. and Conte-Junior, C.A. Valorization of Fermented Food Wastes and Byproducts: Bioactive and Valuable Compounds, Bioproduct Synthesis, and Applications. *Fermentation*. 2023, **9**(10), p.920.
257. Bacovsky, D.-I.K., Birger; Brown, Mark; Bennett, Paul; Pelkmans, Luc; Rossi, Andrea. *Annual Report 2023*. IEA Bioenergy, 2024.
258. EERE. *Hydrogen Production: Biomass Gasification*. [Online]. 2024. [Accessed September 10th]. Available from: <https://www.energy.gov/>

259. Jamradloedluk, J. and Lertsatitthanakorn, C. Characterization and Utilization of Char Derived from Fast Pyrolysis of Plastic Wastes. *Procedia Engineering*. 2014, **69**, pp.1437-1442.
260. Punsuwan, N. and Tangsathitkulchai, C. Product Characterization and Kinetics of Biomass Pyrolysis in a Three-Zone Free-Fall Reactor. *International Journal of Chemical Engineering*. 2014, **2014**, pp.1-10.
261. Li, L., Rowbotham, J.S., Christopher Greenwell, H. and Dyer, P.W. Chapter 8 - An Introduction to Pyrolysis and Catalytic Pyrolysis: Versatile Techniques for Biomass Conversion. In: Suib, S.L. ed. *New and Future Developments in Catalysis*. Amsterdam: Elsevier, 2013, pp.173-208.
262. Wang, Q., Song, H., Pan, S., Dong, N., Wang, X. and Sun, S. Initial pyrolysis mechanism and product formation of cellulose: An Experimental and Density functional theory(DFT) study. *Scientific Reports*. 2020, **10**(1), p.3626.
263. K N, Y., T, P.D., P, S., S, K., R, Y.K., Varjani, S., AdishKumar, S., Kumar, G. and J, R.B. Lignocellulosic biomass-based pyrolysis: A comprehensive review. *Chemosphere*. 2022, **286**, p.131824.
264. Wang, S., Ru, B., Lin, H., Sun, W., Yu, C. and Luo, Z. Pyrolysis mechanism of hemicellulose monosaccharides in different catalytic processes. *Chemical Research in Chinese Universities*. 2014, **30**(5), pp.848-854.
265. Lu, X. and Gu, X. A review on lignin pyrolysis: pyrolytic behavior, mechanism, and relevant upgrading for improving process efficiency. *Biotechnology for Biofuels and Bioproducts*. 2022, **15**(1), p.106.
266. Leng, L., Yang, L., Chen, J., Leng, S., Li, H., Li, H., Yuan, X., Zhou, W. and Huang, H. A review on pyrolysis of protein-rich biomass: Nitrogen transformation. *Bioresource Technology*. 2020, **315**, p.123801.
267. Shen, Q. and Wu, H. Rapid pyrolysis of biochar prepared from slow and fast pyrolysis: The effects of particle residence time on char properties. *Proceedings of the Combustion Institute*. 2023, **39**(3), pp.3371-3378.
268. Hwang, H., Sahin, O. and Choi, J.W. Manufacturing a super-active carbon using fast pyrolysis char from biomass and correlation study on structural features and phenol adsorption. *RSC Advances*. 2017, **7**(67), pp.42192-42202.
269. Lee, Y., Eum, P.-R.-B., Ryu, C., Park, Y.-K., Jung, J.-H. and Hyun, S. Characteristics of biochar produced from slow pyrolysis of Geodae-Uksae 1. *Bioresource Technology*. 2013, **130**, pp.345-350.
270. Pottmaier, D., Costa, M., Farrow, T., Oliveira, A.A.M., Alarcon, O. and Snape, C. Comparison of Rice Husk and Wheat Straw: From Slow and Fast Pyrolysis to Char Combustion. *Energy & Fuels*. 2013, **27**(11), pp.7115-7125.
271. Al-Rumaihi, A., Shahbaz, M., McKay, G., Mackey, H. and Al-Ansari, T. A review of pyrolysis technologies and feedstock: A blending approach for plastic and biomass towards optimum biochar yield. *Renewable and Sustainable Energy Reviews*. 2022, **167**, p.112715.
272. Bridgwater, A.V. Renewable fuels and chemicals by thermal processing of biomass. *Chemical Engineering Journal*. 2003, **91**(2), pp.87-102.
273. Makepa, D.C., Chihobo, C.H., Ruziwa, W.R. and Musademba, D. A systematic review of the techno-economic assessment and biomass supply

- chain uncertainties of biofuels production from fast pyrolysis of lignocellulosic biomass. *Fuel Communications*. 2023, **14**, p.100086.
274. Jerzak, W., Acha, E. and Li, B. Comprehensive Review of Biomass Pyrolysis: Conventional and Advanced Technologies, Reactor Designs, Product Compositions and Yields, and Techno-Economic Analysis. *Energies*. 2024, **17**(20), p.5082.
275. Sharifzadeh, M., Sadeqzadeh, M., Guo, M., Borhani, T.N., Murthy Konda, N.V.S.N., Garcia, M.C., Wang, L., Hallett, J. and Shah, N. The multi-scale challenges of biomass fast pyrolysis and bio-oil upgrading: Review of the state of art and future research directions. *Progress in Energy and Combustion Science*. 2019, **71**, pp.1-80.
276. TradingEconomics. *Crude Oil*. [Online]. 2025. [Accessed January 30th]. Available from: <https://tradingeconomics.com/commodity/crude-oil>
277. Vasireddy, S., Kumar, P., Karri, N., Singh, P., Gandham, S. and Rao, B. Effect of Pressure on In-situ Catalytic Hydropyrolysis of Rice Straw. 2020, **7**, p.1076.
278. Resende, F.L.P. Recent advances on fast hydropyrolysis of biomass. *Catalysis Today*. 2016, **269**, pp.148-155.
279. Lachos-Perez, D., César Torres-Mayanga, P., Abaide, E.R., Zobot, G.L. and De Castilhos, F. Hydrothermal carbonization and Liquefaction: differences, progress, challenges, and opportunities. *Bioresource Technology*. 2022, **343**, p.126084.
280. Gundupalli, M.P., Thomas, A.S.S., Gundupalli, S.P., Bhattacharyya, D. and Sriariyanun, M. Hydrothermal Liquefaction (HTL) of Kraft Lignin (KL) Recovered from Lignocellulosic Biomass: State of the Art. In: Joshi, S.J.Sen, R.Sharma, A.Salam, P.A. eds. *Status and Future Challenges for Non-conventional Energy Sources Volume 1*. Singapore: Springer Singapore, 2022, pp.267-292.
281. Ciuffi, B., Loppi, M., Rizzo, A.M., Chiaramonti, D. and Rosi, L. Towards a better understanding of the HTL process of lignin-rich feedstock. *Scientific Reports*. 2021, **11**(1), p.15504.
282. Feng, L., Li, X., Wang, Z. and Liu, B. Catalytic hydrothermal liquefaction of lignin for production of aromatic hydrocarbon over metal supported mesoporous catalyst. *Bioresource Technology*. 2021, **323**, p.124569.
283. Beims, R.F., Hu, Y., Shui, H. and Xu, C. Hydrothermal liquefaction of biomass to fuels and value-added chemicals: Products applications and challenges to develop large-scale operations. *Biomass and Bioenergy*. 2020, **135**, p.105510.
284. Biller, P. and Ross, A.B. 17 - Production of biofuels via hydrothermal conversion. In: Luque, R.Lin, C.S.K.Wilson, K.Clark, J. eds. *Handbook of Biofuels Production (Second Edition)*. Woodhead Publishing, 2016, pp.509-547.
285. Mishra, R.K., kumar, V., Kumar, P. and Mohanty, K. Hydrothermal liquefaction of biomass for bio-crude production: A review on feedstocks, chemical compositions, operating parameters, reaction kinetics, techno-economic study, and life cycle assessment. *Fuel*. 2022, **316**, p.123377.

286. Ahmad, F., Silva, E.L. and Varesche, M.B.A. Hydrothermal processing of biomass for anaerobic digestion – A review. *Renewable and Sustainable Energy Reviews*. 2018, **98**, pp.108-124.
287. Zhang, L., Champagne, P. and Xu, C. Supercritical water gasification of an aqueous by-product from biomass hydrothermal liquefaction with novel Ru modified Ni catalysts. *Bioresource Technology*. 2011, **102**(17), pp.8279-8287.
288. Biller, P., Madsen, R.B., Klemmer, M., Becker, J., Iversen, B.B. and Glasius, M. Effect of hydrothermal liquefaction aqueous phase recycling on bio-crude yields and composition. *Bioresource Technology*. 2016, **220**, pp.190-199.
289. Hu, Y., Feng, S., Bassi, A. and Xu, C. Improvement in bio-crude yield and quality through co-liquefaction of algal biomass and sawdust in ethanol-water mixed solvent and recycling of the aqueous by-product as a reaction medium. *Energy Conversion and Management*. 2018, **171**, pp.618-625.
290. Guo, Y., Yeh, T., Song, W., Xu, D. and Wang, S. A review of bio-oil production from hydrothermal liquefaction of algae. *Renewable and Sustainable Energy Reviews*. 2015, **48**, pp.776-790.
291. Cao, Y., Zhang, C., Tsang, D.C.W., Fan, J., Clark, J.H. and Zhang, S. Hydrothermal Liquefaction of Lignin to Aromatic Chemicals: Impact of Lignin Structure. *Industrial & Engineering Chemistry Research*. 2020, **59**(39), pp.16957-16969.
292. Usman, M., Cheng, S., Boonyubol, S. and Cross, J.S. From biomass to biocrude: Innovations in hydrothermal liquefaction and upgrading. *Energy Conversion and Management*. 2024, **302**, p.118093.
293. Ponnusamy, V.K., Nagappan, S., Bhosale, R.R., Lay, C.-H., Duc Nguyen, D., Pugazhendhi, A., Chang, S.W. and Kumar, G. Review on sustainable production of biochar through hydrothermal liquefaction: Physico-chemical properties and applications. *Bioresource Technology*. 2020, **310**, p.123414.
294. Sun, X., Atiyeh, H.K., Li, M. and Chen, Y. Biochar facilitated bioprocessing and biorefinery for productions of biofuel and chemicals: A review. *Bioresource Technology*. 2020, **295**, p.122252.
295. Heidari, M., Dutta, A., Acharya, B. and Mahmud, S. A review of the current knowledge and challenges of hydrothermal carbonization for biomass conversion. *Journal of the Energy Institute*. 2019, **92**(6), pp.1779-1799.
296. Kambo, H.S. and Dutta, A. A comparative review of biochar and hydrochar in terms of production, physico-chemical properties and applications. *Renewable and Sustainable Energy Reviews*. 2015, **45**, pp.359-378.
297. Adolfsson, K.H., Yadav, N. and Hakkarainen, M. Cellulose-derived hydrothermally carbonized materials and their emerging applications. *Current Opinion in Green and Sustainable Chemistry*. 2020, **23**, pp.18-24.
298. Puccini, M.S., Eleonara; Tasca, Andrea Luca; Vitolo, Sandra. Pollutant Removal from Gaseous and Aqueous Phases using Hydrochar-based Activated Carbon. *Journal of the Italian Association of Chemical Engineering*. 2018, **67**, pp.637-642.
299. Xia, Y., Yang, T., Zhu, N., Li, D., Chen, Z., Lang, Q., Liu, Z. and Jiao, W. Enhanced adsorption of Pb(II) onto modified hydrochar: Modeling and mechanism analysis. *Bioresource Technology*. 2019, **288**, p.121593.

300. Xu, H., Adolfsson, K.H., Xie, L., Hassanzadeh, S., Pettersson, T. and Hakkarainen, M. Zero-Dimensional and Highly Oxygenated Graphene Oxide for Multifunctional Poly(lactic acid) Bionanocomposites. *ACS Sustainable Chemistry & Engineering*. 2016, **4**(10), pp.5618-5631.
301. Jain, A., Balasubramanian, R. and Srinivasan, M.P. Hydrothermal conversion of biomass waste to activated carbon with high porosity: A review. *Chemical Engineering Journal*. 2016, **283**, pp.789-805.
302. Lei, Y., Su, H. and Tian, F. A Novel Nitrogen Enriched Hydrochar Adsorbents Derived from Salix Biomass for Cr (VI) Adsorption. *Scientific Reports*. 2018, **8**(1), p.4040.
303. Alongi, J., Ferruti, P., Manfredi, A., Carosio, F., Feng, Z., Hakkarainen, M. and Ranucci, E. Superior flame retardancy of cotton by synergetic effect of cellulose-derived nano-graphene oxide carbon dots and disulphide-containing polyamidoamines. *Polymer Degradation and Stability*. 2019, **169**, p.108993.
304. Sollami Delekta, S., Adolfsson, K.H., Benyahia Erdal, N., Hakkarainen, M., Östling, M. and Li, J. Fully inkjet printed ultrathin microsupercapacitors based on graphene electrodes and a nano-graphene oxide electrolyte. *Nanoscale*. 2019, **11**(21), pp.10172-10177.
305. Fang, J., Zhan, L., Ok, Y.S. and Gao, B. Minireview of potential applications of hydrochar derived from hydrothermal carbonization of biomass. *Journal of Industrial and Engineering Chemistry*. 2018, **57**, pp.15-21.
306. Wu, D., Samanta, A., Srivastava, R.K. and Hakkarainen, M. Starch-Derived Nanographene Oxide Paves the Way for Electrospinnable and Bioactive Starch Scaffolds for Bone Tissue Engineering. *Biomacromolecules*. 2017, **18**(5), pp.1582-1591.
307. Erdal, N.B. and Hakkarainen, M. Construction of Bioactive and Reinforced Bioresorbable Nanocomposites by Reduced Nano-Graphene Oxide Carbon Dots. *Biomacromolecules*. 2018, **19**(3), pp.1074-1081.
308. Merzari, F., Langone, M., Andreottola, G. and Fiori, L. Methane production from process water of sewage sludge hydrothermal carbonization. A review. Valorising sludge through hydrothermal carbonization. *Critical Reviews in Environmental Science and Technology*. 2019, **49**(11), pp.947-988.
309. Funke, A. and Ziegler, F. Hydrothermal carbonization of biomass: A summary and discussion of chemical mechanisms for process engineering. *Biofuels, Bioproducts and Biorefining*. 2010, **4**(2), pp.160-177.
310. Wang, F., Wang, J., Gu, C., Han, Y., Zan, S. and Wu, S. Effects of process water recirculation on solid and liquid products from hydrothermal carbonization of Laminaria. *Bioresource Technology*. 2019, **292**, p.121996.
311. Hu, R., Liu, Y., Zhu, G., Chen, C., Hantoko, D. and Yan, M. COD removal of wastewater from hydrothermal carbonization of food waste: Using coagulation combined activated carbon adsorption. *Journal of Water Process Engineering*. 2022, **45**, p.102462.
312. Langone, M. and Basso, D. Process Waters from Hydrothermal Carbonization of Sludge: Characteristics and Possible Valorization Pathways. *Int J Environ Res Public Health*. 2020, **17**(18).
313. VALMET. *LignoBoost® - the process*. [Online]. 2023. [Accessed]. Available from: <https://www.valmet.com/>

314. Parmar, K.R. and Ross, A.B. Integration of Hydrothermal Carbonisation with Anaerobic Digestion; Opportunities for Valorisation of Digestate. *Energies*. 2019, **12**(9), p.1586.
315. Slezak, R., Unyay, H., Szufa, S. and Ledakowicz, S. An Extensive Review and Comparison of Modern Biomass Reactors Torrefaction vs. Biomass Pyrolyzers—Part 2. *Energies*. 2023, **16**(5), p.2212.
316. Lachman, J., Baláš, M., Lisý, M., Lisá, H., Milčák, P. and Elbl, P. An overview of slagging and fouling indicators and their applicability to biomass fuels. *Fuel Processing Technology*. 2021, **217**, p.106804.
317. Shadangi, K.P., Sarangi, P.K. and Behera, A.K. Chapter 3 - Characterization techniques of biomass: physico-chemical, elemental, and biological. In: Shadangi, K.P.Sarangi, P.K.Mohanty, K.Deniz, I.Kiran Gollakota, A.R. eds. *Bioenergy Engineering*. Woodhead Publishing, 2023, pp.51-66.
318. Corporation, L. *Determining Volatile Matter and Ash in Biomass/Plant Tissue*. [Online]. 2016. [Accessed 03/04/2024]. Available from: <https://www.azom.com/>
319. Jabeen, S., Gao, X., Altarawneh, M., Hayashi, J.-i., Zhang, M. and Dlugogorski, B. Analytical Procedure for Proximate Analysis of Algal Biomass: Case Study for Spirulina and Chlorella. *Energy & Fuels*. 2019, **XXXX**.
320. Rheology, T.A. *Thermal Analysis Application Brief: Proximate Analysis of Coal and Coke (Number TA-129)*. [Leaflet]. 2024.
321. ISO, E. 18122: 2015; Solid Biofuels—Determination of Ash Content. *International Organization for Standardization: Geneva, Switzerland*. 2015, pp.1-6.
322. Wilen, C.M., Antero; Kurkela, Esa. *Biomass feedstock analyses*. Technical Research Centre of Finland, 1996.
323. Monti, A., Di Virgilio, N. and Venturi, G. Mineral composition and ash content of six major energy crops. *Biomass and Bioenergy*. 2008, **32**(3), pp.216-223.
324. Mayoral, M.C., Izquierdo, M.T., Andrés, J.M. and Rubio, B. Different approaches to proximate analysis by thermogravimetry analysis. *Thermochimica Acta*. 2001, **370**(1), pp.91-97.
325. García, R., Pizarro, C., Lavín, A.G. and Bueno, J.L. Biomass proximate analysis using thermogravimetry. *Bioresource Technology*. 2013, **139**, pp.1-4.
326. Park, S., Kim, S.J., Oh, K.C., Cho, L., Jeon, Y., Lee, C. and Kim, D. Thermogravimetric analysis-based proximate analysis of agro-byproducts and prediction of calorific value. *Energy Reports*. 2022, **8**, pp.12038-12044.
327. Friedl, A., Padouvas, E., Rotter, H. and Varmuza, K. Prediction of heating values of biomass fuel from elemental composition. *Analytica Chimica Acta*. 2005, **544**(1), pp.191-198.
328. Hosokai, S., Matsuoka, K., Kuramoto, K. and Suzuki, Y. Modification of Dulong's formula to estimate heating value of gas, liquid and solid fuels. *Fuel Processing Technology*. 2016, **152**, pp.399-405.
329. Channiwala, S.A. and Parikh, P.P. A unified correlation for estimating HHV of solid, liquid and gaseous fuels. *Fuel*. 2002, **81**(8), pp.1051-1063.

330. Niu, Y., Tan, H. and Hui, S.e. Ash-related issues during biomass combustion: Alkali-induced slagging, silicate melt-induced slagging (ash fusion), agglomeration, corrosion, ash utilization, and related countermeasures. *Progress in Energy and Combustion Science*. 2016, **52**, pp.1-61.
331. Lowry, H.H. *Chemistry of coal utilization: supplementary volume*. New York: J. Wiley & sons, inc., 1963.
332. Trombley, J.B., Wang, C. and Thennadil, S.N. Model-free measurements of calorific content and ash content of mixed garden wastes using a bomb calorimeter. *Fuel*. 2023, **352**, p.129105.
333. Jeswani, H.K. and Azapagic, A. Assessing the environmental sustainability of energy recovery from municipal solid waste in the UK. *Waste Management*. 2016, **50**, pp.346-363.
334. Parthasarathy, P., Zuhara, S., Al-Ansari, T. and McKay, G. A review on catalytic CO<sub>2</sub> pyrolysis of organic wastes to high-value products. *Fuel*. 2023, **335**, p.127073.
335. AquaCulture. *Analytical Techniques in Aquaculture Research*. [Online]. 2003. [Accessed 03/04/2024]. Available from: <https://aquaculture.ugent.be>
336. SCIENTIFICA, V. *Crude Fiber Determination in Feed (Weende method)*. 2019.
337. Müller, J., Wiedow, D., Chmit, M.S. and Beuerle, T. Utilization of Biomasses from Landscape Conservation Growths Dominated by Common Ragwort (*Jacobaea vulgaris* Gaertn.) for Biomethanization. *Plants (Basel)*. 2022, **11**(6).
338. Quintana-Najera, J., Blacker, A.J., Fletcher, L.A., Bray, D.G. and Ross, A.B. The Influence of Biochar Augmentation and Digestion Conditions on the Anaerobic Digestion of Water Hyacinth. *Energies*. 2022, **15**(7), p.2524.
339. Mariotti, F., Tomé, D. and Mirand, P.P. Converting Nitrogen into Protein—Beyond 6.25 and Jones' Factors. *Critical Reviews in Food Science and Nutrition*. 2008, **48**(2), pp.177-184.
340. Amiri, A. *An investigation on some edible insects as source of human food and animal feed*. thesis, Near East University, 2017.
341. Zang, J., Shih, J.C.H., Cheng, J.J., Liu, Z., Liu, Y. and Lu, W. Thermophilic solid state anaerobic digestion of switchgrass for liquid digestate reuse and organic fertilizer production. *Renewable Agriculture and Food Systems*. 2020, **35**(5), pp.503-512.
342. Jones, D.B. *Factors for Converting Percentages of Nitrogen in Foods and Feeds into Percentages of Protein*. Washington DC, 1941.
343. Wang, W., Lemaire, R., Bensakhria, A. and Luart, D. Review on the catalytic effects of alkali and alkaline earth metals (AAEMs) including sodium, potassium, calcium and magnesium on the pyrolysis of lignocellulosic biomass and on the co-pyrolysis of coal with biomass. *Journal of Analytical and Applied Pyrolysis*. 2022, **163**, p.105479.
344. Zhu, C., Maduskar, S., Paulsen, A.D. and Dauenhauer, P.J. Alkaline-Earth-Metal-Catalyzed Thin-Film Pyrolysis of Cellulose. *ChemCatChem*. 2016, **8**(4), pp.818-829.
345. Hanusa, T.P.P., Courtenay Stanley Goss. *Alkaline-earth metal*. [Online]. 2024. [Accessed July 26th]. Available from: <https://www.britannica.com/>

346. Mohammed, E., Mohammed, T. and Mohammed, A. Optimization of an acid digestion procedure for the determination of Hg, As, Sb, Pb and Cd in fish muscle tissue. *MethodsX*. 2017, **4**, pp.513-523.
347. Chen, K., Han, S., Meng, F., Lin, L., Li, J., Gao, Y., Qin, W. and Jiang, J. Acid controlled washing of municipal solid waste incineration fly ash: Extraction of calcium inhibiting heavy metals and reaction kinetics. *Science of The Total Environment*. 2024, **909**, p.168599.
348. Wang, Y., Guo, X., Bai, Y. and Sun, X. Effective removal of calcium and magnesium sulfates from wastewater in the rare earth industry. *RSC Adv*. 2019, **9**(58), pp.33922-33930.
349. Pecha, B., Arauzo, P. and Garcia-Perez, M. Impact of combined acid washing and acid impregnation on the pyrolysis of Douglas fir wood. *Journal of Analytical and Applied Pyrolysis*. 2015, **114**, pp.127-137.
350. Yoo, K., Kim, B.-S., Kim, M.-S., Lee, J.-c. and Jeong, J. Dissolution of Magnesium from Serpentine Mineral in Sulfuric Acid Solution. *MATERIALS TRANSACTIONS*. 2009, **50**(5), pp.1225-1230.
351. Houzelot, V., Ranc, B., Laubie, B. and Simonnot, M.-O. Agromining of hyperaccumulator biomass: Study of leaching kinetics of extraction of nickel, magnesium, potassium, phosphorus, iron, and manganese from Alyssum murale ashes by sulfuric acid. *Chemical Engineering Research and Design*. 2018, **129**, pp.1-11.
352. Sáenz-Martínez, Á., Pérez-Estébanez, M., San Andrés, M., Alvarez de Buergo, M. and Fort, R. Efficacy of acid treatments used in archaeological ceramics for the removal of calcareous deposits. *The European Physical Journal Plus*. 2021, **136**(8), p.798.
353. Nowakowski, D.J. and Jones, J.M. Uncatalysed and potassium-catalysed pyrolysis of the cell-wall constituents of biomass and their model compounds. *Journal of Analytical and Applied Pyrolysis*. 2008, **83**(1), pp.12-25.
354. Qin, J., Zhang, Y. and Yi, Y. Water washing and acid washing of gasification fly ash from municipal solid waste: Heavy metal behavior and characterization of residues. *Environmental Pollution*. 2023, **320**, p.121043.
355. Scientific, X. *A Beginner's Guide to Thermogravimetric Analysis*. [Online]. 2015. [Accessed 2nd October]. Available from: <https://www.xrfscientific.com/>
356. Shetty, P. 2: *Thermogravimetry*. [Online]. 2024. [Accessed 2nd October]. Available from: <https://chem.libretexts.org/>
357. Dar, O., Lone, S., Malik, M., Wani, M., Talukdar, M., Al-Bogami, A., Hashmi, A.A. and Ahmad, A. Heteroleptic transition metal complexes of Schiff-base-derived ligands exert their antifungal activity by disrupting membrane integrity. *Applied Organometallic Chemistry*. 2019, **33**.
358. El-Sayed, S.A., Khass, T.M. and Mostafa, M.E. Thermal degradation behaviour and chemical kinetic characteristics of biomass pyrolysis using TG/DTG/DTA techniques. *Biomass Conversion and Biorefinery*. 2024, **14**(15), pp.17779-17803.
359. Imtiaz Anando, A., Ehsan, M.M., Karim, M.R., Bhuiyan, A.A., Ahiduzzaman, M. and Karim, A. Thermochemical pretreatments to improve the fuel properties of rice husk: A review. *Renewable Energy*. 2023, **215**, p.118917.

360. Hasan, M.M., Rasul, M.G., Khan, M.M.K., Ashwath, N. and Jahirul, M.I. Energy recovery from municipal solid waste using pyrolysis technology: A review on current status and developments. *Renewable and Sustainable Energy Reviews*. 2021, **145**, p.111073.
361. Li, T., Su, J., Wang, C., Watanabe, A., Teramae, N., Ohtani, H. and Wang, K. Advances in the development and application of analytical pyrolysis in biomass research: A review. *Energy Conversion and Management*. 2022, **271**, p.116302.
362. Wampler, T.P. *Applied Pyrolysis Handbook*. 2nd ed. Boca Rotan: CRC Press, 2006.
363. Moldoveanu, S.C. *Pyrolysis of Organic Molecules: Applications to Health and Environmental Issues*. Elsevier, 2010.
364. Wang, L., Skreiberg, Ø., Gronli, M., Specht, G.P. and Antal, M.J., Jr. Is Elevated Pressure Required to Achieve a High Fixed-Carbon Yield of Charcoal from Biomass? Part 2: The Importance of Particle Size. *Energy & Fuels*. 2013, **27**(4), pp.2146-2156.
365. Selvarajoo, A. and Oochit, D. Effect of pyrolysis temperature on product yields of palm fibre and its biochar characteristics. *Materials Science for Energy Technologies*. 2020, **3**, pp.575-583.
366. Zhang, X., Zhang, P., Yuan, X., Li, Y. and Han, L. Effect of pyrolysis temperature and correlation analysis on the yield and physicochemical properties of crop residue biochar. *Bioresource Technology*. 2020, **296**, p.122318.
367. Babinszki, B., Sebestyén, Z., Jakab, E., Kőhalmi, L., Bozi, J., Várhegyi, G., Wang, L., Skreiberg, Ø. and Czégény, Z. Effect of slow pyrolysis conditions on biocarbon yield and properties: Characterization of the volatiles. *Bioresource Technology*. 2021, **338**, p.125567.
368. Yang, H., Liu, B., Chen, Y., Chen, W., Yang, Q. and Chen, H. Application of biomass pyrolytic polygeneration technology using retort reactors. *Bioresource Technology*. 2016, **200**, pp.64-71.
369. Ochieng, R., Cerón, A.L., Konist, A. and Sarker, S. Experimental and modeling studies of intermediate pyrolysis of wood in a laboratory-scale continuous feed retort reactor. *Bioresource Technology Reports*. 2023, **24**, p.101650.
370. Klavina, K., Klavins, J., Veidenbergs, I. and Blumberga, D. Charcoal Production in a Continuous Operation Retort. Experimental Data Processing. *Energy Procedia*. 2016, **95**, pp.208-215.
371. Garcia-Nunez, J.A., Pelaez-Samaniego, M.R., Garcia-Perez, M.E., Fonts, I., Abrego, J., Westerhof, R.J.M. and Garcia-Perez, M. Historical Developments of Pyrolysis Reactors: A Review. *Energy & Fuels*. 2017, **31**(6), pp.5751-5775.
372. Yunjuan, S., Jianchun, J., Junming, X. and Shuheng, Z. Biomass carbonization industrial process. In: *2011 International Conference on Materials for Renewable Energy & Environment, 20-22 May 2011*, 2011, pp.54-59.
373. Johnson, K.E. *Investigating the Differences between the Self-Heating of Bark and Wood Piles during Storage Through the Use of Computer Modeling*. thesis, University of Toronto, 2017.

374. Yang, H.L., Linda. *Fast Determination of Total Unbound Fat in Snack Foods Using Accelerated Solvent Extraction and the Rocket Evaporator*. Thermo Fisher Scientific, Sunnyvale, CA, USA, 2014.
375. SHU. *Gas Chromatography*. [Online]. 2024. [Accessed 8th Oct]. Available from: <https://teaching.shu.ac.uk/>
376. Turner, D. *Gas Chromatography – How a Gas Chromatography Machine Works, How To Read a Chromatograph and GCxGC*. [Online]. 2024. [Accessed October 8th]. Available from: <https://www.technologynetworks.com/>
377. Noonan, M.J., Tinnesand, H.V. and Buesching, C.D. Normalizing Gas-Chromatography–Mass Spectrometry Data: Method Choice can Alter Biological Inference. *BioEssays*. 2018, **40**(6), p.1700210.
378. Prat, D., Wells, A., Hayler, J., Sneddon, H., McElroy, C.R., Abou-Shehada, S. and Dunn, P.J. CHEM21 selection guide of classical- and less classical-solvents. *Green Chemistry*. 2016, **18**(1), pp.288-296.
379. Europe, M. *Hazard statements*. [Online]. 2024. [Accessed June 23rd]. Available from: <https://www.msds-europe.com/>
380. Helminen, J., Helenius, J., Paatero, E. and Turunen, I. Comparison of sorbents and isotherm models for NH<sub>3</sub>-gas separation by adsorption. *AIChE Journal*. 2000, **46**(8), pp.1541-1555.
381. Sun, Y., Li, S., Sun, R., Yang, S. and Liu, X. Modified Dubinin–Astakhov Model for the Accurate Estimation of Supercritical Methane Sorption on Shales. *ACS Omega*. 2020, **5**(26), pp.16189-16199.
382. NIST. *Ammonia*. [Online]. 2023. [Accessed 16th August]. Available from: <https://webbook.nist.gov/>
383. Stull, D.R. Vapor Pressure of Pure Substances. Organic and Inorganic Compounds. *Industrial & Engineering Chemistry*. 1947, **39**(4), pp.517-550.
384. Ramirez, D., Qi, S., Rood, M.J. and Hay, K.J. Equilibrium and Heat of Adsorption for Organic Vapors and Activated Carbons. *Environmental Science & Technology*. 2005, **39**(15), pp.5864-5871.
385. Haar, L. and Gallagher, J.S. Thermodynamic properties of ammonia. *Journal of Physical and Chemical Reference Data*. 1978, **7**(3), pp.635-792.
386. Biswas, B., Kumar, A., Krishna, B.B. and Bhaskar, T. Effects of solid base catalysts on depolymerization of alkali lignin for the production of phenolic monomer compounds. *Renewable Energy*. 2021, **175**, pp.270-280.
387. Kumar, A., Biswas, B., Kaur, R., Rani, R., Krishna, B.B. and Bhaskar, T. Structure elucidation of prot, alkali and dealkaline lignin(s) by NMR, FT-IR and Py-GC/MS: effect of solid acid and base catalysts. *Sustainable Energy & Fuels*. 2023, **7**(8), pp.1942-1954.
388. Gordobil, O., Moriana, R., Zhang, L., Labidi, J. and Sevastyanova, O. Assesment of technical lignins for uses in biofuels and biomaterials: Structure-related properties, proximate analysis and chemical modification. *Industrial Crops and Products*. 2016, **83**, pp.155-165.
389. Guo, D., Liu, B., Tang, Y., Zhang, J. and Xia, X. Autocatalytic Depolymerization of Alkali Lignin by Organic Bound Sodium in Supercritical Ethanol. *Energy & Fuels*. 2017, **31**(10), pp.10842-10849.
390. Belkheiri, T., Andersson, S.-I., Mattsson, C., Olausson, L., Theliander, H. and Vamling, L. Hydrothermal liquefaction of kraft lignin in sub-critical water:

- the influence of the sodium and potassium fraction. *Biomass Conversion and Biorefinery*. 2018, **8**(3), pp.585-595.
391. Perez, N.D., Lindfors, C., van den Broek, L.A.M., van der Putten, J., Meredith, W. and Robinson, J. Correction to: Comparison of bio-oils derived from crop digestate treated through conventional and microwave pyrolysis as an alternative route for further waste valorization. *Biomass Conversion and Biorefinery*. 2023.
392. Wang, W., Chang, J.-S. and Lee, D.-J. Digestate-derived carbonized char and activated carbon: Application perspective. *Bioresource Technology*. 2023, **381**, p.129135.
393. Monlau, F., Sambusiti, C., Ficara, E., Aboulkas, A., Barakat, A. and Carrère, H. New opportunities for agricultural digestate valorization: current situation and perspectives. *Energy & Environmental Science*. 2015, **8**(9), pp.2600-2621.
394. Ogwang, I., Kasedde, H., Nabuuma, B., Kirabira, J.B. and Lwanyaga, J.D. Characterization of Biogas Digestate for Solid Biofuel Production in Uganda. *Scientific African*. 2021, **12**, p.e00735.
395. Mammarella, D., Di Giuliano, A. and Gallucci, K. Reuse and Valorization of Solid Digestate Ashes from Biogas Production. *Energies*. 2024, **17**(3), p.751.
396. *Digestate Analysis for AD and RNG Projects at Celignis Biomass Lab*. [Online]. [Accessed 18/04/24]. Available from: <https://www.celignis.com/>
397. Feng, Y., Bu, T., Zhang, Q., Han, M., Tang, Z., Yuan, G., Chen, D. and Hu, Y. Pyrolysis characteristics of anaerobic digestate from kitchen waste and availability of Phosphorus in pyrochar. *Journal of Analytical and Applied Pyrolysis*. 2022, **168**, p.105729.
398. Quan, C., Zhou, Y., Gao, N., Yang, T., Wang, J. and Wu, C. Direct CO<sub>2</sub> capture from air using char from pyrolysis of digestate solid. *Biomass and Bioenergy*. 2023, **175**, p.106891.
399. Nisticò, R., Guerretta, F., Benzi, P., Magnacca, G., Mainero, D. and Montoneri, E. Thermal Conversion of Municipal Biowaste Anaerobic Digestate to Valuable Char. *Resources*. 2019, **8**(1), p.24.
400. Peng, W., Zhang, H., Lü, F., Shao, L. and He, P. From food waste and its digestate to nitrogen self-doped char and methane-rich syngas: Evolution of pyrolysis products during autogenic pressure carbonization. *Journal of Hazardous Materials*. 2022, **424**, p.127249.
401. Roy, U.K., Radu, T. and Wagner, J. Hydrothermal carbonisation of anaerobic digestate for hydro-char production and nutrient recovery. *Journal of Environmental Chemical Engineering*. 2022, **10**(1), p.107027.
402. Wang, J., Zhang, S., Chen, M., Feng, Y. and Zhang, H. Fractional condensation of pyrolysis oil from fast pyrolysis of food waste digestate for enrichment of high value-added nitrogen-containing components. *Journal of Analytical and Applied Pyrolysis*. 2022, **166**, p.105609.
403. Ajala, E.O., Ighalo, J.O., Ajala, M.A., Adeniyi, A.G. and Ayanshola, A.M. Sugarcane bagasse: a biomass sufficiently applied for improving global energy, environment and economic sustainability. *Bioresources and Bioprocessing*. 2021, **8**(1), p.87.

404. Zafeer, M.K., Menezes, R.A., Venkatachalam, H. and Bhat, K.S. Sugarcane bagasse-based biochar and its potential applications: a review. *Emergent Materials*. 2024, **7**(1), pp.133-161.
405. Rabiou, S.D., Auta, M. and Kovo, A.S. An upgraded bio-oil produced from sugarcane bagasse via the use of HZSM-5 zeolite catalyst. *Egyptian Journal of Petroleum*. 2018, **27**(4), pp.589-594.
406. Shabbirahmed, A.M., Haldar, D., Dey, P., Patel, A.K., Singhania, R.R., Dong, C.-D. and Purkait, M.K. Sugarcane bagasse into value-added products: a review. *Environmental Science and Pollution Research*. 2022, **29**(42), pp.62785-62806.
407. Caraschi, J.C., Campana Filho, S.P. and Curvelo, A.A.d.S. Preparacao e caracterizacao de polpas para dissolucao obtidas a partir de bagaco de cana-de-acucar. *Polimeros: Ciencia e Tecnologia*. 1996, (9), pp.24-29.
408. Anuchi, S.O., Campbell, K.L.S. and Hallett, J.P. Effective pretreatment of lignin-rich coconut wastes using a low-cost ionic liquid. *Scientific Reports*. 2022, **12**(1), p.6108.
409. Aijen, A., Idris, J., Md Sofwan, N., Husen, R. and Seli, H. Coconut shell and husk biochar: A review of production and activation technology, economic, financial aspect and application. *Waste Manag Res*. 2023, **41**(1), pp.37-51.
410. Pawar, A., Panwar, N.L., Jain, S., Jain, N.K. and Gupta, T. Thermal degradation of coconut husk waste biomass under non-isothermal condition. *Biomass Conversion and Biorefinery*. 2023, **13**(9), pp.7613-7622.
411. Rout, T.K. *Pyrolysis of coconut shell*. Master of Technology thesis, Rourkela National Institute of Technology.
412. Adeyi, O. Proximate composition of some agricultural wastes in Nigeria and their potential use in activated carbon production. *Journal of Applied Sciences and Environmental Management*. 2010, **14**.
413. E, E.D., Dissanayake; S, Udumann; D, Dissanayaka; T, Nuwarapaksha; H, Herath; J. Atapattu. Sustainable Utilization of King Coconut Husk as a Feedstock in Biochar Production with the Highest Conversion Efficiency and Desirable Properties. In: *IOP Conference Series: Earth and Environmental Science, Kuala Lumpur, Malaysia*. 2023.
414. Suman, S. and Gautam, S. Pyrolysis of coconut husk biomass: Analysis of its biochar properties. *Energy Sources, Part A: Recovery, Utilization, and Environmental Effects*. 2017, **39**(8), pp.761-767.
415. Triwibowo, D.S.F.M.C.K.R.A.S.L.B. Producing Bio-Oil from Coconut Shell by Fast Pyrolysis Processing. In: *2018 3rd International Conference on Design, Mechanical and Material Engineering*. 2018.
416. Azeta, O., Ayeni, A.O., Agboola, O. and Elehinafe, F.B. A review on the sustainable energy generation from the pyrolysis of coconut biomass. *Scientific African*. 2021, **13**, p.e00909.
417. Brennan, M., Fritsch, C., Cosgun, S., Dumarcay, S., Colin, F. and Gérardin, P. Quantitative and qualitative composition of bark polyphenols changes longitudinally with bark maturity in *Abies alba* Mill. *Annals of Forest Science*. 2020, **77**(1), p.9.
418. Neumann, M. and Lawes, M.J. Quantifying carbon in tree bark: The importance of bark morphology and tree size. *Methods in Ecology and Evolution*. 2021, **12**(4), pp.646-654.

419. Cardoso, S., Ferreira, J., Quilhó, T. and Pereira, H. Cork of Douglas-fir bark: Impact of structural and anatomical features on usage. *Industrial Crops and Products*. 2017, **99**, pp.135-141.
420. CorkLink. *How cork products are made – from tree bark to stopper*. [Online]. 2023. [Accessed January 30th]. Available from: <https://www.corklink.com/index.php/how-cork-products-are-made-from-tree-bark-to-stopper/#:~:text=The%20cork%20bark%20that%20is,vital%20part%20of%20the%20process>.
421. Wilson, P.L., Funck, J.W. and Avery, R.B. *Fuelwood characteristics of northwestern conifers and hardwoods*. U.S. Department of Agriculture, Forest Service, Pacific Northwest Research Station, 2010.
422. Corder, S.E. *Wood and Bark as Fuel*. Oregon State University, 1973.
423. Neiva, D.M., Araújo, S., Gominho, J., Carneiro, A.C. and Pereira, H. An integrated characterization of *Picea abies* industrial bark regarding chemical composition, thermal properties and polar extracts activity. *PloS one*. 2018, **13**(11), p.e0208270.
424. Sobol, Ł., Sabat, D. and Dyjakon, A. Assessment of Bark Properties from Various Tree Species in Terms of Its Hydrophobicity and Energy Suitability. *Energies*. 2023, **16**(18), p.6586.
425. Reed, T. *Densification - Proximate and Ultimate Analyses*. [Online]. 2009. [Accessed]. Available from: <https://drtlud.com/>
426. project, B. Database for the physico-chemical composition of (treated) lignocellulosic biomass, micro- and macroalgae, various feedstocks for biogas production and biochar. [Online]. 2024. Available from: <https://phyllis.nl/>
427. Fromm, J. Wood formation of trees in relation to potassium and calcium nutrition. *Tree Physiology*. 2010, **30**(9), pp.1140-1147.
428. Andrade, A., Herrera, O.E., Reyes-Contreras, P., Pereira, M. and Vásquez-Garay, F. Eucalyptus globulus bark valorization: Production of fibers by Neutral Sulphite Semi-Chemical Process for Liner Paper Manufacture. *Floresta e Ambiente*. 2021, **28**.
429. Barros, D., Fernandes, É., Jesus, M., Barros, L., Alonso-Esteban, J.I., Pires, P. and Vaz Velho, M. The Chemical Characterisation of the Maritime Pine Bark Cultivated in Northern Portugal. *Plants*. 2023, **12**(23), p.3940.
430. Lourenço, A.P., Helena. Compositional Variability of Lignin in Biomass. In: Matheus, P. ed. *Lignin*. Rijeka, Croatia: IntechOpen, 2017.
431. Ajao, O., Benali, M., Faye, A., Li, H., Maillard, D. and Ton-That, M.T. Multi-product biorefinery system for wood-barks valorization into tannins extracts, lignin-based polyurethane foam and cellulose-based composites: Techno-economic evaluation. *Industrial Crops and Products*. 2021, **167**, p.113435.
432. Engineer, T. *Aston University develops bio-oil technology*. [Online]. 2010. [Accessed 30th April]. Available from: <https://www.theengineer.co.uk/>
433. Zaini, I.N., García López, C., Pretz, T., Yang, W. and Jönsson, P.G. Characterization of pyrolysis products of high-ash excavated-waste and its char gasification reactivity and kinetics under a steam atmosphere. *Waste Management*. 2019, **97**, pp.149-163.

434. Gómez, N., Banks, S.W., Nowakowski, D.J., Rosas, J.G., Cara, J., Sánchez, M.E. and Bridgwater, A.V. Effect of temperature on product performance of a high ash biomass during fast pyrolysis and its bio-oil storage evaluation. *Fuel Processing Technology*. 2018, **172**, pp.97-105.
435. Puri, L., Hu, Y. and Naterer, G. Critical review of the role of ash content and composition in biomass pyrolysis. *Frontiers in Fuels*. 2024, **2**.
436. Açıklın, K. Evaluation of orange and potato peels as an energy source: a comprehensive study on their pyrolysis characteristics and kinetics. *Biomass Conversion and Biorefinery*. 2022, **12**(2), pp.501-514.
437. Cao, W., Li, J., Martí-Rosselló, T. and Zhang, X. Experimental study on the ignition characteristics of cellulose, hemicellulose, lignin and their mixtures. *Journal of the Energy Institute*. 2019, **92**(5), pp.1303-1312.
438. Opatokun, S.A., Kan, T., Al Shoaibi, A., Srinivasakannan, C. and Strezov, V. Characterization of Food Waste and Its Digestate as Feedstock for Thermochemical Processing. *Energy & Fuels*. 2016, **30**(3), pp.1589-1597.
439. Sharifi, M., Baker, S., Hojabri, L. and Hajiaghahi-Kamrani, M. Short-term nitrogen dynamics in a soil amended with anaerobic digestate. *Canadian Journal of Soil Science*. 2019, **99**(2), pp.173-181.
440. Svensson, S. Minimizing the sulphur content in Kraft lignin. In, 2008.
441. Lavallie, A.L. *Characerization, Depolymerization And Fractionation Of Alkali Lignin*. PhD thesis, University of North Dakota, 2021.
442. Mahlie, W.S. Sulphur in Sewage. *Sewage Works Journal*. 1934, **6**(3), pp.547-579.
443. Aich, S., Nandi, B.K. and Bhattacharya, S. Combustion characteristics of high ash Indian thermal, heat affected coal and their blends. *International Journal of Coal Science & Technology*. 2021, **8**(5), pp.1078-1087.
444. Li, Y., Hu, B., Fu, H., Zhang, Z.-x., Guo, Z.-t., Zhou, G.-z., Zhu, L.-j., Liu, J. and Lu, Q. Fast pyrolysis of bagasse catalyzed by mixed alkaline-earth metal oxides for the selective production of 4-vinylphenol. *Journal of Analytical and Applied Pyrolysis*. 2022, **164**, p.105531.
445. García-López, A.M., Delgado, A., Anjos, O. and Horta, C. Digestate Not Only Affects Nutrient Availability but Also Soil Quality Indicators. *Agronomy*. 2023, **13**(5), p.1308.
446. Ejigu, W., Selassie, Y.G., Elias, E. and Molla, E. Effect of lime rates and method of application on soil properties of acidic Luvisols and wheat (*Triticum aestivum*, L.) yields in northwest Ethiopia. *Heliyon*. 2023, **9**(3), p.e13988.
447. Dragicevic, I., Eich-Greatorex, S., Sogn, T.A., Horn, S.J. and Krogstad, T. Use of high metal-containing biogas digestates in cereal production - Mobility of chromium and aluminium. *J Environ Manage*. 2018, **217**, pp.12-22.
448. Robinson, H.D., Knox, K., Formby, R., Bone, B.D. *Testing of residues from incineration of municipal solid waste*. Environment Agency, 2004.
449. Drosch, B., Fuchs, W., Al Seadi, T., Madsen, M. and Linke, B. *Nutrient Recovery by Biogas Digestate Processing*. IEA Bioenergy, 2015.
450. Doyeni, M.O., Stulpinaite, U., Baksinskaite, A., Suproniene, S. and Tilvikiene, V. The Effectiveness of Digestate Use for Fertilization in an Agricultural Cropping System. *Plants (Basel)*. 2021, **10**(8).

451. *Digestate and compost use in agriculture*. 2016.
452. Herath, H.M.I.K. and Wijebandara, D.M.D.I. Potential Use of King Coconut Husk as a Nutrient Source for Organic Coconut Cultivation. *Journal of Food and Agriculture*. 2017.
453. Shrestha, S., Kulandaivelu, J., Rebosura, M.J.R., Yuan, Z. and Sharma, K. Revealing the variations in physicochemical, morphological, fractal, and rheological properties of digestate during the mesophilic anaerobic digestion of iron-rich waste activated sludge. *Chemosphere*. 2020, **254**, p.126811.
454. Ofverstrom, S., Dauknys, R. and Sapkaite, I. The effect of iron salt on anaerobic digestion and phosphate release to sludge liquor. 2011, **3(5)**, pp.123-126.
455. Chester, C.W.a. *Garden waste collection*. [Online]. 2024. [Accessed]. Available from: <https://www.cheshirewestandchester.gov.uk/>
456. Carvalho, A.V.d. *Effects of potassium and calcium on the combustion behaviour of biomass*. Master of Science in Mechanical Engineering thesis, Tecnico Lisboa, 2017.
457. Sillero, L., Prado, R., Welton, T. and Labidi, J. Extraction of flavonoid compounds from bark using sustainable deep eutectic solvents. *Sustainable Chemistry and Pharmacy*. 2021, **24**, p.100544.
458. Service, U.S.F. *Tannins*. [Online]. 2024. [Accessed 08/04/24]. Available from: <https://www.fs.usda.gov/>
459. Akinmoladun, A.C., Falaiye, O.E., Ojo, O.B., Adeoti, A., Amoo, Z.A. and Olaleye, M.T. Effect of extraction technique, solvent polarity, and plant matrix on the antioxidant properties of *Chrysophyllum albidum* G. Don (African Star Apple). *Bulletin of the National Research Centre*. 2022, **46(1)**, p.40.
460. Mächtig, T., Casaretto, R., Moschner, C.R., Born, J., Holm-Nielsen, J.B. and Hartung, E. Anaerobic Biodegradability of Digestates – Influence of and Correlations for Klason lignin. *Chemical Engineering & Technology*. 2020, **43(1)**, pp.39-46.
461. Ress, B.B., Calvert, P.P., Pettigrew, C.A. and Barlaz, M.A. Testing Anaerobic Biodegradability of Polymers in a Laboratory-Scale Simulated Landfill. *Environmental Science & Technology*. 1998, **32(6)**, pp.821-827.
462. Sangian, H.F. and Widjaja, A. The Effect of Alkaline Concentration on Coconut Husk Crystallinity and the Yield of Sugars Released. *IOP Conference Series: Materials Science and Engineering*. 2018, **306(1)**, p.012046.
463. Pagano, M., Hernando, H., Cueto, J., Cruz, P.L., Dufour, J., Moreno, I. and Serrano, D.P. Insights on the acetic acid pretreatment of wheat straw: Changes induced in the biomass properties and benefits for the bio-oil production by pyrolysis. *Chemical Engineering Journal*. 2023, **454**, p.140206.
464. Usino, D.O. *Fast pyrolysis of biomass - primary products and reaction pathways*. thesis, University of Boras, 2023.
465. Ziyun, L., Lihong, W., Yongjun, L. and Zhihe, L. Study On Phenolic Content In Fast Pyrolysis Oil Obtained From The Model Compounds Of Three Major Components In Biomass. In: *Proceedings of the 2016 International*

- Conference on Advances in Energy, Environment and Chemical Science, 2016/05: Atlantis Press, 2016, pp.221-230.*
466. Itabaiana Junior, I., Avelar do Nascimento, M., de Souza, R.O.M.A., Dufour, A. and Wojcieszak, R. Levoglucosan: a promising platform molecule? *Green Chemistry*. 2020, **22**(18), pp.5859-5880.
467. Skrypnik, L., Grigorev, N., Michailov, D., Antipina, M., Danilova, M. and Pungin, A. Comparative study on radical scavenging activity and phenolic compounds content in water bark extracts of alder (*Alnus glutinosa* (L.) Gaertn.), oak (*Quercus robur* L.) and pine (*Pinus sylvestris* L.). *European Journal of Wood and Wood Products*. 2019, **77**(5), pp.879-890.
468. Emiola-Sadiq, T., Zhang, L. and Dalai, A.K. Thermal and Kinetic Studies on Biomass Degradation via Thermogravimetric Analysis: A Combination of Model-Fitting and Model-Free Approach. *ACS Omega*. 2021, **6**(34), pp.22233-22247.
469. RSC. *Calcium*. [Online]. 2024. [Accessed 11/04/24]. Available from: rsc.org
470. RSC. *Iron*. [Online]. 2024. [Accessed 11/04/24]. Available from: rsc.org
471. Life, T.f. *Tree bark*. [Online]. 2024. [Accessed]. Available from: <https://treesforlife.org.uk/>
472. Catry, F.X., Moreira, F., Pausas, J.G., Fernandes, P.M., Rego, F., Cardillo, E. and Curt, T. Cork Oak Vulnerability to Fire: The Role of Bark Harvesting, Tree Characteristics and Abiotic Factors. *PloS one*. 2012, **7**(6), p.e39810.
473. Cukor, J., Vacek, Z., Linda, R., Vacek, S., Marada, P., Šimůnek, V. and Havránek, F. Effects of Bark Stripping on Timber Production and Structure of Norway Spruce Forests in Relation to Climatic Factors. *Forests*. 2019, **10**(4), p.320.
474. Şen, U., Esteves, B. and Pereira, H. Pyrolysis and Extraction of Bark in a Biorefineries Context: A Critical Review. *Energies*. 2023, **16**(13), p.4848.
475. Kusiak, W., Majka, J., Zborowska, M. and Ratajczak, I. Chemical Composition and Related Properties of Lime (*Tilia cordata* Mill.) Bark and Wood as Affected by Tree Growth Conditions. *Materials (Basel)*. 2022, **15**(11).
476. Timber, D. *Hardwood vs. Softwood: What Are The Differences?* [Online]. 2021. [Accessed]. Available from: <https://duffieldtimber.com/>
477. Pásztor, Z., Mohácsiné, I., Gorbacheva, G. and Börcsök, Z. The utilization of tree bark. *BioResources*. 2016, **11**, pp.7859-7888.
478. Ingram, L., Mohan, D., Bricka, M., Steele, P., Strobel, D., Crocker, D., Mitchell, B., Mohammad, J., Cantrell, K. and Pittman, C.U., Jr. Pyrolysis of Wood and Bark in an Auger Reactor: Physical Properties and Chemical Analysis of the Produced Bio-oils. *Energy & Fuels*. 2008, **22**(1), pp.614-625.
479. Jahiding, M., Arsyad, W.O.S., Rif'ah, S.M., Rizki, R.S. and Mashuni. Effect of pyrolysis temperature on bio-fuel quality produced from pine bark (*Pinus merkusii*) by pyro-catalytics method. *Journal of Physics: Conference Series*. 2021, **1825**(1), p.012047.
480. Park, C., Lee, N., Kim, J. and Lee, J. Co-pyrolysis of food waste and wood bark to produce hydrogen with minimizing pollutant emissions. *Environmental Pollution*. 2021, **270**, p.116045.

481. Ben, H., Wu, F., Wu, Z., Han, G., Jiang, W. and Ragauskas, A.J. A Comprehensive Characterization of Pyrolysis Oil from Softwood Barks. *Polymers*. 2019, **11**(9).
482. Lövhall, F. *A Review of Pyrolysis of Bark towards Bio-oil*. Chalmers University of Technology, 2014.
483. Okumura, Y. Quantitative analysis of primary tar yields volatilized from biomass (Effect of heating rate and biomass type on tar components). *Journal of Thermal Science and Technology*. 2021, **16**(2), p.29.
484. Septien, S., Valin, S., Dupont, C., Peyrot, M. and Salvador, S. Effect of particle size and temperature on woody biomass fast pyrolysis at high temperature (1000–1400°C). *Fuel*. 2012, **97**, pp.202-210.
485. Gandrieau, S. *Tannins extraction from bark for industrial applications laboratory study*. 2020.
486. Abilleira, F., Varela, P., Cancela, Á., Álvarez, X., Sánchez, Á. and Valero, E. Tannins extraction from Pinus pinaster and Acacia dealbata bark with applications in the industry. *Industrial Crops and Products*. 2021, **164**, p.113394.
487. Dababi, I., Gimello, O., Elaloui, E. and Brosse, N. Water Extraction of Tannins from Aleppo Pine Bark and Sumac Root for the Production of Green Wood Adhesives. *Molecules*. 2020, **25**(21).
488. Das, A.K., Islam, M.N., Faruk, M.O., Ashaduzzaman, M. and Dungani, R. Review on tannins: Extraction processes, applications and possibilities. *South African Journal of Botany*. 2020, **135**, pp.58-70.
489. Feng, S., Cheng, S., Yuan, Z., Leitch, M. and Xu, C. Valorization of bark for chemicals and materials: A review. *Renewable and Sustainable Energy Reviews*. 2013, **26**, pp.560-578.
490. Ruiz-Aquino, F., Feria-Reyes, R., Rutiaga-Quiñones, J.G., Robledo-Taboada, L.H. and Gabriel-Parra, R. Characterization of tannin extracts derived from the bark of four tree species by HPLC and FTIR. *Forest Science and Technology*. 2023, **19**(1), pp.38-46.
491. Ding, T., Bianchi, S., Ganne-Chedeville, C., Kilpelainen, P., Haapala, A. and Raty, T. Life cycle assessment of tannin extraction from spruce bark. *iForest - Biogeosciences and Forestry*. 2017, **10**(5), pp.807-814.
492. Sartori, C., Mota, G.D., Miranda, I., Mori, F. and Pereira, H. Tannin Extraction and Characterization of Polar Extracts from the Barks of Two Eucalyptus urophylla Hybrids. *BioResources*. 2018, **13**, pp.4820-4831.
493. Davey. *Why Is Bark Falling Off My Tree (Oak, Pine, Ash, Maple)?* [Online]. 2022. [Accessed]. Available from: <https://blog.davey.com/>
494. Murphy, G. *In-forest debarking: a review of the literature*. 2020.
495. V, D. *Why Remove Bark From a Log? How to Debark a Log with a Chainsaw Tool*. [Online]. 2024. [Accessed]. Available from: <https://www.powerequipmentdirect.com/>
496. Adhikari, S. and Ozarska, B. Minimizing environmental impacts of timber products through the production process “From Sawmill to Final Products”. *Environmental Systems Research*. 2018, **7**.
497. Ramasamy, G., Ratnasingam, J., Bakar, E., Halis, R. and Muttiah, N. Assessment of Environmental Emissions from Sawmilling Activity in Malaysia. *BioResources*. 2015, **10**, pp.6643-6662.

498. Venkatesan, T., Choi, Y.W. and Kim, Y.K. Impact of Different Extraction Solvents on Phenolic Content and Antioxidant Potential of *Pinus densiflora* Bark Extract. *Biomed Res Int*. 2019, **2019**, p.3520675.
499. Lopes, P.J.G., Calegari, L., de Medeiros Silva, W.A., Gatto, D.A., de Medeiros Neto, P.N., de Melo, R.R., Bakke, I.A., de Avila Delucis, R. and Missio, A.L. Tannin-based extracts of *Mimosa tenuiflora* bark: features and prospecting as wood adhesives. *Applied Adhesion Science*. 2021, **9**(1), p.3.
500. Raitanen, J.E., Järvenpää, E., Korpinen, R., Mäkinen, S., Hellström, J., Kilpeläinen, P., Liimatainen, J., Ora, A., Tupasela, T. and Jyske, T. Tannins of Conifer Bark as Nordic Piquancy-Sustainable Preservative and Aroma? *Molecules*. 2020, **25**(3).
501. Butor Skulcova, A., Hascicova, Z., Hrdlička, L., Sima, J. and Jablonsky, M. Green solvents based on choline chloride for the extraction of spruce bark (*Picea abies*). *Cellulose Chemistry and Technology*. 2018, **52**.
502. Baldosano, H.Y.C., Ma. Beatriz Micaela G; Elloran, Chantal Danica H; Bacani, Florinda T. Effect of Particle Size, Solvent and Extraction Time on Tannin Extract from *Spondias purpurea* Bark Through Soxhlet Extraction. In: *DLSU Research Congress 2015, De La Salle University, Manila, Philippines*. 2015.
503. Zeppetbauer, F., Süß, R., Nadányi, R., Putz, R.F., Lisý, A., Paulik, C., Šurina, I., Stržincová, P., Huemer, K. and Kamm, B. Environmentally Friendly Extraction from *Picea Abies* Bark as an Approach to Accessing Valuable Antioxidants in Biorefineries. *Processes*. 2023, **11**(7), p.2145.
504. Kwan, I., Huang, T., Ek, M., Seppänen, R. and Skagerlind, P. Bark from Nordic tree species – a sustainable source for amphiphilic polymers and surfactants. *Nordic Pulp & Paper Research Journal*. 2022, **37**(4), pp.566-575.
505. Salem, M.Z.M.N., R.A.; Zeidler, A.; Elansary, H.O; Aref, I.M.; Bohm, M.; Ali, H.M/; Ahmed, A.I. Methylated fatty acids from heartwood and bark of *Pinus sylvestris*, *Abies alba*, *Picea abies*, and *Larix decidua*: Effect of strong acid treatment. *BioResources*. 2015, **10**(4), pp.7715-7724.
506. Ribechini, E., Bacchiocchi, M., Deviese, T. and Colombini, M.P. Analytical pyrolysis with in situ thermally assisted derivatisation, Py(HMDS)-GC/MS, for the chemical characterization of archaeological birch bark tar. *Journal of Analytical and Applied Pyrolysis*. 2011, **91**(1), pp.219-223.
507. Gopalakrishnan, G., Burken, J.G. and Werth, C.J. Lignin and Lipid Impact on Sorption and Diffusion of Trichloroethylene in Tree Branches for Determining Contaminant Fate during Plant Sampling and Phytoremediation. *Environmental Science & Technology*. 2009, **43**(15), pp.5732-5738.
508. Marques, A.V. and Pereira, H. Aliphatic bio-oils from corks: A Py–GC/MS study. *Journal of Analytical and Applied Pyrolysis*. 2014, **109**, pp.29-40.
509. Lourenço, A.G., Jorge; Pereira, Helena. Chemical Characterization of Lignocellulosic Materials by Analytical Pyrolysis. In: Kusch, P. ed. *Analytical Pyrolysis*. Rijeka, Croatia: IntechOpen, 2019, p.Ch. 2.
510. Morar, I.M., Stefan, R., Dan, C., Sestras, R.E., Truta, P., Medeleanu, M., Ranga, F., Sestras, P., Truta, A.M. and Sestras, A.F. FT-IR and HPLC

- analysis of silver fir (*Abies alba* Mill.) bark compounds from different geographical provenances. *Heliyon*. 2024, **10**(5).
511. Bastien, J.-C. *Douglas-fir biomass production and carbon sequestration. 4.2. Douglas-fir – an option for Europe*. European Forest Institute, 2019.
  512. Gil-Moreno, D. *Potential of noble fir, Norway spruce, western red cedar and western hemlock grown for timber production in Great Britain*. Doctor of Philosophy thesis, Edinburgh Napier University, 2018.
  513. Pretzsch, H., Biber, P., Schütze, G., Uhl, E. and Rötzer, T. Forest stand growth dynamics in Central Europe have accelerated since 1870. *Nature Communications*. 2014, **5**, p.4967.
  514. Vangeel, T., Neiva, D., Quilhó, T., Costa, R., Sousa, V., Sels, B. and Pereira, H. Tree bark characterization envisioning an integrated use in a biorefinery. *Biomass Conversion and Biorefinery*. 2021, **13**.
  515. Edwardson, C.F.S., Christopher. *Birch bark pelletization and methods for obtaining natural products from birch bark pellets*. 2007.
  516. Erdem, R.K., Ismail; Cobanoglu, Hatice; Sevik, Hakan. Variation of Magnesium, One of the Macronutrients, in Some Trees Based on Organs and Species. *Forestist*. 2024.
  517. Krutul, D., Zielenkiewicz, T., Radomski, A., Zawadzki, J., Antczak, A., Drożdżek, M. and Makowski, T. Metals accumulation in Scots pine (*Pinus sylvestris* L.) wood and bark affected with environmental pollution. *Wood research*. 2017, **62**, pp.353-364.
  518. Au, J., Youngentob, K.N., Clark, R.G., Phillips, R. and Foley, W.J. Bark chewing reveals a nutrient limitation of leaves for a specialist folivore. *Journal of Mammalogy*. 2017, **98**(4), pp.1185-1192.
  519. Matsuo, M., Kobayashi, T., Singh, T.B., Tsurumi, M. and Ichikuni, M. 57Fe Mössbauer spectroscopic study of Japanese cedar bark — The variation in chemical states of iron due to influence of human activities. *Hyperfine Interactions*. 1992, **71**(1), pp.1255-1258.
  520. Bojórquez-Quintal, E., Escalante-Magaña, C., Echevarría-Machado, I. and Martínez-Estévez, M. Aluminum, a Friend or Foe of Higher Plants in Acid Soils. *Frontiers in Plant Science*. 2017, **8**, p.1767.
  521. Čabalová, I., Bélik, M., Kučerová, V. and Jurčyková, T. Chemical and Morphological Composition of Norway Spruce Wood (*Picea abies*, L.) in the Dependence of Its Storage. *Polymers (Basel)*. 2021, **13**(10).
  522. Siegrist, R.L. Volatile organic compounds in contaminated soils: The nature and validity of the measurement process. *Journal of Hazardous Materials*. 1991, **29**(1), pp.3-15.
  523. Radačovská, L., Holubčík, M., Nosek, R. and Jandačka, J. Influence of Bark Content on Ash Melting Temperature. *Procedia Engineering*. 2017, **192**, pp.759-764.
  524. Singhal, A., Goel, A., Bhatnagar, A., Roslander, C., Wallberg, O., Konttinen, J. and Joronen, T. Improving inorganic composition and ash fusion behavior of spruce bark by leaching with water, acetic acid, and steam pre-treatment condensate. *Chemical Engineering Journal*. 2023, **452**, p.139351.
  525. Ritchie, H. *Forest area*. [Online]. 2021. [Accessed]. Available from: <https://ourworldindata.org/>

526. Maxwell, S. *Tools and Resources: Woodland Statistics*. [Online]. 2023. [Accessed]. Available from: <https://www.forestresearch.gov.uk>
527. Ministry of Agriculture, N.a.F.Q. *Protected nature areas*. [Online]. 2024. [Accessed May 10th]. Available from: <https://www.government.nl/topics/>
528. Ren, X.G., J; Wang, W; Li, Q; Chang, J; Li, B. Optimization of bark fast pyrolysis for the production of phenol-rich bio-oil. *BioResources*. 2013, **8**(4).
529. Jones, J.M., Heineman, K.D. and Dalling, J.W. Soil and species effects on bark nutrient storage in a premontane tropical forest. *Plant and Soil*. 2019, **438**(1), pp.347-360.
530. Terzopoulou, P., Kamperidou, V. and Lykidis, C. Cypress Wood and Bark Residues Chemical Characterization and Utilization as Fuel Pellets Feedstock. *Forests*. 2022, **13**(8), p.1303.
531. Özgenç Keleş, Ö., Durmaz, S. and Kuştaş, S. Chemical Analysis of Tree Barks using ATR-FTIR Spectroscopy and Conventional Techniques. *BioResources*. 2017, **12**, pp.9143-9151.
532. Räisänen, T. and Athanassiadis, D. Basic chemical composition of the biomass components of pine, spruce and birch. In, 2013.
533. Custodis, V.B.F., Hemberger, P., Ma, Z. and van Bokhoven, J.A. Mechanism of Fast Pyrolysis of Lignin: Studying Model Compounds. *The Journal of Physical Chemistry B*. 2014, **118**(29), pp.8524-8531.
534. Jeenpadiphat, S., Mongkolpichayarak, I. and Tungasmita, D.N. Catechol production from lignin by Al-doped mesoporous silica catalytic cracking. *Journal of Analytical and Applied Pyrolysis*. 2016, **121**, pp.318-328.
535. Serra, O. and Geldner, N. The making of suberin. *New Phytologist*. 2022, **235**(3), pp.848-866.
536. Lee, N.-H., Lee, S.-M., Lee, T.-M., Chung, N. and Lee, H.-S. GC-MS Analyses of the Essential Oils Obtained from Pinaceae Leaves in Korea. *Journal of Essential Oil Bearing Plants*. 2015, **18**(3), pp.538-542.
537. Garneau, F.-X., Collin, G., Gagnon, H. and Pichette, A. Chemical Composition of the Hydrosol and the Essential Oil of Three Different Species of the Pinaceae Family : *Picea glauca* (Moench) Voss., *Picea mariana* (Mill.) B.S.P., and *Abies balsamea* (L.) Mill. *Journal of Essential Oil Bearing Plants*. 2012, **15**(2), pp.227-236.
538. Karapandzova, M., Stefkov, G., Cvetkovikj, I., Trajkovska-Dokik, E., Kaftandzieva, A. and Kulevanova, S. Chemical Composition and Antimicrobial Activity of the Essential Oils of *Pinus peuce* (Pinaceae) Growing Wild in R. Macedonia. *Natural Product Communications*. 2014, **9**(11), p.1934578X1400901124.
539. Teh, J.S., Teoh, Y.H., How, H.G. and Sher, F. Thermal Analysis Technologies for Biomass Feedstocks: A State-of-the-Art Review. *Processes*. 2021, **9**(9), p.1610.
540. Naron, D.R. *Catalytic Pyrolysis Conversion of Lignin from Different Sources to Phenols*. Doctor of Philosophy thesis, Stellenbosch University, 2019.
541. Jindo, K., Goron, T.L., Kurebito, S., Matsumoto, K., Masunaga, T., Mori, K., Miyakawa, K., Nagao, S. and Tokunari, T. Sustainable Plant Growth Promotion and Chemical Composition of Pyroligneous Acid When Applied with Biochar as a Soil Amendment. *Molecules*. 2022, **27**(11).

542. Kuo, C.-Y., Schelz, Z., Tóth, B., Vasas, A., Ocsovszki, I., Chang, F.-R., Hohmann, J., Zupkó, I. and Wang, H.-C. Investigation of natural phenanthrenes and the antiproliferative potential of juncusol in cervical cancer cell lines. *Phytomedicine*. 2019, **58**, p.152770.
543. Hasheminejad, S., Moradi, H. and Soleimani, M. Potential of Pinus eldarica Medw. tree bark for biomonitoring polycyclic aromatic hydrocarbons in ambient air. *Scientific Reports*. 2024, **14**(1), p.6259.
544. Hickey, D.T., Hayes, D.J., Pembroke, J.T., Ryan, M.P. and Leahy, J.J. The Importance of Extraction Protocol on the Analysis of Novel Waste Sources of Lignocellulosic Biomass. *Energies*. 2021, **14**(19), p.6406.
545. Abdelhamid, S.A., El-Shatoury, E.H., Asker, M.S., Abd-El-Aal, S.K. and Mohamed, S.S. Hydrolysis of Cellulose Rich Agricultural Waste Using Two Potent Local Bacterial Isolates. *Proceedings of the National Academy of Sciences, India Section B: Biological Sciences*. 2023, **93**(1), pp.225-234.
546. Poulsen, J.S., Macêdo, W.V., Bonde, T. and Nielsen, J.L. Energetically exploiting lignocellulose-rich residues in anaerobic digestion technologies: from bioreactors to proteogenomics. *Biotechnology for Biofuels and Bioproducts*. 2023, **16**(1), p.183.
547. IRENA. *Bioethanol*. [Online]. 2022. [Accessed 12th May]. Available from: <https://www.irena.org/>
548. Redfern, J., Kinninmonth, M., Burdass, D. and Verran, J. Using soxhlet ethanol extraction to produce and test plant material (essential oils) for their antimicrobial properties. *J Microbiol Biol Educ*. 2014, **15**(1), pp.45-46.
549. Willemin, C.R., Geoffroy; Moreno, Angeles Fonolla; Lemoine, Cyril. *Composition containing a Phenanthrenol*. 2008.
550. Ogunwande, I. and Oladosu, I. Anticandidal activity of phenanthrenol from *Blighia sapida* Koenig (Sapindaceae). *Der Pharmacia Lettre*. 2011, **3**, pp.221-227.
551. Kwofie, M. and Gupta, M. Phenanthrene: A versatile molecule; A review. *PLANT ARCHIVES*. 2021, **21**.
552. Li, J., Feng, W., Dai, R. and Li, B. Recent Progress on the Identification of Phenanthrene Derivatives in Traditional Chinese Medicine and Their Biological Activities. *Pharmacological Research - Modern Chinese Medicine*. 2022, **3**, p.100078.
553. Malipeddi, H., Das, P. and Karigar, A. Green technique-solvent free synthesis and its advantages. *IJRAP*. 2011, **2**, pp.1079-1086.
554. Gladysz, J.A. Reaction: Toward Organic-Solvent-free Synthetic Chemistry. *Chem*. 2018, **4**(9), pp.2007-2008.
555. Tan, D. and García, F. Main group mechanochemistry: from curiosity to established protocols. *Chemical Society Reviews*. 2019, **48**(8), pp.2274-2292.
556. Ye, Z. and Ouyang, D. Prediction of small-molecule compound solubility in organic solvents by machine learning algorithms. *J Cheminform*. 2021, **13**(1), p.98.
557. Tantardini, C. and Oganov, A.R. Author Correction: Thermochemical electronegativities of the elements. *Nature Communications*. 2021, **12**(1), p.4406.

558. Rossini, E. and Knapp, E.-W. Erratum: Proton solvation in protic and aprotic solvents [J. Comput. Chem. 2015, 37, 1082–1091]. *Journal of Computational Chemistry*. 2016, **37**(23), pp.2163-2164.
559. Gao, F., Chang, H., Li, J., Wang, R. and Gu, Y. Replacing polar aprotic solvents with water in organic synthesis. *Current Opinion in Green and Sustainable Chemistry*. 2023, **40**, p.100774.
560. Shimizu, K. *Classification of Solvents*. [Online]. 2022. [Accessed 23rd June]. Available from: <https://shimizu-uofsc.net/>
561. Zohuri, B. and Behgounia, F. Chapter 8 - Application of artificial intelligence driving nano-based drug delivery system. In: Philip, A. Shahiwala, A. Rashid, M. Faiyazuddin, M. eds. *A Handbook of Artificial Intelligence in Drug Delivery*. Academic Press, 2023, pp.145-212.
562. Gani, R., Jiménez-González, C. and Constable, D.J.C. Method for selection of solvents for promotion of organic reactions. *Computers & Chemical Engineering*. 2005, **29**(7), pp.1661-1676.
563. Ijardar, S.P., Singh, V. and Gardas, R.L. Revisiting the Physicochemical Properties and Applications of Deep Eutectic Solvents. *Molecules*. 2022, **27**(4), p.1368.
564. Kumar, V.K., Joonam. *What are important factors to select the solvent?* [Online]. 2015. [Accessed 23rd June]. Available from: <https://www.researchgate.net/>
565. Alfonsi, K., Colberg, J., Dunn, P.J., Fevig, T., Jennings, S., Johnson, T.A., Kleine, H.P., Knight, C., Nagy, M.A., Perry, D.A. and Stefaniak, M. Green chemistry tools to influence a medicinal chemistry and research chemistry based organisation. *Green Chemistry*. 2008, **10**(1), pp.31-36.
566. Prat, D., Pardigon, O., Flemming, H.-W., Letestu, S., Ducandas, V., Isnard, P., Guntrum, E., Senac, T., Ruisseau, S., Cruciani, P. and Hosek, P. Sanofi's Solvent Selection Guide: A Step Toward More Sustainable Processes. *Organic Process Research & Development*. 2013, **17**(12), pp.1517-1525.
567. Diorazio, L.J., Hose, D.R.J. and Adlington, N.K. Toward a More Holistic Framework for Solvent Selection. *Organic Process Research & Development*. 2016, **20**(4), pp.760-773.
568. Alder, C.M., Hayler, J.D., Henderson, R.K., Redman, A.M., Shukla, L., Shuster, L.E. and Sneddon, H.F. Updating and further expanding GSK's solvent sustainability guide. *Green Chemistry*. 2016, **18**(13), pp.3879-3890.
569. Byrne, F.P., Jin, S., Paggiola, G., Petchey, T.H.M., Clark, J.H., Farmer, T.J., Hunt, A.J., Robert McElroy, C. and Sherwood, J. Tools and techniques for solvent selection: green solvent selection guides. *Sustainable Chemical Processes*. 2016, **4**(1), p.7.
570. Ashcroft, C.P., Dunn, P.J., Hayler, J.D. and Wells, A.S. Survey of Solvent Usage in Papers Published in Organic Process Research & Development 1997–2012. *Organic Process Research & Development*. 2015, **19**(7), pp.740-747.
571. Stengel, J.P., Lehr, A.L., Aboagye, E.A., Chea, J.D. and Yenkie, K.M. Development of an Interactive Software Tool for Designing Solvent Recovery Processes. *Ind Eng Chem Res*. 2023, **62**(5), pp.2090-2103.

572. Shi, Q. and Liu, W.H. Reactivity Umpolung of Amides in Organic Synthesis. *Asian Journal of Organic Chemistry*. 2023, **12**(12), p.e202300473.
573. Davis, M.C., Fedick, P.W., Lupton, D.V., Ostrom, G.S., Quintana, R. and Woodroffe, J.D. Solubility of hydrocarbon oils in alcohols ( $\leq C(6)$ ) and synthesis of difusel carbonate for degreasing. *RSC Adv*. 2019, **9**(40), pp.22891-22899.
574. Sicaire, A.-G., Vian, M., Fine, F., Joffre, F., Carré, P., Tostain, S. and Chemat, F. Alternative Bio-Based Solvents for Extraction of Fat and Oils: Solubility Prediction, Global Yield, Extraction Kinetics, Chemical Composition and Cost of Manufacturing. 2015, **16**(4), pp.8430-8453.
575. Virost, M., Tomao, V., Ginies, C. and Chemat, F. Total Lipid Extraction of Food Using d-Limonene as an Alternative to n-Hexane. *Chromatographia*. 2008, **68**(3), pp.311-313.
576. Abbot, S.H., Charles; Yamamoto, Hiroshi. *HSPiP Datasets*. [Online]. 2024. [Accessed June 24th]. Available from: <https://www.hansen-solubility.com/HSPiP/datasets.php>
577. Vimala, M., Stella Mary, S., Ramalakshmi, R., Muthu, S. and Irfan, A. Computational prediction of polar and non-polar solvent effect on the electronic property of N-BOC- Piperidine-4-Carboxylic acid. *Journal of Molecular Liquids*. 2021, **341**, p.117222.
578. Scientific, T. *Solvents*. [Online]. 2024. [Accessed July 23rd]. Available from: <https://www.thermofisher.in/>
579. Anon. *Nonpolar Solvents in Nature of Solvents*. [Online]. 2024. [Accessed]. Available from: <https://www.studocu.com/>
580. Ashenhurst, J. *Polar Protic? Polar Aprotic? Nonpolar? All About Solvents*. [Online]. 2022. [Accessed]. Available from: <https://www.masterorganicchemistry.com/>
581. Sollai, S., Porcu, A., Tola, V., Ferrara, F. and Pettinau, A. Renewable methanol production from green hydrogen and captured CO<sub>2</sub>: A techno-economic assessment. *Journal of CO<sub>2</sub> Utilization*. 2023, **68**, p.102345.
582. Hasegawa, F., Yokoyama, S. and Imou, K. Methanol or ethanol produced from woody biomass: Which is more advantageous? *Bioresource Technology*. 2010, **101**(1, Supplement), pp.S109-S111.
583. Zaborniak, I., Klamut, M., Warne, C.M., Kisiel, K., Niemiec, M., Błoniarz, P., Pellis, A., Matyjaszewski, K. and Chmielarz, P. Controlled Polymer Synthesis Toward Green Chemistry: Deep Insights into Atom Transfer Radical Polymerization in Biobased Substitutes for Polar Aprotic Solvents. *ACS Sustainable Chemistry & Engineering*. 2024, **12**(12), pp.4933-4945.
584. Sherwood, J., De bruyn, M., Constantinou, A., Moity, L., McElroy, C.R., Farmer, T.J., Duncan, T., Raverty, W., Hunt, A.J. and Clark, J.H. Dihydrolevoglucosenone (Cyrene) as a bio-based alternative for dipolar aprotic solvents. *Chemical Communications*. 2014, **50**(68), pp.9650-9652.
585. Zhang, J., White, G.B., Ryan, M.D., Hunt, A.J. and Katz, M.J. Dihydrolevoglucosenone (Cyrene) As a Green Alternative to N,N-Dimethylformamide (DMF) in MOF Synthesis. *ACS Sustainable Chemistry & Engineering*. 2016, **4**(12), pp.7186-7192.
586. Sauer, M. Industrial production of acetone and butanol by fermentation-100 years later. *FEMS Microbiol Lett*. 2016, **363**(13).

587. Kumar, A., Anushree, Kumar, J. and Bhaskar, T. Utilization of lignin: A sustainable and eco-friendly approach. *Journal of the Energy Institute*. 2020, **93**(1), pp.235-271.
588. Van Nam, H., Viet, D.Q., Tam, T.T. and Tho, V.D.S. Chemical composition of pyrolysis oil through thermal decomposition of sugarcane biomass. *Vietnam Journal of Chemistry*. 2020, **58**(6), pp.770-778.
589. Balagurumurthy, B. and Bhaskar, T. Hydropyrolysis of lignocellulosic biomass: state of the art review. *Biomass Conversion and Biorefinery*. 2014, **4**(1), pp.67-75.
590. Urland, T.S., Bryan. *Performance Solvents for the Pharmaceutical Industry*. [Online]. 2024. [Accessed 23rd June]. Available from: <https://www.haltermann-carless.com/>
591. Evans, W.C. and Evans, D. Chapter 22 - Volatile oils and resins. In: Evans, W.C. and Evans, D. eds. *Trease and Evans' Pharmacognosy (Sixteenth Edition)*. W.B. Saunders, 2009, pp.263-303.
592. Wildschut, J. Pyrolysis oil upgrading to transportation fuels by catalytic hydrotreatment. In, 2009.
593. Bu, C., Qiao, H., Zou, L., Tao, Y., Fu, J., Liu, C., Zheng, Z. and Ouyang, J. Hydrogenation of biomass pyrolysis oil using enhanced reduction catalytic capacity cellular by expressing excavated carbonyl reductase. *Fuel*. 2023, **332**, p.126108.
594. Struhs, E., Hansen, S., Mirkouei, A., Ramirez-Corredores, M.M., Sharma, K., Spiers, R. and Kalivas, J.H. Ultrasonic-assisted catalytic transfer hydrogenation for upgrading pyrolysis-oil. *Ultrason Sonochem*. 2021, **73**, p.105502.
595. Zhang, M., Pjontek, D., Wang, H., Liu, M., Han, X., Zeng, Y. and Xu, C. Upgrading Fast Pyrolysis Oil with Vacuum Gas Oil by Catalytic Hydrodeoxygenation in Supercritical Ethanol. *Energy & Fuels*. 2024, **38**(11), pp.9794-9803.
596. Venderbosch, R.H. and Heeres, H.J. Pyrolysis Oil Stabilisation by Catalytic Hydrotreatment. In: Marco Aurélio dos Santos, B. ed. *Biofuel's Engineering Process Technology*. Rijeka: IntechOpen, 2011, p.Ch. 17.
597. Catizane, C., Jiang, Y. and Sumner, J. Improving plastic pyrolysis oil quality via an electrochemical process for polymer recycling: a review. *Energy Advances*. 2024, **3**(2), pp.366-388.
598. Mansur, D., Sugiwati, S., Rizal, W.A., Suryani, R. and Maryana, R. Pyrolysis of cajuput (*Melaleuca leucadendron*) twigs and rice (*Oryza sativa*) husks to produce liquid smoke-containing fine chemicals for antibacterial agent application. *Biomass Conversion and Biorefinery*. 2023, **13**(12), pp.10561-10574.
599. Bestonrecycling. *Application of Plastic Pyrolysis Oil*. [Online]. 2024. [Accessed July 23rd]. Available from: <https://medium.com/>
600. Kirkwood, K. and Jackson, S.D. Competitive Hydrogenation and Hydrodeoxygenation of Oxygen-Substituted Aromatics over Rh/Silica: Catechol, Resorcinol and Hydroquinone. *Topics in Catalysis*. 2021, **64**(17), pp.934-944.
601. Chen, X., Zhang, L., Zhang, B., Guo, X. and Mu, X. Highly selective hydrogenation of furfural to furfuryl alcohol over Pt nanoparticles supported

- on g-C<sub>3</sub>N<sub>4</sub> nanosheets catalysts in water. *Scientific Reports*. 2016, **6**(1), p.28558.
602. Zaman, S., Bamufleh, H.S., Al-Zahrani, A., Ahmed Rafiqui, M., Alhamed, Y. and Petrov, L. Acetic acid hydrogenation over silica supported MoP catalyst. *Comptes Rendus de L'Academie Bulgare des Sciences*. 2018, **71**, pp.29-37.
603. Alshehri, F., Feral, C., Kirkwood, K. and Jackson, S.D. Low temperature hydrogenation and hydrodeoxygenation of oxygen-substituted aromatics over Rh/silica: part 1: phenol, anisole and 4-methoxyphenol. *Reaction Kinetics, Mechanisms and Catalysis*. 2019, **128**(1), pp.23-40.
604. Martínez-Klimov, M.E., Yevdokimova, O., Mäki-Arvela, P., Cueto, J., Shcherban, N., Vajglová, Z., Eränen, K. and Murzin, D.Y. Hydrodeoxygenation of isoeugenol in continuous mode using bifunctional Pt-Beta 25-binder catalysts for renewable jet fuel production. *Sustainable Energy & Fuels*. 2024, **8**(1), pp.90-102.
605. Bissantz, C., Kuhn, B. and Stahl, M. A medicinal chemist's guide to molecular interactions. *J Med Chem*. 2010, **53**(14), pp.5061-5084.
606. Palusiak, M. and Grabowski, S.J. Methoxy group as an acceptor of proton in hydrogen bonds. *Journal of Molecular Structure*. 2002, **642**(1), pp.97-104.
607. Properties of Alcohols and Phenols.
608. Singh, A.K. Chapter 2 - Structure, Synthesis, and Application of Nanoparticles. In: Singh, A.K. ed. *Engineered Nanoparticles*. Boston: Academic Press, 2016, pp.19-76.
609. Ducháčková, L., Kadlčíková, A., Kotora, M. and Roithová, J. Oxygen Superbases as Polar Binding Pockets in Nonpolar Solvents. *Journal of the American Chemical Society*. 2010, **132**(36), pp.12660-12667.
610. Abbot, S.H., Charles; Yamamoto, Hiroshi. *The HSP Sphere*. [Online]. 2024. [Accessed 23rd July]. Available from: <https://www.hansen-solubility.com/HSP-science/sphere.php>
611. PubChem. *m-Cresol*. [Online]. 2024. [Accessed 23rd July]. Available from: <https://pubchem.ncbi.nlm.nih.gov/>
612. Separations, M.I. *Dehydration of Tetrahydrofuran*. [Online]. 2024. [Accessed July 23rd]. Available from: <https://www.mtrinc.com/>
613. Regensis. *Methylene Chloride*. [Online]. 2023. [Accessed July 23rd]. Available from: <https://regensis.com/>
614. ITRC. *1,4-Dioxane: History of Use and Potential Sources*. [Online]. 2021. [Accessed July 23rd]. Available from: [www.itrcweb.org](http://www.itrcweb.org).
615. Pauli, G.F., Chen, S.N., Simmler, C., Lankin, D.C., Gödecke, T., Jaki, B.U., Friesen, J.B., McAlpine, J.B. and Napolitano, J.G. Importance of purity evaluation and the potential of quantitative <sup>1</sup>H NMR as a purity assay. *J Med Chem*. 2014, **57**(22), pp.9220-9231.
616. Robles, H. Furan. In: Wexler, P. ed. *Encyclopedia of Toxicology (Fourth Edition)*. Oxford: Academic Press, 2024, pp.875-879.
617. MERCK. *Solvent Stabilizer Systems*. [Online]. 2024. [Accessed July 23rd]. Available from: <https://www.sigmaaldrich.com/>
618. Bušić, A., Mardetko, N., Kundas, S., Morzak, G., Belskaya, H., Ivančić Šantek, M., Komes, D., Novak, S. and Šantek, B. Bioethanol Production from Renewable Raw Materials and Its Separation and Purification: A Review. *Food Technol Biotechnol*. 2018, **56**(3), pp.289-311.

619. Fontes, S.T., Fernández, M.R., Ogliari, F.A., de Carvalho, R.V., de Moraes, R.R., Pinto, M.B. and Piva, E. Tetrahydrofuran as solvent in dental adhesives: cytotoxicity and dentin bond stability. *Clinical Oral Investigations*. 2013, **17**(1), pp.237-242.
620. Said, I. *1,3-Dioxolane*. [Online]. 2013. [Accessed July 23rd].
621. BAUA. *Substance Evaluation Conclusion as required by REACH Article 48 and Evaluation Report for 1,3-dioxolane*. Federal Institute for Occupational Safety and Health, 2022.
622. OPES. Methylene Chloride. 2024.
623. Kumar, S.P.J., Prasad, S.R., Banerjee, R., Agarwal, D.K., Kulkarni, K.S. and Ramesh, K.V. Green solvents and technologies for oil extraction from oilseeds. *Chem Cent J*. 2017, **11**, p.9.
624. EPA. *Fact Sheet: N-Methylpyrrolidone (NMP)*. [Online]. 2015. [Accessed 23rd July]. Available from: <https://www.epa.gov/>
625. Book, C. *Uses of Furan*. [Online]. 2022. [Accessed 23rd July]. Available from: <https://www.chemicalbook.com/>
626. Benítez, J.J., Ramírez-Pozo, M.C., Durán-Barrantes, M.M., Heredia, A., Tedeschi, G., Ceseracciu, L., Guzman-Puyol, S., Marrero-López, D., Becci, A., Amato, A. and Heredia-Guerrero, J.A. Bio-based lacquers from industrially processed tomato pomace for sustainable metal food packaging. *Journal of Cleaner Production*. 2023, **386**, p.135836.
627. Corporation, B. *1,3-Dioxolane*. [Online]. 2024. [Accessed July 23rd]. Available from: <https://www.ulprospector.com/>
628. FisherScientific. *Tetrahydrofuran*. [Online]. 2024. [Accessed].
629. Clifton, J. What is Tetrahydrofuran (THF)? 2019. [Online]. Available from: <https://www.chemicals.co.uk/>
630. Monticelli, F. Diethyl Ether. In: Wexler, P. ed. *Encyclopedia of Toxicology (Third Edition)*. Oxford: Academic Press, 2014, pp.138-139.
631. Radu Dan, R. and Marc, J.M.A. New High-Performance Materials: Bio-Based, Eco-Friendly Polyimides. In: Sombel, D. ed. *Polyimide for Electronic and Electrical Engineering Applications*. Rijeka: IntechOpen, 2020, p.Ch. 15.
632. Sargent, M.V. and Dean, F.M. 3.11 - Furans and their Benzo Derivatives: (ii) Reactivity. In: Katritzky, A.R. and Rees, C.W. eds. *Comprehensive Heterocyclic Chemistry*. Oxford: Pergamon, 1984, pp.599-656.
633. ChemEurope. *Diethyl ether*. [Online]. 2024. [Accessed 23rd July].
634. Jahangiri, F., Mohanty, A.K. and Misra, M. Sustainable biodegradable coatings for food packaging: challenges and opportunities. *Green Chemistry*. 2024, **26**(9), pp.4934-4974.
635. Thakre, D.D., Darsha; Mehar, Chetan; Mungmode, Nikesh; Khobragde, Jayesh; Mustkim, Md; Ghosh, Siddharth. A Review on Metal Cleaning. *Journal for Research in Applied Science and Engineering Technology*. 2021, **9**(1).
636. Tan, K.A., Mohan, Y., Liew, K.J., Chong, S.H. and Poh, P.E. Development of an effective cleaning method for metallic parts using microbubbles. *Journal of Cleaner Production*. 2020, **261**, p.121076.
637. Zang, J. The Preparation and Test of Green Water-Based Metal Cleaning Agent. *Advanced Materials Research*. 2014, **1015**, pp.312-315.

638. MarketsAndMarkets. *Metal Cleaning Chemicals Market*. [Online]. 2022. [Accessed July 24th]. Available from: <https://www.marketsandmarkets.com/>
639. Shen, M.K., Sen; Heurung, Casey. *USDA-certified Biobased, Low VOC and Biodegradable Paint Stripper and Graffiti Remover*. NACE International, 2020.
640. ECHA. *Advice on how to comply with NMP restriction*. [Online]. 2019. [Accessed July 24th]. Available from: <https://echa.europa.eu/>
641. CORTEC. *Surface Preparation Products: EcoLine 4320/4330*. [Leaflet]. Minnesota, 2018.
642. Angerer, J.B., U; Chambers, C; Degen, G; Lilienblum, W; Nielsen, E; Rastogi, S C; Rogiers, V; Sanner, T; van Engelen, J; Waring, R; White, I R. *Opinion on Dichloromethane*. European Commission, 2022.
643. ECSA. *Product Safety Summary on Dichloromethane*. European Chlorinated Solvents Association, 2015.
644. IDEAL. *Ethanol for the Personal Care Industry*. [Online]. 2024. [Accessed July 23rd]. Available from: <https://www.idealchemical.com/>
645. ChemicalSafetyFacts. *Ammonia*. [Online]. 2023. [Accessed July 18th]. Available from: <https://www.chemicalsafetyfacts.org/>
646. Ryan, L. *Ammonia's Potential Role in a Low-Carbon Economy*. Congressional Research Service, 2022.
647. Jones, N. *From Fertilizer to Fuel: Can 'Green' Ammonia Be a Climate Fix?* [Online]. 2022. [Accessed July 18th]. Available from: <https://e360.yale.edu/>
648. Irfan, H.M., Iqbal, K., Taipabu, M.I., You, C.-Y., Mazumdar, D. and Wu, W. Decarbonization frameworks to industrial-scale ammonia production: Techno-economic and environmental implications. *International Journal of Hydrogen Energy*. 2024, **78**, pp.580-593.
649. David, B.A., Fraser; Bowen, Phil; Fowler, David; Irvine, John; Torrente Murciano, Laura. *Ammonia: Zero-carbon fertiliser, fuel and energy store*. The Royal Society, 2020.
650. GrandViewResearch. *Ammonia Market Size & Trends*. [Online]. 2022. [Accessed 18th July]. Available from: <https://www.grandviewresearch.com/>
651. ChemAnalyst. *Ammonia Market Analysis*. [Online]. 2023. [Accessed 18th July]. Available from: <https://www.chemanalyst.com/>
652. ByJu's. *Uses of Ammonia*. [Online]. 2020. [Accessed July 18th]. Available from: <https://byjus.com/>
653. Salonen, H., Salthammer, T., Castagnoli, E., Täubel, M. and Morawska, L. Cleaning products: Their chemistry, effects on indoor air quality, and implications for human health. *Environment International*. 2024, **190**, p.108836.
654. ChemAnalyst. *Exploring Ammonia: Applications, Manufacturing Techniques, and Major Market Players!* [Press release]. 2024. Available from: <https://www.linkedin.com/>
655. EasyChem. *Industrial Uses of Ammonia*. [Online]. 2012. [Accessed July 18th]. Available from: <https://easychem.com.au/>
656. DEFRA. *ENV01 - Emissions of air pollutants*. Department for Environment, Food & Rural Affairs, 2024.

657. Dechojarassri, D., Nishida, K., Ozakiya, R., Furuike, T. and Tamura, H. Adsorption Studies of Ammonia, Protein, and Phytic Acid Using Chitosan Fiber Coated with Oxidized Cellulose Nanofiber. *Fibers*. 2023, **11**(4), p.32.
658. Wang, B., Yang, C., Wang, H., Hu, D., Duan, B. and Wang, Y. Effects of combustion and emission performance of ammonia/natural gas engines ignited by diesel. *Fuel*. 2024, **358**, p.130323.
659. Bourzac, K. *Carbon-free fuels could have a dark side*. [Online]. 2023. [Accessed July 18th]. Available from: <https://www.science.org/>
660. Wang, B., Wang, H., Duan, B., Yang, C., Hu, D. and Wang, Y. Effect of ammonia/hydrogen mixture ratio on engine combustion and emission performance at different inlet temperatures. *Energy*. 2023, **272**, p.127110.
661. Friedmann, J. *Ammonia: Today's Imperative, Tomorrow's Promise*. [Online]. 2023. [Accessed]. Available from: <https://www.carbon-direct.com/>
662. Iberdrola. *Green ammonia: the sustainable revolution in the chemical industry*. [Online]. 2024. [Accessed July 18th]. Available from: <https://www.iberdrola.com/>
663. Le, T.T., Sharma, P., Bora, B.J., Tran, V.D., Truong, T.H., Le, H.C. and Nguyen, P.Q.P. Fueling the future: A comprehensive review of hydrogen energy systems and their challenges. *International Journal of Hydrogen Energy*. 2024, **54**, pp.791-816.
664. Fumoto, E.T., Teruoki; Masuda, Takao. Recovery of Ammonia and Ketones from Biomass Wastes. In: Syed Shahid, S. ed. *Progress in Biomass and Bioenergy Production*. Rijeka: IntechOpen, 2011, p.Ch. 15.
665. Ren, S., Huang, S. and Liu, B. Enhanced removal of ammonia nitrogen from rare earth wastewater by NaCl modified vermiculite: Performance and mechanism. *Chemosphere*. 2022, **302**, p.134742.
666. Chatain, M., Chretien, E., Crunaire, S. and Jantzem, E. Road Traffic and Its Influence on Urban Ammonia Concentrations (France). *Atmosphere*. 2022, **13**(7), p.1032.
667. Hansen, K., Pryor, S.C., Boegh, E., Hornsby, K.E., Jensen, B. and Sørensen, L.L. Background concentrations and fluxes of atmospheric ammonia over a deciduous forest. *Agricultural and Forest Meteorology*. 2015, **214-215**, pp.380-392.
668. Kuntke, P., Sleutels, T.H.J.A., Rodríguez Arredondo, M., Georg, S., Barbosa, S.G., ter Heijne, A., Hamelers, H.V.M. and Buisman, C.J.N. (Bio)electrochemical ammonia recovery: progress and perspectives. *Applied Microbiology and Biotechnology*. 2018, **102**(9), pp.3865-3878.
669. Aung, S.L., Choi, J., Cha, H., Woo, G. and Song, K.G. Ammonia-selective recovery from anaerobic digestate using electrochemical ammonia stripping combined with electrodialysis. *Chemical Engineering Journal*. 2024, **479**, p.147949.
670. Wang, R., Yang, K., Wong, C., Aguirre-Villegas, H., Larson, R., Brushett, F., Qin, M. and Jin, S. Electrochemical ammonia recovery and co-production of chemicals from manure wastewater. *Nature Sustainability*. 2024, **7**(2), pp.179-190.
671. Saltworks. *Ammonia Wastewater Treatment*. [Online]. 2024. [Accessed 18th July]. Available from: <https://www.saltworkstech.com/>

672. Kesari, K.K., Soni, R., Jamal, Q.M.S., Tripathi, P., Lal, J.A., Jha, N.K., Siddiqui, M.H., Kumar, P., Tripathi, V. and Ruokolainen, J. Wastewater Treatment and Reuse: a Review of its Applications and Health Implications. *Water, Air, & Soil Pollution*. 2021, **232**(5), p.208.
673. Gupta, V.K. and Saleh, T.A. Sorption of pollutants by porous carbon, carbon nanotubes and fullerene- An overview. *Environmental Science and Pollution Research*. 2013, **20**(5), pp.2828-2843.
674. Chen, M., Li, J., Zhang, J., Ma, Y., Dong, H., Li, W., Bekyarova, E., Al-Hadeethi, Y.F., Chen, L., Hedhili, M.N., Tian, B. and Zhang, X. Evolution of cellulose acetate to monolayer graphene. *Carbon*. 2021, **174**, pp.24-35.
675. Chen, M., Li, Z. and Chen, L. Highly antibacterial rGO/Cu<sub>2</sub>O nanocomposite from a biomass precursor: Synthesis, performance, and mechanism. *Nano Materials Science*. 2020, **2**(2), pp.172-179.
676. Chen, M., Yengel, E., Zhang, J., Zhu, C., He, X., Zhang, C., Huang, J.-K., Hedhili, M.N., Anthopoulos, T. and Zhang, X. One-step growth of reduced graphene oxide on arbitrary substrates. *Carbon*. 2019, **144**, pp.457-463.
677. Dai, Y., Sun, Q., Wang, W., Lu, L., Liu, M., Li, J., Yang, S., Sun, Y., Zhang, K., Xu, J., Zheng, W., Hu, Z., Yang, Y., Gao, Y., Chen, Y., Zhang, X., Gao, F. and Zhang, Y. Utilizations of agricultural waste as adsorbent for the removal of contaminants: A review. *Chemosphere*. 2018, **211**, pp.235-253.
678. Otero, G.S., Pascucci, B., Branda, M.M., Miotto, R. and Belelli, P.G. Evaluating the size of Fe nanoparticles for ammonia adsorption and dehydrogenation. *Computational Materials Science*. 2016, **124**, pp.220-227.
679. Zhao, Y.-l., Yang, W.-j., Zhou, J.-h., Wang, Z.-h., Liu, J.-z. and Cen, K.-f. Experimental study on ammonia adsorption by coal ashes. *Journal of Fuel Chemistry and Technology*. 2015, **43**(3), pp.266-272.
680. Haroon, M., Wang, L., Yu, H., Ullah, R.S., Zain ul, A., Khan, R.U., Chen, Q. and Liu, J. Synthesis of carboxymethyl starch-g-polyvinylpyrrolidones and their properties for the adsorption of Rhodamine 6G and ammonia. *Carbohydrate Polymers*. 2018, **186**, pp.150-158.
681. Furtado, A.M.B., Wang, Y. and LeVan, M.D. Carbon silica composites for sulfur dioxide and ammonia adsorption. *Microporous and Mesoporous Materials*. 2013, **165**, pp.48-54.
682. Wang, X., Sato, T. and Xing, B. Competitive Sorption of Pyrene on Wood Chars. *Environmental Science & Technology*. 2006, **40**(10), pp.3267-3272.
683. Cheng, C.-H., Lin, T.-P., Lehmann, J., Fang, L.-J., Yang, Y.-W., Menyailo, O.V., Chang, K.-H. and Lai, J.-S. Sorption properties for black carbon (wood char) after long term exposure in soils. *Organic Geochemistry*. 2014, **70**, pp.53-61.
684. Shen, Y. and Zhang, N. Facile synthesis of porous carbons from silica-rich rice husk char for volatile organic compounds (VOCs) sorption. *Bioresource Technology*. 2019, **282**, pp.294-300.
685. Wang, P., Tyndall, S., Rahman, T., Roy, P., Jahromi, H., Adhikari, S. and Boersma, M. Sorption and recovery of phenolic compounds from aqueous phase of sewage sludge hydrothermal liquefaction using bio-char. *Chemosphere*. 2022, **287**, p.131934.
686. Mohan, D., Pittman, C.U., Bricka, M., Smith, F., Yancey, B., Mohammad, J., Steele, P.H., Alexandre-Franco, M.F., Gómez-Serrano, V. and Gong, H.

- Sorption of arsenic, cadmium, and lead by chars produced from fast pyrolysis of wood and bark during bio-oil production. *Journal of Colloid and Interface Science*. 2007, **310**(1), pp.57-73.
687. Ramalingham, S. and Donipathi Mogili Reddy, P. Sorption of Heavy Metals onto Biochar. In: Ahmed, A.A. and Mohammed, H.H.A. eds. *Applications of Biochar for Environmental Safety*. Rijeka: IntechOpen, 2020, p.Ch. 13.
688. Hyder, A.H.M.G., Begum, S.A. and Egiebor, N.O. Sorption studies of Cr(VI) from aqueous solution using bio-char as an adsorbent. *Water Science and Technology*. 2014, **69**(11), pp.2265-2271.
689. Cheung, C.W., McKay, G. and Porter, J.F. The Removal of Metal Ions from Aqueous Solutions by Bone Char Sorption. In: Healy, M.Wise, D.L.Moo-Young, M. eds. *Environmental Monitoring and Biodiagnostics of Hazardous Contaminants*. Dordrecht: Springer Netherlands, 2001, pp.11-26.
690. Choung, S. and Allen-King, R.M. Can Chlorofluorocarbon Sorption to Black Carbon (Char) Affect Groundwater Age Determinations? *Environmental Science & Technology*. 2010, **44**(12), pp.4459-4464.
691. Dorward, C. *The Ammonia Sorption Capacity of Hydrochars from High Lignin Feedstocks: Potential applications within agriculture*. Unpublished, 2016.
692. Ro, K.S., Lima, I.M., Reddy, G.B., Jackson, M.A. and Gao, B. Removing Gaseous NH<sub>3</sub> Using Biochar as an Adsorbent. *Agriculture*. 2015, **5**(4), pp.991-1002.
693. Rong, R., Zheng, Y., Zhang, F., Yang, L. and Li, Z. The Effects of Different Types of Biochar on Ammonia Emissions during Co-composting Poultry Manure with a Corn Leaf. *Polish Journal of Environmental Studies*. 2019, **28**(5), pp.3837-3843.
694. He, Z., Cao, H., Liang, J., Hu, Q., Zhang, Y., Nan, X. and Li, Z. Effects of biochar particle size on sorption and desorption behavior of NH<sub>4</sub><sup>+</sup>-N. *Industrial Crops and Products*. 2022, **189**, p.115837.
695. Trazzi, P.A., Vashishtha, M., Najser, J., Schmalenberger, A., Kannuchamy, V.K., Leahy, J.J. and Kwapinski, W. Adsorption of Ammonium, Nitrate, and Phosphate on Hydrochars and Biochars. *Applied Sciences*. 2024, **14**(6), p.2280.
696. Ulusal, A., Apaydin Varol, E., Bruckman, V.J. and Uzun, B.B. Opportunity for sustainable biomass valorization to produce biochar for improving soil characteristics. *Biomass Conversion and Biorefinery*. 2021, **11**(3), pp.1041-1051.
697. RHS. *Biochar*. [Online]. 2024. [Accessed 26th May]. Available from: <https://www.rhs.org.uk/>
698. Tang, S., Wang, Z., Liu, Z., Zhang, Y. and Si, B. The Role of Biochar to Enhance Anaerobic Digestion: A Review. *Journal of Renewable Materials*. 2020, **8**, pp.1033-1052.
699. Cai, Y., Zhu, M., Meng, X., Zhou, J.L., Zhang, H. and Shen, X. The role of biochar on alleviating ammonia toxicity in anaerobic digestion of nitrogen-rich wastes: A review. *Bioresource Technology*. 2022, **351**, p.126924.
700. Munar-Florez, D.A., Varón-Cardenas, D.A., Ramírez-Contreras, N.E. and García-Núñez, J.A. Adsorption of ammonium and phosphates by biochar

- produced from oil palm shells: Effects of production conditions. *Results in Chemistry*. 2021, **3**, p.100119.
701. Krounbi, L., Enders, A., Anderton, C.R., Engelhard, M.H., Hestrin, R., Torres-Rojas, D., Dynes, J.J. and Lehmann, J. Sequential Ammonia and Carbon Dioxide Adsorption on Pyrolyzed Biomass to Recover Waste Stream Nutrients. *ACS Sustainable Chemistry & Engineering*. 2020, **8**(18), pp.7121-7131.
  702. Fidel, R.B., Laird, D.A. and Spokas, K.A. Sorption of ammonium and nitrate to biochars is electrostatic and pH-dependent. *Scientific Reports*. 2018, **8**(1), p.17627.
  703. Ferrer, V., Flores, M., Grandón, H., Escalona, N. and Segura, C. Ammonia Removal in Activated Carbons Prepared from Olive Oil Industry Waste. *Journal of the Brazilian Chemical Society*. 2023, **34**.
  704. Puragen, C. *What is Activated Carbon?* [Online]. 2024. [Accessed 26th May]. Available from: <https://activated-carbon.com/>
  705. Guo, X., Tak, J.K. and Johnson, R.L. Ammonia removal from air stream and biogas by a H<sub>2</sub>SO<sub>4</sub> impregnated adsorbent originating from waste wood-shavings and biosolids. *Journal of Hazardous Materials*. 2009, **166**(1), pp.372-376.
  706. Rodrigues, C.C. and Moraes, D. Control of the Emission of Ammonia through Adsorption in a Fixed Bed of Activated Carbon. *Adsorption Science & Technology*. 2002, **20**(10), pp.1013-1022.
  707. Ghimire, S., Wang, L., Zhang, B., Li, X. and Shahbazi, A. Production and modification of hydrochar from anaerobically digested cattail for adsorbing ammonium and phosphorous in wastewater. *Water Science and Technology*. 2021, **84**(7), pp.1678-1692.
  708. Parvage, M.M. and Herbert, R. Sequential removal of nitrate and sulfate in woodchip and hematite – coated biochar bioreactor. *Environmental Science: Water Research & Technology*. 2023, **9**(2), pp.489-499.
  709. Lee, Y.-E., Jeong, Y., Shin, D.-C., Ahn, K.-H., Jung, J.-H. and Kim, I.-T. Fabrication of Mg-Doped Sargassum Biochar for Phosphate and Ammonium Recovery. *Sustainability*. 2021, **13**(22), p.12752.
  710. Koopmann, A.K., Schuster, C., Torres-Rodríguez, J., Kain, S., Pertl-Obermeyer, H., Petutschnigg, A. and Hüsing, N. Tannin-Based Hybrid Materials and Their Applications: A Review. *Molecules*. 2020, **25**(21).
  711. Zandi-Darehgharibi, F., Haddadi, H. and Asfaram, A. A new tannin-based adsorbent synthesized for rapid and selective recovery of palladium and gold: Optimization using central composite design. *Heliyon*. 2024, **10**(3), p.e24639.
  712. Chen, B. and Schnoor, J.L. Role of Suberin, Suberan, and Hemicellulose in Phenanthrene Sorption by Root Tissue Fractions of Switchgrass (*Panicum virgatum*) Seedlings. *Environmental Science & Technology*. 2009, **43**(11), pp.4130-4136.
  713. Olivella, M.À., Bazzicalupi, C., Bianchi, A., del Río, J.C., Fiol, N. and Villaescusa, I. Binding interactions between suberin monomer components and pesticides. *Science of The Total Environment*. 2015, **527-528**, pp.159-164.

714. Aroso, I.M., Araújo, A.R., Pires, R.A. and Reis, R.L. Cork: Current Technological Developments and Future Perspectives for this Natural, Renewable, and Sustainable Material. *ACS Sustainable Chemistry & Engineering*. 2017, **5**(12), pp.11130-11146.
715. Azreen, I., Lija, Y. and Zahrim, A.Y. Ammonia nitrogen removal from aqueous solution by local agricultural wastes. *IOP Conference Series: Materials Science and Engineering*. 2017, **206**(1), p.012077.
716. Yang, D., Chen, Q., Liu, R., Song, L., Zhang, Y. and Dai, X. Ammonia recovery from anaerobic digestate: State of the art, challenges and prospects. *Bioresource Technology*. 2022, **363**, p.127957.
717. Peng, Y., Li, L., Dong, Q., Yang, P., Liu, H., Ye, W., Wu, D. and Peng, X. Evaluation of digestate-derived biochar to alleviate ammonia inhibition during long-term anaerobic digestion of food waste. *Chemosphere*. 2023, **311**, p.137150.
718. Riaño, B., Molinuevo-Salces, B., Vanotti, M.B. and García-González, M.C. Ammonia Recovery from Digestate Using Gas-Permeable Membranes: A Pilot-Scale Study. *Environments*. 2021, **8**(12), p.133.
719. Xu, B. and He, Z. Ammonia recovery from simulated anaerobic digestate using a two-stage direct contact membrane distillation process. *Water Environ Res*. 2021, **93**(9), pp.1619-1626.
720. Mutegoa, E., Hilonga, A. and Njau, K.N. Approaches to the mitigation of ammonia inhibition during anaerobic digestion – a review. *Water Practice and Technology*. 2020, **15**(3), pp.551-570.
721. Battista, F., Masala, C., Zamboni, A., Varanini, Z. and Bolzonella, D. Valorisation of Agricultural Digestate for the Ammonium Sulfate Recovery and Soil Improvers Production. *Waste and Biomass Valorization*. 2021, **12**(12), pp.6903-6916.
722. Li, J.-F., Li, Z.-M., Xu, J.-B., Guo, C.-Y., Fang, G.-W., Zhou, Y., Sun, M.-S. and Tao, D.-J. Demethylation of Waste Alkali Lignin for Rapid and Efficient Ammonia Adsorption. *Industrial & Engineering Chemistry Research*. 2024, **63**(7), pp.3282-3289.
723. McNevin, D. and Barford, J. Inter-relationship between adsorption and pH in peat biofilters in the context of a cation-exchange mechanism. *Water Research*. 2001, **35**(3), pp.736-744.
724. Sipponen, M.H. and Österberg, M. Aqueous Ammonia Pre-treatment of Wheat Straw: Process Optimization and Broad Spectrum Dye Adsorption on Nitrogen-Containing Lignin. *Front Chem*. 2019, **7**, p.545.
725. Couillard, D. The use of peat in wastewater treatment. *Water Research*. 1994, **28**(6), pp.1261-1274.
726. Witter, E. and Kirchmann, H. Peat, zeolite and basalt as adsorbents of ammoniacal nitrogen during manure decomposition. *Plant and Soil*. 1989, **115**(1), pp.43-52.
727. Abbès, C., Parent, L. and Karam, A. Ammonia sorption by peat and N fractionation in some peat-ammonia systems. *Nutrient Cycling in Agroecosystems*. 1993, **36**, pp.249-257.
728. IPS. *Peat*. [Online]. 2024. [Accessed July 21st].

729. Klavins, M.P., Oskars Changes of Peat Humic Acid Properties During Peat Genesis Process. In: *14th International Peat Congress: Peatlands in Balance, Stockholm*. 2012.
730. Adey, W.H. and Loveland, K. CHAPTER 6 - The Input of Organic Energy: Particulates and Feeding. In: Adey, W.H. and Loveland, K. eds. *Dynamic Aquaria (Third Edition)*. London: Academic Press, 2007, pp.93-100.
731. Wollina, U. Peat: a natural source for dermatocosmetics and dermatotherapeutics. *J Cutan Aesthet Surg*. 2009, **2**(1), pp.17-20.
732. Pipes, G.T. and Yavitt, J.B. Biochemical components of Sphagnum and persistence in peat soil. *Canadian Journal of Soil Science*. 2022, **102**(3), pp.785-795.
733. Trckova, M., Matlova, L., Hudcova, H., Martin, F., Zraly, Z., Dvorska, L., Beran, V. and Pavlik, I. Peat as a feed supplement for animals: A review. *Vet. Med. – Czech*. 2005, **50**, pp.361-377.
734. Sabiham, S. Properties of Indonesian Peat in Relation to the Chemistry of Carbon Emission. In: *Proc. of Int. Workshop on Evaluation and Sustainable Management of Soil Carbon Sequestration in Asian Countries, Bogor, Indonesia*. 2010.
735. Wen, Y., Wang, S., Mu, W., Yang, W. and Jönsson, P.G. Pyrolysis performance of peat moss: A simultaneous in-situ thermal analysis and bench-scale experimental study. *Fuel*. 2020, **277**, p.118173.
736. Karaca, H., Depci, T., Karta, M. and Coskun, M. Liquefaction Potential of Adiyaman Peat. *IOP Conference Series: Earth and Environmental Science*. 2016, **44**, p.052050.
737. Hossain, M.R., Khalekuzzaman, M., Bari, Q.H., Kabir, S.B. and Islam, M.B. Characterizations of peat biomass for subsequent thermochemical conversion. *AIP Conference Proceedings*. 2023, **2713**(1), p.060012.
738. Skreiberg, O.S., Alexandra. *Characterisation studies on peat*. SINTEF Energy Research, 2009.
739. Schellekens, J., Buurman, P. and Kuyper, T.W. Source and transformations of lignin in Carex-dominated peat. *Soil Biology and Biochemistry*. 2012, **53**, pp.32-42.
740. Strengell, T. *Peat*. [Online]. 2011. [Accessed]. Available from: <https://whiskyscience.blogspot.com>
741. Nahata, M. *Facile Synthesis of Activated Carbon from Cellulose in the Presence of Air for Ammonia Recovery in Resource-Constrained Settings*. Doctor of Philosophy thesis, University of Michigan, 2018.
742. Wonorahardjo, S., Ibnu, M.S. and Budiasih, E. Sulfur dioxide and ammonia gas reduction using coconut cellulose and acetylated cellulose. 2016, **17**, pp.179-188.
743. James, A. and Yadav, D. Valorization of coconut waste for facile treatment of contaminated water: A comprehensive review (2010–2021). *Environmental Technology & Innovation*. 2021, **24**, p.102075.
744. Oktavetri, N., Purnobasuki, H., Kuncoro, E. and Purnamasari, I. Ammonia Removal Using Coconut Shell Based Adsorbent: Effect of Carbonization Duration and Contact Time. *IPTEK Journal of Proceedings Series*. 2017, p.26.

745. Boopathy, R., Karthikeyan, S., Mandal, A.B. and Sekaran, G. Adsorption of ammonium ion by coconut shell-activated carbon from aqueous solution: kinetic, isotherm, and thermodynamic studies. *Environ Sci Pollut Res Int*. 2013, **20**(1), pp.533-542.
746. Dey, S., Charan, S.S., Pallavi, U., Sreenivasulu, A. and Haripavan, N. The removal of ammonia from contaminated water by using various solid waste biosorbents. *Energy Nexus*. 2022, **7**, p.100119.
747. Danley-Thomson, A.A., Robbins, D.M. and Gunsch, C.K. Cocopeat for Wastewater Treatment in the Developing World. II: Field Evaluation of Constructed Wetlands Packed with Cocopeat for Wastewater Treatment in Can Tho, Vietnam. *Journal of Environmental Engineering*. 2016, **142**(2), p.04015070.
748. Van Do, T.C., Pham, T.T.Y. and Pham, T.M.H. Ammonium removal by alkaline-activated coconut coir from synthetic and ground waters. *Asia-Pacific Journal of Chemical Engineering*. 2023, **18**(1), p.e2849.
749. Kasmuri, N., Dzulkifli, N.F.M., Ismail, N.A., Zaini, N. and Yaacob, Z. An investigation of a mixture of coconut husk and rice husk as activated carbon for treatment of wastewater. *IOP Conference Series: Earth and Environmental Science*. 2022, **1019**(1), p.012048.
750. Stirling, R.J., Snape, C.E. and Meredith, W. The impact of hydrothermal carbonisation on the char reactivity of biomass. *Fuel Processing Technology*. 2018, **177**, pp.152-158.
751. Zhu, F., Wang, Z., Huang, J., Hu, W., Xie, D. and Qiao, Y. Efficient adsorption of ammonia on activated carbon from hydrochar of pomelo peel at room temperature: Role of chemical components in feedstock. *Journal of Cleaner Production*. 2023, **406**, p.137076.
752. Wojtowicz, M.C., Jesph; Serio, Michael; Willburn, Monique. Adsorption of Ammonia on Regenerable Carbon Sorbents. In., 2015.
753. Kulaots, I.G., Yu-Ming; Hurt, Robert; Suuberg, Eric. Adsorption of Ammonia on Regenerable Carbon Sorbents. In: *2001 International Ash Utilization Symposium, Center for Applied Energy Research, University of Kentucky*. 2001.
754. Gonçalves, M., Sánchez-García, L., Oliveira Jardim, E.d., Silvestre-Albero, J. and Rodríguez-Reinoso, F. Ammonia Removal Using Activated Carbons: Effect of the Surface Chemistry in Dry and Moist Conditions. *Environmental Science & Technology*. 2011, **45**(24), pp.10605-10610.
755. Hsieh, C.C., Tsai, J.S. and Chang, J.R. Effects of Moisture on NH<sub>3</sub> Capture Using Activated Carbon and Acidic Porous Polymer Modified by Impregnation with H<sub>3</sub>PO<sub>4</sub>: Sorbent Material Characterized by Synchrotron XRPD and FT-IR. *Materials (Basel)*. 2022, **15**(3).
756. Bandosz, T.J. and Petit, C. On the reactive adsorption of ammonia on activated carbons modified by impregnation with inorganic compounds. *J Colloid Interface Sci*. 2009, **338**(2), pp.329-345.
757. Yeh, C.-Y., Chen, Y.-T., Chen, N.-Y. and Chang, J.-R. Air Regeneration of Ethanol-Laden Pellet NaY-SiO<sub>2</sub> and Pt/NaY-SiO<sub>2</sub>: Effects of Air Flow Rate on Pt Morphology and Regeneration Efficiency. *Catalysts*. 2018, **8**(7), p.288.

758. Pick, Š. and Dreyssé, H. Tight-binding study of ammonia and hydrogen adsorption on magnetic cobalt systems. *Surface Science*. 2000, **460**(1), pp.153-161.
759. Roque-Malherbe, R., Marquez-Linares, F., Del Valle, W. and Thommes, M. Ammonia adsorption on nanostructured silica materials for hydrogen storage and other applications. *J Nanosci Nanotechnol*. 2008, **8**(11), pp.5993-6002.
760. Kojima, Y. Ammonia As a Hydrogen Carrier for PEM Fuel Cells. In: *NH3 Fuel Conference 2018*, 2018.
761. Khaleque, A., Alam, M.M., Hoque, M., Mondal, S., Haider, J.B., Xu, B., Johir, M.A.H., Karmakar, A.K., Zhou, J.L., Ahmed, M.B. and Moni, M.A. Zeolite synthesis from low-cost materials and environmental applications: A review. *Environmental Advances*. 2020, **2**, p.100019.
762. Serrano, D.P., Centi, G., Diddams, P.A. and Čejka, J. Outlooks for zeolite catalysts in a low-carbon scenario. *Catalysis Today*. 2024, **426**, p.114365.
763. Tenny, S. and Abdelgawad, I. Statistical Significance. In: *StatPearls*. Treasure Island (FL): StatPearls Publishing, 2024.
764. Hu, D., Cao, G., Du, M., Huang, J., Zhao, J., Li, C. and Fang, Y. Insight into the biomass pyrolysis volatiles reaction with an iron-based oxygen carrier in a two-stage fixed-bed reactor. *Chemical Engineering Journal*. 2023, **465**, p.142860.
765. Na-Lampang, C., Assawasaengrat, P., Phumjan, L., Narkrugsa, W. and Sriprom, P. Optimizing Ammonia Adsorption Using Activated Carbon from Tamarind Pulp. *日本エネルギー学会誌*. 2021, **100**(12), pp.288-293.
766. Parihar, A., Sripada, P., Bambery, K., Garnier, G. and Bhattacharya, S. Investigation of functional group changes in biomass during slow pyrolysis using synchrotron based infra-red microspectroscopy and thermogravimetry-infra-red spectroscopy. *Journal of Analytical and Applied Pyrolysis*. 2017, **127**, pp.394-401.
767. Abdullahi, T., Harun, Z. and Othman, M.H.D. A review on sustainable synthesis of zeolite from kaolinite resources via hydrothermal process. *Advanced Powder Technology*. 2017, **28**(8), pp.1827-1840.
768. Dou, J., Kögler, M., Kesari, K.K., Pitkänen, L. and Vuorinen, T. Seasonal dynamics in structural characteristics within bark stems of cultivated willow (*Salix* sp.) by NMR and time-gated Raman spectroscopy. *Green Chemistry*. 2023, **25**(5), pp.1908-1919.
769. Nie, W., Liu, Y., Tan, C., Wang, Y., Liu, J., Zhao, X., Jiang, Z. and Jia, Z. Characteristics and factors driving the variations in bark thickness of major woody plants in China. *Ecological Indicators*. 2022, **144**, p.109447.
770. Zhou, Q., Jiang, Z., Zhang, X., Lai, Q., Li, Y., Zhao, F. and Zhao, Z. Tree age did not affect the leaf anatomical structure or ultrastructure of *Platycladus orientalis* L. (Cupressaceae). *PeerJ*. 2019, **7**, p.e7938.
771. Ferreira, J.P.A., Miranda, I., Sousa, V.B. and Pereira, H. Chemical composition of barks from *Quercus faginea* trees and characterization of their lipophilic and polar extracts. *PloS one*. 2018, **13**(5), p.e0197135.
772. ArboristNow. *Why is your tree losing bark? Causes and solutions for peeling bark*. [Online]. 2023. [Accessed July 26th]. Available from: <https://www.arboristnow.com/>

773. Vacek, Z., Cukor, J., Linda, R., Vacek, S., Šimůnek, V., Brichta, J., Gallo, J. and Prokúpková, A. Bark stripping, the crucial factor affecting stem rot development and timber production of Norway spruce forests in Central Europe. *Forest Ecology and Management*. 2020, **474**, p.118360.
774. Jager, M.M., Richardson, S.J., Bellingham, P.J., Clearwater, M.J. and Laughlin, D.C. Soil fertility induces coordinated responses of multiple independent functional traits. *Journal of Ecology*. 2015, **103**(2), pp.374-385.
775. Nde, D.B. and Foncha, A.C. Optimization Methods for the Extraction of Vegetable Oils: A Review. *Processes*. 2020, **8**(2), p.209.
776. Wu, M.R., Schott, D.L. and Lodewijks, G. Physical properties of solid biomass. *Biomass and Bioenergy*. 2011, **35**(5), pp.2093-2105.
777. Tumuluru, J.S., Ghiasi, B., Soelberg, N.R. and Sokhansanj, S. Biomass Torrefaction Process, Product Properties, Reactor Types, and Moving Bed Reactor Design Concepts. *Frontiers in Energy Research*. 2021, **9**.
778. Zakaria, M.R., Ahmad Farid, M.A., Andou, Y., Ramli, I. and Hassan, M.A. Production of biochar and activated carbon from oil palm biomass: Current status, prospects, and challenges. *Industrial Crops and Products*. 2023, **199**, p.116767.
779. Tokushige, M. and Ryu, J. Adsorption and Desorption Behaviors of Ammonia on Zeolites at 473 K by the Pressure–Swing Method. *ACS Omega*. 2023, **8**(36), pp.32536-32543.
780. Jiang, Y., Takahashi, A., Kawamoto, T., Asai, M., Zhang, N., Lei, Z., Zhang, Z., Kojima, K. and Nakamura, T. Unique adsorption and desorption behaviour of ammonia gas at heating temperature using the Prussian blue analogue  $Zn_3[Co(CN)_6]_2$ . *Inorganica Chimica Acta*. 2020, **501**, p.119273.
781. Hong, M.W., Park, J.H., Win, M.Z., Yoon, H.C. and Yi, K.B. Enhanced ammonia adsorption performance of  $MgCl_2$ -loaded activated carbon in pressure swing adsorption. *Journal of Industrial and Engineering Chemistry*. 2023, **118**, pp.216-225.
782. Chen, C., Yu, J., Song, G. and Che, K. Desorption performance of commercial zeolites for temperature-swing  $CO_2$  capture. *Journal of Environmental Chemical Engineering*. 2023, **11**(3), p.110253.
783. Sander, R. Compilation of Henry's law constants (version 5.0.0) for water as solvent. *Atmos. Chem. Phys.* 2023, **23**(19), pp.10901-12440.
784. Walker, R. *Density, sg of water at different temps.* [Online]. 2015. [Accessed]. Available from: <https://www.simetric.co.uk/>
785. Dubinin, M.M. and Astakhov, V.A. Development of the concepts of volume filling of micropores in the adsorption of gases and vapors by microporous adsorbents. *Bulletin of the Academy of Sciences of the USSR, Division of chemical science*. 1971, **20**(1), pp.3-7.

## Appendix

In this Appendix, the exhaustive data from across the thesis is presented.

Here, the chemical properties and safety data sheet information of original, methylated, and hydrogenated pyrolysis oil-derived components that pertained to the CHEM21 scoring (in Chapter 6) are presented.

From the ammonia adsorption chapter (Chapter 7), the characterisation data of the samples only analysed for that chapter, examples of the calculation of the partial pressures of ammonia and comparisons with literature values of adsorption capacity (which were performed with the Solver function on Microsoft Excel), and the inputs from Helminen (380) which were used to enable the comparison of literature values are outlined.

Finally, example peak tables from the pyrolysis-gas chromatography/mass spectrometry (py-GC/MS) analysis performed across Chapter 4, Chapter 5 and Chapter 6 are illustrated.

### **A.1 Solvent Hazardousness Justification tables**

This section displays the chemical properties and safety data sheet information of original, methylated, and hydrogenated pyrolysis oil-derived components that pertained to the CHEM21 scoring (in Chapter 6).

**Table A1-1 – Environmental scoring of pyrolysis oil-derived components.**

Compound	CAS	Boiling Point (°C)	H400/H402/H410/H411?	H412/H413?	H420?	Env Score
Catechol	120-80-9	245	N	N	N	7
Furfural	98-01-1	162	N	N	N	5
Acetic acid	64-19-7	117	N	N	N	3
2-methoxy phenol	90-05-1	205	N	N	N	7
Trans-isoeugenol	5932-68-3	268	N	N	N	7
Creosol	93-51-6	221.5	N	N	N	7
Phenol	108-95-2	182	Y	N	N	7
Phenol, 4-ethyl-2-methoxy-	2785-89-9	235	N	N	N	7
1,2-Benzenediol, 4-methyl	452-86-8	251	N	N	N	7
p-Cresol	106-44-5	202	N	Y	N	7

**Table A1-2– Safety scoring of pyrolysis oil-derived components.**

Compound	CAS	Flash point (°C)	H225/ H224?	H226?	Auto-ignition Temperature (°C)	EUH019 ?	Safety Score
Catechol	120-80-9	127	N	N	N	N	1
Furfural	98-01-1	61.7	N	N	N	N	1
Acetic acid	64-19-7	39	N	Y	426	N	3
2-methoxy phenol	90-05-1	90	N	N	N	N	1
Trans-isoeugenol	5932-68-3	134	N	N	N	N	2
Creosol	93-51-6	99	N	N	N	N	2
Phenol	108-95-2	79	N	N	N	N	1
Phenol, 4-ethyl-2-methoxy-	2785-89-9	108	N	N	N	N	2
1,2-Benzenediol, 4-methyl	452-86-8	140	N	N	N	N	2
p-Cresol	106-44-5	86	N	N	559	N	1

**Table A1-3 – Health scoring of pyrolysis oil-derived components.**

Compound	CAS	H340/ H350/ H360 ?	H300/ H310/ H330 ?	H334 ?	H341/ H351/ H361 ?	H370/ H372 ?	H301/ H311/ H331 ?	H314 ?	H318 ?	H304/ H371/ H373 ?	H302/ H312/ H332/ H336/ EUH070 ?	H315/ H317/ H319/ H335/ EUH066 ?	Health Score
Catechol	120-80-9	Y	N	N	Y	N	Y	N	N	N	N	Y	9
Furfural	98-01-1	N	Y	N	Y	N	Y	N	N	N	Y	Y	9
Acetic acid	64-19-7	N	N	N	N	N	N	Y	Y	N	N	N	7
2-methoxy phenol	90-05-1	N	N	N	N	N	N	N	N	N	Y	Y	2
Trans-isoeugenol	5932-68-3	N	N	N	N	N	N	N	N	N	N	Y	2
Creosol	93-51-6	N	N	N	N	N	N	N	N	N	Y	Y	2
Phenol	108-95-2	N	N	N	Y	N	Y	Y	Y	Y	N	N	7
Phenol, 4-ethyl-2-methoxy-	2785-89-9	N	N	N	N	N	N	N	N	N	N	Y	2
1,2-Benzenediol, 4-methyl	452-86-8	N	N	N	N	N	N	N	N	N	N	N	5
p-Cresol	106-44-5	N	N	N	N	N	Y	Y	Y	N	N	N	7

**Table A1-4 – Environmental scoring of methylated pyrolysis oil-derived components.**

Compound	CAS	Boiling Point (°C)	H400/H402/H410/H411?	H412/H413?	H420?	Env Score
Veratrole	91-16-7	206.5	N	N	N	7
Methyl acetate	79-20-9	57	N	N	N	5
4-Propenyl Veratrole	93-16-3	263	N	N	N	7
Homoveratrole	494-99-5	219	N	N	N	7
Anisole	100-66-3	154	N	N	N	5
Methyl anisole	104-93-8	174	N	N	N	5

**Table A1-5 – Safety scoring of methylated pyrolysis oil-derived components.**

Compound	CAS	Flash point (°C)	H225/H224?	H226?	Auto-ignition Temperature (°C)	EUH019?	Safety Score
Veratrole	91-16-7	72	N	N	N	N	1
Methyl acetate	79-20-9	-13	Y	N	502.2	N	5
4-Propenyl Veratrole	93-16-3	113	N	N	N	N	2
Homoveratrole	494-99-5	85	N	N	N	N	2
Anisole	100-66-3	51	N	Y	475	N	3
Methyl anisole	104-93-8	59	N	Y	490	N	3

**Table A1-6 – Health scoring of methylated pyrolysis oil-derived components.**

Compound	CAS	H340/ H350/ H360 ?	H300/ H310/ H330 ?	H334 ?	H341/ H351/ H361 ?	H370/ H372 ?	H301/ H311/ H331 ?	H314 ?	H318 ?	H304/ H371/ H373 ?	H302/ H312/ H332/ H336/ EUH070 ?	H315/ H317/ H319/ H335/ EUH066 ?	Health Score
Veratrole	91-16-7	N	N	N	N	N	N	N	N	N	Y	N	2
Methyl acetate	79-20-9	N	N	N	N	N	N	N	N	N	Y	Y	3
4-Propenyl Veratrole	93-16-3	N	N	N	N	N	N	N	N	N	N	N	5
Homoveratrole	494-99-5	N	N	N	N	N	N	N	N	N	N	Y	2
Anisole	100-66-3	N	N	N	N	N	N	N	N	N	N	N	5
Methyl anisole	104-93-8	N	N	N	Y	N	N	N	N	N	Y	Y	6

**Table A1-7 – Environmental scoring of hydrogenated pyrolysis oil-derived components.**

Compound	CAS	Boiling Point (°C)	H400/H402/H410/ H411?	H412/H413?	H420?	Env Score
Furfuryl alcohol	98-00-0	170	N	N	N	5
Ethanol	64-17-5	78	N	N	N	3
2-methoxy-4-propylphenol	2785-87-7	289.9	N	N	N	7
Methyl cyclohexanone	589-92-4	170	N	N	N	5
Methyl cyclohexanol	590-67-0	168	N	N	N	5
Cyclohexanone	108-94-1	155	N	N	N	5
Cyclohexanol	108-93-0	160.5	N	Y	N	5

**Table A1-8 – Safety scoring of hydrogenated pyrolysis oil-derived components.**

Compound	CAS	Flash point (°C)	H225/H224?	H226?	Auto-ignition Temperature (°C)	EUH019?	Safety Score
Furfuryl alcohol	98-00-0	78	N	N	391.11	N	1
Ethanol	64-17-5	13	Y	N	455	N	5
2-methoxy-4-propylphenol	2785-87-7	113	N	N	374	N	1
Methyl cyclohexanone	589-92-4	48	N	Y	N	N	4
Methyl cyclohexanol	590-67-0	68	N	N	N	N	2
Cyclohexanone	108-94-1	46	N	Y	420	N	3
Cyclohexanol	108-93-0	64	N	N	285	N	1

**Table A1-9** – Health scoring of hydrogenated pyrolysis oil-derived components.

Compound	CAS	H340/ H350/ H360 ?	H300/ H310/ H330 ?	H334 ?	H341/ H351/ H361 ?	H370/ H372 ?	H301/ H311/ H331 ?	H314 ?	H318 ?	H304/ H371/ H373 ?	H302/ H312/ H332/ H336/ EUH070 ?	H315/ H317/ H319/ H335/ EUH066 ?	Health Score
Furfuryl alcohol	98-00-0	N	N	N	Y	N	Y	N	N	N	Y	Y	6
Ethanol	64-17-5	N	N	N	N	N	N	N	N	N	N	Y	3
2-methoxy-4-propylphenol	2785-87-7	N	N	N	N	N	N	N	Y	N	N	Y	4
Methyl cyclohexanone	589-92-4	N	N	N	N	N	N	N	N	N	Y	N	2
Methyl cyclohexanol	590-67-0	N	N	N	N	N	N	N	N	N	Y	Y	2
Cyclohexanone	108-94-1	N	N	N	N	N	N	N	N	N	Y	N	2
Cyclohexanol	108-93-0	N	N	N	N	N	N	N	N	N	Y	Y	2

**Table A1-10 – Environmental scoring of non-polar common solvents.**

Compound	CAS	Boiling Point (°C)	H400/H402/H410/ H411?	H412/H413?	H420?	Env Score
Benzene	71-43-2	80.1	N	Y	N	5
Cyclohexane	110-82-7	80.7	Y	N	N	7
Hexane	110-54-3	69	Y	N	N	7
Xylene	106-42-3	138	N	Y	N	5
Toluene	108-88-3	110.5	N	Y	N	5
1,4-Dioxane	123-91-1	101	N	N	N	3
Furan	110-00-9	32	N	Y	N	7
Diethyl ether	60-29-7	34.6	N	N	N	7
Chloroform	67-66-3	56	N	Y	N	5
Isopropyl Ether	108-20-3	68	N	N	N	5
Methyl Ethyl Ketone	78-93-3	80	N	N	N	3
Pyridine	110-86-1	115	N	N	N	3
Acetonitrile	75-05-8	81	N	N	N	3
Acetone	67-64-1	56	N	N	N	5
Methylene Dichloride	75-09-2	39.9	N	N	N	7
Ethyl acetate	141-78-6	77	N	N	N	3
n-Methyl-2- pyrrolidone	872-50-4	202	N	N	N	7
Tetrahydrofuran	109-99-9	65	N	N	N	5
1,3-Dioxolane	646-06-0	75.5	N	N	N	3
Dimethyl sulphide	75-18-3	38	N	N	N	7
Dimethyl Formamide	68-12-2	153	N	N	N	5

**Table A1-11 – Safety scoring of non-polar common solvents.**

Compound	CAS	Flash point (°C)	H225/H224?	H226?	Auto-ignition Temperature (°C)	EUH019?	Safety Score
Benzene	71-43-2	-11	Y	N	498	N	5
Cyclohexane	110-82-7	-20	Y	N	N	N	7
Hexane	110-54-3	-22	Y	N	N	N	7
Xylene	106-42-3	27	N	Y	529	N	3
Toluene	108-88-3	4	Y	N	N	N	5
1,4-Dioxane	123-91-1	11	Y	N	190.55	N	6
Furan	110-00-9	-36	Y	N		N	8
Diethyl ether	60-29-7	-40	Y	N	N	N	7
Chloroform	67-66-3	85	N	N	N	N	1
Isopropyl Ether	108-20-3	-29	Y	N	441.7	N	7
Methyl Ethyl Ketone	78-93-3	-3	Y	N	N	N	5
Pyridine	110-86-1	20	Y	N	N	N	5
Acetonitrile	75-05-8	2	Y	N	524	N	5
Acetone	67-64-1	-17	Y	N	465	N	5
Methylene Dichloride	75-09-2	39.9	N	N	N	N	3
Ethyl acetate	141-78-6	11	Y	N	N	N	5
n-Methyl-2-pyrrolidone	872-50-4	86	N	N		N	2
Tetrahydrofuran	109-99-9	-21.1	Y	N	215	N	7
1,3-Dioxolane	646-06-0	-3	Y	N	N	N	5
Dimethyl sulphide	75-18-3	-34	Y	N	206.1	N	7
Dimethyl Formamide	68-12-2	58	N	Y		N	4

Table A1-12 – Health scoring of non-polar common solvents.

Compound	CAS	H340/ H350/ H360 ?	H300/ H310/ H330 ?	H334 ?	H341/ H351/ H361 ?	H370/ H372 ?	H301/ H311/ H331 ?	H314 ?	H318 ?	H304/ H371/ H373 ?	H302/ H312/ H332/ H336/ EUH070?	H315/ H317/ H319/ H335/ EUH066 ?	Health Score
Benzene	71-43-2	Y	N	N	N	Y	N	N	N	Y	N	Y	10
Cyclohexane	110-82-7	N	N	N	N	N	N	N	N	Y	Y	Y	3
Hexane	110-54-3	N	N	N	N	N	N	N	N	Y	Y	Y	3
Xylene	106-42-3	N	N	N	N	N	N	N	N	Y	Y	Y	2
Toluene	108-88-3	N	N	N	Y	N	N	N	N	Y	Y	Y	6
1,4-Dioxane	123-91-1	Y	N	N	N	N	N	N	N	N	N	Y	9
Furan	110-00-9	Y	N	N	Y	N	N	N	N	Y	Y	Y	10
Diethyl ether	60-29-7	N	N	N	N	N	N	N	N	N	Y	N	3
Chloroform	67-66-3	N	N	N	Y	Y	Y	N	N	N	Y	Y	7
Isopropyl Ether	108-20-3	N	N	N	N	N	N	N	N	N	Y	N	3
Methyl Ethyl Ketone	78-93-3	N	N	N	N	N	N	N	N	N	Y	Y	3
Pyridine	110-86-1	N	N	N	N	N	N	N	N	N	Y	Y	2
Acetonitrile	75-05-8	N	N	N	N	N	N	N	N	N	Y	Y	3
Acetone	67-64-1	N	N	N	N	Y	Y	N	N	Y	Y	Y	7
Methylene Dichloride	75-09-2	N	N	N	Y	N	N	N	N	N	Y	Y	7
Ethyl acetate	141-78-6	N	N	N	N	Y	Y	N	N	N	N	N	7
n-Methyl-2-pyrrolidone	872-50-4	Y	N	N	N	N	N	N	N	N	N	Y	9
Tetrahydrofuran	109-99-9	N	N	N	Y	N	N	N	N	N	Y	Y	7
1,3-Dioxolane	646-06-0	Y	N	N	N	N	N	N	N	N	N	Y	10
Dimethyl sulphide	75-18-3	N	N	N	N	N	N	N	N	N	N	N	6
Dimethyl Formamide	68-12-2	Y	N	N	N	N	N	N	N	N	Y	Y	9

**Table A1-13 – Environmental scoring of non-polar common solvents.**

Compound	CAS	Boiling Point (°C)	H400/H402/H410/H411?	H412/H413?	H420?	Env Score
Ethanol	64-17-5	78	N	N	N	3
Methanol	67-56-1	64.7	N	N	N	5
Water	7732-18-5	100	N	N	N	3
Isoamyl alcohol	123-51-3	131	N	N	N	3
Hexafluoro Isopropanol	920-66-1	59	N	N	N	5
m-Cresol	108-39-4	203	N	Y	N	7

**Table A1-14 – Safety scoring of non-polar common solvents.**

Compound	CAS	Flash point (°C)	H225/H224?	H226?	Auto-ignition Temperature (°C)	EUH019?	Safety Score
Ethanol	64-17-5	13	Y	N	455	N	5
Methanol	67-56-1	9.7	Y	N	455	N	5
Water	7732-18-5		N	N		N	5
Isoamyl alcohol	123-51-3	43	N	Y	340	N	3
Hexafluoro Isopropanol	920-66-1	7.6	N	N	N	N	4
m-Cresol	108-39-4	86	N	N	N	N	1

**Table A1-15 – Health scoring of non-polar common solvents.**

Compound	CAS	H340/ H350/ H360 ?	H300/ H310/ H330 ?	H334 ?	H341/ H351/ H361 ?	H370/ H372 ?	H301/ H311/ H331 ?	H314 ?	H318 ?	H304/ H371/ H373 ?	H302/ H312/ H332/ H336/ EUH070 ?	H315/ H317/ H319/ H335/ EUH066 ?	Health Score
Ethanol	64-17-5	N	N	N	N	N	N	N	N	N	N	Y	3
Methanol	67-56-1	N	N	N	N	Y	Y	N	N	N	N	N	7
Water	7732-18-5	N	N	N	N	N	N	N	N	N	N	N	5
Isoamyl alcohol	123-51-3	N	N	N	N	N	N	N	Y	N	Y	Y	4
Hexafluoro Isopropanol	920-66-1	N	N	N	Y	N	N	Y	Y	Y	N	N	8
m-Cresol	108-39-4	N	N	N	N	N	Y	Y	Y	N	N	N	7

## A.2 Ammonia adsorption appendices

In this section, the data that was not included within the ammonia adsorption chapter is outlined. This includes the characterisation data of the samples only analysed for that chapter, examples of the calculation of the partial pressures of ammonia and comparisons with literature values of adsorption capacity (which were performed with the Solver function on Microsoft Excel), and the inputs from Helminen (380) which were used to enable the comparison of literature values.

### A.2.1 Characterisation data for samples run specifically for ammonia adsorption testing.

From the comparison of proximate, ultimate and fibre analysis data with the ammonia adsorption capacity of samples in Chapter 7, this data is outlined below.

#### A.2.1.1 Proximate analysis data

This section displays the proximate analysis data for the samples that underwent ammonia adsorption testing.

**Table A2-1** – Proximate Analysis of raw tree barks used in Chapter 7. Error calculated by 1x standard deviation. Samples run in duplicate.

Sample	Moisture Content (%wt, as analysed)	Volatiles (%wt, dry basis)	Fixed Carbon (%wt, dry basis)	Ash (%wt, dry basis)
NF	5.3 ± 0.0	70.3 ± 0.3	29.5 ± 0.3	0.2 ± 0.1
ESF	6.5 ± 0.6	78.9 ± 0.9	20.5 ± 1.5	0.6 ± 0.6
GF	4.8 ± 0.0	79.9 ± 0.0	20.0 ± 0.0	0.1 ± 0.0
DF	5.3 ± 0.1	72.9 ± 0.4	26.8 ± 0.5	0.4 ± 0.1
NC	3.8 ± 0.0	84.4 ± 0.0	13.4 ± 0.0	2.2 ± 0.0
Oak		72.5 ± 6.0	24.7 ± 4.8	4.2 ± 1.3

**Table A2-2 – Proximate Analysis of treated tree barks and activated carbons used in Chapter 7.** 'bc' = biochar, 'HW' = hot water-washed, 'Sox' = solvent extraction solid residue. Error calculated by 1x standard deviation. Samples run in duplicate.

<b>Sample</b>	<b>Moisture Content (%wt, as analysed)</b>	<b>Volatiles (%wt, dry basis)</b>	<b>Fixed Carbon (%wt, dry basis)</b>	<b>Ash (%wt, dry basis)</b>
<b>DFbc</b>	2.2 ± 0.3	27.4 ± 5.1	68.7 ± 4.1	3.9 ± 1.0
<b>HW-DFbc</b>	1.9 ± 0.1	22.1 ± 0.2	73.1 ± 0.6	4.8 ± 0.5
<b>DFSox</b>	4.8 ± 0.0	72.7 ± 0.3	26.0 ± 0.1	1.3 ± 0.4
<b>GFSox</b>	4.6 ± 0.4	76.6 ± 0.6	21.8 ± 0.2	1.6 ± 0.8
<b>NFbc</b>	2.4 ± 0.2	23.2 ± 0.3	74.8 ± 0.9	2.0 ± 1.2
<b>HW-NFbc</b>	3.5 ± 0.5	29.7 ± 0.4	69.8 ± 0.5	1.4 ± 1.1
<b>NCbc</b>	4.6 ± 0.5	25.1 ± 0.5	65.8 ± 0.5	9.1 ± 0.0
<b>ESFbc</b>	2.1 ± 0.2	22.3 ± 0.9	72.9 ± 1.2	4.8 ± 0.3
<b>Oakbc</b>	2.8 ± 0.7	23.9 ± 4.6	69.8 ± 7.0	6.3 ± 2.3
<b>NORIT-AC</b>	1.6 ± 0.3	3.7 ± 0.3	92.2 ± 3.5	8.2 ± 1.0
<b>SIGMA-AC</b>	3.0 ± 0.4	17.5 ± 1.0	74.3 ± 0.0	8.3 ± 1.0

**Table A2-3 – Proximate Analysis of 'miscellaneous' samples used in Chapter 7.** Error calculated by 1x standard deviation. Samples run in duplicate.

<b>Sample</b>	<b>Moisture Content (%wt, as analysed)</b>	<b>Volatiles (%wt, dry basis)</b>	<b>Fixed Carbon (%wt, dry basis)</b>	<b>Ash (%wt, dry basis)</b>
<b>MSWdig</b>	3.1 ± 0.0	36.2 ± 0.1	8.3 ± 0.0	55.5 ± 0.1
<b>VGFDig</b>	4.4 ± 0.0	47.2 ± 1.1	9.0 ± 0.2	43.8 ± 0.8
<b>CH</b>	4.5 ± 0.1	63.7 ± 2.7	28.2 ± 0.5	8.0 ± 3.2
<b>AlkLig</b>	6.0 ± 0.0	47.6 ± 0.1	31.8 ± 0.8	20.6 ± 0.8
<b>PeatSEPO</b>	6.6 ± 0.1	64.0 ± 0.3	31.1 ± 0.0	4.8 ± 0.3
<b>PeatMoss</b>	6.5 ± 0.1	61.3 ± 1.9	28.2 ± 0.3	10.6 ± 1.7
<b>Lignoboost</b>	2.8 ± 0.6	57.5 ± 0.9	37.8 ± 0.1	11.0 ± 1.0
<b>Cellulose</b>	2.6 ± 0.1	93.0 ± 0.1	8.4 ± 0.4	0.5 ± 0.1

### A.2.1.2 Ultimate analysis data

This section displays the ultimate analysis data for the samples that underwent ammonia adsorption testing before the experiment, and the nitrogen values measured after the experiment had finished.

#### A.2.1.2.1. Pre-ammonia adsorption experiment ultimate analysis data

**Table A2-4** – Ultimate Analysis of raw tree barks used in Chapter 7. Error calculated by 1x standard deviation. Samples run in duplicate.

Sample	C (wt%, dry basis)	H (wt%, dry basis)	N (wt%, dry basis)	S (wt%, dry basis)	O (wt%, dry basis)
NF	54.1 ± 0.5	5.7 ± 1.1	0.7 ± 0.0	0.0 ± 0.0	39.4 ± 1.6
ESF	44.7 ± 4.5	5.0 ± 0.5	1.0 ± 0.0	0.0 ± 0.0	48.7 ± 0.5
GF	47.8 ± 0.0	5.9 ± 0.1	0.7 ± 0.0	0.0 ± 0.0	45.6 ± 0.0
DF	49.7 ± 1.0	5.1 ± 0.5	0.6 ± 0.0	0.0 ± 0.0	44.3 ± 0.1
NC	50.0 ± 1.8	6.0 ± 0.3	0.7 ± 0.0	0.0 ± 0.0	43.3 ± 0.1
Oak	43.4 ± 2.1	5.9 ± 0.1	0.3 ± 0.2	0.1 ± 0.0	42.9 ± 1.0

**Table A2-5** – Ultimate Analysis of treated tree barks and activated carbons used in Chapter 7. 'bc' = biochar, 'HW' = hot water-washed, 'Sox' = solvent extraction solid residue. Error calculated by 1x standard deviation. Samples run in duplicate.

Sample	C (wt%, dry basis)	H (wt%, dry basis)	N (wt%, dry basis)	S (wt%, dry basis)	O (wt%, dry basis)
DFbc	75.9 ± 0.0	2.6 ± 0.0	2.7 ± 0.1	0.0 ± 0.0	14.9 ± 0.0
HW-DFbc	73.6 ± 0.9	2.6 ± 0.2	0.7 ± 0.1	0.0 ± 0.0	18.4 ± 1.0
DFSox	47.1 ± 1.1	4.2 ± 0.4	1.2 ± 0.0	0.0 ± 0.0	45.9 ± 1.2
GFSox	44.9 ± 0.7	4.5 ± 0.5	1.2 ± 0.0	0.0 ± 0.0	48.1 ± 0.3
NFbc	74.3 ± 1.5	2.5 ± 0.1	2.4 ± 0.1	0.0 ± 0.0	18.8 ± 1.5
HW-NFbc	75.9 ± 0.3	2.4 ± 0.0	0.6 ± 0.0	0.0 ± 0.0	19.7 ± 0.3
NCbc	70.9 ± 0.8	2.6 ± 0.0	2.6 ± 0.2	0.0 ± 0.0	13.8 ± 1.0
ESFbc	73.1 ± 1.8	2.6 ± 0.1	2.7 ± 0.1	0.0 ± 0.0	16.7 ± 2.0
Oakbc450	74.3 ± 2.6	1.8 ± 0.3	1.3 ± 0.0	0.0 ± 0.0	16.3 ± 2.4
NORIT-AC	85.8 ± 0.9	0.1 ± 0.0	1.3 ± 0.0	0.5 ± 0.0	4.1 ± 0.9
SIGMA-AC	68.4 ± 0.7	0.9 ± 0.1	1.1 ± 0.0	0.0 ± 0.0	21.3 ± 0.6

**Table A2-6** – Ultimate Analysis of 'miscellaneous' samples used in Chapter 7. Error calculated by 1x standard deviation. Samples run in duplicate.

Sample	C (wt%, dry basis)	H (wt%, dry basis)	N (wt%, dry basis)	S (wt%, dry basis)	O (wt%, dry basis)
MSWdig	24.1 ± 0.0	1.7 ± 0.0	1.5 ± 0.0	0.2 ± 0.0	16.9 ± 0.0
VGfdig	29.5 ± 0.1	3.0 ± 0.1	2.0 ± 0.0	0.3 ± 0.0	21.3 ± 0.6
CH	48.4 ± 1.5	3.8 ± 0.1	0.8 ± 0.1	0.0 ± 0.0	38.9 ± 1.8
AlkLig	47.2 ± 0.3	3.5 ± 0.2	0.0 ± 0.0	1.8 ± 0.2	26.9 ± 1.2
PeatSEPO	48.6 ± 0.2	3.9 ± 0.4	2.5 ± 0.0	0.3 ± 0.0	39.8 ± 0.6
PeatMoss	43.3 ± 1.7	3.0 ± 0.3	2.1 ± 0.2	0.1 ± 0.1	41.0 ± 1.9
Lignoboost	61.3 ± 0.5	4.7 ± 0.3	0.9 ± 0.0	1.2 ± 0.1	28.2 ± 1.2

**A.2.1.2.2. Post-ammonia adsorption experiments ultimate analysis data**

**A.2.1.2.2.1. Untreated samples**

**Table A2-7** – Ultimate Analysis of coconut husk after each ammonia adsorption experiment. In XX-A-B-C, A = ammonium sulphate concentration (AMS), B = ammonia adsorption experiment replicate number, C = ultimate analysis replicate number. Uncorr H = hydrogen uncorrected for moisture content.

Sample Name	AMS Conc (M)	N (wt%, dry basis)	C (wt%, dry basis)	Uncorr H (wt%, as received)	S (wt%, dry basis)
CH-0.05-1-1	0.05	1.29	19.25	3.16	0.00
CH-0.05-1-2	0.05	1.42	21.31	2.31	0.00
CH-0.05-2-1	0.05	2.14	29.11	2.67	0.00
CH-0.05-2-2	0.05	2.21	28.63	2.57	0.00
CH-0.5-1-1	0.5	2.47	23.68	2.33	0.00
CH-0.5-1-2	0.5	2.78	31.48	3.34	0.02
CH-0.5-2-1	0.5	3.03	34.58	3.73	0.00
CH-0.5-2-2	0.5	2.72	27.15	2.88	0.00
CH-1.8-1-1	1.8	2.74	30.59	4.22	0.00
CH-1.8-1-2	1.8	3.15	30.53	4.16	0.00
CH-1.8-2-1	1.8	2.82	29.58	4.21	0.00
CH-1.8-2-2	1.8	3.27	31.01	4.44	0.00

**Table A2-8** – Ultimate Analysis of European silver fir tree bark after each ammonia adsorption experiment. In XX-A-B-C, A = ammonium sulphate concentration (AMS), B = ammonia adsorption experiment replicate number, C = ultimate analysis replicate number. Uncorr H = hydrogen uncorrected for moisture content.

Sample Name	AMS Conc (M)	N (wt%, dry basis)	C (wt%, dry basis)	Uncorr H (wt%, as received)	S (wt%, dry basis)
ESF-0.05-1-1	0.05	2.46	34.76	4.36	0.00
ESF-0.05-1-2	0.05	2.52	36.57	4.23	0.00
ESF-0.05-2-1	0.05	2.71	36.63	4.15	0.00
ESF-0.05-2-2	0.05	2.67	34.34	3.92	0.00
ESF-0.05-3-1	0.05	2.45	37.46	4.21	0.00
ESF-0.05-3-2	0.05	2.53	36.35	4.30	0.00
ESF-0.5-1-1	0.5	2.79	38.84	4.20	0.00
ESF-0.5-1-2	0.5	2.46	36.96	4.04	0.00
ESF-0.5-2-1	0.5	2.50	37.36	4.06	0.00
ESF-0.5-2-2	0.5	2.47	37.77	4.21	0.00
ESF-1.8-1-1	1.8	2.47	37.32	4.01	0.00
ESF-1.8-1-2	1.8	2.53	38.09	4.06	0.00
ESF-1.8-2-1	1.8	2.40	38.76	4.10	0.00
ESF-1.8-2-2	1.8	2.65	39.30	4.23	0.00

**Table A2-9** – Ultimate Analysis of noble fir tree bark after each ammonia adsorption experiment. In XX-A-B-C, A = ammonium sulphate concentration (AMS), B = ammonia adsorption experiment replicate number, C = ultimate analysis replicate number. Uncorr H = hydrogen uncorrected for moisture content.

Sample Name	AMS Conc (M)	N (wt%, dry basis)	C (wt%, dry basis)	Uncorr H (wt%, as received)	S (wt%, dry basis)
NF-0.05-1-1	0.05	2.22	33.81	3.68	0.00
NF-0.05-1-2	0.05	2.59	42.03	4.50	0.00
NF-0.05-2-1	0.05	2.84	45.77	5.11	0.00
NF-0.05-2-2	0.05	2.62	44.49	4.84	0.00
NF-0.05-3-1	0.05	2.73	46.86	5.10	0.00
NF-0.05-3-2	0.05	2.24	44.99	4.84	0.00
NF-0.5-1-1	0.5	2.86	35.58	3.87	0.00
NF-0.5-1-2	0.5	3.14	37.74	4.04	0.00
NF-0.5-2-1	0.5	2.58	36.84	3.96	0.00
NF-0.5-2-2	0.5	2.54	39.36	4.24	0.00
NF-1.8-1-1	1.8	2.90	33.57	3.90	0.00
NF-1.8-1-2	1.8	2.74	36.06	3.70	0.00
NF-1.8-2-1	1.8	3.01	35.03	3.68	0.00
NF-1.8-2-2	1.8	2.85	39.85	4.04	0.00

**Table A2-10** – Ultimate Analysis of nootka cypress tree bark after each ammonia adsorption experiment. In XX-A-B-C, A = ammonium sulphate concentration (AMS), B = ammonia adsorption experiment replicate number, C = ultimate analysis replicate number. Uncorr H = hydrogen uncorrected for moisture content.

Sample Name	AMS Conc (M)	N (wt%, dry basis)	C (wt%, dry basis)	Uncorr H (wt%, as received)	S (wt%, dry basis)
NC-0.05-1-1	0.05	2.00	44.17	4.86	0.00
NC-0.05-1-2	0.05	2.09	42.06	4.66	0.00
NC-0.05-2-1	0.05	1.36	38.07	4.71	0.00
NC-0.05-2-2	0.05	1.20	35.57	4.21	0.00
NC-0.5-1-1	0.5	1.96	34.49	4.60	0.07
NC-0.5-1-2	0.5	1.89	34.38	3.96	0.08
NC-0.5-2-1	0.5	1.82	34.05	4.01	0.00
NC-0.5-2-2	0.5	1.80	36.73	4.91	0.07
NC-1.8-1-1	1.8	2.12	42.24	4.88	0.00
NC-1.8-1-2	1.8	2.13	43.74	5.01	0.00
NC-1.8-2-1	1.8	2.11	42.68	4.90	0.00
NC-1.8-2-2	1.8	2.13	44.72	7.61	0.00

**Table A2-11** – Ultimate Analysis of grand fir tree bark after each ammonia adsorption experiment. In XX-A-B-C, A = ammonium sulphate concentration (AMS), B = ammonia adsorption experiment replicate number, C = ultimate analysis replicate number. Uncorr H = hydrogen uncorrected for moisture content.

Sample Name	AMS Conc (M)	N (wt%, dry basis)	C (wt%, dry basis)	Uncorr H (wt%, as received)	S (wt%, dry basis)
GF-0.05-1-1	0.05	1.78	29.17	3.31	0.00
GF-0.05-1-2	0.05	1.91	28.55	3.09	0.00
GF-0.05-2-1	0.05	1.80	33.79	3.65	0.00
GF-0.05-2-2	0.05	1.71	31.57	3.97	0.00
GF-0.5-1-1	0.5	2.3	33.50	3.54	0.00
GF-0.5-1-2	0.5	2.49	34.85	4.45	0.00
GF-0.5-2-1	0.5	2.65	33.69	3.66	0.00
GF-0.5-2-2	0.5	2.77	38.44	4.23	0.00
GF-1.8-1-1	1.8	2.75	35.74	4.38	0.00
GF-1.8-1-2	1.8	3.02	38.63	4.75	0.01
GF-1.8-2-1	1.8	3.13	37.95	4.63	0.00
GF-1.8-2-2	1.8	3.14	36.29	4.50	0.00

**Table A2-12** – Ultimate Analysis of Douglas fir tree bark after each ammonia adsorption experiment. In XX-A-B-C, A = ammonium sulphate concentration (AMS), B = ammonia adsorption experiment replicate number, C = ultimate analysis replicate number. Uncorr H = hydrogen uncorrected for moisture content.

Sample Name	AMS Conc (M)	N (wt%, dry basis)	C (wt%, dry basis)	Uncorr H (wt%, as received)	S (wt%, dry basis)
DF-0.05-1-1	0.05	1.65	28.10	2.70	0.00
DF-0.05-1-2	0.05	1.64	31.00	3.50	0.00
DF-0.05-2-1	0.05	1.86	34.48	3.33	0.00
DF-0.05-2-2	0.05	1.93	37.02	4.27	0.00
DF-0.5-1-1	0.5	3.53	37.85	3.78	0.00
DF-0.5-1-2	0.5	3.13	35.91	3.56	0.00
DF-0.5-2-1	0.5	3.30	35.29	4.16	0.00
DF-0.5-2-2	0.5	3.34	37.18	3.68	0.00
DF-1.8-1-1	1.8	3.96	35.70	4.13	0.00
DF-1.8-1-2	1.8	3.76	35.48	4.05	0.00
DF-1.8-2-1	1.8	3.81	35.16	4.07	0.00
DF-1.8-2-2	1.8	3.79	35.67	4.01	0.00

**Table A2-13** – Ultimate Analysis of oak after each ammonia adsorption experiment. In XX-A-B-C, A = ammonium sulphate concentration (AMS), B = ammonia adsorption experiment replicate number, C = ultimate analysis replicate number. Uncorr H = hydrogen uncorrected for moisture content.

Sample Name	AMS Conc (M)	N (wt%, dry basis)	C (wt%, dry basis)	Uncorr H (wt%, as received)	S (wt%, dry basis)
OAK-0.05-1-1	0.05	2.14	28.45	3.76	0.01
OAK-0.05-1-2	0.05	1.96	29.98	3.33	0.00
OAK-0.05-2-1	0.05	1.63	26.98	2.97	0.00
OAK-0.05-2-2	0.05	1.77	26.77	2.94	0.00
OAK-0.5-1-1	0.5	2.38	36.83	4.51	0.00
OAK-0.5-1-2	0.5	2.64	35.19	4.56	0.00
OAK-0.5-2-1	0.5	2.46	32.12	3.85	0.00
OAK-0.5-2-2	0.5	2.63	33.34	3.99	0.00
OAK-1.8-1-1	1.8	3.61	33.32	4.03	0.00
OAK-1.8-1-2	1.8	3.55	32.98	4.01	0.00
OAK-1.8-2-1	1.8	3.65	33.41	3.93	0.00
OAK-1.8-2-2	1.8	3.58	35.35	4.47	0.00

**Table A2-14** – Ultimate Analysis of peat moss after each ammonia adsorption experiment. In XX-A-B-C, A = ammonium sulphate concentration (AMS), B = ammonia adsorption experiment replicate number, C = ultimate analysis replicate number. Uncorr H = hydrogen uncorrected for moisture content.

Sample Name	AMS Conc (M)	N (wt%, dry basis)	C (wt%, dry basis)	Uncorr H (wt%, as received)	S (wt%, dry basis)
PEATMOSS-0.05-1-1	0.05	2.64	30.22	3.21	0.00
PEATMOSS-0.05-1-2	0.05	2.39	28.49	3.07	0.00
PEATMOSS-0.05-2-1	0.05	2.31	28.07	2.99	0.00
PEATMOSS-0.05-2-2	0.05	2.64	31.19	3.66	0.00
PEATMOSS-0.5-1-1	0.5	3.48	32.66	3.81	0.15
PEATMOSS-0.5-1-2	0.5	3.63	34.82	3.83	0.13
PEATMOSS-0.5-2-1	0.5	3.69	34.14	4.24	0.13
PEATMOSS-0.5-2-2	0.5	3.94	33.10	3.95	0.11
PEATMOSS-1.8-1-1	1.8	4.06	54.18	3.84	0.00
PEATMOSS-1.8-1-2	1.8	3.77	32.24	3.63	0.00
PEATMOSS-1.8-2-1	1.8	4.48	38.98	4.67	0.00
PEATMOSS-1.8-2-2	1.8	4.45	40.17	4.68	0.00

**Table A2-15** – Ultimate Analysis of PeatSEPO after each ammonia adsorption experiment. In XX-A-B-C, A = ammonium sulphate concentration (AMS), B = ammonia adsorption experiment replicate number, C = ultimate analysis replicate number. Uncorr H = hydrogen uncorrected for moisture content.

Sample Name	AMS Conc (M)	N (wt%, dry basis)	C (wt%, dry basis)	Uncorr H (wt%, as received)	S (wt%, dry basis)
PEATSEPO-0.05-1-1	0.05	2.81	32.27	4.35	0.00
PEATSEPO-0.05-1-2	0.05	3.27	34.48	4.18	0.00
PEATSEPO-0.05-2-1	0.05	2.55	31.02	3.35	0.00
PEATSEPO-0.05-2-2	0.05	2.73	32.42	3.90	0.00
PEATSEPO-0.5-1-1	0.5	3.85	34.16	3.98	0.27
PEATSEPO-0.5-1-2	0.5	3.93	33.73	3.96	0.21
PEATSEPO-0.5-2-1	0.5	3.86	33.24	3.83	0.24
PEATSEPO-0.5-2-2	0.5	3.74	32.26	3.71	0.23
PEATSEPO-1.8-1-1	1.8	5.58	34.52	3.95	0.00
PEATSEPO-1.8-1-2	1.8	4.21	34.96	3.83	0.00
PEATSEPO-1.8-2-1	1.8	4.29	36.35	4.28	0.00
PEATSEPO-1.8-2-2	1.8	4.92	40.71	4.67	0.00

**A.2.1.2.2.2. Treated samples**

**Table A2-16** – Ultimate Analysis of European silver fir tree bark biochar after each ammonia adsorption experiment. In XX-A-B-C, A = ammonium sulphate concentration (AMS), B = ammonia adsorption experiment replicate number, C = ultimate analysis replicate number. Uncorr H = hydrogen uncorrected for moisture content.

Sample Name	AMS Conc (M)	N (wt%, dry basis)	C (wt%, dry basis)	Uncorr H (wt%, as received)	S (wt%, dry basis)
ESFbc-0.05-1-1	0.05	1.77	68.56	2.65	0.00
ESFbc-0.05-1-2	0.05	1.93	68.94	2.63	0.00
ESFbc-0.05-2-1	0.05	1.69	57.35	2.15	0.00
ESFbc-0.05-2-2	0.05	1.81	68.72	2.68	0.00
ESFbc-0.05-3-1	0.05	1.46	71.42	2.70	0.00
ESFbc-0.05-3-2	0.05	1.51	71.91	2.81	0.00
ESFbc-0.5-1-1	0.5	2.08	69.88	2.72	0.00
ESFbc-0.5-1-2	0.5	2.10	68.48	2.64	0.00
ESFbc-0.5-2-1	0.5	2.12	69.58	2.81	0.00
ESFbc-0.5-2-2	0.5	2.06	69.94	2.74	0.00
ESFbc-1.8-1-1	1.8	2.22	69.99	2.90	0.00
ESFbc-1.8-1-2	1.8	2.12	69.62	2.82	0.00
ESFbc-1.8-2-1	1.8	2.21	71.18	3.00	0.00
ESFbc-1.8-2-2	1.8	2.13	68.34	2.86	0.00

**Table A2-17** – Ultimate Analysis of noble fir tree bark biochar after each ammonia adsorption experiment. In XX-A-B-C, A = ammonium sulphate concentration (AMS), B = ammonia adsorption experiment replicate number, C = ultimate analysis replicate number. Uncorr H = hydrogen uncorrected for moisture content.

Sample Name	AMS Conc (M)	N (wt%, dry basis)	C (wt%, dry basis)	Uncorr H (wt%, as received)	S (wt%, dry basis)
NFbc-0.05-1-1	0.05	1.79	62.56	2.41	0.00
NFbc-0.05-1-2	0.05	1.90	70.75	2.73	0.00
NFbc-0.05-2-1	0.05	1.53	64.45	2.40	0.00
NFbc-0.05-2-2	0.05	1.60	71.12	2.65	0.00
NFbc-0.05-3-1	0.05	1.48	72.48	2.77	0.00
NFbc-0.05-3-2	0.05	1.58	72.33	2.76	0.00
NFbc-0.5-1-1	0.5	1.86	66.40	2.34	0.00
NFbc-0.5-1-2	0.5	1.89	70.97	2.59	0.00
NFbc-0.5-2-1	0.5	1.67	55.48	2.00	0.00
NFbc-0.5-2-2	0.5	1.84	71.07	2.55	0.00
NFbc-1.8-1-1	1.8	2.03	71.87	2.76	0.00
NFbc-1.8-1-2	1.8	1.78	70.43	2.58	0.00
NFbc-1.8-2-1	1.8	2.04	71.32	2.56	0.00
NFbc-1.8-2-2	1.8	2.01	68.74	2.46	0.00

**Table A2-18** – Ultimate Analysis of Douglas fir tree bark biochar after each ammonia adsorption experiment. In XX-A-B-C, A = ammonium sulphate concentration (AMS), B = ammonia adsorption experiment replicate number, C = ultimate analysis replicate number. Uncorr H = hydrogen uncorrected for moisture content.

Sample Name	AMS Conc (M)	N (wt%, dry basis)	C (wt%, dry basis)	Uncorr H (wt%, as received)	S (wt%, dry basis)
DFbc-0.05-1-1	0.05	1.46	74.88	2.88	0.00
DFbc-0.05-1-2	0.05	1.40	78.54	2.86	0.00
DFbc-0.05-2-1	0.05	1.34	75.25	2.69	0.00
DFbc-0.05-2-2	0.05	1.45	78.87	2.88	0.00
DFbc-0.5-1-1	0.5	1.64	74.21	2.78	0.00
DFbc-0.5-1-2	0.5	1.66	75.57	2.85	0.00
DFbc-0.5-2-1	0.5	1.60	71.12	2.69	0.00
DFbc-0.5-2-2	0.5	1.69	73.88	2.83	0.00
DFbc-1.8-1-1	1.8	1.70	70.63	2.79	0.00
DFbc-1.8-1-2	1.8	1.79	76.87	3.06	0.00
DFbc-1.8-2-1	1.8	1.73	70.38	2.81	0.00
DFbc-1.8-2-2	1.8	1.77	74.29	3.02	0.00

**Table A2-19** – Ultimate Analysis of nootka cypress tree bark biochar after each ammonia adsorption experiment. In XX-A-B-C, A = ammonium sulphate concentration (AMS), B = ammonia adsorption experiment replicate number, C = ultimate analysis replicate number. Uncorr H = hydrogen uncorrected for moisture content.

Sample Name	AMS Conc (M)	N (wt%, dry basis)	C (wt%, dry basis)	Uncorr H (wt%, as received)	S (wt%, dry basis)
NCbc-0.05-1-1	0.05	1.25	70.03	2.72	0.00
NCbc-0.05-1-2	0.05	1.36	75.77	2.94	0.00
NCbc-0.05-2-1	0.05	1.18	64.39	2.41	0.00
NCbc-0.05-2-2	0.05	1.20	67.78	2.54	0.00
NCbc-0.5-1-1	0.5	1.36	52.68	2.38	0.13
NCbc-0.5-1-2	0.5	1.70	69.33	2.89	0.00
NCbc-0.5-2-1	0.5	1.74	67.41	2.91	0.00
NCbc-0.5-2-2	0.5	1.48	55.60	2.29	0.00
NCbc-1.8-1-1	1.8	1.75	66.72	3.06	0.00
NCbc-1.8-1-2	1.8	1.74	67.02	2.87	0.00
NCbc-1.8-2-1	1.8	1.78	69.32	3.17	0.00
NCbc-1.8-2-2	1.8	1.78	67.43	3.02	0.00

**Table A2-20** – Ultimate Analysis of Lawson cypress tree bark biochar after each ammonia adsorption experiment. In XX-A-B-C, A = ammonium sulphate concentration (AMS), B = ammonia adsorption experiment replicate number, C = ultimate analysis replicate number. Uncorr H = hydrogen uncorrected for moisture content.

Sample Name	AMS Conc (M)	N (wt%, dry basis)	C (wt%, dry basis)	Uncorr H (wt%, as received)	S (wt%, dry basis)
LCbc-0.05-1-1	0.05	1.42	76.23	2.78	0.00
LCbc-0.05-1-2	0.05	1.51	83.82	2.97	0.00
LCbc-0.05-2-1	0.05	1.31	79.90	2.78	0.00
LCbc-0.05-2-2	0.05	1.31	79.84	2.89	0.00

**Table A2-21** – Ultimate Analysis of larch tree bark biochar after each ammonia adsorption experiment. In XX-A-B-C, A = ammonium sulphate concentration (AMS), B = ammonia adsorption experiment replicate number, C = ultimate analysis replicate number. Uncorr H = hydrogen uncorrected for moisture content.

Sample Name	AMS Conc (M)	N (wt%, dry basis)	C (wt%, dry basis)	Uncorr H (wt%, as received)	S (wt%, dry basis)
Lbc-0.05-1-1	0.05	1.38	75.93	2.61	0.00
Lbc-0.05-1-2	0.05	1.36	78.15	2.77	0.00
Lbc-0.05-2-1	0.05	1.31	78.33	2.81	0.00
Lbc-0.05-2-2	0.05	1.34	75.25	2.66	0.00

**Table A2-22** – Ultimate Analysis of Norway spruce tree bark biochar after each ammonia adsorption experiment. In XX-A-B-C, A = ammonium sulphate concentration (AMS), B = ammonia adsorption experiment replicate number, C = ultimate analysis replicate number. Uncorr H = hydrogen uncorrected for moisture content.

Sample Name	AMS Conc (M)	N (wt%, dry basis)	C (wt%, dry basis)	Uncorr H (wt%, as received)	S (wt%, dry basis)
NSbc-0.05-1-1	0.05	1.37	60.96	2.44	0.00
NSbc-0.05-1-2	0.05	1.42	66.97	2.67	0.00
NSbc-0.05-2-1	0.05	1.57	67.45	2.68	0.00
NSbc-0.05-2-2	0.05	1.50	64.56	2.49	0.00

**Table A2-23** – Ultimate Analysis of NORIT activated carbon after each ammonia adsorption experiment. In XX-A-B-C, A = ammonium sulphate concentration (AMS), B = ammonia adsorption experiment replicate number, C = ultimate analysis replicate number. Uncorr H = hydrogen uncorrected for moisture content.

Sample Name	AMS Conc (M)	N (wt%, dry basis)	C (wt%, dry basis)	Uncorr H (wt%, as received)	S (wt%, dry basis)
NORIT-AC-0.05-1-1	0.05	1.32	67.62	0.73	0.47
NORIT-AC-0.05-1-2	0.05	1.22	61.70	0.21	0.51
NORIT-AC-0.05-2-1	0.05	1.24	70.13	0.23	0.57
NORIT-AC-0.05-2-2	0.05	1.33	68.62	0.23	0.62
NORIT-AC-0.5-1-1	0.5	1.55	71.18	0.23	0.52
NORIT-AC-0.5-1-2	0.5	1.57	64.01	0.31	0.32
NORIT-AC-0.5-2-1	0.5	1.49	60.49	0.30	0.26
NORIT-AC-0.5-2-2	0.5	1.38	66.39	0.22	0.36
NORIT-AC-1.8-1-1	1.8	1.22	56.33	0.27	0.00
NORIT-AC-1.8-1-2	1.8	1.28	64.84	0.69	0.00
NORIT-AC-1.8-2-1	1.8	1.49	65.68	0.58	0.00
NORIT-AC-1.8-2-2	1.8	1.32	60.69	0.29	0.00

**Table A2-24** – Ultimate Analysis of SIGMA activated carbon after each ammonia adsorption experiment. In XX-A-B-C, A = ammonium sulphate concentration (AMS), B = ammonia adsorption experiment replicate number, C = ultimate analysis replicate number. Uncorr H = hydrogen uncorrected for moisture content.

Sample Name	AMS Conc (M)	N (wt%, dry basis)	C (wt%, dry basis)	Uncorr H (wt%, as received)	S (wt%, dry basis)
SIGMA-AC-0.05-1-1	0.05	0.61	37.89	3.16	0.00
SIGMA-AC-0.05-1-2	0.05	0.44	40.06	2.03	0.00
SIGMA-AC-0.05-2-1	0.05	0.41	41.41	2.59	0.00
SIGMA-AC-0.05-2-2	0.05	0.41	38.57	2.80	0.00
SIGMA-AC-0.5-1-1	0.5	1.44	41.95	1.27	0.00
SIGMA-AC-0.5-1-2	0.5	1.48	41.41	1.86	0.00
SIGMA-AC-0.5-2-1	0.5	1.49	37.91	2.43	0.00
SIGMA-AC-0.5-2-2	0.5	1.51	32.65	0.88	0.00
SIGMA-AC-1.8-1-1	1.8	1.70	50.89	1.28	0.00
SIGMA-AC-1.8-1-2	1.8	1.45	47.02	1.07	0.00
SIGMA-AC-1.8-2-1	1.8	1.64	47.85	1.42	0.00
SIGMA-AC-1.8-2-2	1.8	1.66	48.40	1.37	0.00

**Table A2-25** – Ultimate Analysis of oak biochar after each ammonia adsorption experiment. In XX-A-B-C, A = ammonium sulphate concentration (AMS), B = ammonia adsorption experiment replicate number, C = ultimate analysis replicate number. Uncorr H = hydrogen uncorrected for moisture content.

Sample Name	AMS Conc (M)	N (wt%, dry basis)	C (wt%, dry basis)	Uncorr H (wt%, as received)	S (wt%, dry basis)
OAK450BC-0.05-1-1	0.05	0.47	13.18	0.30	0.00
OAK450BC-0.05-1-2	0.05	0.99	76.43	1.68	0.00
OAK450BC-0.05-2-1	0.05	1.50	66.81	2.89	0.00
OAK450BC-0.05-2-2	0.05	1.42	73.03	3.05	0.00
OAK450BC-0.5-1-1	0.5	1.50	72.90	2.12	0.00
OAK450BC-0.5-1-2	0.5	1.83	73.13	2.28	0.00
OAK450BC-0.5-2-1	0.5	2.08	67.8	2.56	0.00
OAK450BC-0.5-2-2	0.5	3.71	62.03	3.04	0.00
OAK450BC-1.8-1-1	1.8	1.40	63.60	2.19	0.00
OAK450BC-1.8-1-2	1.8	2.92	72.92	3.01	0.00
OAK450BC-1.8-2-1	1.8	2.45	71.96	2.36	0.00
OAK450BC-1.8-2-2	1.8	2.09	66.05	2.35	0.00

**Table A2-26** – Ultimate Analysis of hot water-washed Douglas fir tree bark biochar after each ammonia adsorption experiment. In XX-A-B-C, A = ammonium sulphate concentration (AMS), B = ammonia adsorption experiment replicate number, C = ultimate analysis replicate number. Uncorr H = hydrogen uncorrected for moisture content.

Sample Name	AMS Conc (M)	N (wt%, dry basis)	C (wt%, dry basis)	Uncorr H (wt%, as received)	S (wt%, dry basis)
HW-DFBC-0.05-1-1	0.05	1.14	70.83	2.59	0.00
HW-DFBC-0.05-1-2	0.05	0.99	70.78	2.90	0.00
HW-DFBC-0.05-2-1	0.05	0.94	70.08	2.56	0.00
HW-DFBC-0.05-2-2	0.05	0.86	67.24	2.79	0.00
HW-DFBC-0.5-1-1	0.5	2.44	71.38	2.75	0.00
HW-DFBC-0.5-1-2	0.5	1.93	70.95	2.74	0.00
HW-DFBC-0.5-2-1	0.5	1.93	71.76	2.74	0.00
HW-DFBC-0.5-2-2	0.5	1.97	71.86	2.93	0.00
HW-DFBC-1.8-1-1	1.8	2.04	74.36	2.86	0.00
HW-DFBC-1.8-1-2	1.8	1.94	71.79	2.77	0.00
HW-DFBC-1.8-2-1	1.8	1.93	66.54	2.77	0.00
HW-DFBC-1.8-2-2	1.8	2.12	75.16	3.03	0.00

**Table A2-27** – Ultimate Analysis of hot water-washed noble fir tree bark biochar after each ammonia adsorption experiment. In XX-A-B-C, A = ammonium sulphate concentration (AMS), B = ammonia adsorption experiment replicate number, C = ultimate analysis replicate number. Uncorr H = hydrogen uncorrected for moisture content.

Sample Name	AMS Conc (M)	N (wt%, dry basis)	C (wt%, dry basis)	Uncorr H (wt%, as received)	S (wt%, dry basis)
HW-NFBC-0.05-1-1	0.05	1.04	71.54	2.79	0.00
HW-NFBC-0.05-1-2	0.05	1.01	68.47	2.65	0.00
HW-NFBC-0.05-2-1	0.05	1.13	70.78	2.90	0.00
HW-NFBC-0.05-2-2	0.05	1.07	67.50	2.72	0.00
HW-NFBC-0.5-1-1	0.5	2.03	68.30	2.62	0.00
HW-NFBC-0.5-1-2	0.5	1.94	71.25	2.88	0.00
HW-NFBC-0.5-2-1	0.5	2.07	70.56	2.78	0.00
HW-NFBC-0.5-2-2	0.5	2.06	71.92	2.85	0.00
HW-NFBC-1.8-1-1	1.8	2.00	70.42	2.68	0.00
HW-NFBC-1.8-1-2	1.8	1.83	65.50	2.47	0.00
HW-NFBC-1.8-2-1	1.8	1.86	68.94	2.78	0.00
HW-NFBC-1.8-2-2	1.8	1.84	70.32	2.56	0.00

**Table A2-28** – Ultimate Analysis of Soxhlet-extracted grand fir tree bark after each ammonia adsorption experiment. In XX-A-B-C, A = ammonium sulphate concentration (AMS), B = ammonia adsorption experiment replicate number, C = ultimate analysis replicate number. Uncorr H = hydrogen uncorrected for moisture content.

Sample Name	AMS Conc (M)	N (wt%, dry basis)	C (wt%, dry basis)	Uncorr H (wt%, as received)	S (wt%, dry basis)
GF-SOX-0.05-1-1	0.05	1.29	34.04	4.12	0.00
GF-SOX-0.05-1-2	0.05	1.46	31.83	4.02	0.00
GF-SOX-0.05-2-1	0.05	1.40	29.92	3.71	0.00
GF-SOX-0.05-2-2	0.05	1.51	32.25	4.09	0.00
GF-SOX-0.5-1-1	0.5	2.37	35.9	4.84	0.00
GF-SOX-0.5-1-2	0.5	2.17	37.46	4.17	0.00
GF-SOX-0.5-2-1	0.5	1.96	41.12	5.38	0.00
GF-SOX-0.5-2-2	0.5	2.05	38.67	4.33	0.00
GF-SOX-1.8-1-1	1.8	2.11	36.42	4.46	0.00
GF-SOX-1.8-1-2	1.8	1.90	36.71	4.60	0.00
GF-SOX-1.8-2-1	1.8	1.91	34.43	4.23	0.00
GF-SOX-1.8-2-2	1.8	1.83	32.71	4.05	0.25

**Table A2-29** – Ultimate Analysis of Soxhlet-extracted Douglas fir tree bark after each ammonia adsorption experiment. In XX-A-B-C, A = ammonium sulphate concentration (AMS), B = ammonia adsorption experiment replicate number, C = ultimate analysis replicate number. Uncorr H = hydrogen uncorrected for moisture content.

Sample Name	AMS Conc (M)	N (wt%, dry basis)	C (wt%, dry basis)	Uncorr H (wt%, as received)	S (wt%, dry basis)
DF-SOX-0.05-1-1	0.05	1.52	32.53	3.76	0.00
DF-SOX-0.05-1-2	0.05	1.27	29.41	3.58	0.00
DF-SOX-0.05-2-1	0.05	1.47	32.53	3.73	0.00
DF-SOX-0.05-2-2	0.05	1.35	31.94	3.80	0.00
DF-SOX-0.5-1-1	0.5	2.82	33.50	3.89	0.00
DF-SOX-0.5-1-2	0.5	3.05	32.79	3.99	0.00
DF-SOX-0.5-2-1	0.5	3.02	34.39	4.26	0.00
DF-SOX-0.5-2-2	0.5	3.04	34.52	4.03	0.00
DF-SOX-1.8-1-1	1.8	3.64	39.29	4.69	0.00
DF-SOX-1.8-1-2	1.8	3.45	39.91	4.74	0.00
DF-SOX-1.8-2-1	1.8	3.92	40.90	4.88	0.00
DF-SOX-1.8-2-2	1.8	3.58	41.53	4.92	0.00

**Table A2-30** – Ultimate Analysis of municipal solid waste digestate after each ammonia adsorption experiment. In XX-A-B-C, A = ammonium sulphate concentration (AMS), B = ammonia adsorption experiment replicate number, C = ultimate analysis replicate number. Uncorr H = hydrogen uncorrected for moisture content.

Sample Name	AMS Conc (M)	N (wt%, dry basis)	C (wt%, dry basis)	Uncorr H (wt%, as received)	S (wt%, dry basis)
MSWdig-0.05-1-1	0.05	1.47	12.83	1.01	0.08
MSWdig-0.05-1-2	0.05	1.70	12.53	0.92	0.09
MSWdig-0.05-2-1	0.05	1.37	16.47	1.5	0.22
MSWdig-0.05-2-2	0.05	0.90	16.03	1.29	0.2
MSWdig-0.5-1-1	0.5	1.38	17.26	1.44	0.22
MSWdig-0.5-1-2	0.5	1.23	14.49	1.20	0.21
MSWdig-0.5-2-1	0.5	1.17	16.73	1.30	0.23
MSWdig-0.5-2-2	0.5	1.09	15.28	1.32	0.18
MSWdig-1.8-1-1	1.8	1.26	20.82	2.38	0.30
MSWdig-1.8-1-2	1.8	1.01	16.64	1.76	0.00
MSWdig-1.8-2-1	1.8	1.23	19.37	2.37	0.22
MSWdig-1.8-2-2	1.8	1.29	18.33	2.16	0.25

**Table A2-31** – Ultimate Analysis of vegetable, garden, and fruit residue digestate after each ammonia adsorption experiment. In XX-A-B-C, A = ammonium sulphate concentration (AMS), B = ammonia adsorption experiment replicate number, C = ultimate analysis replicate number. Uncorr H = hydrogen uncorrected for moisture content.

Sample Name	AMS Conc (M)	N (wt%, dry basis)	C (wt%, dry basis)	Uncorr H (wt%, as received)	S (wt%, dry basis)
VGFDig-0.05-1-1	0.05	0.95	10.68	1.21	0.00
VGFDig-0.05-1-2	0.05	1.33	17.9	1.92	0.19
VGFDig-0.05-2-1	0.05	1.32	17.74	2.21	0.18
VGFDig-0.05-2-2	0.05	1.50	17.61	2.01	0.20
VGFDig-0.5-1-1	0.5	1.98	17.29	1.83	0.11
VGFDig-0.5-1-2	0.5	1.8	14.9	1.67	0.10
VGFDig-0.5-2-1	0.5	1.76	15.19	1.66	0.10
VGFDig-0.5-2-2	0.5	1.96	21.23	2.33	0.12
VGFDig-1.8-1-1	1.8	2.28	26.50	3.20	0.72
VGFDig-1.8-1-2	1.8	2.64	26.94	3.19	0.38
VGFDig-1.8-2-1	1.8	1.37	12.72	1.38	0.15
VGFDig-1.8-2-2	1.8	1.83	16.56	1.94	0.20

**A.2.1.2.3. Example of calculation for converting nitrogen content from ultimate analysis into adsorption capacities**

In this section, the calculation from the nitrogen content (from ultimate analysis) to ammonia adsorption capacity of a sample are illustrated using screenshots from Microsoft Excel.

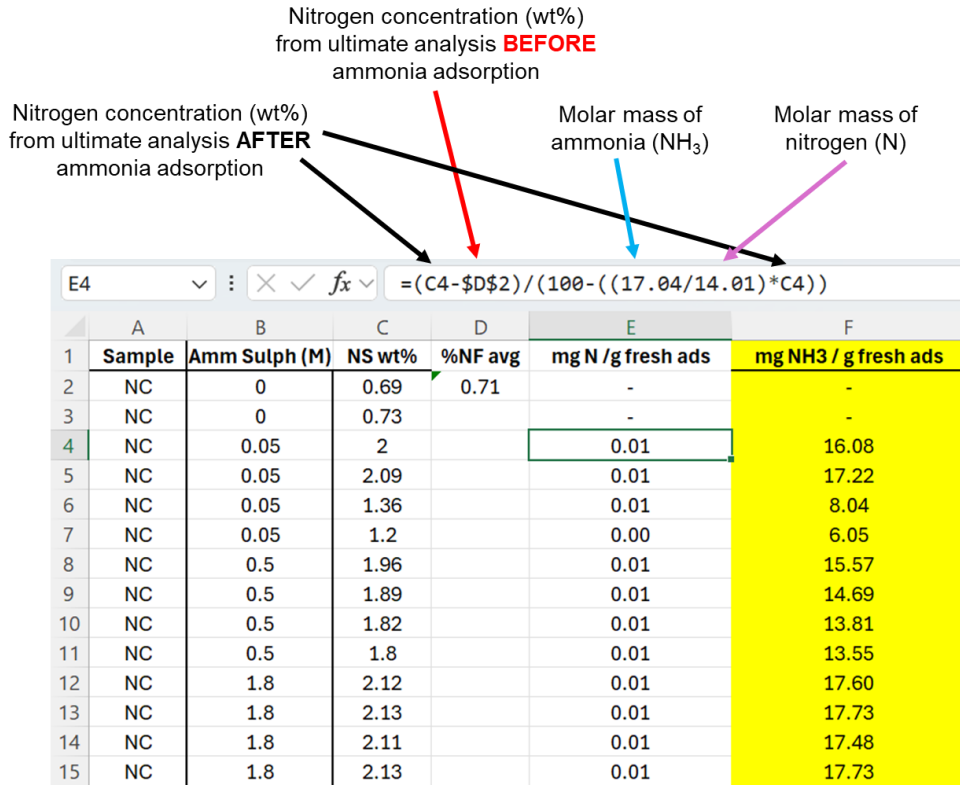


**Figure A2-1** – Screenshot of the Microsoft Excel worksheet (in particular the calculation of mgN/g fresh adsorbent) used for calculating the adsorption capacity of this study's samples after ammonia adsorption testing.

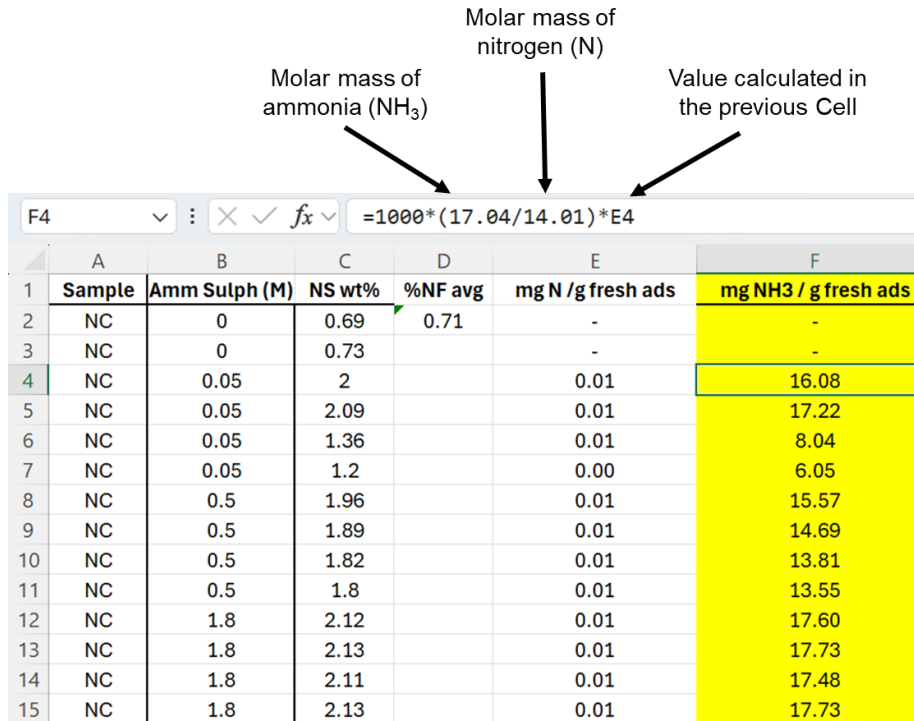


**Figure A2-2**– Screenshot of the Microsoft Excel worksheet (in particular the calculation of mgNH<sub>3</sub>/g fresh adsorbent) used for calculating the adsorption capacity of this study's samples after ammonia adsorption testing.

### A.2.1.3 Fibre analysis data

In this section, the tables presented show the fibre analysis results for the samples that underwent ammonia adsorption testing.

**Table A2-32** – Fibre Analysis of raw tree barks used in Chapter 7. Error calculated by 1x standard deviation. Samples run in duplicate.

Sample	Cellulose (wt%)	Hemicellulose (wt%)	Lignin (wt%)	Unknown (wt%)
NF	23.4 ± 0.0	2.1 ± 0.5	48.3 ± 1.0	22.1
ESF	38.9 ± 0.5	4.5 ± 0.0	45.0 ± 1.0	5.5
GF	39.5 ± 0.1	8.1 ± 0.6	22.2 ± 0.2	26.8
DF	20.0 ± 9.4	4.1 ± 0.3	32.3 ± 0.5	39.8
NC	33.0 ± 0.2	8.8 ± 0.5	14.8 ± 0.6	37.3
Oak	19.6 ± 0.2	0.0 ± 0.0	25.0 ± 1.1	43.8

**Table A2-33** – Fibre Analysis of ‘miscellaneous’ samples used in Chapter 7. Error calculated by 1x standard deviation. Samples run in duplicate.

Sample	Cellulose (wt%)	Hemicellulose (wt%)	Lignin (wt%)	Unknown (wt%)
MSWdig	6.5 ± 1.5	12.3 ± 0.0	17.5 ± 2.0	4.0
VGFdig	13.1 ± 1.2	3.8 ± 0.3	24.1 ± 0.3	6.4
CH	33.4 ± 1.5	2.6 ± 0.0	42.5 ± 2.9	9.0
AlkLig	6.1 ± 0.0	24.5 ± 0.9	39.2 ± 1.7	9.6
PeatSEPO	14.8 ± 0.3	0.5 ± 0.0	57.9 ± 1.8	22.1
PeatMoss	27.6 ± 0.2	0.6 ± 0.0	42.6 ± 0.1	18.7
Lignoboost	3.6 ± 1.5	29.8 ± 0.5	40.9 ± 0.5	9.6

### A.2.2 Calculation of the partial pressures from the mass of ammonia.

This section will describe how the partial pressure of ammonia was calculated for the 1.8M ammonium sulphate solution. The volumes of the pure reagent and the dilution (with water) are outlined in Table A2-34 and Table A2-35.

**Table A2-34** – Dilutions of ammonium sulphate and NaOH at each ammonia adsorption experiment.

Ammonium Sulphate (98.5% purity)				NaOH (97% purity)			
Conc (M)	Vol of dilution (ml)	Solid mass (g)	Vol of water (ml)	Conc (M)	Vol of dilution (ml)	Solid mass (g)	Vol of water (ml)
0.05	25	0.17	24.91	0.1	60	0.25	59.84
0.50	25	1.68	24.05	1	60	2.47	58.37
1.76	25	5.91	21.66	3	60	7.42	55.10

**Table A2-35** – Total volumes of water used in the dilutions of ammonium sulphate and NaOH at each ammonia adsorption experiment.

Desired AMS concentration (M)	Total volume of water used (ml)
0.05	84.74
0.50	82.42
1.76	76.76

This data was inputted into Microsoft Excel (in the yellow cells), with the Solver being run once all of the necessary data was added.

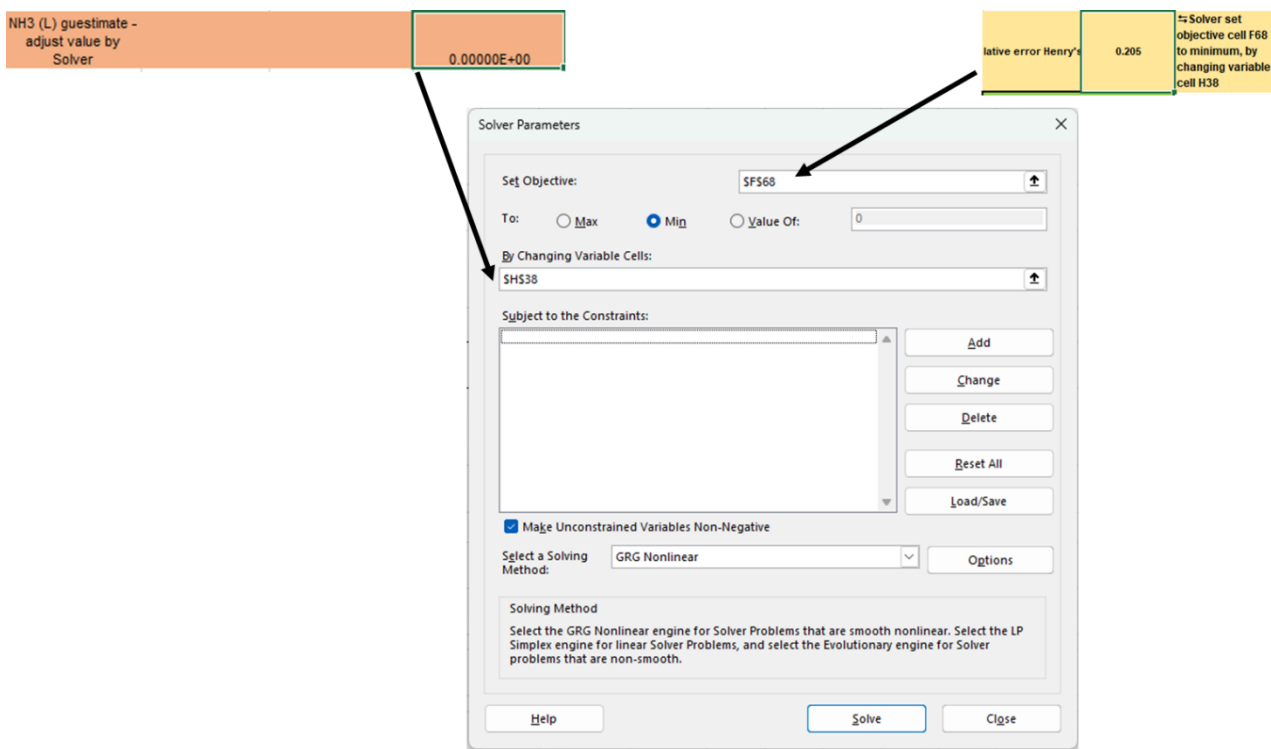
[a]

formula	mass (g)	molar mass (g/mol)	moles compound		
(NH4)2SO4	5.91	132.17	0.0447		
NaOH	7.42	40	0.1855		
Volume H2O in as per expt (ml)	76.76	is 2 N NaOH > AMS ?	YES		
Tads( C)	20				
H2O density at Tads (g/mL)	0.997800	→polynomial of temperature			
H2O mass in (g)	76.59109248	18.02	4.250		
$2 NaOH_{(aq)} + (NH_4)_2SO_{4(aq)} \rightarrow Na_2SO_{4(aq)} + 2H_2O_{(l)} + 2NH_{3(g)}$					
			<b>N moles</b>	<b>mol fraction (L)</b>	
NH3 total - assume no NH4+			8.94303E-02		
NH3 (L) gestimate - adjust value by Solver			8.93287E-02	0.0195473	
NH3(G) calc by difference with tot and (L)			1.01597E-04		
product reaction H2O <sub>R</sub>			8.94303E-02		
total H2O (Liq) before reaction			4.33977E+00	0.9496456	
excess NaOH (Liq) (basic)			9.60697E-02	0.0210224	
product Na2SO4 (Liq) (neutral)			4.47151E-02	0.0097847	
total (Liq)			4.56988E+00	1	
Volume bottle (mL)	250				
Mass H2O <sub>R</sub> (g)	1.61153E+00				
Vol H2O <sub>R</sub> (mL)	1.61509E+00				
Volume Liquid (mL)	78.375				
Volume before reaction (Gas) (cm3)	171.6				
				A	B
			H2O Antoine's constants (NIST)	4.6543	1435.264
Total Pressure before reaction (kPa)	100.00	assumed same as atmospheric pressure	log10 (P0,H2O (bar))	-1.6323904	
total Air moles before reaction and before water-moisture equilibrium (moles)	7.0454E-03	from ideal gas law	P0,H2O (bar)	0.0233136	<b>Antoine Equ</b>
Partial pressure H2O moisture before reaction and after water - moisture equilibrium (kPa)	2.2140E+00	from Raoult's law	P0,H2O (kPa)	2.33	log <sub>10</sub> (P) = A - (B / T) P = vapor pressure T = temperature
moles of H2O moisture after water-moisture equilibrium and before reaction	1.5590E-04	from ideal gas law			

[b]

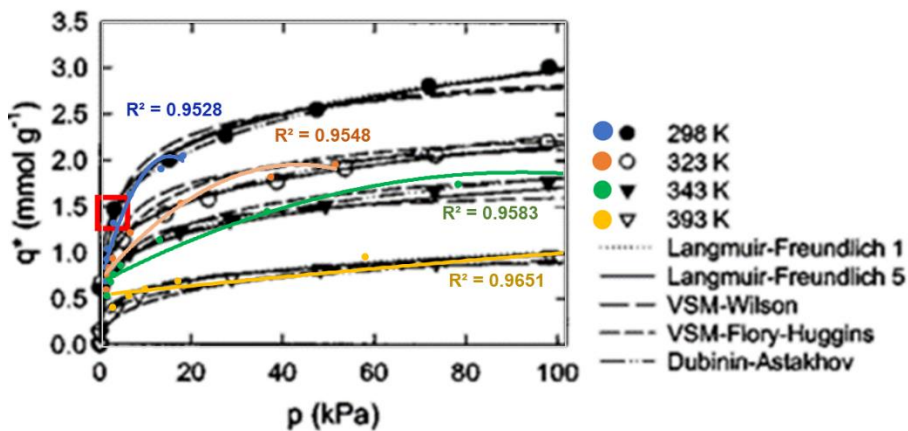
total Gas moles after reaction (air+NH3(G)+moisture)	7.3029E-03			after reaction	
Ptot Total Pressure after reaction (kPa)	103.65	from ideal gas law	mol fraction NH3 gas (y) =	0.01391	mol fraction moisture =
Henry's constant aqueous NH3 at Tads (mol/(m3Pa))	0.750237475	Sander 2015 table 6c	mol fraction NH3 liq (x) =	0.01955	
H cp @ 298K Sander et al 2011 in mol/(m3 Pa)	0.59	Sander 2015 table 6c	is y small (<0.05)?	YES	
d (lnH)/ d(1/T) Sander et al 2011 (K)	4200	Sander 2015 table 6c	is x small (<0.05)?	YES	
Henry's constant aq.NH3 at Tads (1/atm)	1.37360229				
Henry's constant aqNH3 at Tads (kPa)	73.77				
<b>Henry's law: y Ptot = x H</b>					
x H (kPa)	1.44192129E+00				
y Ptot (kPa)	1.44204318E+00		is Solver error acceptable?	YES	
% relative error Henry's law	0.008	⇄ Solver set objective cell F68 to minimum, by changing variable cell H38			
<b>P<sub>NH3</sub> Partial pressure of NH3 (kPa)</b>		<b>1.4420432</b>			

Figure A2-3 [a] and [b] – Screenshot of the Microsoft Excel worksheet used for calculating the partial pressure of ammonia (in this case, for 1.8M of ammonium sulphate).



**Figure A2-4** – Screenshot of Solver used in the Microsoft Excel worksheet used for calculating the partial pressure of ammonia (in this case, for 1.8M of ammonium sulphate).

The outputs of using Solver were validated by comparing them to Helminen et al's initial data, by calculating the adsorption capacity at the four adsorption temperatures tested by Helminen et al (298, 323, 343 and 393 K).



**Figure A2-5** – Validation of Helminen's adsorption capacity of alumina as an adsorbent to values generated by Microsoft Excel in this study.

### A.2.3 List of inputs for D-A models from Helminen et al.'s data.

In this section, the isothermic parameters used by Helminen et al. (380) will be outlined (Table A2-36).

**Table A2-36** – The isotherm parameters of the sorbents investigated by Helminen et al. (380) for the Dubinin-Astakhov ammonia adsorption equilibrium model.

<b>Isotherm Model</b>	<b>Isotherm Parameters</b>	<b>R<sup>2</sup> (%)</b>	<b>Total SS</b>	<b>RSS</b>	<b>Standard Error of Estimate</b>
<b>Alumina</b>	$W_0 = 0.159 \pm 0.012 \text{ cm}^3\text{g}^{-1}$	99.78	24	0.05	0.042
	$E = 10.0 \pm 0.9 \text{ kJmol}^{-1}$				
	$n = 0.844 \pm 0.055$				
<b>4A Zeolite</b>	$W_0 = 252 \pm 6 \times 10^{-3} \text{ cm}^3\text{g}^{-1}$	98.96	269	2.8	0.310
	$E = 24.6 \pm 0.5 \text{ kJmol}^{-1}$				
	$n = 2.47 \pm 0.18$				
<b>13X Zeolite</b>	$W_0 = 262 \pm 7 \times 10^{-3} \text{ cm}^3\text{g}^{-1}$	99.08	289	2.7	0.304
	$E = 24.8 \pm 0.5 \text{ kJmol}^{-1}$				
	$n = 2.26 \pm 0.17$				
<b>Activated Carbon</b>	$W_0 = 2.31 \pm 2.06 \text{ cm}^3\text{g}^{-1}$	98.84	44	0.51	0.125
	$E = 1.51 \pm 1.15 \text{ kJmol}^{-1}$				
	$n = 0.751 \pm 0.187$				
<b>Silica Gel</b>	$W_0 = 159 \pm 10 \times 10^{-3} \text{ cm}^3\text{g}^{-1}$	98.97	62	0.63	0.148
	$E = 16.7 \pm 0.8 \text{ kJmol}^{-1}$				
	$n = 1.62 \pm 0.15$				

### A.2.4. Calculation of the partial pressure of ammonia

The method of generating ammonia in glass bottles (as described in Table 3-10) occurred due to the reaction between ammonium sulphate and sodium hydroxide in a water solution. In the glass bottles, the headspace available for the  $\text{NH}_3$  gas product is therefore finite. For this reason, an equilibrium between gaseous ammonia and dissolved ammonia in the water, as well as moisture in the headspace, was expected to establish themselves. The total pressure in the headspace therefore depends on the equilibrium amounts of gaseous  $\text{NH}_3$ , the air present before the reaction, and the equilibrium amount of moisture. The liquid-vapour equilibrium of  $\text{NH}_3$  was determined by Henry's law, and the liquid-vapour equilibrium of water was determined by Raoult's law.

The calculation of the equilibrium partial pressure of ammonia,  $P_{\text{NH}_3}$ , requires information on ammonia's Henry's constant,  $H$ , which is temperature dependent. Here, Henry's constant for ammonia is calculated using Sander (2023) (783), as outlined later in Error! Reference source not found.. 'H' is then used according to Henry's law as given in **Equation A2-1**. In **Equation A2-1**,  $P_{\text{tot}}$  is the total pressure after reaction, 'y' is the  $\text{NH}_3$  gas molar fraction after reaction, and 'x' is the molar fraction of  $\text{NH}_3$  in equilibrium in the aqueous liquid phase.

**Equation A2-1** – Application of Henry's law for the calculation of the post-reaction ammonia gas molar fraction (y).

$$P_{\text{NH}_3} = xH = yP_{\text{tot}}$$

However, certain assumptions must be made to ensure that  $P_{\text{NH}_3}$  is valid, as the Henry's constant calculation only applies to non-ideal solutions where the solute is very dilute.

#### A.2.4.1. Assumptions necessary for validation of Henry's law

First, the sodium hydroxide (NaOH) added to the Duran bottle must be in excess (in terms of molarity) compared to ammonium sulphate so that it can be assumed that all of the ammonium sulphate reacts. The reacted ammonium sulphate is then completely converted into gaseous and/or dissolved  $\text{NH}_3$  along with liquid-phase  $\text{H}_2\text{O}$  and  $\text{Na}_2\text{SO}_4$ , with some of the excess NaOH remaining in the liquid phase. Through the production of neutral pH  $\text{Na}_2\text{SO}_4$ , alongside the basic (pH > 7) sodium hydroxide, the product solution is also basic. Due to the chemical reaction occurring in Equation 3-10, an alkaline product solution will favour the dissolved ammonia over the ammonium ion ( $\text{NH}_4^+$ ) products in the aqueous

solution. It can then be assumed that the only  $\text{NH}_x$  product in solution is  $\text{NH}_3$  (liq), with no  $\text{NH}_4^+$  co-product present.

In terms of the volumes of compounds ( $\text{NaOH}$  and  $\text{Na}_2\text{SO}_4$ ) that would be present in the bottle during the test, it is assumed that they are negligible compared to the total volume of water, and are both fully dissolved in the water due to their high solubilities. The total volume of water is therefore assumed to be the total volume of liquid in the bottle. The same can be assumed to the sample holder material (the cap) and solid material (the sample), where their volumes are assumed to be negligible to the total volume of liquid in the bottle.

Once the sulphuric acid has been added and the reaction has finished, it is assumed that the molar fraction of ammonia in the gas phase ('y' in **Equation A2-1**) is small, so the ideal gas law applies. The post-reaction gas-phase is assumed to be mostly air with a bit of moisture, with the aqueous and gaseous  $\text{NH}_3$  assumed to be in equilibrium:  $\text{NH}_3(g) \rightleftharpoons \text{NH}_3(l)$ . As the aqueous molar fraction of ammonia ('x' in **Equation A2-1**) is assumed to be small, Henry's law can be applied to the equilibrium.

#### **A.2.4.2. Determination of partial pressure using Henry's law**

The application of Henry's law (**Equation A2-1**) in Microsoft Excel requires a starting guesstimate of the molar fractions of ammonia in the gaseous and vapour phase. 'Solver' is then used to minimise the error between the right hand side and left hand side of Equation A2-1.

First, the volume of liquid water present before the reaction ( $V_{\text{H}_2\text{O},\text{in}}$ ) is converted to the mass of liquid water ( $M_{\text{H}_2\text{O},\text{in}}$ ) using a time-dependent density polynomial fit (784). By applying the data from Walker (784), a temperature-dependent polynomial of order two was fit (with an  $R^2$  of 0.9994165) for the density of pure liquid water ( $\rho_{\text{H}_2\text{O}}$ ), according to Equation A2-1. Here, 'T' is the temperature in °C. At 20 °C, for example, the density of pure liquid water is 0.997800  $\text{gml}^{-1}$ .

**Equation A2-2** – The temperature-dependent polynomial equation to calculate the density of pure liquid water (784).

$$\rho_{\text{H}_2\text{O}}(\text{gml}^{-1}) = -3.985363 \times 10^{-6} \times T^2 - 3.776588 \times 10^{-5} \times T + 1.000149$$

After the estimation of the density, the mass of the liquid water is calculated by **Equation A2-3**. The mass of each component ( $M_{i,\text{in}}$ ) was then converted to moles ( $N_{i,\text{in}}$ ) using **Equation A2-4**.

**Equation A2-3** – Calculation of the mass of liquid water.

$$M_{H_2O,in} = \rho_{H_2O} \times V_{H_2O,in}$$

**Equation A2-4** – Calculation of the number of moles from component masses.  $W_i$  is molar mass. This equation is valid for NaOH ( $N_{NaOH}$ ), ammonium sulphate ( $N_{AMS}$ ) and water ( $N_{H_2O}$ ).

$$N_{i,in} = \frac{M_{i,in}}{W_i}$$

As presented in the chemical reaction in **Equation 3-10**, each mole of ammonium sulphate (AMS) is taken to generate two moles of  $NH_3$ , therefore  $N_{NH_3} = 2N_{AMS,in}$ , where  $N_{NH_3}$  is the total molar amount of  $NH_3$  product. The sodium hydroxide (NaOH) volume is kept in excess by ensuring that the moles of NaOH are always at least double that of AMS ( $N_{AMS,in} < 2 N_{NaOH,in}$ ) via a logical test in Microsoft Excel.

The number of moles of the non- $NH_3$  products, that of  $H_2O$  and  $Na_2SO_4$ , are compared to the moles of  $NH_3$  via **Equation A2-5**, where  $N_{NS}$  and  $N_{H_2O,R}$  are the moles of sodium sulphate water in the reaction, respectively.

**Equation A2-5** – Calculation of the number of moles of sodium sulphate ( $N_{NS}$ ) and water in the reaction ( $N_{H_2O,R}$ ), relative to the moles of ammonia ( $N_{NH_3}$ ).

$$N_{H_2O,R} = N_{NH_3}$$

$$N_{NS} = 0.5N_{NH_3}$$

After the reaction, the remaining number of moles of sodium hydroxide can be calculated by **Equation A2-6**.

**Equation A2-6** – Calculation of the number of moles of NaOH present after reaction.

$$N_{NaOH} = N_{NaOH,in} - N_{NH_3}$$

The total number of moles that is present in the liquid phase after the reaction can be calculated by **Equation A2-7**, where the molar amount of ammonia ( $N_{L,NH_3}$ ) is given an assumed value to begin with. Therefore, the mole fraction of ammonia in the liquid phase (also known as 'x') can be calculated from **Equation A2-8**.

**Equation A2-7** – Calculation of the total number of moles present in the liquid phase after reaction.

$$N_{L,tot} = N_{NaOH} + N_{NS} + N_{H_2O,in} + N_{H_2O,R}$$

**Equation A2-8** – Calculation of mole fraction of ammonia in the liquid phase.

$$x = \frac{N_{L,NH_3}}{N_{L,tot}}$$

The values of 'x' and  $N_{L,NH_3}$  are adjusted in the Microsoft Excel workbook at the final step of this methodology through the use of Solver to minimise the error in the Henry's law equation (**Equation A2-1**). This error is calculated according to **Equation A2-9**, as Henry's law is  $xH - yP_{tot} = 0$  (where  $yP_{tot} = P_{NH_3}$  is from Dalton's law).

**Equation A2-9** – Calculation of error after application of Henry's law.

$$100 \times Abs \frac{(xH - yP_{tot})}{(yP_{tot})} = \% \text{ error}$$

The molar amount of ammonia in the gas phase,  $N_{G,NH_3}$ , is determined by **Equation A2-10**.

**Equation A2-10** – Calculation of the molar amount of ammonia present in the gas phase.

$$N_{G,NH_3} = N_{NH_3} - N_{L,NH_3}$$

The total volume of gas before reaction,  $V_{G,tot, b.r.}$ , was calculated by difference between the bottle volume,  $V_{tot}$ , and total liquid volume before reaction,  $V_{L,tot,b,r.}$ , as described in **Equation A2-11**. Here,  $V_{L,tot,b,r.}$  changes in each experiment whilst  $V_{tot}$  remains constant (250 ml).

**Equation A2-11** – Calculation of the total volume of gas present before reaction.

$$V_{G,tot,b,r.} = V_{tot} - V_{L,tot,b,r.}$$

The ideal gas law applies here also (as shown in **Equation 3-19**), but can be expressed as in **Equation A2-12**. Here,  $P_{tot,b,r.}$  is assumed to be 1 bar (or  $10^5$  Pa) and R is the universal gas constant ( $8.314 \text{ Jmol}^{-1}\text{K}^{-1}$ ). The gas that is present before the reaction is assumed to only be air.

**Equation A2-12** – Application of the ideal gas law for the calculation of the number of moles present in the gas phase before reaction.

$$N_{G,tot,b,r.}(\text{mol}) = \frac{P_{tot,b,r.}(\text{Pa}) \times V_{G,tot,b,r.}(\text{m}^3)}{R(\text{Jmol}^{-1}\text{K}^{-1}) \times T_{ads}(\text{K})}$$

Once the lid is closed on the Duran bottles in the experiment, and a water-moisture equilibrium is established, there is  $N_{H_2O,moist}$  in the gas which obeys Raoult's law (Error! Reference source not found.). Here,  $x_{H_2O,moist}$  is the mole fraction of moisture in the gas phase before reaction,  $P_{0,H_2O,moist}$  is the vapour pressure of  $H_2O$  at the adsorption temperature (which is given by Antoine's equation), and  $P_{H_2O,moist}$  is the partial pressure of moisture in the gas phase.

**Equation A2-13 – Raoult's law**

$$x_{H_2O,moist} \times P_{0,H_2O,moist} = P_{H_2O,moist}$$

The moles of water in the moisture was calculated by another adaptation of the ideal gas law (**Equation A2-14**).

**Equation A2-14 – Application of the ideal gas law for water held in the moisture after sealing the reaction bottle.**

$$N_{H_2O,moist} (mol) = \frac{P_{H_2O,moist} (Pa) \times V_{G,tot,b.r} (m^3)}{R (Jmol^{-1}K^{-1}) \times T_{ads} (K)}$$

After reaction, the moles of gas was considered to be  $N_{G,tot}$ , as with **Equation A2-15**.

**Equation A2-15 – Calculation of number of moles in the gas phase after reaction.**

$$N_{G,tot} = N_{G,tot,b.r} + N_{H_2O,moist} + N_{G,NH_3}$$

The mole fractions of ammonia in the gas phase can therefore be calculated according to **Equation A2-16**.

**Equation A2-16 – Calculation of mole fractions of ammonia in the gas phase.**

$$y = \frac{N_{G,NH_3}}{N_{G,tot}}$$

$$y_{moist} = \frac{N_{H_2O,moist}}{N_{G,tot}}$$

The volume of liquid after reaction,  $V_{L,tot}$ , is the sum of  $V_{L,tot,b.r}$  with the volume of water produced by the reaction,  $V_{H_2O,R}$  (**Equation A2-19**).  $V_{H_2O,R}$  is determined by converting  $N_{H_2O,R}$  into the mass of liquid water produced,  $M_{H_2O,R}$ , via the molar mass of  $H_2O$ ,  $W_{H_2O}$  (**Equation A2-17**). The  $M_{H_2O,R}$  is converted into the volume of liquid water produced,  $V_{H_2O,R}$ , by the density,  $\rho_{H_2O}$ , of liquid water at  $T_{ads}$  (**Equation A2-18**). This was derived earlier in **Equation A2-2**.

**Equation A2-17 – Calculation of mass of liquid water produced from the reaction.**

$$M_{H_2O,R} = W_{H_2O} (18.02 \text{ gmol}^{-1}) \times N_{H_2O,R}$$

**Equation A2-18– Calculation of volume of liquid water produced from the reaction.**

$$V_{H_2O,R} = \frac{M_{H_2O,R}}{\rho_{H_2O}}$$

**Equation A2-19 – Calculation of volume of liquid contained in the Duran bottle after reaction.**

$$V_{L,tot} = V_{L,tot,b.r} + V_{H_2O,R}$$

After the reaction, the total volume of gas can be calculated by **Equation A2-20**.

**Equation A2-20** – Calculation of volume of gas contained in the Duran bottle after reaction.

$$V_{G,tot} = V_{tot} - V_{L,tot}$$

By applying the ideal gas law, the total pressure,  $P_{tot}$ , after the reaction can be calculated by **Equation A2-21**.

**Equation A2-21** – Calculation of the total pressure in the Duran bottle after reaction.

$$P_{tot} = \frac{N_{G,tot} \times R \times T_{ads}}{V_{G,tot}}$$

The partial pressure of ammonia in the Duran bottle is therefore illustrated by **Equation A2-22**.

**Equation A2-22** – Calculation of the partial pressure of ammonia in the Duran bottle after reaction, according to Dalton's law, as a function of the right hand side term of Henry's law

$$(xH = yP_{tot} = P_{NH_3}).$$

$$P_{NH_3} = y \times P_{tot}$$

The following step was to ensure that Henry's law, which describes the equilibrium between ammonia dissolved in the liquid and gaseous ammonia, is observed in the conditions of  $T_{ads}$  and  $P_{NH_3}$ . The Henry's constant for a very dilute  $NH_3$  concentration in water is dependent on the temperature of equilibrium. Sander (783) noted that the Henry's constant for ammonia can be calculated by setting the Henry solubility at the reference temperature ( $H^\ominus$ ) as  $0.590 \text{ molm}^{-3}\text{Pa}^{-1}$  and  $-\Delta_{sol}H/R$  as 4200 K (by  $\text{Jmol}^{-1}/\text{JK}^{-1}\text{mol}^{-1}$ ), for use in **Equation A2-23**.

**Equation A2-23** – Calculation of Henry's constant (783).  $T^\ominus$  is 298.15K.

$$H(T) = H^\ominus \times e^{\frac{-\Delta_{sol}H}{R} \times \left(\frac{1}{T} - \frac{1}{T^\ominus}\right)}$$

The units used for Henry's law constants differ across the literature. For this work, the unit to be used is kPa, as that is the common unit used in adsorption isotherms (384, 785).  $1 \text{ molm}^{-3}\text{Pa}^{-1}$  is equivalent to  $1.83089 \text{ atm}^{-1}$ , where 1 atm equals 101.325 kPa. Therefore, where  $T = 20^\circ\text{C}$ , or 293.15K,  $H(T) = 0.750237475 \text{ molm}^{-3}\text{Pa}^{-1}$ , this can be converted to kPa by **Equation A2-24**.

**Equation A2-24** – Value of Henry's constant (783) at  $20^\circ\text{C}$ , where  $T^\ominus$  is 298.15K.

$$H_{aqNH_3@20^\circ\text{C}}(\text{kPa}) = \frac{1}{1.37360229} \times 101.325 = 73.77 \text{ kPa}$$

All of the equations described so far were based on an estimate of  $N_{L,NH_3}$ . This led to an assumed value of  $x$ , the mole fraction of  $NH_3$  in the liquid phase. The % relative error of the Henry's law equation is then necessary to calculate (**Equation A2-25**).

**Equation A2-25**– Calculation of error in applying Henry's law.

$$\%error = 100 \times Abs \frac{xH - P_{NH_3}}{P_{NH_3}}$$

The final step of this methodology was to utilise the Solver function in Microsoft Excel to minimise the %error from Henry's law by adjusting  $N_{L,NH_3}$ . A logical test has been used so that the solution is only accepted when the %error is less than 0.02. By altering  $N_{L,NH_3}$ , the values of the partial pressure ( $P_{NH_3}$ ), liquid molar fraction of  $NH_3$  ( $x$ ), the total pressure after reaction ( $P_{tot}$ ), gas molar fraction of  $NH_3$  ( $y$ ), and molar fraction of moisture ( $y_{H_2O,moist}$ ) were generated in Solver, thereby updating the remaining calculations.

The assumptions are then checked to ensure that they have remained valid. The solution, after running Solver, is checked so that  $x$  and  $y$  are small (e.g.  $<0.05$ ). This ensures that the ammonia concentrations are still considered 'very dilute' and therefore under ideal gas conditions. Here, the amount of excess NaOH is significant (e.g.  $4N_{NaOH} > N_{AMS}$ ), rendering the aqueous solution as basic ( $pH > 7$ ). This allows the potential ammonium ion co-product to be ignored as the ammonia product is thermodynamically favoured. An example of the use of Microsoft Excel and Solver is presented in the the Appendix (A1.2.2). Due to reactive solutions being used for this methodology, there was a maximum partial pressure of around 2 kPa that was possible.

### A.3 Pyrolysis-Gas Chromatography/Mass Spectrometry peak tables

In this section, examples of the peak tables generated from the pyrolysis-gas chromatography/mass spectrometry of the samples run across Chapter 4, Chapter 5, and Chapter 6 are presented. Here, the py-GC/MS chromatograms (py-gram) of one sample from each category of sample are shown (as described in Table A3-1).

**Table A3-1** – Peak tables of samples representing each category of sample.

<b>Category</b>	<b>Sample</b>
<b>Commercial lignin</b>	Lignoboost at 550 °C
<b>Digestate Residue</b>	Municipal Solid Waste (MSW) digestate at 550 °C
<b>Acid-washed solid sample</b>	Coconut husk at 550 °C
<b>Tree bark</b>	Acid-washed MSWdig at 550 °C
<b>Solvent-extracted solid sample</b>	Grand fir (GF) at 550 °C
	Soxhlet-extracted grand fir (GFSox) at 550 °C

**Table A3-2** – Peak table for py-GC/MS of lignoboost at 550 °C. Highlighted cells denote compounds discussed in the results chapters.

Peak#	Ret.Time	Proc.From	Proc.To	Mass	Area	Height	A/H	Conc.	Name
1	19.896	19.64	19.93	TIC	417701358	44174850	9.46	13.59	Phenol, 2-methoxy-
2	21.473	21.395	21.52	TIC	43588623	14917043	2.92	1.42	Creosol
3	22.441	22.155	22.56	TIC	732873793	63521145	11.54	23.84	Creosol
4	23.31	23.26	23.39	TIC	17246172	6381606	2.7	0.56	Phenol, 3-ethyl-
5	23.765	23.67	23.82	TIC	56954574	18571102	3.07	1.85	Benzene, 1,4-dimethoxy-2-methyl-
6	24.328	24.11	24.36	TIC	306023106	44702734	6.85	9.95	Benzene, 1,4-dimethoxy-2-methyl-
7	25.607	25.42	25.66	TIC	254375976	43795250	5.81	8.27	Benzene, 1-methoxy-2-methyl-3-nitro-
8	26.07	25.96	26.1	TIC	54789348	12629135	4.34	1.78	trans-Isoeugenol
9	26.14	26.1	26.34	TIC	50030581	20273140	2.47	1.63	Homovanillyl alcohol
10	26.436	26.34	26.54	TIC	132098232	28385829	4.65	4.3	Catechol
11	27.05	26.99	27.17	TIC	25084842	10101759	2.48	0.82	trans-Isoeugenol
12	27.277	27.17	27.32	TIC	96153322	17221095	5.58	3.13	Phenol, 2-methoxy-4-(2-propenyl)-, acetate
13	27.38	27.32	27.44	TIC	22625763	7219001	3.13	0.74	3-Methoxybenzyl alcohol
14	28.137	28.03	28.25	TIC	99891183	25179695	3.97	3.25	1,2-Benzenediol, 4-methyl-
15	29.015	28.85	29.05	TIC	115205891	19564668	5.89	3.75	Vanillin
16	29.889	29.81	29.97	TIC	26058185	10191910	2.56	0.85	1,3-Benzenediol, 4-ethyl-
17	30.098	29.97	30.15	TIC	52810280	12482753	4.23	1.72	Homovanillic acid
18	30.639	30.5	30.68	TIC	86042585	16141313	5.33	2.8	Apocynin
19	30.797	30.72	30.86	TIC	29745958	7989373	3.72	0.97	4-Ethoxy-3-anisaldehyde
20	31.597	31.46	31.64	TIC	98907269	19944473	4.96	3.22	2-Propanone, 1-(4-hydroxy-3-methoxyphenyl)-
21	32.188	32.07	32.27	TIC	48822485	12583286	3.88	1.59	4-Ethoxy-3-anisaldehyde
22	34.005	33.74	34.08	TIC	228622144	25369228	9.01	7.44	Homovanillic acid
23	34.7	34.62	34.75	TIC	22291657	7676547	2.9	0.73	Benzeneacetic acid, 3,4-dimethoxy-
24	37.001	36.91	37.04	TIC	29265331	9937311	2.94	0.95	1H-Inden-1-one, 2,3-dihydro-5,6-dimethoxy-3-methyl-
25	41.419	41.33	41.48	TIC	27499825	9191687	2.99	0.89	Retene

**Table A3-3** – Peak table for py-GC/MS of MSW digestate at 550 °C. Highlighted cells denote compounds discussed in the results chapters.

Peak#	Ret.Time	Proc.From	Proc.To	Mass	Area	Height	A/H	Conc.	Name
1	3.764	3.605	3.87	TIC	2536230	405664	6.25	7.4	Ethene, 1,1-difluoro-
2	7.85	7.82	7.95	TIC	175086	33963	5.16	0.51	Isoamyl nitrite
3	7.994	7.95	8.155	TIC	978957	149711	6.54	2.86	Toluene
4	11.362	11.34	11.92	TIC	19151237	2321078	8.25	55.88	Bicyclo[4.2.0]octa-1,3,5-triene
5	18.545	18.5	18.63	TIC	427014	88945	4.8	1.25	Phenol
6	23.115	23.035	23.195	TIC	1397600	214636	6.51	4.08	Benzoic acid
7	23.265	23.195	23.335	TIC	574079	93639	6.13	1.68	Benzoic acid 2-methylpentyl ester
8	24.532	24.455	24.585	TIC	514213	109269	4.71	1.5	3-Methoxyacetophenone
9	24.621	24.585	24.745	TIC	438006	73471	5.96	1.28	Phenol, 2,3,5,6-tetramethyl-
10	25.67	25.64	25.805	TIC	343051	54944	6.24	1	Phenol, 2,6-dimethoxy-
11	27.3	27.245	27.345	TIC	449721	118837	3.78	1.31	Phenol, 2-methoxy-4-(2-propenyl)-, acetate
12	27.362	27.345	27.47	TIC	482242	130274	3.7	1.41	1H-Indole, 3-methyl-
13	28.76	28.715	28.805	TIC	400687	165686	2.42	1.17	1-Dodecanol, 3,7,11-trimethyl-
14	29.81	29.76	29.84	TIC	314757	112604	2.8	0.92	Benzene, 1,1'-(1,3-propanediyl)bis-
15	29.845	29.84	29.91	TIC	207771	84732	2.45	0.61	Hexadecane, 2,6,10,14-tetramethyl-
16	29.957	29.91	30.015	TIC	268781	80514	3.34	0.78	1-Docosene
17	31.042	30.975	31.18	TIC	2747043	695363	3.95	8.02	Benzene, 3-butenyl-
18	31.235	31.18	31.315	TIC	284992	54383	5.24	0.83	2-Tridecanone
19	37.641	37.595	37.68	TIC	224978	86030	2.62	0.66	9-Tetradecen-1-ol, acetate, (Z)-
20	38.102	38.06	38.155	TIC	173983	72247	2.41	0.51	FOSTHIAZATE-1
21	38.912	38.895	39	TIC	718372	198225	3.62	2.1	m-Terphenyl
22	39.685	39.64	39.74	TIC	411646	133643	3.08	1.2	p-Terphenyl
23	39.761	39.74	39.88	TIC	551195	150841	3.65	1.61	1,2-Ethanediol, dibenzoate
24	40.476	40.45	40.565	TIC	207933	63582	3.27	0.61	[1,1':3',1''-Terphenyl]-2'-ol
25	42.51	42.465	42.58	TIC	291286	107376	2.71	0.85	Benzenemethanamine, N-hydroxy-N-(phenylmethyl)-

**Table A3-4** – Peak table for py-GC/MS of coconut husk (CH) at 550 °C. Highlighted cells denote compounds discussed in the results chapters.

Peak#	Ret.Time	Proc.From	Proc.To	Mass	Area	Height	A/H	Conc.	Name
1	3.554	3.38	3.7	TIC	3523549	485392	7.26	8.56	N'-Furfurylidene-4-nitrobenzohydrazide
2	4.302	4.235	4.44	TIC	532762	89579	5.95	1.29	Cyclopropane, (methoxymethyl)-
3	11.455	11.41	11.505	TIC	301839	71640	4.21	0.73	[1,1'-Bicyclopentyl]-2-one
4	17.855	17.81	17.955	TIC	168461	31739	5.31	0.41	2-Cyclopenten-1-one, 2-hydroxy-3-methyl-
5	17.972	17.955	18.36	TIC	9273260	964548	9.61	22.53	Phenol
6	18.464	18.36	18.75	TIC	3292404	350817	9.38	8	Phenol, 2-methoxy-
7	19.398	19.33	19.58	TIC	715981	99307	7.21	1.74	Phenol, 2-methyl-
8	20.22	20.18	20.25	TIC	764607	253540	3.02	1.86	p-Cresol
9	20.255	20.25	20.54	TIC	1741802	230482	7.56	4.23	
10	21.002	20.94	21.09	TIC	770386	135633	5.68	1.87	Creosol
11	21.155	21.09	21.315	TIC	755716	108678	6.95	1.84	6-Nonenal, (Z)-
12	22.674	22.59	22.69	TIC	1600494	528135	3.03	3.89	Benzoic acid
13	22.734	22.69	22.885	TIC	4735804	690603	6.86	11.5	Benzene, 1,4-dimethoxy-2-methyl-
14	22.9	22.885	22.925	TIC	418866	189609	2.21	1.02	Benzoic acid
15	22.935	22.925	23.025	TIC	476040	153813	3.09	1.16	
16	24.114	24.04	24.16	TIC	2015955	550845	3.66	4.9	4-Ethylbenzoic acid
17	24.183	24.16	24.505	TIC	5088680	657263	7.74	12.36	4-Hydroxy-3-methylacetophenone
18	24.638	24.6	24.75	TIC	361762	94673	3.82	0.88	Phenol, 2-methoxy-4-(2-propenyl)-, acetate
19	25.331	25.26	25.49	TIC	1653921	220660	7.5	4.02	Phenol, 2,6-dimethoxy-
20	25.52	25.49	25.615	TIC	248365	66751	3.72	0.6	Diisopropyl adipate
21	25.889	25.84	26.055	TIC	341897	52079	6.56	0.83	trans-Isoeugenol
22	26.985	26.94	27.15	TIC	1452568	224711	6.46	3.53	trans-Isoeugenol
23	27.237	27.15	27.275	TIC	183126	37580	4.87	0.44	Phenol, 2-methoxy-4-(2-propenyl)-, acetate
24	29.208	29.155	29.29	TIC	265166	64364	4.12	0.64	Fluorene
25	30.47	30.44	30.59	TIC	482011	113575	4.24	1.17	Benzophenone

**Table A3-5** – Peak table for py-GC/MS of acid-washed MSW digestate at 550 °C. Highlighted cells denote compounds discussed in the results chapters.

Peak#	Ret.Time	Proc.From	Proc.To	Mass	Area	Height	A/H	Conc.	Name
1	5.729	5.695	5.92	TIC	9773074	1555727	6.28	7.96	Acetic acid
2	8.789	8.725	8.865	TIC	641727	146850	4.37	0.52	p-Xylene
3	9.275	9.225	9.43	TIC	2509342	478457	5.24	2.04	Propanenitrile, 3,3'-oxybis-
4	10.068	9.995	10.34	TIC	25794210	4925273	5.24	21.01	Furfural
5	12.467	12.41	12.56	TIC	968826	280725	3.45	0.79	Cyclohexene, 1-methyl-4-(1-methylethenyl)-, (S)-
6	13.317	13.26	13.385	TIC	709984	161024	4.41	0.58	Cycloheptane
7	13.991	13.945	14.06	TIC	1824246	548692	3.32	1.49	2-Furancarboxaldehyde, 5-methyl-
8	14.098	14.06	14.205	TIC	1201216	315722	3.8	0.98	.alpha.-Acetobutyrolactone
9	14.533	14.48	14.62	TIC	1630188	453747	3.59	1.33	1-Hexanol, 2-ethyl-
10	15.599	15.475	15.755	TIC	21024643	4075540	5.16	17.13	1,4-Butanediamine, 2,3-dimethoxy-N,N,N',N'-tetramethyl-, [S-(R*,R*)]-
11	16.564	16.5	16.685	TIC	2170586	565071	3.84	1.77	2-Propenoic acid, 2-methyl-, 1-methylethyl ester
12	17.602	17.545	17.725	TIC	2206565	526500	4.19	1.8	2,5-Dimethyl-4-hydroxy-3(2H)-furanone
13	19.19	19.12	19.25	TIC	779669	203627	3.83	0.64	2-Nonen-1-ol, (Z)-
14	20.298	20.16	20.375	TIC	33098065	7577690	4.37	26.96	2-Furanmethanol
15	22.186	22.13	22.3	TIC	1359992	320964	4.24	1.11	Methacrylic acid, ethyl ester
16	22.867	22.795	23.055	TIC	4406559	808787	5.45	3.59	Heptanal
17	24.332	24.235	24.455	TIC	4368421	970754	4.5	3.56	3-Methoxyacetophenone
18	24.767	24.72	24.845	TIC	597249	154694	3.86	0.49	4-Hydroxy-3-methylacetophenone
19	24.95	24.905	25.01	TIC	701852	252007	2.79	0.57	trans-Isoeugenol
20	26.656	26.585	26.73	TIC	689326	175677	3.92	0.56	Indan-1,2,3-trione
21	26.842	26.73	26.93	TIC	620112	155770	3.98	0.51	Benzene, (octyloxy)-
22	27.709	27.655	27.865	TIC	3127085	615913	5.08	2.55	Phenol, 2-methoxy-4-(1-propenyl)-
23	30.277	30.23	30.345	TIC	1094279	360445	3.04	0.89	3,6-Dimethylpiperazine-2,5-dione
24	30.385	30.345	30.455	TIC	702383	239750	2.93	0.57	3,6-Dimethylpiperazine-2,5-dione
25	38.126	38.07	38.18	TIC	769393	282116	2.73	0.63	Hexadecane, 1-chloro-

**Table A3-6** - Peak table for py-GC/MS of grand fir (GF) tree bark at 550 °C. Highlighted cells denote compounds discussed in the results chapters.

Peak#	Ret.Time	Proc.From	Proc.To	Mass	Area	Height	A/H	Conc.	Name
1	12.075	12.025	12.12	TIC	31729074	13189157	2.41	1.64	(1R)-2,6,6-Trimethylbicyclo[3.1.1]hept-2-ene
2	12.703	12.65	12.735	TIC	26248634	10749543	2.44	1.35	Camphene
3	13.589	13.515	13.625	TIC	61618321	21257191	2.9	3.18	Bicyclo[3.1.1]heptane, 6,6-dimethyl-2-methylene-, (1S)-
4	15.263	15.21	15.3	TIC	31460422	13515649	2.33	1.62	.beta.-Phellandrene
5	19.23	19.135	19.275	TIC	94077027	24008566	3.92	4.85	Phenol
6	19.776	19.645	19.84	TIC	142079365	27741413	5.12	7.33	Phenol, 2-methoxy-
7	20.353	20.31	20.405	TIC	19165312	7257622	2.64	0.99	Phenol, 2-methyl-
8	21.288	21.225	21.325	TIC	38434399	10229804	3.76	1.98	p-Cresol
9	22.283	22.145	22.32	TIC	145963733	29846968	4.89	7.53	Creosol
10	23.021	22.895	23.07	TIC	288392005	64131435	4.5	14.88	Acetic acid, 1,7,7-trimethyl-bicyclo[2.2.1]hept-2-yl ester
11	23.657	23.61	23.695	TIC	25812683	10711582	2.41	1.33	Copaene
12	24.153	24.085	24.175	TIC	41735870	14657324	2.85	2.15	Phenol, 4-ethyl-2-methoxy-
13	24.2	24.175	24.24	TIC	16062702	8438197	1.9	0.83	1H-Cyclopenta[1,3]cyclopropa[1,2]benzene, octahydro-7-methyl-3-methylene-4-(1-methylethyl)-, [3aS-(3a.alpha.,3b.beta.,4.beta.,7
14	25.548	25.365	25.57	TIC	231832455	40507539	5.72	11.96	4-Hydroxy-3-methylacetophenone
15	25.616	25.57	25.665	TIC	45329965	17199126	2.64	2.34	.alpha.-Cubebene
16	26.017	25.92	26.08	TIC	130028271	30752576	4.23	6.71	Phenol, 2-methoxy-4-(2-propenyl)-, acetate
17	26.593	26.525	26.64	TIC	37324557	14232787	2.62	1.93	.alpha.-Muurolene
18	26.796	26.74	26.825	TIC	28232443	12287563	2.3	1.46	1H-Cyclopenta[1,3]cyclopropa[1,2]benzene, octahydro-7-methyl-3-methylene-4-(1-methylethyl)-, [3aS-(3a.alpha.,3b.beta.,4.beta.,7
19	27.096	26.965	27.12	TIC	140334126	32871398	4.27	7.24	Naphthalene, 1,2,3,5,6,8a-hexahydro-4,7-dimethyl-1-(1-methylethyl)-, (1S-cis)-
20	27.182	27.12	27.205	TIC	37399805	13993363	2.67	1.93	Phenol, 2-methoxy-4-(1-propenyl)-
21	27.23	27.205	27.26	TIC	16710607	9557730	1.75	0.86	Naphthalene, 1,2,4a,5,8,8a-hexahydro-4,7-dimethyl-1-(1-methylethyl)-, [1S-(1.alpha.,4a.beta.,8a.alpha.)]-
22	27.439	27.35	27.485	TIC	71575977	23545046	3.04	3.69	Naphthalene, 1,2,3,4,4a,7-hexahydro-1,6-dimethyl-4-(1-methylethyl)-
23	27.591	27.52	27.635	TIC	22809533	10481622	2.18	1.18	Naphthalene, 1,2,3,4-tetrahydro-1,6-dimethyl-4-(1-methylethyl)-, (1S-cis)-
24	28.343	28.185	28.405	TIC	189184975	37020345	5.11	9.76	trans-Isoeugenol
25	30.358	30.3	30.405	TIC	24435120	10356606	2.36	1.26	1-Naphthalenol, 1,2,3,4,4a,7,8,8a-octahydro-1,6-dimethyl-4-(1-methylethyl)-, [1R-(1.alpha.,4.beta.,4a.beta.,8a.beta.)]-

**Table A3-7 - Peak table for py-GC/MS of solvent-extracted solid grand fir (GFSox) tree bark at 550 °C. Highlighted cells denote compounds discussed in the results chapters.**

Peak#	Ret.Time	Proc.From	Proc.To	Mass	Area	Height	A/H	Conc.	Name
1	5.729	5.69	6.2	TIC	39230393	5228686	7.5	40.05	Acetic acid
2	6.457	6.4	6.72	TIC	3516462	456926	7.7	3.59	2-Propanone, 1-hydroxy-
3	8.501	8.435	8.6	TIC	1487735	300751	4.95	1.52	2-Propanone, 1-hydroxy-
4	9.374	9.32	9.53	TIC	993494	174296	5.7	1.01	1-Pyrrolidinebutyronitrile
5	9.609	9.55	9.715	TIC	1241720	255589	4.86	1.27	Propanoic acid, 2-oxo-, methyl ester
6	10.145	10.075	10.365	TIC	12730426	2568668	4.96	13	Furfural
7	11.307	11.255	11.4	TIC	1876526	414375	4.53	1.92	2-Furanmethanol
8	11.443	11.4	11.56	TIC	1923470	517529	3.72	1.96	
9	12.567	12.52	12.695	TIC	1178664	302033	3.9	1.2	4-Cyclopentene-1,3-dione
10	13.373	13.33	13.545	TIC	1653291	328369	5.03	1.69	Cyclopentanone, 2-methyl-
11	14.089	14.05	14.195	TIC	1572992	429709	3.66	1.61	2-Furancarboxaldehyde, 5-methyl-
12	14.659	14.615	14.775	TIC	747483	179890	4.16	0.76	Butyrolactone
13	15.535	15.485	15.6	TIC	1000355	315644	3.17	1.02	2,5-Furandione, 3-methyl-
14	15.637	15.6	15.77	TIC	1154298	278738	4.14	1.18	1,4-Butanediamine, 2,3-dimethoxy-N,N,N',N'-tetramethyl-, [S-(R*,R*)]-
15	16.334	16.275	16.465	TIC	743824	150497	4.94	0.76	2-Cyclopenten-1-one, 2-hydroxy-3-methyl-
16	16.671	16.63	16.765	TIC	672023	194048	3.46	0.69	2-Propenoic acid, 2-methyl-, 1-methylethyl ester
17	17.104	17.06	17.235	TIC	1547097	460277	3.36	1.58	Phenol
18	17.676	17.625	17.82	TIC	1913766	487178	3.93	1.95	Phenol, 2-methoxy-
19	19.229	19.18	19.385	TIC	1790347	365413	4.9	1.83	Orcinol
20	20.732	20.67	20.795	TIC	4885318	1303833	3.75	4.99	Cyclopropyl carbinol
21	20.817	20.795	20.95	TIC	1428305	344253	4.15	1.46	2-Pentenoic acid, 3-ethyl-, methyl ester
22	24.205	24.065	24.34	TIC	5275556	447900	11.78	5.39	Propylene Carbonate
23	24.43	24.34	24.59	TIC	5032650	1192818	4.22	5.14	4-Hydroxy-3-methylacetophenone
24	27.787	27.735	27.93	TIC	3453278	1111695	3.11	3.53	Phenol, 2-methoxy-4-(1-propenyl)-
25	28.749	28.7	28.865	TIC	899086	251455	3.58	0.92	7-Methoxy-4-methylcoumarin